Photo and Electrochemical Strategies to C–N Bond Formation

A dissertation submitted in partial fulfillment for the degree of

Doctor of Philosophy

Submitted By

Tipu Alam

Roll No. 176122011

Under the supervision of

Prof. Bhisma Kumar Patel

Department of Chemistry

Indian Institute of Technology Guwahati

Guwahati-781039, Assam, India

April, 2024

भारतीय प्रौद्योगिकी संस्थान गुवाहाटी
Indian Institute of Technology Guwahati

DEDICATED WITH LOVE

To my parents and family, for their endless love, support, and encouragement

My supervisor

Prof. Bhisma K. Patel

भारतीय प्रौद्योगिकी संस्थान गुवाहाटी
Indian Institute of Technology Guwahati

INDIAN INSTITUTE OF TECHNOLOGY GUWAHATI

Department of Chemistry

STATEMENT

I do hereby declare that the matter embodied in this thesis is the result of investigations carried out by me in the Department of Chemistry, Indian Institute of Technology Guwahati, India, under the guidance of *Prof. Bhisma K. Patel*.

In keeping with the general practice of reporting scientific observations, due acknowledgements have been made wherever the work described is based on the findings of other investigators.

April, 2024

IIT Guwahati ***Tipu Alam***

भारतीय प्रौद्योगिकी संस्थान गुवाहाटी
Indian Institute of Technology Guwahati

INDIAN INSTITUTE OF TECHNOLOGY GUWAHATI

Department of Chemistry

CERTIFICATE

This is to certify that *Tipu Alam* has been working under my supervision since July 2017 as a regular registered Ph.D. student. His thesis entitled "***Photo and Electrochemical Strategies to C–N Bond Formation***" is an authentic record of the results obtained from the research work in the Department of Chemistry, Indian Institute of Technology Guwahati, Assam, India. I am forwarding his thesis to submit for the Ph.D. (Science) degree from this institute. I certify that he has fulfilled all the requirements according to the rules of this institute regarding the investigations embodied in his thesis and this work has not been submitted elsewhere for a degree.

April, 2024
IIT Guwahati

Prof. Bhisma K. Patel
(Thesis Supervisor)
Department of Chemistry

भारतीय प्रौद्योगिकी संस्थान गुवाहाटी
Indian Institute of Technology Guwahati

ACKNOWLEDGEMENT

As the highest academic qualification, a Ph.D. degree can not be completed alone. So, standing at the final stage of a truly unforgettable journey, I would like to acknowledge and thank the people who supported me, believed in me, and encouraged me to complete the journey.

First and foremost, I want to express my deepest respect and profound gratitude to my supervisor, Prof. Bhisma K. Patel, for allowing me to work under his guidance. His continuous support and inspiration through creative and unique scientific ideas helped me to explore the domain of my work assembled in this thesis. I feel blessed to have him as my mentor, who gave me moral support and full freedom throughout the journey.

I would also like to extend my heartiest thanks to the doctoral committee members, Prof. Abu Taleb Khan, Prof. Vaibhav V. Goud, and Dr. Krishna Pada Bhabak, for their timely evaluation of my Ph.D. work, encouragement, and precious suggestions.

I sincerely thank all the faculty and staff members of the Department of Chemistry, IIT Guwahati, for their cooperative nature. I would like to thank Babulal da for single-crystal XRD, Imdadul da for NMR, Aniruddha da for HRMS, and Diganta da, Basab da, Tapu, and Michel for various official work and support in the Department of Chemistry.

I wish to express sincere gratitude to MHRD for financial support and to IIT Guwahati for all the facilities that were made available to me for learning several analytical instruments required during my research work. I would also like to especially thank the Central Instruments Facility, IIT Guwahati, for allowing me to become an operator of the NMR (600 MHz) instrument. I am grateful to the single-crystal XRD facilities, MHRD for the 400 MHz NMR facility under the COE-FAST program, DST for the 500 MHz NMR facility under the DST-FIST program, NECBH, IIT Guwahati, and DBT, Govt. of India for the 400 MHz NMR and single-crystal XRD facilities.

I would like to express my gratitude and a big thanks to all the operators inside and outside IIT Guwahati for successfully carrying out all the instrumental experiments required during my research work. Further, I am extremely thankful to all the co-authors, editors, associate editors, and reviewers for their valuable comments and suggestion.

The most unforgettable journey of my academic life wouldn't have been possible without the support of the incredible BKP warriors I've had the privilege to know personally. I want to express my deepest gratitude to my Ph.D. senior, Dr. Anjali Dahiya, for her guidance during the initial stages of my lab work. However, such a remarkable journey in academia is not a solo effort. I also want to extend my heartfelt thanks to Dr. Wajid Ali, who not only provided overall training but also supported me through the most challenging stages of this journey. I am also immensely grateful to Dr. Amitava Rakshit, who has constantly supported me throughout this journey. He's not just a helpful lab senior but also a great friend and tea partner.

I am immensely grateful to my outstanding lab seniors, Subendhu bhai, Prakash bhai, Dr. Anju Modi, Dr. Suresh Rajamanickam, Dr. Bilal Ahmed Mir, and Dr. Prasenjit Sau, for their invaluable help, precious suggestions, and constant encouragement. I also want to extend my heartfelt thanks to my postdoctoral lab seniors, Dr. Gaurav Shukla, Dr. C.B. Singh, Dr. Suman Pal, Dr. Ritush Kumar, Dr. Pakiza Begum, Dr. Gongutri Borah, Dr. Bhaskar Deka, Dr. Binoyargha Dam, and Dr. Kamal Krishna Rajbongshi, for their unwavering support and assistance. Special thanks to Kamal bhai and Binoy bhai, who have been exceptionally supportive and friendly throughout my journey.

I am also fortunate to have Ashish and Nikita as batchmates, whose enormous support and encouragement have been invaluable to me. I can't forget the countless healthy discussions, picnics, and parties we shared throughout this journey. During this journey, our fights and love were as evident as the head and tail of a coin in a friendship. I deeply appreciate all the talented juniors - Bubul, Hiru, Tamanna, Pritishree, Raju, Dinabandhu, Shalini, Deepjyoti, Supriya, and Manjunath- for their hard work, diligence, and for maintaining a friendly atmosphere in the lab. With these fellow warriors, I have experienced the happiest and most memorable moments of my life. I've also had the pleasure of working with dedicated summer and M.Sc. trainees such as Sreyashi, Angshu, Abhishek, Gaurav, Priyabrata, Prashant, Poonam, Garima, Rani, Arihant, Kunika, Pankaj, Akshar, Abhishek, Sourasish, Kaustav, and Pratip.

I want to extend my heartfelt thanks to my M.Sc. seniors, Jabed bhai, Atikur bhai, Mofijur bhai, Sahel bhai, and Samim bhai, for their outstanding contribution before my journey even began. I am extremely grateful to my friends Nurujaman and Adnan for their unwavering help, support, and for always being by my side. They made good times even better and made the hard times a whole lot easier. Our healthy gossip sessions

throughout the journey are truly unforgettable. Thank you, Nurujaman and Adnan, for motivating me at every stage of this journey.

I would like to thank my Ph.D. friends, seniors, and juniors here at IITG. Adil bhai, Shaad bhai, Akhtar bhai, Shoaib bhai, Rabindranath, Mihir, Abu, Bipin, Bitan, Araghni, Arindom, Rupa, Khadimul, Avijit, Tapas, Raktim, Kisan, Biman, Subhamoy, Amit, Manideepa, Sonbidya, Arup, Santa, Sourav, Sudip, Surya, Pallav, Vinoy, Jagnyesh, Paresh, Manmath, Shubhajit, Kangkan, Srimanta, Ahmad, Dr. Archana Kumari Sahoo, Dr. Kundan, Dr. Subhasish, Dr. Tariq, Dr. Sourav, and Dr. Rashid, thank you for making this journey much better, easier, and entertaining.

I am deeply grateful to my teachers, to whom I owe immense gratitude for their invaluable teachings and the philosophy they imparted on being a good human being. Prof. Shamsuzzaman, Prof. Syed Mashhood Ali, Prof. Suhail Sabir, Prof. Lutfullah, Dr. Palashuddin Sk, and Dr. Md. Musawwer Khan, your guidance has been instrumental in shaping not just my academic journey but also my values as a person. Thank you for everything.

Lastly, and most importantly, my Ph.D. journey would not have been possible without the endless love, unwavering support, patience, and blessings from my family. I am profoundly grateful to my Mom, Dad, Sister, and Brother for their unconditional support, affection, and deep concern for my career. I want to express my deepest gratitude to my parents, whose unconditional love at every stage of my life motivated me to overcome all challenges. I owe my entire life to them. Dedicating this thesis to them is a small recognition of their love, support, and encouragement.

Last but not the least; I am thankful to Almighty for continuous blessing during my research carrier to accomplish this remarkable journey.

Tipu Alam

SYNOPSIS

The contents of this thesis have been divided into six chapters based on the experimental works performed and results obtained during the research period. The introductory chapter of the thesis represents a summary of '**Photo and Electrochemical Strategies to C–N Bond Formation'**. For simplicity and brevity, **Chapter I** is divided into two parts. **Chapter IA** includes a photochemical C–N bond formation *via* difunctionalization of alkenes and indoles, whereas, **Chapter IB** deals with electrochemical approach for the C–N bond construction. The subsections of **Chapter IA** and **IB** are based on the mode of reactivity of difunctionalization and cross-coupling reactions.

Chapter II demonstrates a visible-light-induced synthesis of *N*-hydroxybenzimidoyl cyanides from aromatic terminal alkenes using Eosin Y as an organic photoredox catalyst. The process goes via a radical pathway with successive incorporation of two nitrogen atoms, one each from *tert*-butyl nitrite and ammonium acetate. The final product is achieved by the concomitant installation of an oxime and a nitrile group. DFT calculation supports a bi-radical pathway and all the proposed steps. A few useful synthetic transformations of *N*-hydroxybenzimidoyl cyanide have also been illustrated.

Chapter III describes a visible-light-mediated concomitant C3 oxidation and C2 amination of indoles at room temperature using Ir (III) photocatalyst. This reaction proceeds without any isatin intermediate via the attack of singlet oxygen at the C3 position followed by C2 amination leading to difunctionalization of indoles.

Chapter IV describes an electrochemical amidation of benzoyl hydrazine/carbazate and primary/secondary amine as coupling partners via concomitant cleavage and formation of $C(sp^2)$–N bonds. This methodology proceeds under metal and exogenous oxidant-free conditions producing N_2 and H_2 as by-products. Mechanistic studies reveal the *in situ* generations of both acyl and *N*-centered radicals from benzoyl hydrazines and amines respectively. The utility of this protocol is demonstrated in the large-scale, and synthesis of bezafibrate, a hyperlipidemic drug.

Chapter V delineates a robust electrochemical cross-coupling between aroyl hydrazine and *NH*-sulfoximine via concomitant cleavage and formation of C(sp^2)–N bond with the evolution of H_2 and N_2 as innocuous by-products. This sustainable protocol avoids the use of toxic reagents and occurs at room temperature. The reaction proceeds via the generation of an aroyl and a sulfoximidoyl radical via anodic oxidation under constant current electrolysis (CCE), affording *N*-aroylated sulfoximine. The strategy is applied to late-stage sulfoximidation of L-menthol, (–)-borneol, D-glucose, vitamin-E derivatives, and marketed drugs such as probenecid, ibuprofen, flurbiprofen, ciprofibrate, and sulindac. In addition, the present methodology is mild, high functional group tolerance with broad substrate scope and scalable.

Chapter VI describes a robust electrochemical cross-coupling between α-keto acids and *NH*-sulfoximines is established. This process cleaves the C–C bond and forms a C(sp^2)–N bond with the evolution of by-products H_2 and CO_2. This sustainable approach eliminates the need for hazardous reagents and operates at room temperature. In this process, *N*-aroylated sulfoximines are produced through the generation of aroyl and sulfoximidoyl radicals by anodic oxidation in constant current electrolysis (CCE). This approach is successfully employed for the late-stage sulfoximidation of various compounds, including L-menthol, (-)-borneol, D-glucose, derivatives, and commercial drugs such as probenecid, ibuprofen, and flurbiprofen. This methodology features good functional group compatibility, a broad scope, and a detailed mechanistic investigation.

Each of these chapters comprises seven subsections which include an introduction, previous work, present work, experimental section, references, spectral data, and a few representative spectra.

CHAPTER I. Photo and Electrochemical Strategies to C–N Bond Formation

Part A:

The introductory chapter includes a brief understanding of difunctionalization strategies, their advantages, limitations, and applications in synthetic organic chemistry. The first part of this chapter includes the photochemical difunctionalization of alkenes for the construction of C–N bonds.

The past decades have witnessed rapid progress in radical-mediated carbon-heteroatom bond formations which have been established as powerful tools to access various organic frameworks. Despite several existing methods for the C–X bond formations, there is a need to develop newer methodologies. In this regard, visible-light-mediated C–X bond formations have gained immense popularity due to their operational simplicity, minimization of by-products, easy handling, mild reaction conditions, etc. Besides offering a sustainable way to synthesize molecules, photochemistry has the potential to unlock reaction manifolds that are unavailable to conventional thermal pathways.

Since the pioneering work from the group of MacMillan, Koenig, Stephenson, Rueping, Ritter, Yoon, and others, photocatalysis has experienced renascence over the past decades. This field is mainly categorized based on the catalytic systems involved. (i) The use of photocatalyst (transition metal complexes or organic dyes) which in its excited state activates the organic molecules via either single electron transfer (SET) energy transfer (EnT), (Figure I.1). (ii) Synergistic combination of photocatalyst and transition metal catalyst. (iii) The use of only transition metal complexes in combination with visible light which plays a dual role of harnessing photon energy as a photocatalyst followed by bond-breaking and making process. Mostly the use of visible-light irradiation, in combination with photosensitizer (transition metal complexes or organic dyes), has been a well-established reaction promoter for many organic transformations. In this direction, transition metal complexes as well as organic dyes have gained enough popularity due to their outstanding reactivities and selectivity in various photochemical reactions. Most of these photochemical reaction proceeds through a single-electron transfer (SET) process from the excited photocatalyst to the organic substrate or reagent which usually involves two pathways either an oxidative quenching or a reductive quenching (Figure I.1).

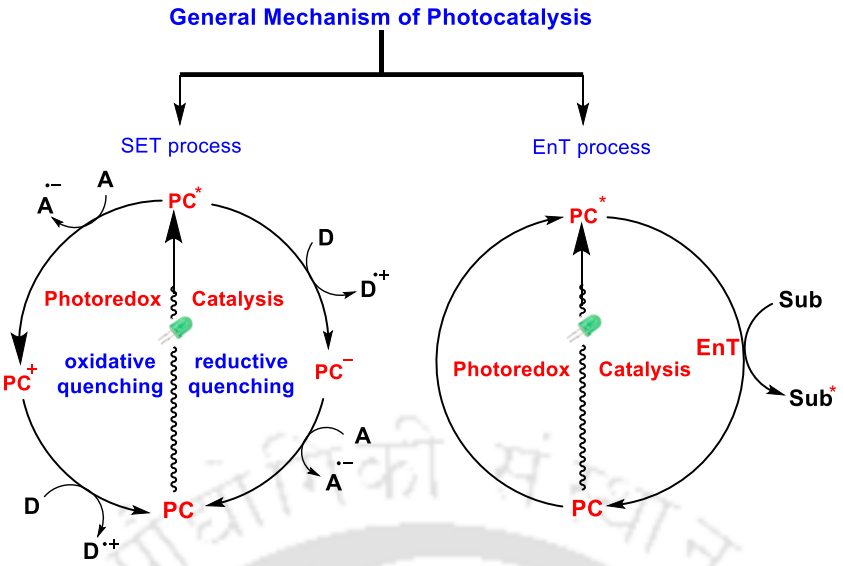

Figure I.1. *General mechanism of visible-light-induced transformations.*

IA. Difunctionalization Strategy for C–C Double Bond

The difunctionalization approach is widely used in modern organic synthesis because of its high regioselectivity, allowing the simultaneous incorporation of two functional groups onto a C–C double bond. This method provides a straightforward route to constructing complex molecular frameworks.

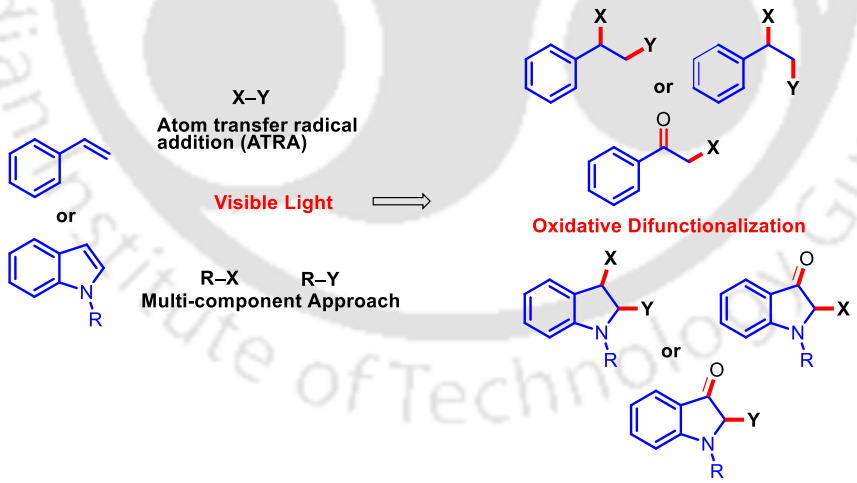

Figure IA.1. *Different difunctionalization strategies*

IA.1. Photochemical C–N Bond Formation via Difunctionalization of Alkene

In recent years, C–N bond formation via the difunctionalization of alkenes has gained much reputation, where the simultaneous introduction of two functional groups is achieved in

a single step. In this endeavour development of newer methodologies in the direction of difunctionalization of alkene remains an important topic of research in organic synthesis.

.

IA.2. Photochemical C–N Bond Formation via Difunctionalization of Indole

Indoles are the backbones of many natural products as well as pharmaceuticals hence the development of newer methodologies for the synthesis of complex indole frameworks is always demanding. Though photocatalysis is well-established in organic synthesis but electrochemical approach stands out as a greener and advanced method that can precisely control reaction potentials to enable complex reactions. Since this approach aligns with the broad goal of achieving greener and sustainable protocols, hence the development of newer electrochemical methodologies is always welcome in organic synthesis.

Part B:

The second part of this chapter gives a brief synopsis of the exploration of electrochemical strategies toward the construction of C–N bonds *via* traditional and radical-radical cross-coupling approaches. Over the past decades, cross-coupling reactions have gained enough popularity for the construction of various organic molecules. But traditionally cross-coupling reaction often requires high temperatures, oxidants, and other additives. The electrochemical C–H/N–H oxidative cross-coupling normally occurs in anodic oxidation mode. Specifically, no external oxidant is needed and the surplus hydrogen is evolved in the form of dihydrogen. With the choice of appropriate anode, cathode, and other reaction conditions, some transformations can be attained just through direct electrolysis. Compared with the easily available constant current electrolysis, constant potential electrolysis can control the activation of substrates and supply other ways to inhibit the reduction of transition-metal catalysts. Owing to the above-mentioned advantages scientists are gradually directed more towards electro oxidative cross-coupling.

IB.1. Development of Electrochemistry Battery to Modern Electrochemical Cell

Ongoing advancements in electro-organic synthesis, with a focus on sustainable and green methodologies. This timeline provides a brief overview of the major developments in electro-organic chemistry over the years.

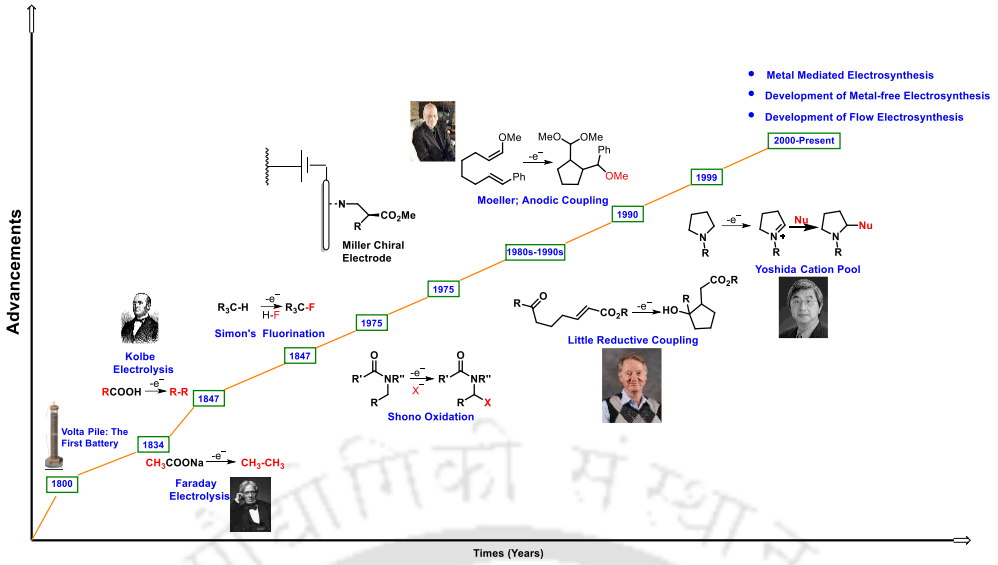

Figure IB.1: *Timeline showing the revolution of electro-organic chemistry from 1800-2023.*

IB.2. Challenges in Electro-organic Synthesis

Analogous to the potential of an oxidizing agent (to oxidize a substrate), the electric potential can be tuned to achieve the oxidation of substrates to facilitate selective coupling. Potentials for the desired redox process can be obtained from tables with standard potentials (E°) or by measuring cyclic voltammograms. Tables of standard reduction potentials E° for an oxidized species (Ox) being reduced to a reduced species (Red) can be found in the literature. By definition, these standard potentials are obtained under standard conditions (25 °C, 1 mol L^{-1},1 atm) against a standard calomel electrode (SCE). Typical potential ranges for organic functional groups, redox mediators, and solvents are depicted in Figure IB.2.

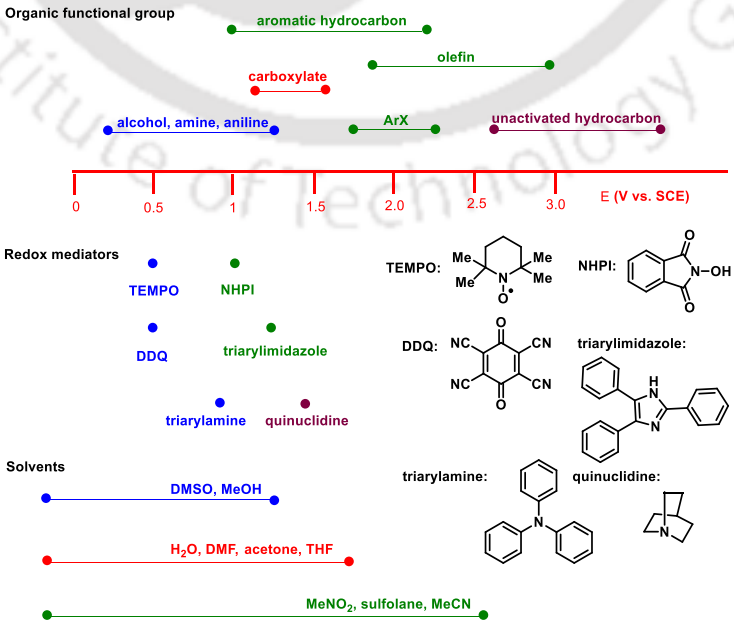

Figure IB.2. *Oxidation potentials for organic functional groups, redox mediators, and solvents.*

IB.3. Traditional and Modern Approach for the C–N Bond Formation Resulting Amide Framework

IB.3.1. Synthesis of Amide

Amides are prevalent in biomolecules such as peptides, and proteins, and are found in natural products, pharmaceuticals, polymers, and fine chemicals. In 2014, an analysis by Brown *et al*. revealed that 50% of medicinally relevant compounds possess at least one amidic linkage.

IB.3.2. Electrochemical Oxidative Cross-coupling Strategy

Oxidative cross-coupling has been developed into a robust method for carbon-carbon (C–C), carbon-heteroatom (C–X), and heteroatom-heteroatom (X–Y) bond formation. Over the past two decades, tremendous efforts have been devoted to this field and significant advancements have been achieved. Electrochemical synthesis is a powerful and environmentally benign approach, which not only achieves oxidative cross-couplings under external-oxidant-free conditions but also releases valuable hydrogen gas during the chemical bond formation. Recently, the electrochemical oxidative cross-coupling with hydrogen evolution reactions has been significantly explored.

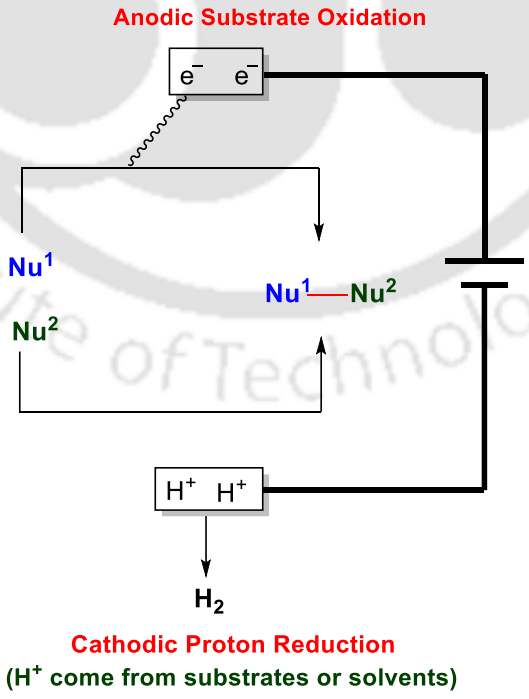

Figure IB.3. *Electrochemical oxidative cross-coupling.*

In summary, the use of visible light and electrochemical C–N bond formation has brought a paradigm shift in contemporary organic chemistry. Despite existing traditional methodologies in the direction of C–N bond formations, the visible-light-induced and electrifying synthesis of the nitrogen-containing framework is still ongoing and will be of immediate interest soon. The above-mentioned literature paves the way to generate radicals via photochemical and electrochemical methods to attain nitrogenous frameworks. Hence further improvement in this field may open up new avenues to straightforward and efficient synthesis of various molecular frameworks that may find applications not only in pharmaceuticals but also in other industries.

CHAPTER II: Visible-Light-Induced Difunctionalization of Styrenes: Synthesis of *N*-Hydroxybenzimidoyl Cyanides

This chapter demonstrates a visible-light-induced synthesis of *N*-hydroxybenzimidoyl cyanides from aromatic terminal alkenes which is achieved using Eosin Y as an organic photoredox catalyst. The process goes via a radical pathway with successive incorporation of two nitrogen atoms, one each from *tert*-butyl nitrite and ammonium acetate. The concomitant installation of an oxime and a nitrile group achieves the final product. DFT calculation supports a bi-radical pathway and all the proposed steps. A few useful synthetic transformations of *N*-hydroxybenzimidoyl cyanide is also illustrated.

Visible-light mediated photocatalytic functionalization has attracted considerable attention in modern organic synthesis because of sustainable energy sources to promote chemical reactions. Of late difunctionalization of alkenes has become a popular and competent chemical transformation by which two functional groups can be introduced simultaneously across the double bond. Normally, difunctionalization of alkenes requires transition-metal catalysts and proceeds via radical-mediated processes. However, the synthesis of functionalized oxime via difunctionalization using *tert*-butyl nitrite as a N-synthon has attained some special attention in organic synthesis.

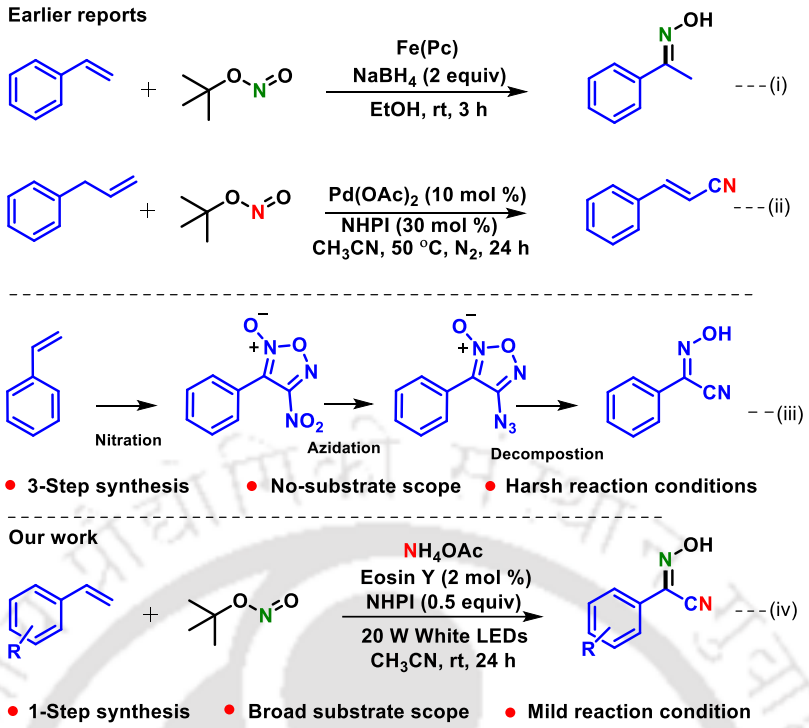

Scheme II.1 *Oximation and cyanation of terminal alkenes.*

In this context, an elegant synthesis of oxime in reported by the Beller group in 2009 from styrene and *tert*-butyl nitrite in the presence of Fe(II) catalyst [Scheme II.1, (i)]. Later Wang group introduce a CN group to an allyl benzene using a Pd(II) catalyst and *tert*-butyl nitrite serving as the nitrogen source in the presence of *N*-hydroxy phthalimide as the co-catalyst [Scheme II.1, (ii)]. The synthesis of 2-hydroxyimino-2-phenyl acetonitrile starting from styrene was first reported by Kunai group via a three-step process involving nitration of styrene to 4-nitro-3-phenylfurazan-2-oxide, an azidation step followed by photolytic decomposition [Scheme II.1, (iii)].

In continuation of our efforts towards functionalization of alkene, we were curious to see the reactivity of an alkene with *tert*-butyl nitrite in the presence of NH_4OAc under 2 x 10 W white LEDs mediated by an organophotoredox catalyst [Scheme II.1, (iv)]. To reach the suitable conditions for the synthesis of *N*-hydroxybenzimidoyl cyanide (**2a**), various solvents, photocatalysts, and light sources, were screened. The ideal condition for the synthesis of **2a** was the use of *p*-methyl styrene (**2**) (0.25 mmol), *tert*-butyl nitrite (**a**) (1.25 mmol), Eosin Y (2 mol %), NH_4OAc (4 equiv), and NHPI (50 mol %) in 2 mL CH_3CN under irradiation of 2 x 10 W white LEDs. With the optimized condition in hand, this protocol was subsequently applied for the synthesis of various *N*-hydroxybenzimidoyl cyanide (**2a**). It was observed that the reaction underwent smooth reaction in the presence of both electron-withdrawing as well

as electron-donating groups in styrenes. The tri-substituted and di-substituted aromatic terminal alkenes underwent efficient conversion to their desired *N*-hydroxybenzimidoyl cyanides. The biphenyl styrenes having electron-donating substituents, electron-withdrawing substituents, and disubstituted all were successfully converted to their hydroxyaminoacetonitriles. Based on control experiments and from DFT calculations a tentative mechanism has been proposed (Scheme II.2).

In the presence of white LEDs, Eosin Y (EY) is first photoexcited. This is followed by the photooxidation of NHPI to a PINO radical by the activated Eosin Y via HAT (hydrogen atom transfer) mechanism. This process regenerates back the Eosin Y producing a HO_2• radical, which on disproportionation produces oxygen and hydrogen peroxide. The PINO radical then attacks the terminal sp^2-carbon of alkene (**1**) to generate a benzylic radical intermediate (**A**). Photochemical decomposition of *tert*-butyl nitrite generates a NO and a *tert*-butoxyradicals. The benzylic position of the intermediate (**A**) is attacked by the NO radical to generate intermediate (**B**). The *in situ* generated nitroso intermediate (**B**) is tautomerized to an oxime intermediate (**C**). The *tert*-butoxyl radical sequentially abstracts two hydrogen atoms from the oxime intermediate (**C**) to first generate a mono radical (**D1**) followed by a 1,4-biradical intermediate (**D**). An intramolecular coupling of biradical (**D**) generates a four-membered cyclic intermediate (**E**). The hydrogen peroxide produced *in situ*, decomposes to a hydroxyl radical in the presence of light. The strained cyclic intermediate (**E**) undergoes ring-opening via attack of an OH radical to form a hemiacetal radical intermediate (**F**). The N–O radical intermediate (**F**) abstracts a proton from the *tert*-butanol to generate a neutral hemiacetal intermediate (**G**). The neutral hemiacetal intermediate loses NHPI providing an oxime aldehyde (**H**). Condensation between ammonia (generated from ammonium acetate) and the aldehydic intermediate (**H**) forms an iminium intermediate (**I**), which is perhaps the rate-determining step of the process. Abstraction of an iminium N–H from the intermediate (**I**) by ^{t}BuO radical produces a nitrogen-centered radical (**J**). Finally, the abstraction of the aldehydic proton from intermediate (**J**) by *tert*-butoxy radical provided the desired cyano functionality (Scheme II.2).

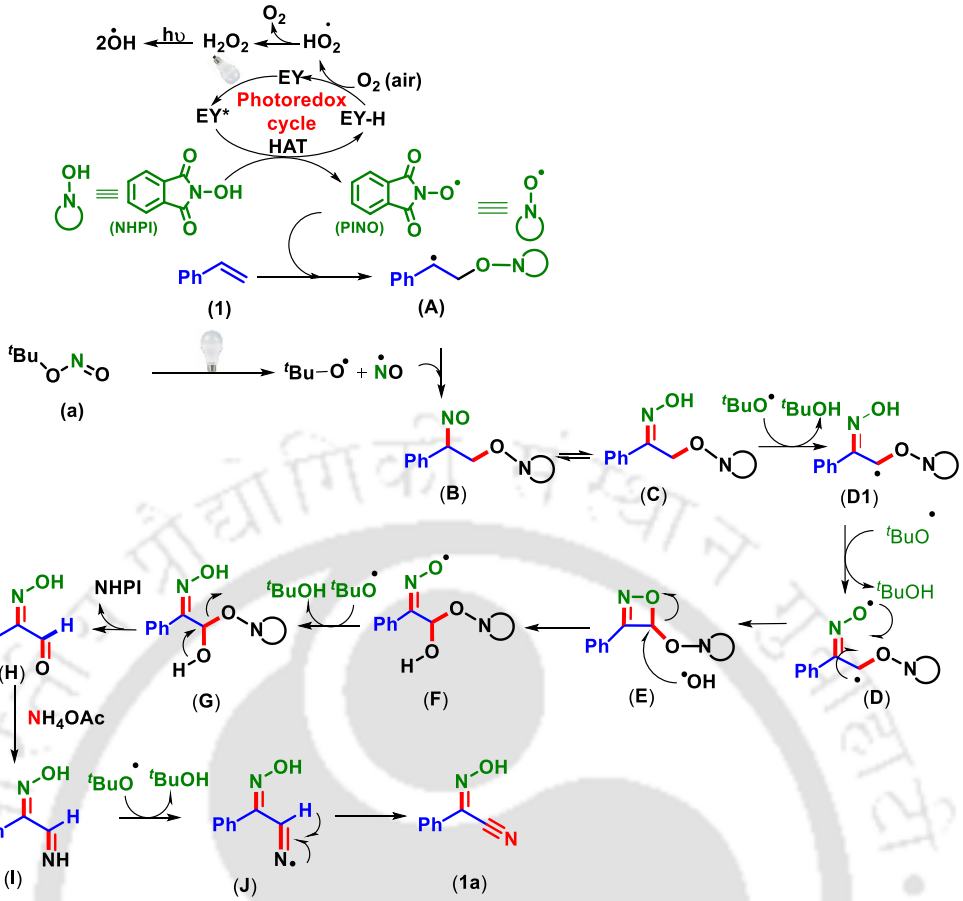

Scheme II.2. *Plausible mechanism for the synthesis of N-hydroxybenzimidoyl cyanides.*

In summary, a visible light-mediated synthesis of *N*-hydroxybenzimidoyl cyanides have been accomplished from styrenes in the presence of an organic photoredox catalyst. The bifunctionalized moiety possesses two important functionalities *viz.* an oxime and a nitrile group, which originate from *tert*-butyl nitrite and ammonium acetate respectively. This reaction proceeds through a biradical reaction path. The proposed mechanism is supported by the detection of some of the reaction intermediates and each of the steps is supported by DFT calculation. Some useful post-synthetic modifications were performed to show the synthetic utility of the difunctionalized hydroxyaminoacetonitrile thereby expanding the further scope of this methodology.

CHAPTER III: Visible-Light-Mediated Ir(III)-Catalyzed Concomitant C3-Oxidation and C2-Amination of Indoles

The photocatalytic functionalizations of indoles have attracted considerable attention since functionalized indole motifs have found significant applications in biological and medicinal chemistry and are present in various natural and artificial bioactive molecules. Hence the development of newer methodologies to make functionalized indole is always demanding. In this respect, Borhan *et al.* published an elegant C3-oxidation and C2-amination of indoles involving Cu(I) catalyst and an acyl nitroso reagent such as hydroxycarbamate [Scheme III.1(a)]. This method has advantages in terms of peroxide-free oxidation, and the use of hydroxycarbamate as the source of both oxygen and the amide making this protocol advantageous over previous methodologies involving difuctionalization of indoles. Nevertheless, this method has an inherent limitation as it is applicable only to C2-protected indoles and C2-free indoles failed to functionalize.

This chapter demonstrates a visible-light-mediated concomitant C3 oxidation and C2 amination of indoles at room temperature using an Ir(III) photocatalyst. This reaction proceeds without an isatin intermediate via the attack of singlet oxygen at the C3 position followed by C2 amination leading to the difunctionalization of indoles [Scheme III.1.(b)].

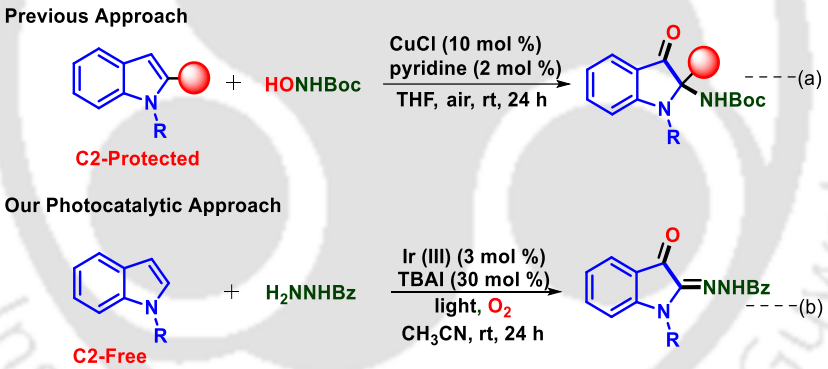

Scheme III.1. *Approaches towards difunctionalization of indoles via selective C3 oxidation and C2 amination.*

After the screening of several parameters, the optimal condition for this transformation was found to be (**1f**) (0.25 mmol), benzohydrazide (**2a**) (0.25 mmol), catalyst **P1** (3 mol %) and TBAI (30 mol %) in 5mL CH_3CN under an atmosphere of oxygen by irradiation of 20 W white LEDs at room temperature. A diverse array of *N*-substituted and mono and di (1,5 and 1,7) substituted indoles could be transformed to their corresponding 3-oxindoles in good yields. Further the compatibility of various benzyl substituents was tested as they are often prone to oxidation. Substrates having *N*-benzyl substituents, bearing either electron-donating or electron-withdrawing groups reacted efficiently with benzohydrazide (**2a**) to give good

yields of their products. From the control experiments and from the DFT calculations a plausible mechanism for the formation of difunctionalization of indole is proposed (Scheme III.2).

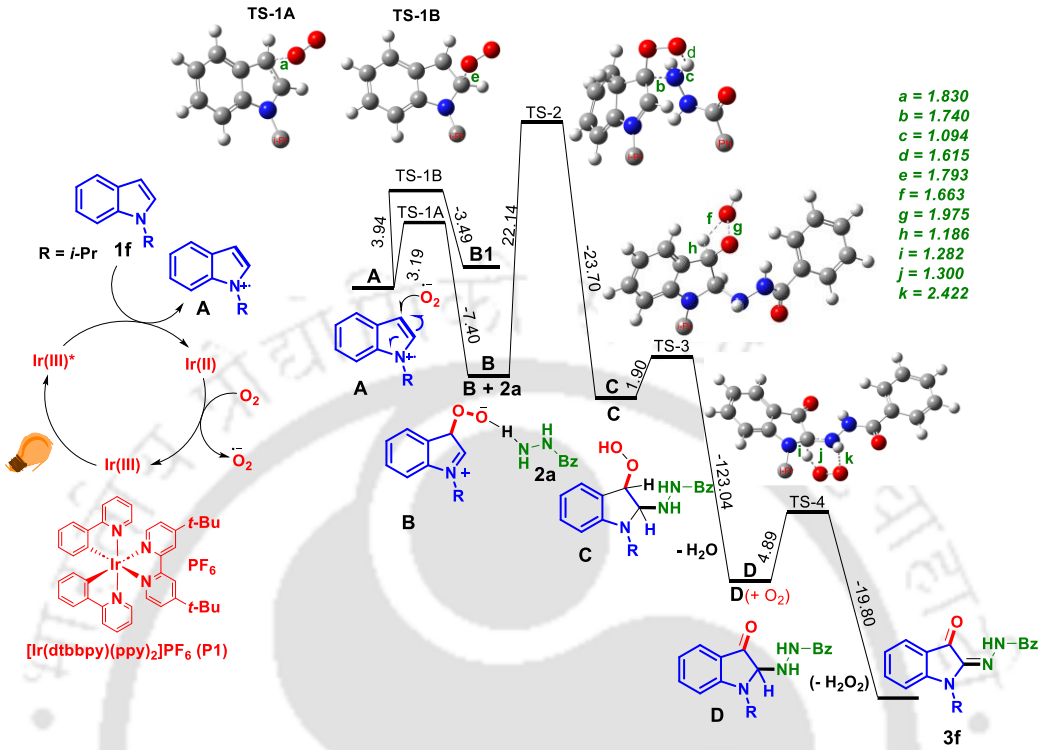

Scheme III.2. *Plausible mechanism for the formation of 3-oxindoles.*

In the first step indole (**1f**) is oxidized to an indole radical cation (**A**) through a reductive quenching process by the photocatalyst Ir (III)* (**P1**). Simultaneously, the molecular oxygen is reduced to a superoxide ion $O_2^{\bullet-}$ by Ir (II) and the catalyst is regenerated. Next, we compared the possibility of attack of $O_2^{\bullet-}$ on two possible sites (C_3 and C_2) of the radical cation **A** through TS-1A and TS-1B (Scheme III.2). Clearly, TS-1A, *i.e* attack at the C3-site has a lower barrier and lower stabilization compared to TS-1B involving a C-2 attack as depicted in Scheme III.2. Further, the forward reaction is preferred for TS-1A and the reverse reaction is preferred for TS-1B. Thus the formation of transition state TS-1B via the C-2 attack of $O_2^{\bullet-}$ is ruled out. The highly reactive $O_2^{\bullet-}$ then attacks at the C-3 site of the intermediate **A** to form a peroxy iminium species **B**. The benzohydrazide **2a** attacks at the C-2 site of intermediate **B** to form intermediate **C** through TS-2. This is perhaps the rate-determining step for this reaction having an activation barrier of 22.14 kcal/mol. The intermediate **C** is around 1.56 kcal/mol more stable compared to intermediate **B**. As expected, the barrier for the removal of a molecule of water is very low (1.90 kcal/mol) from intermediate **C** to form intermediate **D** which is associated with higher stabilization. Finally, the removal of two hydrogens, one each from

indole and benzohydrazide (**2a**). The final step seems to be a facile one with an activation barrier of 4.89 kcal/mol. Moreover, the final product (**3f**) is 14.91 kcal/mol more stable compared to the intermediate **D**. Thus all the proposed steps are highly favorable which leads to a stable bi-functionalized product (Scheme III.2).

In summary, a mild and efficient photocatalytic regioselective method has been developed for the selective difunctionalization of indoles by visible-light-induced photo redox Ir(III) catalysis. A wide range of indoles, as well as benzohydrazides, participate competently in the free-radical reaction to afford structurally diverse oxindoles in good yields. Based on control experiments carried out plausible mechanism has been proposed which is well supported by DFT calculation.

CHAPTER IV: Electrochemical Amidation: Benzoyl Hydrazine/Carbazate and Amine as Coupling Partners

This chapter focuses on the electrochemical amidation of benzoyl hydrazine/carbazate and primary/secondary amine as coupling partners via concomitant cleavage and formation of C(sp^2)–N bonds. The reaction proceeds under metal and exogenous oxidant-free conditions producing N_2 and H_2 as by-products. The reaction also proceeds the *in situ* generations of both acyl and *N*-centered radicals from benzoyl hydrazines and amines. To show the practical usefulness of the protocol a large-scale, synthesis of Bezafibrate, a hyperlipidemic drug is also performed.

The coupling of amine with carboxylic acid, ester, and acyl chloride using transition-metals or activating agents and transition-metal-catalyzed carbonylative amidation are the frequently used method [Scheme IV.1 (a)]. Further, N-heterocyclic carbenes (NHCs) have been effectively used as catalysts for metal-free amidation of activated esters. However, these amidation protocols often generate stoichiometric quantities of toxic waste and a few of the strategies suffer from limitations such as the use of expensive transition-metal catalysts having limited substrate scope.

The easily accessible air and moisture-stable benzoyl hydrazine is an ideal precursor of acyl radicals by the expulsion of N_2 and H_2. However, the reported methodologies for the generation of acyl radical from benzoyl hydrazine uses an excess of catalyst and chemical oxidants such as $(NH_4)_2S_2O_8$ and PbO_2, thereby generating waste [Scheme IV.1 (b)]. The

generation of acyl radicals is important in various biochemical and synthetic processes. Thus, the development of a waste-free and milder method for its generation from benzoyl hydrazine is highly desirable. Recently, the Zou group developed a Cu(II)/TBHP-catalyzed oxidative coupling of amines and carbazates leading to carbamates [Scheme IV.1 (c)]. Following the same strategy, they subsequently developed a Fe(III)/TBHP-catalyzed synthesis of amides from benzoyl hydrazines and amines [Scheme IV.1 (c)]. These reactions proceed through an *in situ* generation of alkoxy carbonyl/acyl radicals involving metal complexation via an oxidative addition followed by a reductive elimination leading to carbamates or amides. The reported amidation strategies for the synthesis of amides are neither atom-economical nor sustainable, thus constructing amide bonds under mild conditions would be much more alluring [Scheme IV.1(d)]. Hence we developed an electrochemical condition leading to amides using benzoylhydrazide and amines under electrochemical conditions.

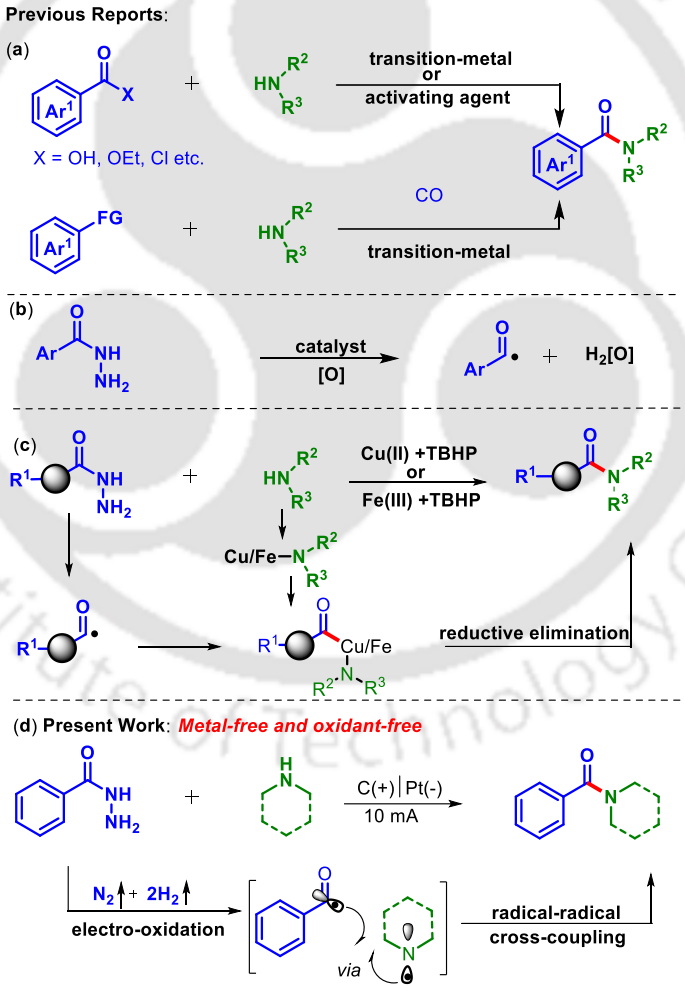

Scheme IV.1. *Amide bond formation strategies*

To find out the optimal reaction condition for this electrochemical transformation, other reaction parameters such as solvents, electrolytes, and electrodes were screened. After screening several parameters, the optimal condition for this transformation was found to be the use of benzoylhydrazine (**a**) (0.5 mmol), morpholine (**1**) (0.75 mmol, 1.5 equiv) in tetrabutylammonium hexafluorophosphate ($^{n}Bu_4NPF_6$) (50 mol %) in 2:3 ratios of 1,2-dichloroethane (DCE) and 1,1,1,3,3,3-hexafluoro-2-propanol (HFIP) (5 mL) at room temperature applying a 10 mA constant current using a carbon rod anode and a platinum plate cathode in an undivided cell under N_2 atmosphere for 18 h.

The scope of benzoyl hydrazines was explored using morpholine as the other coupling partner. Benzoyl hydrazine possesses electron-donating groups and electron-withdrawing groups are smoothly coupled giving their respective product good to moderate yield. Both secondary and primary amines are proved to be a good coupling partner, giving their respective products.

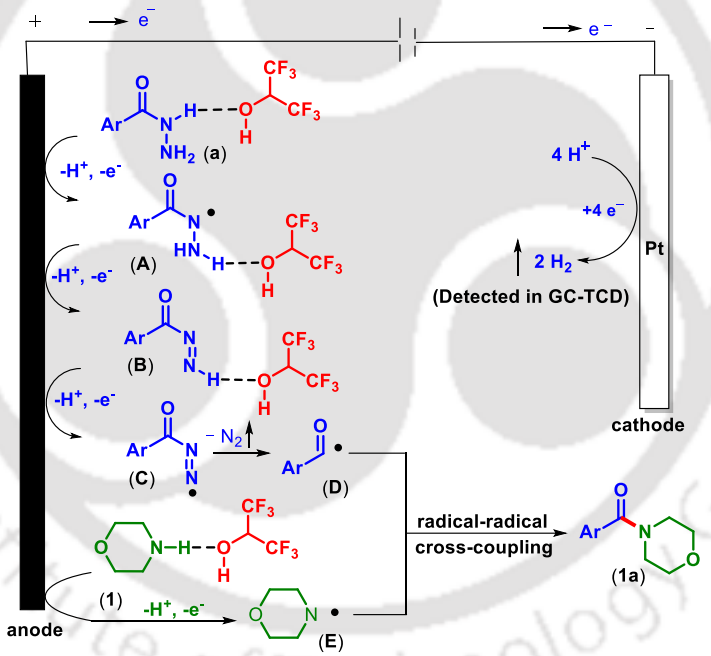

Scheme IV.2. *Plausible mechanism for the formation of amides*

Based on the control experiments, the results obtained from cyclic voltammetry, linear sweep voltammetry measurements, and previous literature reports, a plausible mechanism is depicted (Scheme IV.2). The solvent HFIP interacts via hydrogen bonding with the N–H of the benzoyl hydrazine (**a**). Next, this activated benzoyl hydrazine (**a**) undergoes electrochemical anodic oxidation to generate a *N*-centered diazaneyl radical intermediate (**A**). Further, a sequential two-step oxidation from the radical intermediate (**A**) produces a diazene

radical intermediate (**C**) via intermediate (**B**). Next, C–N bond cleavage of intermediate (**C**) generates a benzoyl radical intermediate (**D**) with concurrent releases of N_2. Similarly, the morpholine (**a**) is activated via H-bonding interaction with the HFIP and subsequent anodic oxidation generates a N-centered radical intermediate (**E**). Finally, radical-radical cross-coupling between intermediates (**D**) and (**E**) afforded the amide (**1a**). During the cathodic reduction, molecular H_2 is released which has been detected by GC analysis (Scheme IV.2).

In summary, an electrochemical amidation/carbamidation under metal and external oxidant-free condition is developed. The process involves radical-radical cross-coupling between benzoyl hydrazines/carbazates and amines leading to the formation of a C–N bond. The protocol is compatible with a wide range of benzoyl hydrazines/carbazates and aromatic/aliphatic amines. Alkyl amines are selectively amidated in the presence of arylamines but the method is unsuccessful for substrates where the *N*-centered radical is part of conjugated systems. Thus chemo-selective amidation can be achieved in substrates having multiple aminating sites. A plausible mechanism has been proposed based on control experiments and CV measurements. Finally, the synthetic utility is demonstrated through a large-scale and biologically active 'Bezafibrate' drug.

CHAPTER V: Electrochemical *N*-Aroylation of Sulfoximines using Benzoyl Hydrazines with H_2 Generation

This chapter focuses on the development of a robust electrochemical cross-coupling between aroyl hydrazine and *NH*-sulfoximine via concomitant cleavage and formation of C(sp^2)–N bond with the evolution of H_2 and N_2 as innocuous by-products. This sustainable protocol avoids the use of toxic reagents and occurs at room temperature. The reaction proceeds via the generation of an aroyl and a sulfoximidoyl radical via anodic oxidation under constant current electrolysis (CCE), affording *N*-aroylated sulfoximine. The strategy is applied to late-stage sulfoximidation of L-menthol, (-)-borneol, D-glucose, Vitamin-E derivatives, and marketed drugs such as probenecid, ibuprofen, flurbiprofen, ciprofibrate, and sulindac. In addition, the present methodology is mild, high functional group tolerance with broad substrate scope and scalable.

The potential applications of organosulfur compounds viz. sulfoximines in pharmaceuticals and pesticides have been well recognized. Sulfoximine-containing compounds such as atuveciclib, BAY1251152, and AZD6738 have progressed into clinical

trials. Sulfoxaflor, a sulfoximine-containing compound was first developed by Dow AgroSciences as a potential insecticide and introduced into the market. Thus, a significant effort has been devoted to establishing efficient strategies for the synthesis of *N*-acylated sulfoximines. In this context, carboxyl activating agents have been employed for the coupling of carboxylic acid and *NH*-sulfoxamine leading to *N*-acylated sulfoximine. The transition-metal-catalyzed synthesis of *N*-aroyl sulfoximine has been achieved using aryl halide and carbon monoxide [Scheme V.1(a)].

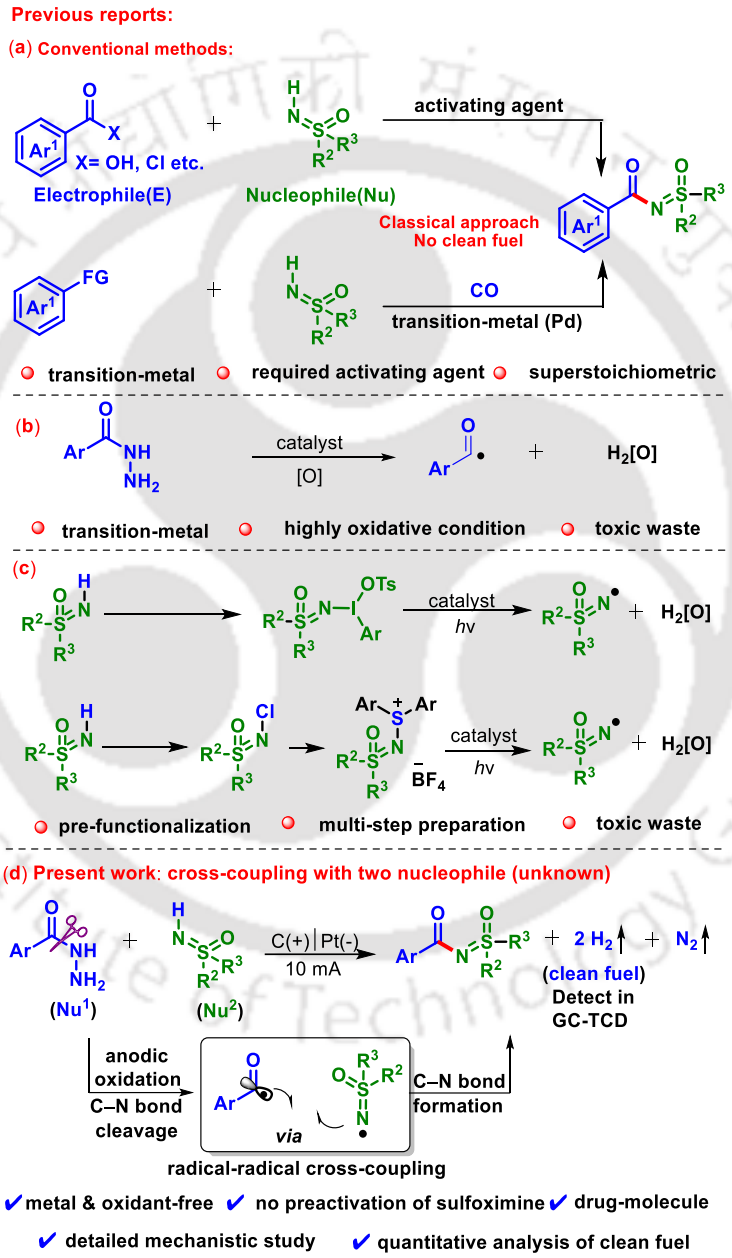

Scheme V.1. *Strategies for N-aroylation of sulfoximines*

However, the existing methods for their generation rely on stoichiometric use of chemical oxidants under transition-metal catalysis producing chemical waste making them environmentally unacceptable [Scheme V.1 (b)]. Recently, a visible-light-induced α-keto acylation of sulfoximines using hypervalent iodine reagent and aryl alkynes has been achieved. Following this, several other strategies involving the generation of *N*-centered sulfoximidoyl radicals under photocatalytic conditions have been adopted. The success of these strategies relies on the preactivation or *in situ* activation of *NH*-sulfoximines, using hypervalent iodine(III) and *N*-halogenated sulfoximines via mesolytic or homolytic cleavage of a weak nitrogen-heteroatom bond. Considering all these, we envisioned sulfoximidation via anodic oxidation of benzoyl hydrazine and *NH*-sulfoximine [Scheme V.1(d)]. Hence we developed a method that is more efficient as compared to other methods.

To find out an appropriate reaction condition for this electrochemical transformation, other reaction parameters such as solvents, electrolytes, and electrodes were screened. After the screening of several parameters, the optimal condition for this transformation was found to be the use of benzoyl hydrazine (**a**) (0.5 mmol), sulfoximine (**1**) (0.75 mmol, 1.5 equiv.), and $^{n}Bu_4NOAc$ (1 equiv.) in a co-solvent of HFIP/CH_3CN (1:4) 5 mL and applying a 10 mA current, carbon rod as anode and platinum plate as cathode under N_2 atmosphere at room temperature for 10 h in an undivided cell.

Having established the optimized reaction conditions, we sought to examine the generality of this transformation by exploring the scope of various sulfoximines with benzoyl hydrazine (**a**). Aryl sulfoximines possessing electron-donating groups (EDGs) and electron-withdrawing-groups (EWGs) smoothly reacted with benzoyl hydrazine. Benzoyl hydrazine possesses electron-donating groups and electron-withdrawing groups are smoothly coupled giving their respective product good to moderate yield.

Based on the electrochemical studies, the results obtained from control experiments, and previous literature reports, a plausible mechanism is depicted. It is well documented and demonstrated here as well, that tetrabutylammonium acetate ($^{n}Bu_4NOAc$) plays a vital role in this electrosynthesis. The initial step involves hydrogen bonding between $^{n}Bu_4NOAc$ and the N–H of benzoyl hydrazine (**a**). Subsequently, the resulting adduct of benzoyl hydrazine (**a**) undergoes an electrochemical anodic oxidation, leading to selective homolysis of the amidic N–H bond. This process generates a *N*-centered diazanyl radical intermediate (**A**).

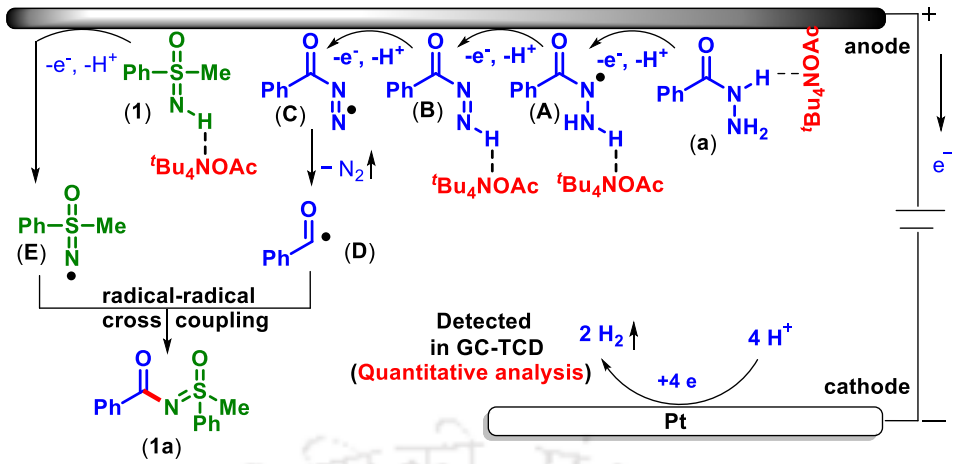

Scheme V.2. *Plausible mechanism for the formation of sulfoximidation product.*

Next, through a sequential two-step transformation involving intermediate (**B**), a diazene radical intermediate (**C**) is produced from radical intermediate (**A**). Further, the cleavage of the initial C–N bond of benzoyl hydrazine (**a**) releases a molecule of N_2 as the by-product and produces a benzoyl radical intermediate (**D**). In a similar fashion, the sulfoximine (**1**) is activated by H-bonding interaction with tetrabutylammonium acetate and via anodic oxidation generates sulfoximidoyl radical intermediate (**E**). Finally, the radical-radical cross-coupling between intermediates (**D**) and (**E**) affords the sulfoximidated product (**1a**). On the other hand, at the platinum plate cathode surface, the overall redox process is balanced by the reduction of four protons with four electrons producing hydrogen gas. Further, quantitative analysis of hydrogen production is also illustrated with the help of the GC-TCD method (Scheme V.2).

In summary, developed here is an electrochemical sulfoximidation under metal and external oxidant-free conditions between benzoyl hydrazine and *NH*-sulfoximine. The process involves a radical-radical cross-coupling between the *in-situ* generated benzoyl and sulfoximidoyl radicals. The developed electrochemical approach features mild reaction conditions, operational simplicity, and remarkable scope, particularly in the late-stage modifications of complex and sensitive pharmaceuticals and natural products. The method is scalable and provides H_2 and N_2 as the only by-products that can be utilized as a clean energy source. The sequential cleavage and formation of a new C(sp^2)–N bond under the same condition offers opportunities to pursue fundamental mechanistic studies, which may lead to the discovery of new cross-coupling in synthetic electrochemistry.

CHAPTER VI: Electrochemical Sulfoximidation: The Phenyl Glyoxylic Acid and *NH*-Sulfoximines as Coupling Partners with H_2 Evolution

This chapter focuses on developing a robust electrochemical cross-coupling between α-keto acids and *NH*-sulfoximines. This process simultaneously breaks the C–C bond and forms a C(sp^2)–N bond, with the evolution of H_2 and CO_2. In this process, *N*-aroylated sulfoximines are produced through the generation of aroyl and sulfoximidoyl radicals by anodic oxidation in constant current electrolysis (CCE). This approach is successfully employed for the late-stage sulfoximidation of various compounds, including L-menthol, (-)-borneol, and D-glucose, derivatives, and commercial drugs such as probenecid, ibuprofen, and flurbiprofen. This blueprint features good functional group compatibility, a broad scope, and a detailed mechanistic investigation.

Discovered from the "agenized" proteins in the early 1950s, sulfoximines are recognized as isosteres of sulfones, where one "=O" on sulfur(VI) is substituted by a "=NR". The sulfur(VI) linkages are subsequently expanded by the additional imino vector, bringing about unprecedented physical, chemical, and biological properties in comparison to sulfones. In this context, sulfoximines have found wide use in pharmaceuticals, agrochemicals, materials, and organic synthesis. The *N*-functionalization of free sulfoximines (=NH) is an important route to enrich the chemical space of the parent skeletons, which contributes directly to their downstream applications. In this regard, there is no doubt that a massive amount of effort has been devoted to the construction of N-acylated sulfoximines. The carboxyl activating agents like 1-ethyl-3-(3-dimethylaminopropyl)carbodiimide (EDC) or N,N′-dicyclohexylcarbodiimide (DCC) have been used to facilitate the coupling between carboxylic acids and *NH*-sulfoximine, resulting in the formation of *N*-acylated sulfoximines. A similar sulfoximidation reaction has been established utilizing different activating agents such as boric acid or 1,3-dioxa-5-aza-2,4,6-triborinane (DATB). The synthesis of *N*-aroyl sulfoximines has also been achieved via transition-metal-catalyzed processes using aryl halides and carbon monoxide. Given their significance, there is a strong demand for the development of sustainable synthetic methods that possess broad functional group tolerance and reaction flexibility, allow for late-stage modifications of biologically relevant molecules, and offer a clean energy source (H_2) as a by-product. However, the current method for producing acyl

radicals typically depends on the stoichiometric use of chemical oxidants in the presence of transition-metal catalysts, which generate chemical waste and are not environmentally friendly. In this context, there is a strong need for a gentler and more sustainable approach to generating acyl radicals from α-keto acids [Scheme VI.1 (b)].

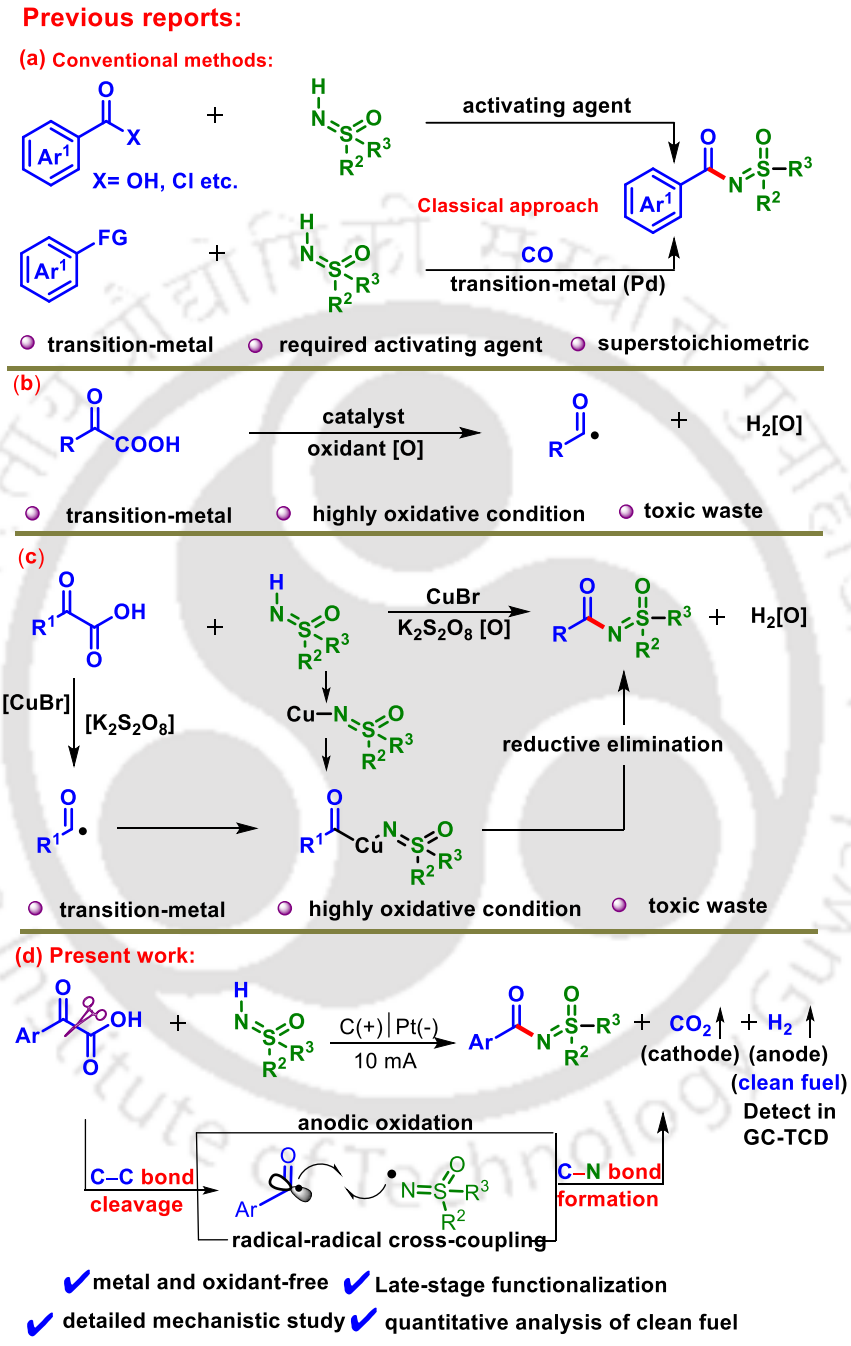

Scheme VI.1. *Different strategies for the sulfoximidation*

The electrochemical cross-coupling of NH-sulfoximine remains uncharted territory, likely due to the high oxidation potential of NH-sulfoximine (Eox = +1.92 to +2.00 V vs. SCE) and

its strong *N*-centre bond with a high bond dissociation energy (BDE_{N-H} =104–106 kcal/mol), making it challenging to generate *N*-centre radicals. The Yotphan group developed a Cu(I)/$K_2S_2O_8$-catalyzed oxidative decarboxylative coupling of *α*-keto acids and sulfoximines [Scheme VI.1 (c)]. These reactions proceed through an *in situ* generation of benzoyl radical involving metal complexation via an oxidative addition followed by a reductive elimination leading to *N*-acylated sulfoximines. The reported sulfoximidation strategies for the synthesis of *N*-acylated sulfoximines are neither atom-economical nor sustainable. Therefore, the use of any transition metal or oxidant can be avoided by using this proposed strategy. Nevertheless, designing a metal-free methodology for radical cross-coupling that accepts the challenge of generating two distinct radicals has to overcome the homo-cross-coupling of two individual open-shell radicals. We envisioned that sulfoximidation through anodic oxidation of readily available α-keto acids and sulfoximine as shown [Scheme VI.1(d)].

To find out an appropriate reaction condition for this electrochemical transformation, other reaction parameters such as solvents, electrolytes, and electrodes were screened. After the screening of several parameters, the optimal condition for this transformation was found to be the use of α-keto acid (**a**) (1 mmol, 2.0 equiv), sulfoximine (**1**) (0.5 mmol), and $^{n}Bu_4NClO_4$ (1.5 equiv) in a DCE solvent 5 mL applying a 10 mA current, carbon rod as anode and platinum plate as a cathode under N_2 atmosphere at room temperature for 6 h in an undivided cell.

Having established the optimized reaction conditions, we sought to examine the generality of this transformation by exploring the scope of various sulfoximines with α-keto acids (**a**). Arylsulfoximines possessing electron-donating groups (EDGs) and electron-withdrawing groups (EWGs) smoothly react with α-keto acid. After demonstrating the compatibility of various sulfoximines, we examined the nature of various substituents (EDG and EWG) presenting the α-keto acids smoothly couple giving their respective product moderate to good yield. Based on electrochemical studies, the results obtained from control experiments, and previous literature reports, a mechanism for sulfoximidation is proposed. It is demonstrated here that K_2CO_3 (base) plays a vital role in this electrosynthesis. Initially base-mediated deprotonation of α-keto acid provided α-oxocarboxylate intermediate (**A**). Then, upon anodic oxidation α-oxocarboxylate (**A**) through a single electron transfer and decarboxylation to give benzoyl radical species (**C**). Meanwhile, similarly sulfoximine (**1**) in the presence of K_2CO_3 gave sulfoximidoyl anione intermediate (**D**) and via anodic oxidation generated sulfoximidoyl radical intermediate (**E**). Finally, the radical-radical cross-coupling

between intermediate (**C**) and intermediate (**E**) affords the sulfoximidation product (**1a**). On the other hand, platinum plate cathode surface, the overall redox process is balanced by the reduction of protons with two electrons producing the hydrogen gas. Further, quantitative analysis of hydrogen production is also illustrated with the help of the GC-TCD method (Scheme IV.2).

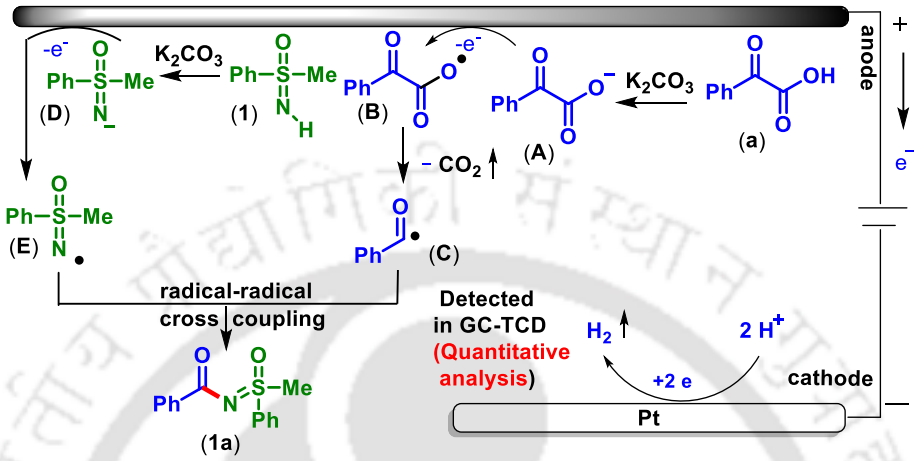

Scheme VI.2. *Plausible mechanism for the formation of sulfoximidation product*.

In summary, this study presents an electrochemical sulfoximidation method that operates without the use of metal catalysts or external oxidants. The process involves a cross-coupling reaction between *in situ* generated benzoyl and sulfoximidoyl radicals. The electrochemical method developed offers mild reaction conditions, simplicity in operation, and a wide range of applications, particularly in modifying complex pharmaceuticals and natural products in the later stages. This approach is scalable and produces only H_2 and CO_2 as by-products, which can serve as a clean energy source.

CONTENTS

Chapter I. Photo and Electrochemical Strategies to C–N Bond Formation

CHAPTER IA

Photo and Electrochemical Strategies to C–N Bond Formation

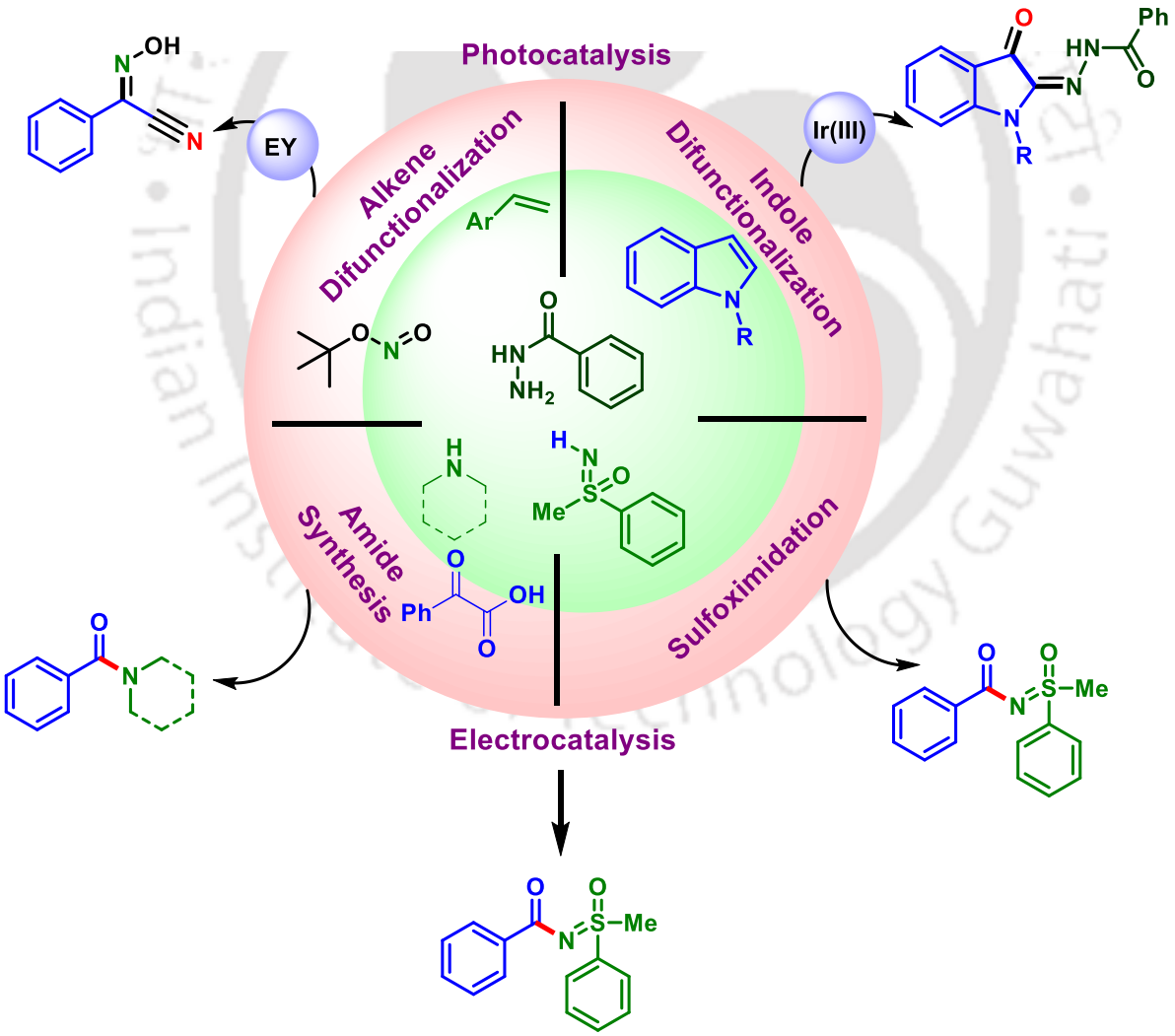

भारतीय प्रौद्योगिकी संस्थान गुवाहाटी
Indian Institute of Technology Guwahati

CHAPTER IA

Photochemical C–N Bond Formation *via* Difunctionalization of Alkenes and Indoles

IA.1 Introduction

Recent decades have witnessed notable progress in the field of radical-mediated carbon-heteroatom bond formations, offering potent strategies for the synthesis of diverse organic structures.[1] Despite the availability of numerous methods for C–X bond formations, there remains a need to develop new methodologies.[2] Visible-light-mediated C–X bond formations have gained tremendous reputation due to their simple operation, minimized by-product formation, ease of handling, and mild reaction conditions. In addition to providing an eco-friendly approach for synthesizing molecules, photochemistry paves the way for the synthesis of complex frameworks that are not accessible through traditional thermal conditions.[3,4] Following the groundbreaking research by MacMillan, König, Stephenson, Rueping, Ritter, Yoon, and other researchers, photocatalysis has witnessed a resurgence in recent decades.[5] The field is primarily classified based on the catalytic systems employed: (a) Utilizing a photocatalyst, such as transition metal complexes or organic dyes, which, in its excited state, activates organic molecules through either single electron transfer (SET) or energy transfer (EnT) mechanisms (Figure IA.2). (b) A synergistic approach combining both a photocatalyst and a transition metal catalyst. (c) Employing only transition metal complexes in conjunction with visible light, serving a dual role by harnessing photon energy as a photocatalyst and catalyzing bond-breaking and formation processes.[6] Mostly, combining visible light with a photosensitizer (either transition metal complexes or organic dyes) has been widely acknowledged as an effective approach for numerous organic transformations. In this context, the use of transition metal complexes, as well as organic dyes, has garnered significant attention for their remarkable reactivity and selectivity in diverse photochemical reactions.[7,8] Many of these photochemical reactions typically proceed either through a single-electron transfer (SET) process (oxidative quenching or reductive quenching) or via a hydrogen atom transfer (HAT) process.[9]

Among the different approaches to C–X bond formations, the C–N bond formations have grabbed the attention of chemists owing to the widespread availability of the nitrogenous

framework as the principal core of many biologically active molecules. Scientists are actively working to develop elegant methodologies for the synthesis of useful nitrogenous frameworks (nitrogenous heterocycles, amides, oximes) (Figure IA. 1).[10]

Intensive research has been directed toward the C–N bond formation. There are several traditional ways, such as amidation, C–H amination, ring annulation, copper-catalyzed Ullmann reaction, palladium-catalyzed Buchwald-Hartwig reaction, and Chan-Lam coupling, etc., that provide excellent selectivity. Besides the traditional approach, the photochemical approach has brought a paradigm shift in the C–N bond construction.[11]

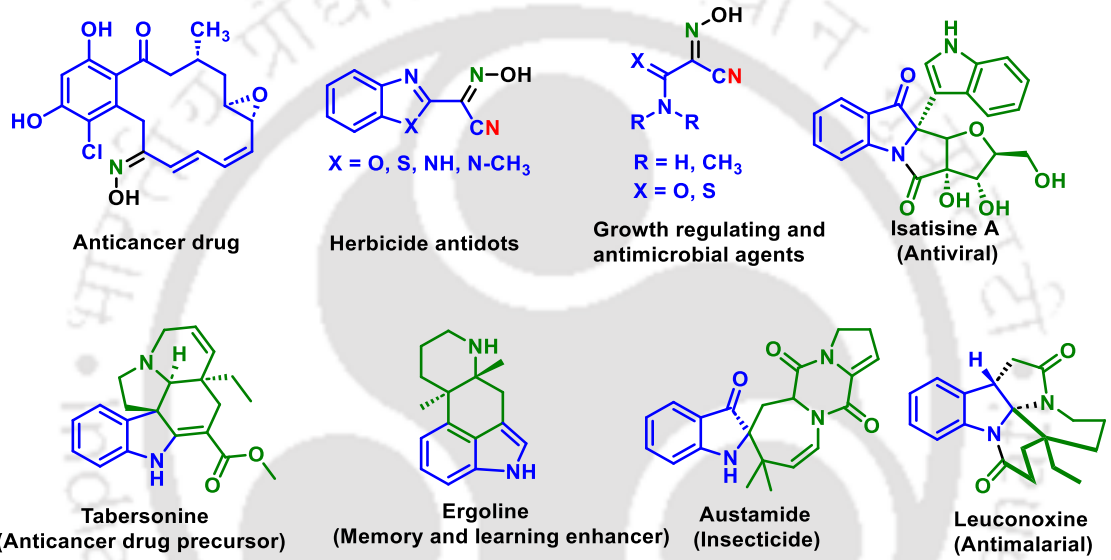

Figure IA.1. *Biologically active nitrogen compounds*

IA.2. Historical Background

Light-induced reactions have been fundamental since the early days of the universe, existing long before life on Earth. The sunlight-mediated photochemistry emerged alongside the development of life on our planet. A prime example is the formation of a protective ozone layer through the photolysis of oxygen. This crucial mechanism safeguards human and animal life from the harmful effects of solar UV radiation.[12] For billions of years, these photoreactions have unfolded unnoticed, unaffected by human intervention. The intriguing concept that light interaction with materials can not only impact their physical properties but also alter their chemical properties has spurred chemists to develop photochemical reactions.[13]

IA.3. Basic Concepts of Photocatalysis

Photocatalysis is all about light interacting with molecules, catalysts, or additives, sparking chemical reactions. By using LEDs with different wavelengths, one can selectively excite specific components. The selection of LEDs plays a crucial role in achieving various selectivities, focusing on absorbance maxima for optimal energy absorption (λmax). The choice of a light source is determined by the absorption maxima, tailored to a specific photoredox catalyst.[7] The λmax value is a crucial parameter, providing insights into the energy required for photoinduced electron transfer. In this realm, ruthenium and iridium photocatalysts, as well as organic dyes, have proven powerful in creating diverse molecular structures demonstrating efficient reactivity in numerous photochemical transformations.[8]

IA.4. General Mechanistic Schemes for Photocatalysis

Photocatalysis operates primarily through energy transfer, electron transfer, and hydrogen atom transfer (Figure IA.2.).

1) Electron transfer
2) Energy transfer
3) Hydrogen atom transfer

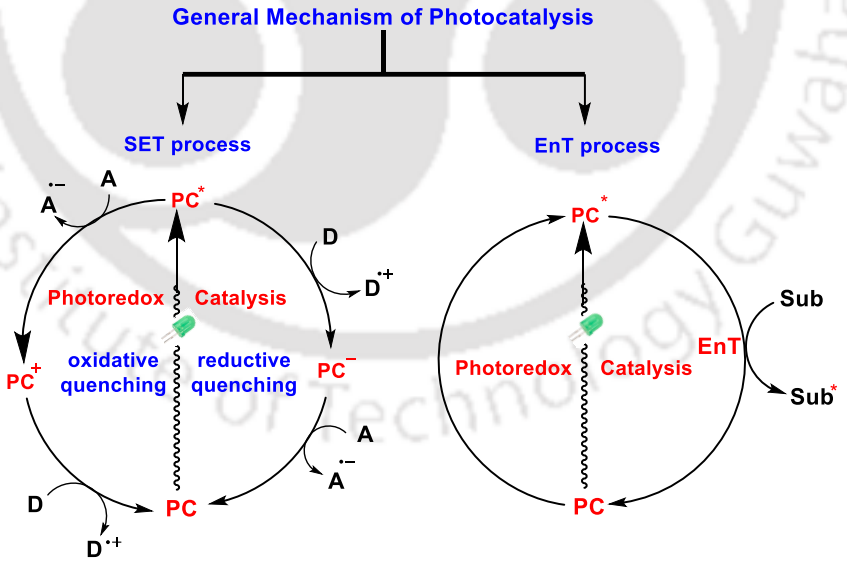

Figure IA.2. *General mechanism for energy and electron transfer.*

IA.4.1. Electron Transfer

In an electron transfer reaction, the catalysts initially remain redox neutral in their ground state. However, in the excited state, they either accept or lose an electron to the substrate, acting

as either an oxidizing or a reducing agent. Various types of electron transfer processes are involved in most photochemical reactions, including (1) oxidative and reductive quenching, (2) proton-coupled electron transfer (PCET), (3) proton transfer followed by electron transfer (PT/ET), (4) electron-donor-acceptor complexes (EDA complexes).[14]

IA.4.2. Oxidative and Reductive Quenching

In an oxidative quenching cycle, the excited state photocatalyst [PC*] is quenched by donating an electron to either the substrate or an oxidant [ox] in the reaction. Conversely, in a reductive quenching cycle, the excited state of the photocatalyst [PC*] accepts an electron from the substrate or a reductant [red]. The oxidative cycle maintains catalytic turnover by reducing the oxidized form $[PC]^{\bullet+}$, while the reductive cycle involves oxidizing the reduced form $[PC]^{\bullet-}$ to sustain catalytic turnover. Substrates, intermediates, or external redox-active reagents (light-absorbing species) primarily drive the catalyst turnover.[15]

IA.4.3. Proton-Coupled-Electron Transfer

The proton-coupled electron transfer (PCET) is a process where electrons and protons are exchanged in a concerted manner. The essential condition for PCET is establishing a hydrogen bond between the substrate and a proton donor/acceptor before the charge transfer occurs. The PCET mechanisms typically fall into two categories: reductive PCET and oxidative PCET. The reductive PCET pathway is primarily associated with the formation of ketyl radicals, while the oxidative PCET pathway is involved in the generation of amidyl radicals (Figure IA.3).[16a]

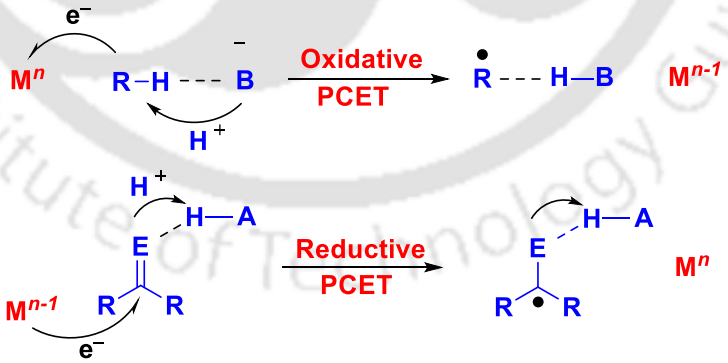

Figure IA.3. *General mechanism for oxidative and reductive PCET.*

IA.4.4. Proton Transfer Followed by Electron Transfer (PT/ET)

The PT/ET process involves the electron transfer mechanism, where the initial step is deprotonation, followed by a subsequent single-electron process. Unlike concerted processes, in PT/ET, proton transfer and electron transfer do not occur simultaneously (Figure IA. 4).[16b]

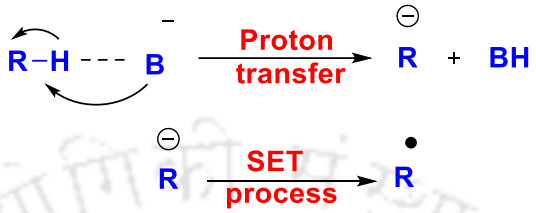

Figure IA.4. *General mechanism for PT/ET.*

IA.4.5. Electron Donor-Acceptor Complexes

While transition metal complexes or organic dyes are frequently employed in photocatalysis, photocatalytic transformations can occur without the presence of any photocatalyst. In such scenarios, the individual reacting partners cannot absorb light within the irradiation wavelength range. Nevertheless, when mixed, these reacting components undergo a change in color, signaling the formation of an electron donor-acceptor (EDA) complex or a charge-transfer complex.[17]

IA.4.6. Hydrogen Atom Transfer Process (HAT)

Direct photocatalyzed hydrogen atom transfer (d-HAT) can be considered a method of choice for elaborating C–H bonds. In this manifold, a photocatalyst (PC_{HAT}) exploits the energy of a photon to trigger the homolytic cleavage of bonds in organic compounds. The selective C–H bond elaboration may be achieved by a judicious choice of the hydrogen abstractor (key parameters are the electronic character and the molecular structure), as well as reaction additives.

IA.5. Importance of C–N Bond Formation

The C–N bond formation reactions have become highly favored owing to the widespread applications of nitrogenous products in pharmaceuticals and various industries. The utilization of C–N bond formation methods in medicinal chemistry constitutes around 23% of reported reactions in recent publications, underscoring the pervasive nature of this transformation. Among the C–N bond-forming strategies difunctinalization has gain importance.[19]

IA.5.1. Difunctionalization Strategy for C–C Double Bond

The difunctionalization approach is widely appreciated in modern organic synthesis for its impressive regioselectivity, allowing the simultaneous incorporation of two functional groups onto a carbon-carbon double bond. This method provides a straightforward route to constructing complex molecular frameworks.[20]

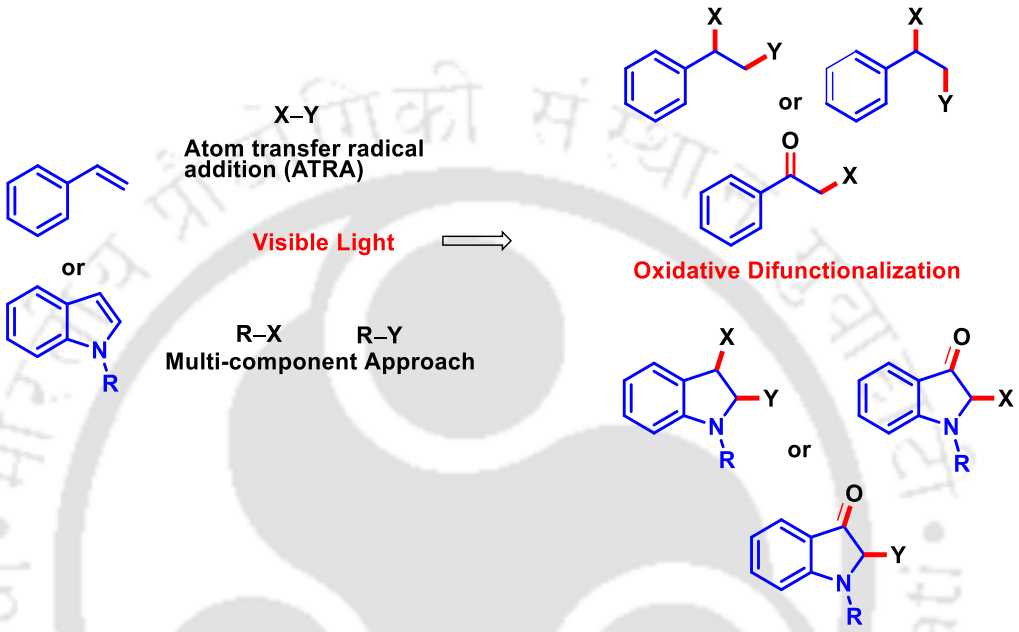

Figure IA.5. *Different difunctionalization strategies.*

Difunctionalization is commonly achieved through various methods, including atom transfer radical addition and the multi-component approach. In the atom transfer radical addition approach, both coupling partners originate from a single radical precursor, while in the multi-component approach, the coupling partners originates from different radical precursors. In the multi-component approach, if one of the radicals is trapped by O_2 or moisture, this type of difunctionalization is termed oxidative difunctionalization. Significant progress has been made in the oxidative difunctionalization of alkenes and indoles using thermal and photochemical approaches to construct diverse frameworks (Figure IA. 5). The photochemical difunctionalization reactions have gained considerable recognition for the construction of C–N bonds.[21] Usually, the difunctionalization mechanism initiates with the attack of one radical precursor on the alkenes, forming a vinyl radical intermediate. This radical is subsequently trapped either directly by another radical or undergoes a SET (single-electron transfer) process, leading to the formation of a

carbocation intermediate. The carbocation is then captured by a nucleophilic partner, resulting in the formation of the desired difunctionalized product (Figure IA. 6).

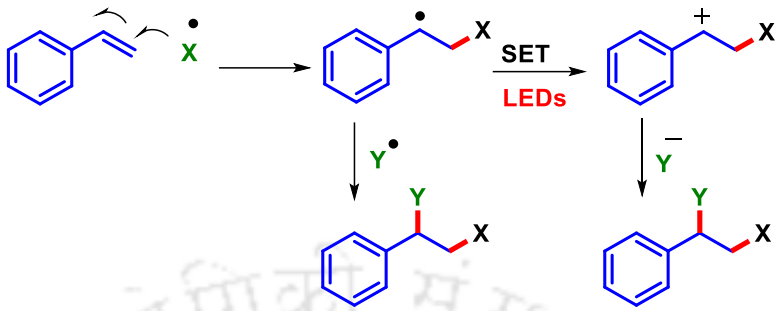

Figure IA.6. *General mechanism for the difunctionalization of alkenes.*

IA.5.1.1. Photochemical C–N Bond Formation *via* Difunctionalization of Alkene

The difunctionalization of alkene has become the focus of chemists as a complex molecular framework via the simultaneous installation of two functional groups onto a carbon-carbon double bond. In particular, styrenes have been frequently used as an important and commercially available building block of many pharmaceuticals, natural products, and materials. In this context, styrene difunctionalization via visible light irradiation has gained importance in modern organic synthesis. The oxime group is a privileged scaffold for preparing amines, amides, and nitrogen-containing heterocyclic compounds.[20] Oxime functionality is found in compounds having anti-inflammatory, antibiotic, and pesticidal activities. Similarly, nitrile serves as a synthetic precursor of many functional groups, such as amine, amide, aldehyde, tetrazole, and carboxylic acid, which are also found. in a variety of compounds having numerous biological activity.[22]

Numerous methodologies are employed to achieve C–N bond formation via visible-light irradiation. In this context, in 2021, the Zhu group demonstrated a photocatalytic 1,2-diamination of 1,3-dienes using N-aminopyridinium and TMSNCS, leading to the formation of 1,2-aminoisothiocyanation products, showcasing high chemo- and regio-selectivity. The broad substrate scope and good functional group tolerance further highlight the versatility and potential applications of diverse compounds (Scheme 1A.1).[23]

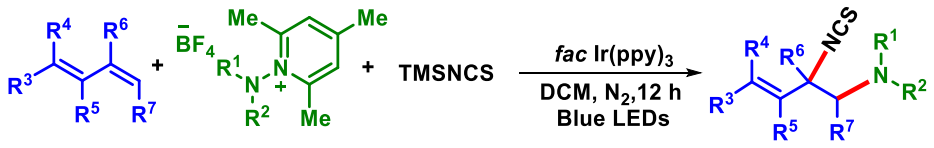

Scheme IA.1. *Synthesis of 1,2-diamination product.*

Gong *et al*. developed a visible-light-induced intermolecular azido-hydrazination method. This innovative approach enables the synthesis of β-azido alkyl hydrazines from unactivated alkenes. A key feature of this transformation is its metal-free and redox-neutral conditions, which enhance its applicability to a wide range of alkenes. The resulting β-azido alkyl hydrazines serve as valuable synthetic building blocks (Scheme 1A.2).[24]

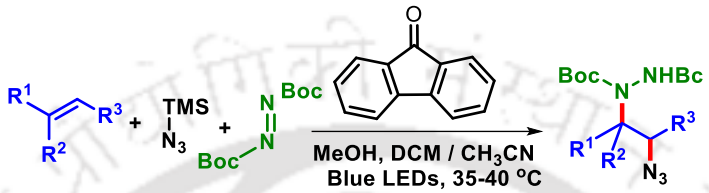

Scheme IA.2. *Synthesis of β-azido alkyl hydrazines.*

Zhang and co-workers in 2021 reported a photo-induced multi-component cascade reaction involving aryldiazonium salts, unactivated alkenes, and trimethylsilyl azide ($TMSN_3$) under oxidant-free conditions. This innovative protocol introduces a synthetic method for unsymmetrical azo compounds, showcasing versatility with different aryldiazonium salts and alkenes (Scheme 1A.3).[25]

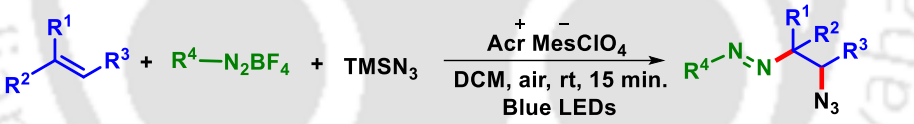

Scheme IA.3. *Synthesis of unsymmetrical azo compounds.*

The work by the Yu group in 2019 presents a notable advancement in organic synthesis, showcasing a visible-light-mediated Cu-catalyzed difunctionalization of alkenes to yield azidation products. Here, azidobenziodoxole acts as the azidating agent, with acetonitrile and $[Cu(dap)_2]PF_6$ complex serving as the photocatalyst. The reactions produce three types of difunctionalized products, such as amido-azidation, diazidation, and benzoyloxy-azidation. The electronic properties of the aryl group attached to the alkene play a crucial role in determining the reaction outcome (Scheme 1A.4).[26]

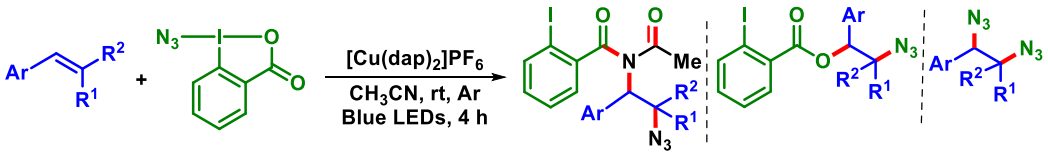

Scheme IA.4. *Synthesis of azidation derivative.*

In 2018 Yang *et al*. established a facile visible-light-mediated synthesis of α-azido ketones. The oxyazidation of alkenes with $TMSN_3$ is achieved in ambient conditions, in the presence of air, and employs Rose Bengal as a metal-free photocatalyst. This approach facilitates the formation of C–N and C–O bonds, yielding α-azido ketones in moderate to excellent yields. (Scheme 1A.5).[27]

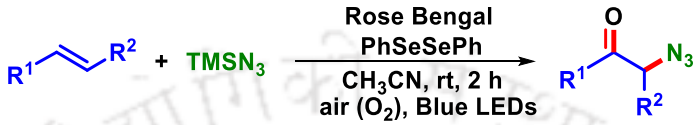

Scheme IA.5. *Synthesis of azido ketones.*

Masson *et al*. demonstrated a visible-light-mediated synthesis of carbotrifluoromethylation product using enecarbamates, and Togni's reagent as the CF_3 and NaN_3 as the azide source (Scheme 1A.6).[28]

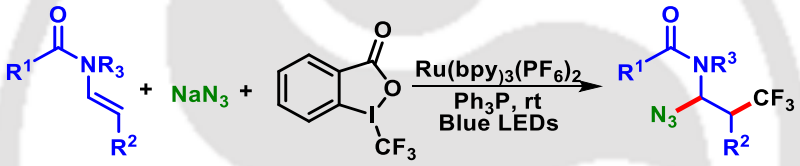

Scheme IA.6. *Strategy for synthesis of carbotrifluoromethylation*.

In 2018, Li and co-workers developed a photo-induced three-component reaction for the synthesis of 1,2-alkylamines using styrenes, alkyl N-hydroxy phthalimide (NHP) esters, and amines. Here, the alkyl NHP esters play a crucial role as alkylating agents, facilitating the generation of 1,2-alkylamine products from the corresponding alkenes (Scheme 1A.7).[29]

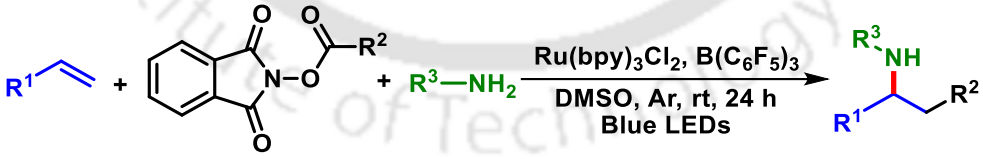

Scheme IA.7. *Strategy for synthesis of 1,2-alkyl amine products.*

In 2019, the Chu group detailed an Ir-catalyzed visible-light-mediated azidoarylation of alkenes, employing pyridines and $TMSN_3$. The reactions were conducted in the presence of *tert*-butanol and irradiated with 90 W blue LEDs. Herein, electron-withdrawing and electron-donating groups of the alkene and cyanopyridine substrates exhibited smooth reactivity, yielding the desired products (Scheme 1A.8).[30]

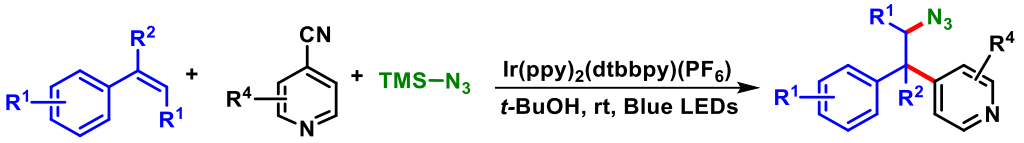

Scheme IA.8. *Strategy for the synthesis of β–azidopyridines.*

Shen *et al*. described a scandium(III) trifluoromethanesulfonate [$Sc(OTf)_3$] and [fac-$Ir(ppy)_3$]-catalyzed synthesis of trifluoromethylative amination product *via* three-components gathering of alkenes, selenium ylides-based trifluoromethylation reagents, and nucleophiles such as azide, amines. The reaction was conducted under mild conditions, and various nucleophiles, including amine, azide, alcohol, water, and electron-rich arenes were tolerated (Scheme 1A.9).[31]

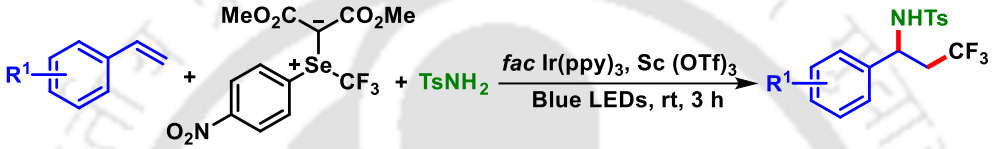

Scheme IA.9. *Synthesis of trifluoromethylative amination product.*

In 2015, the Yu group demonstrated an Ir-catalyzed visible-light-mediated synthesis of chloroamines from activated olefins. Here, N-chlorosulfonamides served as both the nitrogen and chlorine sources. The methodology offered a regioselective, efficient, and atom-economic strategy for preparing vicinal halo amines (Scheme 1A.10).[32]

Scheme IA.10. *Synthesis of chlroamination derivative.*

In 2015, Greaney *et al*. introduced a method for synthesizing azidation derivatives from activated alkenes. Here, the reaction is light-switchable; in the presence of light, it gives methoxyazidated products, and in the absence of light, a diazidation product is obtained. This methodology uses a sustainable and cheap copper-based photocatalyst to enable electron transfer under mild reaction conditions, thus affecting the formation of double C–N bonds in the dark and C–N/C–O formation in the presence of light (Scheme 1A.11).[33]

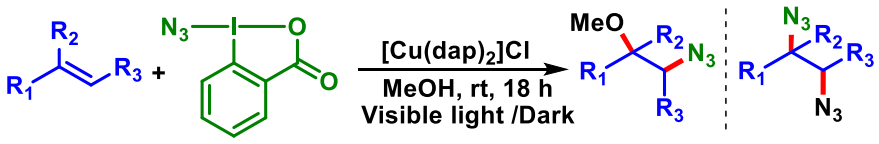

Scheme IA.11. *Synthesis of azidation derivative.*

In 2018, the Reiser group introduced a visible-light-photocatalytic strategy for synthesizing azido ketones from vinyl arenes and $TMSN_3$. The reactions proceeded in a step-economic fashion under aerobic conditions without the need for additional oxidants (Scheme 1A.12).[34]

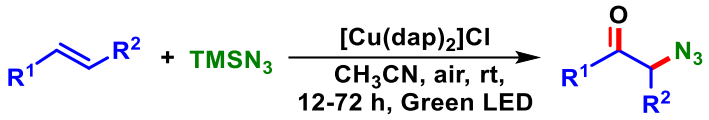

Scheme IA.12. *Synthesis of azido ketones.*

In 2019 Zhang's group reported a Cu-catalyzed visible-light-mediated synthesis of amino alkylated derivatives in the presence of alkene, alkyl iodides, and carbazole. The reaction easily couples with the readily available alkenes, a wide variety of halides, and a broad range of amines (Scheme 1A.13).[35]

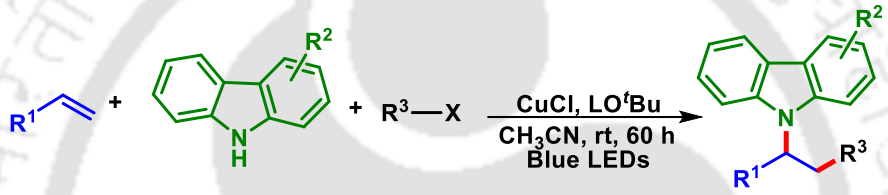

Scheme IA.13. *Synthesis of carboaminations product.*

In 2020, the Gevorgyan group disclosed a Pd-catalyzed visible-light-mediated synthesis of amino alkylated derivatives through the 1,2-carbofunctionalization of conjugated dienes using alkyl iodides and amines as coupling partners. This versatile methodology was further applied for the late-stage derivatization of complex molecules, which is useful in drug discovery. The multi-component reaction utilized readily available reaction partners with a broad substrate scope and did not require exogenous photosensitizers or external oxidants (Scheme 1A.14).[36]

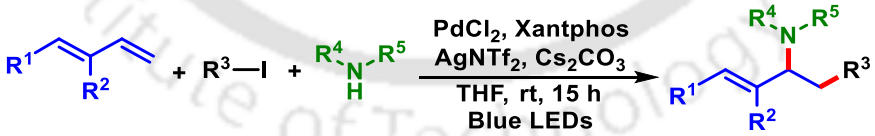

Scheme IA.14. *Synthesis of aminoalkylations derivative.*

Hong *et al.* demonstrated an atom-economical visible-light-mediated synthesis of aminopyridines using alkenes and N-aminopyridinium ylides. This environmentally friendly method demonstrated applicability to a wide range of substrates with good functional group tolerance. The activated and unactivated alkenes, as well as pyridine, smoothly participated in the reaction, yielding the desired products in moderate to good yields at room temperature (Scheme 1A.15).[37]

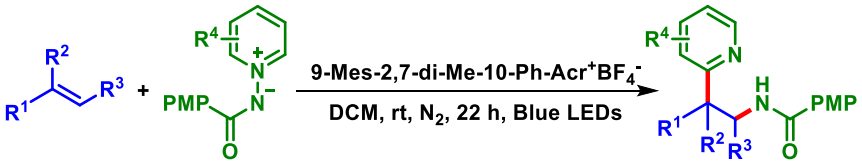

Scheme IA.15. *Synthesis of aminopyridylation product*.

IA.5.1.2. Photochemical C–N Bond Formation *via* Difunctionalization of Indole

Indole and its derivatives are pivotal in bioactive molecules, natural products, and advanced materials. Consequently, the quest for functionalizing simple indoles to construct intricate derivatives is a significant area of research. Photocatalysis is considered a synthetically attractive for driving the single electron oxidation of indoles. Indole-derived radical cations, open-shell reactive species, display distinctive dual reactivity due to the carbon-centered radical and more electrophilic carbocation. It has been applied in various single electron oxidation reactions for synthesizing structurally diverse functionalized indoles and indolines. Remarkable achievements in indole-derived radical cation-mediated indole functionalization have been realized so far.[38] Although 2,3-difunctionalization of indoles has been extensively explored, reported examples are predominantly confined to synthesizing 2,3-disubstituted indole derivatives. Up to date, the 2,3-difunctionalization of simple indoles for synthesizing dearomatized molecules is rare. Here, we have discussed the applications of indole radical cations and dearomative 2,3-difunctionalization, emphasizing the vital single electron oxidation steps of indoles.[39]

Liang's group demonstrated an iodine-mediated C2,3–H aminoheteroarylation of indoles using azoles and quinoxalinones as the reacting partners. This method offers several advantages, including metal-free, straightforward operation, mild reaction conditions, and good tolerance toward various functional groups. This methodology features the versatility of one-pot difunctionalization strategy (Scheme 1A.16).[40]

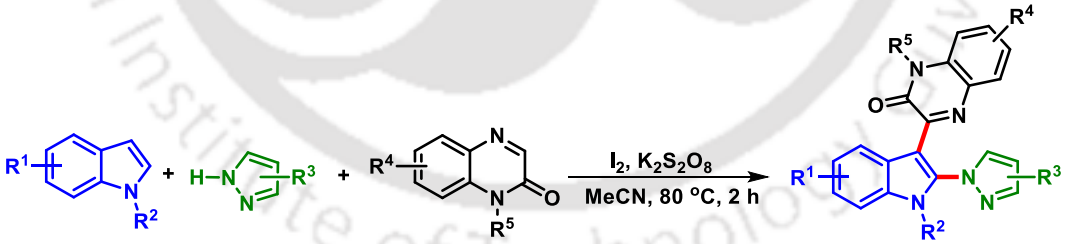

Scheme IA.16. *Synthesis of aminoheteroarylationof indoles derivatives.*

In 2020, Sen *et al*. introduced an iodine-catalyzed aerobic diazenylation-amination of indole. Here, the aromatic amines are generated in situ by the reaction of aryl hydrazine with iodine. The reaction is compatible with both these substrates and various functional groups. This methodology provides a practical route to access C2/C3 aminated indoles (Scheme 1A.17).[41]

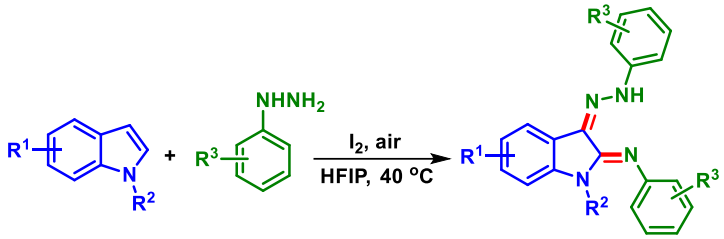

Scheme IA.17. *Synthesis of azenyl-aminated indole derivatives*.

Liang group disclosed a palladium-/copper-catalyzed regioselective amination and chloroamination of indoles. This reaction produces good to excellent yields to give a variety of 2-amino-substituted indoles and exhibits excellent regioselectivity at room temperature. Similarly, an intermolecular direct C–H amination of indoles is obtained using chlorosulfonamides as the nitrogen source (Scheme 1A.18).[42]

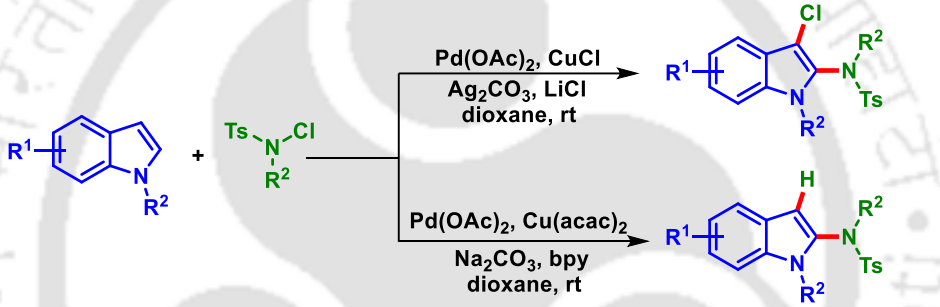

Scheme IA.18. *Synthesis of azenyl-aminated indole derivatives*.

In 2020 the Zheng group presented an electrochemical iodoamination method for indoles that employed unactivated amines. This electrochemical approach facilitates the iodoamination of diverse indole derivatives with various unactivated amines, amino acid, and benzotriazoles derivatives. This strategy is further extended in gram-scale synthesis and its utility in the radioactive of ^{131}I-labeled compounds (Scheme 1A.19).[43]

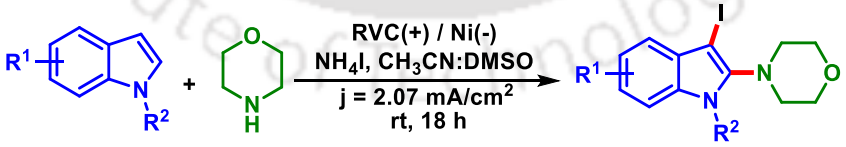

Scheme IA.19. *Synthesis of iodoamination indole derivatives.*

In 2018 Borhan group demonstrated a Cu-catalyzed oxidation of C2 and C3 alkyl-substituted indole via acyl nitroso reagents. The selective oxidation of C2-alkyl-substituted indoles to 3-oxindole and the selective C–H oxygenation or amination of C2,C3-dialkyl-substituted

indoles at C2 are achieved under mild conditions. The strongly electron-donating and electron-withdrawing groups are compatible with this reaction (Scheme 1A.20).[44]

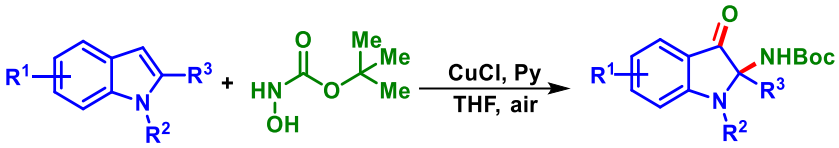

Scheme IA.20. *Synthesis of 3-oxindole derivatives.*

In 2019, the Ji group unveiled the dearomatization of indoles through azido radical addition and dioxygen trapping, resulting in the synthesis of 2 azidoindolin-3-ols. Here, the molecular oxygen played a dual role as an oxygen-atom source and a trapping agent. The reaction demonstrated exceptional site- and diastereoselectivity, showcasing its versatility across a wide substrate scope (Scheme 1A.21).[45]

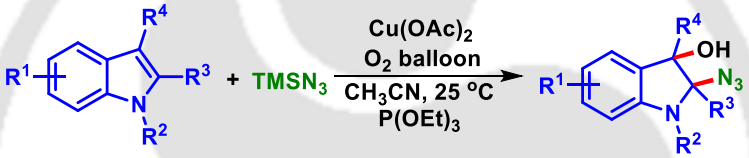

Scheme IA.21. *Synthesis of 2-azidoindolin-3-ols derivatives*.

Tu *et al*. presented a TBHP/TBAI-catalyzed oxidative coupling reaction of C2,C3-unsubstituted indoles with arylsulfonyl hydrazide. The methodology provided a mild and practical route to polyfunctionalized indoles with good to excellent yields via the simultaneous formation of C–S and C–N bonds (Scheme 1A.22).[46]

Pan group introduced an environmentally benign electrochemical method for the chemoselective sulfonylation and hydrazination of C2, and C3-unsubstituted indoles. This approach involved the use of aryl sulfonyl hydrazide in the presence of ammonium bromide as a redox catalyst and electrolyte (Scheme 1A.22.).[47]

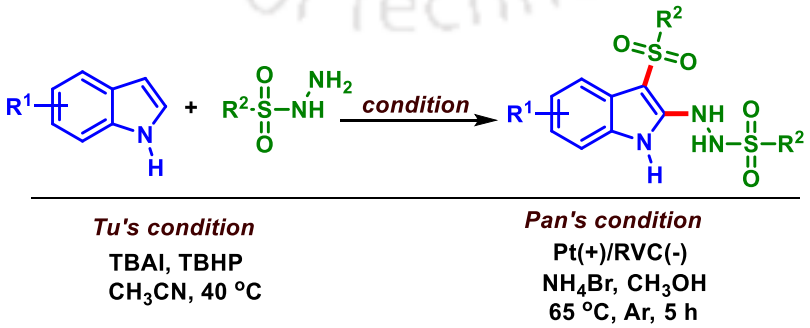

Scheme IA.22. *Synthesis of sulfonylation and hydrazination of indoles derivatives*.

In 2019, the Vincent group disclosed an interesting electrochemical dearomative 2,3-difunctionalization of indoles. This operationally simple electro-oxidative procedure avoids the use of an external oxidant and displays excellent functional group compatibility (Scheme 1A.23).[48]

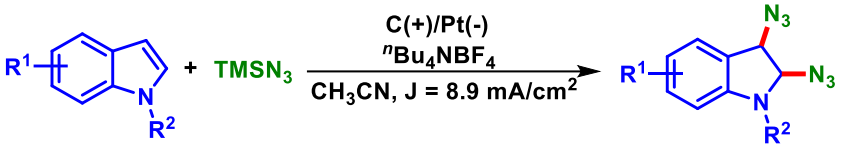

Scheme IA.23. *Synthesis of diazidation of indoles derivatives*.

Zhu and co-workers developed a copper-catalyzed 2,3-diazidation of indole derivatives *via* C–H activation using azidotrimethylsilane as the azide source. The methodology synthesizes a variety of 2,3-diazide-substituted indoles in high yields. The resulting 2,3-diazides exhibit facile conversion into various functional groups, such as vicinal diamines, triazoles, and benzotriazoles (Scheme 1A.24).[49]

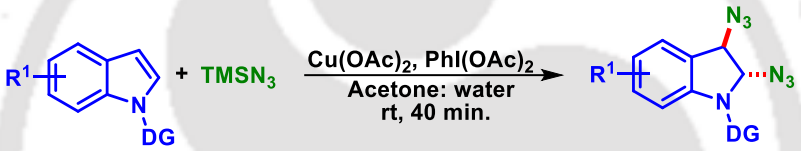

Scheme IA.24. *Synthesis of 2,3-diazidation of indoles derivatives*.

In 2023, Chandrasekhar's group demonstrated a metal-free strategy for the regioselective of 2,3-difunctionalization of indoles to access trans-2-azido-3-arylselenyl indolines under mild conditions. The reaction proceeds via oxidation of N-substituted indole involving the formation of C–N and C–Se bonds (Scheme 1A.25).[50]

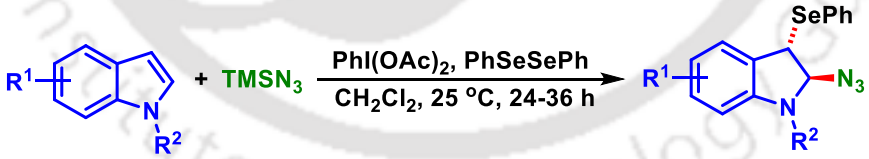

Scheme IA.25. *Synthesis of 2-azido-3-arylselenyl indolines derivatives*.

Ji *et al*. demonstrated a visible-light-promoted radical cyclization and N–N bond cleavage relay of N-aminopyridinium ylides to access 2,3-difunctionalized indoles. The electrophilic pyridyl and nucleophilic amino groups were installed simultaneously into a wide range of indoles under mild and metal-free conditions. The protocol shows high levels of step and atom economy (Scheme 1A.26).[51]

Scheme IA.26. *Synthesis of 2,3- difunctionalized indoles derivatives.*

IA.6. Conclusion

In summary, the literature, as mentioned earlier, gives the idea of how C–N bond formation takes place *via* difunctionalization of alkene and indole under thermal and photochemical conditions. With the current momentum of development, a more significant impact of photocatalytic C–N bond-formations reactions is foreseeable, for example, in the late-stage modifications of natural products, large-scale syntheses, and enantioselective C–N bond formations reactions, visible-light-mediated reactions provide a greener and sustainable approach and mild reaction condition towards the construction of complex molecules. Taking cues from the above literature, the photochemical C–N bond formation *via* difunctionalization of alkene and dearomative 2,3-difunctionalization of indole have been designed.

IA.7. References

[1] (a) Yi, H.; Zhang, G.; Wang, H.; Huang, Z.; Wang, J.; Singh, A. K.; Lei, A. *Chem. Rev.* **2017**, *117*, 9016−9085. (b) Togo, H. Advanced Free Radical Reactions for Organic Synthesis, 1st ed.; Elsevier: Amsterdam, Boston, **2004**. (c) Fontecave, M.; Ollagnier-de-Choudens, S.; Mulliez, E. *Chem. Rev.* **2003**, *103*, 2149−2166.

[2] (a) Holmberg-Douglas, N.; Nicewicz, D. A. *Chem. Rev.* **2022**, *122*, 1925−2016. (b) Zeitler, K. *Angew. Chem., Int. Ed.* **2009**, *48*, 9785−9789. (c) Narayanam, J. M. R.; Stephenson, C. R. J. *Chem. Soc. Rev.* **2011**, *40*, 102−113. (c) Shi, L.; Xia, W. *Chem. Soc. Rev.* **2012**, *41*, 7687−7697.

[3] (a) Nicewicz, D. A.; Nguyen, T. M. *ACS Catal.* **2014**, *4*, 355−360. (b) Zhang, G.; Bian, C.; Lei, A. *Chin. J. Catal.* **2015**, *36*, 1428−1439. (c) Angnes, R. A.; Li, Z.; Correia, C. R. D.; Hammond, G. B. *Org. Biomol. Chem.* **2015**, *13*, 9152−9167.

[4] (a) Romero, N. A.; Nicewicz, D. A. *Chem. Rev.* **2016**, *116*, 10075−10166. (b) Tóth, B. L.; Tischler, O.; Novák, Z. *Tetrahedron Lett.* **2016**, *57*, 4505−4513. (c) Siddiqui, R.; Ali, R. *Beilstein J. Org. Chem.* **2020**, *16*, 248−280. (d) Amos, S. G. E.; Garreau, M.; Buzzetti, L.; Waser, J. *Beilstein J. Org. Chem.* **2020**, *16*, 1163−1187.

[5] (a) Prier, C. K.; Rankic, D. A.; MacMillan, D. W. C. *Chem. Rev.* **2013**, *113*, 5322−5363. (b) Yoon, T. P.; Ischay, M. A.; Du, J. *Nat. Chem.* **2010**, *2*, 527−532. (c) Hopkinson, M. N.; Sahoo, B.; Li, J.-L.; Glorius, F. *Chem. Eur. J.* **2014**, *20*, 3874−3886.

[6] (a) Koike, T.; Akita, M. *Inorg. Chem. Front.* **2014**, *1,* 562−576. (b) Skubi, K. L.; Blum, T. R.; Yoon, T. P. *Chem. Rev.* **2016**, *116*, 10035−10074. (c) Levin, M. D.; Kim, S.; Toste, F. D. *ACS Cent. Sci.* **2016**, *2*, 293−301.

[7] (a) Teply, F. *Chem. Commun.* **2011**, *76*, 859−917. (b) Xuan, J.; Xiao, W.-J. *Angew. Chem., Int. Ed.* **2012**, *51*, 6828−6838. (c) Brachet, E.; Ghosh, T.; Ghosh, I.; König, B. *Chem. Sci.* **2015**, *6*, 987−992. (d) Chen, J.-R.; Hu, X.-Q.; Lu, L.-Q.; Xiao, W.-J. *Chem. Soc. Rev.* **2016**, *45*, 2044−2056.

[8] (a) Karkas, M. D. *ACS Catal.* **2017**, *7*, 4999−5022. (b) Zhao, Y.; Xia, W. *Chem. Soc. Rev.* **2018**, *47*, 2591−2608. (c) Jiang, H.; Studer, A. *Angew. Chem., Int. Ed.* **2017**, *56*, 12273−12276.

[9] (a) Penzkofer, A.; Beidoun, A.; Daiber, M. *J. Lumin.* **1992**, *51*, 297−314. (b) Majek, M.; Filace, F.; von Wangelin, A. J. *Beilstein J. Org. Chem.* **2014**, *10*, 981−989. (c) Timpe, H.-J.; Neuenfeld, S. *J. Chem. Soc. Faraday Trans.* **1992**, *88*, 2329−2336. (d) Yoshioka, E.; Kohtani, S.; Jichu, T.; Fukazawa, T.; Nagai, T.; Takemoto, Y.; Miyabe, H. *Synlett* **2015**, *26*, 265−270.

[10] Zhao, Y.; Xia, W.; *Chem. Soc. Rev.*, **2018**, *47*, 2591-2608.

[11] Chan, C.-M.; Chow, Y.-C.; Yu, W.-Y. *Synthesis* **2020**, *52*, 2899–2921.

[12] Canuto, V. M.; Levine, J. S.; Augustsson, T. R.; Imhoff, C. L.; Giam-papa, M. S. *Nature* **1983**, *305*, 281–286.

[13] (a) Blake, A. J.; Carver, J. H.; *J. Atmos. Sci.* **1977**, *34,*720–728. (b) Levine, J. S.; Hays, P. B.; Walker, J. C. G. *Icarus* **1979**, *39* 295–309.

[14] Ni, T.; Caldwell, R. A.; Melton, L. A. *J. Am. Chem. Soc.* **1989**, *111*, 457−464.

[15] (a) Mangion, D.; Kendall, J.; Arnold, D. R. *Org. Lett.* **2001**, *3*, 45−48. (b) Griesbeck, A. G.; Hundertmark, T.; Steinwascher, J. *Tetrahedron Lett.* **1996**, *37*, 8367−8370. (c) Davies,

J.; Booth, S. G.; Essafi, S.; Dryfe, R. A. W.; Leonori, D. *Angew*. *Chem*. **2015**, *127*, 14223−14227. (d) Yang, D.-T.; Meng, Q.-Y.; Zhong, J.-J.; Xiang, M.; Liu, Q.; Wu, L.-Z. *Eur*. *J*. *Org*. *Chem*. **2013**, *2013*, 7528−7532.

[16] (a) Gentry, E. C.; Knowles, R. R. *Acc*. *Chem*. *Res*. **2016**, *49*, 1546−1556. (b) Dahiya, A.; Das, B.; Sahoo, A. K.; Patel, B. K. *Adv. Synth. Catal*. **2022**,*364*, 966–973.

[17] (a) Rosokha, S. V.; Kochi, J. K. *Acc*. *Chem*. *Res*. **2008**, *41*, 641−653. (b) Rosokha, S. V.; Kochi, J. K. *J*. *Am*. *Chem*. *Soc*. **2007**, *129*, 3683−3697. (c) Kochi, J. K. *Pure Appl*. *Chem*. **1991**, *63*, 255−264. (d) Silvi, M.; Arceo, E.; Jurberg, I. D.; Cassani, C.; Melchiorre, P. *J*. *Am*. *Chem*. *Soc*. **2015**, *137*, 6120−6123. (e) Wozniak,́ Ł.; Murphy, J. J.; Melchiorre, P. *J*. *Am*. *Chem*. *Soc*. **2015**, *137*, 5678−568.

[18] Capaldo, L.; Ravelli, D.; Fagnoni, M. *Chem. Rev.* **2022**, *122*, 1875–1924.

[19] Chan, C.-M.; Chow, Y.-C.; Yu, W.-Y. *Synthesis* **2020**, *52*, 2899–2921.

[20] (a) Patel, M.; Saunthwal, R. K.; Verma, A. K. *Acc*. *Chem. Res*. **2017**, *50*, 240−254. (b) Wille, U. *Chem*. *Rev*. **2013**, *113*, 813−853. (c) Yue, H.; Zhu, C.; Kancherla, R.; Liu, F.; Rueping, M. *Angew*. *Chem*., *Int*. *Ed.* **2020**, *59*, 5738−5746. (d) Huang, L.; Rudolph, M.; Rominger, F.; Hashmi, A. S. K. *Angew*. *Chem*., *Int*. *Ed*. **2016**, *55*, 4808−4813. (e) Xu, T.; Cheung, C. W.; Hu, X. *Angew*. *Chem*., *Int*. *Ed*. **2014**, *53*, 4910−4914.

[21] (a) Li, Z.; Wang, S.; Huo, Y.; Wang, B.; Yan J.; Guo, Q. *Org*. *Chem*. *Front*. **2021**, *8*, 3076–3081. (b) Hossain, A.; Engl, S.; Lutsker, E.; Reiser, O. *ACS Catal*. **2019**, *9*, 1103–1109. (c) Lei, W.-L.; Wang, T.; Feng, K.-W.; Wu, L.-Z.; Liu, Q. *ACS Catal*. **2017**, *7,* 7941–7945. (d) Reddy, M. B.; Anandhan, R. *Chem*. *Commun*. **2020**, *56*, 3781–3784. (e) Shi, P.; Tu, Y.; Zhang, D.; Wang, C.; Truong, K.-N.; Rissanen K.; Bolm, C. *Adv. Synth. Catal*. 2021, 363, 2552–2556.

[22] (a) Furuya, Y.; Ishihara, K.; Yamamoto, H. *J. Am. Chem. Soc.* **2005**, *127*, 11240. (b) Hong, W. P.; Iosub, A. V.; Stahl, S. S. *J. Am. Chem. Soc*. **2013**, *135*, 13664. (c) Ferris, J. P.; Antonucci, F. R. *J. Am. Chem. Soc*. **1972**, 8091. (d) Himo, F.; Demko, Z. P.; Noodleman, L.; Sharpless, K. B. *J. Am. Chem. Soc*. **2002**, *124*, 12210.

[23] Guo, W.; Wang, Q.; Zhu, J. *Angew. Chem. Int. Ed*. **2021**, 60, 4085–4089.

[24] Wang, P.; Luo, Y.; Zhu, S.; Lu, D.; Gong, Y. *Adv. Synth.Catal*. **2019**, *361*, 5565–5575

[25] Shen, J.; Xu, J.; He, L.; Ouyang, Y.; Huang, L.; Li, W.; Zhu, Q.; Zhang, P. *Org. Lett*. **2021**, *23*, 1204–1208.

[26] Wu, D.; Cui, S.-S.; Lin, Y.; Li, L.; Yu, W. *J. Org. Chem*. **2019**, *84*, 10978–10989.

[27] Wei, W.; Cui, H.; Yue, H.; Yang, D. *Green Chem*., **2018**, *20*, 3197–3202.

[28] Carboni, A.; Dagousset, G.; Magnier, E.; Masson, G. *Org. Lett*. **2014**, *16*, 1240–1243.

[29] Ouyang, X.-H.; Li, Y.; Song, R.-J.; Li, J.-H. *Org. Lett*. **2018**, *20*, 6659–6662.

[30] Chen, J.; Zhu, S.; Qin, J.; Chu, L. *Chem. Commun*., **2019**, *55*, 2336–2339.

[31] Ge, H.; Wu, B.; Liu, Y.; Wang, H.; Shen, Q. *ACS Catal*. **2020**, *10*, 12414–12424.

[32] Qin, Q.; Ren, D.; Yu, S. *Org. Biomol. Chem*., **2015**, *13*, 10295–10298.

[33] Fumagalli, G.; Rabet, P. T. G.; Boyd, S.; Greaney, M. F. *Angew. Chem. Int. Ed*. **2015**, *54*, 11481–11484.

[34] Hossain, A.; Vidyasagar, A.; Eichinger, C.; Lankes, C.; Phan, J.; Rehbein, J.; Reiser, O. *Angew. Chem. Int. Ed*. **2018**, *57*, 8288–8292.

[35] Xiong, Y.; Ma, X.; Zhang, G. *Org. Lett*. **2019**, *21*, 1699–1703.

[36] Cheung, K. P. S.; Kurandina, D.; Yata, T.; Gevorgyan, V. *J. Am. Chem. Soc.* **2020**, *142*, 9932–9937.

[37] Moon, Y.; Lee, W.; Hong, S. *J. Am. Chem. Soc.* **2020**, *142*, 12420–12429.

[38] (a) Petrini, M.; *Adv. Synth. Catal*. **2020**, *362*, 1214–1232. (b) Zheng, L.; Tao, K.; Guo, W. *Adv. Synth. Catal*. **2021**, *363*, 62–119.

[39] (a) Bugaenko, D. I.; Karchava, A. V.; Yurovskaya, M. A. *Russ. Chem. Rev*., **2019**, *2*, 99–159. (b) Dai, L.; Sun, Y.-L.; Guo, J.; Zhou, X.; Huang, Q.; Lu, Y. DOI: 10.31635/ccschem.023.202303434. (c) Zhou, W.; Chen, X.; Lu, L.; Song, X.-R.; Luo, M.-J.; Xiao, Q.; *Chin. Chem. Lett.* **2024**, *35,* 108902–108920. (d) Liu, S.; Zhao, F.; Chen, X.; Deng, G.-J.; Huang, H. *Adv. Synth. Catal*. **2020**, *362*, 3795–3823.

[40] Dai, M.; Zhang, Y.; Zhang, X.; Wang, R.; Wei, W.; Zhang, Z.; Liang, T. *J. Org. Chem.* **2023**, *88*, 15106–15117.

[41] Sar, S.; Tripathi, A.; Dubey, K. D.; Sen, S. *J. Org. Chem*. **2020**, *85*, 3748–3756.

[42] Liu, X.-Y.; Gao, P.; Shen, Y.-W.; Liang, Y.-M. *Org. Lett*. **2011**, *16*, 4196–4199.

[43] Lei, N.; Shen, Y.; Li, Y.; Tao, P.; Yang, L.; Su, Z.; Zheng, K. *Org. Lett*. **2020**, *22*, 9184–9189.

[44] Zhang, J.; Kohlbouni, S. T.; Borhan, B. *Org. Lett.* **2019**, *21*, 14–17.

[45] Xu, M.-M.; Cao, W.-B.; Ding, R.; Li, H.-Y.; Xu, X.-P.; Ji, S.-J. *Org. Lett*. **2019**, *21*, 6217–6220.

[56] Qiu, J.-K.; Hao, W.-J.; Wang, D.-C.; Wei, P.; Sun, J.; Jiang, B.; Tu, S.-J. *Chem. Commun*., **2014**, *50*, 14782–14785.

[46] Zhang, Y.-Z.; Mo, Z.-Y.; Wang, H.-S.; Wen, X.-A.; Tang, H.-T.; Pan, Y.-M. *Green Chem*., **2019**, 21, 3807–3811.

[48] Wu, J.; Dou, Y.; Guillot, R.; Kouklovsky, C.; Vincent, G. *J. Am. Chem. Soc*. **2019**, *141*, 2832–2837.

[49] Liu, J.; Fang, Z.; Liu, X.; Dou, Y.; Jiang, J.; Zhang, F.; Qu, J.; Zhu, Q. *Chin. Chem. Lett.* **2020**, *31*, 1332–1336.

[50] Pal, P.; Goud, G. K.; Sridhar, B.; Mainkar, P. S.; Nayani, K.; Chandrasekhar, S. *Tetrahedron Lett.* **2023**, *121*,154478-154483.

[51] Xu, M.-M.; Cao, W.-B.; Xu, X.-P.; Ji, S.-J. *Adv. Synth. Catal*. **2022**, *364*, 2211–2220.

CHAPTER IB

CHAPTER IB

Electrochemical Approach for the C–N Bond Construction

IB.1. Introduction

Though the photochemical strategies have been well-established, providing ample nitrogenous framwork in a sustainble manner but the development of newer strateges in this direction will always welcome in the scintific community. In recent years electrochemical reactions gathered anough popularity in achieving various molecular framework. Particularly, the C–N bond construction *via* electrochemical approach has proven to be a powerful tool. Thus, within the realm of green and sustainable chemistry, there is a notable push for the acknowledgment and adoption of environmentally friendly methodologies that employ sustainable approaches in facilitating C–N bond formation reactions.

This approach aligns with the broader goal of achieving greener and more sustainable practices in organic synthesis.[1] Synthetic organic chemists are continuously exploring innovative techniques to enhance selectivity and productivity for the synthesis of pharmaceutical compounds. This approach can potentially reduce chemical usage, minimize waste, and reduce operational costs, safety, and sustainability. Electro-organic synthesis involves the direct use of electrons from a power source to drive redox transformations.[2]

Mostly, electrochemical methods employ constant voltage or current to facilitate chemical transformations. This approach, known as direct current electrolysis (DCE), ensures that the electric current flows in a single direction. The alternating current electrolysis (ACE) has not been explored much, where the flow of charge periodically changes its direction. The adoption of electrochemical methods, whether using DCE or ACE, represents a promising avenue for achieving greener and more efficient organic synthesis.[3] In this part, we will explore traditional and modern approaches for the C–N bond formation resulting in an amide framework. The discussion will begin with the basic concept of electro-organic synthesis and the formation of the C–N bond, followed by an examination of the electrochemical approach specifically for cross-coupling reactions.[4]

IB.2. Development of Electrochemistry Battery to Modern Electrochemical Cell

Terminology

Power supply:–electricity source

Current:– electrons movement (I in ampere)

Potential:–voltage difference between two electrodes, provides energy to move electrons (U in volt)

Charge:–current passed within time (Q in coulomb)

Electrode:– A conducting material that transfers electrical current into the reaction solution

Cathode:–reduction electrode

Anode:–oxidation electrode

Working electrode:– the electrode where the desired reaction takesplace(WE)

Counter electrode:–electrode opposite to working electrode (CE)

Counter reaction:–reaction on the counter electrode

Cyclic voltammetry:–an electrochemical analytical tool (CV)

Overpotential:–additional potential required, dependent on e.g. the electrode material

Standard potential:–the potential of a redox reaction under standard conditions.

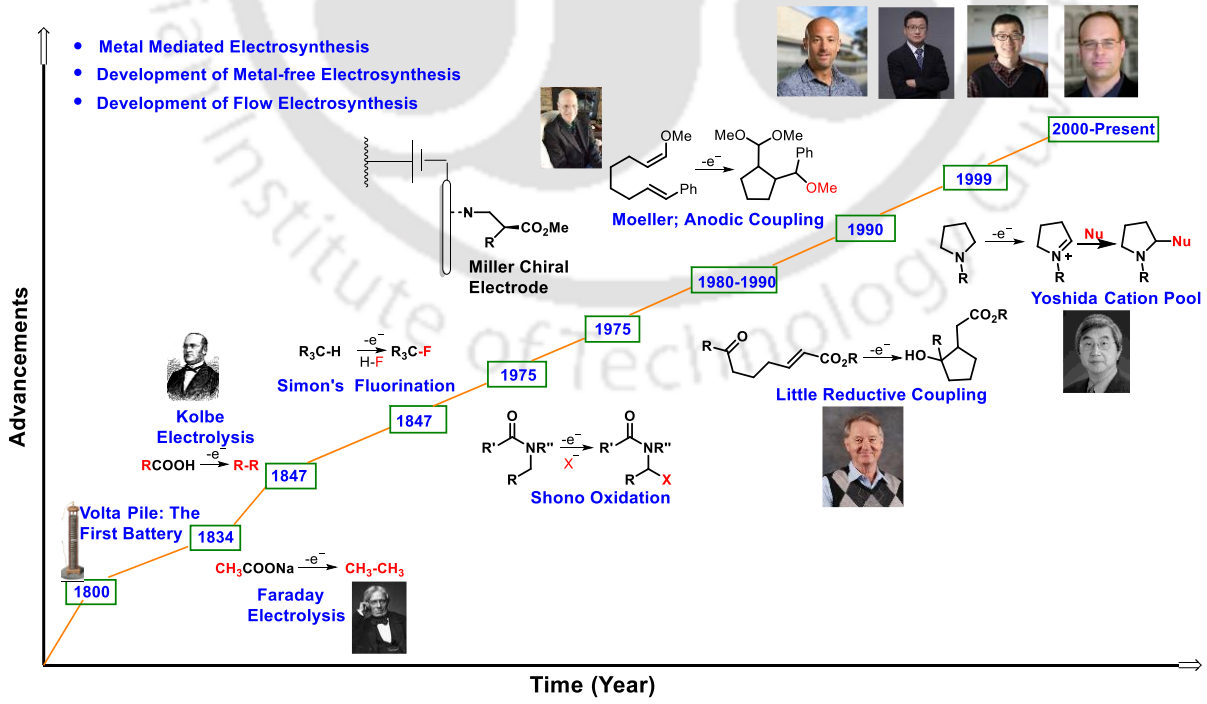

Figure IB.1. *Timeline showing the revolution of electro-organic chemistry from 1800-2023.*

Ongoing advancements in electro-organic synthesis, focusing on sustainable and green methodologies. Advancements in electro-organic chemistry from 1800 to 2023 have been driven by significant technological and methodological innovations. The invention of the voltaic pile by Alessandro Volta in 1800 laid the foundational principles, which were further refined by Michael Faraday's laws of electrolysis in the early 19th century. The mid-20th century saw the introduction of controlled potential electrolysis and potentiostatic methods, enhancing the precision and scope of electro-organic reactions. In recent decades, the integration of computational chemistry, electrocatalysis, and flow electrochemistry has vastly improved reaction efficiency and scalability. The contemporary focus on green chemistry and the use of renewable energy sources has made electro-organic processes more sustainable and environmentally friendly. This timeline provides a brief overview of the significant developments in electro-organic chemistry over the years (Figure IB.1).[2]

IB.2.1. Electric Battery in Electrochemical Reaction

The era of electro-organic synthesis began in 1800 with the introduction of the Volta Pile. Serving as the inaugural electric battery, the Volta Pile marked a significant milestone by enabling a continuous flow of electrons through a circuit, laying the foundation for electrochemical reaction in organic synthesis.[5]

IB.2.2. Faraday’s Contribution to Electrochemistry

Michael Faraday, one of the world's greatest physicists, is also known as the father of the electric motor, electric generator, and electric transformer. He introduced the concept of electrolysis to the world, the well-known terms cathode and anode, and the observation of ions moving through electrolyte solutions. This led to the development of Faraday’s Laws of electrolysis.[6]

IB.2.3. Kolbes Electrolysis

Faraday's legacy in electro-organic chemistry is further solidified by his description of the electrolysis of sodium acetate. This pioneering work served as inspiration for the development of the renowned Kolbe electrolysis, which involves the electrochemical generation of alkyl radicals from carboxylic acids (Figure IB.2).[7]

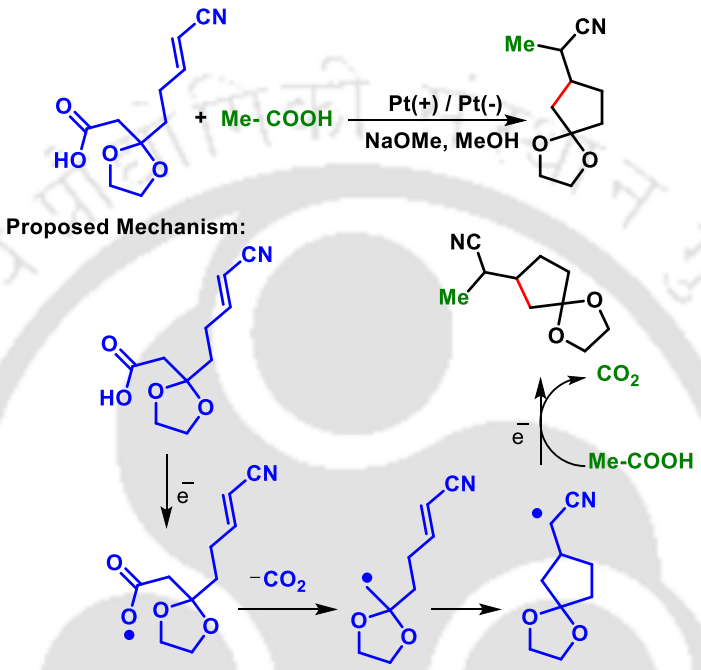

Figure IB.2. *Cyclisation using mixed-kolbe electrolysis strategy and a plausible mechanism.*

In addition to the pioneering early advancements in electro-organic synthesis, significant progress has emerged over the past six decades.[2,3] Noteworthy contributions include Lund's[8] 1969 breakthrough in electrochemical generation of bases, along with the establishment of the Shono oxidation[9] in 1975, enabling the α-functionalization of alkyl amides. Furthermore, the past thirty years have witnessed a proliferation of groundbreaking research in electro-organic synthesis spearheaded by luminaries such as Little[10] in electro-reductive cyclization. The Moeller[11] in anodic olefin coupling, Yoshida[12] in electro-auxiliaries employing S and Si, Baran's[13] achievement in total synthesis of dixiamycin, Waldvogel's[14] innovations in the biaryl coupling, among numerous others.[15]

IB.2.4. Introduction of CyclicVoltamtery

Randles in 1948 reported the world's first cyclic voltammetry(CV) experiment. This groundbreaking technique allowed the accurate determination of redox potentials for various specific functional groups and remained a valuable tool in electrochemical studies.

In a cyclic voltammetry (CV) setup, there is a working electrode, a counter electrode, and a reference electrode. During the experiment, the current is monitored as the potential at the working electrode is scanned in a cyclic manner using a triangular waveform, resulting in a cyclic voltammogram. When the potential is increased without any active reaction occurring, there will be no rise in current observed. However, if a species can undergo oxidation or reduction at the applied voltage, current will flow until the species is depleted at the electrode surface, resulting in a peak formation.[16]

IB.2.5. Current and Potential

In electrochemical reactions, the current (I) and potential (U) are key factors. The current shows the movement of electrons, while the potential represents the energy needed to facilitate this electron movement. The current regulates the electron transfer rate into the reaction medium, thereby controlling the reaction rate in an electrochemical context. Charge (Q), which is current over a certain period, aligns with the total electrons transferred, which is close to the stoichiometry of a reagent. The potential (U), representing the energy of the electrons, must be adjusted to match the potential required for the desired electrochemical approach. The precise control of the potential is crucial for achieving the desired reaction outcomes in electrochemical synthesis.

The current and potential in an electrochemical reaction are connected through the system's resistance (R), which stems from components like wiring, electrodes, the reaction solution, and the reaction itself. Given their intrinsic link, any modification in one parameter, like its potential, resistance, or current, affects the others. Consequently, in electrochemical systems, any adjustments in potential or current must account for the corresponding alterations in resistance to uphold the desired reaction conditions.[17]

$$U = R \times I$$

U: potential in volt [V], R: resistance in ohm [Ω], I: current in ampere [A].

IB.2.6. Set-up of Electrochemical Reaction

IB.2.6.1. Equipments Needed

The apparatus and example electrodes are used for conducting reactions in either an undivided cell or a divided cell. The primary components in all setups include:

i. An electrolyte solution containing a charged species dissolved in a solvent, facilitating the transfer of charges between electrodes (e.g., $LiClO_4$ dissolved in MeCN).

ii. Electrodes immersed in the electrolyte solution, conducting electrons to or from the potentiostat.

iii. A potentiostat.

iv. A reaction vessel or cell, which can be either divided or undivided.

IB.2.6.2. Choice of Electrode

The electrodes play a crucial role in electrochemical reactions, and the choice of electrode material, size, and shape can significantly impact the reaction outcome. Since reactions occur on the electrode surface, surface area is a key factor. Materials with higher surface areas, such as foams or meshes, offer more active sites for reaction, leading to enhanced reaction rates than solid plates or rods. Therefore, selecting electrodes with appropriate surface characteristics is essential for optimizing reaction performance in the electrochemical approach. A standard three-electrode system is employed in electrochemical experiments, featuring a working electrode (WE), a reference electrode (RE), and a counter electrode (CE).

IB.2.6.3. Choice of Solvents and Electrolytes

The choice of solvent in an electrochemical cell significantly influences reducing resistance or increasing conductivity. In electro synthesis, organic solvents, particularly polar aprotic ones, are commonly used. These solvents dissolve substrates, electrolytes, and reactants

effectively. The solvent is frequently exposed to electrodes at high oxidizing or reducing potentials during electrochemical reactions. Therefore, selecting a solvent with appropriate properties is essential for ensuring the success and efficiency of the electrochemical reaction. To ensure the cell's charge neutrality, having charged species (electrolytes) is crucial. Electrolytes also play a role in altering the electrode surface during reactions. These electrolytes vary from ionic liquids to polar solvents, aiding conductivity through soluble organic salts like Bu_4NBF_4 and Bu_4NPF_6.

IB.2.6.4. Electrochemical Cell Design

Electrolysis can be conducted using standard laboratory glassware such as beakers or round-bottom flasks. In addition to self-made setups utilizing regular batteries, there are also commercially available setups for electrolysis. Flow electrolysis is particularly important for scaling up the process. Electrochemical cells come in two varieties: undivided cells and divided cells.

IB.2.6.4.1. Undivided Cell

In an undivided electrochemical cell, the cathode and anode are housed in the same chamber. This setup is easy to carry out, as no elaborate glassware/reactor is needed. In addition, the distance between the two electrodes can be easily adjusted, and ionic species can move freely between the electrodes (Figure IB.3).

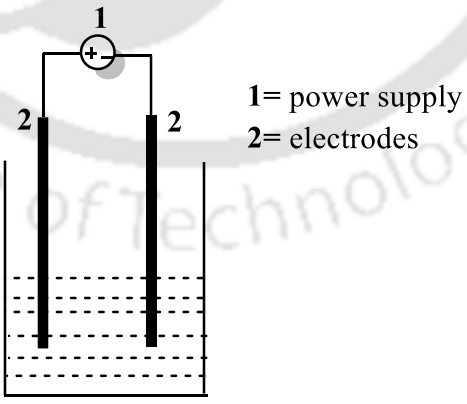

Figure IB.3. *Undivided cell.*

IB.2.6.4.2. Divided Cell

In a divided electrochemical cell, the cathode and anode are kept in different chambers, separated by an ion-permeable membrane or salt bridge. A semipermeable membrane or porous glass frit is used in divided cells to separate the anolyte and catholyte to suppress nondesired diffusion to the counter electrode (Figure IB.4).

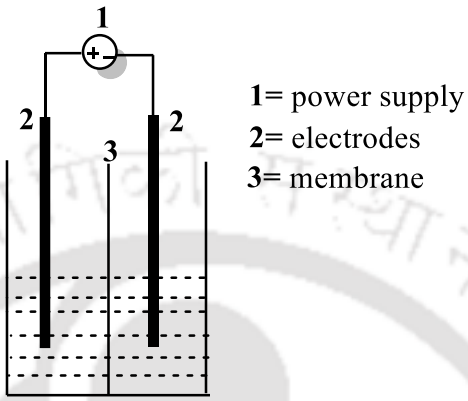

Figure IB.4. *Divided cell*

IB.2.7. Galvanostatic Conditions

Electrolysis can be carried out galvanostatically using a constant current, which can be achieved with a simple, low-cost setup using equipment commonly found in hardware stores. This method enables rapid reactions and is particularly useful for scaling up organic synthesis. In a galvanostatic setup, only the working and counter electrodes are needed, along with a clear understanding of the electrons involved in the process. By tracking the current (I) over time (t), the total charge (Q) involved in the reaction can be calculated. This total charge is derived from factors such as the number of electrons per substrate (z), the moles (N) of the substrate, and the Faraday constant.

$$Q = I \times t$$

$$Q = n \times F \times N$$

Q: charge in Coulomb [C = A s], z: number of electrons per substrate, N: number of moles [mol], F: Faraday constant [96 485 s A mol^{-1}].

The time needed for the required charge to pass into the reaction at a specific current can be calculated

$$t = \frac{Z \times N \times F}{I}$$

The calculated time corresponds to the time necessary for one electron equivalent (1 F or 1 F mol^{-1}) to pass, and this duration can be extended to achieve higher electron equivalents.

IB.2.8. Potentiostatic Conditions

The application of constant potential to perform electrolysis is known as potenstiostatic electrolysis. The potential, or voltage, represents the energy needed to transfer electrons from the anode to the cathode, generating a potential difference. When this difference is significant, electrons can move from the cathode into the reaction solution. Concurrently, electrons are extracted from the reaction solution at the anode, leading to the current flow. There are different types of moods of electrolysis depicted in Figure IB.5.

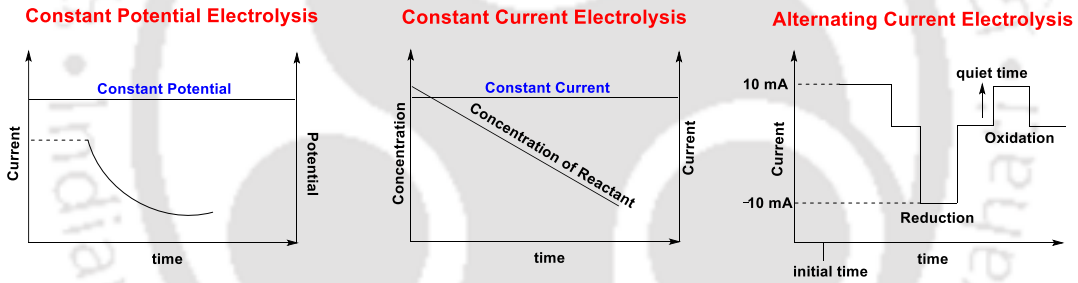

Figure IB.5. *Different modes of elctrolysis*.

IB.2.9. Challenges in Electro-organic Synthesis

Analogous to the potential of an oxidizing agent (to oxidize a substrate), the electric potential can be tuned to achieve the oxidation of substrates to facilitate selective coupling. Potentials for the desired redox process can be obtained from tables with standard potentials (E°) or by measuring cyclic voltammograms. Tables of standard reduction potentials E° for an oxidized species (Ox) being reduced to a reduced species (Red) can be found in the literature. By definition, these standard potentials are obtained under standard conditions (25 ^{o}C, 1 mol L^{-1}, 1 atm) against a standard calomel electrode (SCE). Typical potential ranges for organic functional groups, redox mediators, and solvents are depicted in Figure IB.6.[17]

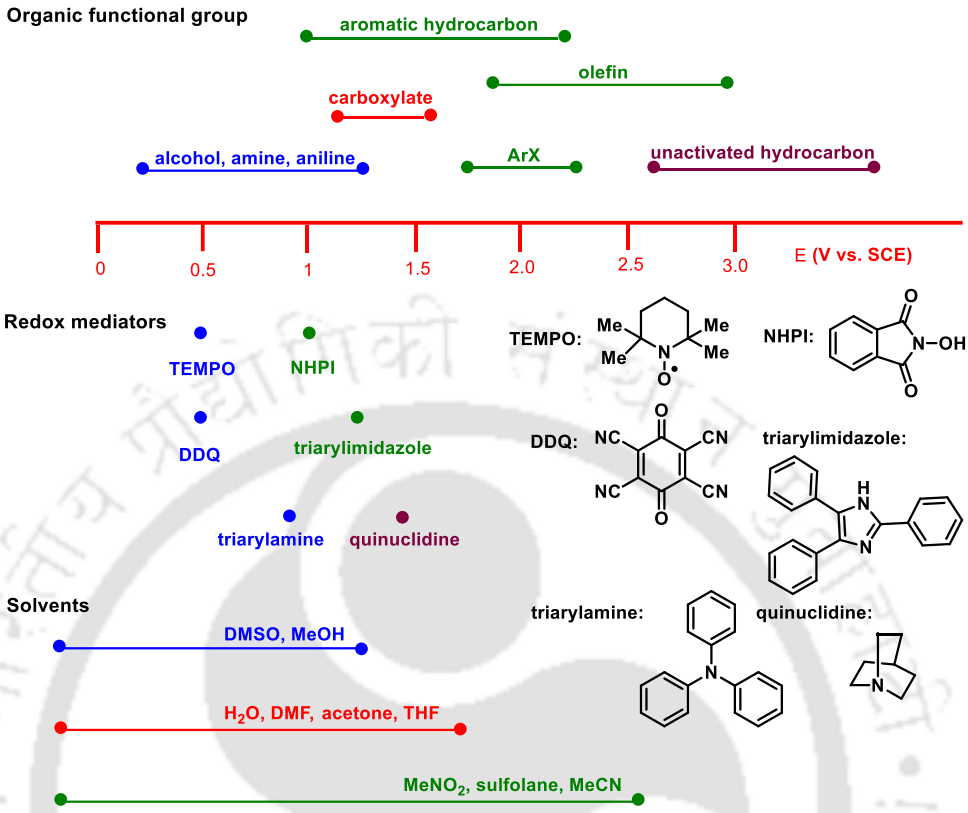

Figure IB.6. *Oxidation potentials for organic functional groups, redox mediators, and solvents.*

IB.3. Electrochemical Oxidative Cross-coupling Strategy

Oxidative cross-coupling has been developed into a robust method for carbon-carbon (C–C), carbon-heteroatom (C–X), and heteroatom-heteroatom (X–Y) bond formation. Over the past two decades, tremendous efforts have been devoted to this field, and significant advancements have been achieved. Electrochemical synthesis is a powerful and environmentally benign approach, which not only achieves oxidative cross-couplings under external-oxidant-free conditions but also releases valuable hydrogen gas during the chemical bond formation. Recently, the electrochemical oxidative cross-coupling with hydrogen evolution reactions has been significantly explored.[18,19]

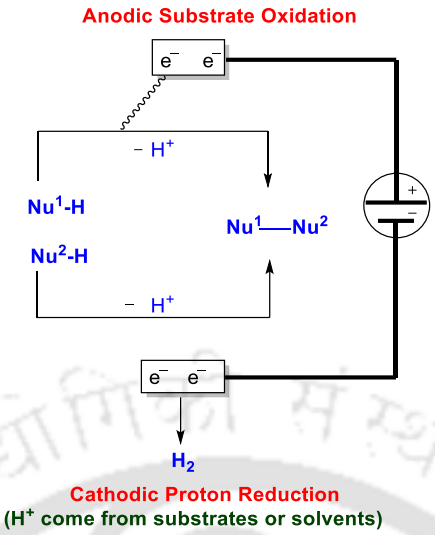

Figure IB.7. *Electrochemical oxidative cross-coupling.*

IB.3.1. Oxidative Cross-coupling for the C–N Bond Formation

Oxidative cross-coupling for C–N bond formation represents a powerful synthetic strategy in organic chemistry, enabling the construction of complex molecular structures with high efficiency. This method involves the direct coupling of carbon and nitrogen through the oxidative process, often employing transition metal catalysts. The oxidative C–N bond formation allows for the synthesis of various nitrogen-containing compounds, such as amines and amides, which are essential building blocks in pharmaceuticals, agrochemicals, and materials sciences.[20]

IB.3.2 Traditional and Modern Approach for the C–N Bond Formation Resulting Amide Framework

Amides are prevalent in biomolecules such as peptides and proteins and are found in natural products, pharmaceuticals, polymers, and fine chemicals. In 2014, an analysis by Brown *et al*. revealed that 50% of medicinally relevant compounds possess at least one amidic linkage. In this context, in 2014, the Lei group disclosed a visible-light-mediated $[Ru(phen)_3]Cl_2$-catalyzed decarboxylation/oxidative amidation of α-keto acids with amines under mild reaction conditions using O_2 as the terminal oxidant. This protocol is compatible with a wide range of

substrates, leading to the formation of corresponding product in good to excellent yields (Scheme 1B.1).[21]

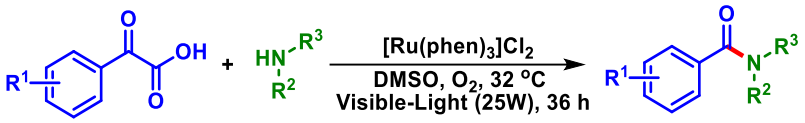

Scheme 1B.1. *Visible-light-induced acylation of amines with α-keto acids.*

In 2021, the Cibulka group disclosed a riboflavin catalyzed coupling between aldehydes and amines for synthesizing diverse amides. This approach demonstrated high functional group tolerance and relatively low oxidation potential of the hemiaminal formed by amine to aldehyde addition underscoring its synthetic versatility and potential impact on organic synthesis (Scheme 1B.2).[22]

An electrochemical method for amide bond formation using benzaldehydes and amines was developed by the Chiba group in 2020. The oxidation step is facilitated by cathodic-generated hydrogen peroxide (Scheme 1B.2).[23]

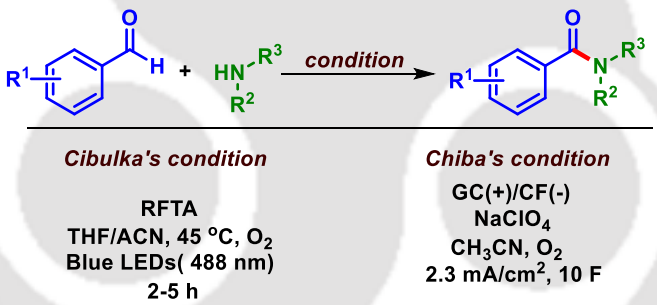

Scheme 1B.2. *N-acylation of amines with aldehyde.*

In 2012, Luca's group demonstrated the direct conversion of aldehydes to amides using iron(III) chloride as a catalyst and *tert*-butyl hydroperoxide (TBHP) as an oxidant. This protocol is compatible with a range of aliphatic and aromatic aldehydes, reacting successfully with both mono-and di-substituted N-chloramines (Scheme 1B.3).[24]

In 2013, Singh *et al*. presented an AIBN-initiated metal-free amidation of aldehydes using N-chloroamines. This method provides a metal and base-free approach, featuring mild reaction conditions, high yields, and good functional group tolerance (Scheme 1B.3).[25]

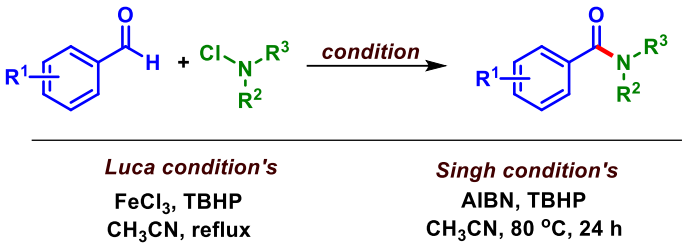

Scheme 1B.3. Iron-catalyzed *N-acylation of amines with aldehyde*.

In 2018, Saito's group unveiled a diboron-catalyzed dehydrative amidation reaction, facilitating the coupling of aromatic carboxylic acids with amines. This protocol's hallmark lies in its simplicity and remarkable efficiency demonstrated across many substrates. It offers a compelling avenue for leveraging diboron catalysts in amide synthesis, eliminating the requirement for stoichiometric or additional dehydrating agents (Scheme 1B.5).[26]

In 2018, the Fussell group presented a significant advancement employing tetramethyl orthosilicate (TMOS) as a highly effective reagent for the direct amidation of aliphatic and aromatic carboxylic acids with amines and anilines. This methodology offers the advantage of yielding amidesin good to excellent yields. Additionally, the products can be obtained in a pure form directly after workup, obviating the necessity for further purification steps (Scheme 1B.5).[27]

In 2021, the Cobb group established a pentafluoropyridine (PFP) catalyzed deoxyfluorination of carboxylic acid for the construction of amides. Here, PFP offers several advantages, being cost-effective, commercially available, non-corrosive, and stable on the bench. Furthermore, PFP can facilitate one-pot amide bond formation by enabling the in situ generation of acyl fluorides. This reaction involving the unactivated carboxylic acids with amines affords amides in good to excellent yields (Scheme 1B.5).[28]

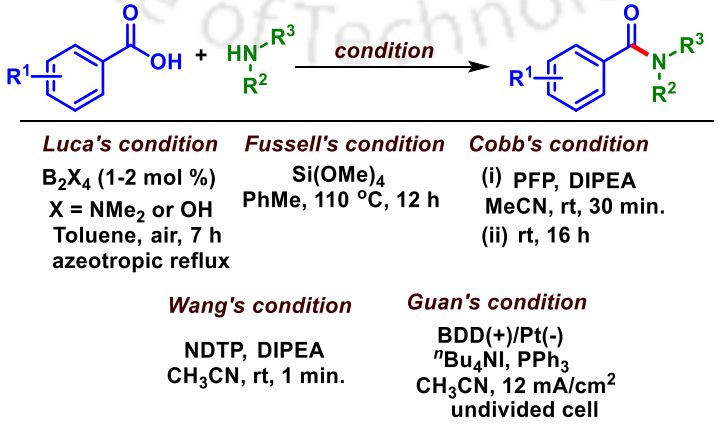

Scheme 1B.5. *N-acylation of amines with carboxylic acid*

Wang *et al*. developed an NDTP (N,N-dimethylthiophosphoryl chloride) catalyzed synthesis of amide and peptide. This methodology enables direct and rapid synthesis of peptides without inducing epimerization. The reaction condition is mild, and the coupling reagent NDTP is recyclable (Scheme 1B.5).[29]

In 2019, Guan group introduced a catalyst-free method for forming amide bonds using thiocarboxylic acids and amines. The mechanistic investigations highlighted the pivotal role of disulfide intermediates in this reaction. The thiobenzoic acids undergo spontaneous oxidation to disulfides in the presence of air, while thioaliphatic acids electro-oxidized to generate disulfides. Subsequently, these disulfides reacted with amines to yield the desired amides (Scheme 1B.5).[30]

Newman group reported the construction of amide *via* a Ni-catalyzed C–N coupling using esters and amines. This method has the advantage of its mild reaction condition, excellent functional group tolerance, and broad substrate scope (Scheme 1B.6).[31]

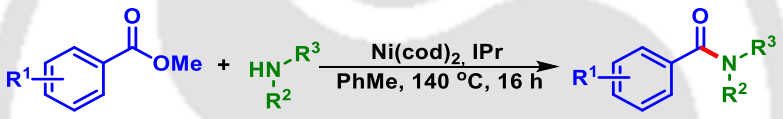

Scheme 1B.6. *N-acylation of amines with aldehyde*

Brown *et al.* introduced a ball-milling methodology for the direct amidation of esters through mechanochemistry. This operationally straightforward procedure entails combining ester, amine, and sub-stoichiometric KO^{t}Bu, resulting in the synthesis of a broad and diverse array of amides with modest to excellent yield. This reaction offers a convenient route to assembling large libraries of amides, showcasing the potential of mechanochemical techniques in organic synthesis (Scheme 1B.7).[32]

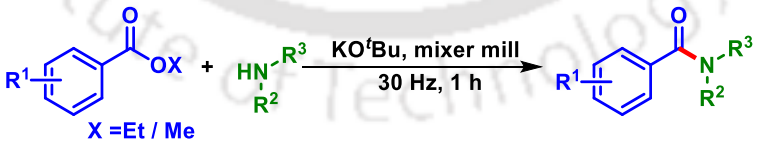

Scheme 1B.7. *N-acylation of amines with aldehyde*

In 2013 the Dyson group demonstrated an efficient method for the synthesis of amides *via* Pd-catalyzed oxidative carbonylation of C(sp^3)–H bonds with CO and amines. The route efficiently provides substituted phenyl amides from alkanes (Scheme 1B.8).[33]

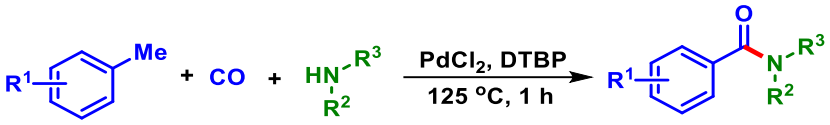

Scheme 1B.8. Pd-catalyzed *N-acylation of amines with toluene*

In 2019, Szostak's group presented an elegant and highly chemoselective method via a transition-metal-free transamidation of unactivated amides and direct amidation of alkyl esters through N–C/O–C cleavage (Scheme 1B.9).[34]

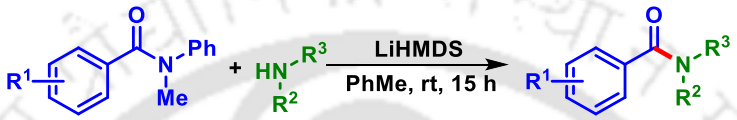

Scheme 1B.9. *N-acylation of amines with unactivated amide*

In 2018, Liu's group demonstrated the synthesis of α-benzylated amides *via* the electrocatalytic Favorskii rearrangement of 1,3-diarylacetones. This electrocatalytic transformation favored the Favorskii rearrangement of 1,3-diaryl acetones, even with electron-withdrawing substituents, yielding α-benzylated amides in good yields. The method was effective with various unsymmetrical ketones, showing moderate regioselectivity. Additionally, this approach introduced a chiral center at the α-position of the amide (Scheme 1B.11).[35]

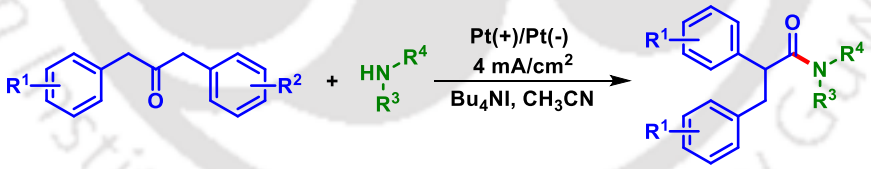

Scheme 1B.10. *Electrochemical synthesis of α-benzylated amides derivatives*

In 2013, Yuan's group developed an electrochemical method for synthesizing amides directly. This approach involved the transformation of methyl ketones with formamides, leveraging the in situ generation of iodine through the electrolysis of sodium iodide. This metal-free, mild-condition electrochemical strategy delivers the desired amide products in good to excellent yields (Scheme 1B.12).[36]

Scheme 1B.11. *Electrochemical synthesis of dimethylamine derivatives.*

Gong group accomplished an electrochemical method for synthesizing α-ketoamides *via* decarboxylative acylation of isocyanides using α-ketoacids as an acyl source. The method is compatible with various α-ketoacids under mild conditions for synthesizing highly functionalized α-ketoamides (Scheme 1B.12).[37]

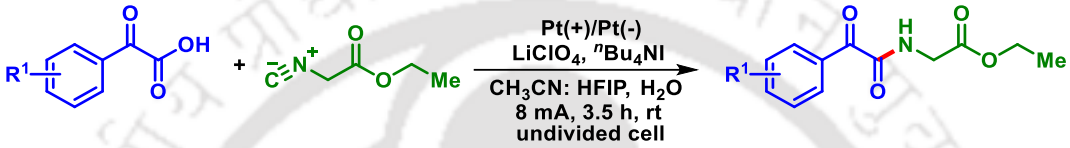

Scheme 1B.12. *Electrochemical synthesis of α-ketoamides using α-ketoacids.*

Wang's group described a one-pot methodology for the preparation of α-ketoamides through anodic oxidation. This transformation is highly versatile, has a broad substrate scope, and has excellent functional group tolerance (Scheme 1B.13).[38]

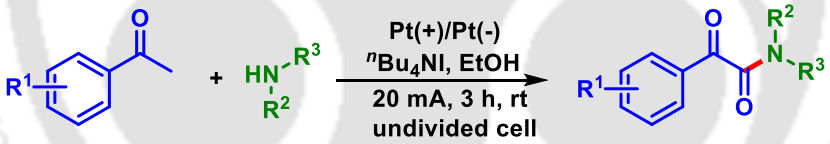

Scheme 1B.13. *Electrochemical synthesis of α-ketoamides using acetophenone.*

In 2019, the Vannucci group presented an electrochemical anion pool synthesis for the concurrent generation of amides and benzyl esters. This method involved the electrochemical generation of strong nucleophiles from amine substrates, then reacting with acid anhydrides to form amides. These one-pot reactions were operationally simple, conducted at room temperature, and eliminated the use of transition metal and base (Scheme 1B.14).[39]

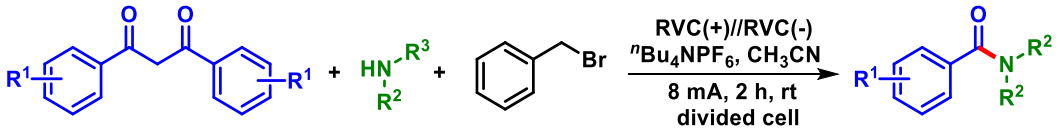

Scheme 1B.14. *Electrochemical synthesis of amide derivatives.*

In 2019, Wang's group demonstrated an efficient cross-coupling reaction involving carbon dioxide, amines, and arylketones. This reaction was achieved through straightforward electrochemical oxidation under mild and metal-free conditions, yielding a variety of O-β-oxoalkyl carbamates with moderate to good yields (Scheme 1B.15).[40]

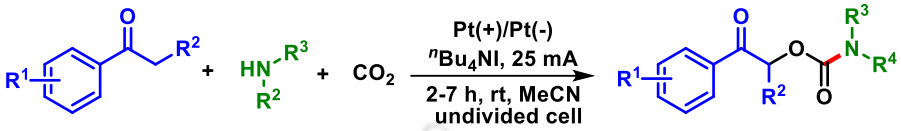

Scheme 1B.15. *Electrochemical synthesis of O-β-oxoalkyl carbamates derivatives*.

In 2022, the Opatz group introduced an iodide-mediated anodic amide coupling method. This approach utilizes commercially available PPh_3 as the coupling reagent and Bu_4NI as a redox mediator to facilitate the direct coupling of carboxylic acids with amines (Scheme 1B.16**)**.[41]

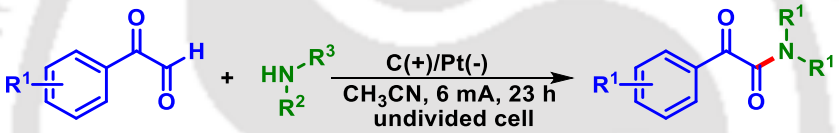

Scheme 1B.16. *Electrochemical synthesis of α-ketoamides derivatives*.

In 2020, He *et al*. disclosed the electrochemical synthesis of α-ketoamides under catalyst, oxidant, and electrolyte-free conditions. The reaction proceeds under mild conditions, excellent functional-group tolerance, high atom economy, and scalability, making it suitable for various applications in pharmaceutical chemistry (Scheme 1B.17).[42]

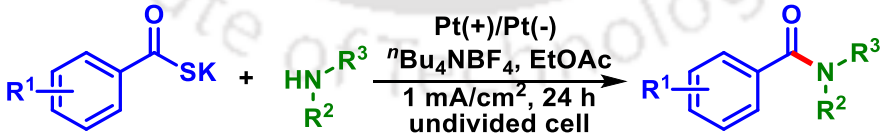

Scheme 1B.17. *Electrochemical synthesis of amide using thioacid.*

In 2019, Vannucci's group demonstrated an electrochemical synthesis for selective N^1-acylation of indazoles. The methodology, known as the "anion pool," involved electrochemically reducing indazole molecules to generate indazole anions and H_2. The procedure is base-free, with

acid anhydrides used as the acylation substrate. This procedure can also be applied to acylation of benzimidazoles and indoles (Scheme 1B.19).[43]

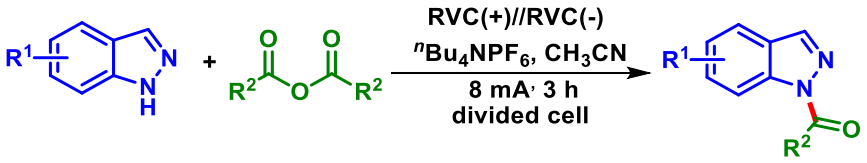

Scheme 1B.18. *Electrochemical N^1-acylation of indazoles.*

In 2023, the Luo group introduced an electrochemical oxidative transamidation of tertiary amines with *N*-acyl imides for the construction of amide. This protocol is environmentally friendly and easy to handle, as tertiary amines are used as surrogates for secondary amines. The C–N bond of tertiary amines is cleaved, allowing for the preparation of amide compounds with yields ranging from 11% to 80% (Scheme 1B.19).[44]

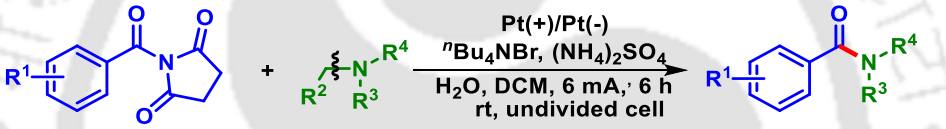

Scheme 1B.19. *Electrochemical synthesis of amide using N-acyl imides*

In 2022, the Li group reported an amidation reaction for the constructing amides through electro-oxidative C–C cleavage. This electro-oxidative reaction was conducted under constant current conditions in a simple undivided cell using NH_4I as a mediator and derived amides in moderate to good yields (Scheme 1B.20).[45]

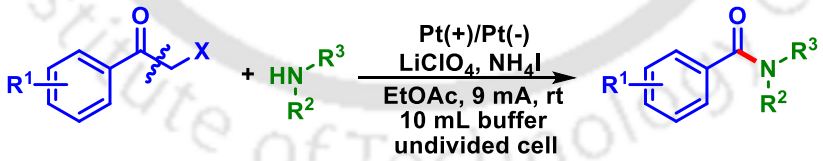

Scheme 1B.20. *Electrochemical Synthesis of amide using phenacyl bromide*.

The *N*-acylations of NH-sulfoximines utilize acyl halides, anhydrides, aldehydes, or carboxylic acids as the primary acylating agents. An early illustration of *N*-acylation involves a reaction catalyzed by DMAP (4-dimethylaminopyridine) between acyl halides and NH-sulfoximines in the presence of a base such as Et_3N (triethylamine) or pyridine. This approach leads to the efficient formation of *N*-acylated products in high-yield (Scheme 1B.21).[46]

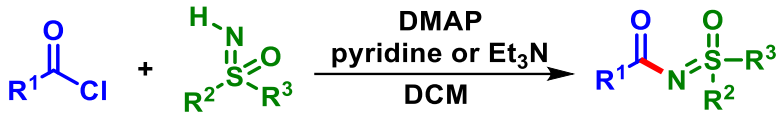

Scheme 1B.21. *N-Acylation of sulfoximines with acyl halides.*

In 2004, Bolm's group disclosed a method for carbodiimide-mediated coupling between NH-sulfoximines and acyl halides, leading to the synthesis of *N*-acylated products. Despite the typically weak nucleophilicity of sulfoximines, NH-sulfoximines proved amenable to coupling with carboxylic acids utilizing DCC (dicyclohexylcarbodiimide) or EDC [1-ethyl-3-(3-dimethylaminopropyl)carbodiimide] (Scheme 1B.22).[46] Garimallaprabhakaran and Harmata further advanced this field by introducing a boric acid-mediated *N*-acylation of sulfoximines with carboxylic acids (Scheme 1B.22).[47]

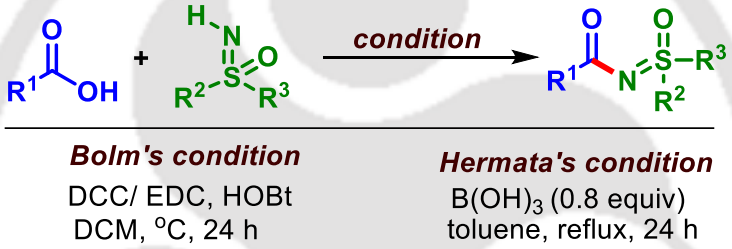

Scheme 1B.22. *N-Acylation of sulfoximines with carboxylic acids.*

In 2013, the Bolm group reported an oxidative cross-coupling reaction between aldehydes and sulfoximines involving dual C–H/N–H functionalization. This reaction was facilitated copper catalyst and *tert*-butyl hydroperoxide (TBHP) as the oxidant. This method proceeded under mild reaction conditions to afford a series of valuable *N*-acylated sulfoximine derivatives in excellent yield (Scheme 1B.23).[48]

Deng *et al.* introduced a C–H/N–H cross-coupling reaction targeting *N*-aroylated sulfoximines using a TBAI/TBHP catalytic system with n-hexane as the solvent (Scheme 1B.23).[49]

In the subsequent year, Guin and colleagues unveiled an NHC-catalyzed acylation of NH-sulfoximines with aldehydes, employing DBU as the base and bisquinone as the oxidant. This methodology facilitated the amidation of numerous unactivated aliphatic and heteroaromatic aldehydes, providing high yields (Scheme 1B.23).[50]

Zeng's group disclosed the visible light-mediated synthesis of *N*-aroyl sulfoximines, utilizing a combination of TBHP and $K_2S_2O_8$ as oxidants, without requiring any photosensitizer, metal catalyst, or base (Scheme 1B.23).[51]

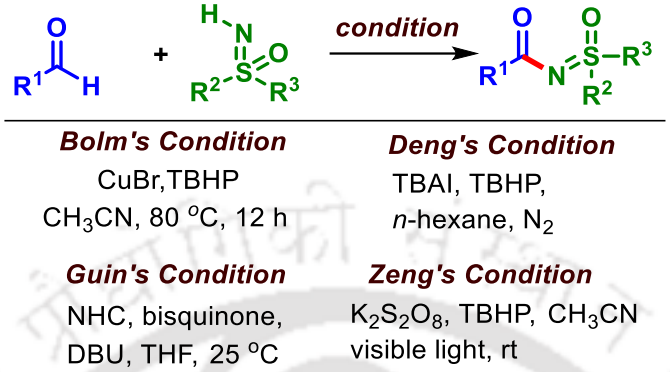

Scheme 1B.23. *N-Acylation of sulfoximines with aldehyde*.

In 2017, the Yuan group demonstrated a Pd-catalyzed aroylation of NH-sulfoximines with aryl halides, employing chloroform as the CO source. Under the standard reaction conditions, various aryl halides and sulfoximines demonstrated efficient reactivity, resulting in the formation of the products in moderate to good yields (Scheme 1B.24).[52]

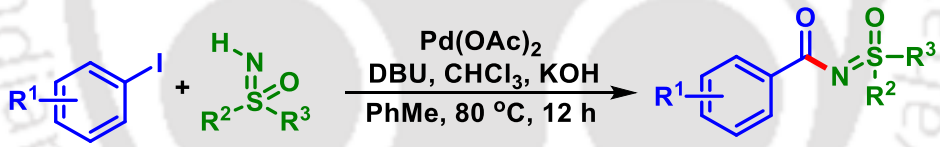

Scheme 1B.24. *N-Acylation of sulfoximines with aryl halides.*

Bolm *et al*. introduced a fascinating approach for C–H activation of methyl arenes in the MnO_2-mediated aroylation of *N*-chlorosulfoximines. This method entailed manganese oxide promoted C–H activation of methyl arenes to generate an aroyl intermediate, which subsequently underwent smooth reaction with *N*-chlorosulfoximines, affording a range of valuable aroyl sulfoximine in high yields (Scheme 1B.25).[53]

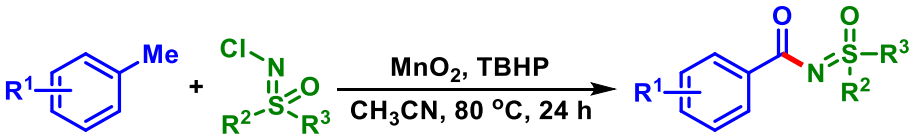

Scheme 1B.25. *N-Acylation of sulfoximines with toluene*

In 2016, Sekar's group unveiled an innovative method for the aroylation of NH-sulfoximines utilizing Pd nanoparticles stabilized by a binaphthyl backbone (Pd-BNP). This synthetic strategy involved the carbon monoxide insertion into aryl iodides by Pd-BNP, resulting in the formation of an aroyl intermediate. Subsequently, this intermediate reacted with NH-sulfoximines, yielding N-aroyl sulfoximine in good to excellent yields (Scheme 1B.26).[54]

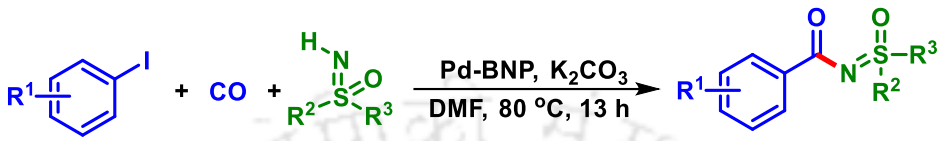

Scheme 1B.26. *N-Acylation of sulfoximines with aryl halides.*

In 2015, An's group disclosed the transition metal-free aroylation of *NH*-sulfoximines with methyl arenes. The reaction proceeds in the presence of elemental iodine, requiring no external organic solvents, transition metal catalysts, or ligands (Scheme 1B.27).[55]

In 2016 Sekar's group introduced an iron-catalyzed one-pot *N*-aroylation of NH-sulfoximines with methylarenes through benzylic C–H bond oxidation. This protocol involves the oxidation of benzylic C–H bonds of toluenes to generate aroyl radical intermediates followed by oxidative coupling with NH-sulfoximines to form *N*-aroylated sulfoximines in good to excellent yields (Scheme 1B.27).[56]

In 2015, the Zhao group disclosed an oxidative acylation of sulfoximines with methylarenes as an acyl donor. The reaction was carried out in neat condition. Both electron-donating and withdrawing groups on methyl arenes are well-tolerated (Scheme 1B.27).[57]

Hou *et al*. demonstrated a copper-catalyzed synthesis of *N*-aroylated sulfoximines from methyl arenes. This methodology excluded the requirement for additional solvents or ligands assistedby external oxidant *tert*-butyl hydroperoxide (Scheme 1B.27).[58]

In 2024, our group revealed a visible light and PIDA/I_2-promoted acylation of NH-sulfoximines with methylarenes. This approach is devoid of transition metal catalysts and photosensitizers. It is achieved by oxidative coupling sulfoximines with readily accessible methylarenes, eliminating the peroxide sources. Mechanistic inquiries indicate the involvement of radicals, with molecular oxygen playing a crucial role in the reaction mechanism (Scheme 1B.27).[59]

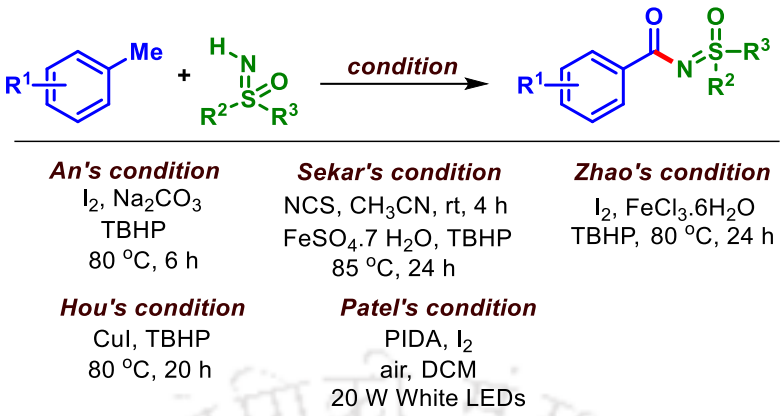

Scheme 1B.27. *N-Acylation of sulfoximines with toluene.*

In 2021, the Bolm group disclosed a palladium-catalyzed carbonylation method for the synthesis of *N*-ynonylsulfoximines. This methodology proceeds at room temperature with a wide range of substrate combinations, which affords the products in good yields (Scheme 1B.28).[60]

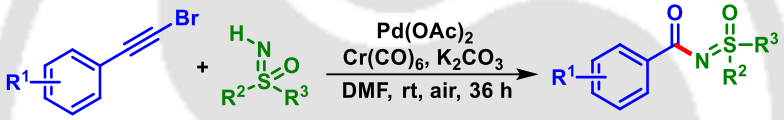

Scheme 1B.28. *N-Acylation of sulfoximines with bromoalkynes.*

In 2017, the Yotphan group demonstrated a copper-catalyzed oxidative decarboxylative coupling of α-keto acids and sulfoximine. A variety of aryl α-oxocarboxylic acids and sulfoximine substrates were well-compatible. The mechanistic investigation suggested that this transformation involves the radical pathway, and the reactive aroyl radical is generated under standard conditions (Scheme 1B.29).[61]

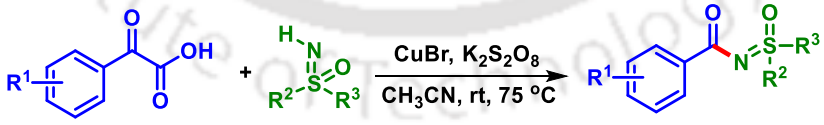

Scheme 1B.29. *N-Acylation of sulfoximines with α-keto acids.*

The Bolm group developed a NBS-catalyzed visible-light promoted strategy for synthesizing *N*-acyl sulfoximines using ketone *via* the oxidative cleavage of C–C bonds. The reaction proceeds through the radicals generated *via* a Norrish Type I bond cleavage mechanism.

This methodology has success across a wide range of NH-sulfoximines and ketones, delivering the products in good to excellent yields (Scheme 1B.30).[62]

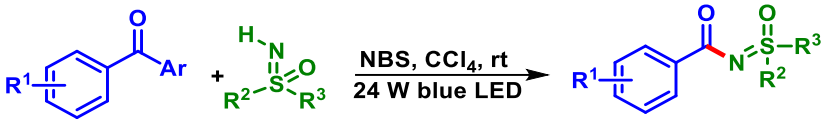

Scheme 1B.30. *Visible-light-induced acylation of sulfoximines with ketones*

The Ji group in 2023 discribe an electrochemical *N*-acylation and *N*-α-ketoacylation of sulfoximines via the selective decarboxylation and dehydration of α-ketoacids. These two reactions use electricity as a "traceless" oxidant and α-ketoacid as a selective "acyl" or "α-ketoacyl" source. A broad range of acylated- and α-ketoacylated sulfoximines were isolated in good to excellent yields (Scheme 1B.31).[63]

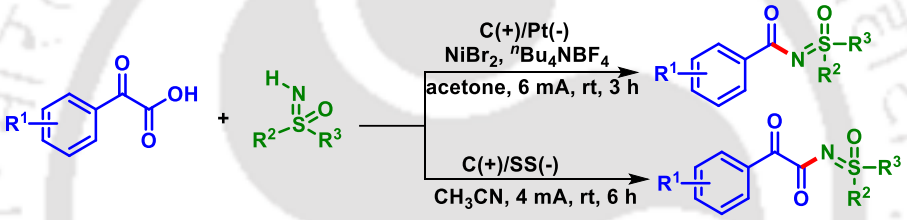

Scheme 1B.31. *N-acylation and N-α-ketoacylation of sulfoximines with*. α-ketoacids.

IB.4. Conclusion

In summary, the above-mentioned literature gives the idea of how *N*-centered radicals can be generated under visible-light irradiation and electrochemical conditions. The C–N bond formation occurs *via* the conventional method and the radical-radical cross-coupling reaction leading to the amidic frameworks. Taking cues from the above literature the cross-coupling strategy and the generation of *N*-centered radicals for the synthesis of amidic frameworks have been designed.

IA.5. References

[1] (a) Yan, M.; Kawamata, Y.; Baran, P. S. *Angew.Chem. Int.Ed*. **2018**, *57*, 4149–4155.

[2] (a) Yan, M.; Kawamata, Y.; Baran, P. S. *Chem. Rev*. **2017**, *117*, 13230–13319. (b) Xiong, P.; Xu, H.-C. *Acc. Chem. Res*. **2019**, *52*, 3339–3350. (c) Shi, S.-H.; Liang, Y.; Jiao, N. *Chem. Rev*. **2021**, *121*, 485–505. (d) Li, M.; Peng, M.; Huang, W.; Zhao, L.; Wang, S.; Kang, C.; Jiang, G.; Ji, F. *Org. Lett*. **2023**, 25, 7529–7534.

[3] (a) Yang, D.; Guan, Z.; Peng, Y.; Zhu, S.; Wang, P.; Huang, Z.; Alhumade, H.; Gu, D.; Yi, H.; Lei, A. *Nat. Commun* **2023**, *14*, 1476–1484.

[4] (a) Harwood, S. J.; Palkowitz, M. D.; Gannett, C. N.; Perez, P.; Yao, Z.; Sun, L.; Abruña, H. D.; Anderson, S. L.; Baran, P. S. *Science* **2022**, *375*, 745–752. [5] Volta, A. *Philos. Trans. R. Soc*., **1800**, *90*, 403–431.

[6] Faraday, M. *Philos. Trans. R. Soc*., **1834**, *124*, 77–122.

[7] Kolbe, H. *J. Prakt. Chem*., **1847**, *41*, 137–139.

[8] Iversen, P. E.; Lund, H.; *Tetrahedron Lett*., **1969**, *40*, 3523–3524.

[9] Shono, T.; Hamaguchi, H.; Matsumura, Y. *J. Am. Chem. Soc*., **1975**, *97*, 4264–4268.

[10] Little, R. D.; Fox, D. P.; Hijfte, L. V.; Dannecker, R.; Sowell, G.; Wolin, R. L.; Moens, L.; Baizer, M. M. *J. Org. Chem*., **1988**, *53*, 2287–2294.

[11] Moeller, K. D. *Tetrahedron*, **2000**, *56*, 9527–9554.

[12] Yoshida, J. I.; Murata, T.; Isoe, S. *Tetrahedron Lett*., **1986**, *27*, 3373–3376.

[13] Rosen, B. R.; Werner, E. W.; O'Brien, A. G.; Baran, P. S. *J. Am. Chem. Soc*., **2014**, *136*, 5571–5574.

[14] Elsler, B.; Schollmeyer, D.; Dyballa, K. M.; Franke, R. L; Waldvogel, S. R. *Angew. Chem. Int. Ed*., **2014**, *53*, 5210–5213.

[15] (a) Liu, X.; Yang, D.; Liu, Z.; Wang, Y.; Liu, Y.; Wang, S.; Wang, P.; Cong, H.; Chen, Y.-H.; Lu, L.; Qi, X.; Yi, H.; Lei, A. *J. Am. Chem. Soc*. **2023**, *145*, 3175–3186. (b) Novaes, L. F. T.; Liu, J.; Shen, Y.; Lu, L.; Meinhardt, J. M.; Lin, S. *Chem. Soc. Rev*., **2021**, *50*, 7941–8002. (c) Sadowski, B.; Yuan, B.; Lin, Z.; Ackermann, L. *Angew. Chem., Int. Ed*. **2022**, *61*, e202117188.

[16] Randles, J. E. B. *Trans. Faraday Soc*., **1948**, *44*, 327–338.

[17] Schotten, C.; Nicholls, T. P.; Bourne, R. A.; Kapur, N.; Nguyen, B. N.; Willans, C. E. *Green Chem*., **2020**, *22*, 3358–3375.

[18] Y. Yuan, A. Lei, *Acc. Chem. Res*. **2019**, *52*, 3309-3324.

[19] Y. Yuan, J. Yang, A. Lei, *Chem. Soc. Rev.*, **2021**, *50*, 10058-10086.

[20] Zhao, Y.; Xia, W.; *Chem. Soc. Rev*., **2018**, *47*, 2591–2608.

[21] Liu, J.; Liu, Q.; Yi, H.; Qin, C.; Bai, R.; Qi, X.; Lan, Y.; Lei, A. *Angew. Chem. Int. Ed.* **2014**, *53*, 502–506.

[22] Tolba, A. H.; Krupicka, M.; Chudoba, J.; Cibulka, R. *Org. Lett*. **2021**, *23*, 6825–6830.

[23] Kurose, Y.; Imada, Y.; Okada, Y.; Chiba, K. *Eur. J. Org. Chem*. **2020**, 3844–3846.

[24] Porcheddua, A.; Luca, L. D. *Adv. Synth. Catal*. **2012**, *354*, 2949–2953.

[25] Vanjari, R.; Guntreddi, T.; Singh, K. N. *Green Chem*., **2014**, *16*, 351–356.

[26] Sawant, D. N.; Bagal, D. B.; Ogawa, S.; Selvam, K.; Saito, S. *Org. Lett*. **2018**, *20*, 4397–4400.

[27] Braddock, D. C.; Lickiss, P. D.; Rowley, B. C.; Pugh, D.; Purnomo, T.; Santhakumar, G.; Fussell, S. J. *Org. Lett*. **2018**, 20, 950–953.

[28] Brittain, W. D. G. Cobb, S. L. *Org. Lett*. **2021**, *23*, 5793–5798.

[29] Li, Y.; Li, J.; Bao, G.; Yu, C.; Liu, Y.; He, Z.; Wang, P.; Ma, W.; Xie, J.; Sun, W.; Wang, R. *Org. Lett*. **2022**, *24*, 1169−1174.

[30] Tang, L.; Matuska, J. H.; Huang, Y.-H.; He, Y.-H.; Guan, Z. *ChemSusChem* **2019**, *12*, 2570–2575.

[31] Halima, T. B.; Masson-Makdissi, J.; Newman, S. G. *Angew. Chem. Int. Ed*. **2018**, *57*, 12925–12929.

[32] Nicholson, W. I.; Barreteau, F.; Leitch, J. A.; Payne, R.; Priestley, I.; Godineau, E.; Battilocchio, C.; Browne, D. L. *Angew. Chem. Int. Ed*. **2021**, *60*, 21868–21874.

[33] Liu, H.; Laurenczy, G.; Yan, N.; Dyson, P. J. *Chem. Commun*., **2014**, *50*, 341–343.

[34] Li, G.; Ji, C.-L.; Hong, X.; Szostak, M. *J. Am. Chem. Soc*. **2019**, *141*, 11161–11172.

[35] Liu, W.; Huang, W.; Lan, T.; Qin, H.; Yang, C. *Tetrahedron* **2018**, *74*, 2298–2305.

[36] Huang, H.; Yuan, G.; Li, X.; Jiang, H. *Tetrahedron Lett.* **2013**, *54*, 7156–7159.

[37] Zhao, Y.; Meng, X.; Cai, C.; Wang, L.; Gong, H. *Asian J. Org. Chem*. **2022**, *11*, e202100748.

[38] Zhang, Z.; Su, J.; Zha, Z.; Wang, Z. *Chem. Commun*., **2013**, *49*, 8982–8984.

[39] Dissanayake, D. M. M. M.; Melville, A. D.; Vannucci, A. K. *Green Chem*., **2019**, *21*, 3165–3171.

[40] Wang, J.; Qian, P.; Hu, K.; Zha, Z.; Wang, Z. https://doi.org/10.1002/celc.201801724

[41] Großmann, L. M.; Beier, V.; Duttenhofer, L.; Lennartz, L.; Opatz, T. *Chem. Eur. J*. **2022**, *28*, e202201768.

[42] Chen, J.-Y.; Wu, H.-Y.; Gui, Q.-W.; Han, X.-R.; Wu, Y.; Du, K.; Cao, Z.; Lin, Y.-W.; He, W.-M. *Org. Lett*. **2020**, *22*, 2206–2209.

[43] Dissanayake, D. M. M. M.; Vannucci, A. K. *Org. Lett*. **2019**, *21*, 457–460.

[44] Lin, H.; Liu, S.; Li, Q.; Zhang, Q.; Yang, L.; Wang, T.; Luo, J. *Synth. Commun* **2023**, *17*, 1412–1425.

[45] He, Y.; Zeng, L.; Li, M.; Gu, L.; Zhang, S.; Li, G. *J. Org. Chem*. **2022**, *87*, 12622–12631.

[46] Hackenberger, C. P. R.; Raabe, G.; Bolm, C. *Chem. Eur. J*., **2004**, 10, 2942–2952.

[47] Garimallaprabhakaran, A.; Harmata, M. *Synlett*, **2011**, *3*, 361–364.

[48] Wang, L.; Priebbenow, D. L.; Zou, L.-H.; Bolm, C. *Adv. Synth. Catal*. **2013**, *355*, 1490–1494.

[49] W.-J. Qin, Y. Li, X. Yu and W.-P. Deng, *Tetrahedron*, 2015, **71**, 1182–1186.

[50] Porey, A.; Santra, S.; Guin, J. *Asian J. Org. Chem*., **2016**, *5*, 870–873.

[51] Jiang, W.; Huang, Y.; Zhou, L.; Zeng, Q. *Sci. China Chem*., **2019**, *62*, 1213–1220.

[52] Guo, S.-r.; Kumar, P. S.; Yuan, Y.-q.; Yang, M.-h. *Tetrahedron Letters* **2017**, *58*, 2681–2684.

[53] Priebbenow, D. L.; Bolm, C. *Org. Lett*. **2014**, *16*, 1650–1652.

[54] Sharma, N.; Sekar, G. *RSC Adv*.,**2016**, *6*, 37226–37235.

[55] Zou, Y.; Xiao, J.; Peng, Z.; Dong, W.; An, D. *Chem. Commun*., **2015**, *51*, 14889–14892.

[56] Muneeswara, M.; Kotha, S. S.; Sekar, G. *Synthesis* **2016**, *48*, 1541–1549.

[57] Zhao, Z.; Wang, T.; Yuan, L.; Jia, X.; Zhao, J. *RSC Adv*., **2015**, *5*, 75386–75389.

[58] Hou, A.; Zhao, Z.; *Synth. Commun* **2017**, *13*, 1201–1208.

[59] Chakraborty, N.; Rajbongshi, K. K.; Gondaliya, A.; Patel, B. K. *Org. Biomol. Chem*., **2024**, *22*, 2375–2379.

[60] Ma, D.; Wang, C.; Kong, D.; Tu, Y.; Shi, P.; Bolm, C. *Adv. Synth. Catal*. **2021**, *363*, 1330–1334.

[61] Pimpasri, C.; Sumunnee, L.; Yotphan, S. *Org. Biomol. Chem*.,**2017**, *15*, 4320–4327.

[62] Tu, Y.; Zhang, D.; Shi, P.; Wang, C.; Ma, D.; Bolm, C. *Org. Biomol. Chem*., **2021**, *19*, 8096–8101.

[63] Kang, C.; Li, M.; Huang, W.; Wang, S.; Peng, M.; Zhao, L.; Jiang, G.; Ji, F. *Green Chem*., **2023**, *25*, 8838–8844.

CHAPTER-II

Visible-Light-Induced Difunctionalization of Styrenes: Synthesis of *N*-Hydroxybenzimidoyl Cyanides

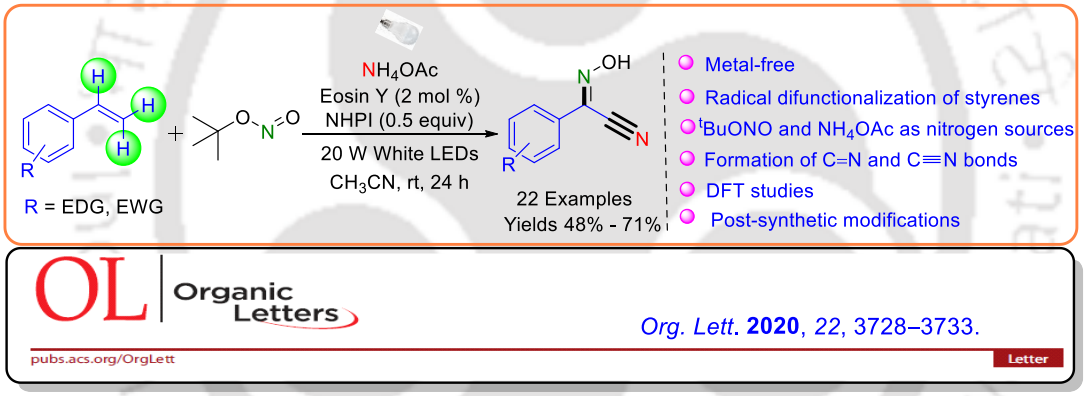

Abstract: *A visible-light-induced synthesis of N-hydroxybenzimidoyl cyanides from aromatic terminal alkenes is achieved by using Eosin Y as an organic photoredox catalyst. The process goes via a radical pathway with successive incorporation of two nitrogen atoms, one each from tert-butyl nitrite and ammonium acetate. The final product is achieved by the concomitant installation of an oxime and a nitrile group. DFT calculation supports a biradical pathway and all the proposed steps. A few useful synthetic transformations of N-hydroxybenzimidoyl cyanide are also illustrated.*

भारतीय प्रौद्योगिकी संस्थान गुवाहाटी
Indian Institute of Technology Guwahati

CHAPTER II

Visible-Light-Induced Difunctionalization of Styrenes: Synthesis of *N*-Hydroxybenzimidoyl Cyanides

II.1. Introduction

Visible-light-mediated photocatalytic functionalization has attracted considerable attention in modern organic synthesis because of sustainable energy sources that promote chemical reactions.[1] Usually, the photoredox process via a single-electron transfer (SET) under mild reaction conditions is utilized to synthesize numerous organic compounds.[2] In this context, Ru- and Ir-based complexes are well-explored photocatalysts for several organic transformations mediated by visible light.[3] However, despite their extraordinary photophysical properties, their use is discouraged because of their scant availability, toxicity, and high cost.[4] Lately, organic dyes such as Rose Bengal, Eosin Y, Eosin B, etc., have been used in lieu of transition metals since they are inexpensive, less toxic, and easy to handle. In particular, Eosin Y is used as an organophotoredox catalyst in many radical-based organic transformations.[5] Of late difunctionalization of alkenes has become a popular and competent chemical transformation by which two functional groups can be introduced simultaneously across the double bond.[6] Normally, difunctionalization of alkenes requires transition-metal catalysts and proceeds via radical-mediated processes. This increases the molecular complexity in a step-economical fashion.[7] Among various methods, the radical-mediated difunctionalization of alkenes has made great progress recently, particularly the visible-light-mediated photoredox SET process.[8,9] On the other hand, oxime is a privileged scaffold for preparing amines, amides, and nitrogen-containing heterocyclic compounds.[10] Oxime functionality is found in compounds that have anti-inflammatory, antibiotic, and pesticidal activities.[11] Similarly, nitrile serves as a synthetic precursor of many functional groups such as amine, amide, aldehyde, tetrazole, and carboxylic acid, which are also found in a variety of compounds having numerous biological activity.[12] The presence of these two important functional groups in a single molecule may further augment its activity against various targets (Figure II.1).[13] Conventionally, nitrile group is introduced by Sandmeyer and Rosenmund-von Braun

reactions, as well as by the use of traditional cyanating reagents such as NaCN, CuCN, KCN, TMSCN, $Zn(CN)_2$, and $K_4[Fe(CN)_6]$.[14] However, many of the cyanation processes suffer from certain drawbacks, because of the direct use of the toxic cyanide anion, which releases fatal and volatile HCN under the reaction conditions.[15]

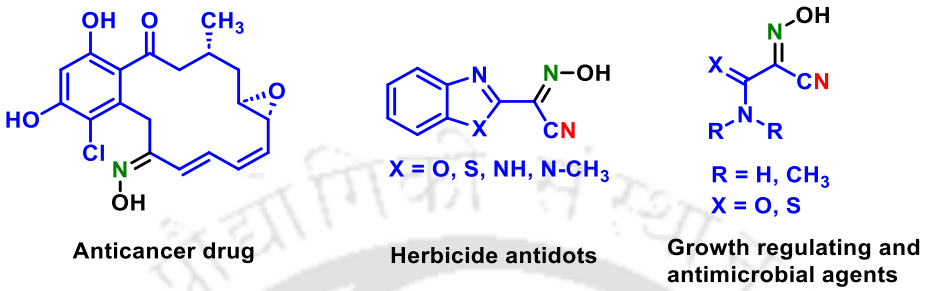

Figure II.1. *Representative biologically active oximes and N-hydroxybenzimidoyl cyanides.*

II.2. Ideas Toward the Synthesis of N-Hydroxybenzimidoyl Cyanides

Oh, group's represents a significant breakthrough in organic synthesis, introducing a visible-light-induced photoaddition of N-nitroso alkylamines to alkenes. This one-pot tandem approach enables the 1,2-diamination of alkenes from secondary amines. The method combines the visible-light-promoted photo-addition reaction of N-nitroso amines to alkenes with the o-NQ-catalyzed aerobic oxidation protocol of amines. This strategy eliminates the direct handling of harmful N-nitroso compounds, resulting in the efficient synthesis of α-amino oxime (Scheme II.1).[16a]

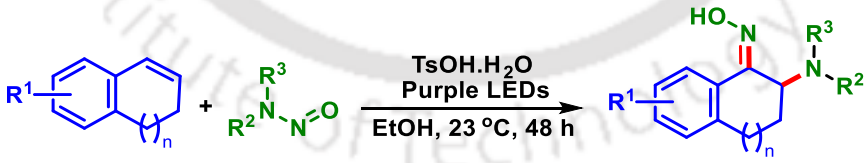

Scheme II.1. *Strategy for the N-nitrosoamines to indene.*

In 2019, the Hong group presented a strategy for the synthesis of aminoethyl pyridine derivatives using Eosin Y as a photocatalysis in the presence of alkenes. Various N-aminopyridinium salts were employed as aminating and pyridylating agents, respectively. The method enabled the concurrent incorporation of amino and pyridyl groups into alkenes under

mild reaction conditions. Here, alkene substrates with both electron-withdrawing and electron-donating groups were well tolerated in this protocol (Scheme II.2).[16b]

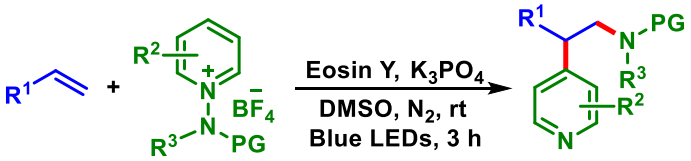

Scheme II.2. *Synthesis of aminoethyl pyridine derivatives.*

Yu *et al*. reported a photo-redox-catalyzed diamidation and oxidative amidation of alkenes. This approach utilizes $Ir(ppy)_3$ as the photocatalyst under visible light irradiation, allowing the synthesis of a diverse range of 1,2-diamidates and α-amino ketones with various functional groups. The choice of solvent, CH_3CN for diamidation and DMSO for oxidative amidation, plays a crucial role in providing a versatile method for the selective formation of 1,2-diamides and α-amino ketones (Scheme II.3).[16c]

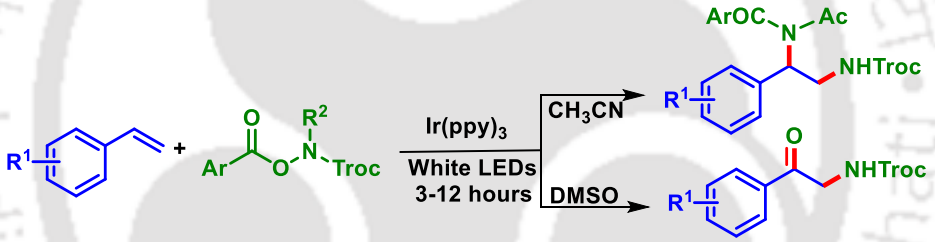

Scheme II.3. *Strategy for 1,2-diamidation and synthesis of α-amino ketones.*

The Leonori and co-workers reported the synthesis of vicinal diamines, compounds widely present in pharmaceuticals and biologically active substances. They developed a Ru-catalyzed diamination of alkenes under blue LED. The *in-situ* generation of *N*-chloroamines leads to an aminium radical capable of adding anti-Markovnikov alkenes. The study underscores the potential of transition metal catalysis and photochemical techniques in advancing complex molecule synthesis (Scheme II.4).[16d]

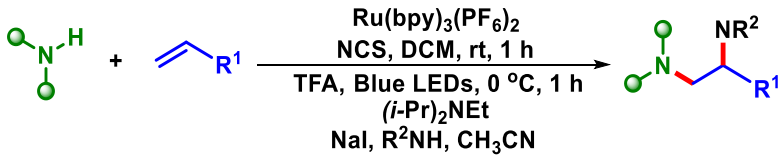

Scheme II.4. *Synthesis of 1, 2-diamination product.*

An elegant synthesis of oxime has been reported by the Beller group in 2009 from styrene and *tert*-butyl nitrite in the presence of Fe(II) catalyst [Scheme II.5,(i)].[17] Later, the Wang group introduced a CN group to an allyl benzene using Pd(II) catalyst and *tert*-butyl nitrite serving as the nitrogen source in the presence of *N*-hydroxyphthalimide as the co-catalyst [Scheme II.5,(ii)].[18] However, only a limited method is available for the synthesis of hydroxyimino-acetonitriles. Bohle and co-workers demonstrated the synthesis of 2-hydroxyimino-2-phenyl acetonitrile from benzyl cyanide, potassium methoxide, and nitric oxide.[19] Hydroxyiminoacetonitriles can also be synthesized from aldoxime *via* chlorination, followed by a reaction with alkali cyanide.[20]

Scheme II.5. Oximation and cyanation of terminal alkenes

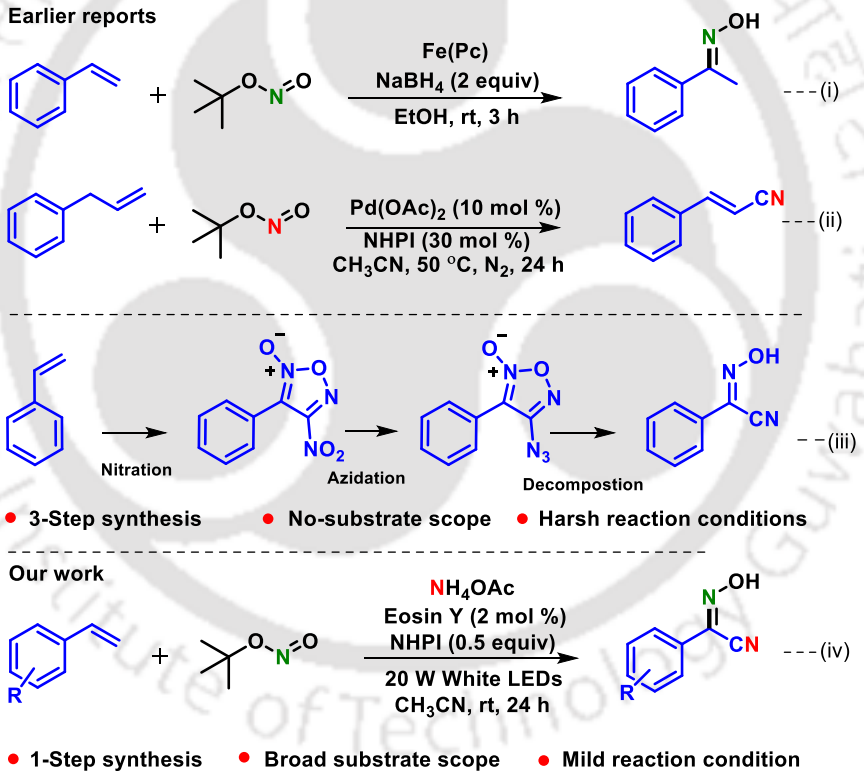

The synthesis of 2-hydroxyimino-2-phenyl acetonitrile starting from styrene was first reported by the Kunai group via a three-step process involving nitration of styrene to 4-nitro-3-phenylfurazan-2-oxide, an azidation step followed by photolytic decomposition [Scheme II.5,(iii)].[21] Although the above processes provide access to hydroxyiminoacetonitriles, these methods have inherent limitations, such as the requirement of prefunctionalized starting

materials, multistep process, limited substrate scope, and harsh reaction conditions. Therefore, designing routes for the synthesis of hydroxyiminoacetonitriles that are efficient, cost-effective, and atom economy is highly desirable. In recent times our group has been actively involved in the functionalization of alkenes using *tert*-butyl nitrite, which gave a variety of functionalized products under different reaction conditions.[22]

The reagent *tert*-butyl nitrite (TBN) is emerging as a versatile synthon in organic synthesis.[22a] TBN serves as an "N–O" synthon during the construction of isoxazolines from terminal aryl alkenes[22b] and as an "N1" synthon in the construction of imidazo[1,2-a]quinolines.[22c] Interestingly, TBN serves the dual role of "N1" and "N–O" synthons in the construction of 1,2,4-oxaziazole-5(4*H*)-ones from terminal aryl alkenes.[22d] In continuation of our efforts toward functionalization of alkene, we were curious to see the reactivity of an alkene with *tert*-butyl nitrite in the presence of NH_4OAc under 2 × 10 W white LEDs mediated by an organophotoredox catalyst [Scheme II.5,(iv)].

II.3. Present Work

The visible-light-mediated difunctionalization of alkenes were initiated by taking *p*-Me styrene (**2**) (0.25 mmol), *tert*-butyl nitrate (**a**), (4 equiv), Eosin Y (1 mol %) as the photocatalyst, NH_4OAc (4 equiv), *N*-hydroxyphthalimide (NHPI) (40 mol %) as cocatalyst in the presence of 2 × 10 W white LEDs in acetonitrile at room temperature. A new product was isolated in 40% yield. Standard spectroscopic analysis of the isolated product and subsequent single-crystal X-ray analysis reveal its structure to be *N*-hydroxybenzimidoyl cyanide (**2a)** (Figure II.2). To the best of our knowledge, this is a unique concomitant oximation–cyanation of alkene using *tert*-butyl nitrite as the N–O and ammonium acetate as the nitrogen (N1) synthon. Thrilled by this visible-light-mediated synthesis of hydroxyiminoacetonitrile, subsequent tuning of reaction parameters were attempted to enhance the productivity, taking *p*-Me styrene (**2**) as the prototypical substrate. The details optimization of various reaction parameters are summarized in Table II.1. Finally, the ideal condition for the synthesis of **2a** was the use of *p*-methylstyrene (**2**) (0.25 mmol), *tert*-butyl nitrite (**a**) (1.25 mmol), Eosin Y (2 mol %) NH_4OAc (4 equiv), and NHPI (50 mol %) in 2 mL CH_3CN under irradiation of 2 × 10 W white LEDs.

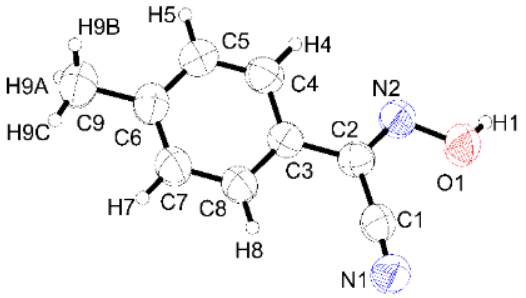

Figure II.2. *ORTEP diagram of (**2a**) with 40% ellipsoid probability (CCDC 1979124).*

II.3.1. Optimization of Reaction Conditions

Other organic dyes *viz* Eosin B (32%) and Rose Bengal (35%) were found to be mediocre compared to Eosin Y (Table II.1, entries 2–3). On the other hand, transition-metal based photocatalysts such as $[Ir(dtbbpy)(ppy)_2]PF_6$ (28%) $Ir[dF(CF_3)ppy]_2(dtbpy)PF_6$ (25%) were far less effective (Table II.1, entries 4–5). Therefore, we continue to use Eosin Y for this oximation-cyanation process. Next, increasing the loading Eosin Y to 2 mol %, an enhancement in the product yield (53%) was found (Table II.1, entry 6). Still, a further 1% surge in the catalyst loading (3 mol %) did not show any noteworthy increase in the yield (55%) (Table II.1, entry 7). Other ammonium salts, such as NH_4HCO_3 (22%) and NH_4Br (10%), both provided inferior yields as compared to NH_4OAc (Table II.1, entries 8–9). To see the effect of the solvent, various solvents were screened on the reaction. Solvent DCE (5%, Table II.1, entry 10) was found to be less effective than DCM (15%, Table II.1, entry 11). On the other hand, the use of polar aprotic solvents (DMSO, 00%), (DMF, 00%), and polar-protic solvents (MeOH, 00%) were completely ineffective (Table II.1, entries 12–14). However, polar aprotic solvent CH_3CN is the perfect solvent for this bifunctionalization. Both decreasing [(3 equiv, (27%)] or increasing [(5 equiv, (33%)] in the amount of NH_4OAc gave unsatisfactory yields (Table II.1, entries 15–16). Incidentally, increasing the loading of *tert*-butyl nitrite (TBN) to 5 equiv under otherwise identical conditions improved the yield to 60% (Table II.1, entry 17). However, any improvement in the yield (49%) was not observed with a further increase in TBN loading to 6 equiv (Table II.1, entry 18). The reaction, when carried out with different NO sources such as isobutyl nitrite (IBN) under identical conditions, provided a 52% yield of (**2a**) (Table II.1, entry 19). Incidentally, increasing the NHPI loading from 40 mol % to 50 mol % improved the yield to 65% (Table II.1, entry 20). However, any further increase in its loading was not beneficial

(Table II.1, entry 21). Other additives, such as *N*-hydroxysuccinamide (NHS) and hydroxybenzotrizole (HOBt), provided 42% and 32% yields, respectively (Table II.1, entries 22–23).

Table II.1. *Optimization of the reaction conditions*[a-e]

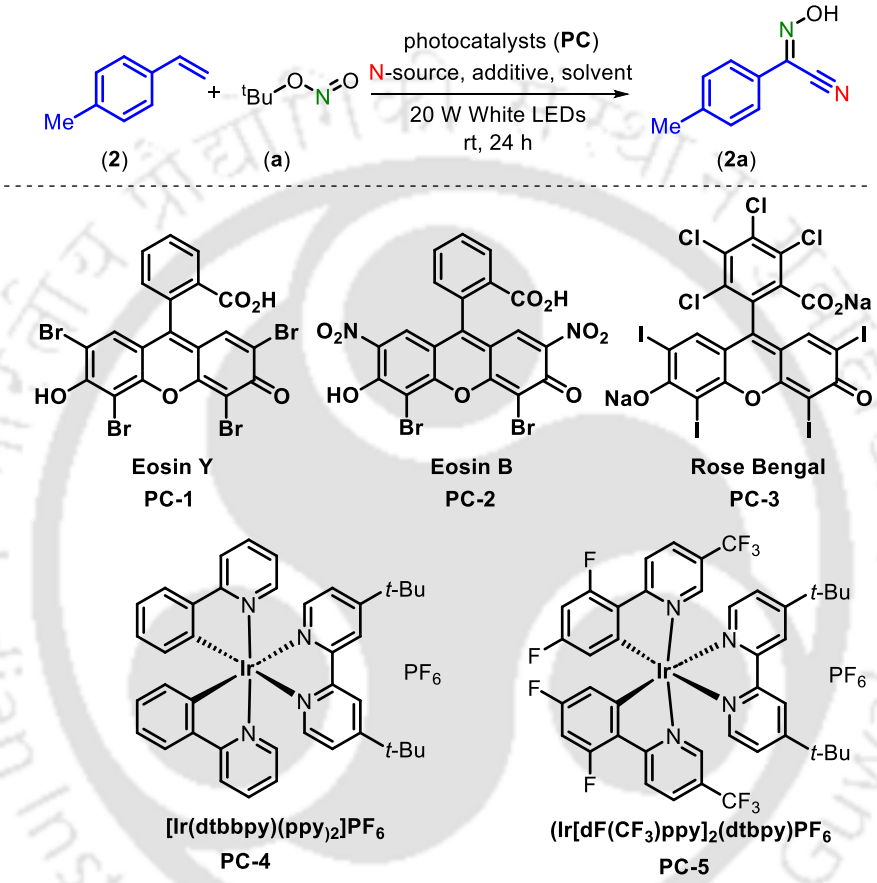

Entry	PC (mol%)	N-Source (eq.)	NO-Source (eq.)	Additive (mol%)	Solvent	Yield[b] (%)
1	**PC-1** (1)	NH_4OAc (4)	TBN (4)	NHPI (40)	CH_3CN	40
2	**PC-2** (1)	NH_4OAc (4)	TBN (4)	NHPI (40)	CH_3CN	32
3	**PC-3** (1)	NH_4OAc (4)	TBN (4)	NHPI (40)	CH_3CN	35
4	**PC-4** (1)	NH_4OAc (4)	TBN (4)	NHPI (40)	CH_3CN	28
5	**PC-5** (1)	NH_4OAc (4)	TBN (4)	NHPI (40)	CH_3CN	25
6	**PC-1** (2)	NH_4OAc (4)	TBN (4)	NHPI (40)	CH_3CN	53
7	**PC-1** (3)	NH_4OAc (4)	TBN (4)	NHPI (40)	CH_3CN	55
8	**PC-1** (2)	NH_4HCO_3 (4)	TBN (4)	NHPI (40)	CH_3CN	22

9	**PC-1** (2)	NH_4Br (4)	TBN (4)	NHPI (40)	CH_3CN	10
10	**PC-1** (2)	NH_4OAc (4)	TBN (4)	NHPI (40)	DCE	5
11	**PC-1** (2)	NH_4OAc (4)	TBN (4)	NHPI (40)	DCM	15
12	**PC-1** (2)	NH_4OAc (4)	TBN (4)	NHPI (40)	DMSO	ND[c]
13	**PC-1** (2)	NH_4OAc (4)	TBN (4)	NHPI (40)	DMF	ND[c]
14	**PC-1** (2)	NH_4OAc (4)	TBN (4)	NHPI (40)	MeOH	ND[c]
15	**PC-1** (2)	NH_4OAc (3)	TBN (4)	NHPI (40)	CH_3CN	27
16	**PC-1** (2)	NH_4OAc (5)	TBN (4)	NHPI (40)	CH_3CN	33
17	**PC-1** (2)	NH_4OAc (4)	TBN (5)	NHPI (40)	CH_3CN	60
18	**PC-1** (2)	NH_4OAc (4)	TBN (6)	NHPI (40)	CH_3CN	49
19	**PC-1** (2)	NH_4OAc (4)	IBN(5)	NHPI (40)	CH_3CN	52
20	**PC-1** (2)	NH_4OAc (4)	TBN (5)	NHPI (50)	CH_3CN	65
21	**PC-1** (2)	NH_4OAc (4)	TBN (5)	NHPI (60)	CH_3CN	62
22	**PC-1** (2)	NH_4OAc (4)	TBN (5)	NHS (50)	CH_3CN	42
23	**PC-1** (2)	NH_4OAc (4)	TBN (5)	HOBt (50)	CH_3CN	32
24		NH_4OAc (4)	TBN (5)	NHPI (50)	CH_3CN	18
25	**PC-1** (2)		TBN (5)	NHPI (50)	CH_3CN	ND[c]
26	**PC-1** (2)	NH_4OAc (4)	TBN (5)		CH_3CN	Trace
27	**PC-1** (2)	NH_4OAc (4)	TBN (5)	NHPI (50)	CH_3CN	12[d]
28	**PC-1** (2)	NH_4OAc (4)	TBN (5)	NHPI (50)	CH_3CN	60[e]
29	**PC-1** (2)	NH_4OAc (4)	TBN (5)	NHPI (50)	CH_3CN	37[f]
30	**PC-1** (2)	NH_4OAc (4)	TBN (5)	NHPI (50)	CH_3CN	44[g]
31	**PC-1** (2)	NH_4OAc (4)	TBN (5)	NHPI (50)	CH_3CN	33[h]

[a]Reaction conditions: 1a (0.25 mmol), 2a (equiv), Catalyst (mol %), *N*-Source (equiv), and additive (mol %) in 2 mL solvent with a 2 x 10 W white LEDs irradiation at room temperature. [b]Yield of isolated product. [c]ND = Not detected. [d]Reaction performed in the dark. [e]Reaction performed using 10 W White LEDs light. [f]Reaction performed using 10 W (513 nm) green LED light. [g]Reaction performed using 10 W (632 nm) red LEDs light. [h]Reaction performed using 10 W (430 nm) blue LEDs light.

TBN= *tert*-butyl nitrite, IBN= isobutyl nitrite, NHPI= *N*-hydroxyphthalimide, NHS= *N*-hydroxysuccinimide, HOBt= Hydroxybenzotriazole

The reaction in the absence of photo-catalyst (Eosin Y) provides a much lesser yield (18%) under otherwise similar conditions (Table II.1, entry 24). Whereas the reaction in the absence of N-source NH_4OAc does not proceed at all (Table II.1, entry 25). Reactions performed without NHPI, provided a meagre amount of the product (Table II.1, entry 26). These results suggest the necessity of photo-catalyst, *N*-source, and additives in the difunctionalization of styrenes. The reaction when carried out in the dark gave only 12% yield of product **2a** (Table II.1, entry 27). The use of a single 10W white LED light provided a slightly lesser yield (60%) of the product compared to that of a 2 x 10 W white LED light (Table II.1, entry 28).

The temperature in the vicinity of the reaction was almost identical to that of room temperature (~28 ^oC) during the entire process due to the usage of (2 x 10 W) LEDs as it was well-ventilated, confirming the photochemical pathways for this transformation. When the reaction was performed with 10 W LED light of other wavelengths, such as green (513 nm), red (632 nm), and blue (430 nm), all provided reduced yields of 37%, 44%, and 33%, respectively (Table II.1 entry 29–31).

II.3.2. Substrates scope for the Synthesis of *N*-Hydroxybenzimidoyl Cyanides from Aryl Alkenes

The substrate scope of the methodology was applied to various aromatic terminal alkenes adopting the optimized reaction condition (Scheme II.6). Simple styrene (**1**), having no substituent in the phenyl ring, provided a 61% yield of the difunctionalized product (**1a**). Styrenes having electron-donating groups, namely, *p*-Me (**2**), *m*-Me (**3**), *o*-Me (**4**), *p*-^{t}Bu (**5**), *p*-OMe (**6**), and *p*-CH_2Cl (**7**) yielded their corresponding *N*-hydroxybenzimidoyl cyanides (**2a**, 65%), (**3a**, 62%), (**4a**, 59%), (**5a**, 67%,), (**6a**, 69%) and (**7a**, 63%), respectively (Scheme II.6). Styrenes possessing substituents such as *p*-F (**8**), *m*-F (**9**), *p*-Cl (**10**), *m*-Cl (**11**), *o*-Cl (**12**), and *p*-Br (**13**) having moderate electron-withdrawing ability, all underwent successfully difunctionalizations to produce *N*-hydroxybenzimidoyl cyanides (**8a**, 60%), (**9a**, 58%), (**10a**, 59%), (**11a**, 55%), (**12a**, 52%), and (**13a**, 57%), respectively, in acceptable yields (Scheme II.6). A meta-substituted nitrostyrene (**14**) having a strongly electron-withdrawing group also reacted smoothly, affording the corresponding product (**14a**, 48%) (Scheme II.6).

Scheme II.6. Substrates scope for the synthesis of N-hydroxybenzimidoyl cyanides from aryl alkenes.[a,b]

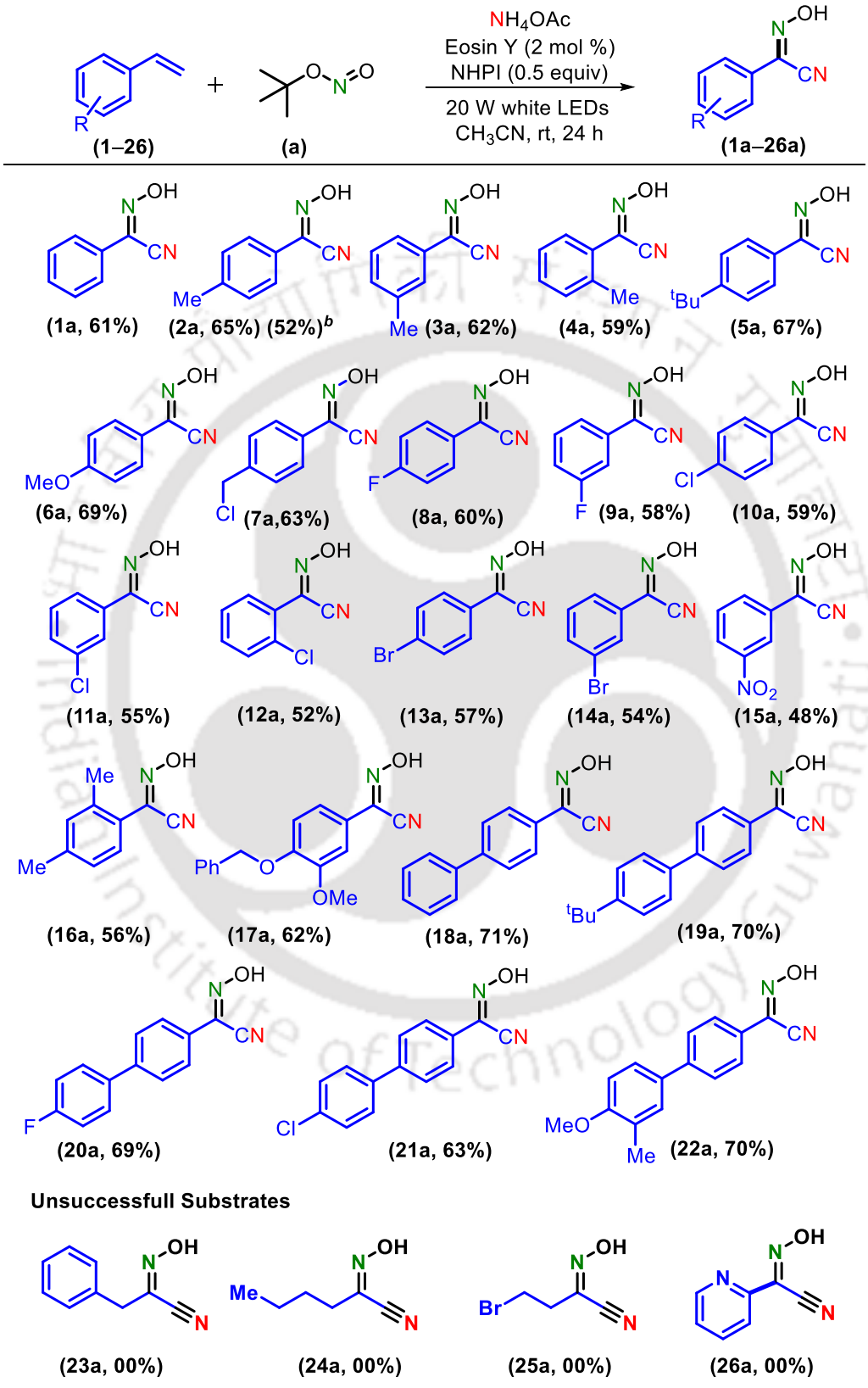

[a]Reaction conditions:(i) 1–26 (0.25 mmol), [t]BuONO (1.25 mmol), NH_4OAc (1 mmol), NHPI (0.125 mmol), Eosin Y (0.005 mmol), and CH_3CN (2 mL) for 24 h. [b]Yield reported for 5 mmol scales.

Trisubstituted and disubstituted aromatic terminal alkenes such as 2,4,6-trimethylstyrene (**15**), 2,4-dimethylstyrene (**16**), and 3-methoxy-4-benzyloxystyrene (**17**) underwent efficient conversion to their desired *N*-hydroxybenzimidoyl cyanides (**15a**, 51%), (**16a**, 56%), and (**17a**, 62%), respectively (Scheme II.6). A biphenyl styrene (**18**) reacted smoothly, giving hydroxyaminoacetonitrile (**18a**) in 71% yield. Other biphenyl styrenes having electron-donating substituent [*p*-[t]Bu (**19**)], electron-withdrawing substituents [*p*-F (**20**), and *p*-Cl (**21**)] and disubstituted such as 3-Me-4-OMe (**22**) all were successfully converted to their hydroxyaminoacetonitriles (**19a**, 70%), (**20a**, 69%), (**21a**, 63%), and (**22a**, 70%), respectively.

Unlike terminal aromatic alkenes, aliphatic terminal alkenes, such as ally benzene (**23**), 1-hexene (**24**), 4-bromo-1-butene (**25**), and heteroaryl alkene (**26**) all failed to provide any product, which is possibly due to the instability of the radicals produced in the medium (Scheme II.6). A successful large-scale reaction was performed using 4-methylstyrene (**2**) (5 mmol, 590 mg), *tert*-butyl nitrite (25 mmol, 2.57g) ammonium acetate (20 mmol, 1.54 g), and NHPI (50 mol %, 407 mg), which provided product (**2a)** in 52% yield.

II.4. Mechanistic Investigation

II.4.1. Control Experiments

After an excellent demonstration of a useful synthesis of *N*-hydroxybenzimidoyl cyanides, it is time to suggest a plausible mechanism. To ascertain the radical nature of the reaction, two independent reactions were performed: one in the presence of 2,2,6,6-tetramethylpiperidine-1-oxyl (TEMPO, 2 equiv) and the other with 2,6-di-tertbutyl-4-methyl phenol (BHT, 2 equiv). In the former case, no formation of the product (**1a**, 00%) was observed, but the latter scavenger provided <10% yield of (**1a**), thereby approving the radical nature of the reaction (Scheme II.7).

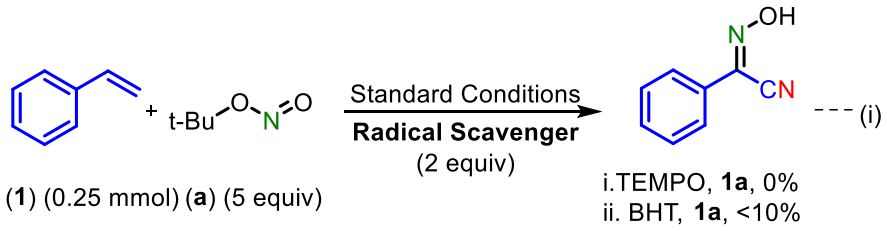

Scheme II.7. *Control experiments.*

(ii) To prove the role of aerial oxygen, a standard experiment between (**1**) and (**a**) was carried out in an N_2 atmosphere under otherwise identical conditions. No formation of the desired product (**1a**, 0%) was observed, suggesting the involvement of aerial oxygen (Scheme II.8).

Scheme II.8. *Control experiments.*

ESI-MS study for the detection of reaction intermediates during the synthesis of (Z)-*N*-hydroxybenzimidoyl cyanide (1a) from styrene (1) and *tert*-butyl nitrite (a) at different time intervals (30 and 45 minutes):

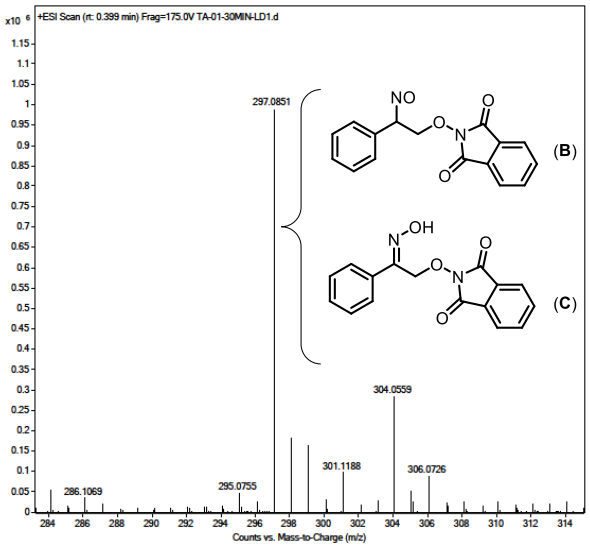

Figure II.3. *HRMS spectrum of the reaction mixture after 30 minutes.*

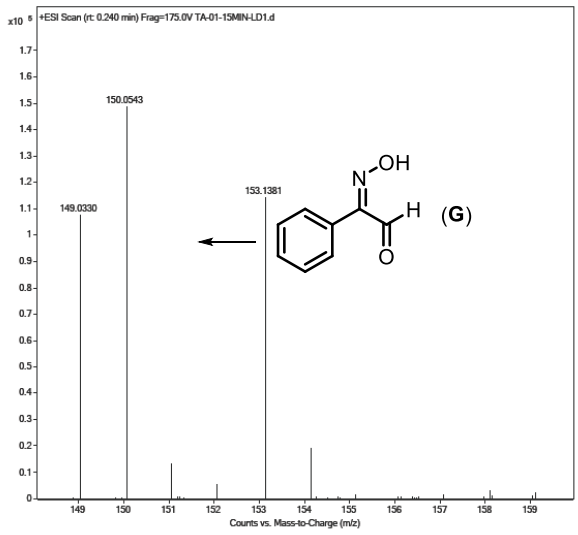

Figure II.4. *HRMS spectrum of the reaction mixture after 45 minutes.*

II.4.2. Plausible Reaction Mechanism

Based on the control experiments and intermediates identified by the HRMS analysis of the reaction aliquots at various times, a logical mechanism is suggested (Scheme II.9). In the presence of white LED light, Eosin Y (EY) is first photoexcited. This is followed by photo-oxidation of NHPI to a PINO radical by the activated Eosin Y via HAT (hydrogen atom transfer) mechanism. This process regenerates the Eosin Y back, producing an HO_2• radical, which upon disproportionation, produces oxygen and hydrogen peroxide.[23a,b] The PINO radical then attacks at the terminal sp^2-carbon of alkene (**1**) to generate a benzylic radical intermediate (**A**). Photochemical decomposition of *tert*-butyl nitrite generates NO and *tert*-butoxyradicals.[23c] The benzylic position of the intermediate (**A**) is attacked by the NO radical to generate intermediate (**B**). Although PINO and NO radicals exist in the reaction medium, only the PINO attacks at the terminal carbon of styrene (**1**) and the NO at the benzylic carbon. This type of preferential attack of one of the radicals over others (NO and NO_2) has been observed earlier.[22b–d] To get an insight into this preferential attack by these radicals on styrene, DFT calculations were performed and modeled the reaction profile at the M06/6-31+G(d) level of theory; no symmetry constraints were imposed during geometry optimization. Furthermore,

single-point energy calculations were performed using the M06/cc-pVTZ method, and these energies were subsequently used in the analyses of chemical mechanisms. Transition states were established by their characteristic solo imaginary frequency in normal vibrational mode. As shown from Scheme II.9, the attack of NO radical at the terminal sp^2-carbon goes through a high activation barrier of 13.75 kcal/mol, generating an unstable intermediate (**A′**). On the other hand, an identical attack of the PINO radical required 8.53 kcal/mol less energy, generating a comparatively stable radical intermediate (**A**). The in-situ-generated nitroso intermediate (**B**) is tautomerized to an oxime intermediate (**C**). The *tert*-butoxyl radical sequentially abstracts two H atoms from the oxime intermediate (**C**) to first generate a mono radical (**D1**), followed by a 1,4-biradical intermediate (**D**). An intramolecular coupling of biradical (**D**) generates a four-membered cyclic intermediate (**E**). The hydrogen peroxide produced in situ decomposes to a hydroxyl radical in the presence of light.[23d,e] The strained cyclic intermediate (**E**) undergoes ring-opening via attack of an OH radical to form a hemiacetal radical intermediate (**F**). The N–O radical intermediate (**F**) abstracts a proton from *tert*-butanol to generate a neutral hemiacetal intermediate (**G**). The neutral hemiacetal intermediate loses NHPI providing an oxime aldehyde (**H**). Condensation between ammonia (generated from ammonium acetate) and the aldehydic intermediate (**H**) forms an iminium intermediate (**I**),[24] which is perhaps the rate-determining step of the process. Abstraction of an iminium N–H from the intermediate (**I**) by the ^{t}BuO radical produces a nitrogen-centered radical (**J**). Finally, the abstraction of the aldehydic proton from intermediate (**J**) by *tert*-butoxy radical provided the desired cyano functionality. As can be seen from the DFT calculation (Figure.II.5).

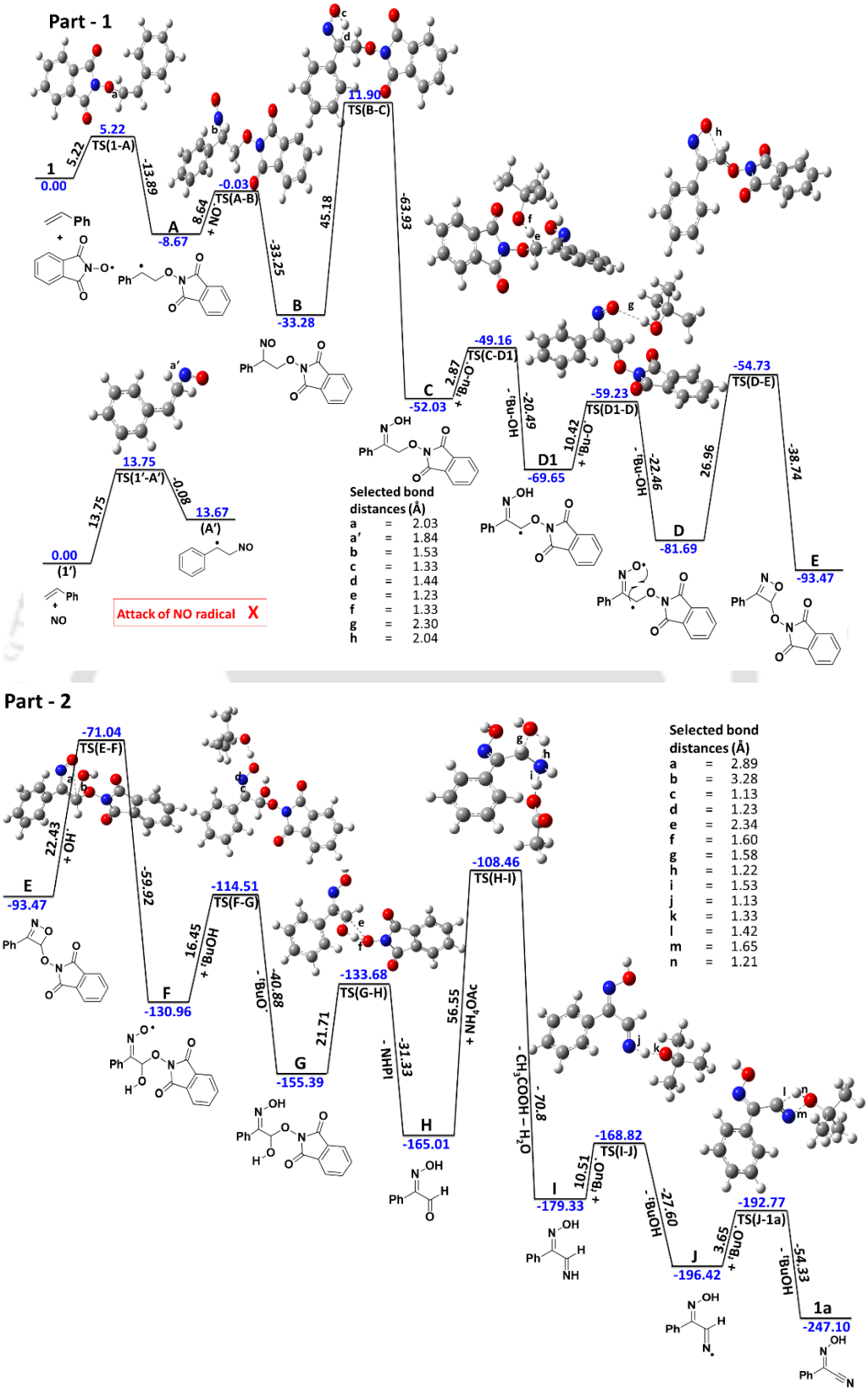

Figure II.5. *[a]Calculated energy profile diagrams for the photolytic difunctionalization of alkene. The relative energies from DFT calculations are in kcal.mol^{-1} and bond lengths in Å, done at M06/6-31g+(d,p) level of theory. Single-point calculations were done using the M06/cc-pVTZ method, and these energies were subsequently used in the analyses of chemical mechanisms. The relative energies are shown in blue color; the activation barrier is shown in italic, bold font, and stabilization energy is shown in the normal font; all are given are units of kcal.mol^{-1}. The cross sign in red color (X) indicates the unfavorable reaction with a higher activation barrier and lower stabilization.*

Scheme II.9. *Proposed reaction pathway for the formation of N-hydroxybenzimidoyl cyanides.*

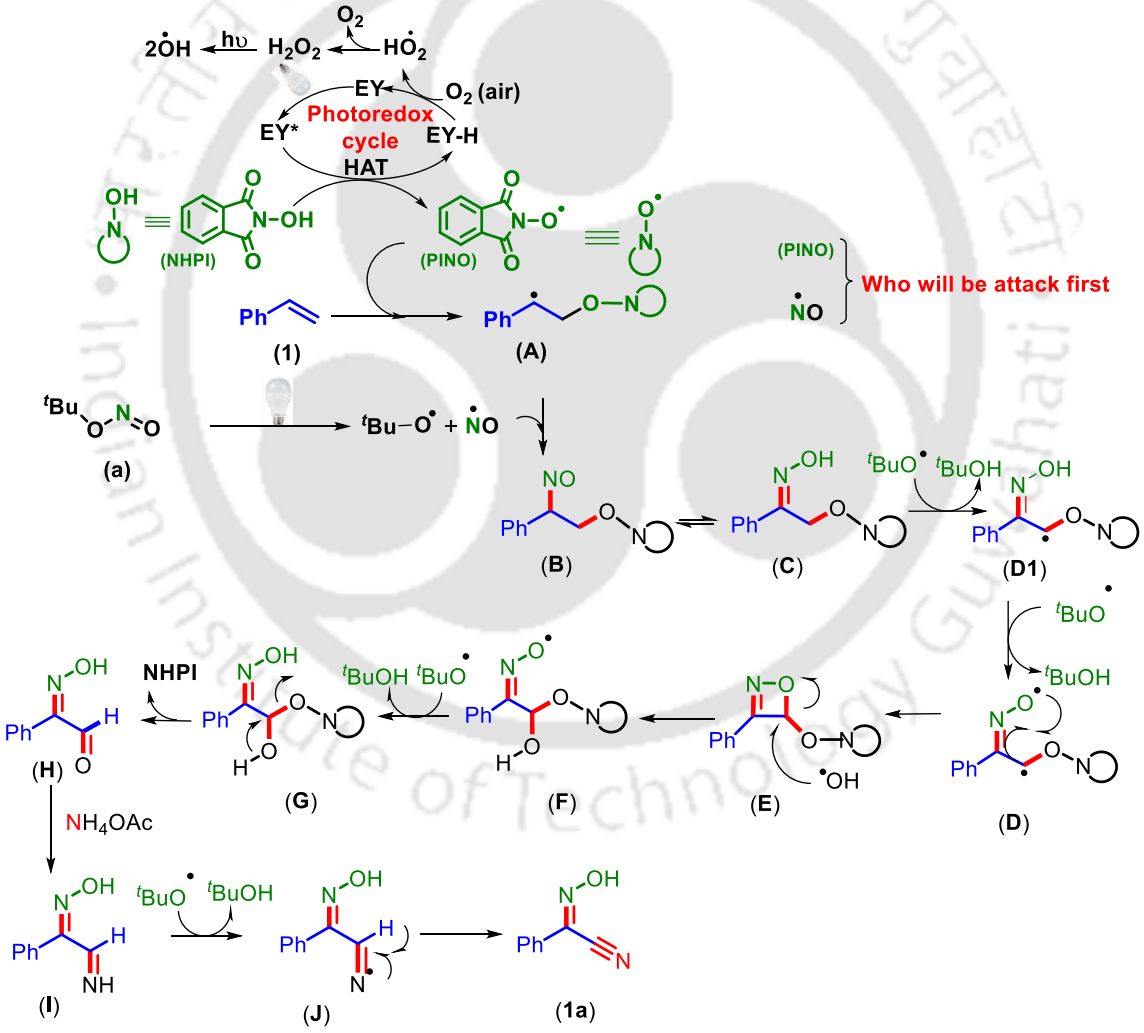

II.5. Post-Synthetic Applications

The difunctionalized hydroxyaminoacetonitrile having an oxime (=NOH) and a reactive nitrile (C≡N) group can be transformed to a variety of other functionalized products. When (**2a**) was heated in an aqueous H_2SO_4, the nitrile group was converted to an acid functionality (**2b**) (Scheme II.10).[25]

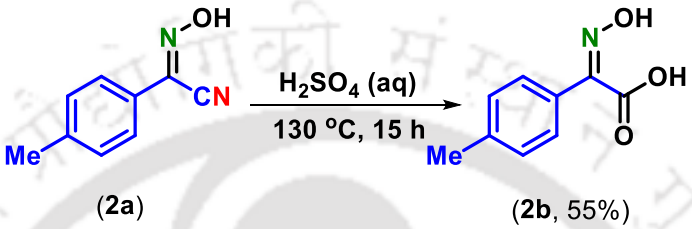

Scheme II.10. *Synthesis of acid derivative.*

Conversely, when (**2a**) was treated with concentrated H_2SO_4, the nitrile functionality was converted to an amide (**2c**) (Scheme II.11).[26]

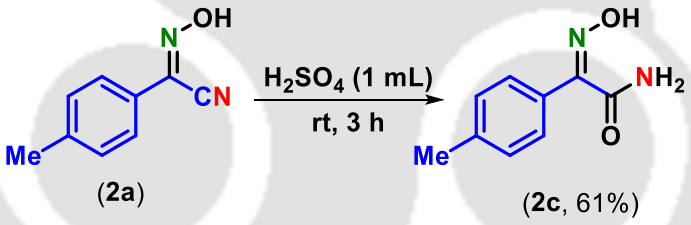

Scheme II.11. *Synthesis of amide derivative.*

Furthermore, in the treatment of (**2a**) with a phenylboronic acid in the presence of a Pd(II) catalyst, both the oxime and cyano functionality were converted to a keto group (**2d**) with concurrent incorporation of a phenyl group (Scheme II.12).[27]

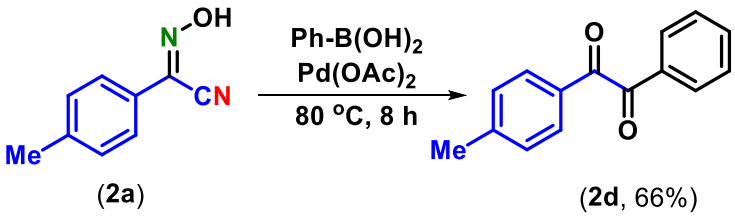

Scheme II.12. *Synthesis of ketone derivative.*

The cyano substrate (**2a**) on treatment with NaN_3 is transformed to a tetrazole moiety (**2e**) without affecting the oxime functionality (Scheme II.13).[28]

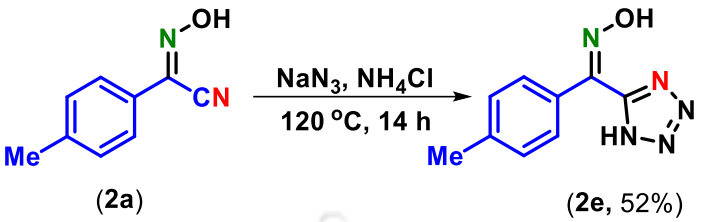

(**2a**) (**2e**, 52%)

Scheme II.13. *Synthesis of tetrazole derivative.*

II.6. Conclusion

In conclusion, a visible-light-mediated synthesis of *N*-hydroxybenzimidoyl cyanides have been accomplished from styrenes in the presence of an organic photoredox catalyst. The bifunctionalized moiety possesses two important functionalities, *viz*, an oxime and a nitrile group, which originate from *tert*-butyl nitrite and ammonium acetate, respectively. This reaction proceeds through a biradical reaction path. The proposed mechanism detects some of the reaction intermediates, and a DFT calculation supports each of the steps. Some useful post-synthetic modifications were performed to show the synthetic utility of the difunctionalized hydroxyaminoacetonitrile, thereby expanding the scope of this methodology further.

II.7. Experimental Section

II.7.1. General Information: All the reagents were commercial grade and purified according to the established procedures. Organic extracts were dried over anhydrous sodium sulfate. Solvents were removed in a rotary evaporator under reduced pressure. Silica gel (60-120 mesh size) was used for the column chromatography. TLC monitored reactions on silica gel 60 F_{254} (0.25 mm). NMR spectra were recorded in $CDCl_3$ and DMSO-d_6 as the internal standard for ^1H NMR (400 MHz) and ^{13}C NMR (100 MHz). MS spectra were recorded using ESI mode. IR spectra were recorded in KBr or neat.

Light Information:

A Philips 10W white LED bulb was used as a light source for this light-promoted reaction. We have not used any filters. For a wavelength of 400-700 nm, borosilicate glass was

used as an irradiation vessel. Distance from the light source to the irradiation vessel ~6-8 cm. The regular fan was used to maintain the temperature at 28-30 ^{o}C.

II.7.2. Crytallographic Description

Sample preparation: We dissolved 15 mg of the compound (**2a**) in 1 mL of Methanol: Hexane (5: 1).

Diffraction data were collected at 292 K with MoKα radiation (λ = 0.71073 Å) using a Bruker Nonius SMART APEX CCD diffractometer equipped with graphite monochromator and Apex CD camera. The SMART software was used for data collection for indexing the reflections and determining the unit cell parameters. Data reduction and cell refinement were performed using SAINT[1,2] software, and the space groups of these crystals were determined from systematic absences by XPREP and further justified by the refinement results. The structures were solved by direct methods and refined by full-matrix least-squares calculations using SHELXTL-97[3] software. All the non-H atoms were refined in the anisotropic approximation against F^2 of all reflections.

Crystallographic description of (Z)-*N*-hydroxy-4-methylbenzimidoyl cyanide (2a)

$C_9H_8N_2O$, crystal dimensions 0.27 x 0.23 x 0.14 mm, M_r = 160.17, triclinic space, group P -1, a=6.143(6), b=7.196(6), c=10.502(10) Å, α = 105.05 ^{o} (3), β = 92.92 ^{o} (4) , γ = 109.32 ^{o} (3) , V = 418.2 (7) Å^3, Z = 2, ρ_{calcd} = 1.272 mg/m^3, μ = 0.086 mm^{-1}, F(000) = 168.0, refinement method = full-matrix least-squares on F^2, final R indices [$I > 2\sigma(I)$]: R_1 = 0.0793 (521), wR_2 = 0.3090 (1475), goodness of fit = 1.000. CCDC 1979124 for (Z)-*N*-hydroxy-4-methylbenzimidoyl cyanide (**2a**) contains the supplementary crystallographic data for this paper. These data can be obtained free of charge from The Cambridge Crystallographic Data Centre via www.ccdc.cam.ac.uk/data_request/cif.

II.7.3. General Procedure for the Synthesis of *N*-Hydroxybenzimidoyl Cyanides (1a–22a) from Styrene (1–22) and *tert*-Butyl nitrite (a)

To an oven-dried 10 mL round bottom flask was added styrene (**1**–**22**) (0.25 mmol), *tert*-butyl nitrite (**a**) (1.25 mmol, 128.9 mg), Eosin Y (2 mol %, 3.23 mg), NH_4OAc (4 equiv, 154 mg) and NHPI (50 mol %, 20.37 mg) in 2 mL CH_3CN. The reaction mixture was stirred at room temperature for 24 h, maintaining an approximate distance of ~6–8 cm from two 10W

white LED bulbs (Flux 46 mw/cm^2). After completion of the reaction (monitored by TLC analysis), the solvent was removed in vacuo, and the mixture was admixed with ethyl acetate (25 mL). The organic layer was washed with a saturated solution of aqueous $MgSO_4$ (1 x 5 mL). The organic layer was dried over anhydrous Na_2SO_4, and the solvent was evaporated under reduced pressure. The crude product so obtained was purified over a column of silica gel using an increasing percentage of ethyl acetate in hexane to afford the *N*-hydroxybenzimidoyl cyanide (**1a–22a**). The identity and purity of the product were confirmed by spectroscopic analysis.

II.7.4. General Procedure for 5 mmol Scale Reaction of 2a

To an oven-dried 50 mL round bottom flask was added 4-methyl styrene (**2**) (5 mmol, 590 mg), *tert*-butyl nitrite (25 mmol, 2.57g) ammonium acetate (20 mmol, 1.54 g), and NHPI (50 mol %, 407 mg) in 6 mL CH_3CN. The reaction mixture was stirred at room temperature for 24 h, maintaining an approximate distance of ~6–8 cm from two 10W white LED bulbs (Flux 46 mw/cm^2). After completion of the reaction (monitored by TLC analysis), the solvent was removed in vacuo, and the mixture was admixed with ethyl acetate (50 mL). The organic layer was washed with a saturated solution of aqueous $MgSO_4$ (1 x 10 mL). The organic layer was dried over anhydrous Na_2SO_4, and the solvent was evaporated under reduced pressure. The crude product so obtained was purified over a column of silica gel using an increasing percentage of ethyl acetate in hexane to afford the (Z)-*N*-Hydroxy-4-methylbenzimidoyl cyanide (**2a**) 52% yield.

II.7.5. Procedure for the Formation (Z)-2-(Hydroxyimino)-2-(*p*-tolyl)acetic acid (2b)

To an oven-dried 10 mL round bottom flask fitted with a magnetic bar was added (Z)-*N*-hydroxy-4-methylbenzimidoyl cyanide (**2a**) (40 mg, 0.25 mmol) and 15 N H_2SO_4 (1.5 mL). The reaction mixture was stirred in an oil bath preheated at 130 ^oC for 15 h. Next, the reaction mixture was cooled to room temperature and admixed with CH_2Cl_2 (25 mL). The organic layer was washed with saturated sodium bicarbonate solution (1 x 5 mL) and dried over Na_2SO_4. The CH_2Cl_2 solvent was removed under a reduced pressure. The crude product so obtained was purified over a column of silica gel (hexane/ethyl acetate, 8.5:1.5) to afford the (Z)-2-

(hydroxyimino)-2-(*p*-tolyl)acetic acid (25 mg, yield 55%) (**2b**). The identity and purity of the product were confirmed by spectroscopic analysis.

II.7.6. Procedure for the Formation of (Z)-2-(Hydroxyimino)-2-(*p*-Tolyl)acetamide (2c)

An oven-dried 10 mL round bottom flask containing a magnetic bar was added (Z)-*N*-hydroxy-4-methylbenzimidoyl cyanide (**2a**) (40 mg, 0.25 mmol) and conc. H_2SO_4 (1.0 mL) under a nitrogen atmosphere. Maintaining the nitrogen atmosphere, the reaction mixture was stirred at room temperature for 3 h. After completion of the reaction, it was diluted with water (10 mL). The organic product in water was extracted with ethyl acetate (25 mL). The organic layer was washed with saturated $NaHCO_3$ solution (1 x 5 mL) and dried over Na_2SO_4. The ethyl acetate was removed under a reduced pressure. The crude product so obtained was purified over a column of silica gel (hexane/ethylacetate, 8:2) to afford the (Z)-2-(hydroxyimino)-2-(*p*-tolyl)acetamide (**2c**) (27 mg, yield 61%). The identity and purity of the product were confirmed by spectroscopic analysis.

II.7.7. Procedure for the Formation 1-Phenyl-2-(*p*-tolyl)ethane-1,2-dione (2d)

To an oven-dried 10 mL round bottom flask containing a magnetic bar was added (Z)-*N*-hydroxy-4-methylbenzimidoyl cyanide (**2a**) (40 mg, 0.25 mmol), phenylboronic acid (91 mg, 0.75 mmol), $Pd(OAc)_2$ (5.6 mg, 10 mol %,), 2,2´-bipyridyl (7.8 mg, 20 mol %,), PTSA.H_2O (475.5 mg, 10 equiv) and toluene (2 mL). The reaction mixture was stirred in an oil bath preheated at 80 ^oC for 12 h. After completion of the reaction, it was cooled to room temperature and admixed with ethyl acetate (25 mL). The organic layer was washed with a saturated solution of $NaHCO_3$ (1 x 5 mL), dried over Na_2SO_4, and the solvent was removed under a reduced pressure. The crude product so obtained was purified over a column of silica gel (hexane/ethyl acetate, 9:1) to afford the 1-phenyl-2-(*p*-tolyl)ethane-1,2-dione (**2d**) (37 mg, yield 66%) pure product. The identity and purity of the product were confirmed by spectroscopic analysis.

II.7.8. Procedure for the Formation of (Z)-(1*H*-Tetrazol-5-yl)(*p*-tolyl)methanone oxime (2e)

To an oven-dried 10 mL round bottom flask containing a magnetic bar was added (Z)-*N*-hydroxy-4-methylbenzimidoyl cyanide (**2a**) (40 mg, 0.25 mmol), NaN_3 (32.5 mg, 0.5

mmol), and NH_4Cl (13.37 mg, 0.25 mmol). A rubber septum was fitted to the flask, which was subjected to vacuum for 10 minutes and purged with nitrogen. Next, DMF (2 mL) was introduced through a syringe, maintaining the nitrogen atmosphere. The reaction mixture was stirred in an oil bath preheated at 120 ^oC for 14 h. After completion of the reaction, it was cooled to room temperature and admixed with cold water (15 mL). The aqueous reaction mixture was acidified with 2N HCl, and the product was extracted with ethyl acetate (25 mL). The organic layer was washed with a saturated solution of NaHCO3 (1 x 5 mL) and dried over Na_2SO_4. The solvent was removed under reduced pressure, and the crude product thus obtained was purified by column chromatography over silica gel (hexane/ethyl acetate, 6:4) to afford the (Z)-(1*H*-tetrazol-5-yl)(*p*-tolyl)methanone oxime (**2e**) (26 mg, yield 52%) pure product. The identity and purity of the product were confirmed by spectroscopic analysis.

II.8. References

[1] (a) Ma, J.; Rosales, A. R.; Huang, X.; Harms, K.; Riedel, R.; Wiest, O.; Meggers, E. *J. Am. Chem. Soc*. **2017**, *139*, 17245–17248. (b) Kim, I.; Kang, G.; Lee, K.; Park, B.; Kang, D.; Jung, H.; He, Y.-T.; Baik, M.-H.; Hong, S. *J. Am. Chem. Soc.* **2019**, *141*, 9239–9248. (c) Patra, T.; Mukherjee, S.; Ma, J.; Strieth-Kalthoff, F.; Glörius, F. *Angew. Chem., Int. Ed*. **2019**, *58*, 10514. (d) Yu, W.-L.; Luo, Y.-C.; Yan, L.; Liu, D.; Wang, Z.-Y.; Xu, P.-F. *Angew. Chem.* **2019**, *131*, 11057–11061.

[2] (a) Hou, J.; Ee, A.; Cao, H.; Ong, H.-W.; Xu, J.-H.; Wu, J. *Angew. Chem., Int. Ed.* **2018**, *57*, 17220–17224. (b) Jung, S.; Lee, H.; Moon, Y.; Jung, H.-Y.; Hong, S. *ACS Catal.* **2019**, *9*, 9891–9896. (c) Wang, P.-Z.; He, B.-Q.; Cheng, Y.; Chen, J.-R.; Xiao, W.-J. *Org. Lett*. **2019**, *21*, 6924–6929. (d) Song, C.; Yi, H.; Dou, B.; Li, Y.; Singh, A. K.; Lei, A. *Chem. Commun*. **2017**, *53*, 3689–3692.

[3] (a) Allen, L. J.; Cabrera, P. J.; Lee, M.; Sanford, M. S. *J. Am. Chem. Soc.* **2014**, *136*, 5607–5610. (b) Speckmeier, E.; Fuchs, P. J. W.; Zeitler, K. *Chem. Sci*. **2018**, *9*, 7096–7103. (c) Li, H.; Cheng, Z.; Tung, C.-H.; Xu, Z. *ACS Catal*. **2018**, *8*, 8237–8243. (d) Chalotra, N.; Rizvi, M. A.; Shah, B. A. *Org. Lett*. **2019**, *21*, 4793–4797. (e) Cheng, J.; Cheng, Y.; Xie, J.; Zhu, C. *Org. Lett*. **2017**, *19*, 6452–6455.

[4] Li, G.; Yan, Q.; Gan, Z.; Li, Q.; Dou, X.; Yang, D. *Org. Lett*. **2019**, *21*, 7938–7942. (b) Pramanik, M. M. D.; Rastogi, N. *Chem. Commun*. **2016**, *52*, 8557–8560. (c) Chaturvedi, A. K.; Rastogi, N. *Org. Biomol. Chem*. **2018**, *16*, 8155–8159.

[5] (a) Srivastava, V.; Singh, P. P. *RSC Adv*. **2017**, *7*, 31377–31392. (b) Hari, D. P.; König, B. *Chem. Commun*. **2014**, *50*, 6688–6699. (c) Yadav, A. K.; Sharma, A. K.; Singh, K. N. *Org. Chem. Front*. **2019**, *6*, 989–993. (d) Gu, L; Jin, C.; Wang, W.; He, Y.; Yang, G.; Li, G. *Chem. Commun*. **2017**, *53*, 4203–4206. (e) Yadav, A. K.; Yadav, L. D. S. *Green. Chem*. **2015**, *17*, 3515–3520. (f) Yang, W.; Yang, S.; Li, P.; Wang, L. *Chem. Commun*. **2015**, *51*, 7520–7523. (g) Pramanik, M. M. D.; Nagode, S. B.; Kant, R.; Rastogi, N. *Org. Biomol. Chem*. **2017**, *15*, 7369–7373. (h) Nagode, S. B.; Kant, R.; Rastogi, N. *Org. Lett*. **2019**, *21*, 6249–6254. (i) Li, R.; Chen, X.; Wei, S.; Sun, K.; Fan, L.; Liu, Y.; Qu, L.; Zhao, Y.; Yua, B. *Adv. Synth. Catal*. **2018**, *360*, 4807–4813. (j) Xiao, T.; Li, L.; Lin, G.; Mao, Z.-w.; Zhou, L. *Org. Lett*. **2014**, *16*, 4232–4235.

[6] (a) Jensen, K. H.; Sigman, M. S. *Org. Biomol. Chem*. **2008**, *6*, 4083–4088. (b) Ciesielski, J.; Dequirez, G.; Retailleau, P.; Gandon, V.; Dauban, P. *Chem. Eur. J*. **2016**, *22*, 9338–9347. (c) Pathak, T. P.; Gligorich, K. M.; Welm, B. E.; Sigman, M. S. *J. Am. Chem. Soc*. **2010**, *132*, 7870–7871. (d) Ashikari, Y.; Shimizu, A.; Nokami, T.; Yoshida, J.-i. *J. Am. Chem. Soc*. **2013**, *135*, 16070–16073. (e) Rosen, B. R.; Ney, J. E.; Wolfe, J. P. *J. Org. Chem*. **2010**, *75*, 2756–2759.

[7] (a) Zhou, S.-F.; Pan, X.; Zhou, Z.-H.; Shoberu, A.; Zou, J.-P. *J. Org. Chem*. **2015**, *80*, 3682–3687. (b) Xue, Q.; Xie, J.; Xu, P.; Hu, K.; Cheng, Y.; Zhu, C. *ACS Catal*. **2013**, *3*, 1365–1368. (c) Oh, S. H.; Malpani, Y. R.; Ha, N.; Jung, Y.-S.; Han, S. B. *Org. Lett*. **2014**, *16*, 1310–1313. (d) Huang, L.; Zheng, S.-C.; Tan, B.; Liu, X.-Y. *Org. Lett*. **2015**, *17*, 1589–1592.

[8] (a) Tang, S.; Liu, K.; Liu, C.; Lei, A. *Chem. Soc. Rev*. **2015**, *44*, 1070–1082. (b) Lan, X.-W.; Wang, N.-X.; Xing, Y. *Eur. J. Org. Chem*. **2017**, 5821–5851. (c) Sauer, G. S.; Lin, S. *ACS Catal*. **2018**, *8*, 5175–5187. (d) Qiu, G.; Lai, L.; Cheng, J.; Wu, J. *Chem. Commun*. **2018**, *54*, 10405–10414.

[9] (a) Niu, T.-f.; Cheng, J.; Zhuo, C.-l.; Jiang, D.-y.; Shu, X.-g.; Ni, B.-q. *Tetrahedron Lett.* **2017**, *58*, 3667–3671. (b) Hoque, I. U.; Chowdhury, S. R.; Maity, S. *J. Org. Chem*. **2019**, *84*, 3025–3035. (c) Li, L.; Huang, M.; Liu, C.; Xiao, J.-C.; Chen, Q.-Y.; Guo, Y.; Zhao, Z.-G. *Org. Lett*. **2015**, *17*, 4714–4717. (d) Noto, N.; Koike, T.; Akita, M. *ACS Catal*. **2019**, *9*, 4382–4387. (e) Li, L.; Chen, H.; Mei M.; Zhou, L. *Chem. Commun*. **2017**, *53*, 11544–11547.

[10] (a) Furuya, Y.; Ishihara, K.; Yamamoto, H. *J. Am. Chem. Soc.* **2005**, *127*, 11240–11241. (b) Hong, W. P.; Iosub, A. V.; Stahl, S. S. *J. Am. Chem. Soc*. **2013**, *135*, 13664–13667. (c) Ramón, R. S.; Bosson, J.; Díez-González, S.; Marion, N.; Nolan, S. P. *J. Org. Chem.* **2010**, *75*, 1197–1202. (d) Kong, W.; Guo, Q.; Xu, Z.; Wang, G.; Jiang, X.; Wang, R. *Org. Lett*. **2015**, *17*, 3686–3689. (e) Peng, X.; Tong, B. M. K.; Hirao, H.; Chiba, S. *Angew. Chem. Int. Ed*. **2014**, *53*, 1959–1963. (f) Yu, J.; Lu, M. *Org. Biomol. Chem*. **2015**, *13*, 7397–7401.

[11] Bolotin, D. S.; Bokach, N. A.; Demakova, M. Y.; Kukushkin, V. Y. *Chem. Rev*. **2017**, *117*, 13039–13122.

[12] (a) Caddick, S.; Haynes, A. K. de K.; Judd, D. B.; Williams, M. R. V. *Tetrahedron Lett.* **2000**, *41*, 3513–3516. (b) Yamaguchi, K.; Matsushita, M.; Mizuno, N. *Angew. Chem. Int. Ed*. **2004**, *43*, 1576–1580. (c) Ferris, J. P.; Antonucci, F. R. *J. Am. Chem. Soc*. **1972**, *94*, 8091–8092. (d) Himo, F.; Demko, Z. P.; Noodleman, L.; Sharpless, K. B. *J. Am. Chem. Soc*. **2002**, *124*, 12210–12216. (e) Gutmann, B.; Roduit, J.-P.; Roberge, D.; Kappe, C. O. *Angew. Chem. Int. Ed*. **2010**, *49*, 7101–7105. (f) Jiang, X.-b.; Minnaard, A. J.; Feringa, B. L.; Vries, J. G. d. *J. Org. Chem*. **2004**, *69*, 2327–2331.

[13] (a) Gerasimchuk, N.; Goeden, L.; Durham, P.; Barnes, C.; Cannon, J. F.; Silchenko, S.; Hidalgo, I. *Inorg. Chim. Acta.* **2008**, *361*, 1983–2001. (b) El-Faham, A.; Elnakdy, Y. A.; Gazzar, S. A. M. E.; El-Rahman, M. M. A.; Khattab, S. N. *Chem. Pharm. Bull*. **2014**, *62*, 373–378. (c) Soliman, S. M.; Ghabbour, H. A.; Khattab, S. N.; Siddiqui, M. R. H.; El-Faham, A. *J. Chem. Sci.* **2017**, *129*, 1469–1481. (d) Aakeröy, C. B.; Smith, M. M.; Desper, J. *CrystEngComm* 2012, 14, 71–74. (e) Robertson, D.; Cannon, J. F.; Gerasimchuk, N. *Inorg. Chem*. **2005**, *44*, 8326–8342.

[14] (a) Lee, H.-Y.; Lee, L.-W.; Nien, C.-Y.; Kuo, C.-C.; Lin, P.-Y.; Chang, C.-Y.; Chang, J.-Y.; Liou, J.-P. *Org. Biomol. Chem*. **2012**, *10*, 9593–9600. (b) Wu, J. X.; Beck, B.; Ren, R. X. *Tetrahedron Lett.* **2002**, *43*, 387–389. (c) Nauth, A. M.; Opatz, T. *Org. Biomol. Chem*. **2019**, *17*, 11–23. (d) Wang, T.; Jiao, N. *Acc. Chem. Res*. **2014**, *47*, 1137–1145. (e) Khan, N. H.; Agrawal, S.; Kureshy, R. I.; Abdi, S. H. R.; Mayani, V. J.; Jasra, R. V. *Eur. J. Org. Chem*. **2006**, 3175–3180. (f) Ilchenko, N. O.; Janson, P. G.; Szabó, K. J. *J. Org. Chem*. **2013**, *78*, 11087–11091. (g) Jiao, Y.; Chiou, M.-F.; Li, Y.; Bao, H. *ACS Catal*. **2019**, *9*, 5191–5197. (h) Guo, Q.; Wang, M.; Wang, Y.; Xu, Z.; Wang, R. *Chem. Commun*. **2017**, *53*, 12317–12320.

[15] (a) McKinney, R. J.; Roe, D. C. *J. Am. Chem. Soc*. **1986**, *108*, 5167–5173. (b) Bini, L.; Müller, C.; Wilting, J.; Chrzanowski, L. v.; Spek, A. L.; Vogt, D. *J. Am. Chem. Soc*. **2007**, *129*, 12622–12623.

[16] (a) Patil, D. V.; Si, T.; Kim, H. Y.; Oh, K. *Org. Lett*. **2021**, *23*, 3105–3109. (b) Moon, Y.; Park, B.; Kim, I.; Kang, G.; Shin, S.; Kang, D.; Baik, M.-H.; Hong, S. *Nat. Commun*. **2019**, *10*, 4117–4126. (c) Qin, Q.; Han, Y.-Y.; Jiao, Y.-Y.; He, Y.; Yu, S. *Org. Lett*. **2017**, *19*, 2909–2912. (d) Govaerts, S.; Angelini, L.; Hampton, C.; Malet-Sanz, L.; Ruffoni, A.; Leonori, D. *Angew. Chem. Int. Ed*. **2020**, *59*, 15021–15028.

[17] Prateeptongkum, S.; Jovel, I.; Jackstell, R.; Vogl, N.; Weckbecker, C.; Beller, M. *Chem. Commun*. **2009**, 1990–1992.

[18] Shu, Z.; Zhou, Y.; Zhang, Y.; Wang, J. *Org. Chem. Front*. **2014**, *1*, 1123–1127.

[19] Bohle, D. S.; Chua, Z.; Perepichka, I.; Rosadiuk, K. *Chem. Eur. J*. **2013**, *19*, 4223–4229.

[20] Ma, J.-A.; Ma, Z.-H.; Ma, H.-M.; Huang, R.-Q.; Shao, R.-L. *Synth. Commun*, **2000**, *30*, 1563–1567.

[21] Kunai, A.; Doi, T.; Nagaoka, T.; Yagi, H.; Sasaki, K. *Bull. Chem. Soc. Jpn*. **1990**, *63*, 1843–1847.

[22] (a) Dahiya, A.; Sahoo, A. K.; Alam, T.; Patel, B. K. *Chem. Asian J*. **2019**, *14*, 4454–4492. (b) Sau, P.; Santra, S. K.; Rakshit, A.; Patel, B. K. *J. Org. Chem*. **2017**, *82*, 6358–6365. (c) Sau, P.; Rakshit, A.; Modi, A.; Behera, A.; Patel, B. K. *J. Org.*

Chem. **2018**, *83*, 1056–1064. (d) Sau, P.; Rakshit, A.; Alam, T.; Srivastava, H. K.; Patel, B. K. *Org. Lett*. **2019**, *21*, 4966–4970.

[23] (a) Luo, J.; Zhang, J.; *J. Org. Chem.* **2016**, *81*, 9131–9137. (b) Ansari, M. A.; Yadav, D.; Soni, S.; Srivastava, A.; Singh, M. S. *J. Org. Chem*. **2019**, *84*, 5404–5412. (c) Pan, D.; Wang, Y.; Li, M.; Hu, X.; Sun, N.; Jin, L.; Hu, B.; Shen, Z. *Synlett* **2019**, *30*, 218–224. (d) Li, N.; Yan, W.; Yang, P.; Zhang, H.; Wang, Z.; Zheng, J.; Jia, S.; Zhu, Z. *Green Chem*. **2016**, *18*, 6029–6034. (e) Coleman, H. M.; Vimonses, V.; Leslie, G.; Amal, R. *J. of Hazard. Mater*. **2007**, *146*, 496–501.

[24] Wu, X.; Li, K.; Wang, S.; Liu, C.; Lei, A. *Org. Lett*. **2016**, *18*, 56–59.

[25] Gao, D.-W.; Vinogradova, E. V.; Nimmagadda, S. K.; Medina, J. M.; Xiao, Y.; Suciu, R. M.; Cravatt, B. F.; Engle, K. M. *J. Am. Chem.* Soc. **2018**, *140*, 8069–8073.

[26] Israr, M.; Xiong, H.; Li, Y.; Bao, H. *Org. Lett*. **2019**, *21*, 7078-7083.

[27] Qi, L.; Hu, K.; Yu, S.; Zhu, J.; Cheng, T.; Wang, X.; Chen, J.; Wu, H. *Org. Lett*. **2017**, *19*, 218–221.

[28] Zhang, M.; Lin, J.-H.; Xiao, J.-C. *Angew. Chem*. **2019**, *131*, 6140–6144.

II.9. Spectral Data

(Z)-N-Hydroxybenzimidoyl cyanide (1a):

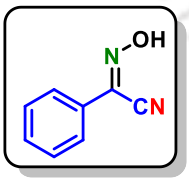

Yield: 61% (22 mg) as a white solid, mp 120–122 °C; ^{1}H NMR ($CDCl_3$, 400 MHz): δ 9.23 (s, 1H), 7.80 (dd, 2H, J_1 = 7.6 Hz, J_2 = 1.2 Hz), 7.48–7.45 (m, 3H); ^{13}C NMR ($CDCl_3$, 100 MHz): δ 134.1, 131.6, 129.3, 129.2, 126.5, 109.4; IR (KBr, cm^{-1}): 3309, 2981, 2242, 1495, 1063, 925; HRMS (ESI/Q-TOF) (m/z): calcd for $C_8H_6N_2O$, $[M + NH_4]^+$: 164.0818, found 164.0824.

(Z)-N-Hydroxy-4-methylbenzimidoyl cyanide (2a):

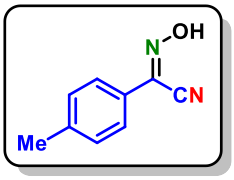

Yield: 65% (26 mg) as a white solid, mp 150–152 °C; ^{1}H NMR ($CDCl_3$, 400 MHz): δ 9.51 (s, 1H), 7.67 (d, 2H, J = 8.0 Hz), 7.25 (d, 2H, J = 8.8 Hz), 2.39 (s, 3H); ^{13}C NMR ($CDCl_3$, 100

MHz): δ 142.1, 134.0, 130.0, 126.6, 126.4, 109.6, 21.7; IR (KBr, cm^{-1}): 3332, 2925, 2239, 1513, 1058, 965; HRMS (ESI/Q-TOF) (m/z): calcd for $C_9H_8N_2O$, $[M + NH_4]^+$: 178.0975, found 178.0979.

(Z)-N-Hydroxy-3-methylbenzimidoyl cyanide (3a):

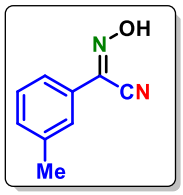

Yield: 62% (25 mg) as a gummy; ^1H NMR ($CDCl_3$, 400 MHz): δ 9.12 (s, 1H), 7.59 (d, 2H, J = 6.8 Hz), 7.36–7.29 (m, 2H), 2.40 (s, 3H); ^{13}C NMR ($CDCl_3$, 100 MHz): δ 139.2, 134.3, 132.4, 129.21, 129.20, 127.0, 123.7, 109.5, 21.6; IR (KBr, cm^{-1}): 3288, 2921, 2232, 1587, 1069, 980; HRMS (ESI/Q-TOF) (m/z): calcd for $C_9H_8N_2O$, $[M + NH_4]^+$: 178.0975, found 178.0988.

(Z)-N-Hydroxy-2-methylbenzimidoyl cyanide (4a):

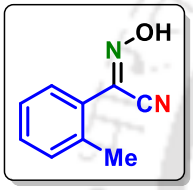

Yield: 59% (23 mg) as a gummy; ^1H NMR ($CDCl_3$, 400 MHz): δ 7.46–7.44 (m, 1H), 7.29–7.27 (m, 1H), 7.22–7.18 (m, 2H) 2.42 (s, 3H); ^{13}C NMR ($CDCl_3$, 100 MHz): δ 137.5, 134.4, 131.9, 130.9, 129.8, 128.5, 126.6, 110.1, 21.4; IR (KBr, cm^{-1}): 3263, 2926, 2227, 1455, 1043, 964; HRMS (ESI/Q-TOF) (m/z): calcd for $C_9H_8N_2O$, $[M + NH_4]^+$: 178.0975, found 178.0982.

(Z)-4-(tert-Butyl)-N-hydroxybenzimidoyl cyanide (5a):

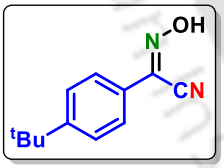

Yield: 67% (34 mg) as a white solid, mp 158–160 °C; ^1H NMR ($CDCl_3$, 400 MHz): δ 8.97 (s, 1H), 7.72 (d, 2H, J = 8.4 Hz), 7.47 (d, 2H, J = 8.4 Hz), 1.34 (s, 9H); ^{13}C NMR ($CDCl_3$, 100 MHz): δ 155.1, 133.9, 126.3, 126.1, 126.0, 109.3, 35.0, 31.1; IR (KBr, cm^{-1}): 3317, 2962, 2237, 1463, 1060, 966; HRMS (ESI/Q-TOF) (m/z): calcd for $C_{12}H_{14}N_2O$, $[M + H]^+$: 203.1179, found 203.1188.

(Z)-N-Hydroxy-4-methoxybenzimidoyl cyanide (6a):

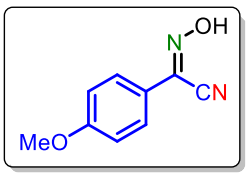

Yield: 69% (30 mg) as a white solid, mp 72–74 °C; ^1H NMR ($CDCl_3$, 400 MHz): δ 7.73 (d, 2H, J = 8.8 Hz), 6.96 (d, 2H, J = 8.8 Hz), 3.86 (s, 3H); ^{13}C NMR ($CDCl_3$, 100 MHz): δ 162.1, 133.5, 127.9, 121.7, 114.5, 109.4, 55.5; IR (KBr, cm^{-1}): 3326, 2843, 2235, 1606, 1062, 966; HRMS (ESI/Q-TOF) (m/z): calcd for $C_9H_8N_2O_2$, $[M + H]^+$: 177.0659, found 177.0657.

(Z)-4-(Chloromethyl)-N-hydroxybenzimidoyl cyanide (7a):

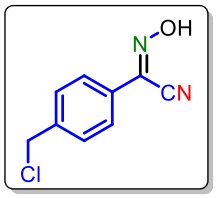

Yield: 63% (31 mg) as a gummy; ^{1}H NMR ($CDCl_3$, 400 MHz): δ 9.23 (s, 1H), 7.79 (d, 2H, J = 8.4 Hz), 7.48 (d, 2H, J = 8.0 Hz), 4.60 (s, 2H); ^{13}C NMR ($CDCl_3$, 100 MHz): δ 141.0, 133.5, 129.4, 129.3, 126.9, 109.3, 45.5; IR (KBr, cm^{-1}): 3291, 2962, 2234, 1565, 1063, 969; HRMS (ESI/Q-TOF) (m/z): calcd for $C_9H_7ClN_2O$, $[M + NH_4]^+$: 212.0585, found 212.0590.

(Z)-4-Fluoro-N-hydroxybenzimidoyl cyanide (8a):

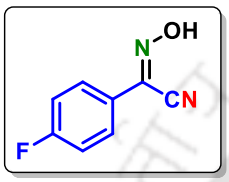

Yield: 60% (25 mg) as a white solid, mp 112–114 ^{o}C; ^{1}H NMR ($CDCl_3$, 400 MHz): δ 9.49 (s, 1H), 7.80–7.77 (m, 2H), 7.14 (t, 2H, J = 8.6 Hz); ^{13}C NMR ($CDCl_3$, 100 MHz): δ 166.4, 163.9, 133.3, 128.9 (d, J = 8.7 Hz), 126.0 (d, J = 3.4 Hz), 117.0 (d, J = 22.2 Hz), 109.8; ^{19}F NMR ($CDCl_3$, 377 MHz): δ –107.7 (s); IR (KBr, cm^{-1}): 3307, 2922, 2233, 1511, 1062, 969; HRMS (ESI/Q-TOF) (m/z): calcd for $C_8H_5FN_2O$, $[M + H]^+$: 165.0459, found 165.0486.

(Z)-3-Fluoro-N-hydroxybenzimidoyl cyanide (9a):

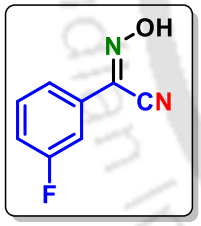

Yield: 58% (24 mg) as a white solid, mp 120–122 ^{o}C; ^{1}H NMR ($CDCl_3$, 400 MHz): δ 9.29 (s, 1H) 7.59–7.54 (m, 1H), 7.53–7.51 (m, 1H), 7.47–7.41 (m, 1H), 7.22–7.17 (m, 1H); ^{13}C NMR ($CDCl_3$, 100 MHz): δ 164.1, 161.6, 132.9, 131.2 (d, J = 8.3 Hz), 130.8 (d, J = 8.3 Hz), 122.4 (d, J = 3.1 Hz), 118.5 (d, J = 21.3 Hz), 112.9 (d, J = 24.2 Hz), 108.9; ^{19}F NMR ($CDCl_3$, 377 MHz): δ –111.1 (s); IR (KBr, cm^{-1}): 3288, 2843, 2245, 1575, 1061, 868; HRMS (ESI/Q-TOF) (m/z): calcd for $C_8H_5FN_2O$, $[M + H]^+$: 165.0459, found 165.0479.

(Z)-4-Chloro-N-hydroxybenzimidoyl cyanide (10a):

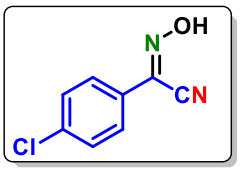

Yield: 59% (27 mg) as a white solid, mp 139–141 ^{o}C; ^{1}H NMR ($CDCl_3$, 400 MHz): δ 9.23 (s, 1H), 7.74 (dd, 2H, J_1 = 6.8 Hz, J_2 = 2.0 Hz), 7.43 (dd, 2H, J_1 = 6.8 Hz, J_2 = 1.6 Hz); ^{13}C NMR ($CDCl_3$, 100 MHz): δ 137.6, 132.9, 129.4, 127.6, 127.5, 108.9; IR (KBr, cm^{-1}): 3133, 2922, 2231, 1595, 1064, 968; HRMS (ESI/Q-TOF) (m/z): calcd for $C_8H_5ClN_2O$, $[M + NH_4]^+$: 198.0429, found 198.0440.

(Z)-3-Chloro-N-hydroxybenzimidoyl cyanide (11a):

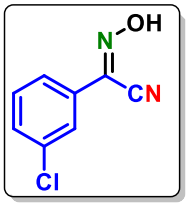

Yield: 55% (25 mg) as a gummy; ^{1}H NMR ($CDCl_3$, 400 MHz): δ 9.24 (s, 1H), 7.81 (d, 1H, J = 1.6 Hz), 7.68 (d, 1H, J = 7.6 Hz), 7.52–7.38 (m, 2H); ^{13}C NMR ($CDCl_3$, 100 MHz): δ 135.3, 132.8, 131.4, 130.8, 130.3, 126.0, 124.6, 108.8; IR (KBr, cm^{-1}): 3295, 2919, 2240, 1597, 1061, 988; HRMS (ESI/Q-TOF) (m/z): calcd for $C_8H_5ClN_2O$, $[M + NH_4]^+$: 198.0429, found 198.0439.

(Z)-2-Chloro-N-hydroxybenzimidoyl cyanide (12a):

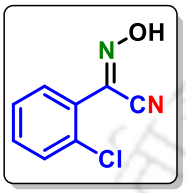

Yield: 52% (23 mg) as a gummy; ^{1}H NMR ($CDCl_3$, 400 MHz): δ 9.43 (s, 1H), 7.53–7.46 (m, 3H), 7.45–7.36 (m, 1H); ^{13}C NMR ($CDCl_3$, 100 MHz): δ 133.6, 132.36, 132.33, 131.2, 130.9, 128.4, 127.5, 109.2; IR (KBr, cm^{-1}): 3135, 2919, 2232, 1591, 1087, 972; HRMS (ESI/Q-TOF) (m/z): calcd for $C_8H_5ClN_2O$, $[M + NH_4]^+$: 198.0429, found 198.0446.

(Z)-4-Bromo-N-hydroxybenzimidoyl cyanide (13a):

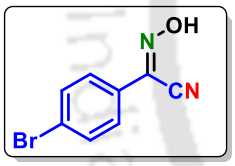

Yield: 57% (32 mg) as a white solid, mp 123–125 °C; ^{1}H NMR ($CDCl_3$, 400 MHz): δ 9.31 (s, 1H), 7.67 (dd, 2H, J_1 = 6.8 Hz, J_2 = 2.0 Hz), 7.59 (dd, 2H, J_1 = 6.8 Hz, J_2 = 2.0 Hz); ^{13}C NMR ($CDCl_3$, 100 MHz): δ 133.0, 132.4, 128.1, 127.6, 125.9, 108.9; IR (KBr, cm^{-1}): 3295, 2922, 2233, 1589, 1061, 966; HRMS (ESI/Q-TOF) (m/z): calcd for $C_8H_5BrN_2O$, $[M + NH_4]^+$: 241.9924, found 241.9932.

(Z)-N-Hydroxy-3-nitrobenzimidoyl cyanide (14a):

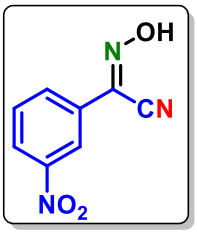

Yield: 48% (23 mg) as a white solid, mp 63–65 °C; ^{1}H NMR ($CDCl_3$, 400 MHz): δ 8.68 (s, 1H), 8.34 (d, 1H, J = 8.4 Hz), 8.12 (d, 1H, J = 7.6 Hz), 7.69 (t, 1H, J = 8.0 Hz); ^{13}C NMR ($CDCl_3$, 100 MHz): δ 148.7, 131.9, 131.8, 131.0, 130.3, 125.6, 120.9, 108.6; IR (KBr, cm^{-1}): 3296, 2922, 2333, 1527, 1075, 807; HRMS (ESI/Q-TOF) (m/z): calcd for $C_8H_5N_3O_3$, $[M + NH_4]^+$: 209.0669, found 209.0677.

(Z)-N-hydroxy-2,4,6-trimethylbenzimidoyl cyanide (15a):

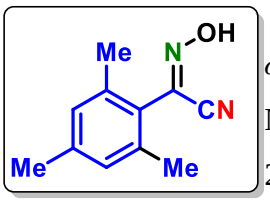

Yield: 51% (24 mg) as a gummy; ^{1}H NMR ($CDCl_3$, 400 MHz): δ 6.92 (d, 2H, J = 2.8 Hz), 2.30 (s, 3H), 2.27 (s, 3H), 2.24 (s, 3H); ^{13}C NMR ($CDCl_3$, 100 MHz): δ 140.5, 137.7, 135.9, 128.9, 128.6, 114.3, 21.2, 19.7, 19.4; IR (KBr, cm^{-1}): 2920, 2855, 1611, 1034, 940; HRMS (ESI/Q-TOF) (m/z): calcd for $C_{11}H_{12}N_2O$, $[M + NH_4]^+$: 206.1288, found 206.1293.

(Z)-N-Hydroxy-2,4-dimethylbenzimidoyl cyanide (16a):

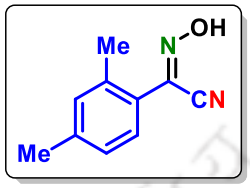

Yield: 56% (24 mg) as a gummy; ^{1}H NMR ($CDCl_3$, 400 MHz): δ 7.43 (d, 1H, J = 8.0 Hz), 7.09 (d, 2H, J = 7.6 Hz), 2.45 (s, 3H), 2.35 (s, 3H); ^{13}C NMR ($CDCl_3$, 100 MHz): δ 141.0, 137.1, 134.3, 132.5, 129.6, 127.1, 125.4, 109.9, 21.3, 21.2; IR (KBr, cm^{-1}): 3312, 2966, 2232, 1612, 1046, 967; HRMS (ESI/Q-TOF) (m/z): calcd for $C_{10}H_{10}N_2O$, $[M + H]^+$: 175.0866, found 175.0872.

(Z)-4-(Benzyloxy)-N-hydroxy-3-methoxybenzimidoyl cyanide (17a):

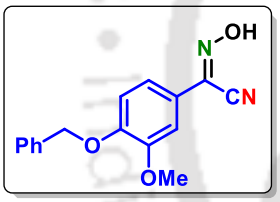

Yield: 62% (44 mg) as a white solid, mp 79–81 ^{o}C; ^{1}H NMR ($CDCl_3$, 400 MHz): δ 9.21 (s, 1H), 7.34–7.28 (m, 4H), 7.22–7.16 (m, 3H), 6.82 (d, 1H, J = 8.4 Hz), 5.11 (s, 2H), 3.81 (s, 3H); ^{13}C NMR ($CDCl_3$, 100 MHz): δ 150.9, 149.9, 136.2, 133.4, 128.7, 128.2, 127.3, 122.3, 120.6, 113.1, 109.4, 108.1, 70.9, 56.1; IR (KBr, cm^{-1}): 2919, 2224, 1510, 1029, 808; HRMS (ESI/Q-TOF) (m/z): calcd for $C_{16}H_{14}N_2O_3$, $[M + Na]^+$: 305.0897, found 305.0902.

(Z)-N-Hydroxy-[1,1'-biphenyl]-4-carbimidoyl cyanide (18a):

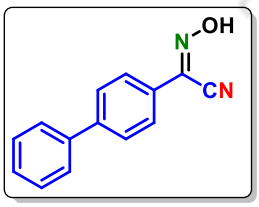

Yield: 71% (39 mg) as a white solid, mp 141–143 ^{o}C; ^{1}H NMR ($CDCl_3$, 400 MHz): δ 7.74–7.68 (m, 4H), 7.61–7.58 (m, 2H), 7.51–7.47 (m, 2H), 7.45–7.41 (m, 1H); ^{13}C NMR ($CDCl_3$, 100 MHz): δ 145.9, 139.4, 132.8, 129.3, 128.9, 128.2, 127.9, 127.4, 119.1, 111.1; IR (KBr, cm^{-1}): 3031, 2963, 2225, 1605, 1037, 841; HRMS (ESI/Q-TOF) (m/z): calcd for $C_{14}H_{10}N_2O$, $[M + H]^+$: 223.0866, found 223.1008.

(Z)-4'-(tert-Butyl)-N-hydroxy-[1,1'-biphenyl]-4-carbimidoyl cyanide (19a):

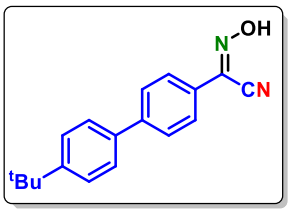

Yield: 70% (49 mg) as a white solid, mp 178–180 °C; ^{1}H NMR ($CDCl_3$, 400 MHz): δ 9.23 (s, 1H), 7.86 (d, 2H, J = 8.4 Hz), 7.68 (d, 2H, J = 8.8 Hz), 7.57 (d, 2H, J = 8.8 Hz), 7.50 (d, 2H, J = 8.4 Hz), 1.37 (s, 9H); ^{13}C NMR ($CDCl_3$, 100 MHz): δ 152.0, 144.7, 137.4, 134.4, 130.9, 128.1, 127.4, 127.3, 126.6, 109.9, 35.3, 31.9; IR (KBr, cm^{-1}): 3319, 2921, 2237, 1606, 1064, 849; HRMS (ESI/Q-TOF) (m/z): calcd for $C_{18}H_{18}N_2O$, $[M + H]^+$: 279.1492, found 279.1494.

(Z)-4'-Fluoro-N-hydroxy-[1,1'-biphenyl]-4-carbimidoyl cyanide (20a):

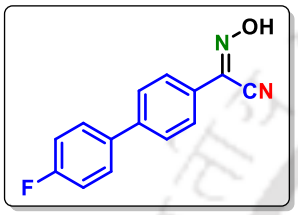

Yield: 69% (41 mg) as a white solid, mp 135–137 °C; ^{1}H NMR ($CDCl_3$, 400 MHz): δ 9.13 (s, 1H), 7.86 (d, 2H, J = 8.4 Hz), 7.64–7.56 (m, 4H), 7.16 (t, 2H, J = 8.6 Hz); ^{13}C NMR ($CDCl_3$, 100 MHz): δ 164.8, 162.4, 143.8, 136.5, 134.2, 129.4 (d, J = 8.1 Hz), 128.7, 128.2 127.4, 116.6 (d, J = 21.4 Hz), 109.8; ^{19}F NMR ($CDCl_3$, 377 MHz): δ –114.1 (s); IR (KBr, cm^{-1}): 3106, 2922, 1603, 1098, 815; HRMS (ESI/Q-TOF) (m/z): calcd for $C_{14}H_9FN_2O$, $[M + NH_4]^+$: 258.1037, found 258.1037.

(Z)-4'-Chloro-N-hydroxy-[1,1'-biphenyl]-4-carbimidoyl cyanide (21a):

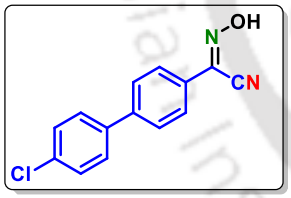

Yield: 63% (40 mg) as a white solid, mp 137–139 °C; ^{1}H NMR ($CDCl_3$, 400 MHz): δ 9.26 (s, 1H), 7.87 (d, 2H, J = 8.4 Hz), 7.63 (d, 2H, J = 8.4 Hz), 7.54 (d, 2H, J = 8.4 Hz), 7.44 (d, 2H, J = 8.4 Hz); ^{13}C NMR ($CDCl_3$, 100 MHz): δ 143.1, 138.4, 134.6, 133.8, 130.6, 129.4, 128.6, 127.8, 127.1, 109.4; IR (KBr, cm^{-1}): 2923, 2219, 1664, 1095, 822; HRMS (ESI/Q-TOF) (m/z): calcd for $C_{14}H_9ClN_2O$, $[M + H]^+$: 257.0476, found 257.0480.

(Z)-N-Hydroxy-4'-methoxy-3'-methyl-[1,1'-biphenyl]-4-carbimidoyl cyanide (22a):

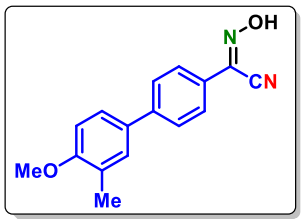

Yield: 70% (46 mg) as a white solid, mp 113–115 °C; ^{1}H NMR ($CDCl_3$, 400 MHz): δ 9.37 (s, 1H), 7.96 (dd, 2H, J_1 = 8.4 Hz, J_2 = 8.4 Hz), 7.63 (d, 2H, J = 8.4 Hz), 7.42 (d, 2H, J = 8.4 Hz), 6.91 (d, 1H, J = 8.0 Hz), 3.89 (s, 3H) 2.29 (s, 3H); ^{13}C NMR ($CDCl_3$, 100 MHz): δ 158.7, 144.6, 134.4, 132.3, 130.9, 129.9, 127.9, 127.8, 127.7, 127.3, 126.1, 110.9, 56.1, 17.0; IR (KBr, cm^{-1}): 3306, 2959, 2232, 1604,

1066, 968; HRMS (ESI/Q-TOF) (m/z): calcd for $C_{16}H_{14}N_2O_2$, [M + H]$^+$: 267.1128, found 267.1129.

(Z)-2-(Hydroxyimino)-2-(p-tolyl)acetic acid (2b):

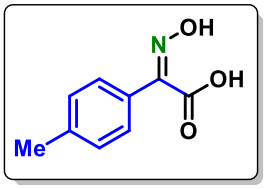

Yield: 55% (25 mg) as a white solid, mp 176–178 °C; ^{1}H NMR ($CDCl_3$, 400 MHz): δ 7.93 (d, 2H, J = 8.4 Hz), 7.19 (d, 2H, J = 8.0 Hz), 2.35 (s, 3H); ^{13}C NMR ($CDCl_3$, 100 MHz): δ 173.1, 145.3, 130.9, 129.8, 127.2, 22.4; IR (KBr, cm^{-1}): 2919, 2549, 1670, 1283, 1117, 840; HRMS (ESI/Q-TOF) (m/z): calcd for $C_9H_9NO_3$, [M + H]$^+$: 180.0655, found 180.0660.

(Z)-2-(Hydroxyimino)-2-(p-tolyl)acetamide (2c):

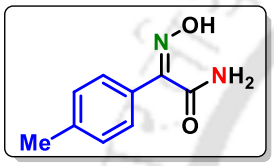

Yield: 61% (27 mg) as a white solid, mp 174–176 °C; ^{1}H NMR (DMSO-d_6, 400 MHz): δ 11.31 (s, 1H), 7.90 (s, 1H), 7.68 (s, 1H), 7.44 (d, 2H, J = 8.0 Hz), 7.22 (d, 2H, J = 8.0 Hz), 2.31 (s, 3H); ^{13}C NMR (DMSO-d_6, 100 MHz): δ 166.1, 153.4, 139.4, 129.9, 129.6, 126.1, 21.3; IR (KBr, cm^{-1}): 2923, 2859, 1672, 1186, 969, 756; HRMS (ESI/Q-TOF) (m/z): calcd for $C_9H_{10}N_2O_2$, [M + H]$^+$: 179.0815, found 179.0838.

1-Phenyl-2-(p-tolyl)ethane-1,2-dione (2d):

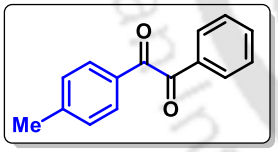

Yield: 66% (37 mg) as a gummy; ^{1}H NMR ($CDCl_3$, 400 MHz): δ, 7.89–7.87 (m, 2H), 7.78 (d, 2H, J = 8.0 Hz), 7.56 (t, 1H, J = 7.4 Hz), 7.42 (t, 2H, J = 7.8 Hz), 7.22 (d, 2H, J = 8.4 Hz), 2.35 (s, 3H); ^{13}C NMR ($CDCl_3$, 100 MHz): δ 194.8, 194.3, 146.2, 134.8, 133.1, 130.6, 130.0, 129.9, 129.7, 129.0, 21.9; IR (KBr, cm^{-1}): 2923, 1667, 1603, 1214, 1173; HRMS (ESI/Q-TOF) (m/z): calcd for $C_{15}H_{12}O_2$, [M + H]$^+$: 225.0910, found 225.0915.

(Z)-(1H-Tetrazol-5-yl)(p-tolyl)methanone oxime (2e):

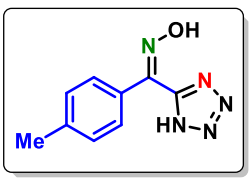

Yield: 52% (26 mg) as a white solid, mp 210–212 °C; ^{1}H NMR (DMSO-d_6, 400 MHz): δ 12.9 (s, 1H), 7.44 (d, 2H, J = 8.4 Hz), 7.24 (d, 2H, J = 8.0 Hz), 2.32 (s, 3H); ^{13}C NMR (DMSO-d_6, 100 MHz): δ 147.3, 143.2, 139.9, 130.9 129.6, 127.6, 21.3; IR (KBr, cm^{-1}): 2923,

2855, 1719, 1607, 1456, 1183, 989, 821; HRMS (ESI/Q-TOF) (m/z): calcd for $C_9H_9N_5O$, $[M + H]^+$: 204.0880, found 204.0889.

II.10. Representative Spectra

(Z)-N-Hydroxybenzimidoyl cyanide (1a): **^{1}H NMR ($CDCl_3$, 400 MHz)**

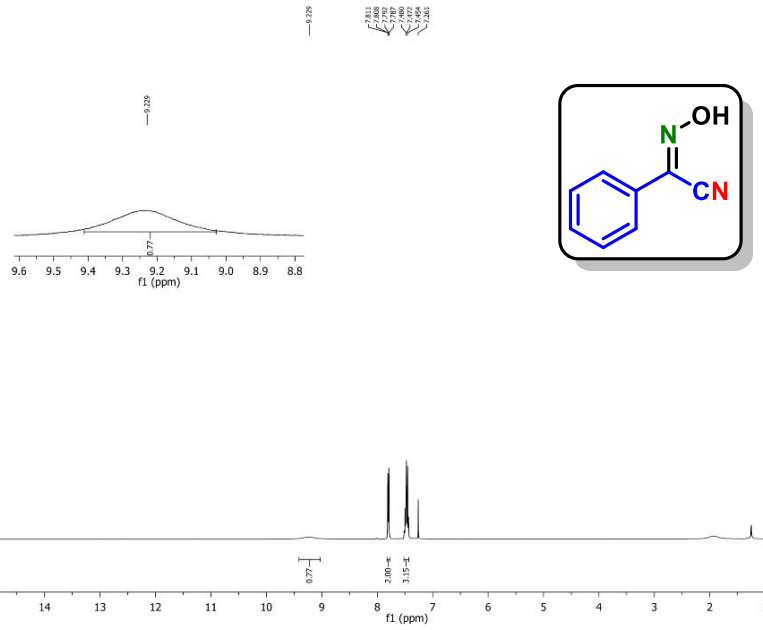

(Z)-N-Hydroxybenzimidoyl cyanide (1az): **^{13}C{^{1}H} NMR ($CDCl_3$, 100 MHz)**

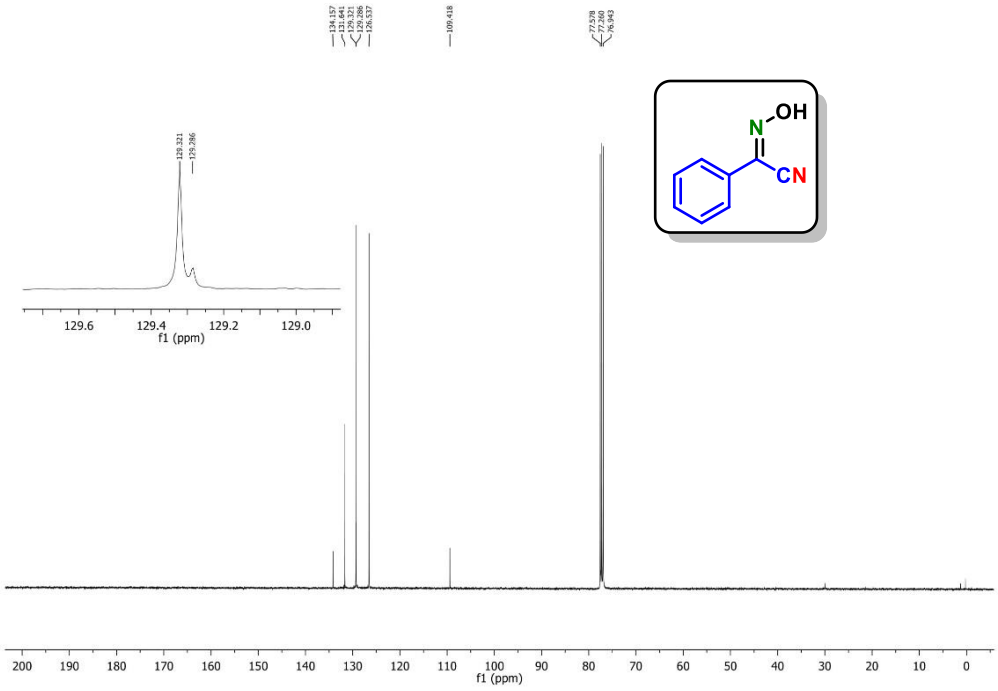

***(Z)-N-Hydroxy-4-methylbenzimidoyl cyanide (2a)*:^{1}H NMR ($CDCl_3$, 400 MHz)**

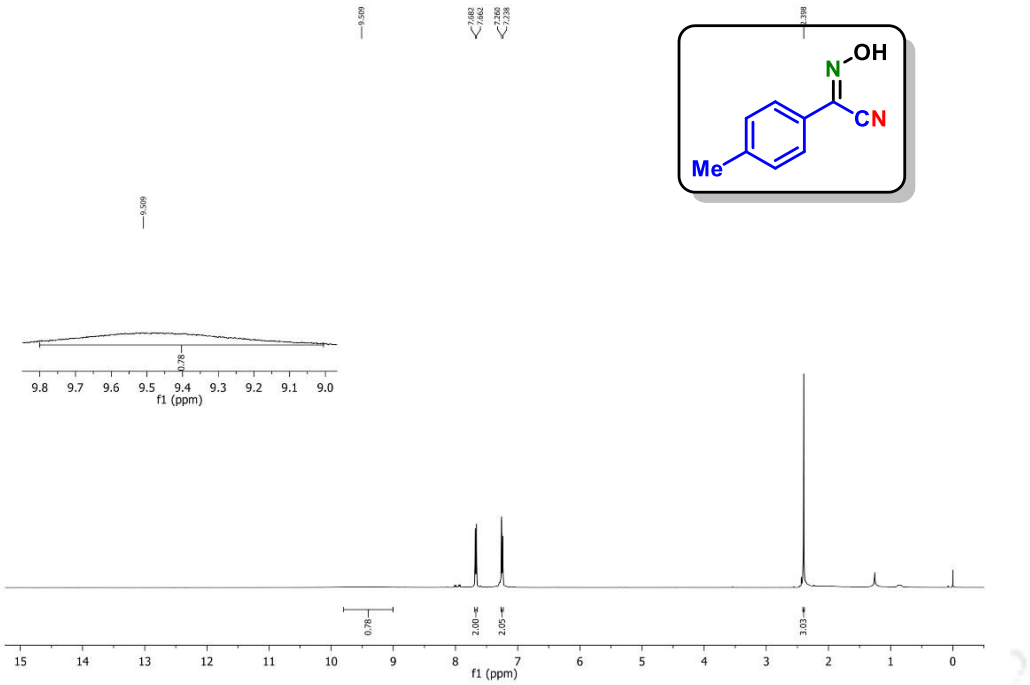

***(Z)-N-Hydroxy-4-methylbenzimidoyl cyanide (2a)*:^{13}C{^{1}H} NMR ($CDCl_3$, 100 MHz)**

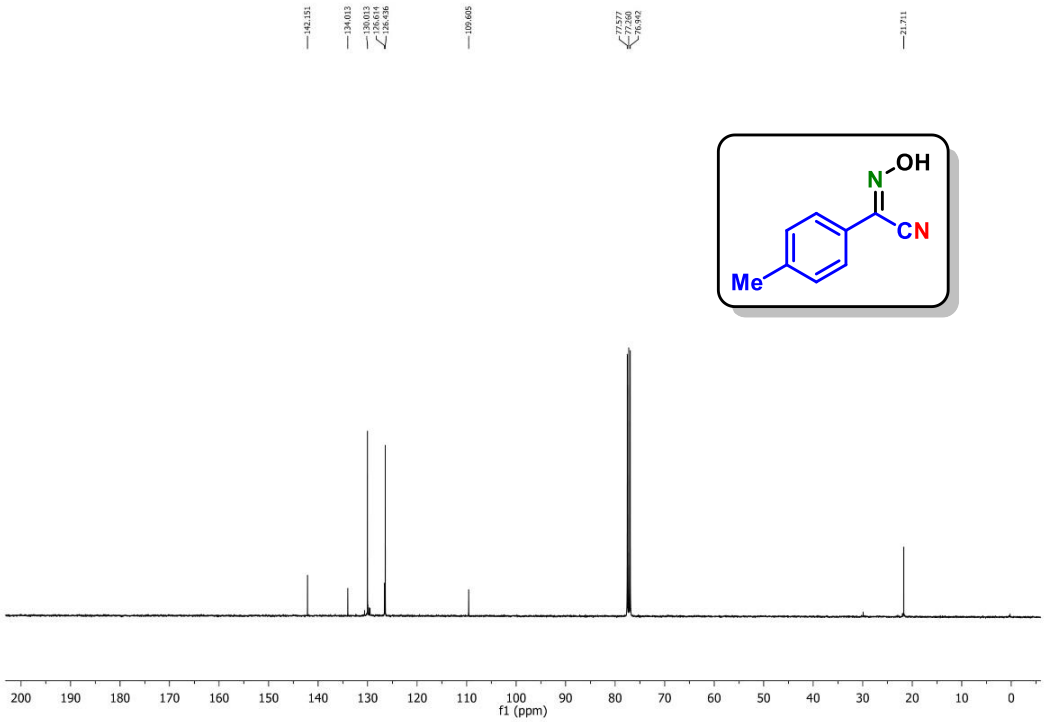

(Z)-4-(Chloromethyl)-N-hydroxybenzimidoyl cyanide (7a): **^{1}H NMR ($CDCl_3$, 400 MHz)**

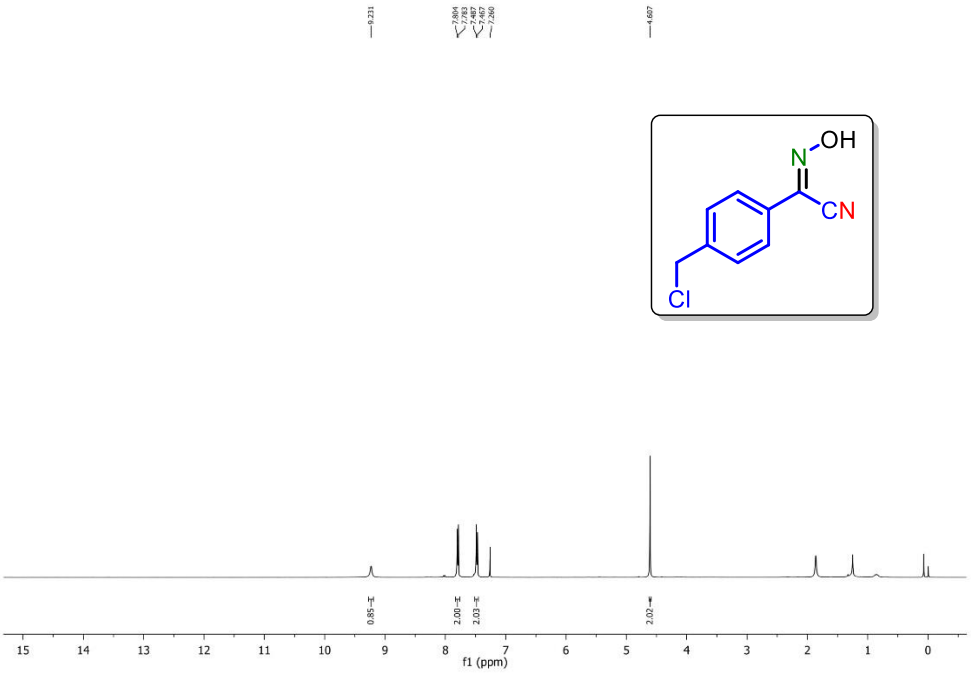

(Z)-4-(Chloromethyl)-N-hydroxybenzimidoyl cyanide (7a): **^{13}C{^{1}H} NMR ($CDCl_3$, 100 MHz)**

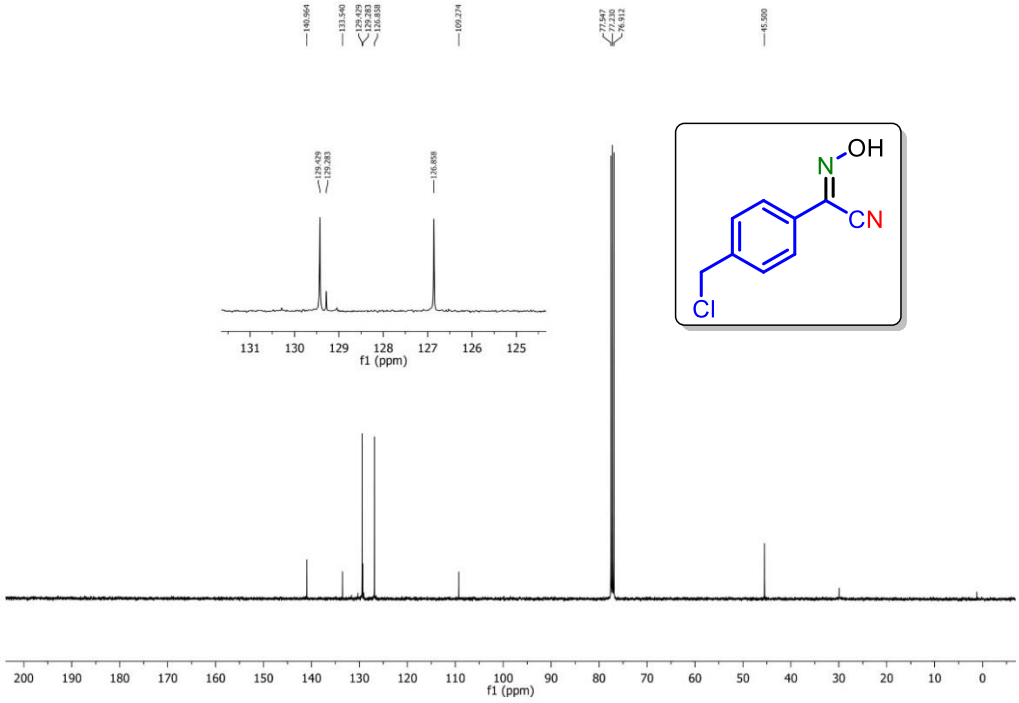

***(Z)-4-Chloro-N-hydroxybenzimidoyl cyanide (10a)*: ^{1}H NMR ($CDCl_3$, 400 MHz)**

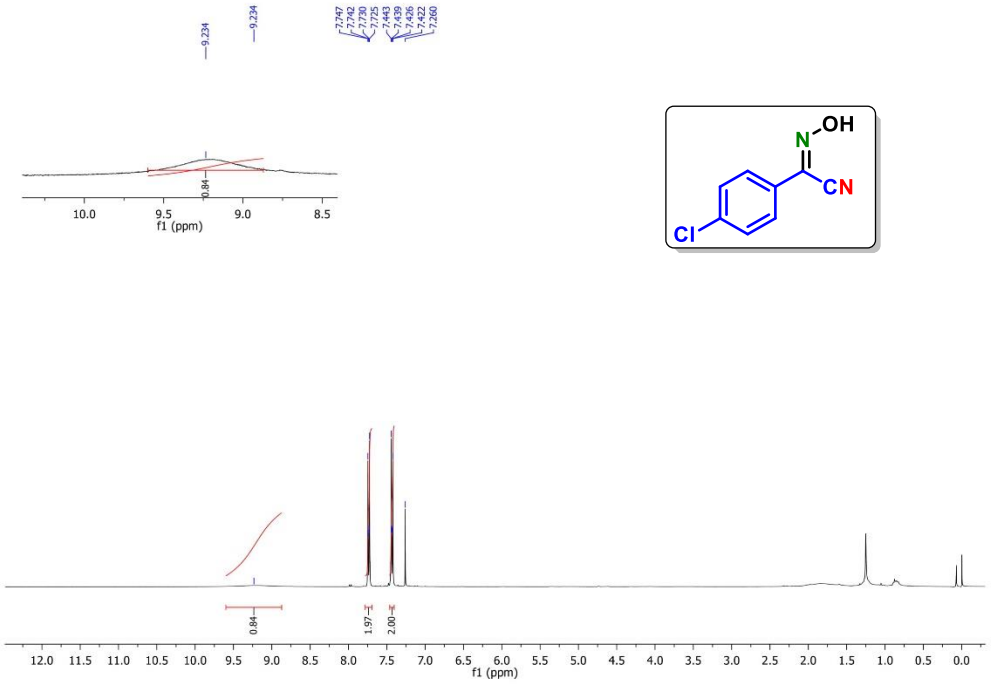

***(Z)-4-Chloro-N-hydroxybenzimidoyl cyanide (10a)*: ^{13}C{^{1}H} NMR ($CDCl_3$, 100 MHz)**

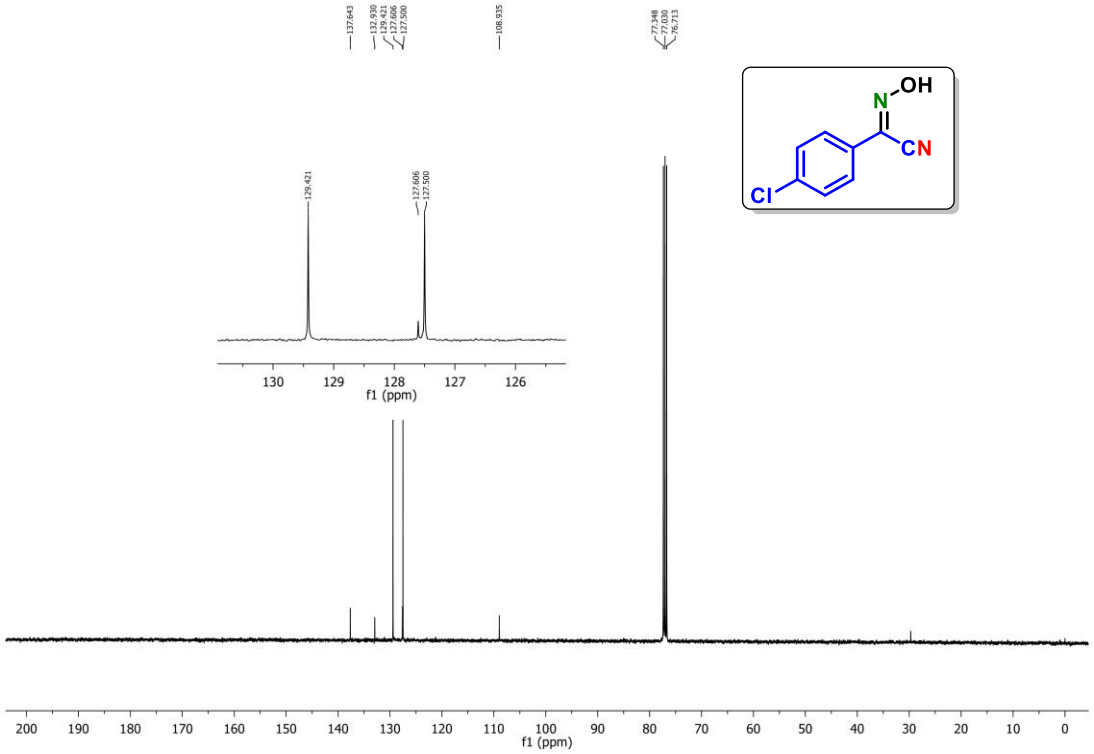

***(Z)-N-Hydroxy-3-nitrobenzimidoyl cyanide (14a)*: ^{1}H NMR ($CDCl_3$, 400 MHz)**

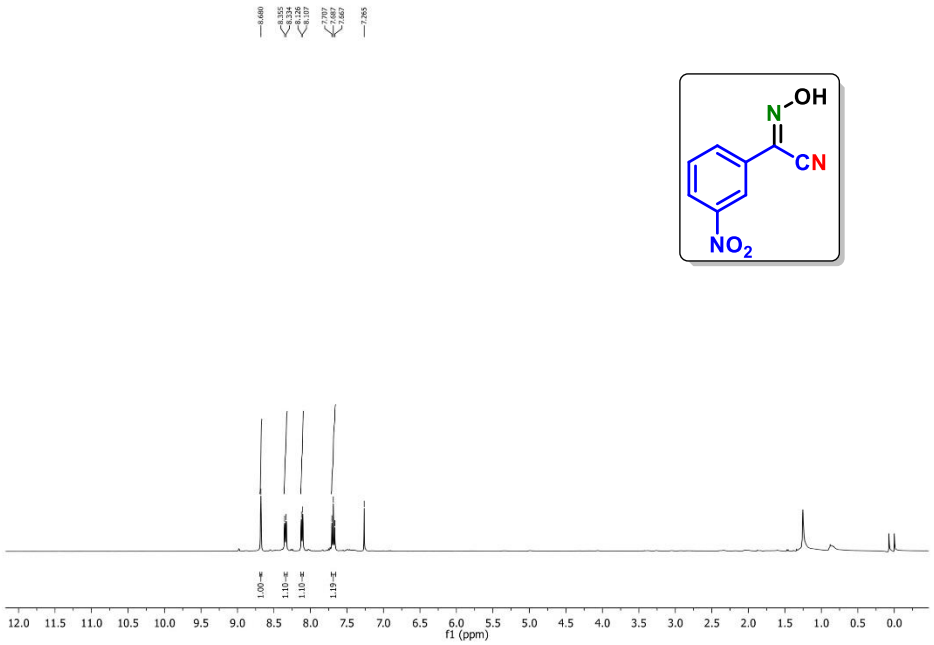

***(Z)-N-Hydroxy-3-nitrobenzimidoyl cyanide (14a)*: ^{13}C{^{1}H} NMR ($CDCl_3$, 100 MHz)**

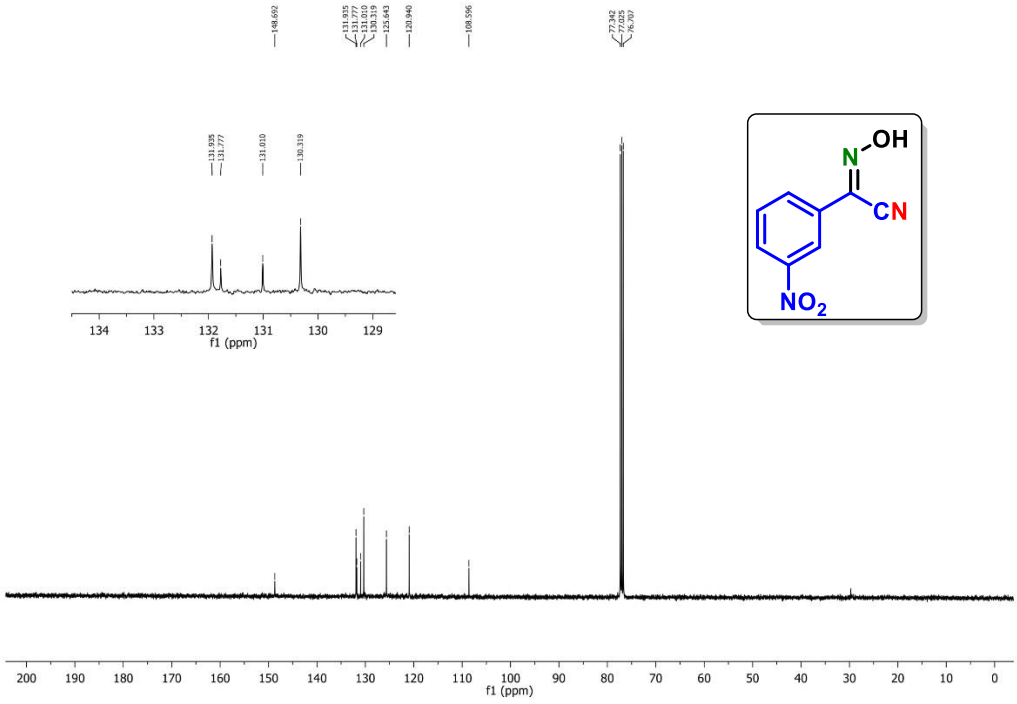

***(Z)-4'-(tert-Butyl)-N-hydroxy-[1,1'-biphenyl]-4-carbimidoyl cyanide (19a)*: ^{1}H NMR (CDCl$_3$, 400 MHz)**

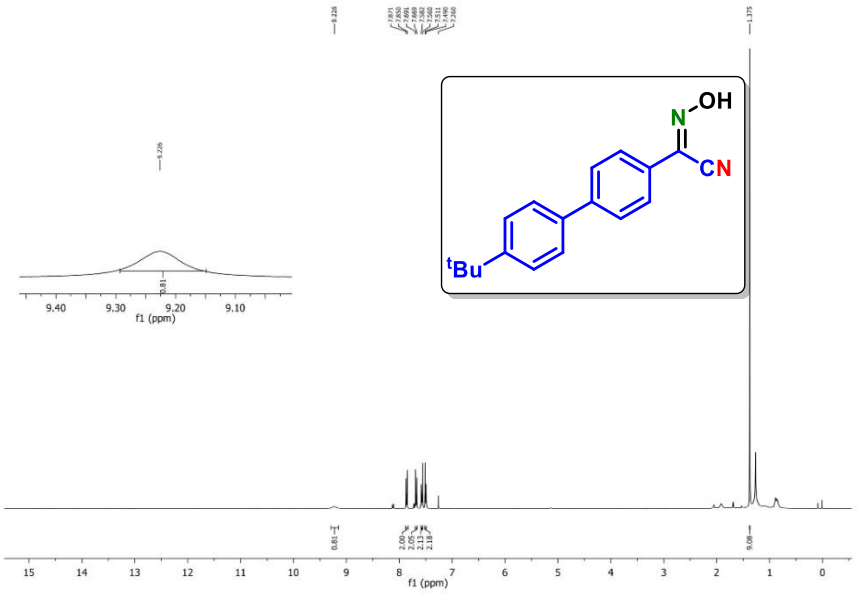

***Z)-4'-(tert-Butyl)-N-hydroxy-[1,1'-biphenyl]-4-carbimidoyl cyanide (19a)*: ^{13}C{^{1}H} NMR (CDCl$_3$, 100 MHz)**

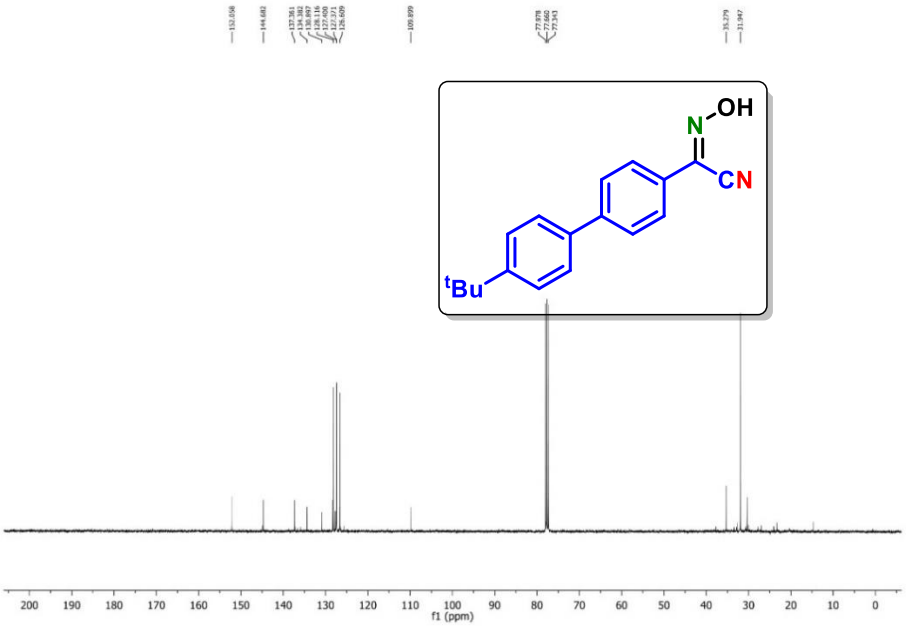

CHAPTER-III

Visible-Light-Mediated Ir(III)-Catalyzed Concomitant C3-Oxidation and C2-Amination of Indoles

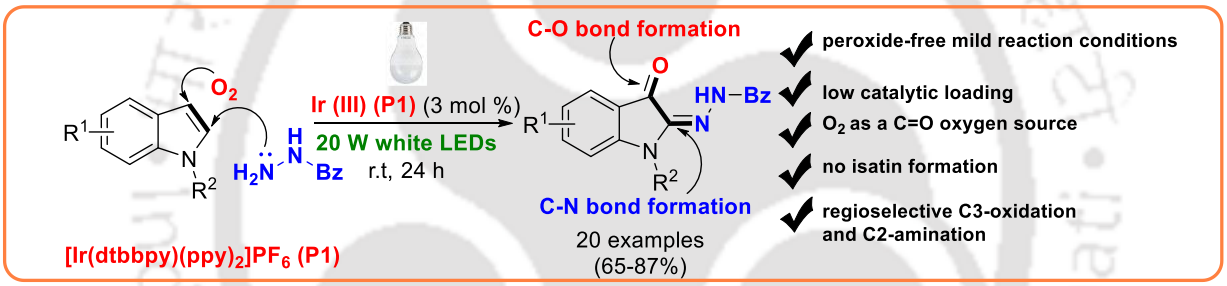

OL | Organic Letters
pubs.acs.org/OrgLett
Org. Lett. **2019**, *21*, 3543–3547
Letter

Abstract: *A visible-light-mediated concomitant C3 oxidation and C2 amination of indoles have been achieved at room temperature using an Ir (III) photocatalyst. This reaction proceeds without an isatin intermediate via the attack of a singlet oxygen at the C3 position followed by C2 amination leading to difunctionalization of indoles.*

CHAPTER III

Visible-Light-Mediated Ir(III)-Catalyzed Concomitant C3-Oxidation and C2-Amination of Indoles

III.1. Introduction

Recently, photocatalytic functionalizations have emerged as powerful synthetic tools in modern organic chemistry/synthesis.[1] Compared to traditional functionalizations, the photocatalytic strategy has emerged as an alternative method for rapidly constructing highly functionalized structures by amplifying their chemical diversity.[2] In particular, the photocatalytic functionalizations of indoles have attracted considerable attention since functionalized indole motifs have found significant applications in biological and medicinal chemistry and are present in various natural and artificial bioactive products (Figure III.1).[3]

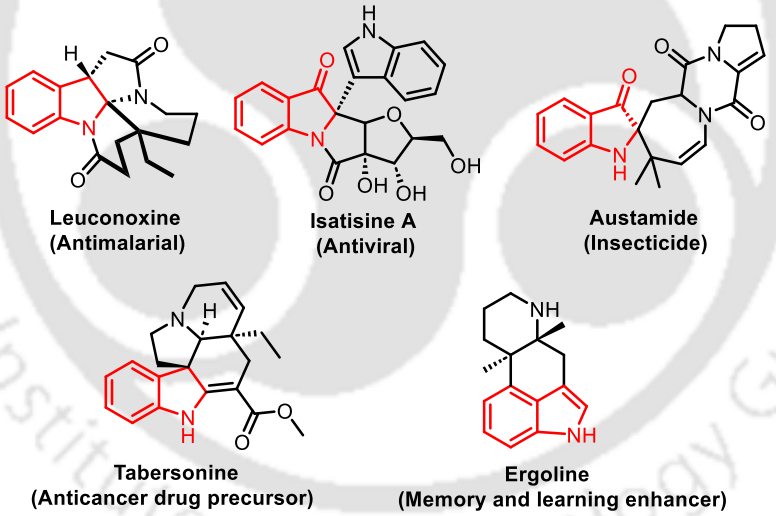

Figure III.1. *Representative bioactive products containing functionalized indoles.*

III.2. Ideas Toward the Synthesis of 2,3-Difunctionalization of Indoles

In 2013, Ji's group demonstrated the I_2/TBHP-catalyzed chemoselective amination of indoles. This method offers several benefits, including utilizing an aqueous medium, tolerance

to air, cost-effectiveness, low toxicity, and environmental friendliness. This reaction applies to the production of tryptanthrin, a compound prevalent in various plant species (Scheme III.1).[4a]

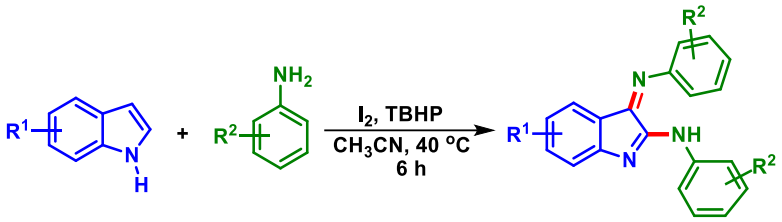

Scheme III.1. *Synthesis of amination of indoles derivatives.*

In 2018, Jiang's group presented an efficient and cost-effective protocol for a copper-mediated aerobic oxidative of C–H iodination and nitration of indoles. This process was conducted smoothly under mild aerobic conditions, enabling the direct synthesis of 3-iodo-2-nitroindoles in a single step. The reaction exhibited high regioselectivity and displayed a broad substrate scope, underscoring its versatility for diverse indole derivatives (Scheme III.2).[4b]

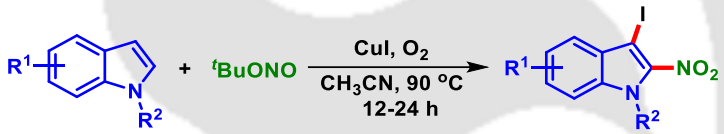

Scheme III.2. *Synthesis of iodination and nitration of indole derivatives.*

Ji group reported a visible-light-mediated synthesis of 2-azidoindolin-3-yl 2-aminobenzoates *via* dearomatization/ring-opening cascade reaction of indole. Here, the photocatalyst played the driving force and triethylamine in the ring-opening step. This reaction features mild conditions and controllable multi-step reactions, providing a new route for the construction of indoline skeletons (Scheme III.3).[4c]

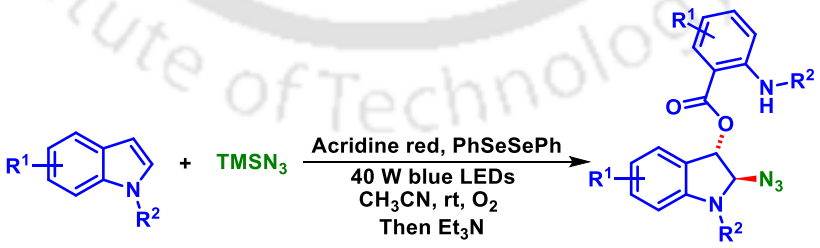

Scheme III.3. *Synthesis of 2-azidoindolin-3-yl 2-aminobenzoates derivatives.*

Among significant photocatalytic reactions of indoles, in 2017, Yoon *et al.* reported a Diels–Alder cycloaddition with dienes leading to tetrahydro-1,4-ethanocarbazoles.[5] A chemo divergent oxygenation of indole to isatins and formylformanilides under visible-light photocatalysis has been developed by Jiang *et al.*[6] The Stephenson reported an efficient addition of malonyl radicals to indoles under Ru-photocatalysis.[7] To the best of our knowledge, there is no photocatalytic functionalization of indoles leading to selective C3 oxidation and C2 amination. Our group is actively involved in the design and development of operationally simple and efficient methodologies for the functionalizations of various heterocycles.[8] Herein, we report a visible-light mediated protocol for the selective difunctionalization of *N*-substituted indoles using benzo hydrzides in an oxygen atmosphere leading to concurrent C3 oxidation and C2 amination of indoles.

By judicious selection of photocatalysts and other reaction parameters, a concomitant *bis*-functionalization of indoles has been accomplished [Scheme III.4 (b)]. While our manuscript was under preparation, Borhan *et al.* published an elegant C3-oxidation and C2-amination of indoles involving Cu(I) catalyst and an acyl nitroso reagent such as hydroxycarbamate [Scheme III.4 (a)].[9] This method has advantages in terms of peroxide-free oxidation use of hydroxycarbamate as the source of oxygen and the amide, making this protocol advantageous over previous methodologies involving difuctionalization of indoles.[10] Nevertheless, this method has an inherent limitation as it is applicable only to C2-protected indoles, and C2-free indoles failed to functionalize.

Scheme III.4. Approaches towards difunctionalization of indoles via selective C3 oxidation and C2 amination

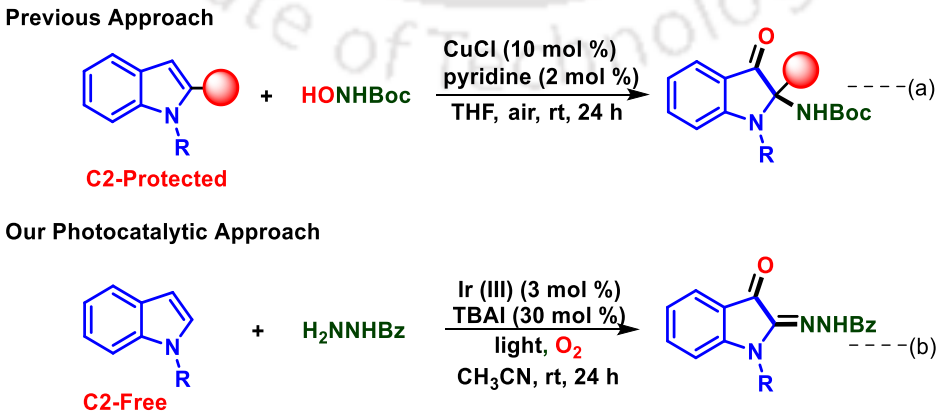

Our initial investigation started using indole (**1f**) (0.25 mmol), benzohydrzide (**2a**) (0.25 mmol), $[Ir(dtbbpy)(ppy)_2]PF_6$ (**P1**, 1 mol %), and TBAI (10 mol%), in 1,2-dichloroethane (DCE) at room temperature, in an oxygen atmosphere under irradiation of visible light (2 x 10 W white LEDs). Interestingly, the reaction resulted in the formation of a new product (**3f**, 30%). Spectroscopic (IR, ^1H, and ^{13}C), HRMS, and crystallographic analysis of the isolated product confirmed its structure to be (*E*)-*N'*-(1-isopropyl-3-oxoindolin-2-ylidene)benzohydrazide (**3f**) (Figure III.2).

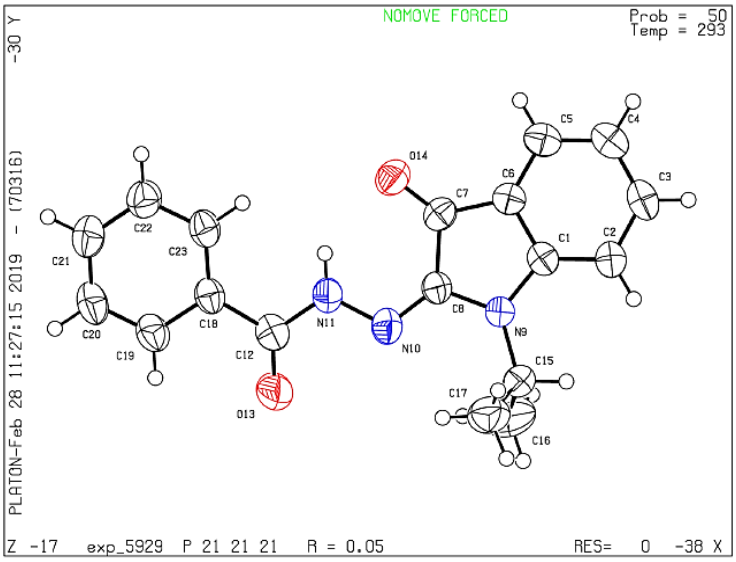

Figure III.2. *ORTEP (with 50% probability) diagram for the structure (E)-N'-(1-isopropyl-3-oxoindolin-2-ylidene)benzohydrazide 3f (CCDC* 1901162*).*

In contrast to other preparations of 3-oxindoles, here formation of this product (**3f**) is accompanied by the regioselective C3-oxidation and C2-amination.[11] Oxindoles are an important class of heterocycles and have attracted considerable attention in the field of antimicrobial and anticancer research.[12] The classical, as well as photocatalytic approaches for the synthesis of 2-oxindoles frameworks, are well documented,[13,14] whereas there are only limited reports on the synthesis of 3-oxindoles.[11,15,16] The two well-established strategies are; (i) a Pd-catalyzed, MnO_2/TBHP-mediated oxidative dearomatization of indoles,[15] and (ii) a redox annulation of nitro-alkynes with indoles in the presence of Au(III)/chiralphosphoric acid dual catalysis.[16] To the best of our knowledge, there is no report for the direct synthesis of 3-oxoindole involving indole with benzohydrazide and oxygen under photocatalysis.

III.3. Present Work

III.3.1. Optimization of the Reaction Conditions

Inspired by this photocatalytic approach, extensive optimization studies involving the selection of different catalytic systems and solvents were carried out. Using different transition metal-based photocatalysts such as $Ir[dF(CF_3)ppy]_2(dtbpy))PF_6$ (**P2**) (20%) and $Ru(bpy)_3(PF_6)_2$ (**P3**)(10%) did not show any improvement in the reaction yields (Table III.1, entries 2–3). On the other hand, organic dyes such as Eosin B, Eosin Y, and Rose Bengal were completely ineffective, leaving the starting material unreacted even after 24 h (Table III.1, entries 4–6). Hence, it was found that the catalyst $[Ir(dtbby)(ppy)_2]PF_6$(**P1**) is more suitable for the formation of (**3f**). Next, the catalyst loading was varied, and it was found that 3 mol % of $[Ir(dtbbpy)(ppy)_2]PF_6$(**P1**) is ideal for the transformation, yielding product (**3f**) in 55% yield (Table III.1, entries 7–9). Further, an increase in the catalytic loading (3.5 mol%) did not show any significant enhancement in the yield (56%) (Table III.1, entry 10). Subsequently, the effect of solvents on the reaction was examined. Solvent DCM (55%, Table III.1, entry 11) was found to be equally effective to that of DCE. The use of polar aprotic solvents such as DMSO (40%) and DMF (45%) were found to be inferior to that of DCE (Table III.1, entries 12–13). However, polar-protic solvents such as MeOH (60%) and EtOH (65%) were superior to DCE (Table III.1, entries 14–15). Incidentally, the polar aprotic solvent CH_3CN was found to be the best in terms of yield (70%) with fewer side products (Table III.1, entry 16). After the optimization of both catalyst and solvent, we next scrutinized the loading of various additives. Increasing the loading of TBAI from 10 to 15, 20, and 30 mol%, the yield of (3f) increased to 70%, 72%, and 75%, respectively (Table III.1, entries 17–19). However, no more improvement in the yield (76%) was observed by further increasing the TBAI loading to 40 mol%. Other organic and inorganic halo additives, such as tetrabutyl ammonium bromide, sodium iodide, and lithium bromide, were completely ineffective (Table III.1, entries 20–23). Reaction without the photocatalyst $[Ir(dtbbpy)(ppy)_2]PF_6$ (**P1**) did not provide any trace of the product (**3f**) (Table III.1, entry 24). The reaction in the dark, under otherwise identical reaction conditions, provided a trace (5%) of the desired product (**3f**) (Table III.1, entry 25). Reaction in open air yielded the desired product in 40% after 24 h; however, it was associated with the formation of some

fluorescent impurities (Table III.1 entry 26). Thus, the optimum condition for the synthesis of (**3f**) was the use of (**1f**) (0.25 mmol), benzo hydrazide (**2a**) (0.25 mmol), catalyst **P1** (3 mol%), and TBAI (30 mol%) in 5mL CH_3CN under an atmosphere of oxygen by irradiation of 20 W white LEDs at room temperature.

Table III.1. Optimization of the reaction conditions[a,b]

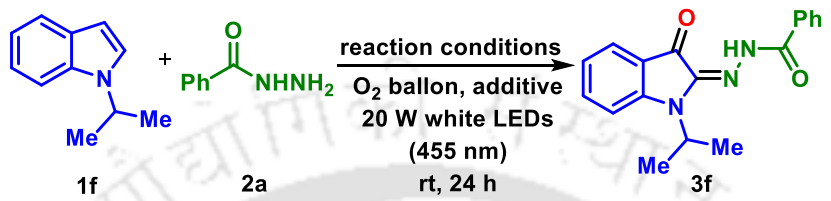

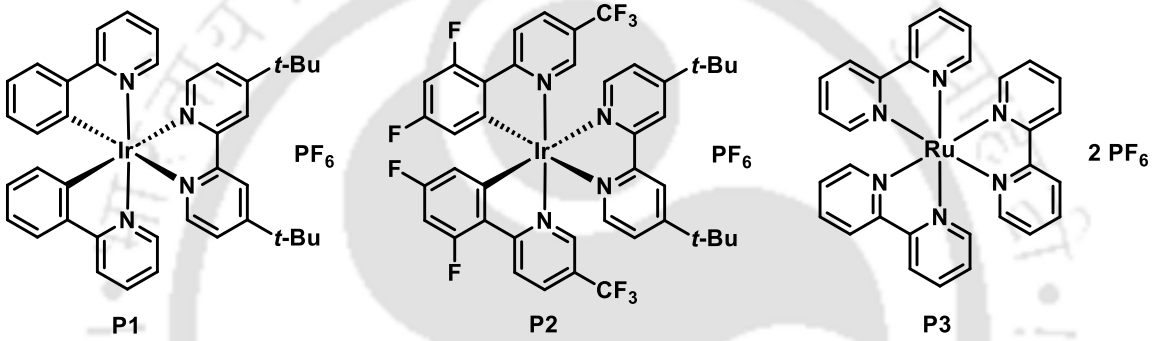

Entry	Catalyst (mol%)	Additive (mol%)	Solvent (5 mL)	Yield[b](%)
1.	$[Ir(dtbbpy)(ppy)_2]PF_6$(1) **P1**	TBAI (10)	DCE	30
2.	$(Ir[dF(CF_3)ppy]_2(dtbpy))PF_6$ (1) **P2**	TBAI (10)	DCE	20
3.	$Ru(bpy)_3(PF_6)_2$ (1) **P3**	TBAI (10)	DCE	10
4.	Eosin B (1)	TBAI (10)	DCE	ND[c]
5.	Eosin Y (1)	TBAI (10)	DCE	ND[c]
6.	Rose Bengal (1)	TBAI (10)	DCE	ND[c]
7.	$[Ir(dtbbpy)(ppy)_2]PF_6$(2) **P1**	TBAI (10)	DCE	45
8.	$[Ir(dtbbpy)(ppy)_2]PF_6$(2.5) **P1**	TBAI (10)	DCE	50
9.	$[Ir(dtbbpy)(ppy)_2]PF_6$(3) **P1**	TBAI (10)	DCE	55
10.	$[Ir(dtbbpy)(ppy)_2]PF_6$(3.5) **P1**	TBAI (10)	DCE	56
11.	$[Ir(dtbbpy)(ppy)_{2]}PF_6$(3) **P1**	TBAI (10)	DCM	55
12.	$[Ir(dtbbpy)(ppy)_2]PF_6$(3) **P1**	TBAI (10)	DMSO	40

13.	[Ir(dtbbpy)(ppy)$_2$]PF$_6$(3) **P1**	TBAI (10)	DMF	45
14.	[Ir(dtbbpy)(ppy)$_2$]PF$_6$(3) **P1**	TBAI (10)	MeOH	60
15.	[Ir(dtbbpy)(ppy)$_2$]PF$_6$(3) **P1**	TBAI (10)	EtOH	65
16.	[Ir(dtbbpy)(ppy)$_2$]PF$_6$(3) **P1**	TBAI (10)	CH_3CN	70
17.	[Ir(dtbbpy)(ppy)$_2$]PF$_6$(3) **P1**	TBAI (15)	CH_3CN	70
18.	[Ir(dtbbpy)(ppy)$_2$]PF$_6$(3) **P1**	TBAI (20)	CH_3CN	72
19.	[Ir(dtbbpy)(ppy)$_2$]PF$_6$(3) **P1**	TBAI (30)	CH_3CN	75
20.	[Ir(dtbbpy)(ppy)$_2$]PF$_6$(3) **P1**	TBAI (40)	CH_3CN	76
21.	[Ir(dtbbpy)(ppy)$_2$]PF$_6$(3) **P1**	TBAB (30)	CH_3CN	50
22.	[Ir(dtbbpy)(ppy)$_2$]PF$_6$(3) **P1**	NaI (30)	CH_3CN	55
23.	[Ir(dtbbpy)(ppy)$_2$]PF$_6$(3) **P1**	LiBr (30)	CH_3CN	40
24	-	TBAI (30)	CH_3CN	ND[c]
25.	[Ir(dtbbpy)(ppy)$_2$]PF$_6$(3) **P1**	TBAI (30)	CH_3CN	Trace[d]
26.	[Ir(dtbbpy)(ppy)$_2$]PF$_6$(3) **P1**	TBAI (30)	CH_3CN	40[e]
27.	[Ir(dtbbpy)(ppy)$_2$]PF$_6$(3) **P1**	TBAI (30)	CH_3CN	25[f]
28.	[Ir(dtbbpy)(ppy)$_2$]PF$_6$(3) **P1**	TBAI (30)	CH_3CN	50[g]
29.	[Ir(dtbbpy)(ppy)$_2$]PF$_6$(3) **P1**	TBAI (30)	CH_3CN	60[h]
30.	[Ir(dtbbpy)(ppy)$_2$]PF$_6$(3) **P1**	TBAI (30)	CH_3CN	ND[i]
31.	[Ir(dtbbpy)(ppy)$_2$]PF$_6$(3) **P1**	TBAI (30)	CH_3CN	ND[j]
32.	[Ir(dtbbpy)(ppy)$_2$]PF$_6$(3) **P1**	TBAI (30)	CH_3CN	45[k]

Reaction conditions: **1f** (0.25 mmol), benzohydrazides**2a** (0.25 mmol), P1 (mol %), and TBAI (mol %) in 5 mL solvent with an oxygen balloon and 2 x 10 W white LEDs irradiation at room temperature. [b]Yield of isolated product. [c]ND = Not detected. [d]Reaction performed in the dark. [e]Reaction in an open atmosphere. [f]Reaction performed using 2W LED light. [g]Reaction performed using 5W LED light (449 nm, FWHM). [h]Reaction performed using 10W LED light. [i]Reaction performed using 5W red LED light. [j]Reaction performed using 5W green LED light. [k]Reaction performed using 5W blue LED light.

TBAI= tetra butyl ammonium iodide, TBAB= tetra butyl ammonium bromide.

II.3.2. Substrate Scope for the Synthesis of 3-Oxindoles

The scope and generality of the visible-light-mediated reaction were extended to various substituted indoles and benzohydrazides under the optimized reaction condition. As shown in Scheme III.5, a diverse array of *N*-substituted and mono and di (1,5 and 1,7) substituted indoles (**1a-m**, **1s-t**) could be transformed to their corresponding 3-oxindoles (**3a-t)** in good yields. At first, the effect of various alkyl substituents (R^2) at the indole nitrogen were examined, and the results are summarized in Scheme III.5. It was found that the isolated yields of the product improved as the alkyl chain length increased. Alkyl substituents such as methyl (**1a**), ethyl (**1b**), n-propyl (**1c**), n-butyl (**1d**), and n-pentyl (**1e**) provided their corresponding bi-functionalized products (**3a**), (**3b**), (**3c**), (**3d**) and (**3e**) in 65%, 68%, 72%, 74% and 80% yields respectively. These primary alkyl groups are expected to stabilize the nitrogen radicals to similar extents and, hence, should provide equal yields. The better-isolated yields for higher alkyl chains could be because of easy elution (isolation) due to the enhanced hydrophobic character during silica gel column chromatographic purification, as highly nitrogenous compounds often stick to the column. Similarly, secondary *N*-alkyl substituents such as isopropyl (**1f**) and cyclopentyl (**1g**) substituted indoles yielded their corresponding products (**3f**) and (**3g**) in 75 and 78% yields, respectively.

Next, the compatibility of various benzyl substituents (R^2) was tested as they are often prone to oxidation.[17] Substrates having *N*-benzyl substituents, bearing either electron-donating *p*-CH_3 (**1h**) or electron-withdrawing *p*-Cl (**1i**), o-Br (**1j**) groups reacted efficiently with benzohydrazide (**2a**) to give good yields of their products (**3h**, 70%), (**3i**, 72%) and (**3j**, 70%) in almost identical yields without undergoing oxidation at the benzylic position. An *N*-allyl substituted indole (**1k**) underwent the present photocatalytic bi-functionalization giving the product (**3k**) a 65% yield without affecting the oxidation-sensitive allylic group. After demonstrating the compatibility of various *N*-protected indoles, we examine the nature of various substituents (EDG and EWG) present either on the homocyclic ring of indoles or on the phenyl rings of benzohydrazides. Irrespective of the nature of the substituents [electron-donating 5-Me (**1l**) or electron-withdrawing 5-Br (**1m** and **1s**) or 7-F (**1t**) in the indolyl moiety and electron-donating *p*-Me (**2b**), *p*-OMe (**2c**), *m*-OMe (**2d**) or electron-withdrawing *p*-CF_3 (**2e**), *p*-Br (**2f**), in the benzo hydrazide ring] or their positions of attachments all provided moderate to good yields of their products (**3l**, 68%), (**3m**, 75%), (**3n**, 75%), (**3o**,

74%), (**3p**, 72%), (**3q**, 85%), (**3r**, 82%), (**3s**, 87%), (**3s**, 85%), revealing no obvious electronic impact from the substituents.

Scheme III.5. Substrate scope for the synthesis of 3-oxindoles [a,b]

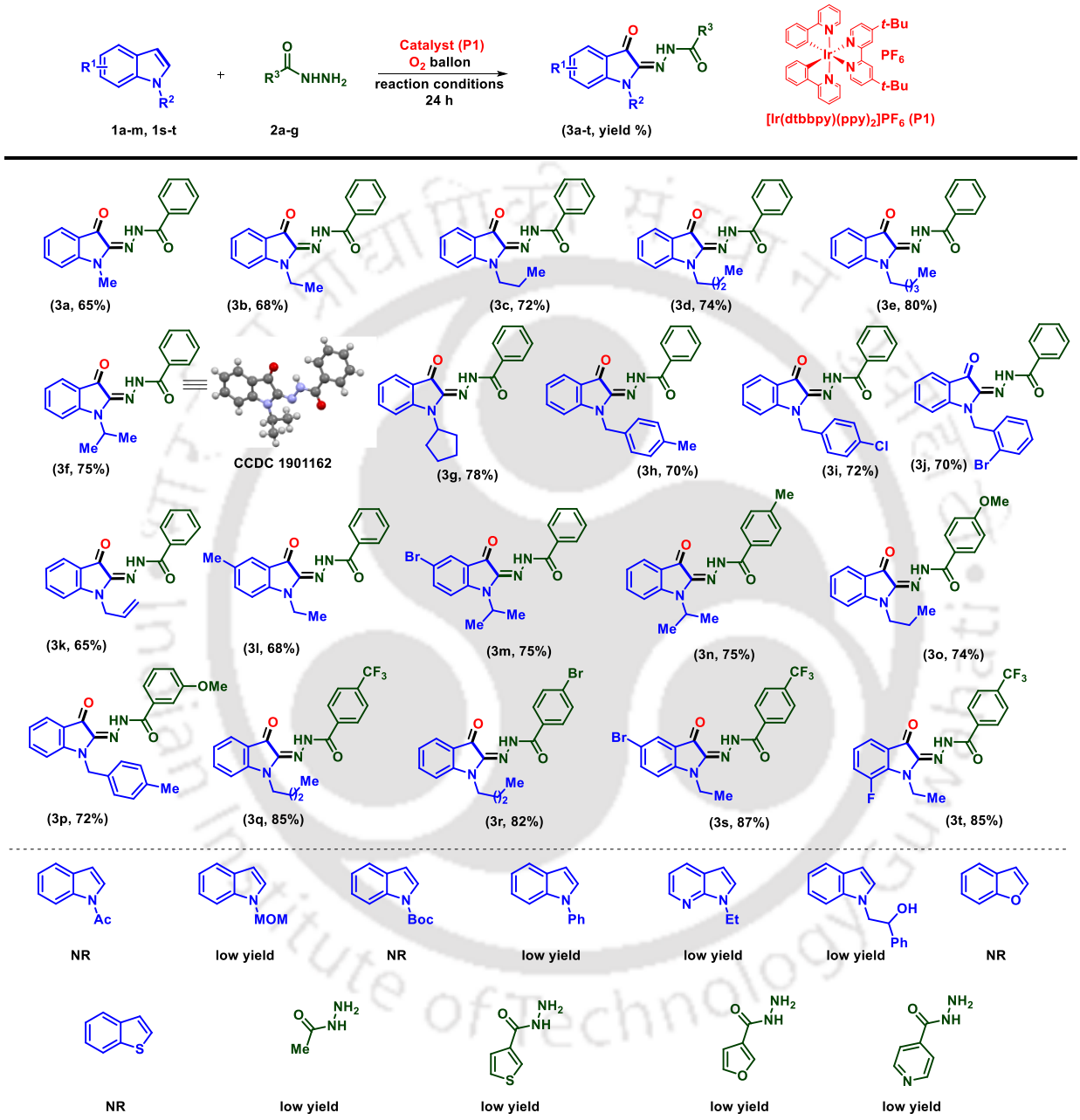

[a]Reaction conditions: **1a–m, 1s–t** (0.25 mmol), **2a–g** (0.25 mmol), P1 (3 mol %), CH_3CN (5 mL), 2 x 10 W Whote LEDs, under O_2. [b]Isolated yield. NR= no reaction.

Reaction with an alkyl hydrazide gave a very poor yield of the product, which is also associated with an inseparable mixture of uncharacterized impurities. In contrast, sulfonyl hydrazide failed to give the anticipated oxidative amination product (Scheme III.5). Unlike benzimidazoles, this photocatalytic process was not successful for the functionalization of analogous heterocycles, such as benzothiazoles, benzoxazoles, and many other *N*-bearing heterocycles (Scheme III.5)

III.4. Mechanistic Investigation

III.4.1. Control Experiments

To gain insight into the mechanism of this regioselective bis functionalization, a series of control experiments were conducted. To ascertain the origin of the carbonyl oxygen in the product, whether it is originating from O_2 or other sources (moisture from the solvent) in the reaction mixture, a standard reaction of **1a** and **2a** was performed under a nitrogen atmosphere. The reaction failed to proceed efficiently, giving just 5% yield of the product **3a** after 24 h. Further, to rule out the possibility of water as the source of carbonyl oxygen of the indole ring, a standard reaction was carried out in the presence of 5 equiv of H_2O^{18}. The HRMS analysis of the isolated product revealed no traces of O^{18} incorporation, suggesting that water is not the source of the carbonyl oxygen in the product. These observations suggest that molecular oxygen is the only possible oxygen source of the carbonyl oxygen as in its absence the reaction is unsuccessful (Scheme III.6).

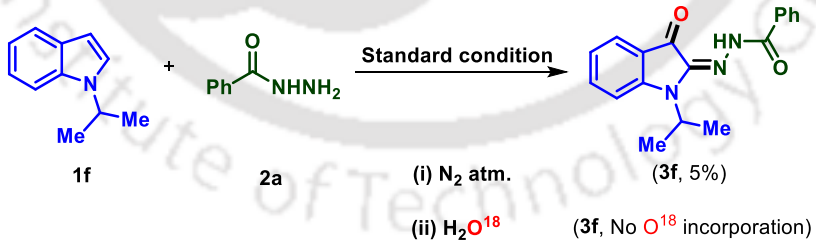

Scheme III.6. *Nitrogen atmosphere and O^{18} labeling experiments.*

To prove the photocatalytic radical pathway, a standard experiment between **1a** and **2a** was carried out in the presence of TEMPO (1 equiv) under otherwise identical conditions, which provided **3a** in only a trace amount (Scheme III.7).

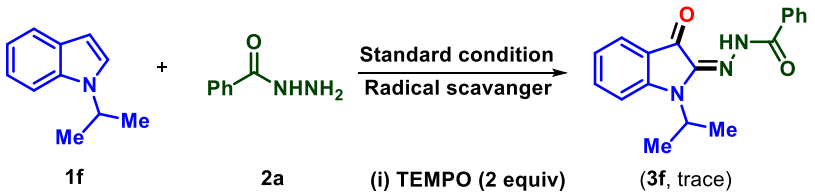

Scheme III.7. *TEMPO experiment.*

Most oxidations of indoles proceed *via* an isatin (indoline-2,3-dione) intermediate.[18] Thus, a question arises whether this oxidative bifunctionalization is proceeding *via* a similar isatin intermediate. An isatin analogue, 1 methyl indoline-2,3-dione in lieu of **1a**, was reacted with **2a** under identical reaction conditions and gave no trace of **3a**, confirming isatin not to be intermediate in this reaction (Scheme III.8).

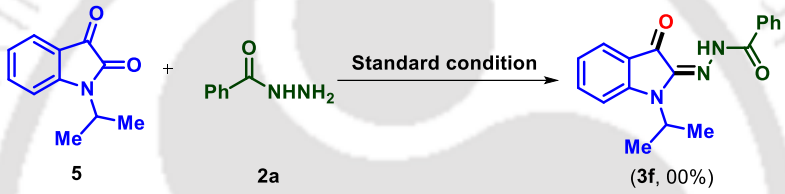

Scheme III.8. *Intermediate detection experiment*.

The reaction mixture was colorless initially and turned violet as the reaction progressed. This is because of the oxidation of the iodide from tetrabutylammonium iodide to molecular iodine due to the generation of hydrogen peroxide in the medium. Two methods have been employed to detected the formation of H_2O_2.

Method-1: When a solution of Fe(II), i.e. $(NH_4)_2FeSO_4.6H_2O$, was added to the reaction mixture, a rapid setting of $Fe(OH)_3$ floc was observed. This is because of the rapid oxidation of Fe(II) to Fe(III) due to the presence of hydrogen peroxide in the medium.

Method-2: The UV absorption of the reaction mixture in acetonitrile shifter from 510 nm to 526 nm upon addition of $TiCl_4$ due to the formation of peroxo complex of titanium (IV) (Figure III.3).

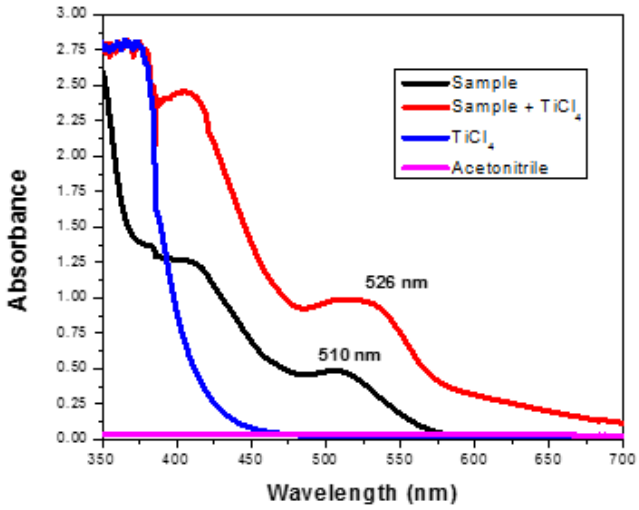

Figure III.3. UV absorption spectrum.

II.4.2. Plausible Reaction Mechanism

Based on the control experiments carried out and from the DFT calculation, a plausible mechanistic path is depicted in Scheme III.9. To clearly understand the mechanism of the reaction, we performed DFT calculations and modeled the reaction profile at M06/6-31+G(d) level of theory. In the first step, indole (**1f**) is oxidized to an indole radical cation (**A**) through a reductive quenching process by the photocatalyst Ir(III)* (**P1**). Simultaneously, the molecular oxygen is reduced to a superoxide ion $O_2^{\bullet-}$ by Ir(II), and the catalyst is regenerated.[20a] Next, we compared the possibility of attack of $O_2^{\bullet-}$ on two possible sites (C_3 and C_2) of the radical cation **A** through TS-1A and TS-1B. Clearly, TS-1A, i.e., attack at the C3-site, has a lower barrier and lower stabilization compared to TS-1B involving a C-2 attack as depicted in Scheme III.9. Further, the forward reaction is preferred for TS-1A, and the reverse reaction is preferred for TS-1B. Thus, the formation of transition state TS-1B *via* the C-2 attack of $O_2^{\bullet-}$ is ruled out. The highly reactive $O_2^{\bullet-}$ then attacks at the C-3 site of the intermediate **A** to form a peroxy iminium species **B**. The benzohydrazide **2a** attacks at the C-2 site of intermediate **B** to form intermediate **C** through TS-2. This is perhaps the rate-determining step for this reaction, having an activation barrier of 22.14 kcal/mol. Intermediate C is around 1.56 kcal/mol, which is more stable than intermediate **B**. As expected, the barrier for removing a water molecule is very low (1.90 kcal/mol) from intermediate C to form intermediate D, which is associated with higher stabilization. Finally, two hydrogens, one

from indole and benzohydrazide (2a), were removed. The final step seems to be a facile one with an activation barrier of 4.89 kcal/mol. Moreover, the final product (**3f**) is 14.91 kcal/mol more stable compared to the intermediate **D**. Thus, all of the proposed steps are highly favorable, which leads to a stable bi-functionalized product. Some of the selected interatomic distances found in the geometries of various transition states are depicted in Scheme III.9.

Scheme III.9. *Plausible mechanism for the formation of 3f supported by DFT calculated energy profile (relative energies (kcal/mol) and bond distances (Å) are calculated at M06/6-31+G(d) level of theory)*

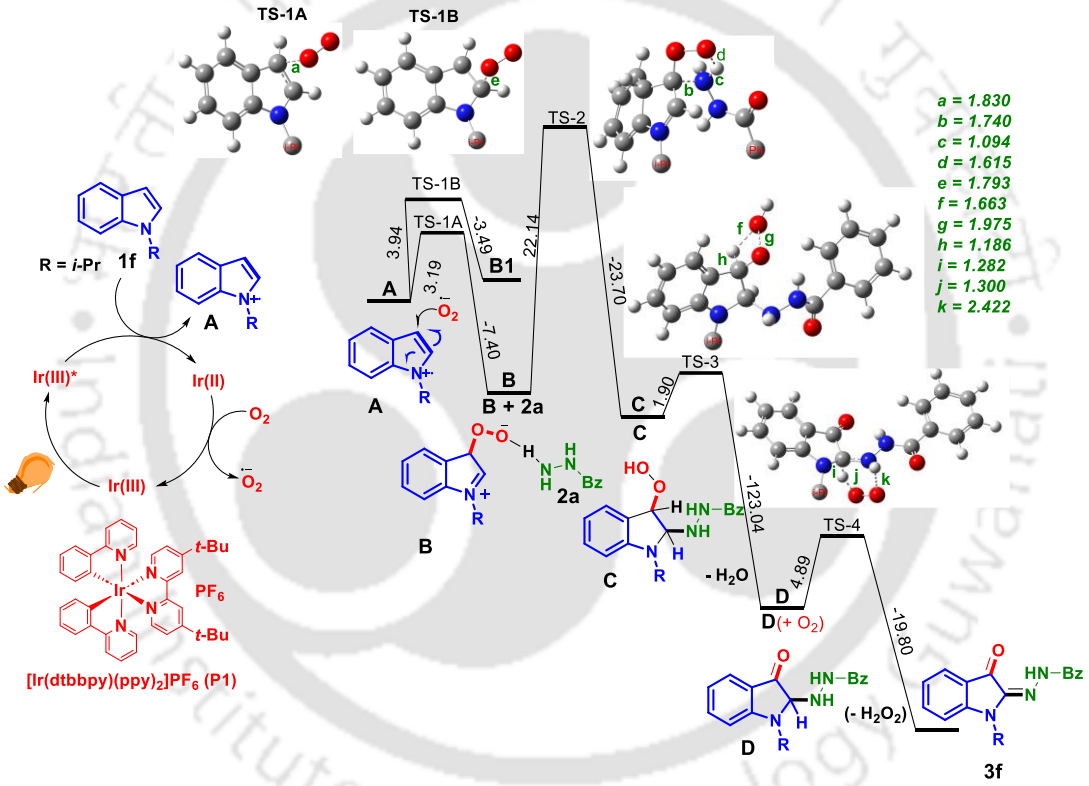

III.5. Post-Synthetic Application

To demonstrate the applicability of the present photochemical approach, the compound (**1a**) was subjected to some useful organic transformations (Scheme III.10). Acidic hydrolysis of difunctionalized product **3f** in MeOH:H_2O (1:1, 3 mL) solvent system and *p*-TSA catalyzed (20 mol %) reaction conditions yielded 1-isopropylindoline-2,3-dione **5** in moderate yield (40%) along with few fluorescent impurities.[20b]

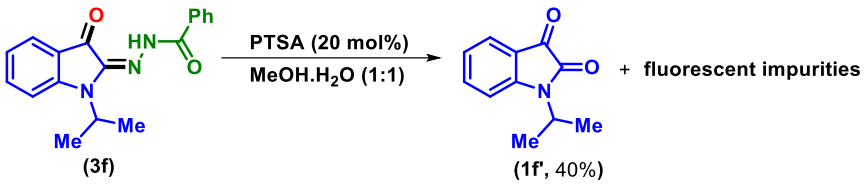

Scheme III.10. *Post-synthetic application.*

III.6. Conclusion

In summary, a mild and efficient photocatalytic regioselective method has been developed for the selective difunctionalization of indoles by visible-light-induced photoredox Ir(III) catalysis. A wide range of indoles, as well as benzohydrazides, participate competently in the free-radical reaction to afford structurally diverse oxindoles in good yields. Based on control experiments carried out plausible mechanism has been proposed which is well supported by DFT calculation.

III.7. Experimental Section

III.7.1. General Information: The starting materials were commercially available and were used without further purification. 1-Substituted indoles were synthesized following the reported procedures.[1] Glassware were dried in an oven at 100°C or flame-dried and cooled under a dry atmosphere before use. Unless otherwise indicated, reactions were performed under an oxygen balloon and 2 x 10 W white LED bulbs irradiation at room temperature. All the reactions were monitored by TLC using precoated sheets of silica gel G/UV-254 of 0.25 mm thickness (Merck $60F_{254}$) using UV light for visualization. Column chromatography was performed using 100-200 mesh silica gels. NMR spectra were recorded on Bruker 400 MHz NMR spectrometer. Chemical shifts for ^{1}H NMR were reported as δ, parts per million, relative to the signal of $CHCl_3$. Chemical shifts for ^{13}C NMR were reported as δ, parts per million, relative to the center line signal of the $CDCl_3$ triplet. The abbreviations s, br. s, d, t, q, and m stand for the resonance multiplicity singlet, broad singlet, doublet, triplet, quartet, and multiplet, respectively. IR spectra were recorded in KBr. HRMS spectra were recorded using ESI mode (Q-TOF type Mass Analyser).

III.7.2. Crytallographic Description:

Crystallographic Description of (E)-N'-(1-isopropyl-3-oxoindolin-2-ylidene)benzohydrazide (3f):

$C_{18}H_{17}N_3O_2$, crystal dimensions 0.24 x 0.20 x 0.16 mm, orthorhombic, space group P 21, a = 6.5705(3), b = 12.6811(6), c = 18.9314(9) Å, α = 90°, β = 90°, γ = 90°, V = 15.7739(13) Å^3, Z = 4. CCDC-2118561 for **(E)-N'-(1-isopropyl-3-oxoindolin-2-ylidene)benzohydrazide (3f)** contains the supplementary crystallographic data for this paper. These data can be obtained free of charge from The Cambridge Crystallographic Data Centre via www.ccdc.cam.ac.uk/data_request/cif.

III.7.3. General Procedure for the Preparation of (3a-t) at 0.25 mmol Scale

An oven-dried 10 mL round bottom flask equipped with a magnetic stir bar and rubber septum were added $Ir(ppy)_2(dtbbpy)PF_6$P1 (3 mol %, 7 mg), TBAI (30 mol %, 27 mg), indole (**1**) (0.25 mmol), and benzohydrazides (**2**) (0.25 mmol) and subjected to the vacuum for 5 minutes. Next, CH_3CN (5 mL) was introduced to the flask through a cannula under an oxygen atmosphere. The reaction mixture was stirred at room temperature at a distance of ~8-10 cm from two 10 W white LED bulbs (455 nm). After completion of the reaction (monitored by TLC analysis), the solvent was removed in vacuoand the mixture was diluted with ethyl acetate (10 mL) followed by washing with aqueous $NaHCO_3$ (2 x 5 mL). The organic layer was dried over anhydrous Na_2SO_4, and the solvent was evaporated under reduced pressure. The crude residue thus obtained was purified by column chromatography over silica gel (100-200 mesh) using an increasing percentage of ethyl acetate in hexane as eluent to afford the pure products (**3**).

III.7.4. Procedure for the Preparation of (3f) at 1 mmol Scale

An oven dried 25 mL round bottom flask equipped with a magnetic stir bar and rubber septum were added $Ir(ppy)_2(dtbbpy)PF_6$P1 (3 mol %, 28 mg), TBAI (30 mol %, 110 mg), indole (**1f**) (1 mmol, 159 mg), and benzohydrazides (**2a**) (1 mmol, 136 mg) and subjected to the vacuum for 5 minutes. Next, CH_3CN (10 mL) was introduced to the flask through a cannula under an oxygen atmosphere. The reaction mixture was stirred at room temperature at a distance of ~8-10 cm from two 10 W white LED bulbs (455 nm). After completion of the

reaction (monitored by TLC analysis), the solvent was removed in vacuo and the mixture was diluted with ethyl acetate (30 mL) followed by washing with aqueous $NaHCO_3$ (2 x 10 mL). The organic layer was dried over anhydrous Na_2SO_4, and solvent was evaporated under reduced pressure. The crude residue thus obtained was purified by column chromatography over silica gel (100-200 mesh) using increasing percentage of ethyl acetate in hexane as eluent to afford the pure products (**3b**, 72 %, 221 mg).

III.7.5. General Procedure for the Acidic Hydrolysis of (*E*)-N'-(1-Isopropyl-3-oxoindolin-2-ylidene)benzohydrazide (3f)

To an oven-dried 10 mL round bottom flask fitted with a reflux condenser were added (*E*)-N'-(1-Isopropyl-3-oxoindolin-2-ylidene)benzohydrazide (**3f**, 0.25 mmol, 76 mg), p-TSA (20 mol %, 8.6 mg) and MeOH:H_2O (1:1, 3mL). Then the reaction mixture was heated at reflux temperature for 24 h. After the completion of the reaction (monitored by TLC) the reaction mixture was mixed with ethyl acetate 10 mL and washed with aq. Na_2CO_3 (2 x 10 mL). The separated organic layer was dried over anhydrous sodium sulphate (Na_2SO_4), and evaporated under reduced pressure. The crude product so obtained was purified by silica gel column chromatography using hexane and ethyl acetate as the eluent to give pure 1-isopropylindoline-2,3-dione **5** (red solid, 40% yield, 19 mg). The identity and purity of the product was confirmed by spectroscopic analysis. ^{1}H NMR (400 MHz, $CDCl_3$): δ 7.60-7.53 (m, 2H), 7.09-7.01 (m, 2H), 4.55-4.48 (m, 1H), 1.51 (d, J = 6.8 Hz, 6H); ^{13}C NMR (100 MHz, $CDCl_3$): δ 183.8, 157.8, 150.5, 138.1, 125.5, 123.2, 117.9, 111.3, 44.8, 19.3.

^{1}H and ^{13}C NMR spectra of 5

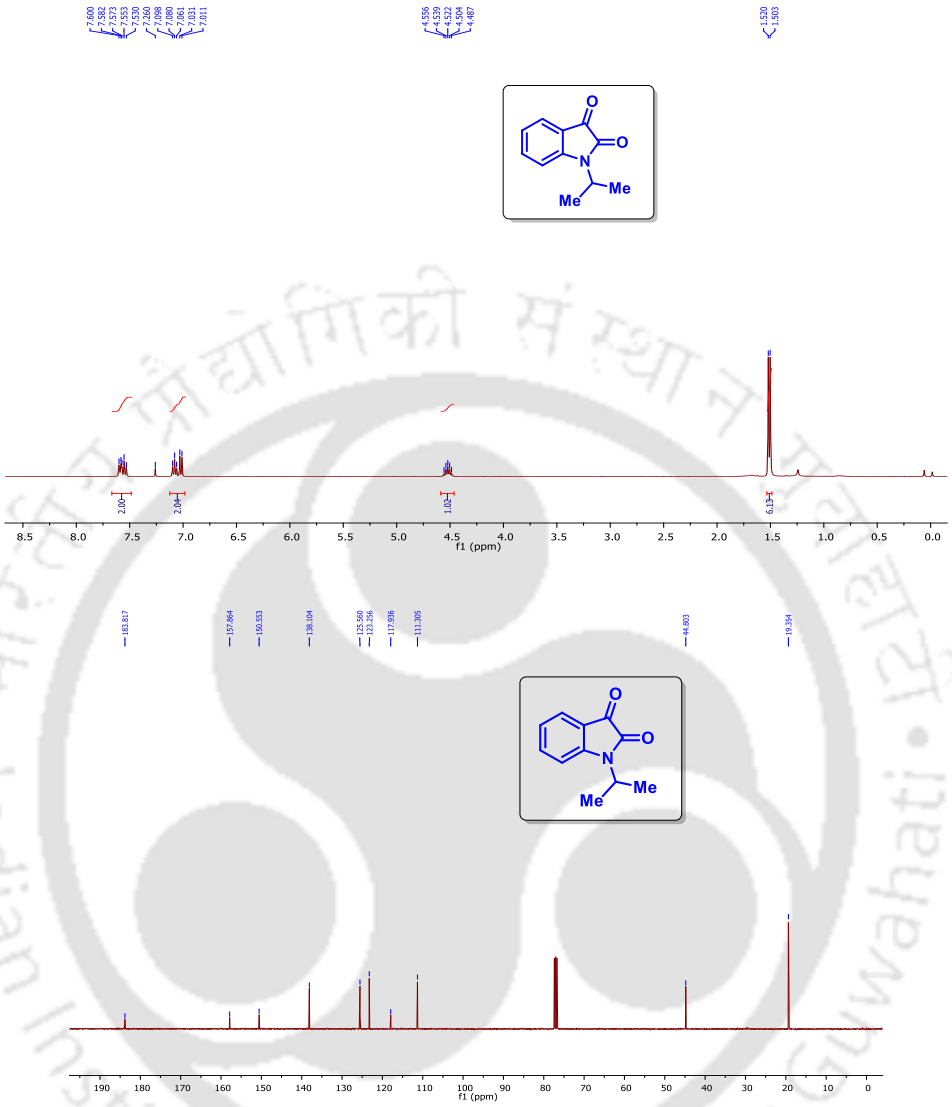

III.8. References

[1] (a) Arora, A.; Weaver, J. D. *Acc. Chem. Res.* **2016**, *49*, 2273–2283. (b) Beeler, A. B. *Chem. Rev.* **2016**, *116*, 9629–9630. (c) Wang, L.-M.; Jenikinson, K.; Wheatley, A. E. H.; Kuwata, K.; Saito, S.; Naka, H. *ACS Sustainable Chem. Eng.* **2018**, *6*, 15419–15424. (d) Prier, C. K.; Rankic, D. A.; MacMillan, D. W. C. *Chem. Rev.* **2013**, *113*, 5322–5363. (e) Qvortrup, K.; Rankic, D. A.; MacMillan, D. W. C. *J. Am. Chem. Soc*. **2014**, *136*, 626–629. (f) Arora, A.; Weaver, J. D. *Org.*

Lett. **2016**, *18*, 3996–3999. (g) Yadav, A. K.; Singh, K. N. *Chem. Commun*. **2018**, *54*, 1976–1979. (h) Liu, K.; Zou, M. Z.; Lei, A. W. *J. Org. Chem.* **2016**, *81*, 7088–7092.

[2] (a) Yang, X.; Li, L.; Li, Y.; Zhang, Y. *J. Org. Chem.* **2016**, *81*, 12433–12442. (b) Senaweera, S.; Weaver, J. D. *J. Am. Chem. Soc*. **2016**, *138*, 2520–2523. (c) Carreira, E. M.; Hastings, C. A.; Shepard, M. S.; Yerkey, L. A.; Millward, D. B. *J. Am. Chem. Soc*. **1994**, *116*, 6622–6630. (d) Wei, G.; Basheer, C.; Tan, C.-H.; Jiang, Z. *Tetrahedron Lett*. **2016**, *57*, 3801–3809. (e) Tóth, B. L.; Tischler, O.; Novák, Z.; *Tetrahedron Lett.* **2016**, *57*, 4505–4513. (f) Hering, T.; Meyer, A. U.; König, B. *J. Org. Chem*. **2016**, *81*, 6927–6936. (g) Douglas, J. J.; Sevrin, M. J.; Stephenson, C. R. J. *Org. Process Res. Dev*. **2016**, *20*, 1134–1147. (h) Romero, N. A.; Nicewicz, D. A. *Chem. Rev.* **2016**, *116*, 10075–10166.

[3] (a) Li, M.; Yang, J.; Ouyang, X.-H.; Yang, Y.; Hu, M.; Song, R.-J.; Li, J-H. *J. Org. Chem*. **2016**, *81*, 7148–7154. (b) Zhu, M.; Zhou, K.; Zhang, X.; You, S.-L. *Org. Lett*. **2018**, *20*, 4379–4383. (c) Muliang, Z.; Duan, Y.; Li, W.; Cheng, Y.; Zhu, C. *Chem. Commun*. **2016**, *52*, 4761–4763. (d) MacMillan, K. S.; Boger, D. L. *J. Am. Chem. Soc*. **2008**, *130*, 16521–16523. (e) Kaushik, N. K.; Kaushik, N.; Attri, P.; Kumar, N.; Kim, C. H.; Verma, A. K.; Choi, E. H. *Molecules* **2013**, *18*, 6620–6662. (f) Wu, W.; Xiao, M.; Wang, J.; Li, Y.; Xie, Z. *Org. Lett.* **2012**, *14*, 1624–1627. (g) Umehara, A.; Ueda, H.; Tokuyama, H. *Org. Lett*. **2014**, *16*, 2526–2529. (h) Baran, P. S.; Corey, E. J. *J. Am. Chem. Soc.* **2002**, *124*, 7904–7905. (i) Deluca, V.; Balsevich, J.; Tyler, R. T.; Eilert, U.; Panchuk, B. D.; Kurz, W. G. W. *J. Plant Physiol*. **1986**, *125*, 147–156. (j) Schiff, P. L. *Am. J. Pharm. Educ.* **2006**, *70*, 98–108. (k) Jadhav, A. P.; Ali, A.; Singh, R. P. *Adv. Synth. Catal*. **2017**, *359*, 1508–1514. (l) Rao, V. U. B.; Kumar, K.; Singh, R. P. *Org. Biomol. Chem*. **2015**, *13*, 9755–9759.

[4] (a) Cai, Z.-J.; Wang, S.-Y.; Ji, S.-J. *Org. Lett*. **2013**, *20*, 5226–5229. (b) Tu, D.; Luo, J.; Jiang, C. *Chem. Commun*., **2018**, *54*, 2514–2517. (c) Zhang, L.-L.; Ji, S.-J.; Xu, M.-M.; Cao, W.-B.; Xu, X.-P.; Ji. S.-J. *Adv. Synth. Catal*. **2020**, *362*, 3131–3136.

[5] Pitre, S. P.; Scaiano, J. C.; Yoon, T. P. *ACS Catal.* **2017**, *7*, 6440–6444.

[6] Zhang, C.; Li, S.; Bureš, F.; Lee, R.; Ye, X.; Jiang, Z. *ACS Catal.* **2016**, *6*, 6853–6860.

[7] Furst, L.; Matsuura, B. S.; Narayanam, J. M. R.; Tucker, J. W.; Stephenson, C. R. J. *Org. Lett.* **2010**, *12*, 3104–3107.

[8] (a) Gogoi, A.; Guin, S.; Rout, S. K.; Patel, B. K. *Org. Lett***. 2013**, *15*, 1802–1805. (b) Gogoi, A.; Modi, A.; Guin, S.; Rout, S. K.; Das, D.; Patel, B. K. *Chem. Commun.* **2014**, *50*, 10445–10447.

[9] Zhang, J.; Kohlbouni, S. T.; Borhan, B. *Org. Lett*. **2019**, *21*, 14–17.

[10] (a) Wu, J.; Dou, Y.; Guillot, R.; Kouklovsky´, C.; Vincent, G. *J. Am. Chem. Soc.* **2019,** *141*, 2832–2837. (b) Xu, D.; Sun, W.W.; Xie, Y.; Liu, J. K.; Liu, B.; Zhou Y.; Wu, B. *J. Org. Chem.* **2016**, *81*, 11081–11094.

[11] (a) Zhang, M.; Duan, Y.; Li, W.; Cheng Y.; Zhu, C. *Chem. Commun.* **2016**, *52*, 4761–4763. (b) Tsai, A, -I.; Lin, C. H.; Chuang, C.-P.; *Hetrocycles* **2005**, *65*, 2381–2394.

[12] (a) Kamal, A.; Ramakrishna, G.; Raju, P.; Rao, A. V.; Viswanath, A.; Nayak, V. L.; Ramakrishna, S. *Eur. J. Med. Chem*. **2011**, *46*, 2427–2435. (b) Romagnoli, R.; Baraldi, P. G.; Prencipe, F.; Oliva, P.; Baraldi, S.; Salvador, M. K.; Lopez-Cara, L. C.; Bortolozzi, R.; Mattiuzzo, E.; Basso, G.; Viola, G. *Eur. J. Med. Chem*. **2017**, *134*, 258–270. (c) Ribeiro, C. J. A.; Amaral, J. D.; Rodrigues, C. M. P. Moreira, R.; Santos M. M.M. *Bioorg. Med. Chem.* **2014**, *22*, 577–584. (d) Rindhe, S. S.; Karale, B. K.; Gupta, R. C.; Rode, M. A. *Indian J. Pharm. Sci.* **2011**, *73*, 292–296.

[13] (a) Jang, Y. J.; Yoon, H.; Lautens, M. *Org. Lett.* **2015**, *17*, 3895–3897. (b) Bhunia, S.; Chang, C.-J.; Liu, R.-S. *Org. Lett.* **2012**, *14*, 5522–5525.

[14] (a) Ju, X.; Liang, Y.; Jia, P.; Li, W.; Yu, W. *Org Biomol Chem*. **2012**, *10*, 498–501. **(b)** Zhang, M.; Fu, Q.-Y.; Gao, G.; He, H.-Y.; Zhang, Y.; Wu, Y.-S.; Zhang, Z.-H. *ACS Sustainable Chem. Eng.* **2017**, *5*, 6175–6182.

[15] Guchhait, S. K.; Chaudhary, V.; Rana, V. A.; Priyadarshani, G.; Kandekar, S.; Kashyap, M. *Org. Lett*. **2016**, *18*, 1534–1537.

[16] Liu, R.-R.; Ye, S.-C.; Lu, C.-J.; Zhuang, G.-L.; Gao, J.-R.; Jia, Y.-X. *Angew.Chem.* **2015**, *127*, 11357–11360.

[17] (a) Guin, S.; Rout, S. K.; Banerjee, A.; Nandi, S.; Patel, B. K. *Org. Lett*., **2012**, *14*, 5294–5297. (b) Rajamanickam, S.; Majji, G.; Santra, S. K.; Patel, B. K. *Org. Lett*. **2015**, *17*, 5586–5589.

[18] Crystal detail (CCDC No. 1901162).

[19] (a) Luo, J.; Gao, S.; Ma, Y.; Ge, G. *Synlett* **2018**, *29*, 969–973. (b) Zi, Y.; Cai, Z.-J.; Wang, S.-Y.; Ji, S.-J. *Org. Lett*. **2014**, *16*, 3094–3097. (c) Bredenkamp, A.; Mohr, F.; Kirsch S. F. *Synthesis* **2015**, *47*, 1937–1943.

[20] (a) Condie, A. G.; Jose, C.; Gonza,´l.-G.; Stephenson, C. R. J. *J. Am. Chem. Soc*. **2010**, *132*, 1464–1465. (b) Shiraishi, Y.; Kanazawa, S.; Sugano, Y.; Tsukamoto, D.; Sakamoto, H.; Ichikawa, S.; Hirai, T. *ACS Catal*. **2014**, *4*, 774–780.

III.9. Spectral Data

(E)-N'-(1-Methyl-3-oxoindolin-2-ylidene)benzohydrazide (3a):

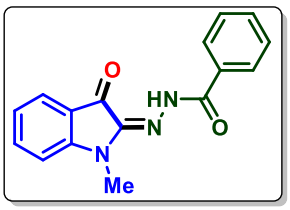

Red solid (45 mg, 65% yield); mp 170-172 °C; ^{1}H NMR (400 MHz, $CDCl_3$): δ 13.49 (s, br, 1H), 7.98 (d, J = 7.6 Hz, 2H), 7.68 (d, J = 7.6 Hz, 1H), 7.60-7.49 (m, 4H), 6.98-6.92 (m, 2H), 3.41 (s, 3H); ^{13}C NMR (100 MHz, $CDCl_3$): δ 182.0, 164.0, 153.9, 140.5, 138.3, 132.6, 132.3, 128.9, 127.5, 127.2, 125.6, 120.5, 118.4, 109.6, 27.7; IR (KBr,cm^{-1}): 3437, 2923,2852, 1691, 1668, 1621, 1538, 1477, 1253, 704, 442; HRMS (ESI) calcd. for $C_{16}H_{13}N_3NaO_2^+$, $[M+Na]^+$, 302.0905, found 302.0923.

***(E)-N'-(1-Ethyl-3-oxoindolin-2-ylidene)benzohydrazide (3b)*:**

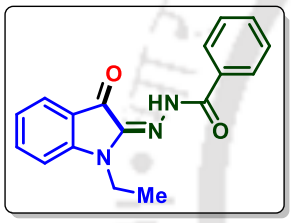

Red solid (49 mg, 68% yield); mp 150-152 °C; ^{1}H NMR (400 MHz, $CDCl_3$): δ 13.55 (s, br, 1H), 7.98 (d, J = 7.2 Hz, 2H), 7.68 (d, J = 7.6 Hz, 1H), 7.59-7.49 (m, 4H), 6.97-6.93 (m, 2H), 3.95 (q, J = 6.8 Hz, 2H), 1.33 (t, J = 7.2 Hz, 3H); ^{13}C NMR (100 MHz, $CDCl_3$): δ 182.2, 163.9, 153.1, 139.7, 138.2, 132.7, 132.3, 128.9, 128.6, 127.7, 127.5, 125.8, 120.3, 118.5, 109.7, 36.0, 12.5; IR (KBr, cm^{-1}): 3438, 3058, 2925, 1696, 1668, 1620, 1532, 1472, 1263, 699, 443; HRMS (ESI) calcd. for $C_{17}H_{15}N_3NaO_2^+$,$[M+Na]^+$, 316.1062, found 316.1079.

***(E)-N'-(3-Oxo-1-propylindolin-2-ylidene)benzohydrazide (3c)*:**

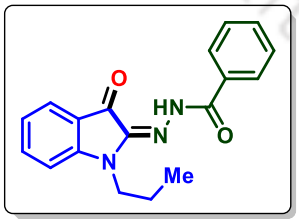

Red gummy liquid (55 mg, 72% yield); ^{1}H NMR (400 MHz, $CDCl_3$): δ 13.57 (s, br, 1H), 7.98 (d, J = 7.2 Hz, 2H), 7.67 (d, J = 7.2 Hz, 1H), 7.57-7.49 (m, 3H), 7.37-7.36 (m, 1H), 6.95-6.92 (m, 2H), 3.83 (t, J = 6.8 Hz, 2H) 1.82-1.76 (m, 2H), 0.98 (t, J = 7.2 Hz, 3H); ^{13}C NMR (100 MHz, $CDCl_3$): δ 182.1, 163.9, 153.6, 140.2, 138.2, 132.7, 132.3, 128.8, 128.6, 127.5, 125.7, 123.6, 120.3, 118.3, 109.9, 42.9, 20.7, 11.4; IR (KBr, cm^{-1}): 3440, 2930, 2854, 1693, 1672, 1619, 1546, 1497, 1249, 699,

452; HRMS (ESI) calcd. for $C_{18}H_{17}N_3NaO_2^+$,[M+Na]$^+$, 330.1218, found 330.1230.

***(E)-N'-(1-Butyl-3-oxoindolin-2-ylidene)benzohydrazide (3d)*:**

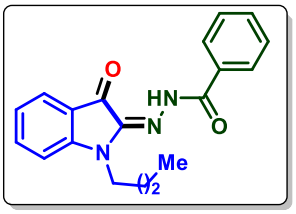

Red gummy liquid (59 mg, 74% yield); ^{1}H NMR (400 MHz, $CDCl_3$): δ 13.56 (s, br, 1H), 7.97 (d, J = 7.6 Hz, 2H), 7.68 (d, J = 7.2 Hz, 1H), 7.59-7.49 (m, 4H), 6.96-6.93 (m, 2H), 3.89 (t, J = 7.2 Hz, 2H), 1.77-1.73 (m, 2H), 1.45-1.40 (m, 2H), 0.97 (t, J = 7.2 Hz, 3H); ^{13}C NMR (100 MHz, $CDCl_3$): δ 182.1, 163.8, 153.5, 140.6, 140.1, 138.2, 132.7, 132.3, 128.8, 127.5, 125.7, 120.2, 118.4, 109.8, 41.2, 29.5, 20.2, 13.8; IR (KBr, cm^{-1}): 2957, 2853, 1696, 1669, 1619, 1472, 1129, 707, 612; HRMS (ESI) calcd. for $C_{19}H_{20}N_3O_2^+$,[M+H]$^+$, 322.1556, found 322.1560.

***(E)-N'-(3-Oxo-1-pentylindolin-2-ylidene)benzohydrazide (3e)*:**

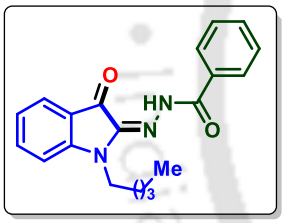

Red gummy liquid, (67 mg, 80% yield); ^{1}H NMR (400 MHz, $CDCl_3$): δ 13.56 (s, br, 1H), 7.97 (d, J = 7.6 Hz, 2H), 7.68 (d, J = 7.2 Hz, 1H), 7.57-7.49 (m, 4H), 6.96-6.92 (m, 2H), 3.88 (t, J = 7.2 Hz, 2H), 1.78-1.76 (m, 2H), 1.38-1.37 (m, 4H), 0.90 (t, J = 6.4 Hz, 3H); ^{13}C NMR (100 MHz, $CDCl_3$): δ 182.1, 163.8, 153.5, 140.1, 138.3, 138.2, 132.7, 132.3, 128.8, 127.5, 125.7, 120.2, 118.3, 109.9, 41.4, 29.0, 27.1, 22.4, 14.0; IR (KBr, cm^{-1}): 2956, 2854, 1696, 1670, 1620, 1472, 1130, 707, 613; HRMS (ESI) calcd. for $C_{20}H_{22}N_3O_2^+$,[M+H]$^+$, 336.1712, found 336.1723.

***(E)-N'-(1-Isopropyl-3-oxoindolin-2-ylidene)benzohydrazide (3f)*:**

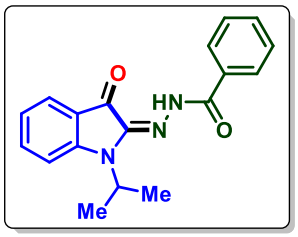

Red solid (57 mg, 75% yield); mp 141-143 ^{o}C; ^{1}H NMR (400 MHz, $CDCl_3$): δ 13.69 (s, br, 1H), 7.99 (d, J = 7.6 Hz, 2H), 7.69 (d, J = 7.6 Hz, 1H), 7.59-7.49 (m, 4H), 7.11 (d, J = 8.4 Hz, 1H), 6.93 (t, J = 7.6 Hz, 1H), 4.85-4.78 (m, 1H), 1.55 (d, J = 7.2 Hz, 6H); ^{13}C NMR (100 MHz, $CDCl_3$): δ 182.3, 163.9, 152.5, 139.8, 137.9, 132.7, 132.3, 128.8, 127.5, 125.9, 120.0, 118.8,

111.5, 45.2, 19.5; IR (KBr, cm^{-1}): 3440, 2972, 2924, 1693, 1670, 1617, 1524, 1468, 1225, 976, 706, 462; HRMS (ESI) calcd. for $C_{18}H_{18}N_3O_2^+$,$[M+H]^+$, 308.1399, found 308.1392.

***(E)-N'-(1-Cyclopentyl-3-oxoindolin-2-ylidene)benzohydrazide (3g)*:**

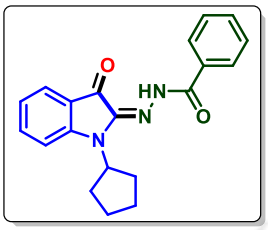

Red solid (64 mg, 78% yield); mp 127-129 ^oC, ^1H NMR (400 MHz, $CDCl_3$): δ 13.69 (s, br, 1H), 7.99 (d, J = 7.2 Hz, 2H), 7.70 (d, J = 7.2 Hz, 1H), 7.57-7.49 (m, 4H), 7.03 (d, J = 8.4 Hz, 1H), 6.94 (t, J = 7.2 Hz, 1H), 5.01-4.94 (m, 1H), 2.21-2.01 (m, 6H), 1.74 (s, br, 2H); ^{13}C NMR (100 MHz, $CDCl_3$): δ 182.3, 163.9, 152.2, 140.1, 137.8, 132.8, 132.2, 128.8, 127.5, 125.8, 120.0, 118.8, 111.3, 53.5, 27.6, 25.0; IR (KBr, cm^{-1}): 3432, 2923,2853, 1695, 1669, 1611, 1533, 1484, 1221, 751, 471; HRMS (ESI) calcd. for $C_{20}H_{19}N_3NaO_2^+$,$[M+Na]^+$, 356.1375, found 356.1383.

***(E)-N'-(1-(4-Methylbenzyl)-3-oxoindolin-2-ylidene)benzohydrazide (3h)*:**

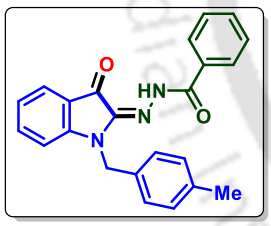

Red solid (66 mg, 72% yield); mp160-162 ^oC; ^1H NMR (400 MHz, $CDCl_3$): δ 13.49 (s, br, 1H), 7.91 (d, J = 7.6 Hz, 2H), 7.62 (d, J = 7.6 Hz, 1H), 7.52-7.39 (m, 4H), 7.15-6.99 (m, 4H), 6.87 (t, J = 7.6 Hz, 1H), 6.78 (d, J = 8.0 Hz, 1H), 4.99 (s, 2H), 2.24 (s, 3H); ^{13}C NMR (100 MHz, $CDCl_3$): δ 180.8, 162.8, 152.2, 139.1, 137.5, 137.2, 134.4, 131.6, 131.3, 127.8, 127.6, 127.5, 127.0, 126.5, 124.6, 123.4, 119.6, 117.5, 109.6, 43.9, 20.4; IR (KBr, cm^{-1}): 3244, 3043,2961, 2921, 2852, 1739, 1577, 1684, 1662, 1618, 1538, 1475, 1261, 798, 442; HRMS (ESI) calcd. for$C_{23}H_{20}N_3O_2^+$,$[M+H]^+$, 370.1556, found 370.1553.

***(E)-N'-(1-(4-Chlorobenzyl)-3-oxoindolin-2-ylidene)benzohydrazide (3i)*:**

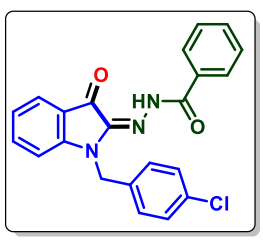

Red solid (68 mg, 70% yield); mp191-193 ^oC; ^1H NMR (400 MHz, $CDCl_3$); δ 13.52 (s, br, 1H), 7.99 (d, J = 7.6 Hz, 2H),7.71 (d, J = 7.2 Hz, 1H), 7.60-7.49 (m, 4H), 7.30 (s, br, 4H), 6.98 (t, J

= 7.6 Hz, 1H), 6.84 (d, *J* = 8.0 Hz, 1H), 5.07 (s, 2H); ^{13}C NMR (100 MHz, $CDCl_3$): δ 181.7, 163.8, 152.8, 139.9, 138.2, 134.1, 133.6, 133.2, 132.5, 132.4, 130.8, 130.0, 129.2, 129.0, 128.9, 128.8, 127.5, 125.8, 120.9, 118.6, 110.3, 44.2; IR (KBr, cm^{-1}): 3441, 3236, 3062, 2923,2853,1740, 1685, 1658, 1618, 1534, 1475, 1267, 752, 447; HRMS (ESI) calcd. for $C_{22}H_{17}ClN_3O_2^+$,$[M+H]^+$, 390.1009, found 390.1004.

***(E)-N'-(1-(2-Bromobenzyl)-3-oxoindolin-2-ylidene)benzohydrazide (3j)*:**

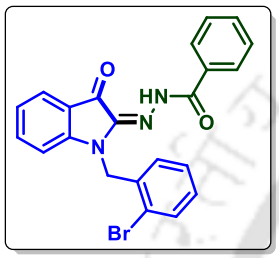

Red solid (75 mg, 70% yield); mp 187-189 ^{o}C ;^{1}H NMR (400 MHz, $CDCl_3$): δ 13.57 (s, br, 1H), 7.97 (d, *J* = 7.2 Hz, 2H), 7.74 (d, *J* = 7.6 Hz, 1H), 7.61-7.56 (m, 2H), 7.53-7.48 (m, 3H), 7.23-7.20 (m, 1H), 7.14 (t, *J* = 7.2 Hz, 2H), 6.99 (t, *J* = 7.6 Hz, 1H), 6.76 (d, *J* = 8.4 Hz, 1H), 5.21 (s, 2H); ^{13}C NMR (100 MHz, $CDCl_3$):δ 181.7, 163.8, 152.9, 140.1, 138.4, 134.3, 133.1, 132.5, 132.4, 129.2, 128.9, 127.8, 127.5, 125.7, 122.6, 121.0, 118.6, 110.8, 45.2; IR (KBr, cm^{-1}): 3428, 3270, 3057, 2922,2851, 1691, 1665, 1621, 1619, 1574, 1529, 1473, 1258, 748, 447; HRMS (ESI) calcd. for $C_{22}H_{17}BrN_3O_2^+$,$[M+H]^+$, 434.0504, found 434.0502.

***(E)-N'-(1-Allyl-3-oxoindolin-2-ylidene)benzohydrazide (3k)*:**

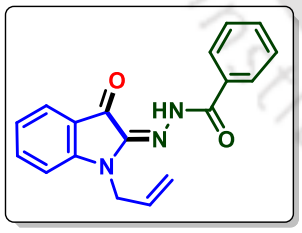

Red solid (49 mg, 65% yield); mp 133-135 ^{o}C; ^{1}H NMR (400 MHz, $CDCl_3$): δ 13.54 (s, br, 1H), 7.98 (d, *J* = 7.6 Hz, 2H), 7.70 (d, *J* = 7.2 Hz, 1H), 7.58-7.49 (m, 4H), 6.99-6.93 (m, 2H), 5.93-5.85 (m, 1H), 5.35-5.23 (m, 2H), 4.53 (d, *J* = 5.2 Hz, 2H); ^{13}C NMR (100 MHz, $CDCl_3$): δ 181.9, 163.9, 153.3, 139.7, 138.2, 132.6, 132.3, 131.1, 128.9, 127.5, 125.6, 123.8, 120.6, 118.6, 118.5, 117.8, 110.5, 43.6; IR (KBr, cm^{-1}): 3425, 2924, 2860, 1618, 1532, 1469, 1261, 801, 699, 468; HRMS (ESI) calcd. for $C_{18}H_{16}N_3O_2^+$,$[M+H]^+$, 306.1243, found 306.1238.

***(E)-N'-(1-Ethyl-5-methyl-3-oxoindolin-2-ylidene)benzohydrazide (3l)*:**

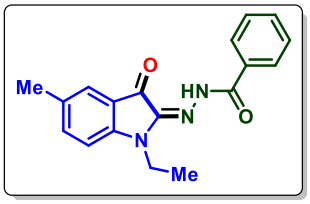

Red solid (52 mg, 68% yield); mp 143-145 ^{o}C; ^{1}H NMR (400 MHz, $CDCl_3$): δ 13.55 (s, br, 1H), 7.98 (d, J = 7.2 Hz, 2H), 7.57 (t, J = 7.2 Hz, 1H), 7.51 (t, J = 7.6 Hz, 2H), 7.46 (s, 1H), 7.39 (d, J = 7.6 Hz, 1H), 6.85 (d, J= 8.4 Hz, 1H), 3.92 (q, J = 6.8 Hz, 2H), 2.33 (s, 3H), 1.31 (t, J = 7.2 Hz, 3H); ^{13}C NMR (100 MHz, $CDCl_3$): δ 182.3, 163.9, 151.4, 140.1, 139.5, 132.8, 132.2, 130.0, 128.8, 128.7, 127.5, 125.4, 118.5, 109.6, 36.0, 20.5, 12.5; IR (KBr, cm^{-1}): 3433, 2922,2852, 1690, 1664, 1628, 1488, 1264, 794, 689, 452; HRMS (ESI) calcd. for $C_{18}H_{18}N_3O_2^+$,[M+H]$^+$, 308.1399, found 308.1396.

***(E)-N'-(5-Bromo-1-isopropyl-3-oxoindolin-2-ylidene)benzohydrazide (3m)*:**

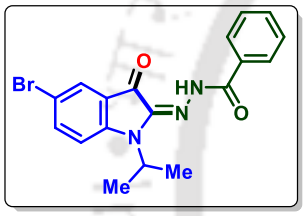

Red solid (72 mg, 75% yield); mp 166-168 ^{o}C; ^{1}H NMR (400 MHz, $CDCl_3$): δ 13.58 (s, br, 1H), 7.96 (d, J = 7.6 Hz, 2H), 7.80-7.79 (m, 1H), 7.63-7.58 (m, 2H), 7.54-7.50 (m, 2H), 7.03 (d, J = 8.8 Hz, 1H), 4.82-4.79 (m, 1H), 1.54 (d, J = 6.8 Hz, 6H); ^{13}C NMR (100 MHz, $CDCl_3$): δ 185.0, 162.1, 151.0, 140.2, 134.4, 132.5, 128.9, 128.2, 127.6, 120.2, 113.0, 112.6, 45.5, 19.5; IR (KBr, cm^{-1}): 3437, 2925, 1616, 1466, , 1262, 1107, 703; HRMS (ESI) calcd. for $C_{18}H_{17}BrN_3O_2^+$,[M+H]$^+$, 386.0504, found 386.0514.

***(E)-N'-(1-Isopropyl-3-oxoindolin-2-ylidene)-4-methylbenzohydrazide (3n)*:**

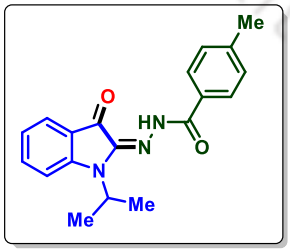

Red solid (60 mg, 75% yield); mp 153-155 ^{o}C; ^{1}H NMR (400 MHz, $CDCl_3$): δ 13.67 (s, br, 1H), 7.88 (d, J = 8.0 Hz, 2H), 7.69 (d, J = 8.0 Hz, 1H), 7.55-7.51 (m, 1H), 7.30 (d, J = 8.0 Hz, 2H), 7.11 (d, J = 8.0 Hz, 1H), 6.93 (t, J = 7.6 Hz, 1H), 4.85-4.78 (m, 1H), 2.43 (s, 3H), 1.54 (d, J = 7.2 Hz, 6H); ^{13}C NMR (100 MHz, $CDCl_3$): δ 182.2, 163.9, 152.4, 142.9, 139.6, 137.9, 129.9, 129.5, 127.6, 125.8, 119.9, 118.8, 111.5, 45.2, 21.6, 19.5; IR (KBr,cm^{-1}): 3435, 2924,2852, 1687, 1667, 1614, 1531, 1568, 1498, 1266,

750, 456; HRMS (ESI) calcd. for $C_{19}H_{20}N_3O_2^+$,[M+H]$^+$, 322.1556, found 322.1551.

***(E)-4-Methoxy-N'-(3-oxo-1-propylindolin-2-ylidene)benzohydrazide (3o)*:**

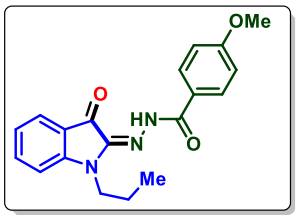

Red solid (62 mg, 74% yield); mp 140-142 ^oC; ^1H NMR (400 MHz, $CDCl_3$): δ 13.54 (s, br, 1H), 7.96 (d, J = 8.8 Hz, 2H), 7.68 (d, J = 8.0 Hz, 1H), 7.55 (t, J = 7.6 Hz, 1H), 6.99 (d, J = 8.0 Hz, 2H), 6.93 (t, J = 8.0 Hz, 2H), 3.88-3.83 (m, 5H, OMe x 3H, -NCH_2 x 2H), 1.85-1.76 (m, 2H), 0.99 (t, J = 7.2 Hz, 3H); ^{13}C NMR (100 MHz, $CDCl_3$): δ 181.9, 163.3, 162.8, 153.5, 138.0, 129.5, 125.6, 125.0, 120.1, 118.3, 114.0, 109.8, 55.4, 42.9, 20.8, 11.4; IR (KBr, cm^{-1}): 3434, 3266, 3013, 2957, 2925, 2853, 1691, 1669, 1621, 1605, 1500, 1484, 1252, 835, 750, 448; HRMS (ESI) calcd. for $C_{19}H_{20}N_3O_3^+$,[M+H]$^+$, 338.1505, found 338.1498.

***(E)-3-Methoxy-N'-(1-(4-methylbenzyl)-3-oxoindolin-2-ylidene)benzohydrazide (3p)*:**

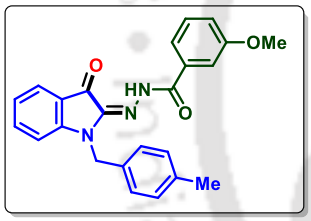

Red solid (71 mg, 72% yield); mp 173-175 ^oC;^1H NMR (400 MHz, $CDCl_3$) δ 13.55 (s, br, 1H), 7.96 (d, J = 8.8 Hz, 2H), 7.70 (d, J = 7.6 Hz, 1H), 7.50-7.46 (m, 1H), 7.22-7.18 (m, 1H), 7.15 (s, 2H), 7.07 (d, J = 7.2 Hz, 1H), 7.00-6.93 (m, 3H), 6.86 (d, J = 8.4 Hz, 1H), 5.07 (s, 2H), 3.88 (s, 3H), 2.31 (s, 3H); ^{13}C NMR (100 MHz, $CDCl_3$): δ 181.8, 163.3, 162.9, 153.2, 138.5, 138.1, 135.6, 129.5, 128.6, 128.5, 128.0, 125.5, 124.9, 124.4, 120.5, 118.5, 114.1, 110.6, 55.5, 44.9, 21.4; IR (KBr, cm^{-1}): 3425, 2922, 2851, 1685, 1662, 1620, 1606, 1569, 1502, 1473, 1255, 838, 745, 443; HRMS (ESI) calcd. for $C_{24}H_{22}N_3O_3^+$,[M+H]$^+$, 400.1661, found 400.1668.

***(E)-N'-(1-Butyl-3-oxoindolin-2-ylidene)-4-(trifluoromethyl)benzohydrazide (3q)*:**

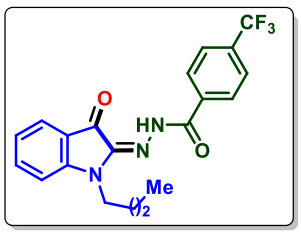

Red gummy liquid (82 mg, 85% yield); ^1H NMR (400 MHz, $CDCl_3$): δ 13.61 (s, br, 1H), 8.09 (d, J = 8.0 Hz, 2H), 7.77 (d, J = 8.0 Hz, 2H), 7.68 (d, J = 7.6 Hz, 1H), 7.58 (t, J = 7.6 Hz, 1H), 6.96 (d, J = 8.0 Hz, 2H), 3.86 (t, J = 7.2 Hz, 2H), 1.77-1.73 (m, 2H), 1.45-1.40 (m, 2H), 0.97 (t, J = 7.6 Hz, 3H); ^{13}C NMR (100

MHz, $CDCl_3$): δ 182.4, 162.5, 153.6, 140.5, 138.5, 136.0, 133.7, 127.9, 125.96, 125.93, 125.88, 120.5, 118.2, 109.9, 41.2, 29.5, 20.2, 13.8; IR (KBr, cm^{-1}): 2920, 1697, 1672, 1620, 1531, 1473, 1326, 1130, 980, 614; ^{19}F NMR ($CDCl_3$ + Hexafluorobenzene): δ –63.0; HRMS (ESI) calcd. for $C_{20}H_{19}F_3N_3O_2^+$,$[M+H]^+$, 390.1429, found 390.1440.

***(E)-4-Bromo-N'-(1-butyl-3-oxoindolin-2-ylidene)benzohydrazide (3r)*:**

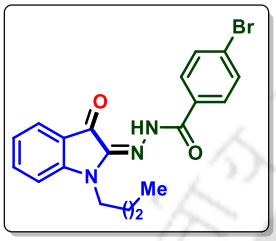

Red solid (82 mg, 82% yield); mp 126-128 ^oC; ^1H NMR (400 MHz, $CDCl_3$): δ 13.49 (s, br, 1H), 7.78 (d, J = 8.4 Hz, 2H), 7.61-7.56 (m, 3H), 7.50 (t, J = 8.4 Hz, 1H), 6.88 (t, J = 8.0 Hz, 2H), 3.81 (t, J = 6.8 Hz, 2H), 1.69-1.63 (m, 2H), 1.37-1.32 (m, 2H), 0.89 (t, J = 7.6 Hz, 3H); ^{13}C NMR (100 MHz, $CDCl_3$): δ 182.3, 162.8, 153.6, 140.3, 138.3, 132.1, 131.6, 129.1, 127.1, 125.8, 120.4, 118.3, 109.9, 41.1, 29.5, 20.2, 13.8; IR (KBr, cm^{-1}): 3430, 2924, 2854, 1622, 1465, 1104; HRMS (ESI) calcd. for$C_{19}H_{19}BrN_3O_2^+$,$[M+H]^+$, 400.0661, found 400.0663.

***(E)-N'-(5-Bromo-1-ethyl-3-oxoindolin-2-ylidene)-4-(trifluoromethyl)benzohydrazide (3s)*:**

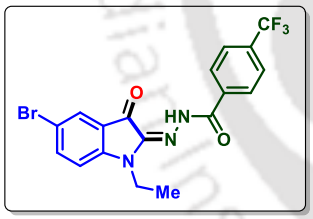

Red solid (95 mg, 87% yield); mp 177-179 ^oC;^1H NMR (400 MHz, $CDCl_3$) δ 13.41 (s, br, 1H), 8.00 (d, J = 8.0 Hz, 2H), 7.77-7.70 (m, 3H), 7.60-7.57 (m, 1H), 6.80 (d, J = 8.8 Hz, 1H), 3.85 (q, J = 6.8 Hz, 2H), 1.25 (t, J = 6.8 Hz, 3H); ^{13}C NMR (100 MHz, $CDCl_3$): δ 180.9, 162.5, 151.7, 140.7, 139.6, 135.8, 128.3, 128.0, 125.9, 124.9, 122.2, 119.7, 113.0, 111.4, 36.2, 12.4; ^{19}F NMR ($CDCl_3$ + Hexafluorobenzene): δ–63.0; IR (KBr, cm^{-1}): 3430, 2926, 1554, 1467, 1390, 1316, 1272, 1100, 881, 790, 622, 459; HRMS (ESI) calcd. for $C_{18}H_{14}BrF_3N_3O_2^+$,$[M+H]^+$, 440.0221, found: 440.0228.

***(E)-N'-(1-Ethyl-7-fluoro-3-oxoindolin-2-ylidene)-4-(trifluoromethyl)benzohydrazide (3t)*:**

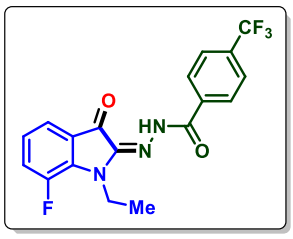

Red solid (80 mg, 85% yield); mp 175-177 ^oC;^1H NMR (400 MHz, $CDCl_3$): δ 13.58 (s, br, 1H), 8.09 (d, J = 7.6 Hz, 2H), 7.78 (d, J = 8.0 Hz, 2H), 7.51 (d, J = 7.6 Hz, 1H), 7.35-7.26 (m,

1H), 6.93-6.89 (m, 1H), 4.13 (q, *J* = 6.8 Hz, 2H), 1.37 (t, *J* = 6.8 Hz, 3H); ^{13}C NMR (100 MHz, $CDCl_3$):*δ* 181.7, 162.5, 150.0, 147.5, 140.3, 140.0, 135.8, 128.0, 126.0, 125.9, 125.1, 125.0, 121.7, 121.6, 120.9, 120.8, 38.7, 13.9; ^{19}F NMR ($CDCl_3$ + Hexafluorobenzene): δ –134.8, –63.0;IR (KBr,cm^{-1}): 3429, 3274, 3044, 2924, 2852, 1693, 1671, 1630, 1591, 1569, 1504, 1469, 1262, 760, 433; HRMS (ESI) calcd. for $C_{18}H_{14}F_4N_3O_2^+$,$[M+H]^+$, 380.1022, found 380.1031.

III.10. Representative Spectra

(E)-N'-(1-Methyl-3-oxoindolin-2-ylidene)benzohydrazide (3a): ^{1}H NMR (CDCl$_3$, 400 MHz)

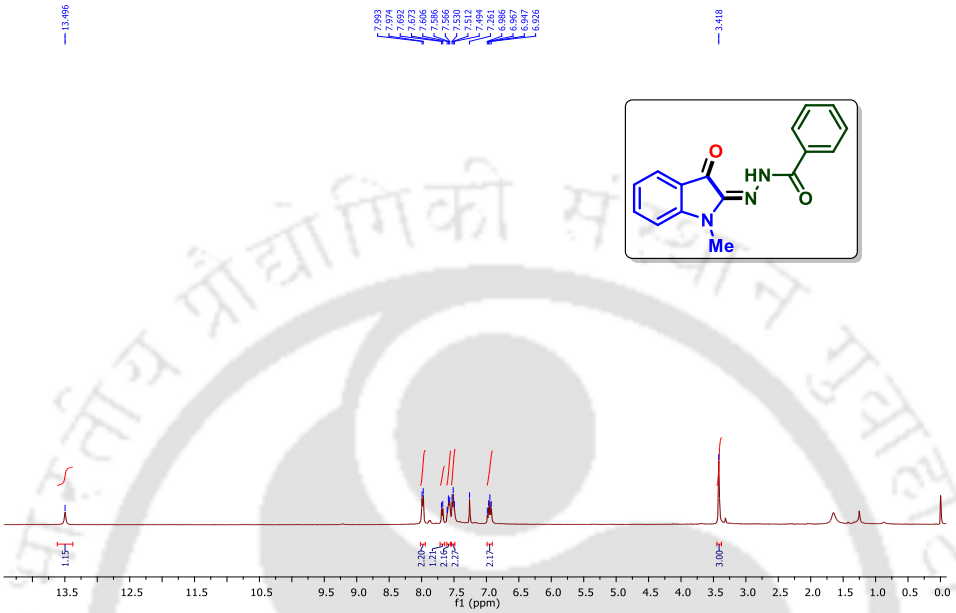

(E)-N'-(1-Methyl-3-oxoindolin-2-ylidene)benzohydrazide (3a: ^{13}C{^{1}H} NMR (CDCl$_3$, 100 MHz)

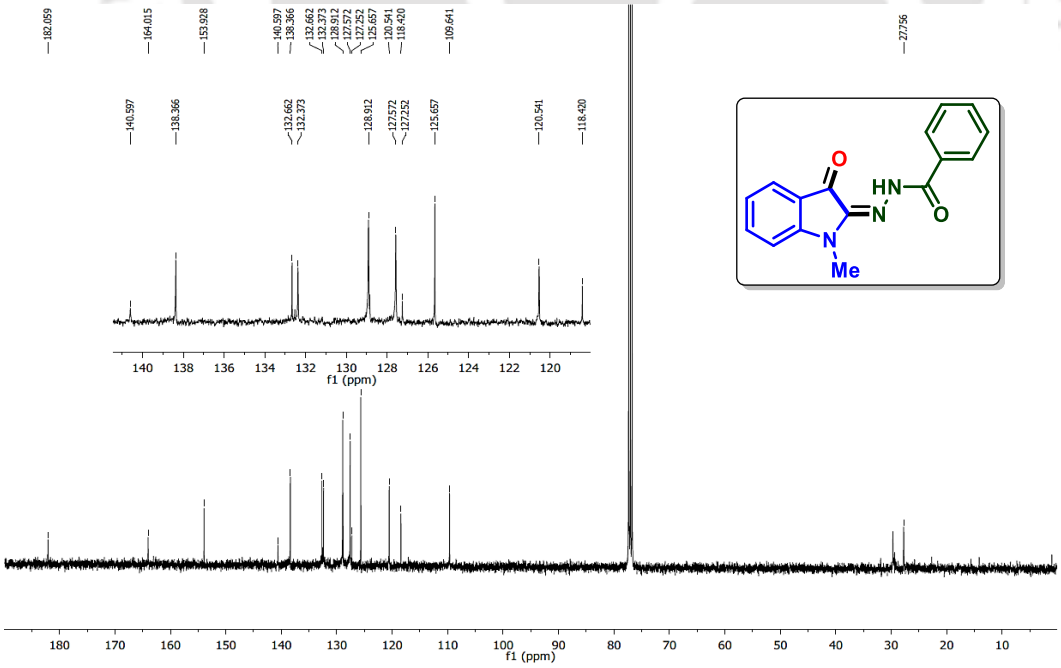

(E)-N'-(1-Isopropyl-3-oxoindolin-2-ylidene)benzohydrazide (3f):^{1}H NMR (CDCl$_3$, 400 MHz)

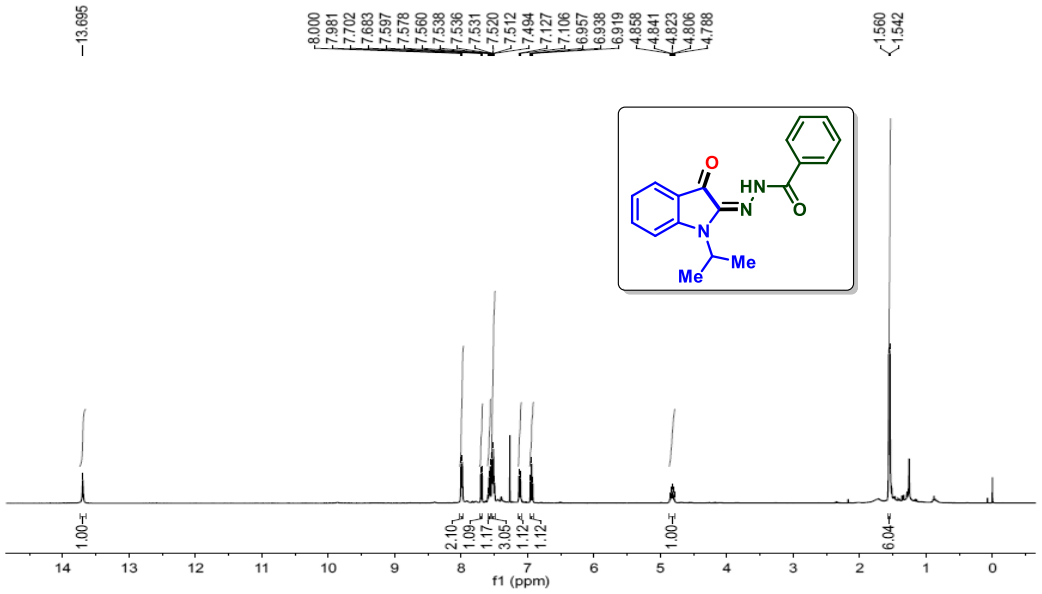

(E)-N'-(1-Isopropyl-3-oxoindolin-2-ylidene)benzohydrazide (3f):^{13}C{^{1}H} NMR (CDCl$_3$, 100 MHz)

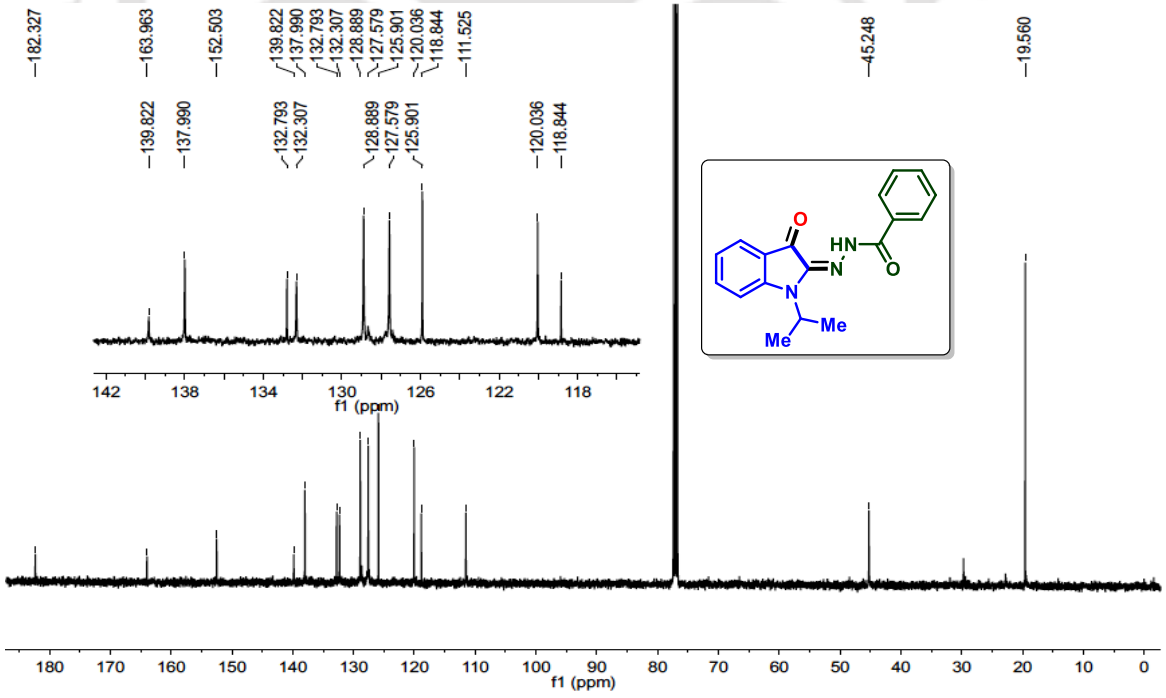

(E)-N'-(5-Bromo-1-isopropyl-3-oxoindolin-2-ylidene)benzohydrazide (3m):^{1}H NMR ($CDCl_3$, 400 MHz)

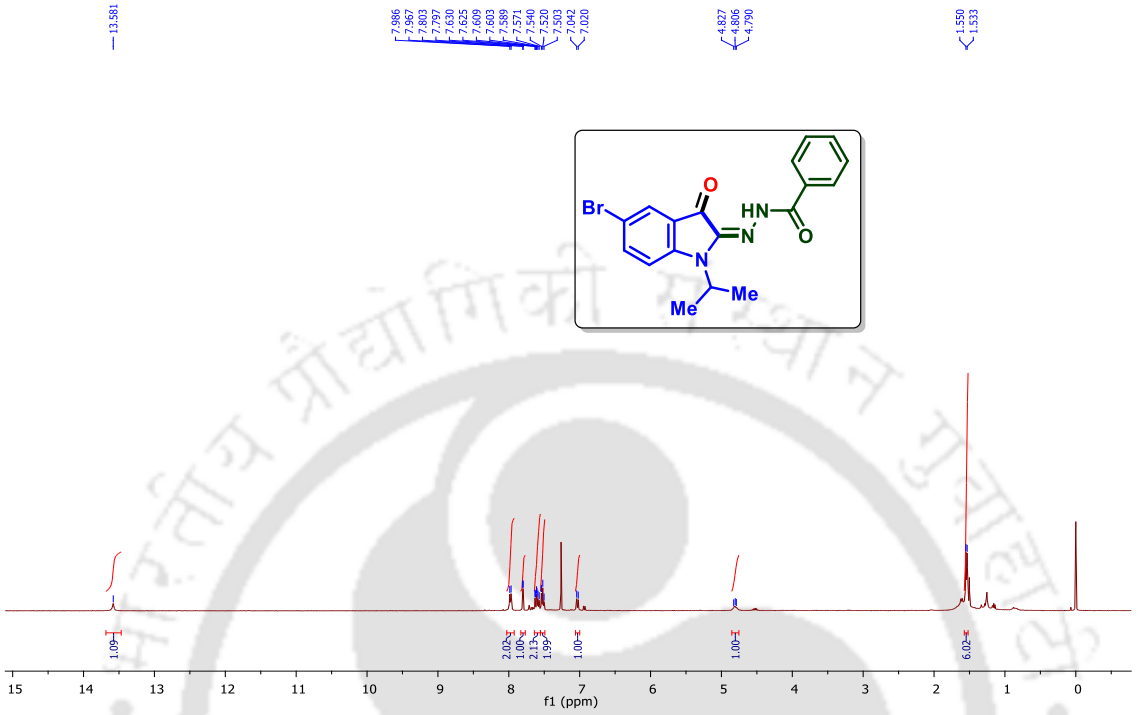

(E)-N'-(5-Bromo-1-isopropyl-3-oxoindolin-2-ylidene)benzohydrazide (3m):$^{13}C\{^{1}H\}$ NMR ($CDCl_3$, 100 MHz)

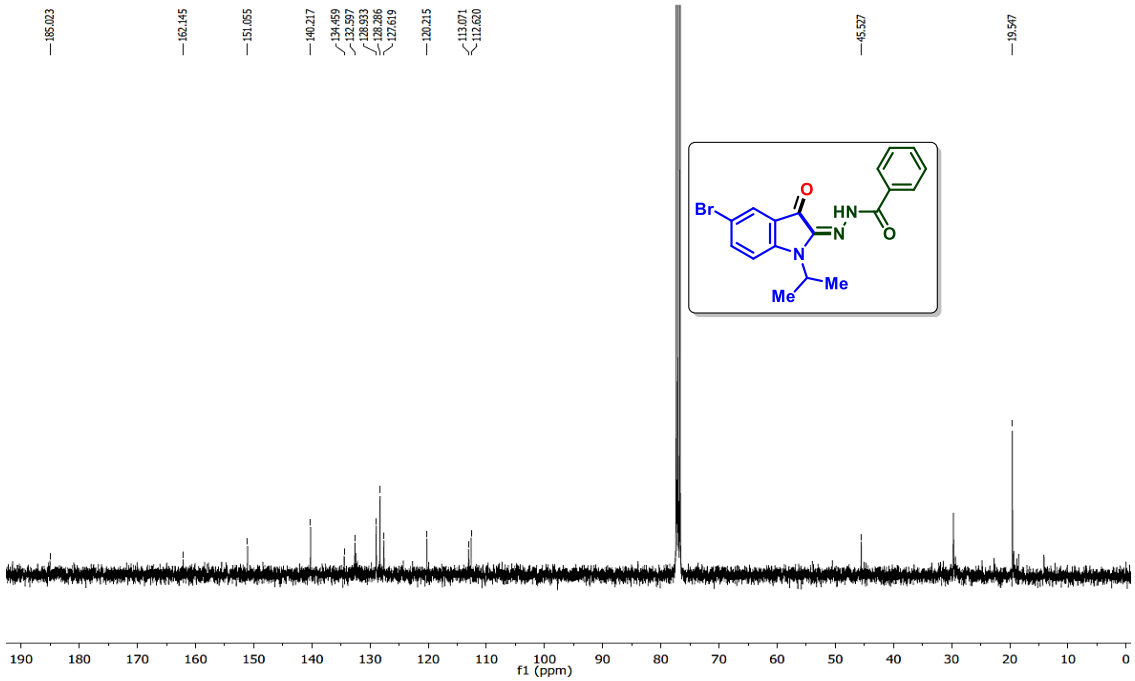

(E)-N'-(1-Butyl-3-oxoindolin-2-ylidene)-4-(trifluoromethyl)benzohydrazide (3q)*: *^{1}H NMR (CDCl$_3$, 400 MHz)

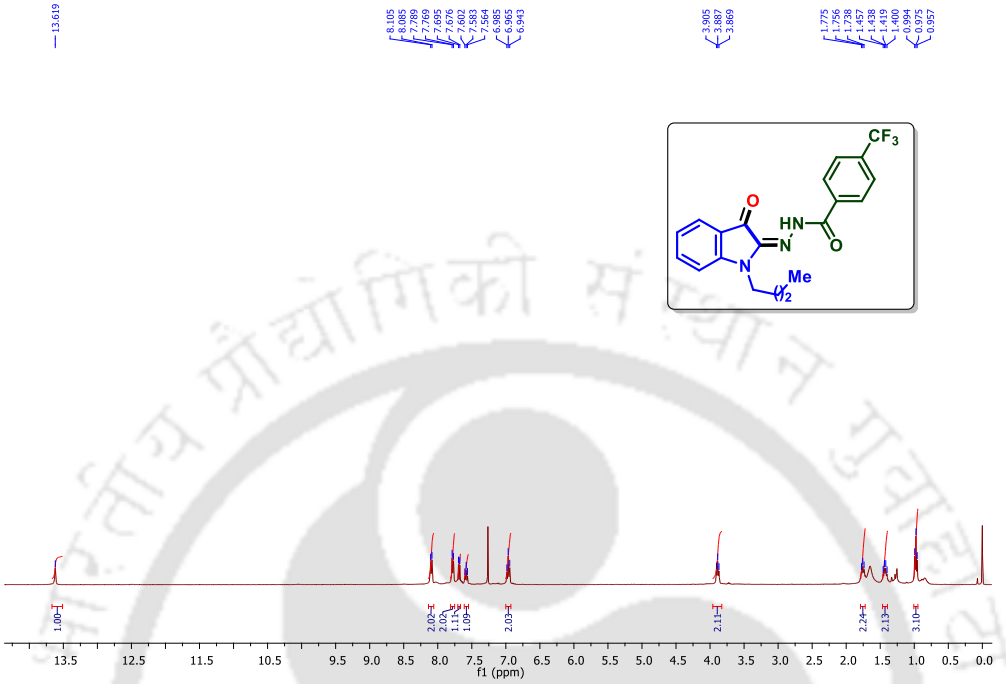

(E)-N'-(1-Butyl-3-oxoindolin-2-ylidene)-4-(trifluoromethyl)benzohydrazide (3q)*: *^{13}C{^{1}H} NMR (CDCl$_3$, 100 MHz)

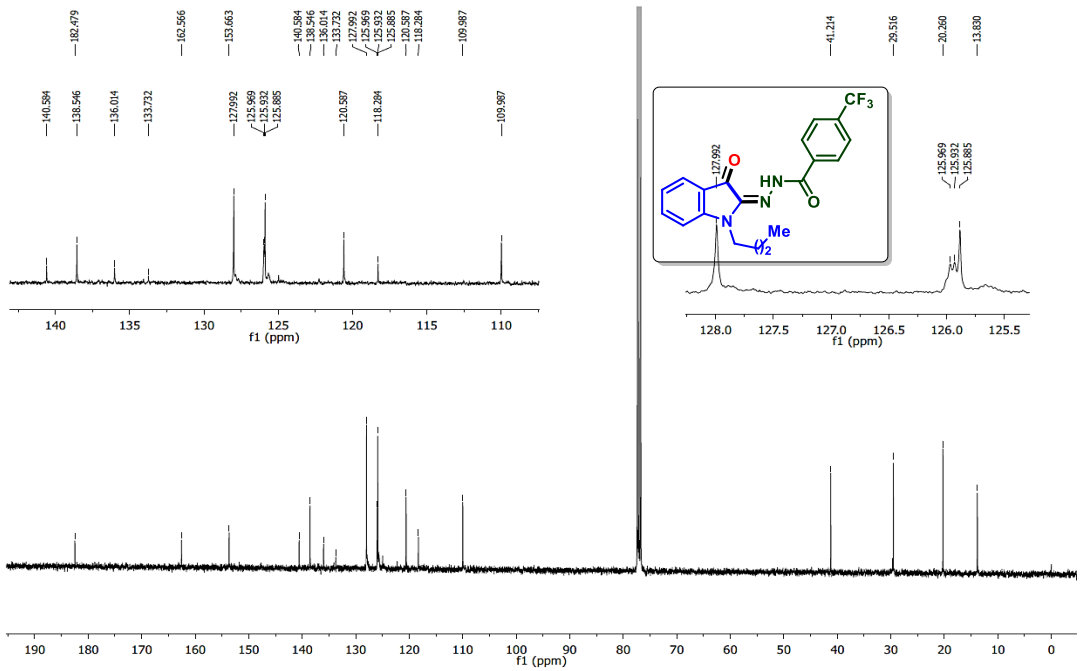

***(E)-N'-(1-Ethyl-7-fluoro-3-oxoindolin-2-ylidene)-4-(trifluoromethyl)benzohydrazide (3t)*:**

^{1}H NMR ($CDCl_3$, 400 MHz)

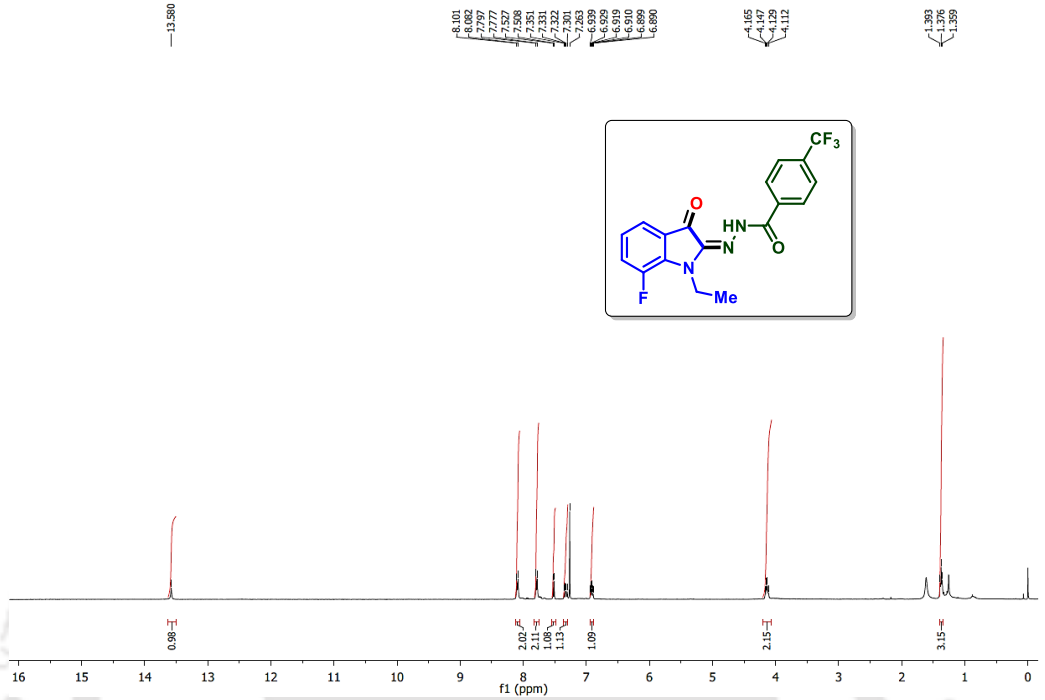

***(E)-N'-(1-Ethyl-7-fluoro-3-oxoindolin-2-ylidene)-4-(trifluoromethyl)benzohydrazide (3t)*:**

^{13}C{^{1}H} NMR ($CDCl_3$, 100 MHz)

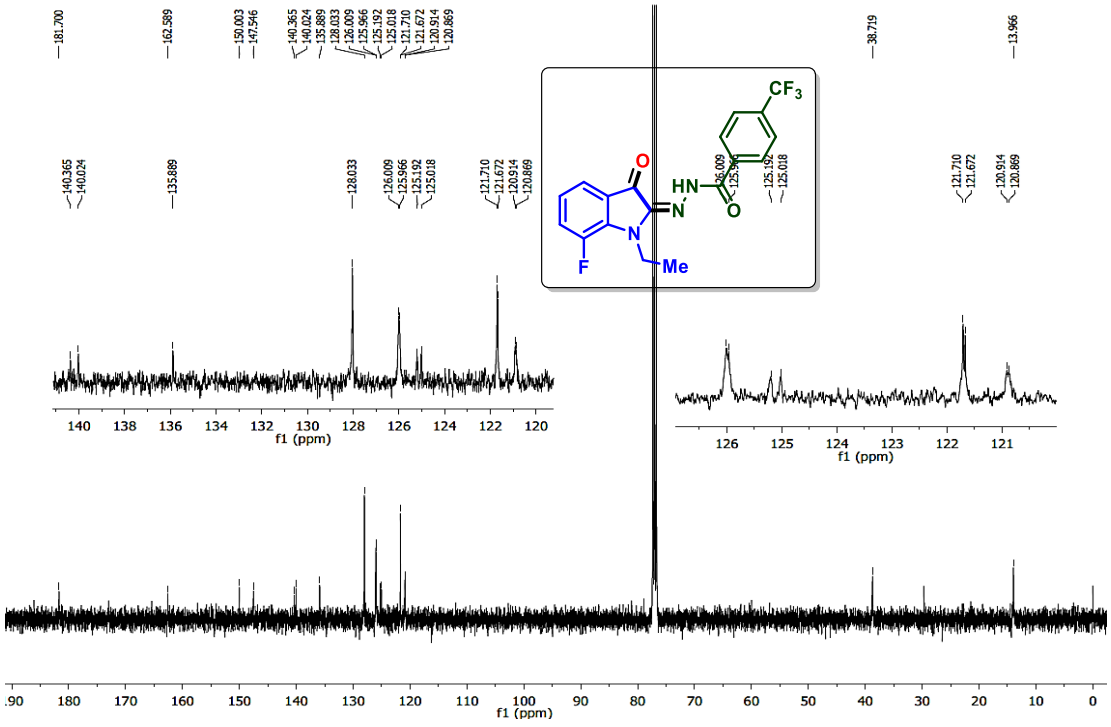

***(E)-N'-(1-Ethyl-7-fluoro-3-oxoindolin-2-ylidene)-4-(trifluoromethyl)benzohydrazide (3t)*:**

^{19}F NMR ($CDCl_3$, 376 MHz)

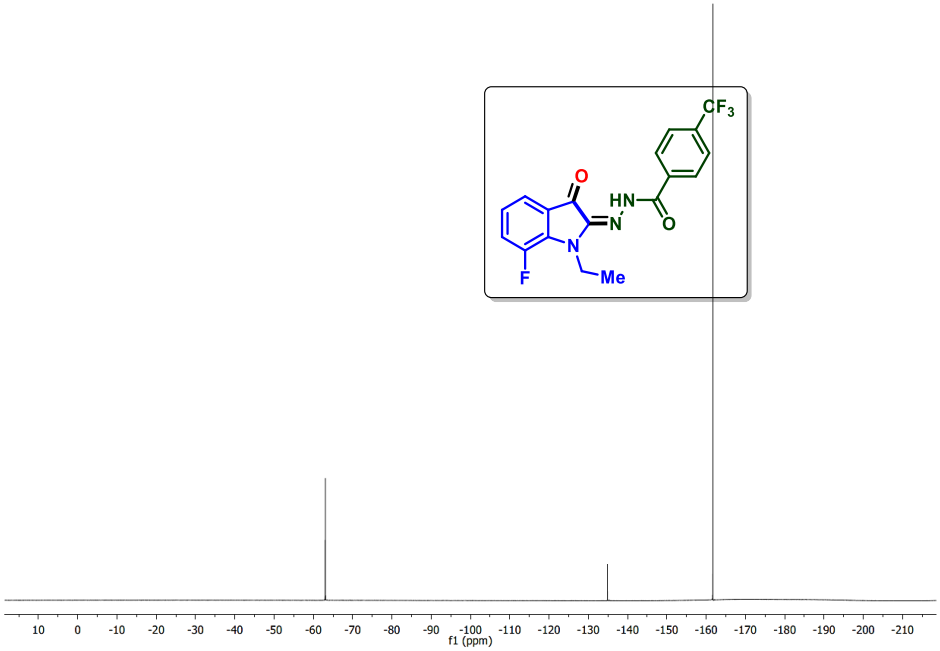

CHAPTER-IV

Electrochemical Amidation: Benzoyl Hydrazine/ Carbazate and Amine as Coupling Partners

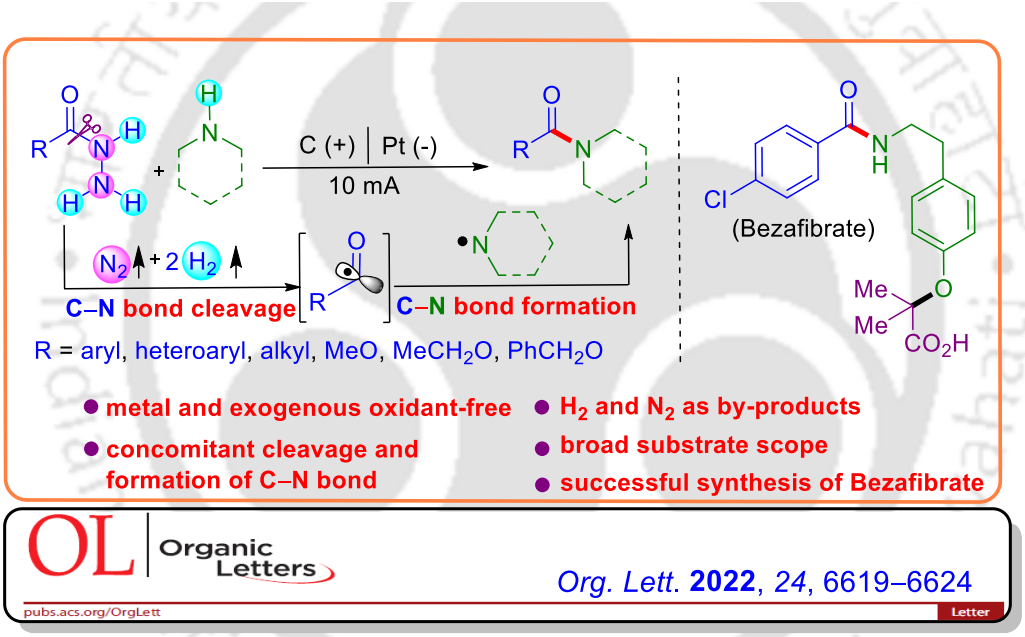

Abstract: *An electrochemical amidation of benzoyl hydrazine/carbazate and primary/secondary amine as coupling partners via concomitant cleavage and formation of C(sp^2)-N bonds has been achieved. This methodology proceeds under metal-free and exogenous oxidant-free conditions producing N_2 and H_2 as byproducts. Mechanistic studies reveal the in situ generations of both acyl and N-centered radicals from benzoyl hydrazines and amines. The utility of this protocol is demonstrated through a large-scale, and synthesis of bezafibrate a hyperlipidemic drug.*

भारतीय प्रौद्योगिकी संस्थान गुवाहाटी
Indian Institute of Technology Guwahati

CHAPTER IV

Electrochemical Amidation: Benzoyl Hydrazine/Carbazate and Amine as Coupling Partners

IV.1. Introduction

Amides are prevalent in biomolecules such as peptides and proteins and are found in natural products, pharmaceuticals, polymers, and fine chemicals (Figure IV.1).[1,2] In 2014, an analysis by Brown *et al*. revealed that 50% of medicinally relevant compounds possess at least one amidic linkage.[3] The coupling of amine with carboxylic acid, ester, and acyl chloride using transition metals or activating agents[4] and transition-metal-catalyzed carbonylative amidation are the frequently used methods.[5] Further, *N*-heterocyclic carbenes (NHCs) have been effectively used as catalysts for metal-free amidation of activated esters [Scheme IV.1 (a)].[6] However, these amidation protocols often generate stoichiometric quantities of toxic waste, and a few of the strategies suffer from limitations such as the use of expensive transition-metal catalysts having limited substrate scope. The generation of acyl radicals is important in various biochemical and synthetic processes.[9] Thus, the development of a waste-free and milder method for its generation from benzoyl hydrazine is highly desirable.

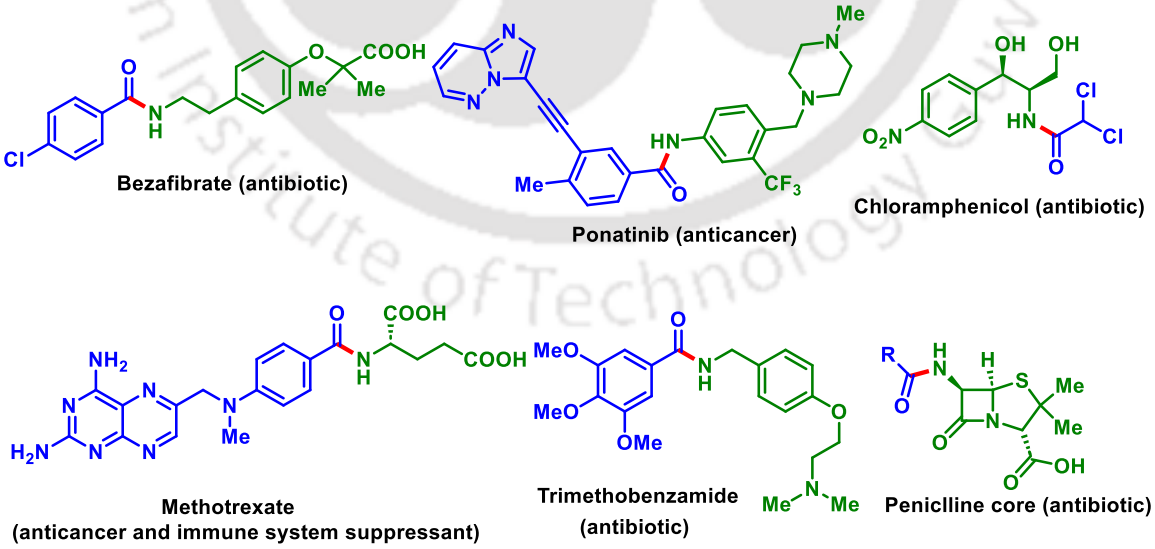

Figure IV.1. *Representative bioactive amides.*

The easily accessible air- and moisture-stable benzoyl hydrazine is an ideal precursor of acyl radicals obtained by the expulsion of N_2 and H_2.[7] However, the reported methodologies for the generation of acyl radical from benzoyl hydrazine use an excess of catalyst and chemical oxidants such as $(NH_4)_2S_2O_8$ and PbO_2, thereby generating waste [(Scheme IV.1.(b)].[8] The generation of acyl radicals is important in various biochemical and synthetic processes.[9] Thus, the development of a waste-free and milder method for its generation from benzoyl hydrazine is highly desirable.

Scheme IV.1. Amide bond formation strategies

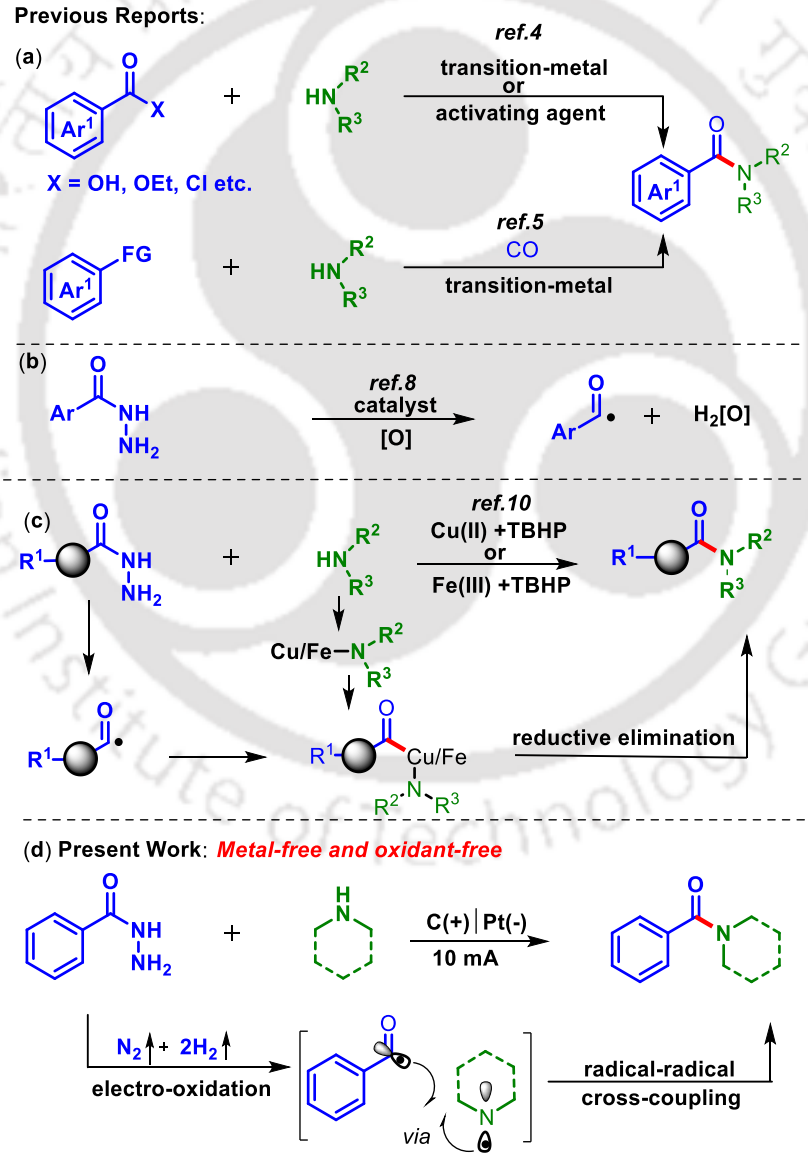

Recently, Zou group developed a Cu(II)/TBHP-catalyzed oxidative coupling of amines and carbazates leading to carbamates [(Scheme IV.1.(c)].[10a] Following the same strategy, they subsequently developed a Fe(III)/TBHP-catalyzed synthesis of amides from benzoyl hydrazines and amines [Scheme IV.1.(c)].[10b] These reactions proceed through an *in situ* generation of alkoxy carbonyl/acyl radicals involving metal complexation *via* an oxidative addition followed by a reductive elimination leading to carbamates or amides. The reported amidation strategies for the synthesis of amides are neither atom-economical nor sustainable;[11] thus, constructing amide bonds under mild conditions would be much more alluring. Recently, electrochemical approaches have emerged as powerful synthetic tools for various organic transformations, such as C–H bond activation/functionalizations and heterocyclizations.[12] With the developing electrochemical techniques, the electrode is deemed as an atomless substitute to conventional stoichiometric oxidizing and reducing agents, thereby minimizing other side reactions and byproducts.[13]

In this context, Lei,[14] Lin,[15] Baran,[16] Ackermann,[17] and others[18] independently developed various electrochemical methods for the construction of C–C, C–X, and X–X (X = N, P, O, and S) bonds. Inspired by the electrochemical synthesis and the propensity of benzoyl hydrazine as an acyl radical and amine as the *N*-centered radical, herein, we report an electrochemical amide bond formation [Scheme IV.1.(d)].

IV.2. Different Strategies for the Synthesis of Amide

In 2012, Wang's group introduced a method for synthesizing amides through the cross-coupling of acyl and aminyl radicals. In this method, Bu_4NI and TBHP served as the internal oxidant. The mechanistic investigation reveals the generation of acyl and aminyl radicals, then both radicals cross-couple to form the desired amide (Scheme IV.2).[19a]

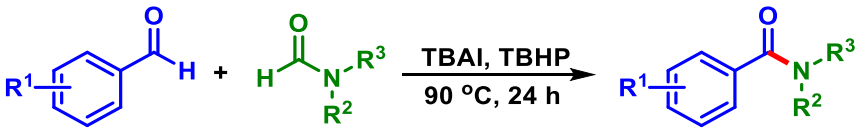

Scheme IV.2. *TBHP-catalyzed N-acylation of amines with aldehyde.*

In 2019, the Xiao group explored a photoinduced copper-catalyzed radical amino carbonylation of cyclo ketone oxime esters. This mild catalytic system, featuring CuCl and

N,N,N-tridentate ligands (L1), exhibited good reactivity and chemoselectivity. The method tolerated a broad range of cyclic ketone oxime esters and alkyl/aryl amines, yielding the corresponding cyano alkylated amides in moderate to good yields (Scheme IV.3).[19b]

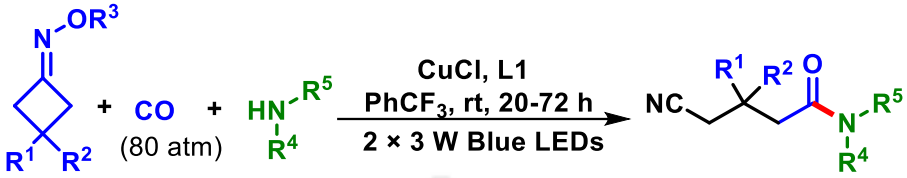

Scheme IV.3. *Cu-catalyzed N-acylation of amines.*

In 2021, the Wacharasindhu group presented a novel electroorganic synthetic method for the NaI-mediated oxidative amidation of benzyl alcohols and aromatic aldehydes to form benzamides. This process utilized NaI as a redox mediator, conducted under ambient temperature in an undivided cell. The reaction occurred in aqueous media, offering the advantages of one-pot synthesis, open-air conditions, and eliminating the need for external conducting salt, base, and oxidant. The resulting amide products were obtained in moderate to good yields (Scheme IV.4).[19c]

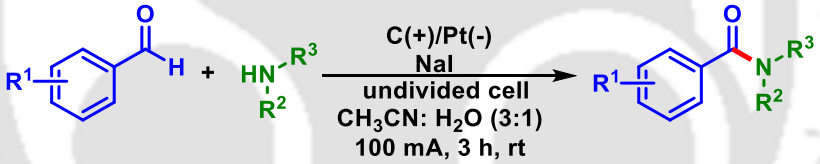

Scheme IV.4. *Electrochemical synthesis of amides derivatives using aldehyde.*

In 2019, the Ke group presented an electrochemical method for synthesizing amides *via* *N*-acylation under aqueous medium. This approach utilized tetrabutylammonium bromide (TBAB) as the electrolyte. The reaction proceeded under mild conditions at room temperature. The utility of this method was exemplified through the synthesis of melatonin, showcasing its potential for the preparation of amide (Scheme IV.5).[19d]

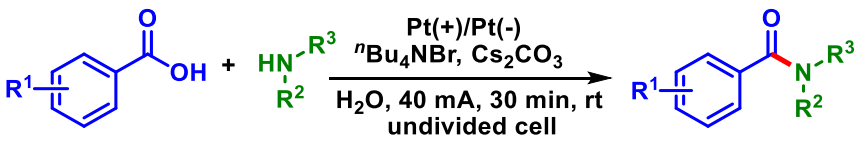

Scheme IV.5. *Electrochemical synthesis of amides derivatives using acid.*

IV.3. Present Work

IV.3.1. Optimization of the Reaction Conditions

To verify our hypothesis, a preliminary reaction was carried out between the benzoylhydrazine (**a**) (0.5 mmol) and morpholine (**1**) (0.75 mmol, 1.5 equiv) in tetrabutylammonium hexafluorophosphate ($^{n}Bu_4NPF_6$) (50 mol %) in a 2:3 ratio of 1,2-dichloroethane (DCE) and 1,1,1,3,3,3-hexafluoro-2-propanol (HFIP) (5 mL) at room temperature, applying a 10 mA constant current using a carbon rod anode and a platinum plate cathode in an undivided cell under N_2 atmosphere for 18 h. During the reaction, a new spot (viewed under 365 nm UV lamp) was observed in the TLC, and the product (**1a**) was isolated in 78% yield after column chromatography (Table 1, entry 1). From the spectroscopic analysis, the structure was assigned as morpholino(phenyl)methanone (**1a**) and further reconfirmed by a single-crystal X-ray diffraction analysis of one of its derivatives (**1d**) (Figure IV.2).

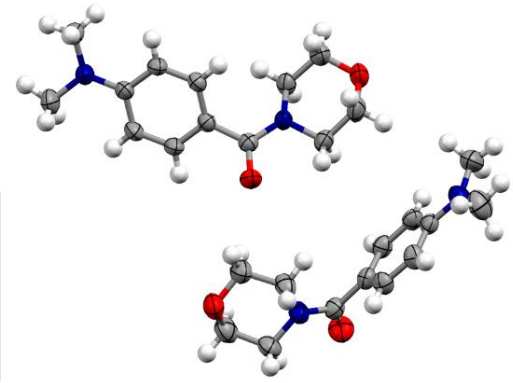

Figure IV.2. *ORTEP diagram of (4-(dimethylamino)phenyl)(morpholino)methanone (**1d**) with 50% ellipsoid probability (**CCDC 2194432**).*

Inspired by this electrochemical approach, further tuning of reaction variables such as solvents, electrolytes, electrodes, and electric current were altered, and the results are summarized in Table IV.1.

Table IV.1. Optimization of the reaction conditions[a,b]

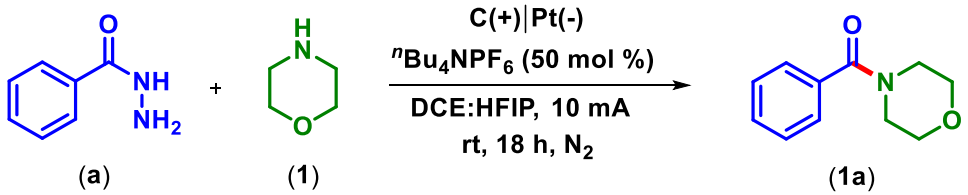

Entry	Variation from the standard conditions	Yield[b] (%)
1	**None**	**78**
2	Without HFIP	<10
3	Without DCE	49
4	MeOH, isopropanol, ethylene glycol instead of HFIP	N.D
5	DMSO, DMA, 1, 4 -dioxane, THF instead of DCE	N.D
6	DCE:HFIP = 4:1, 3:2, 2:4	32, 56, 77
7	DCE:TFE = 4:1, 2:3	10, 35
8	RVC, nickel, platinum anode instead of C rod anode	55, 33, 65
9	Stainless steel, carbon cloth instead of platinum cathode	23, 47
10	^{n}Bu$_4$NBF$_4$, ^{n}Bu$_4$NOAc instead of ^{n}Bu$_4$NPF$_6$	65, 29
11	25 mol %, 100 mol % instead of 50 mol % ^{n}Bu$_4$NPF$_6$	40, 69
12	1 equiv, 2 equiv instead of 1.5 equiv amine	45, 34
13	15 mA, 5 mA instead of 10 mA,	42, 62
14	12 h, 24 h instead of 18 h	49, 40
15	No electric current	N.D
16	No electrolyte	N.D
17	air atmosphere	70

[a]Reaction conditions: **a** (0.5 mmol), **1** (1.5 equiv), ^{n}Bu$_4$NPF$_6$ (50 mol %) in 2:3 ratios of 1, 2-DCE and HFIP (5 mL) solvent with a carbon rod anode (Φ 6 mm), platinum plate cathode (10 mm x 10 mm x 0.3 mm), constant current = 10 mA, at room temperature under N_2 atm, 18 h in undivided cell. [b]yield of isolated product. N.D = not detected.

The use of 1,2-DCE without the fluorinated solvent HFIP was not beneficial as the reaction gave less than 10% yield (Table IV.1, entry 2) while using neat HFIP provided the

product with a 49% yield (Table IV.1, entry 3). Thus, using a mixed solvent significantly enhances the yield of the reaction. The reaction was unproductive when the solvent HFIP was replaced with MeOH, isopropanol, and ethylene glycol (Table IV.1, entry 4). Further, when the DCE solvent was replaced with DMSO, DMA, 1,4-dioxane, and THF (Table IV.1, entry 5) all gave unsuccessful results. In most electrochemical reactions, the solvent HFIP plays a crucial role *via* hydrogen-bond interaction between the *N*–H of the reacting partner {in this case benzoyl hydrazine (**a**)} with the *O*-atom of the HFIP.[1] Next, the ratio of solvents was optimized using fluorinated solvents TFA and HFIP in combination with DCE. The ratio of DCE: HFIP 4:1, 3:2, and 2:4 provides 32%, 56%, and 77% yields, respectively (Table IV.1, entry 6), while the ratio of DCE: TFE 4:1 and 2:3 gave 10% and 35% yields respectively (Table IV.1, entry 7). Replacement of carbon rod anode with other anodes such as RVC, nickel, and platinum plate showed no significant increase in the product yield (Table IV.1, entry 8). Similarly, swapping other cathodes, such as stainless steel and carbon cloth, in lieu of the platinum plate was found less effective (Table IV.1, entry 9). The substitute of alternative organic electrolytes, such as $^{n}Bu_4NBF_4$ (65%) and $^{n}Bu_4NOAc$ (29%) showed less efficacy than $^{n}Bu_4NPF_6$ (Table IV.1, entry 10). The loading of organic electrolyte $^{n}Bu_4NPF_6$ either in lower (25 mol %, 40%) or higher (100 mol %, 69%) was found to be counterproductive (Table IV.1, entry 11). Keeping all reaction parameters constant, increasing the amount of amine to 2 equiv did not improve the yield significantly (34%), while a decrease in the loading to 1 equiv adversely affected the yield (45%) (Table IV.1, entry 12). The reaction failed to improve the yield while performing both at higher (15 mA) and lower (5 mA) operating currents (Table IV.1, entry 13). The electrolysis carried out for 12 h gave a lower yield (49%), which did not improve beyond 40%, even prolonging up to 24 h (Table IV.1, entry 14). A blank experiment showed that no product could be obtained without the application of electric current and electrolyte, which confirms the electro-oxidation process for this coupling process (Table IV.1, entries 15 and 16). Importantly, the reaction could be conducted under an air atmosphere with a slightly decreased yield of 70% (Table IV.1, entry 17). Therefore, the best condition was found to be the use of benzoyl hydrazine (**a**) (0.5 mmol), morpholine (**1**) (0.75 mmol, 1.5 equiv) in tetrabutylammonium hexafluorophosphate ($^{n}Bu_4NPF_6$) (50 mol %) in 2:3 ratios of 1,2-dichloroethane (DCE) and 1,1,1,3,3,3-hexafluoro-2-propanol (HFIP) (5 mL) at room temperature applying a 10 mA

constant current using a carbon rod anode and a platinum plate cathode in an undivided cell under N_2 atmosphere for 18 h (Table IV.1, entry 1)

IV.3.2. Substrates Scopes for the Synthesis of Amides

After establishing the optimized electroamidation process, the scope of the reaction with respect to amines (**1**–**33**) was examined using benzoyl hydrazine (**a**) as the coupling partner (Scheme IV.6).

Scheme IV.6. Substrate scope for various amines.[a]

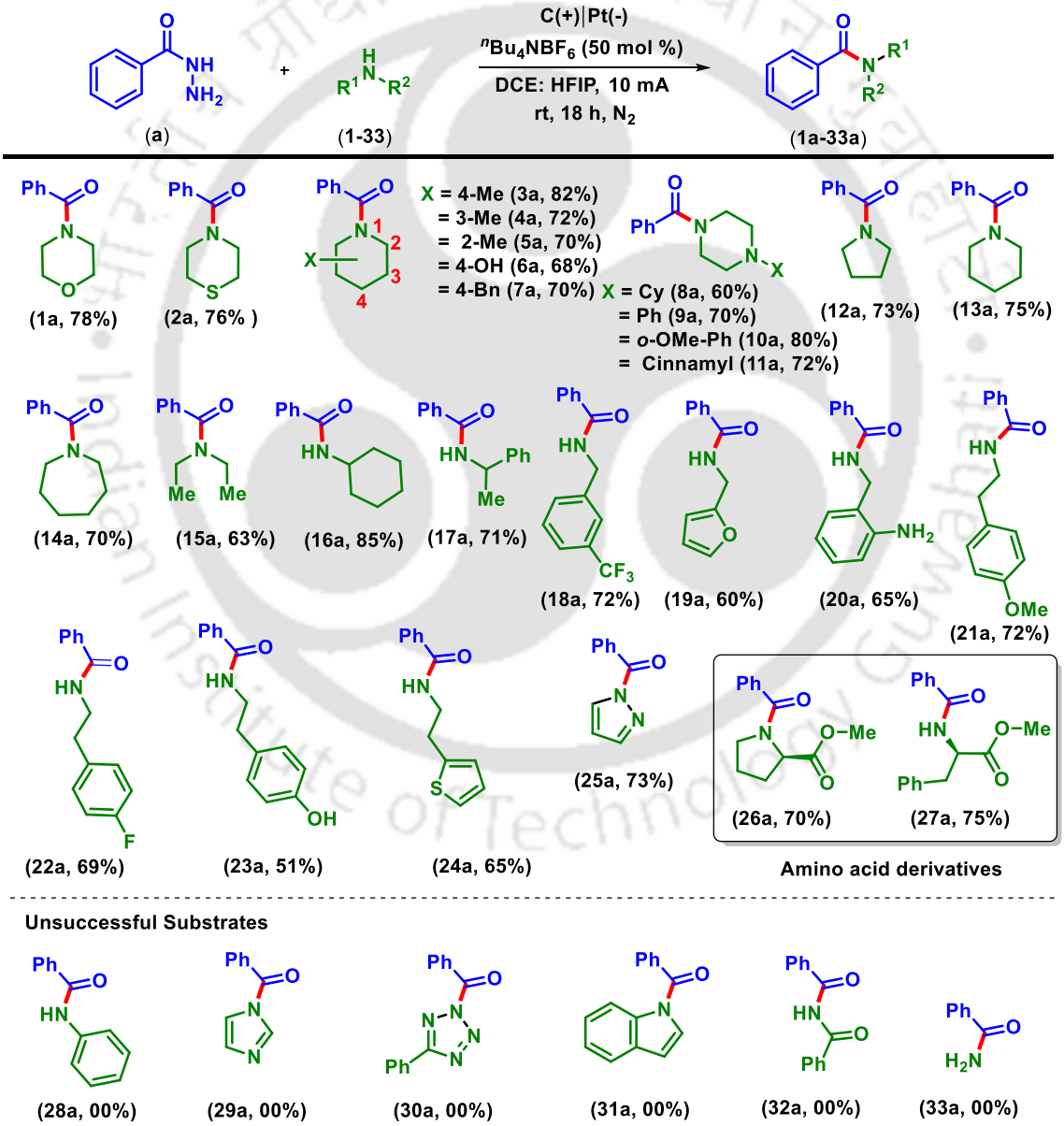

[a]Reaction conditions: **1**-**33** (0.75 mmol), benzoyl hydrazine (**a**) (0.5 mmol), $^{n}Bu_4NPF_6$ (50 mol %) in 2:3 of 1,2-DCE and HFIP (5 mL) utilizing a 10 mA constant current, carbon rod (Φ 6 mm) as an anode and platinum plate (10 mm x 10 mm x 0.3 mm) as a cathode at room temperature under N_2 atmosphere for 18 h in undivided cell.

Morpholine (**1**) and thiomorpholine (**2**) reacted smoothly to give the corresponding amides **1a** (78%) and **2a** (76%) respectively. The effect of substituents on piperidine (**3**–**7**) was inspected with benzoyl hydrazine (**a**). Piperidine having substituents *viz*. 4-Me (**3**), 3-Me (**4**), 2-Me (**5**), 4-hydroxy (**6**), and 4-benzyl (**7**) all reacted effectively with benzoyl hydrazine (**a**), yielding their anticipated amides **3a** (82%), **4a** (72%), **5a** (70%), **6a** (68%), and **7a** (70%), respectively (Scheme IV.6). Similarly, mono-*N*-substituted piperazines such as cyclohexyl (**8**), phenyl (**9**), 2-methoxyphenyl (**10**), and cinnamyl (**11**) provided their respective amides **8a** (60%), **9a** (70%), **10a** (80%), and **11a** (72%) (Scheme IV.6). Other secondary amines such as pyrrolidine (**12**), piperidine (**13**), and azepane (**14**) all effectively provided their amides **12a** (73%), **13a** (75%), and **14a** (70%) in good yields. An acyclic secondary amine (**15**) was also proved to be a good coupling partner, giving the product **15a** in 63% yield. In addition to secondary amines, this method is equally successful for aliphatic primary amines. Cyclohexylamine (**16**) provided amidic product **16a** in 85% yield.

Aromatic primary amines also participate well in this transformation. Benzyl amines such as 1-phenylethane-1-amine (**17a**, 71%), (3-(trifluoromethyl)phenyl)methanamine (**18a**, 72%), and furan-2-ylmethanamine (**19a**, 60%) provided their benzoylated products when reacted with benzoyl hydrazine (**a**). The 2-(aminomethyl)aniline (**20**) having two primary amino groups, one attached to the aryl moiety and the other at the benzylic position, preferentially benzoylated at the benzylic site giving the product (**20a**) in 65% yield without affecting the aromatic amine. This methodology was equally successful for other primary alkyl amines having substituted aromatic (**21**–**23**) and heteroaromatic (**24**) pendants, and all effectively underwent amidation giving their amides **21a** (72%), **22a**, (69%), **23a**, (51%) and **24a**, (65%), respectively. This methodology was equally effective for pyrazole (**25**), an *N*-containing five-membered heterocycle giving its amidic product (**25a**, 73%).

Amidic bonds have been successfully constructed using C-protected amino acids such as L-proline methyl ester (**26**) and L-phenylalanine methyl ester (**27**), giving amides **26a** (70%)

and **27a** (75%) in good yields. The primary aromatic amine, such as aniline (**28**), failed to react, which is consistent with the selectivity observed for the substrate 2-(aminomethyl)aniline (**20**), where one of the amino groups was selectively benzoylated using benzoyl hydrazine (**a**). Besides aniline (**28**), other N-H-containing heterocycles such as imidazole (**29**), tetrazole (**30**), indole (**31**), benzamide (**32**), and ammonia (**33**) were completely unsuccessful. The generated *N*-centered radicals in these substrates are conjugated and possibly undergo delocalization (except ammonia), forming other radical centers making the process unproductive. This selective reactivity has advantages as it permits chemoselective amidation. However, in unsubstituted pyrazole (**25**), one of the N^1-centered radicals, even though conjugated, can form an equivalent N^2-radical species, thereby undergoing effective radical coupling.

Next, the scope of benzoyl hydrazines (**b**–**r**) was explored using morpholine (**1**) as the other coupling partner (Scheme IV.7).

Scheme IV.7. Substrate scope for various benzoyl hydrazines.[a]

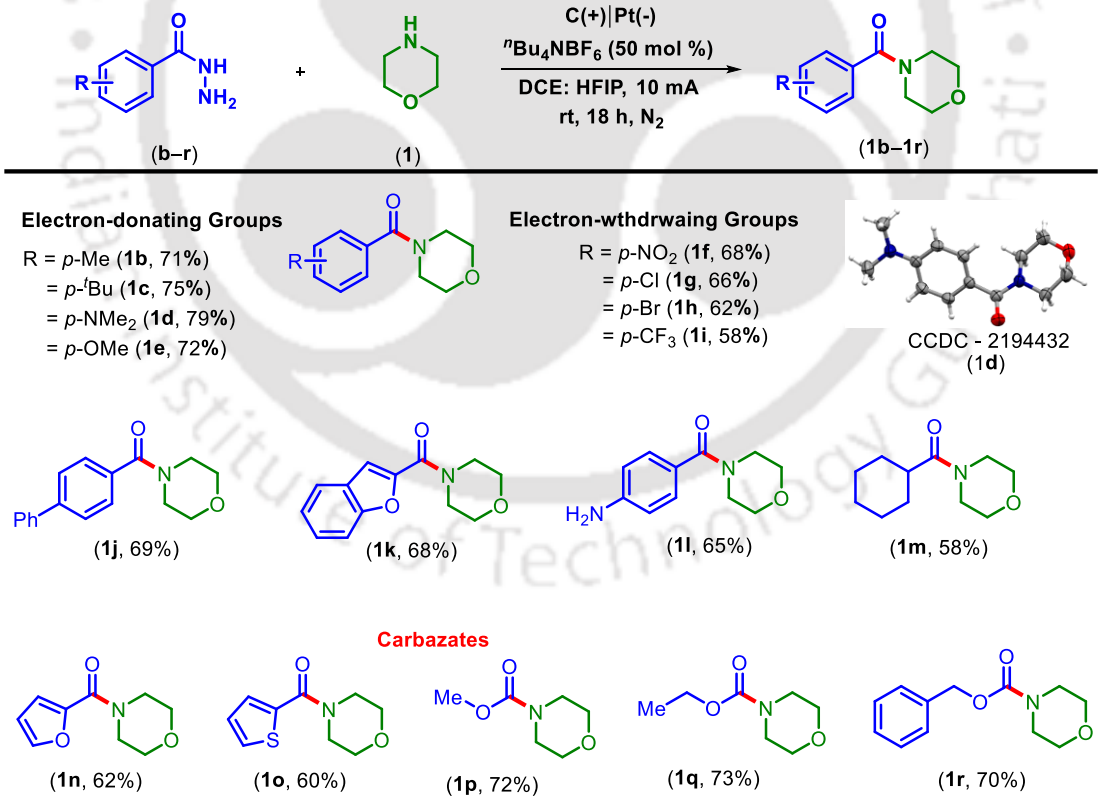

[a]Reaction conditions: (**b–r**) (0.5 mmol), morpholine (**1**) (0.75 mmol), ^{n}Bu$_4$NPF$_6$ (50 mol %) in 2:3 of 1,2-DCE and HFIP (5 mL) utilizing a 10 mA constant current, carbon rod (Φ 6

mm) as an anode and platinum plate (10 mm x 10 mm x 0.3 mm) as a cathode at room temperature under N_2 atmosphere for 18 h in undivided cell.

Benzoyl hydrazine possessing electron-donating groups such as *p*-Me (**b**), *p*-^{t}Bu (**c**), *p*-NMe_2 (**d**), and *p*-OMe (**e**) positively responded to this protocol, providing their amides **1b**, (71%), **1c**, (75%), **1d**, (79%), and **1e**, (72%), respectively (Scheme IV.7).

Benzoyl hydrazine possessing electron-withdrawing groups *p*-NO_2 (**f**), *p*-Cl (**g**), *p*-Br (**h**), and *p*-CF_3 (**i**) also underwent affective amidation when reacted with morpholine (**a**) providing their anticipated products **1f**, (68%), **1g**, (66%), **1h**, (62%), and **1i**, (58%), respectively (Scheme IV.7). In addition, biphenylhydrazine (**j**) and benzofuran-2-carbohydrazide (**k**) yielded their respective products **1j**, (69%), and **1k**, (68%) in similar yields. The 4-aminobenzoylhydrazine (**1l**), when subjected to the electrolytic conditions with morpholine (**1**), provided amide **1l** (65%), without affecting the amino group. The aliphatic hydrazine cyclohexane hydrazine (**1m**) and heteroaromatic hydrazines such as furan (**1n**) and thiophene (**1o**) all coupled efficiently, giving their amides **1m**, (58%), **1n**, (62%), and **1o**, (60%). Besides benzoyl hydrazines, the present electrochemical method is equally successful with carbazates as the coupling partners with morpholine. Carbazates having Me (**p**), Et (**q**), and benzyl (**r**) substituents reacted proficiently with morpholine (**1**), providing corresponding carbamates **1p**, (72%), **1q**, (73%), and **1r**, (70%), respectively.

IV.4. Mechanistic Investigations

IV.4.1. Control Experiments

To gain insight into the nature of the reaction mechanism, a few control experiments were performed (Scheme IV.8). Whether the reaction proceeds *via* a radical mechanism or not, radical-trapping experiments were carried out using (2,2,6,6-tetramethylpiperidine-1-yl)oxyl (TEMPO) and butylated hydroxytoluene (BHT). When TEMPO was added to the reaction of benzoyl hydrazine (**a**) with morpholine (**1**), the formation of **1a** was significantly inhibited. The benzoyl radical was trapped by TEMPO, giving a TEMPO adduct (**1s**) in 33% yield (Scheme IV.8). The identity and purity of the product were confirmed by NMR and HRMS analysis (Figure IV.3), ^{1}H NMR (Figure IV.4), and ^{13}C{1H} (Figure IV.5) analyses.

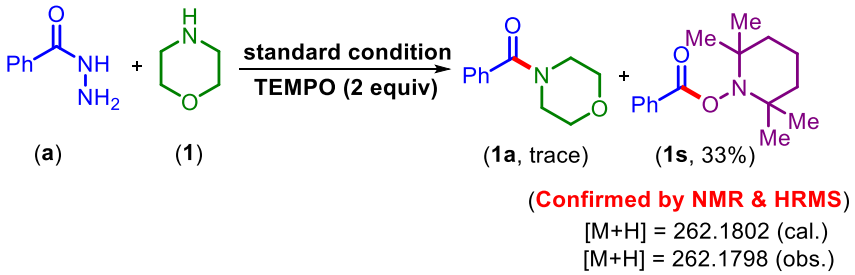

Scheme IV.8. *Radical trapping experiments using TEMPO.*

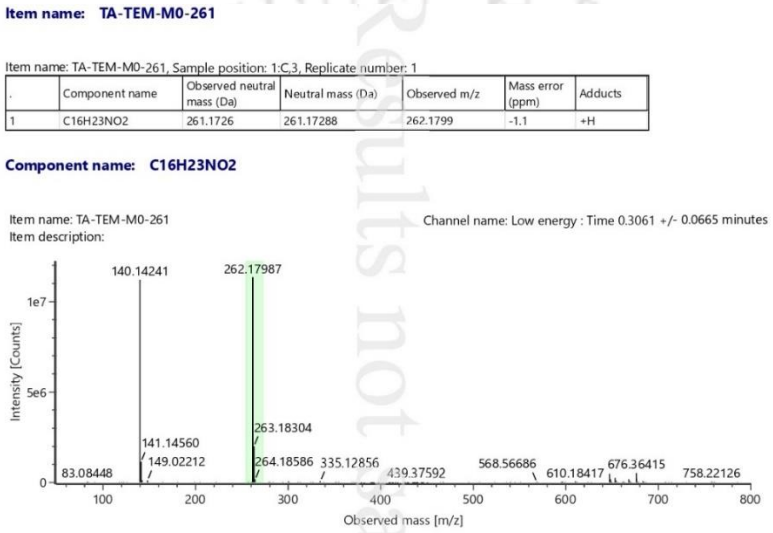

.	Component name	Observed neutral mass (Da)	Neutral mass (Da)	Observed m/z	Mass error (ppm)	Adducts
1	C16H23NO2	261.1726	261.17288	262.1799	-1.1	+H

Figure IV.3 *HRMS spectra of benzoyl-radical trapped adduct (**1s**).*

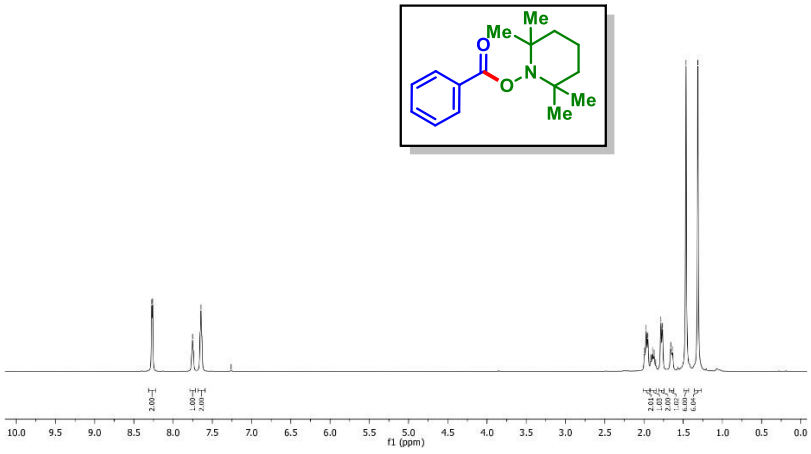

Figure IV.4 *^{1}H-NMR spectra of benzoyl-radical trapped adduct (**1s**).*

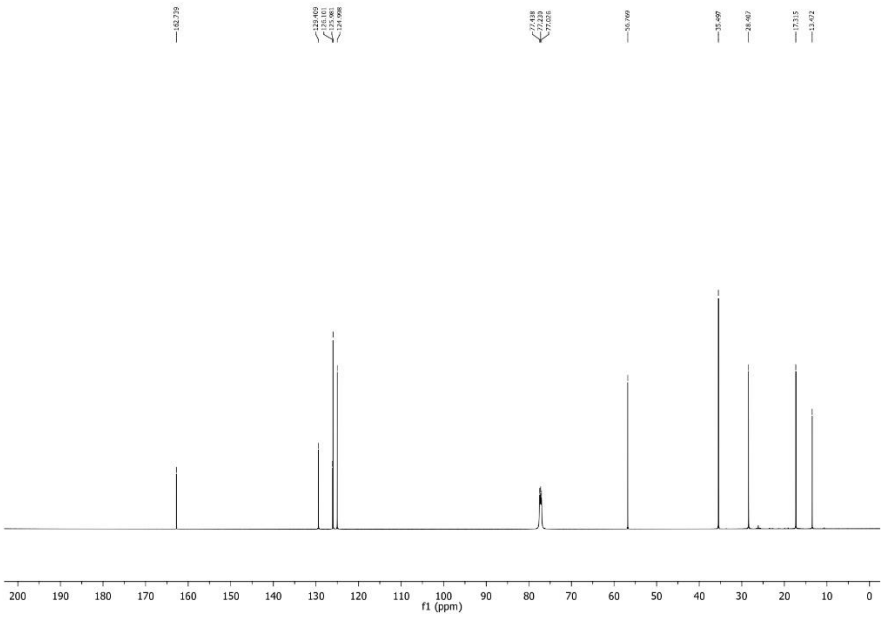

Figure IV.5 *^{13}C{1H} NMR spectra of benzoyl-radical trapped adduct (**1s**).*

The addition of radical scavenger BHT also suppressed this reaction giving the product **1a** in <15% yield along with a BHT adduct (**t**) (Scheme IV.9). The formation of the BHT-adduct, 2,6-di-tert-butyl-4(morpholinomethyl)phenol (t) was confirmed by HRMS analysis of the reaction mixture (Figure IV.6).

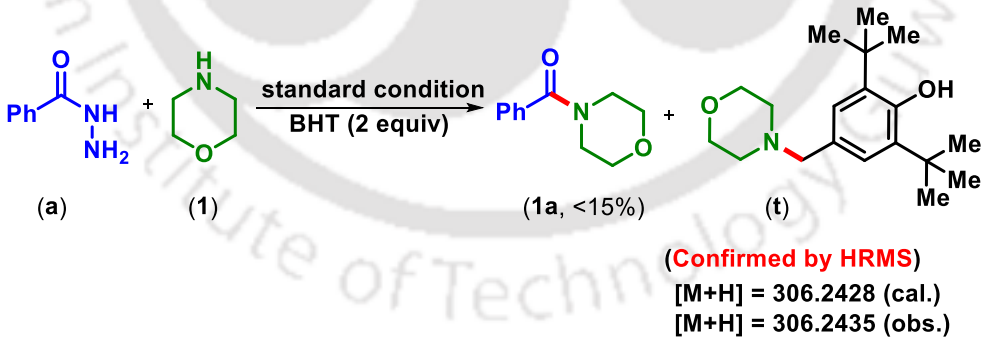

Scheme IV.9. *Radical trapping experiments with BHT.*

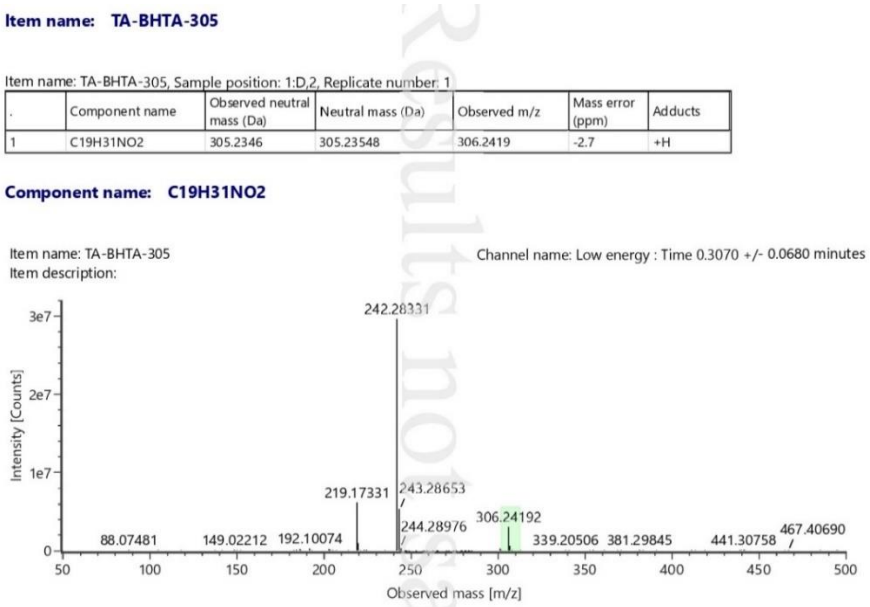

Figure IV.6. *HRMS spectrum of BHT-adduct (t).*

This result suggests the radical nature of both of the coupling partners under electrochemical conditions. Next, to see whether the benzoyl hydrazine (**a**) under these conditions proceeds through aldehyde (**a′**), carboxylic acid (**a′′**), or benzamide (**32**) intermediate, three independent reactions with amine (**1**) were performed. None of them gave the desired product (Scheme IV.10). Thus, the benzoyl radical only originates from benzoyl hydrazine (**a**) *via* the C–N bond cleavage to release N_2 and H_2.

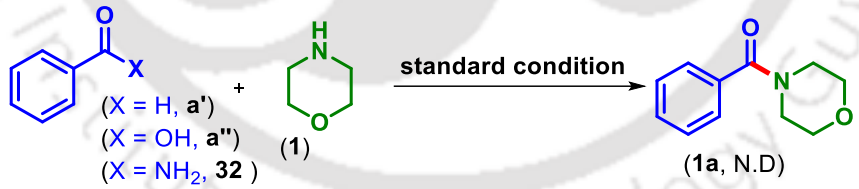

Scheme IV.10. *Possible intermediate detection experiment.*

To identify the mechanistic pathway and understand the electrochemical properties, a series of CV measurements were performed (Figure IV.7). In DCE solvent, the oxidation peaks for (**a)** were observed at 1.58 and 2.63 V vs. SCE, and for morpholine (**1**) found at 1.28 V vs SCE, suggesting the easy oxidation of (**a**) and (**1**) at the anode to generate an acyl and an *N*-centered radical. In a mixed solvent (DCE:HFIP), the oxidation peaks for (**a**) were observed at 1.51 and 2.55 V vs. SCE, and for morpholine (**1**), it was at 1.22 V vs. SCE, suggesting the easy oxidation of both (**a**) and (**1**) through HFIP activation. The oxidation of benzoyl hydrazine (**a**)

and morpholine (**1**) at the anode was further verified by linear sweep voltammetry measurements (Figure IV.7) in a mixed solvent (DCE:HFIP). The onset potentials for (**a**) and (**1**) were observed at 0.99 and 0.63 V vs SCE, and the anodic potential was found at 1.47 and 0.99 V vs SCE. This confirms the oxidation of both of the reacting partners at the anode.

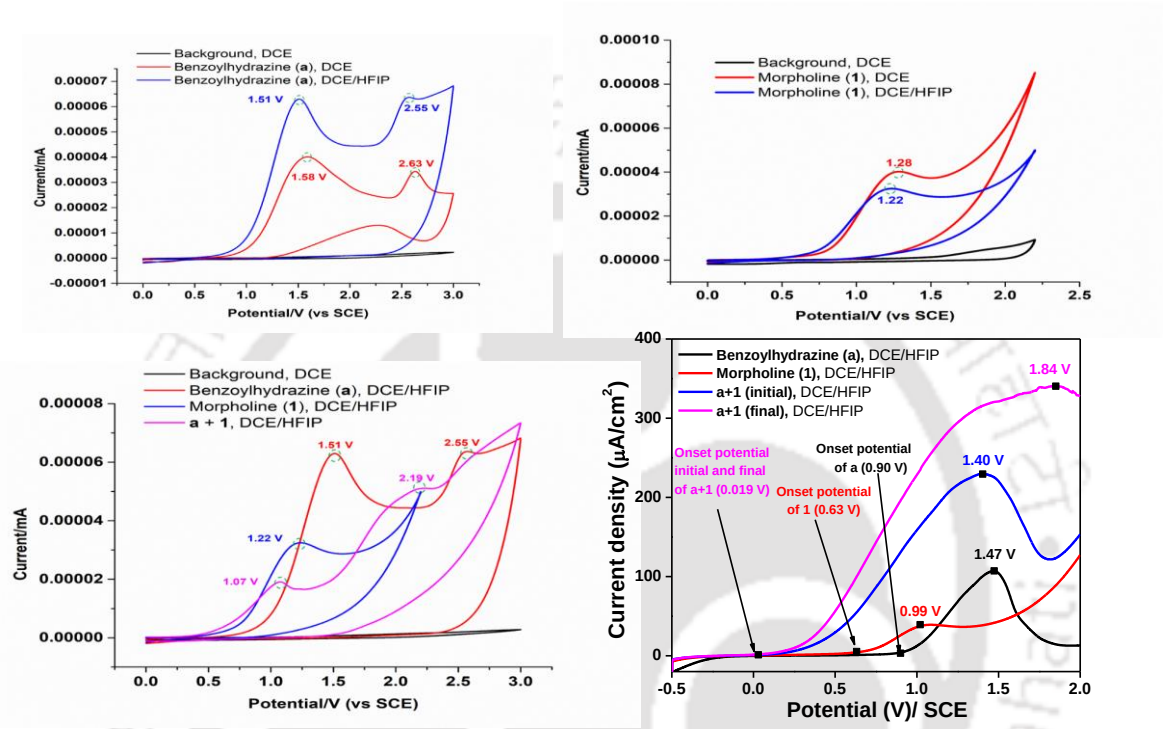

Figure IV.7 *Cyclic voltammetry studies. (I) Cyclic voltammograms of benzoyl hydrazine (a). (II) Cyclic voltammograms of morpholine (1). (III) Cyclic voltammograms of benzoyl hydrazine (a) and morpholine (1). (IV) Linear sweep voltammetry studies.*

IV.4.2. Plausible Reaction Mechanism:

Based on the control experiments, the results obtained from cyclic voltammetry, linear sweep voltammetry measurements, and previous literature reports,[20] a plausible mechanism is depicted in Scheme IV.11.

Scheme IV.11 Plausible mechanisms

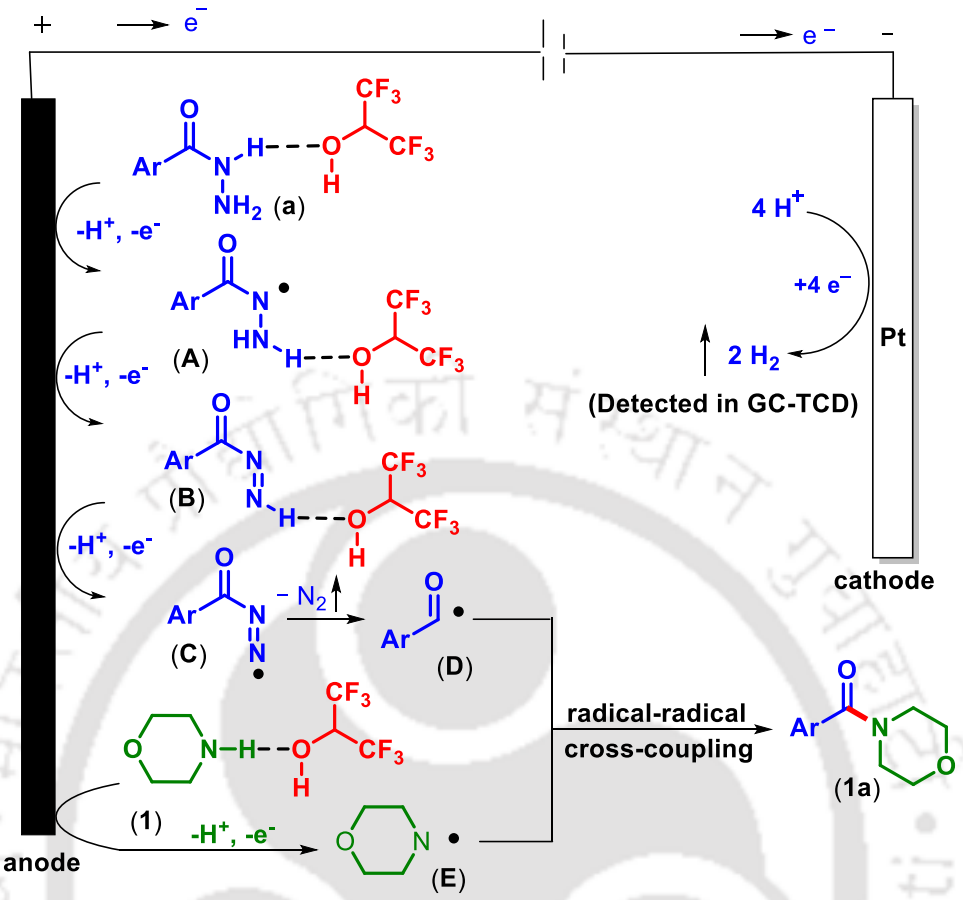

The solvent HFIP interacts via hydrogen bonding with the *N*-H of the benzoyl hydrazine (**a**).[21] Next, this activated benzoyl hydrazine (**a**) undergoes electrochemical anodic oxidation to generate an *N*-centered diazanyl radical intermediate (**A**). Further, a sequential two-step oxidation from the radical intermediate (**A**) produces a diazene radical intermediate (**C**) via intermediate (**B**). Next, C–N bond cleavage of intermediate (**C**) generates a benzoyl radical intermediate (**D**) with concurrent releases of N_2. Similarly, the amine morpholine (**a**) is activated *via* an H-bonding interaction with the HFIP, and subsequent anodic oxidation generates an *N*-centered radical intermediate (**E**).[20a] Finally, radical–radical cross-coupling between intermediates (**D**) and (**E**) afforded the amide (**1a**).[22] During the cathodic reduction, molecular H_2 is released, which has been detected by GC analysis.

IV.5. Gram-scale and Synthesis of Bezafibrate Drug

The synthetic utility of this method is then demonstrated by a gram-scale synthesis of morpholino(phenyl)methanone (**1a**). When the standard electrochemical reaction between

benzoyl hydrazine (**a**) and morpholine (**1**) is carried out on a 10 mmol scale, the amide (**1a**) is obtained after 32 h of reaction with an isolated yield of 70% (Scheme IV.5.1, i). The practical utility of this electrochemical radical coupling is successfully applied for the synthesis of Bezafibrate (**23g′′**), a marketed fibrate drug used in the treatment of hyperlipidemia (Scheme IV.5.1, ii)

Scheme IV.12. ***Gram-scale and synthesis of bezafibrate***

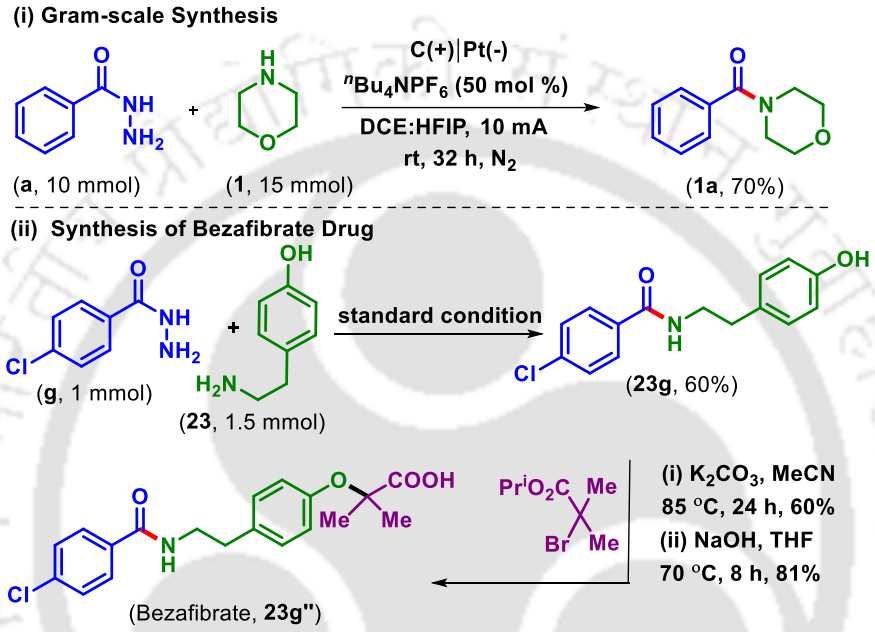

IV.6. Conclusion

In summary, an electrochemical amidation/carbamidation under metal and external oxidant-free pathways is developed. The process involves, radical–radical cross-coupling between benzoyl hydrazines/carbazates and amines, leading to the formation of a C–N bond. The protocol is compatible with a wide range of benzoyl hydrazines/carbazates and aromatic/aliphatic amines. Alkyl amines are selectively amidated in the presence of arylamines, but the method is unsuccessful for substrates where the *N*-centered radical is part of conjugated systems. Thus chemoselective amidation can be achieved in substrates having multiple aminating sites. The reaction mechanism is confirmed by control experiments and CV, and

LSV measurements, and the liberation of H_2 is detected by GC analysis. Finally, the synthetic utility is demonstrated through a large-scale and biologically active 'bezafibrate' drug.

IV.7. Experimental Section

IV.7.1. General Information: All the reagents were commercial grade and purified according to the established procedures. All the reagents were commercial grade and used without further purification unless otherwise stated. Preparation of the starting materials was carried out in an oven-dried 100 mL or 50 mL round bottom flask. Reactions were monitored by thin layer chromatography (TLC) on 0.25 mm silica gel plates ($60F_{254}$) and visualized under UV illumination at 254 nm. Organic extracts were dried over anhydrous sodium sulfate (Na_2SO_4). Column chromatography was performed to purify the crude product on silica gel 60−120 mesh using a mixture of hexane and ethyl acetate as eluent. The isolated compounds were characterized by spectroscopic [^{1}H, ^{13}C{1H} NMR, and IR] techniques and HRMS analysis. NMR spectra were recorded in deuterochloroform ($CDCl_3$) or deuterated dimethyl sulfoxide (DMSO-d^6). ^{1}H, ^{13}C{^{1}H} were recorded in 600 (150) or 500 (125) MHz spectrometer and were calibrated using tetramethylsilane or residual undeuterated solvent for ^{1}H NMR, deuterochloroform for ^{13}C NMR as an internal reference {$Si(CH_3)_4$: 0.00 ppm or $CHCl_3$: 7.260 ppm for ^{1}H NMR, 77.230 ppm for ^{13}C NMR or $(CH_3)_2SO$: 2.50 ppm for ^{1}H NMR, 39.50 ppm for ^{13}C NMR}. ^{19}F NMR was calibrated without any internal standard in $CDCl_3$ and DMSO-d^6 in a 500 MHz spectrometer. The chemical shifts are quoted in δ units, parts per million (ppm). ^{1}H NMR data is represented as follows: Chemical shift, multiplicity (s = singlet, d = doublet, t = triplet, q = quartet, m = multiplet), integration and coupling constant(s) *J* in hertz (Hz). High-resolution mass spectra (HRMS) were recorded on a mass spectrometer using electrospray ionization-time of flight (ESI-TOF) reflection experiments. FT-IR spectra were recorded in KBr or neat and reported in the frequency of absorption (cm^{-1}). The instrument used for the electrolysis is a dual-display METRAVI RPS-6005/RPS-6002 adjustable 60V/5A DC Power Supply (Made in India). The anodic electrode was a carbon rod (Φ 6 mm), and the cathodic electrode was a platinum plate (10 mm ×10 mm × 0.3 mm). All the reactions were carried out using an oven-dried three-neck cell under a nitrogen atmosphere. IUPAC names were obtained

using the ChemDraw Professional 16.0 software. The amine and benzoyl hydrazine/carbazate was purchased from Sigma-Aldrich, TCI, and Alfa aesar.

IV.7.2. Crystallographic Information

(A) Sample Preparation:

The single crystal of compound **1d** was prepared by the slow evaporation method, for which 15 mg of the compound (**1d**) was dissolved in 1 mL of methanol in a clean and dry 10 mL glass vial. DCM (1 mL) was added to this solution slowly with a dropper. The mouth of the glass vial was covered with a cap having a small hole and kept for slow evaporation at room temperature. Crystals of **1d** were obtained as a transparent colorless needle-like shape after around 5 days.

(B) Crystallographic description of (4-(dimethylamino)phenyl)(morpholino)methanone (1d):

Diffraction data were collected at 292 K with MoKα radiation (λ = 0.71073 Å) using a Bruker Nonius SMART APEX CCD diffractometer equipped with graphite monochromator and Apex CD camera. The SMART software was used for data collection for indexing the reflections and determining the unit cell parameters. Data reduction and cell refinement were performed using SAINT[1,2] software, and the space groups of these crystals were determined from systematic absences by XPREP and further justified by the refinement results. The structures were solved by direct methods and refined by full-matrix least-squares calculations using SHELXTL-97[3] software. All the non-H atoms were refined in the anisotropic approximation against F^2 of all reflections.

1. G. M. Sheldrick, SADABS, 1996, based on the method described in: R. H. Blessing, *Acta Crystallogr.* 1995, **A51**, 33–38.
2. SMART and SAINT, Siemens Analytical X-ray Instruments Inc., Madison, WI, 1996.
3. G. M. Sheldrick, *Acta Crystallogr.*, 2008, **A64**, 112–122.

$C_{13}H_{18}N_2O_2$, crystal dimensions 0.34 x 0.24 x 0.20 mm, M_r = 234.29, monoclinic space, group P 21/c, a=9.857 (3), b=10.758 (4), c=23.461 (8) Å, α = 90, β = 99.802° (12) , γ = 90 , V = 2451.6 (15) Å^3, Z = 4, ρ_{calcd} = 1.272 mg/m^3, μ = 0.086 mm^{-1}, $F(000)$ = 168.0, refinement method = full-matrix least-squares on F^2, final R indices [$I > 2\sigma(I)$]: R_1 = 0.0793 (521), wR_2 = 0.3090 (1475), goodness of fit = 1.000. CCDC 2194432 for (4-

(dimethylamino)phenyl)(morpholino)methanone (**1d**) contains the supplementary crystallographic data for this paper. These data can be obtained free of charge from The Cambridge Crystallographic Data Centre via www.ccdc.cam.ac.uk/data_request/cif.

IV.7.3. General Procedure for the Synthesis of Benzofuran-2-carbohydrazide (k)

Compound (**k**) were synthesized as per the following the method described in Rodrigues, D. A.; Guerra, F. S.; Sagrillo, F. S.; Pinheiro, P. de S. M.; Alves, M. A.; Thota, S.; Chaves, L. S.; Sant'Anna, C. M. R.; Fernandes, P. D.; Fraga C. A. M. *ChemMedChem*, **2020**, *15*, 539–551

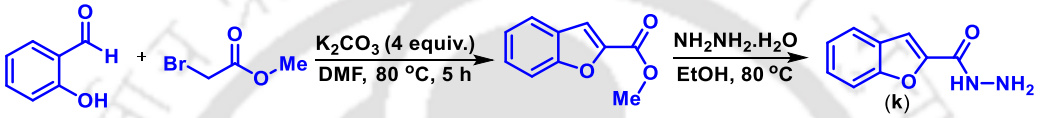

Scheme IV.13. *Synthesis of benzofuran-2-carbohydrazide (k).*

To an oven-dried 100 mL round bottom flask was added a solution of salicylaldehyde (0.610 g, 5 mmol) anhydrous potassium carbonate (2.76 g, 20 mmol) in DMF (20 mL) and was cooled to 0 ^{o}C. Then to the reaction mixture methyl bromoacetate (1.53 g, 10 mmol) was added dropwise. The resulting mixture was stirred at 0 ^{o}C for 30 min and then at 80 ^{o}C in a preheated oil bath for 5 h. After confirming that the reaction was complete by TLC analysis, the solution was cooled to room temperature, and water (15 mL) was added. The reaction mixture was extracted with ethyl acetate (50 mL) and washed with brine (1 x 5 mL). The organic phase was dried over Na_2SO_4, and the solvent was removed under vacuum. The crude product was purified by silica gel column chromatography to give the methyl benzofuran-2-carboxylate product (Scheme IV.13).

To an oven-dried 50 mL round bottom flask was added a methyl benzofuran-2-carboxylate (0.528 g, 3 mmol), and hydrazine hydrate (1.50 g, 30 mmol) was added in absolute ethanol (30 mL). The mixture was kept under stirring and reflux for 18 h. After cooling to room temperature, the ethanol was concentrated in a vacuum. When precipitation was observed, the solid was collected through filtration and washed with 50 mL of hexane and 50 mL of ethyl ether to give benzofuran-2-carbohydrazide (**k**) (Scheme IV.13).

IV.7.4. General Procedure for the Synthesis of Morpholino(phenyl)methanone (1a) from Benzoyl hydrazine (a) and Morpholine (1)

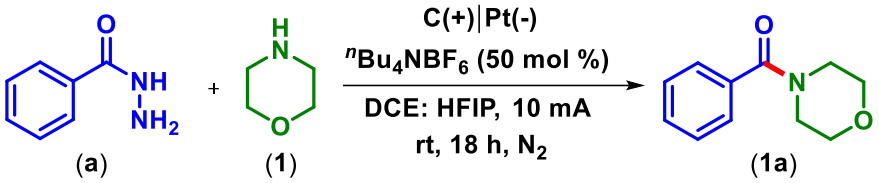

Scheme IV.14. *Synthesis of morpholino(phenyl)methanone (1a).*

To an oven-dried undivided three-necked flask (40 mL) equipped with a magnetic bar, added benzoyl hydrazine (a) (68 mg, 0.5 mmol) and tetrabutylammonium hexafluorophosphate ($^{n}Bu_4NPF_6$) (96.7 mg, 0.25 mmol). Then the flask was equipped with the graphite rod (Φ 6 mm; immersion depth in solution about 15 mm) as the anode, the platinum plate (10 mm ×10 mm × 0.3 mm) as the cathode maintaining an approximate distance of ~6 mm between the electrodes and was flushed with nitrogen (N_2). Then morpholine (**1**) (65 mg, 0.75 mmol, 1.5 equiv) in 2:3 ratios of 1,2-dichloroethane (DCE) and 1,1,1,3,3,3-hexafluoro-2-propanol (HFIP) (5 mL) was added via syringes under nitrogen atmosphere. The reaction mixture was stirred and electrolyzed at a constant current of 10 mA under room temperature for 18 h. After completion of the reaction (monitored by TLC analysis), the solvent was removed in vacuo; the mixture was admixed with ethyl acetate (25 mL), and the organic layer was washed with brine (1 x 10 mL). The organic layer was dried over anhydrous Na_2SO_4, and the solvent was evaporated under reduced pressure. The crude product so obtained was purified over a column of silica gel using 25% ethyl acetate in hexane to afford the morpholino(phenyl)methanone (**1a**) in 78% yield (74 mg) (Scheme IV.14). The identity and purity of the product were confirmed by spectroscopic analysis.

Reaction Set-up:

For the electrolysis, an undivided three-neck cell (40 mL), three rubber septa, a teflon-coated magnetic bar, a carbon rod (Φ 6 mm) as an anode, a platinum plate (10 mm × 10 mm × 0.3 mm) as a cathode and a dual display METRAVI RPS-6002 adjustable 60V/2A DC power supply were used (Figure IV.8).

Figure IV.8. *Electrochemical reaction set-up.*

IV.7.5. General Procedure for 10 mmol Scale Reaction

To an oven-dried undivided two-necked flask (100 mL) equipped with a magnetic bar, was added benzoyl hydrazine (**a**) (1.36 g, 10 mmol), and tetrabutylammonium hexafluorophosphate ($^{n}Bu_4NPF_6$) (1.93 g, 5 mmol). Then the flask was equipped with the graphite rod (Φ 6 mm; immersion depth in solution about 15 mm) as the anode, the platinum plate (10 mm ×10 mm × 0.3 mm) as the cathode maintaining an approximate distance of ~8 mm between the electrodes and was flushed with nitrogen (N_2). Morpholine (**1**) (1.30 g, 15 mmol, 1.5 equiv) in 2:3 ratios of 1, 2-dichloroethane (DCE) and 1,1,1,3,3,3-hexafluoro-2-propanol (HFIP) (50 mL) was added *via* syringes under N_2 atmosphere. The reaction mixture was stirred and electrolyzed at a constant current of 10 mA under room temperature for 32 h. After completion of the reaction (monitored by TLC analysis), the solvent was removed in vacuo, the mixture was admixed with ethyl acetate (100 mL), and the organic layer was washed with brine (50 mL). The organic layer was dried over anhydrous Na_2SO_4, and the solvent was evaporated under reduced pressure. The crude product so obtained was purified over a column of silica gel using increasing 25% ethyl acetate in hexane to afford the morpholino(phenyl)methanone (**1a**) in 70% yield (1.34 g). The identity and purity of the product were confirmed by spectroscopic analysis.

IV.7.6. Synthesis of 'Bezafibrate' Drug

(A) Procedure for the Synthesis of 4-Chloro-*N*-(4-hydroxyphenethyl)benzamide (23g)

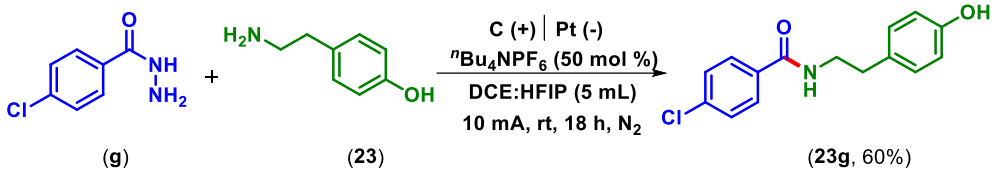

Scheme IV.15. *Synthesis of 4-chloro-N-(4-hydroxyphenethyl)benzamide (23g).*

To an oven-dried undivided three-necked flask (40 mL) equipped with a magentic bar, 4-chloro-benzoyl hydrazine (**g**) (85.3 mg, 0.5 mmol), tyramine (**23**) (102.7 mg, 0.75 mmol, 1.5 equiv) and tetrabutylammonium hexafluorophosphate (^{n}Bu$_4$NPF$_6$) (96.7 mg, 0.25 mmol). Then, the bottle was equipped with the graphite rod (Φ 6 mm; immersion depth in solution about 15 mm) as the anode and the platinum plate (10 mm ×10 mm × 0.3 mm) as the cathode, maintaining an approximate distance of ~6 mm between two electrodes and was flushed with nitrogen. Then 2:3 ratios of 1,2-dichloroethane (DCE) and 1,1,1,3,3,3-hexafluoro-2-propanol (HFIP) (5 mL) were combined and added via syringes under a nitrogen atmosphere. The reaction mixture was stirred and electrolyzed at a constant current of 10 mA under room temperature for 18 h. After completion of the reaction (monitored by TLC analysis), the solvent was removed in vacuo; the mixture was admixed with ethyl acetate (25 mL), and the organic layer was washed with brine (10 mL). The organic layer was dried over anhydrous Na_2SO_4, and the solvent was evaporated under reduced pressure. The crude product so obtained was purified over a column of silica gel using 2% of MeOH in CH_2Cl_2 to afford the 4-chloro-*N*-(4-hydroxyphenethyl)benzamide (**23g**, 60%) (Scheme IV.15). The identity and purity of the product was confirmed by spectroscopic analysis.

(B) Procedure for the Synthesis of Isopropyl 2-(4-(2-(4-chlorobenzamido)ethyl)phenoxy)-2-methylpropanoate (23g′).

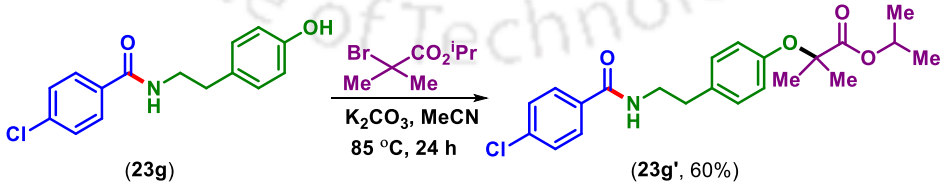

Scheme IV.16. *Synthesis of isopropyl 2-(4-(2-(4-chlorobenzamido)ethyl)phenoxy)-2-methylpropanoate (23g')*

To an oven-dried 10 mL round bottom flask fitted with a magnetic bar was added 4-chloro-*N*-(4-hydroxyphenethyl)benzamide (**23g**) (120.9 mg, 0.3 mmol) in acetonitrile (10 mL) was added potassium carbonate (188 mg, 1.36 mmol) and the mixture was stirred at room temperature for 10 minutes. Isopropyl 2-bromo-2-methylpropanoate (125 mg, 0.6 mmol) was added, and the reaction mixture was stirred under reflux for 16 h. A further portion of isopropyl 2-bromo-2-methylpropanoate (125 mg, 0.6 mmol) and potassium carbonate (69 mg, 0.5 mmol) was added, and the mixture was stirred under reflux for 6 h. The reaction mixture was cooled to room temperature and quenched by adding 1 M aq. HCl (10 mL). The mixture was extracted with CH_2Cl_2 (3 × 20 mL), and the combined organic extracts were washed with brine (50 mL), dried over $MgSO_4$, filtered, and concentrated in a vacuo. The crude product so obtained was purified over a column of silica gel (hexane/ethyl acetate, 8:2) to afford the isopropyl 2-(4-(2-(4-chlorobenzamido)ethyl)phenoxy)-2-methylpropanoate (**23g′**) (72 mg, 60%) (Scheme IV.16) as a colorless oil.

(C) Procedure for the Formation of 2-(4-(2-(4-Chlorobenzamido)ethyl)phenoxy)-2-methylpropanoic acid, Bezafibrate (23g″)

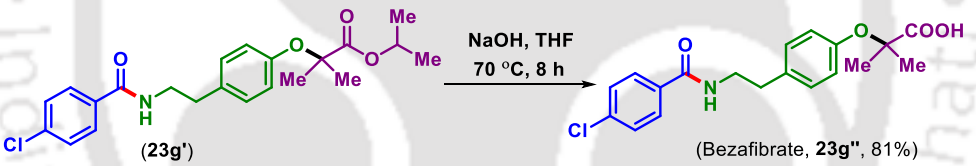

Scheme IV.17. *Synthesis of bezafibrate (23g")*

To an oven-dried 10 mL round bottom flask containing a magnetic bar was added isopropyl 2-(4-(2-(4-chlorobenzamido)ethyl)phenoxy)-2-methylpropanoate (**23g′**) (68 mg, 0.17 mmol) in THF (10 mL) was added 4 M aq. NaOH (2 mL) and the resulting mixture was stirred at reflux for 8 h. Further portions of NaOH (100 mg, 2.50 mmol) were added at 2 h intervals throughout the course of the reaction. The reaction mixture was cooled to room temperature and concentrated in a vacuum. The residue was dissolved in water (20 mL), and concentrated HCl was added dropwise. The resulting precipitate was filtered, washed with water, and dried under a high vacuum to afford 2-(4-(2-(4-chlorobenzamido)ethyl)phenoxy)-2- methylpropanoic acid, bezafibrate (**23g″**) (50 mg, 81%) as an off-white solid (Scheme IV.17). The identity and purity of the product was confirmed by spectroscopic analysis.

IV.7.7. Mechanistic Investigations

Radical-trapping Experiments

(i) To an oven-dried undivided three-necked flask (40 mL) equipped with a magnetic bar was added benzoyl hydrazine (**a**) (68 mg, 0.5 mmol), tetrabutylammonium hexafluorophosphate ($^{n}Bu_4NPF_6$) (96.7 mg, 0.25 mmol) and (2,2,6,6-tetramethylpiperidin-1-yl)oxyl (TEMPO) (156 mg, 1.0 mmol, 2 equiv). Then, the flask was equipped with the graphite rod (Φ 6 mm; immersion depth in solution about 15 mm) as the anode, the platinum plate (10 mm ×10 mm × 0.3 mm) as the cathode maintaining an approximate distance of ~6 mm between the electrodes and was flushed with nitrogen. Then morpholine (**1**) (65 mg, 0.75 mmol, 1.5 equiv) in 2:3 ratios of 1,2-dichloroethane (DCE) and 1,1,1,3,3,3-hexafluoro-2-propanol (HFIP) (5 mL) was added *via* syringes under nitrogen atmosphere. The reaction mixture was stirred and electrolyzed at a constant current of 10 mA under room temperature for 18 h. After completion of the reaction (monitored by TLC analysis), the solvent was removed in vacuo; the mixture was admixed with ethyl acetate (25 mL), and the organic layer was washed with brine (10 mL). The organic layer was dried over anhydrous Na_2SO_4, and the solvent was evaporated under reduced pressure. The crude product so obtained was purified over a column of silica gel using an increasing percentage of ethyl acetate in hexane to afford the TEMPO-adduct, 2,2,6,6-tetramethylpiperidin-1-yl benzoate (**1s**) in 33% yield (43 mg) and a trace amount of morpholino(phenyl)methanone (**1a**).

(ii) To an oven-dried undivided three-necked flask (40 mL) equipped with a magnetic bar was added benzoyl hydrazine (**a**) (68 mg, 0.5 mmol), tetrabutylammonium hexafluorophosphate ($^{n}Bu_4NPF_6$) (96.7 mg, 0.25 mmol) and Butylated hydroxytoluene (BHT) (220 mg, 1.0 mmol, 2 equiv). Then, the flask was equipped with the graphite rod (Φ 6 mm; immersion depth in solution about 15 mm) as the anode, the platinum plate (10 mm ×10 mm × 0.3 mm) as the cathode maintaining an approximate distance of ~6 mm between the electrodes and was flushed with nitrogen. Then morpholine (**1**) (65 mg, 0.75 mmol, 1.5 equiv) in 2:3 ratios of 1,2-dichloroethane (DCE) and 1,1,1,3,3,3-hexafluoro-2-propanol (HFIP) (5 mL) was added *via* a syringes under nitrogen atmosphere. The reaction mixture was stirred and electrolyzed at a constant current of 10 mA under room temperature for 18 h. After completion of the reaction (monitored by TLC analysis), the solvent was removed in vacuo; the mixture was admixed with

ethyl acetate (25 mL), and the organic layer was washed with brine (10 mL). The organic layer was dried over anhydrous Na_2SO_4, and the solvent was evaporated under reduced pressure. The crude product so obtained was purified over a column of silica gel using 25% ethyl acetate in hexane to afford morpholino(phenyl)methanone (**1a**) in <15% yield.

(I) Reaction with benzaldehyde

Scheme IV.18. *Experiments with benzaldehyde.*

(iv) To an oven-dried undivided three-necked flask (40 mL) equipped with a magnetic bar was added tetrabutylammonium hexafluorophosphate ($^nBu_4NPF_6$) (96.7 mg, 0.25 mmol). Then, the flask was equipped with the graphite rod (Φ 6 mm; immersion depth in solution about 15 mm) as the anode, the platinum plate (10 mm ×10 mm × 0.3 mm) as the cathode, maintaining an approximate distance of ~6 mm between the electrodes and was flushed with nitrogen. Then benzaldehyde (**a′**) (53 mg, 0.5 mmol) and morpholine (**1**) (65 mg, 0.75 mmol, 1.5 equiv) in 2:3 ratios of 1,2-dichloroethane (DCE) and 1,1,1,3,3,3-hexafluoro-2-propanol (HFIP) (5 mL) were added *via* syringes under nitrogen atmosphere. The reaction mixture was stirred and electrolyzed at a constant current of 10 mA under room temperature for 18 h. The formation of morpholino(phenyl)methanone (**1a**) was not detected (Scheme IV.18), which suggests that aldehyde is not the intermediate of this reaction.

(II) Reaction with benzoic acid

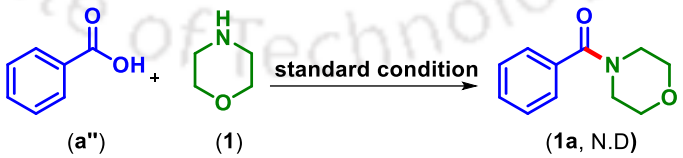

Scheme IV.19. *Experiment with benzoic acid.*

(v) To an oven-dried undivided three-necked flask (40 mL) equipped with a magnetic bar was added benzoic acid (**a″**) (61 mg, 0.5 mmol) and tetrabutylammonium hexafluorophosphate ($^nBu_4NPF_6$) (96.7 mg, 0.25 mmol). Then, the flask was equipped with the

graphite rod (Φ 6 mm; immersion depth in solution about 15 mm) as the anode, the platinum plate (10 mm ×10 mm × 0.3 mm) as the cathode, maintaining an approximate distance of ~6 mm between the electrodes and was flushed with nitrogen. Then morpholine (**1**) (65 mg, 0.75 mmol, 1.5 equiv) in 2:3 ratios of 1,2-dichloroethane (DCE) and 1,1,1,3,3,3-hexafluoro-2-propanol (HFIP) (5 mL) were added *via* syringes under nitrogen atmosphere. The reaction mixture was stirred and electrolyzed at a constant current of 10 mA under room temperature for 18 h. The formation of morpholino(phenyl)methanone (**1a**) was not observed (Scheme IV.19), which suggested that benzoic acid was not the intermediate of this reaction.

(III) Reaction with benzamide

Scheme IV.20. *Experiment with benzamide.*

To an oven-dried undivided three-necked flask (40 mL) equipped with a magnetic bar was added benzamide (**32**) (60 mg, 0.50 mmol) and tetrabutylammonium hexafluorophosphate ($^{n}Bu_4NPF_6$) (96.7 mg, 0.25 mmol). Then the flask was equipped with the graphite rod (Φ 6 mm; immersion depth in solution about 15 mm) as the anode, the platinum plate (10 mm ×10 mm × 0.3 mm) as the cathode maintaining an approximate distance of ~6 mm between the electrodes and was flushed with nitrogen. Then morpholine (**1**) (65 mg, 0.75 mmol, 1.5 equiv) in 2:3 ratios of 1,2-dichloroethane (DCE) and 1,1,1,3,3,3-hexafluoro-2-propanol (HFIP) (5 mL) were added *via* syringes under nitrogen atmosphere. The reaction mixture was stirred and electrolyzed at a constant current of 10 mA under room temperature for 18 h. The formation of morpholino(phenyl)methanone (**1a**) was not observed (Scheme IV.20), which suggests that benzamide is also not the intermediate of this reaction.

IV.7.8. Detection of H_2 gas Under the Standard Condition:

To check the release of H_2 gas in the reaction, we performed GC analysis under standard conditions using benzoyl hydrazine (**a**) (68 mg, 0.5 mmol), tetrabutylammonium hexafluorophosphate ($^{n}Bu_4NPF_6$) (96.7 mg, 0.25 mmol). The flask was equipped with the graphite rod (Φ 6 mm) as the anode, and the platinum plate (10 mm ×10 mm × 0.3 mm) as the

cathode and was flushed with nitrogen. Then morpholine (**1**) (65 mg, 0.75 mmol, 1.5 equiv) in 2:3 ratios of 1,2-dichloroethane (DCE) and 1,1,1,3,3,3-hexafluoro-2-propanol (HFIP) (5 mL) was added *via* syringes under nitrogen atmosphere. The reaction mixture was stirred and electrolyzed at a constant current of 10 mA under room temperature for 18 h. After the reaction, the mixture was examined by gas chromatography (GC) equipped with a TCD detector and the release of H_2 was detected (Figure IV.9).[6].

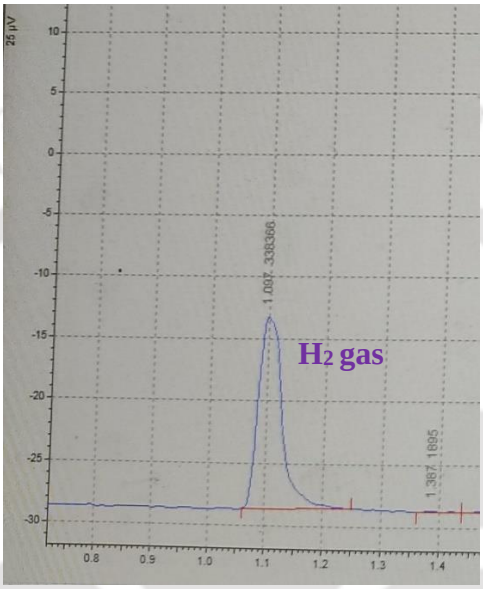

Figure IV.9. *GC chromatogram of hydrogen gas (H_2) evolved after the course of reaction.*

IV.7.9. Cyclic Voltammetry (CV) and Linear Sweep Voltammetry (LSV) Experiments:

Cyclic voltammetry and linear sweep voltammetry (LSV) experiments were performed using Gamry instrument in a three-electrode cell connected to an undivided three-necked bottle with a stir bar under a nitrogen atmosphere at room temperature. The working electrode was a platinum electrode and the counter electrode a platinum wire. The reference was a saturated calomel electrode submerged in a saturated aqueous KCl solution.

(i) Cyclic Voltammetry Studies of Benzoyl Hydrazine (a) to Explore the Reaction at the Anode

Test conditions: A cyclic voltammograms in solvent (5 mL) using platinum as the working electrode, Pt wire as the counter electrode, and saturated calomel electrode (SCE) as

the reference electrode under N_2 at room temperature (Figure IV.10). The scan rate was 0.1 V/s.

Black line: 5 mL DCE and $TBAPF_6$ (0.1 M).

Red line: 10 mM benzoyl hydrazine (**a**) with 5 mL DCE solvent. The two oxidation peaks for (**a**) were observed at 1.58 V (vs. SCE), and 2.63 V (vs. SCE).

Blue line: 10 mM benzoyl hydrazine (**a**) with 2:3 ratio 5 mL DCE:HFIP solvent. The two-oxidation peaks of the benzoyl hydrazine (**a**) were observed at 1.51 V (vs. SCE) and 2.55 V (vs. SCE).

Therefore, it can be concluded that, after adding HFIP to the reaction mixture, the oxidation potentials decreased from 1.58 V to 1.51 V and 2.63 V to 2.55 V, suggesting the easy oxidation of (**a**) through HFIP activation.

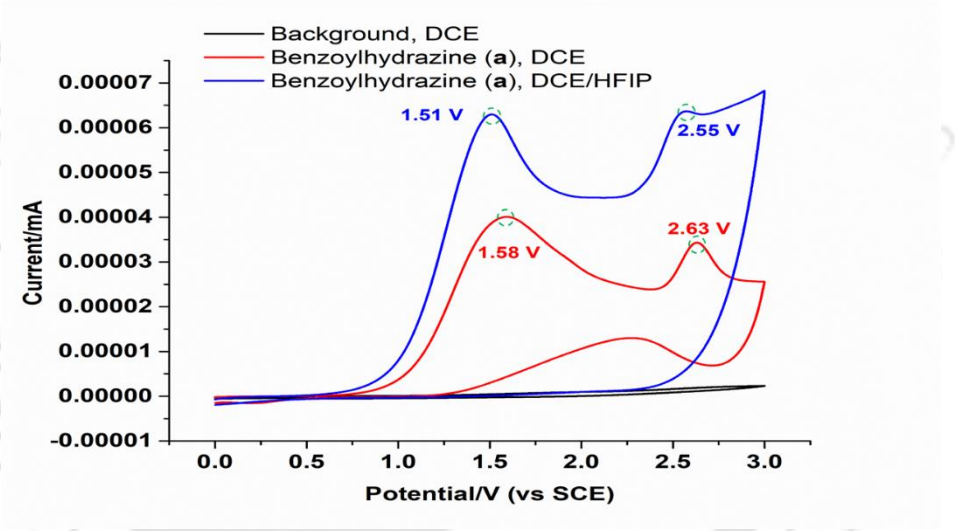

Figure IV.10. *Cyclic voltammograms of benzoyl hydrazine (a).*

(ii) Cyclic Voltammetry Studies of Morpholine (1) to Explore the Reaction at the Anode

Test conditions: A cyclic voltammograms in solvent (5 mL) using platinum as the working electrode, Pt wire as the counter electrode, and saturated calomel electrode (SCE) as the reference electrode under N_2 at room temperature (Figure IV.11). The scan rate is 0.1 V/s.

Black line: 5 mL DCE and $TBAPF_6$ (0.1 M).

Red line: 10 mM morpholine (**1**) with 5 mL DCE solvent. The oxidation peaks of (**1**) were observed at 1.28 V (vs SCE).

Blue line: 10 mM morpholine (**1**) with 2:3 ratio 5 mL DCE:HFIP solvent. The oxidation peak of (**1**) was observed at 1.22 V (vs SCE).

Therefore, it can be concluded that after the addition of HFIP to the reaction mixture, the oxidation potential decreased from 1.28 V to 1.22 V, suggesting the easy oxidation of (**1**) through HFIP activation.

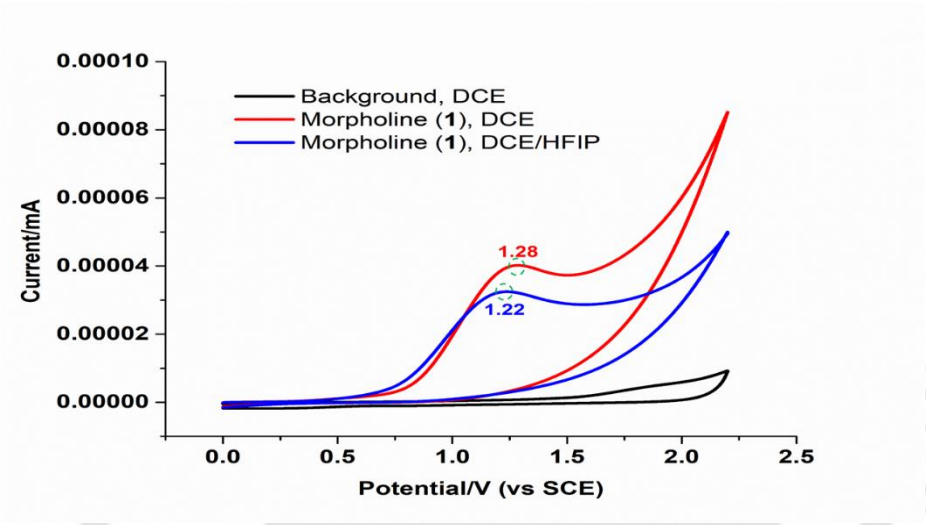

Figure IV.11. *Cyclic voltammograms of morpholine (1).*

(iii) Cyclic Voltammetry Studies of Mixture of Benzoyl Hydrazine (a) and Morpholine (1) to Explore the Reaction at the Anode

Test conditions: A cyclic voltammograms in solvent (5 mL) by using platinum as the working electrode, Pt wire as the counter electrode and saturated calomel electrode (SCE) as the reference electrode under N_2 at room temperature (Figure IV.12). The scan rate is 0.1 V/s.

Black line: 5 mL DCE and $TBAPF_6$ (0.1 M).

Red line: 10 mM Benzoyl hydrazine (**a**) with 2:3 ratio 5 mL DCE:HFIP solvent. The two oxidation peaks of (**a**) were observed at 1.51 V (vs SCE) and 2.55 V (vs SCE).

Blue line: 10 mM Morpholine (**1**) with 2:3 ratio 5 mL DCE:HFIP solvent. The oxidation peak of (**1**) was observed at 1.22 V (vs SCE).

Pink line: 10 mM Benzoyl hydrazine (**a**) and morpholine (**1**) with 2:3 ratio 5 mL DCE:HFIP solvent The two oxidation peaks for the mixture (**a +1**) were observed at 1.07 V (vs. SCE) and 2.19 V (vs. SCE).

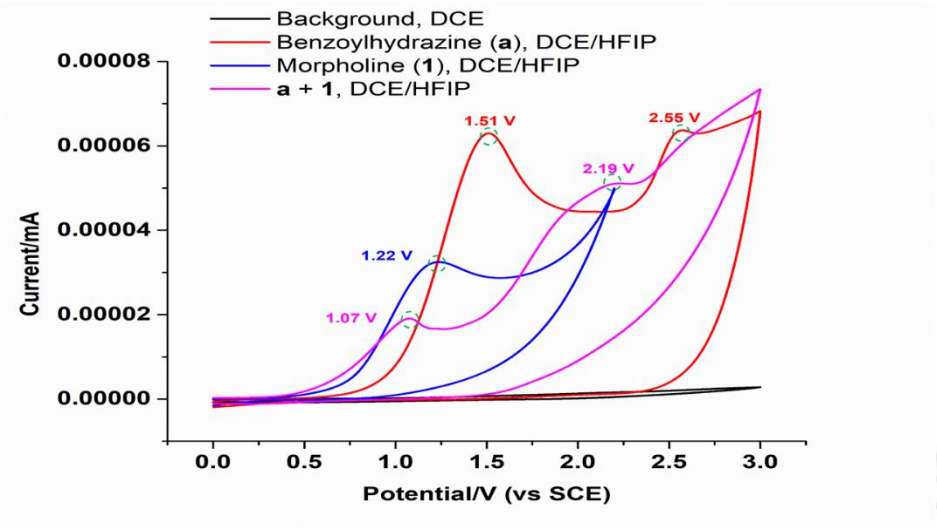

Figure IV.12. *Cyclic voltammograms of benzoyl hydrazine (a) and morpholine (1).*

(iv) Linear Sweep Voltammetry (LSV) Measurements of Benzoyl Hydrazine (a) and Morpholine (1) to Explore the Reaction at the Anode

Test conditions: A linear sweep voltammetry in solvent DCE:HFIP (2:3) (5 mL) and $TBAPF_6$ (0.1 M) by using platinum as the working electrode, Pt wire as the counter electrode and saturated calomel electrode (SCE) as the reference electrode under N_2 at room temperature (Figure IV.13). The scan rate is 0.1 V/s.

Black line: 10 mM benzoyl hydrazine (**a**): Onset potential at 0.90 V vs. (SCE) and anodic potential at 1.47 V vs. SCE.

Red line: 10 mM morpholine (**1**): Onset potential at 0.63 V vs SCE and anodic potential at 0.99 V vs SCE.

Blue line: Initial mixture of 10 mM benzoyl hydrazine (**a**) and morpholine (**1**): Onset potential at 0.019 V vs SCE and the anodic oxidation peaks of (**a** + **1**) were observed at 1.40 V vs SCE.

Pink line: Final mixture of 10 mM benzoyl hydrazine (**a**) and morpholine (**1**): Onset potential at 0.019 V vs SCE and the anodic oxidation peaks for (**a** + **1**) were observed at 1.84 V vs. SCE.

This confirms the oxidation of both the reacting partners at the anode.

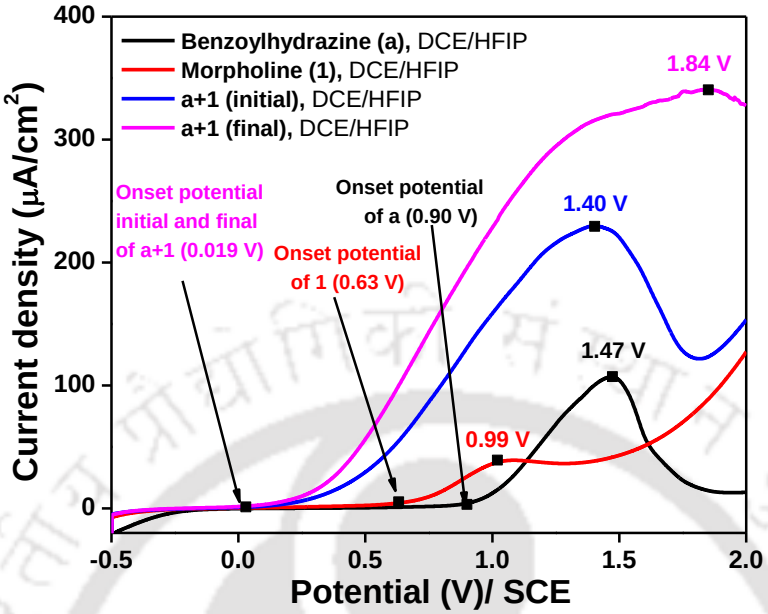

Figure IV.13. *Linear sweep voltammetry (LSV) measurements of benzoyl hydrazine (a) and morpholine (1).*

IV.8. References

[1] (a) Alcaide, B.; Almendros, P.; Aragoncillo, C. *Chem. Rev*. **2007**, *107*, 4437–4492. (b) Humphrey, J. M.; Chamberlin, A. R. *Chem. Rev*. **1997**, *97*, 2243–2266. (c) Tani, K.; Stoltz, B. M. *Nature* **2006**, *441*, 731–734. (d) Pattabiraman, V. R.; Bode, J. W. *Nature* **2011**, *480*, 471–479. (e) Hughes, A. B. Amino Acids, Peptides and Proteins in Organic Chemistry; Wiley-VCH: Weinheim, Germany, **2011**.

[2] (a) Brown, D. G.; Boström, J. *J. Med. Chem*. **2016**, *59*, 4443–4458. (b) Marchildon, K. *Macromol. React. Eng*. **2011**, *5*, 22–54.

[3] Roughley, S. D.; Jordan, A. M. *J. Med. Chem*. **2011**, *54*, 3451–3479.

[4] (a) Halima, T. B.; Masson-Makdissi, J.; Newman, S. G. *Angew. Chem*. **2018**, *130*, 13107–13111. (b) Nicholson, W. I.; Barreteau, F.; Leitch, J. A.; Payne, R.; Priestley, I.; Godineau, E.; Battilocchio, C.; Browne, D. L. *Angew. Chem., Int. Ed*. **2021**, *60*,

21868–21874. (c) Li, Y.; Li, J.; Bao, G.; Yu, C.; Liu, Y.; He, Z.; Wang, P.; Ma, W.; Xie, J.; Sun, W.; Wang, R. *Org. Lett*. **2022**, *24*, 1169–1174. (d) Li, G.; Ji, C.-L.; Hong, X.; Szostak, M. *J. Am. Chem. Soc*. **2019**, *141*, 11161–11172. (e) Brittain, W. D. G.; Cobb, S. L. *Org. Lett*. **2021**, *23*, 5793–5798. (f) Braddock, D. C.; Lickiss, P. D.; Rowley, B. C.; Pugh, D.; Purnomo, T.; Santhakumar, G.; Fussell, S. J. *Org. Lett*. **2018**, *20*, 950–953. (g) Dunetz, J. R.; Magano, J.; Weisenburger, G. A. *Org. Process Res. Dev*. **2016**, *20*, 140–177.

[5] (a) Lu, B.; Cheng, Y.; Chen, L.-Y.; Chen, J.-R.; Xiao, W.-J. *ACS Catal*. **2019**, *9*, 8159–8164. (b) Tien, C.-H.; Trofimova, A.; Holownia, A.; Kwak, B. S.; Larson, R. T.; Yudin, A. K. *Angew. Chem., Int. Ed*. **2021**, *60*, 4342–4349. (c) Liu, H.; Laurenczy, G.; Yan, N.; Dyson, P. J. *Chem. Commun*. **2014**, *50*, 341–343.

[6] (a) Green, R. A.; Pletcher, D.; Leach, S. G.; Brown, R. C. D. *Org. Lett.* **2016**, *18*, 1198–1201. (b) Zhang, B.; Feng, P.; Cui, Y.; Jiao, N. *Chem. Commun*., **2012**, *48*, 7280–7282.

[7] Braslau, R.; Anderson, M. O.; Rivera, F.; Jimenez, A.; Haddad, T.; Axon, J. R. *Tetrahedron* **2002**, *58*, 5513–5523.

[8] (a) Xie, S.; Su, L.; Mo, M.; Zhou, W.; Zhou, Y.; Dong, J. *J. Org. Chem*. **2021**, *86*, 739–749. (b) Xu, X.; Tang, Y.; Li, X.; Hong, G.; Fang, M.; Du, X. *J. Org. Chem*. **2014**, *79*, 446–451. (c) Amos, R. I. J.; Gourlay, B. S.; Yates, B. F.; Schiesser, C. H.; Lewis, T. W.; and Smith, J. A. *Org. Biomol. Chem.* **2013**, *11*, 170–176.

[9] (a) Banerjee, A.; Sarkar, S.; Shah, J. A.; Frederiks, N. C.; Bazan- Bergamino,E. A.; Johnson, C. J.; Ngai, M.-Y. *Angew. Chem., Int. Ed*. **2022**, *61*, e202113841. (b) Banerjee, A.; Lei, Z.; Ngai, M.-Yu. *Synthesis* **2019**, *51*, 303–333. (c) Liu, J.; Liu, Q.; Yi, H.; Qin, C.; Bai, R.; Qi, X.; Lan, Y. Lei, A. *Angew. Chem., Int. Ed*. **2014**, *53*, 502–506. (d) Vanjari, R.; Guntreddi, T.; Singh, K. N. *Green Chem*. **2014**, *16*, 351–356.

[10] (a) Wang, S.-N.; Zhang, G.-Y. Shoberu, A.; Zou, J.-P. *J. Org. Chem*. **2021**, *86*, 9067–9075. (b) Wang, Y.-J.; Zhang, G.-Y.; Shoberu, A.; Zou, J.-P. *Tetrahedron Lett.* **2021**, *80*, 153316–153321.

[11] (a) Piszel, P. E.; Vasilopoulos, A.; Stahl, S. S. *Angew. Chem., Int. Ed*. **2019**, *58*, 12211–12215. (b) Xu, Z.; Yang, T.; Tang, N.; Ou, Y.; Yin, S.-F.; Kambe, N.; Qiu, R.

Org. Lett. **2021**, *23*, 5329–5333. (c) Tolba, A. H.; Krupička, M.; Chudoba, J.; and Cibulka, R. *Org. Lett*. **2021**, *23*, 6825–6830. (d) Gu, C.; Wang, S.; Zhang, Q.; Xie, J. *Chem. Commun*. **2022**, *58*, 5873–5876.

[12] (a) Shi, S.-H.; Liang, Y.; Jiao, N. *Chem. Rev*. **2021**, *121*, 485–505. (b) Baidya, M.; Maiti, D.; Roy, L.; Sarkar, S. D. *Angew. Chem., Int. Ed*. **2022**, *61*, e202111679. (c) Liu, D.; Liu, Z.-R.; Ma, C.; Jiao, K.-J.; Sun, B.; Wei, L.; Lefranc, J.; Herbert, S.; Mei, T.-S. *Angew. Chem.* **2021**, *133*, 9530–9535.

[13] Cantillo, D. *Chem. Commun*. **2022**, *58*, 619–628.

[14] (a) Yuan, Y.; Lei, A. *Acc. Chem. Res*. **2019**, *52*, 3309–3324. (b) Liu, Y.; Shi, B.; Liu, Z.; Gao, R.; Huang, C.; Alhumade, H.; Wang, S.; Qi, X.; Lei, A. *J. Am. Chem. Soc*. **2021**, *143*, 20863–20872. (c) Yuan, Y.; Yang, J.; Lei, A. *Chem. Soc. Rev.* **2021**, *50*, 10058–10086

[15] (a) Novaes, L. F. T.; Liu, J.; Shen, Y.; Lu, L.; Meinhardt, J. M.; Lin, S. *Chem. Soc. Rev*., **2021**, *50*, 7941–8002. (b) Novaes, L. F. T.; Ho, J. S. K.; Mao, K.; Liu, K.; Tanwar, M.; Neurock, M.; Villemure, E.; Terrett, J.; A. Lin, S. *J. Am. Chem. Soc.* **2022**, *144*, 1187–1197. (c) Lu, L.; Siu, J. C.; Lai, Y.; Lin, S. *J. Am. Chem. Soc*. **2020**, *142*, 21272–21278.

[16] Harwood, S. J.; Palkowitz, M. D.; Gannett, C. N.; Perez, P.; Yao, Z.; Sun, L.; Abruña, H. D.; Anderson, S. L.; Baran, P. S. *Science* **2022**, *375*, 745–752.

[17] Sadowski, B.; Yuan, B.; Lin, Z.; Ackermann, L. *Angew. Chem., Int. Ed*. **2022**, *61*, e202117188.

[18] (a) Klein, M.; Waldvogel, S. R. *Angew. Chem., Int. Ed*. **2021**, *60*, 23197–23201. (b) Baidya, M.; Mallick, S.; and Sarkar S. D. *Org. Lett*. **2022**, *24*, 1274–1279. (c) Sen, P. P.; Prakash, R.; Roy, S. R. *Org. Lett*. **2022**, *24*, 4530–4535.

[19] (a) Liu, Z.; Zhang, J.; Chen, S.; Shi, E.; Xu, Y.; Wan, X. *Angew. Chem. Int. Ed*. **2012**, *51*, 3231–3235. (b) Chen, J.; He, B.-Q.; Wang, P.-Z.; Yu, X.-Y.; Zhao, Q.-Q.; Chen, J.-R.; Xiao, W.-J. *Org. Lett*. **2019**, *21*, 4359–4364. (c) Rerkrachaneekorn, T.; Tankam, T.; Sukwattanasinitt, M.; Wacharasindhu, S. *Tetrahedron Lett.* **2021**, *70*, 153017–153023. (d) Ke, F.; Xu, Y.; Zhu, S.; Lin, X.; Lin, C.; Zhou, S.; Su, H. *Green Chem*., **2019**, *21*, 4329–4333.

[20] (a) Qiu, Y.; Struwe, J.; Meyer, T. H.; Oliveira, J. C. A.; Ackermann, L. *Chem. Eur. J.* **2018**, *24*, 12784–12789. (b) Li, K.-J.; Xu, K.; Liu, Y.-G.; Zeng, C.-C.; Sun, B.-G. *Adv. Synth. Catal*. **2019**, *361*, 1033–1041.

[21] Wan, H.; Li, D.; Xia, H.; Yang, L.; Alhumade, H.; Yi, H.; Lei, A. *Chem. Commun*. **2022**, *58*, 665–668.

[22] Liu, Z.; Zhang, J.; Chen, S.; Shi, E.; Xu, Y.; Wan, X. *Angew. Chem., Int. Ed*. **2012**, *51*, 3231–3235.

IV.9. Spectral Data

Morpholino(phenyl)methanone (1a):

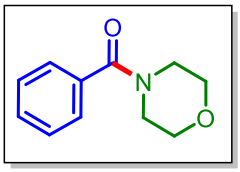

Yield: 78% (74 mg) as a colourless gummy solid; Purification over a column of silica gel (25% EtOAc in hexane); ^{1}H NMR ($CDCl_3$, 600 MHz): δ 7.39–7.37 (m, 5H), 3.74–3.41 (m, 8H); ^{13}C{1H} NMR ($CDCl_3$, 150 MHz): δ 170.6, 135.4, 130.0, 128.7, 127.2, 66.9, 48.3, 42.7; IR (KBr, cm^{-1}): 2977, 2858, 1623, 1255, 708; HRMS (ESI/Q-TOF) (m/z) calcd for $C_{11}H_{14}NO_2$, $[M + H]^+$: 192.1019, found 192.1006.

***Phenyl(thiomorpholino)methanone (2a)*:**

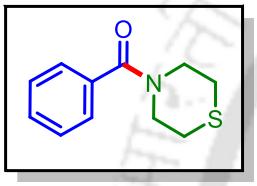

Yield: 76% (79 mg) as a brown oil liquid; Purification over a column of silica gel (25% EtOAc in hexane); ^{1}H NMR ($CDCl_3$, 500 MHz): δ 7.39–7.34 (m, 5H), 3.98–3.64 (m, 4H), 2.68–2.55 (m, 4H); ^{13}C{^{1}H} NMR ($CDCl_3$, 125 MHz): δ 170.8, 135.9, 129.8, 128.7, 126.8, 50.2, 44.7; IR (KBr, cm^{-1}): 2911, 2862, 1625, 1258, 706; HRMS (ESI/Q-TOF) (m/z) calcd for $C_{11}H_{14}NOS$, $[M + H]^+$: 208.0791, found 208.0788.

***(4-Methylpiperidin-1-yl)(phenyl)methanone (3a)*:**

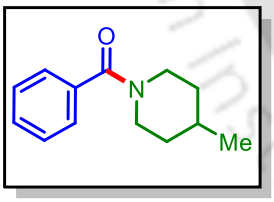

Yield: 82% (83 mg) as a white solid; Purification over a column of silica gel (25% EtOAc in hexane); ^{1}H NMR ($CDCl_3$, 500 MHz): δ 7.38-7.37 (m, 5H), 4.67 (s, br, 1H,), 3.70 (s, br, 1H), 2.96–2.77 (m, 2H); 1.75–1.56 (m, 4H), 1.25 (s, 1H), 0.97 (d, 3H, J = 6.5 Hz); ^{13}C{^{1}H} NMR ($CDCl_3$, 125 MHz): δ 170.5, 136.8, 129.5, 128.6, 127.0, 48.3, 42.7, 34.9, 34.1, 31.4, 21.9; IR (KBr, cm^{-1}): 2903, 2865, 1625, 1116, 703; HRMS (ESI/Q-TOF) (m/z) calcd for $C_{13}H_{18}NO$, $[M + H]^+$: 204.1383, found 204.1379.

***(3-Methylpiperidin-1-yl)(phenyl)methanone (4a)*:**

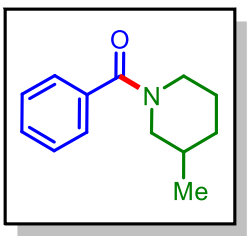

Yield: 72% (73 mg) as a brown liquid; Purification over a column of silica gel (25% EtOAc in hexane); ^{1}H NMR ($CDCl_3$, 600 MHz): δ 7.33 (s, 5H), 4.49 (s, 1H), 3.60–3.53 (m, 1H), 2.88–2.34 (m, 2H),

1.82–1.54 (m, 4H), 1.14–1.10 (m, 1H), 0.92–0.74 (m, 3H); $^{13}C\{^{1}H\}$ NMR ($CDCl_3$, 150 MHz): δ 170.3, 136.5, 129.4, 128.4, 126.8, 55.1, 48.2, 42.7, 33.1, 31.1, 26.0, 19.1; IR (KBr, cm^{-1}): 2922, 2815, 1635, 1125, 721; HRMS (ESI/Q-TOF) (m/z) calcd for $C_{13}H_{18}NO$, $[M + H]^+$: 204.1383, found 204.1380.

***(2-Methylpiperidin-1-yl)(phenyl)methanone (5a)*:**

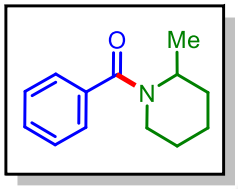

Yield: 70% (71 mg) as a brown liquid; Purification over a column of silica gel (25% EtOAc in hexane); ^{1}H NMR ($CDCl_3$, 600 MHz): δ 7.38–7.34 (m, 5H), 2.97 (s, 1H), 1.87–1.46 (m, 7H), 1.27–1.22 (m, 4H); $^{13}C\{^{1}H\}$ NMR ($CDCl_3$, 150 MHz): δ 170.7, 137.2, 129.3, 128.6, 126.5, 30.5, 26.2, 19.1, 16.3; IR (KBr, cm^{-1}): 2969, 2863, 1620, 1115, 705; HRMS (ESI/Q-TOF) (m/z) calcd for $C_{13}H_{18}NO$, $[M + H]^+$: 204.1383, found 204.1379.

***(4-Hydroxypiperidin-1-yl)(phenyl)methanone (6a)*:**

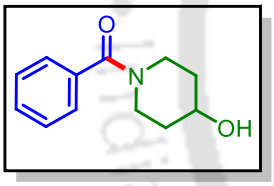

Yield: 68% (70 mg) as a brown liquid; Purification over a column of silica gel (25% EtOAc in hexane); ^{1}H NMR ($CDCl_3$, 600 MHz): δ 7.38–7.36 (m, 3H), 7.35 (m, 2H), 4.14 (s, 1H), 3.88–3.86 (m, 1H), 3.61 (s, 1H), 3.33–3.13 (m, 2H), 2.60 (s, br, 1H), 1.90–1.75 (m, 2H), 1.56–1.44 (m, 2H); $^{13}C\{^{1}H\}$ NMR ($CDCl_3$, 150 MHz): δ 170.6, 136.1, 129.8, 128.6, 126.9, 66.9, 45.1, 39.6, 34.7, 33.9; IR (KBr, cm^{-1}): 2947, 2862, 1598, 1069, 709; HRMS (ESI/Q-TOF) (m/z) calcd for $C_{12}H_{16}NO_2$, $[M + H]^+$: 206.1176, found 206.1174.

***(4-Benzylpiperidin-1-yl)(phenyl)methanone (7a)*:**

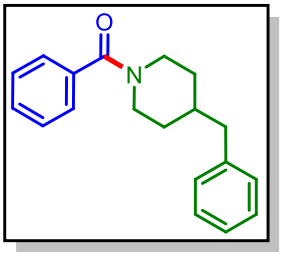

Yield: 70% (98 mg) as a brown liquid; Purification over a column of silica gel (25% EtOAc in hexane); ^{1}H NMR ($CDCl_3$, 600 MHz): δ δ 7.39–7.37 (m, 5H), 7.28 (t, 2H, J = 7.5 Hz), 7.21–7.20 (m, 1H), 7.14 (d, 2H, J = 7.8 Hz), 4.70–4.65 (m, 1H), 3.73–3.71 (m, 1H), 2.92–2.57 (m, 4H), 1.81–1.77 (m, 2H), 1.60–1.58 (m, 1H), 1.27 (s, 1H), 1.18–1.15 (m, 1H); $^{13}C\{^{1}H\}$ NMR ($CDCl_3$, 150 MHz): δ 170.5, 140.1, 136.5, 129.6, 129.2, 128.6, 128.5, 128.1,127.2, 126.9, 126.2, 48.2, 43.1, 42.6, 38.5, 32.8, 31.9; IR (KBr, cm^{-1}): 2954, 2858, 1614,

1255, 698; HRMS (ESI/Q-TOF) (m/z) calcd for $C_{19}H_{22}NO$, $[M + H]^+$: 280.1696, found 280.1696.

***(4-Cyclohexylpiperazin-1-yl)(phenyl)methanone (8a)*:**

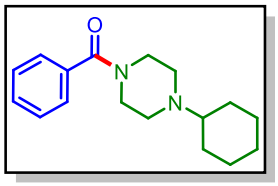

Yield: 60% (81 mg) as a brown liquid; Purification over a column of silica gel (25% EtOAc in hexane); ^{1}H NMR ($CDCl_3$, 600 MHz): δ 7.42–7.38 (m, 5H), 4.03–3.72 (m, 4H), 2.94–2.70 (m, 2H), 2.04–1.99 (m, 1H), 1.85 (d, 2H, J = 12.6 Hz), 1.65 (d, 1H, J = 13.8 Hz), 1.37–1.31 (m, 2H), 1.27–1.23 (m, 3H), 1.14–1.07 (m, 1H); ^{13}C{^{1}H} NMR ($CDCl_3$, 150 MHz): δ 170.4, 134.9, 130.4, 128.8, 127.3, 65.1, 49.0, 48.4, 46.1, 40.6, 27.7, 25.6, 25.5; IR (KBr, cm^{-1}): 2928, 2809, 1614, 1012, 709; HRMS (ESI/Q-TOF) (m/z) calcd for $C_{17}H_{25}N_2O$, $[M + H]^+$: 274.2040, found 274.2043.

***Phenyl(4-phenylpiperazin-1-yl)methanone (9a)*:**

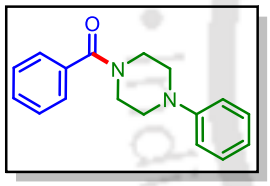

Yield: 70% (93 mg) as a white solid; Purification over a column of silica gel (25% EtOAc in hexane); ^{1}H NMR ($CDCl_3$, 600 MHz): δ 7.43 (s, 5H), 7.29 (t, 2H, J = 8.0 Hz), 6.94–6.91 (m, 3H), 3.93 (s, 2H), 3.58 (s, 2H), 3.18 (d, 4H, J = 83.4 Hz); ^{13}C{^{1}H} NMR ($CDCl_3$, 150 MHz): δ 170.5, 151.0, 135.6, 129.9, 129.3, 128.6, 127.2, 120.7,116.8, 49.9, 49.6, 47.7, 42.2.; IR (KBr, cm^{-1}): 2922, 2853, 1597, 1154, 693; HRMS (ESI/Q-TOF) (m/z) calcd for $C_{17}H_{19}N_2O$, $[M + H]^+$: 267.1492, found 267.1493.

***(4-(2-Methoxyphenyl)piperazin-1-yl)(phenyl)methanone (10a)*:**

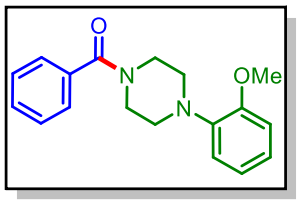

Yield: 80% (118 mg) as a brown liquid; Purification over a column of silica gel (25% EtOAc in hexane); ^{1}H NMR ($CDCl_3$, 600 MHz): δ 7.43–7.40 (m, 5H), 7.04–7.01(m, 1H), 6.93–6.91 (m, 2H), 6.88 (d, 1H, J = 7.8 Hz), 3.97 (s, 2H), 3.86 (s, 3H), 3.61 (s, 2H), 3.12–2.98 (m, 4H); ^{13}C{^{1}H} NMR ($CDCl_3$, 150 MHz): δ 170.5, 152.3, 140.7, 135.8, 129.8, 128.6, 127.2, 123.7,121.2, 118.6,111.4, 55.5, 51.3, 50.8, 48.1, 42.5; IR (KBr, cm^{-1}): 2928, 2816, 1626, 1238,

709; HRMS (ESI/Q-TOF) (m/z) calcd for $C_{18}H_{21}N_2O_2$, $[M + H]^+$: 297.1598, found 297.1598.

***(E)-Phenyl(4-styrylpiperazin-1-yl)methanone (11a)*:**

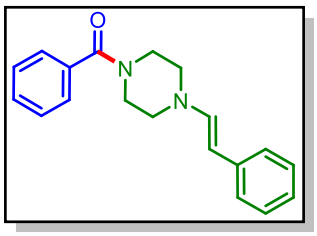

Yield: 72% (105 mg) as a brown liquid; Purification over a column of silica gel (25% EtOAc in hexane); ^{1}H NMR ($CDCl_3$, 500 MHz): δ 7.40–7.36 (m, 7H), 7.30 (t, 2H, J = 7.5 Hz), 7.23 (t, 1H, J = 7.2 Hz), 6.53 (d, 1H, J = 16.0 Hz), 6.24 (dt, 1H, J = 16.0, 6.8 Hz), 3.81–3.45 (m, 4H), 2.58–2.44 (m, 4H); ^{13}C{^{1}H} NMR ($CDCl_3$, 125 MHz): δ 170.5, 136.9, 135.9, 133.7, 129.8, 128.8, 128.6, 127.8,127.2, 126.5,125.9, 61.0, 53.5, 53.0, 47.8, 42.3; IR (KBr, cm^{-1}): 2932, 2812, 1621, 1275, 692; HRMS (ESI/Q-TOF) (m/z) calcd for $C_{19}H_{21}N_2O$, $[M + H]^+$: 293.1648, found 293.1653.

***Phenyl(pyrrolidin-1-yl)methanone (12a)*:**

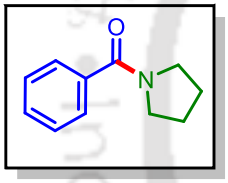

Yield: 73% (64 mg) as a colourless oil; Purification over a column of silica gel (25% EtOAc in hexane); ^{1}H NMR ($CDCl_3$, 500 MHz): δ 7.50–7.48 (m, 2H), 7.38–7.37 (m, 3H), 3.63 (t, 2H, J = 7.0 Hz), 3.40 (t, 2H, J = 6.7 Hz), 1.96–1.91 (m, 2H), 1.88–1.83 (m, 2H); ^{13}C{^{1}H} NMR ($CDCl_3$, 125 MHz): δ 169.9, 137.4, 129.9, 128.4, 127.2, 49.7, 46.3, 26.5, 24.6; IR (KBr, cm^{-1}): 2971, 2876, 1611, 1235, 699; HRMS (ESI/Q-TOF) (m/z) calcd for $C_{11}H_{14}NO$, $[M + H]^+$: 176.1070, found 176.1070.

***Phenyl(piperidin-1-yl)methanone (13a)*:**

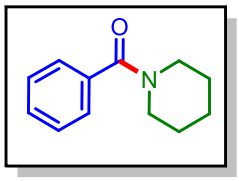

Yield: 75% (71 mg) as a pale yellow liquid; Purification over a column of silica gel (25% EtOAc in hexane); ^{1}H NMR ($CDCl_3$, 600 MHz): δ 7.37–7.36 (m, 5H), 3.69–3.31 (m, 4H), 1.65–1.48 (m, 6H); ^{13}C{^{1}H} NMR ($CDCl_3$, 150 MHz): δ 170.5, 136.6, 129.5, 128.6, 126.9, 48.9, 43.3, 26.7, 25.8, 24.8; IR (KBr, cm^{-1}): 2935, 2854, 1622, 1274, 706; HRMS (ESI/Q-TOF) (m/z) calcd for $C_{12}H_{16}NO$, $[M + H]^+$: 190.1226, found 190.1228.

***Azepan-1-yl(phenyl)methanone (14a)*:**

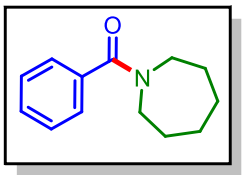

Yield: 70% (71 mg) as a colourless oil; Purification over a column of silica gel (25% EtOAc in hexane); ^{1}H NMR ($CDCl_3$, 600 MHz): δ 7.39–7.37 (m, 5H), 3.67 (t, 2H, J = 6.0 Hz), 3.36 (t, 2H, J = 5.7 Hz), 1.86–1.82 (m, 2H), 1.64–1.62 (m, 6H); ^{13}C{^{1}H} NMR ($CDCl_3$, 150 MHz): δ 171.8, 137.6, 129.2, 128.6, 126.6, 49.9, 46.5, 29.7, 28.1, 27.5, 26.7; IR (KBr, cm^{-1}): 2925, 2855, 1622, 1280, 703; HRMS (ESI/Q-TOF) (m/z) calcd for $C_{13}H_{18}NO$, $[M + H]^+$: 204.1383, found 204.1389.

***N, N-Diethylbenzamide (15a)*:**

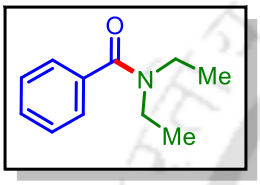

Yield: 63% (56 mg) as a colourless oil; Purification over a column of silica gel (25% EtOAc in hexane); ^{1}H NMR ($CDCl_3$, 600 MHz): δ 7.39-7.36 (m, 5H), 3.55–3.25 (m, 4H), 1.25–1.11 (m, 6H); ^{13}C{^{1}H} NMR ($CDCl_3$, 150 MHz): δ 171.5, 137.5, 129.3, 128.6, 126.5, 43.5, 39.4, 14.4, 13.1; IR (KBr, cm^{-1}): 2974, 2937, 1632, 1260, 749; HRMS (ESI/Q-TOF) (m/z) calcd for $C_{11}H_{16}NO$, $[M + H]^+$: 178.1226, found 178.1232.

***N-Cyclohexylbenzamide (16a)*:**

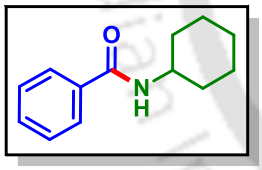

Yield: 85% (86 mg) as a white solid; Purification over a column of silica gel (25% EtOAc in hexane); ^{1}H NMR ($CDCl_3$, 600 MHz): δ 7.74 (d, 2H, J = 7.8 Hz), 7.47 (t, 1H, J = 7.2 Hz), 7.42 (t, 2H, J = 7.5 Hz), 5.98 (s, 1H), 4.00–3.96 (m, 1H), 2.04–2.01 (m, 2H), 1.77–1.73 (m, 2H), 1.66–1.63 (m, 1H), 1.45–1.39 (m, 2H), 1.27–1.19 (m, 3H); ^{13}C{^{1}H} NMR ($CDCl_3$, 150 MHz): δ 166.9, 135.3, 131.4, 128.7, 127.0, 48.9, 33.4, 25.8, 25.1; IR (KBr, cm^{-1}): 2928, 2852, 1625, 1260, 750; HRMS (ESI/Q-TOF) (m/z) calcd for $C_{13}H_{18}NO$, $[M + H]^+$: 204.1383, found 204.1381.

***N-(1-Phenylethyl)benzamide (17a)*:**

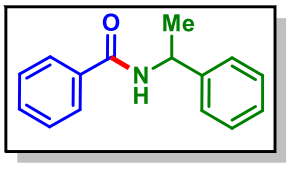

Yield: 71% (80 mg) as a white solid; Purification over a column of silica gel (25% EtOAc in hexane); ^{1}H NMR (DMSO-d_6, 600 MHz): δ 8.82 (d, 1H, J = 8.4 Hz), 7.91–7.90 (m, 2H), 7.53 (t, 1H, J = 7.5 Hz), 7.47 (t, 2H, J = 7.5 Hz), 7.41 (d, 2H, J = 6.6 Hz), 7.33 (t, 2H, J

= 7.8 Hz), 7.22 (t, 1H, *J* = 7.2 Hz), 5.19 (p, 1H, *J* = 7.2 Hz), 1.49 (d, 3H, *J* = 7.2 Hz); $^{13}C\{^{1}H\}$ NMR (DMSO-d_6, 150 MHz): δ 165.5, 144.9, 134.5, 131.1, 128.2, 128.1, 127.4, 126.6, 126.0, 48.4, 22.2; IR (KBr, cm^{-1}): 3012, 2914, 1632, 1189, 763; HRMS (ESI/Q-TOF) (m/z) calcd for $C_{15}H_{16}NO$, $[M + H]^+$: 226.1226, found 226.1225.

***N-(3-(Trifluoromethyl)benzyl)benzamide (18a)*:**

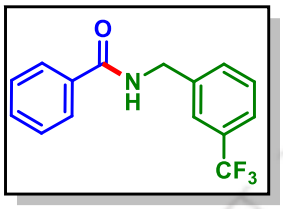

Yield: 72% (100 mg) as a white solid; Purification over a column of silica gel (25% EtOAc in hexane); ^{1}H NMR (DMSO-d_6, 600 MHz): δ 9.16 (t, 1H, *J* = 5.7 Hz), 7.91 (d, 2H, *J* = 7.8 Hz), 7.68 (s, 1H), 7.64 (d, 1H, *J* = 7.2 Hz), 7.61 (d, 1H, *J* = 7.8 Hz), 7.58 (d, 1H, *J* = 7.8 Hz), 7.57–7.53 (m, 1H), 7.49 (t, 2H, *J* = 7.5 Hz), 4.58 (d, 2H, *J* = 6.0 Hz); $^{13}C\{^{1}H\}$ NMR (DMSO-d_6, 150 MHz): δ 166.4, 141.2, 134.1, 131.4, 131.3, 129.3, 129.0 (d, *J* = 31.2 Hz), 128.4, 127.2, 125.2, 123.7 (q, *J* = 3.85 Hz), 123.5 (q, *J* = 3.8 Hz), 123.4, 42.3; ^{19}F NMR (DMSO-d_6, 565 MHz): δ –61.04 (s); IR (KBr, cm^{-1}): 2985, 2862, 1652, 1208, 723; HRMS (ESI/Q-TOF) (m/z) calcd for $C_{15}H_{13}F_3NO$, $[M + H]^+$: 280.0944, found 280.0948.

***N-(Furan-2-ylmethyl)benzamide (19a)*:**

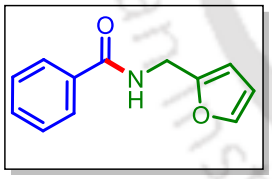

Yield: 60% (60 mg) as a white solid; Purification over a column of silica gel (25% EtOAc in hexane); ^{1}H NMR ($CDCl_3$, 600 MHz): δ 7.78 (d, 2H, *J* = 7.2 Hz), 7.50 (t, 1H, *J* = 7.2 Hz), 7.43 (t, 2H, *J* = 7.5 Hz), 7.38 (s, 1H), 6.44 (s, 1H), 6.35–6.30 (m, 2H), 4.64 (d, 2H, *J* = 5.4 Hz); $^{13}C\{^{1}H\}$ NMR ($CDCl_3$, 150 MHz): δ 167.4, 151.3, 142.5, 134.4, 131.8, 128.8, 127.2, 110.7, 107.9, 37.2; IR (KBr, cm^{-1}): 3062, 2925, 1635, 1110, 747; HRMS (ESI/Q-TOF) (m/z) calcd for $C_{12}H_{12}NO_2$, $[M + H]^+$: 202.0863, found 202.0858.

***N-(2-Aminobenzyl)benzamide (20a)*:**

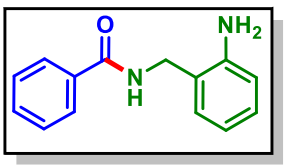

Yield: 65% (73 mg) as a gummy solid; Purification over a column of silica gel (30% EtOAc in hexane); ^{1}H NMR ($CDCl_3$, 600 MHz): δ 7.74 (d, 2H, *J* = 7.8 Hz), 7.46 (t, 1H, *J* = 7.5 Hz), 7.37 (t, 2H, *J* = 7.8 Hz), 7.12–7.09 (m, 2H), 6.76 (s, 1H), 6.70–6.65 (m, 2H), 4.54

(d, 2H, *J* = 6.0 Hz), 3.94 (s, 2H); $^{13}C\{^{1}H\}$ NMR ($CDCl_3$, 150 MHz): *δ* 168.1, 145.7, 134.1, 131.8, 130.8, 129.4, 128.7, 127.1, 121.9, 117.9, 115.9, 41.4; IR (KBr, cm^{-1}): 3062, 2926, 1626, 1290, 691; HRMS (ESI/Q-TOF) (m/z) calcd for $C_{14}H_{15}N_2O$, $[M + H]^+$: 227.1179, found 227.1182.

***N-(4-Methoxyphenethyl)benzamide (21a)*:**

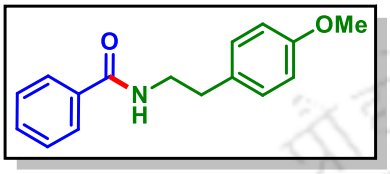

Yield: 72% (92 mg) as a white solid; Purification over a column of silica gel (25% EtOAc in hexane); ^{1}H NMR ($CDCl_3$, 600 MHz): *δ* 7.69 (d, 2H, *J* = 7.8 Hz), 7.46 (t, 1H, *J* = 7.5 Hz), 7.39 (t, 2H, *J* = 8.1 Hz), 7.14 (d, 2H, *J* = 7.2 Hz), 6.86 (d, 2H, *J* = 7.8 Hz), 6.27 (s, 3H), 3.79 (s, 3H), 3.66 (q, 2H, *J* = 6.8 Hz), 2.86 (t, 2H, *J* = 7.2 Hz); $^{13}C\{^{1}H\}$ NMR ($CDCl_3$, 150 MHz): *δ* 167.7, 158.5, 134.8, 131.6, 131.0, 129.9, 128.7, 126.9, 114.3, 55.4, 41.5, 34.9; IR (KBr, cm^{-1}): 2956, 2841, 1642, 1263, 683; HRMS (ESI/Q-TOF) (m/z) calcd for $C_{16}H_{18}NO_2$, $[M + H]^+$: 256.1332, found 256.1329.

***N-(4-Fluorophenethyl)benzamide (22a)*:**

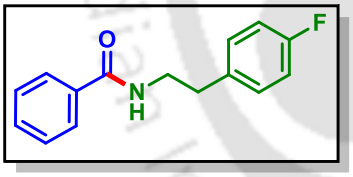

Yield: 69% (84 mg) as a white solid; Purification over a column of silica gel (25% EtOAc in hexane); ^{1}H NMR ($CDCl_3$, 600 MHz): *δ* 7.70 (d, 2H, *J* = 7.8 Hz), 7.46 (t, 1H, *J* = 7.5 Hz), 7.37 (t, 2H, *J* = 7.5 Hz), 7.14 (m, 2H, *J* = 6.6 Hz), 6.96 (t, 2H, *J* = 8.4 Hz), 6.55 (s, 1H), 3.63 (q, 2H, *J* = 6.6 Hz), 2.87 (t, 2H, *J* = 7.2 Hz); $^{13}C\{^{1}H\}$ NMR ($CDCl_3$, 150 MHz): *δ* 167.8, 161.7 (d, *J* = 241.3 Hz), 134.7 (d, *J* = 3.3 Hz), 131.6, 130.3 (d, *J* = 7.9 Hz), 128.7, 126.9, 115.5 (d, *J* = 20.8 Hz), 41.4, 34.9; ^{19}F NMR ($CDCl_3$, 565 MHz): *δ* –116.54 (s); IR (KBr, cm^{-1}): 3066, 2933, 1637, 1290, 705; HRMS (ESI/Q-TOF) (m/z) calcd for $C_{15}H_{15}FNO$, $[M + H]^+$: 244.1132, found 244.1138.

***N-(4-Hydroxyphenethyl)benzamide (23a)*:**

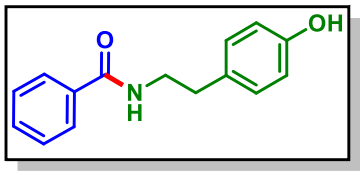

Yield: 51% (61 mg) as a brown liquid; Purification over a column of silica gel (35% EtOAc in hexane); ^{1}H NMR (DMSO-d_6, 500 MHz): δ 9.19 (s, 1H), 8.50 (t, 1H, J = 5.7 Hz), 7.81 (d, 2H, J = 7.5 Hz), 7.50 (t, 1H, J = 7.25 Hz), 7.44 (t, 2H, J = 7.25 Hz), 7.02 (d, 2H, J = 8.0 Hz), 6.68 (d, 2H, J = 8.0 Hz), 3.53 (q, 2H, J = 6.8 Hz), 2.72 (t, 2H, J = 7.5 Hz); ^{13}C{^{1}H} NMR (DMSO-d_6, 125 MHz): δ 166.2, 155.6, 134.7, 131.0, 129.6, 129.5, 128.3, 127.1, 115.1, 41.2, 34.3; IR (KBr, cm^{-1}): 3215, 2950, 2848, 1650, 643; HRMS (ESI/Q-TOF) (m/z) calcd for $C_{15}H_{16}NO_2$, $[M + H]^+$: 242.1176, found 242.1172.

***N-(2-(Thiophen-2-yl)ethyl)benzamide (24a)*:**

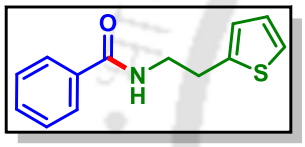

Yield: 65% (75 mg) as a colourless oil; Purification over a column of silica gel (25% EtOAc in hexane); ^{1}H NMR ($CDCl_3$, 600 MHz): δ 7.76–7.75 (m, 2H), 7.45 (t, 1H, J = 7.5 Hz), 7.36 (t, 2H, J = 7.5 Hz), 7.13-7.12 (m, 1H), 7.03 (s, 1H), 6.92–6.91 (m, 1H), 6.82 (d, 1H, J = 3.0 Hz), 3.67 (q, 2H, J = 6.6 Hz), 3.11 (t, 2H, J = 6.9 Hz); ^{13}C{^{1}H} NMR ($CDCl_3$, 150 MHz): δ 167.8, 141.3, 134.5, 131.4, 128.5, 127.1, 127.0, 125.3, 123.9, 41.5, 29.8; IR (KBr, cm^{-1}): 2929, 2854, 1639, 1275, 685; HRMS (ESI/Q-TOF) (m/z) calcd for $C_{13}H_{14}NOS$, $[M + H]^+$: 232.0791, found 232.0796.

***Phenyl(1H-pyrazol-1-yl)methanone (25a)*:**

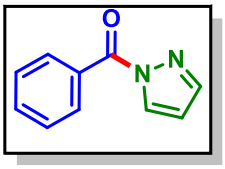

Yield: 73% (63 mg) as a colourless oil; Purification over a column of silica gel (25% EtOAc in hexane); ^{1}H NMR ($CDCl_3$, 600 MHz): δ 8.43 (d, 1H, J = 3.0 Hz), 8.11 (d, 2H, J = 7.2 Hz), 7.79 (s, 1H), 7.60 (t, 1H, J = 7.5 Hz), 7.49 (t, 2H, J = 7.5 Hz), 6.51–6.50 (m, 1H); ^{13}C{^{1}H} NMR ($CDCl_3$, 150 MHz): δ 166.5, 144.6, 133.1, 131.6, 130.5, 128.2, 109.5; IR (KBr, cm^{-1}): 3061, 2989, 1697, 1277, 709; HRMS (ESI/Q-TOF) (m/z) calcd for $C_{10}H_9N_2O$, $[M + H]^+$: 173.0709, found 173.0703.

***(S)-(2-Methoxypyrrolidin-1-yl)(phenyl)methanone (26a)*:**

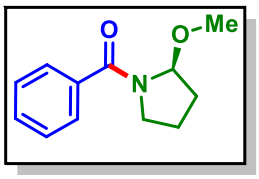

Yield: 70% (72 mg) as a colourless oil; Purification over a column of silica gel (25% EtOAc in hexane); ^{1}H NMR ($CDCl_3$, 600 MHz): δ 7.55 (d, 2H, J = 7.2 Hz), 7.41–7.37 (m, 3H), 4.67–4.64 (m, 1H), 3.76 (s, 3H), 3.65–3.61 (m, 1H), 3.54–3.49 (m, 1H), 2.32–2.29 (m, 1H), 2.02–1.98 (m, 2H), 1.89–1.85 (m, 1H); ^{13}C{^{1}H} NMR ($CDCl_3$, 150 MHz): δ 172.9, 136.2, 130.3, 128.4, 127.4, 59.3, 52.4, 50.1, 29.5, 25.5; IR (KBr, cm^{-1}): 2954, 2929, 1629, 1276, 749; HRMS (ESI/Q-TOF) (m/z) calcd for $C_{12}H_{16}NO_2$, $[M + H]^+$: 206.1176, found 206.1177.

***Methyl benzoyl-L-phenylalaninate (27a)*:**

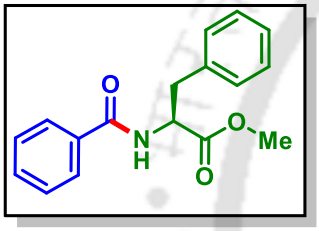

Yield: 75% (106 mg) as a brown liquid; Purification over a column of silica gel (25% EtOAc in hexane); ^{1}H NMR ($CDCl_3$, 600 MHz): δ 7.75 (d, 2H, J = 7.2 Hz), 7.52 (t, 1H, J = 7.5 Hz), 7.43 (t, 2H, J = 7.5 Hz), 7.31 (t, 2H, J = 7.5 Hz), 7.28 (d, 1H, J = 6.6 Hz), 7.16 (d, 2H, J = 7.8 Hz), 6.66 (d, 1H, J = 1.8 Hz), 5.12 (q, 1H, J = 6.4 Hz), 3.78 (s, 3H), 3.33– 3.23(m, 2H); ^{13}C{^{1}H} NMR ($CDCl_3$, 150 MHz): δ 172.2, 167.0, 136.0, 134.0, 131.9, 129.5, 128.8, 128.7, 127.4, 127.2, 53.7, 52.6, 38.1; IR (KBr, cm^{-1}): 3029, 2952, 2924, 1740, 1640, 1225, 699; HRMS (ESI/Q-TOF) (m/z) calcd for $C_{17}H_{18}NO_3$, $[M + H]^+$: 284.1281, found 284.1286.

***Morpholino(p-tolyl)methanone (1b)*:**

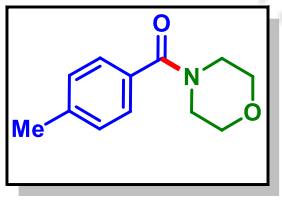

Yield: 71% (73 mg) as a colourless liquid; Purification over a column of silica gel (20% EtOAc in hexane); ^{1}H NMR ($CDCl_3$, 600 MHz): δ, 7.29 (d, 2H, J = 8.0 Hz), 7.19 (d, 2H, J = 7.9 Hz), 3.67–3.46 (m, 8H), 2.35 (s, 3H); ^{13}C{^{1}H} NMR ($CDCl_3$, 150 MHz): δ 170.7, 140.2, 132.4, 129.2, 127.3, 66.9, 48.4, 42.7, 21.5; IR (KBr, cm^{-1}): 2921, 2855, 1612, 1111, 751; HRMS (ESI/Q-TOF) (m/z) calcd for $C_{12}H_{16}NO_2$, $[M + H]^+$: 206.1176, found 206.1171.

(4-(Tert-butyl)phenyl)(morpholino)methanone (1c):

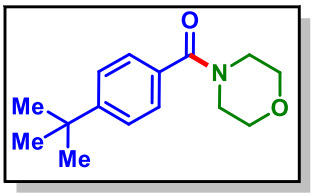

Yield: 75% (93 mg) as a colourless oil; Purification over a column of silica gel (20% EtOAc in hexane); ^{1}H NMR ($CDCl_3$, 500 MHz): δ 7.42 (d, 2H, J = 8.0 Hz), 7.34 (d, 2H, J = 8.5 Hz), 3.69–3.50 (m, 8H), 1.32 (s, 9H); ^{13}C{^{1}H} NMR ($CDCl_3$, 125 MHz): δ 170.5, 153.1, 132.3, 126.9, 125.4, 66.8, 48.2, 42.5, 34.7, 31.1; IR (KBr, cm^{-1}): 2961, 2861, 1630, 1112, 787; HRMS (ESI/Q-TOF) (m/z) calcd for $C_{15}H_{22}NO_2$, $[M + H]^+$: 248.1645, found 248.1651.

***(4-(Dimethylamino)phenyl)(morpholino)methanone (1d)*:**

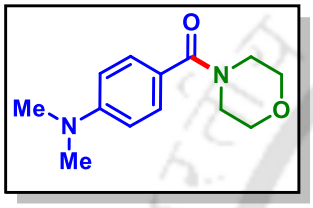

Yield: 79% (92 mg) as a colourless solid; Purification over a column of silica gel (20% EtOAc in hexane); ^{1}H NMR ($CDCl_3$, 600 MHz): δ 7.33 (d, 2H, J = 9.0 Hz), 6.64 (d, 2H, J = 9.0 Hz), 3.66–3.63 (m, 8H), 2.97 (s, 6H); ^{13}C{^{1}H} NMR ($CDCl_3$, 150 MHz): δ 171.3, 151.6, 129.4, 121.7, 111.2, 67.1, 40.3; IR (KBr, cm^{-1}): 2920, 2852, 1608, 1109, 760; HRMS (ESI/Q-TOF) (m/z) calcd for $C_{13}H_{19}N_2O_2$, $[M + H]^+$: 235.1441, found 235.1434.

(4-Methoxyphenyl)(morpholino)methanone (1e):

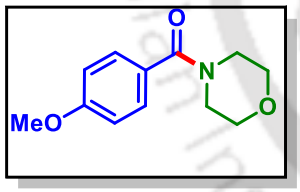

Yield: 72% (80 mg) as a colourless oil; Purification over a column of silica gel (20% EtOAc in hexane); ^{1}H NMR ($CDCl_3$, 500 MHz): δ 7.35 (d, 2H, J = 8.5 Hz), 6.89 (d, 2H, J = 8.5 Hz), 3.80 (s, 3H), 3.66–3.61 (m, 8H); ^{13}C{^{1}H} NMR ($CDCl_3$, 125 MHz): δ 170.5, 161.0, 129.3, 127.5, 113.9, 67.0, 55.5; IR (KBr, cm^{-1}): 2920, 2854, 1606, 1110, 762; HRMS (ESI/Q-TOF) (m/z) calcd for $C_{12}H_{16}NO_3$, $[M + H]^+$: 222.1125, found 222.1124.

Morpholino(4-nitrophenyl)methanone (1f):

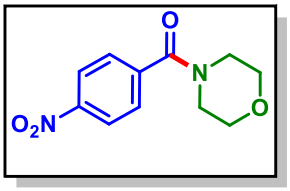

Yield: 68% (80 mg) as a white solid; Purification over a column of silica gel (20% EtOAc in hexane); ^{1}H NMR ($CDCl_3$, 600 MHz): δ 8.16 (d, 2H, J = 9.0 Hz), 7.50 (d, 2H, J = 9.0 Hz), 3.68 (s, 4H), 3.53–3.29 (m, 4H); ^{13}C{^{1}H} NMR ($CDCl_3$, 150 MHz): δ 167.9, 148.2, 141.3, 128.1, 123.8, 66.5, 47.8, 42.3; IR (KBr, cm^{-1}): 2974,

2867, 1621, 1106, 748; HRMS (ESI/Q-TOF) (m/z) calcd for $C_{11}H_{13}N_2O_4$, $[M + H]^+$: 237.0870, found 237.0875.

***(4-Chlorophenyl)(morpholino)methanone (1g)*:**

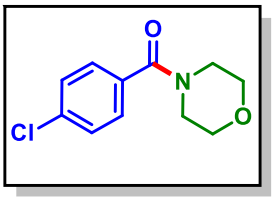

Yield: 66% (74 mg) as a white solid; Purification over a column of silica gel (20% EtOAc in hexane); ^{1}H NMR ($CDCl_3$, 500 MHz): δ 7.37 (d, 2H, J = 8.0 Hz), 7.33 (d, 2H, J = 8.5 Hz), 3.67–3.42 (m, 8H); $^{13}C\{^1H\}$ NMR ($CDCl_3$, 125 MHz): δ 169.5, 136.2, 133.8, 129.0, 128.8, 66.9, 48.3, 42.8; IR (KBr, cm^{-1}): 2921, 2852, 1629, 1111, 754; HRMS (ESI/Q-TOF) (m/z) calcd for $C_{11}H_{13}ClNO_2$, $[M + H]^+$: 226.0629, found 226.0632.

***(4-Bromophenyl)(morpholino)methanone (1h)*:**

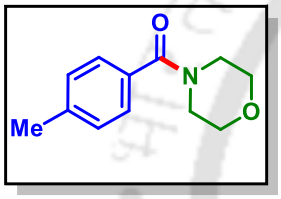

Yield: 62% (84 mg) as a brown liquid; Purification over a column of silica gel (20% EtOAc in hexane); ^{1}H NMR ($CDCl_3$, 500 MHz): δ 7.41 (d, 2H, J = 8.0 Hz), 7.14 (d, 2H, J = 8.5 Hz), 3.55–3.29 (m, 8H); $^{13}C\{^1H\}$ NMR ($CDCl_3$, 125 MHz): δ 169.6, 134.3, 131.9, 129.0, 124.4, 66.9, 48.5, 42.8; IR (KBr, cm^{-1}): 2900, 2855, 1626, 1256, 751; HRMS (ESI/Q-TOF) (m/z) calcd for $C_{11}H_{13}BrNO_2$, $[M + H]^+$: 270.0124, found 270.0131.

***Morpholino(4-(trifluoromethyl)phenyl)methanone (1i)*:**

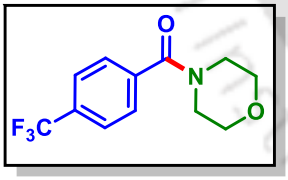

Yield: 58% (75 mg) as a colourless liquid; Purification over a column of silica gel (20% EtOAc in hexane); ^{1}H NMR ($CDCl_3$, 500 MHz): δ 7.64 (d, 2H, J = 8.0 Hz), 7.49 (d, 2H, J = 8.0 Hz), 3.73–3.36 (m, 8H); $^{13}C\{^1H\}$ NMR ($CDCl_3$, 125 MHz): δ 169.0, 138.9, 131.9 (q, J = 32.5 Hz), 130.3, 127.6, 125.7 (q, J =3.75 Hz), 124.8, 122.7, 66.8, 48.2, 42.7; ^{19}F NMR ($CDCl_3$, 471 MHz): δ –62.9 (s) IR (KBr, cm^{-1}): 2952, 2857, 1642, 1265, 755; HRMS (ESI/Q-TOF) (m/z) calcd for $C_{12}H_{13}F_3NO_2$, $[M + H]^+$: 260.0893, found 260.0894.

***[1,1'-Biphenyl]-4-yl(morpholino)methanone (1j)*:**

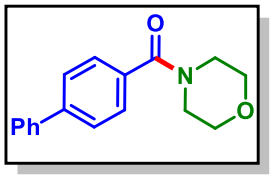

Yield: 69% (92 mg) as a white solid; Purification over a column of silica gel (20% EtOAc in hexane); ^{1}H NMR ($CDCl_3$, 600 MHz): δ 7.63 (d, 2H, J = 8.4 Hz), 7.59 (d, 2H, J = 7.2 Hz), 7.49 (d, 2H, J = 8.4

Hz), 7.45 (t, 2H, *J* = 7.5 Hz), 7.37 (t, 1H, *J* = 7.2 Hz), 3.80–3.51 (m, 8H); $^{13}C\{^{1}H\}$ NMR ($CDCl_3$, 150 MHz): δ 170.4, 142.9, 140.2, 134.0, 129.0, 128.0, 127.8, 127.4, 127.3, 67.0, 48.4, 42.7; IR (KBr, cm^{-1}): 2937, 2847, 1632, 1265, 745; HRMS (ESI/Q-TOF) (m/z) calcd for $C_{17}H_{18}NO_2$, $[M + H]^+$: 268.1332, found 268.1323.

Benzofuran-2-yl(morpholino)methanone (1k):

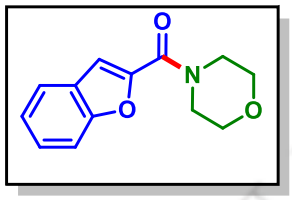

Yield: 68% (79 mg) as a white solid; Purification over a column of silica gel (20% EtOAc in hexane); ^{1}H NMR ($CDCl_3$, 600 MHz): δ 7.64 (d, 1H, *J* = 7.8 Hz), 7.51 (d, 1H, *J* = 7.8 Hz), 7.40–7.37 (m, 1H), 7.34 (s, 1H), 7.27 (t, 1H, *J* = 6.9 Hz) 3.88–3.76 (m, 8H); $^{13}C\{^{1}H\}$ NMR ($CDCl_3$, 150 MHz): δ 159.7, 154.6, 148.7, 126.8, 126.7, 123.7, 122.3, 112.6, 111.9, 66.9, 47.3, 43.2; IR (KBr, cm^{-1}): 2927, 2861, 1608, 1260, 749; HRMS (ESI/Q-TOF) (m/z) calcd for $C_{13}H_{14}NO_3$, $[M + H]^+$: 232.0968, found 232.0965.

(4-Aminophenyl)(morpholino)methanone (1l):

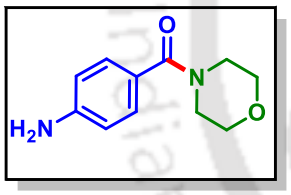

Yield: 65% (67 mg) as a brown liquid; Purification over a column of silica gel (30% EtOAc in hexane); ^{1}H NMR ($CDCl_3$, 500 MHz): δ 8.28 (d, 2H, *J* = 8.5 Hz), 7.57 (d, 2H, *J* = 9.0 Hz), 3.79–3.63 (m, 8H), 3.38 (s, 2H); $^{13}C\{^{1}H\}$ NMR ($CDCl_3$, 125 MHz): δ 168.3, 148.7, 141.6, 128.3, 124.2, 66.9, 48.2, 42.8; IR (KBr, cm^{-1}): 2989, 2860, 1636, 1264, 731; HRMS (ESI/Q-TOF) (m/z) calcd for $C_{11}H_{15}N_2O_2$, $[M + H]^+$: 207.1128, found 207.1132.

***Cyclohexyl(morpholino)methanone (1m)*:**

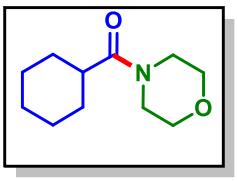

Yield: 58% (57 mg) as a white solid; Purification over a column of silica gel (20% EtOAc in hexane); ^{1}H NMR ($CDCl_3$, 500 MHz): δ 3.62–3.46 (m, 8H), 2.42–2.36 (m, 1H), 1.77–1.64 (m, 5H), 1.53–1.45 (m, 2H), 1.24–1.20 (m, 3H); $^{13}C\{^{1}H\}$ NMR ($CDCl_3$, 125 MHz): δ 174.9, 67.1, 67.0, 46.0, 42.1, 40.4, 29.4, 25.9; IR (KBr, cm^{-1}): 2852, 1624, 1425, 1250, 743; HRMS (ESI/Q-TOF) (m/z) calcd for $C_{11}H_{20}NO_2$, $[M + H]^+$: 198.1489, found 198.1495.

Furan-2-yl(morpholino)methanone (1n):

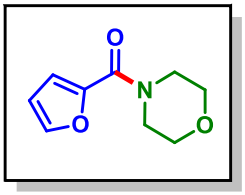

Yield: 62% (56 mg) as a brown liquid; Purification over a column of silica gel (20% EtOAc in hexane); ^{1}H NMR ($CDCl_3$, 600 MHz): δ 7.47 (s, 1H), 7.02 (d, 1H, J = 3.0 Hz), 6.48 (s, 1H), 3.81–3.74 (m, 8H); $^{13}C\{^{1}H\}$ NMR ($CDCl_3$, 150 MHz): δ 159.3, 147.9, 143.9, 117.0, 111.6, 67.1; IR (KBr, cm^{-1}): 2924, 2858, 1615, 1276, 750; HRMS (ESI/Q-TOF) (m/z) calcd for $C_9H_{12}NO_3$, $[M + H]^+$: 182.0812, found 182.0808.

***Morpholino(thiophen-2-yl)methanone (1o)*:**

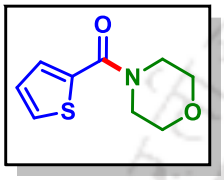

Yield: 60% (59 mg) as a white solid; Purification over a column of silica gel (20% EtOAc in hexane); ^{1}H NMR ($CDCl_3$, 600 MHz): δ 7.45 (d, 1H, J = 4.8 Hz), 7.28 (d, 1H, J = 3.6 Hz), 7.04 (t, 1H, J = 4.5 Hz), 3.77–3.71 (m, 8H); $^{13}C\{^{1}H\}$ NMR ($CDCl_3$, 150 MHz): δ 163.9, 136.8, 129.2, 129.0, 126.9, 67.1; IR (KBr, cm^{-1}): 2912, 2851, 1630, 1279, 759; HRMS (ESI/Q-TOF) (m/z) calcd for $C_9H_{12}NO_2S$, $[M + H]^+$: 198.0583, found 198.0581.

Methyl morpholine-4-carboxylate (1p):

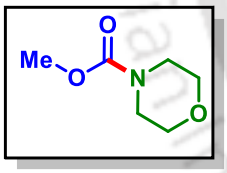

Yield: 72% (52 mg) as a gummy; Purification over a column of silica gel (15% EtOAc in hexane); ^{1}H NMR ($CDCl_3$, 600 MHz): δ 3.69 (s, 3H), 3.64–3.45 (m, 8H); $^{13}C\{^{1}H\}$ NMR ($CDCl_3$, 150 MHz): δ 156.1, 66.8, 66.6, 52.9, 44.4, 43.9; IR (KBr, cm^{-1}): 2923, 2854, 1628, 1262, 752; HRMS (ESI/Q-TOF) (m/z) calcd for $C_6H_{12}NO_3$, $[M + H]^+$: 146.0812, found 146.0815.

Ethyl morpholine-4-carboxylate (1q):

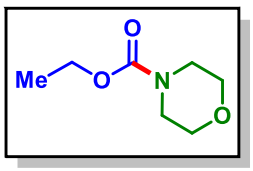

Yield: 73% (58 mg) as a colourless oil; Purification over a column of silica gel (15% EtOAc in hexane); ^{1}H NMR ($CDCl_3$, 600 MHz): δ 4.12 (q, 2H, J = 7.0 Hz), 3.62 (s, 4H), 3.43 (t, 4H, J = 5.1 Hz), 1.23 (t, 3H, J = 6.9 Hz); $^{13}C\{^{1}H\}$ NMR ($CDCl_3$, 150 MHz): δ 155.7, 66.7, 61.6, 44.1, 14.7; IR (KBr, cm^{-1}): 2970, 2858, 1694, 1240, 767; HRMS (ESI/Q-TOF) (m/z) calcd for $C_7H_{14}NO_3$, $[M + H]^+$: 160.0968, found 160.0972.

***Benzyl morpholine-4-carboxylate (1r)*:**

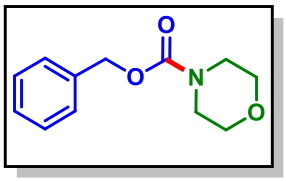

Yield: 70% (77 mg) as a colourless oil; Purification over a column of silica gel (15% EtOAc in hexane); ^{1}H NMR ($CDCl_3$, 500 MHz): δ 7.30–7.27 (m, 5H), 5.1 (s, 2H), 3.59 (s, 4H) 3.45–3.43 (m, 4H); $^{13}C\{^{1}H\}$ NMR ($CDCl_3$, 125 MHz): δ 155.4, 136.7, 129.3, 128.6, 128.4, 128.2, 128.1, 67.4, 66.7, 63.5, 53.7, 44.3; IR (KBr, cm^{-1}): 2898, 2857, 1697, 1114, 697; HRMS (ESI/Q-TOF) (m/z) calcd for $C_{12}H_{16}NO_3$, $[M + H]^+$: 222.1125, found 222.1121.

***2,2,6,6-Tetramethylpiperidin-1-yl benzoate (1s)*:**

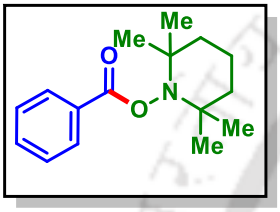

Yield: 33% (43 mg) as a white solid; Purification over a column of silica gel (10% EtOAc in hexane); ^{1}H NMR ($CDCl_3$, 600 MHz): δ 8.27 (d, 2H, J = 7.2 Hz), 7.75 (s, 1H), 7.64 (s, 2H), 1.97 (t, 2H, J = 12.3 Hz), 1.91–1.85 (m, 1H), 1.77 (d, 2H, J = 12.6 Hz), 1.64 (d, 1H, J = 12.0 Hz), 1.46 (s, 6H), 1.31 (s, 6H); $^{13}C\{^{1}H\}$ NMR ($CDCl_3$, 150 MHz): δ 162.7, 129.4, 126.1, 125.9, 124.9, 56.8, 35.5, 28.4, 17.3, 13.5; IR (KBr, cm^{-1}): 2927, 2856, 1750, 1254, 707; HRMS (ESI/Q-TOF) (m/z): calcd for $C_{16}H_{24}NO_2$, $[M + H]^+$: 262.1802, found 262.1798.

***4-Chloro-N-(4-hydroxyphenethyl)benzamide (23g)*:**

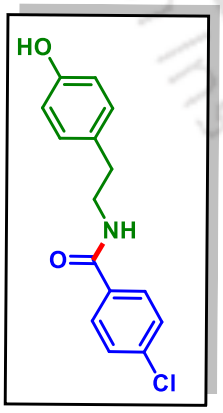

Yield: 60% (83 mg) as a brown solid; Purification over a column of silica gel (2% of MeOH in CH_2Cl_2); ^{1}H NMR (DMSO-d_6, 500 MHz): δ 9.16 (s, 1H), 8.58 (t, 1H, J = 5.2 Hz), 7.83 (d, 2H, J = 8.5 Hz), 7.52 (d, 2H, J = 8.5 Hz), 7.01 (d, 2H, J = 8.5 Hz), 6.67 (d, 2H, J = 8.5 Hz), 3.40–3.35 (m, 2H), 2.71 (t, 2H, J = 7.5 Hz); $^{13}C\{^{1}H\}$ NMR (DMSO-d_6, 125 MHz): δ 165.0, 155.6, 135.8, 133.4, 129.5, 129.0, 128.3, 115.1, 41.2, 34.2; IR (KBr, cm^{-1}): 3009, 2857, 1640, 1275, 750; HRMS (ESI/Q-TOF) (m/z) calcd for $C_{15}H_{15}ClNO_2$, $[M + H]^+$: 276.0786, found 276.0789.

***Isopropyl 2-(4-(2-(4-chlorobenzamido)ethyl)phenoxy)-2-methylpropanoate (23g')*:**

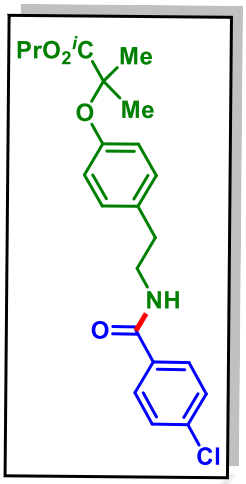

Yield: 60% (72 mg) as a colourless oil; Purification over a column of silica gel (20% EtOAc in hexane); ^{1}H NMR ($CDCl_3$, 600 MHz): δ 7.60 (d, 2H, J = 8.4 Hz), 7.30 (d, 2H, J = 8.4 Hz), 7.02 (d, 2H, J = 8.4 Hz), 6.75 (d, 2H, J = 8.4 Hz), 6.59 (s, 1H), 5.07–5.01 (m, 1H), 3.56 (q, 2H, J = 6.6 Hz), 2.79 (t, 2H, J = 6.9 Hz), 1.54 (s, 6H), 1.18 (d, 6H, J = 6.6 Hz); ^{13}C{^{1}H} NMR ($CDCl_3$, 150 MHz): δ 173.9, 166.6, 154.1, 137.6, 133.0, 132.3, 129.4, 128.8, 128.4, 119.3, 79.1, 69.1, 41.4, 34.8, 25.4, 21.6; IR (KBr, cm^{-1}): 3012, 2924, 2854, 1652, 1023, 759; HRMS (ESI/Q-TOF) (m/z) calcd for $C_{22}H_{27}ClNO_4$, [M + H]$^{+}$: 404.1623, found 404.1631.

***2-(4-(2-(4-Chlorobenzamido)ethyl)phenoxy)-2-methylpropanoic acid (Bezafibrate) (23g")*:**

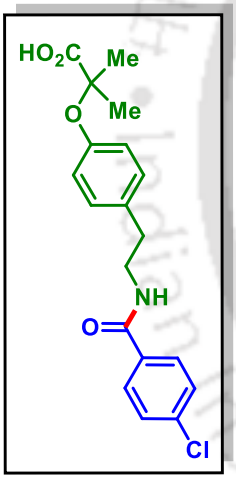

Yield: 81% (50 mg) as a white solid; ^{1}H NMR (DMSO-d_6, 600 MHz): δ 8.63 (t, 1H, J = 5.4 Hz), 7.82 (d, 2H, J = 8.4 Hz), 7.52 (d, 2H, J = 8.4 Hz), 7.12 (d, 2H, J = 8.4 Hz), 6.75 (d, 2H, J = 8.4 Hz), 3.42 (t, 2H, J = 6.6 Hz), 2.76 (t, 2H, J = 7.5 Hz), 1.47 (s, 6H); ^{13}C{^{1}H} NMR (DMSO-d_6, 150 MHz): δ 175.1, 165.1, 153.7, 135.9, 133.3, 132.6, 129.4, 129.1, 128.4, 118.5, 78.3, 41.0, 34.2, 25.1; IR (KBr, cm^{-1}): 3295, 3015, 2914, 2874, 1725, 1642, 1014, 711; HRMS (ESI/Q-TOF) (m/z) calcd for $C_{19}H_{21}ClNO_4$, [M + H]$^{+}$: 362.1154, found 362.1151.

IV.10. Representative Spectra

Morpholino(phenyl)methanone (1a) : ^{1}H NMR ($CDCl_3$, 600 MHz)

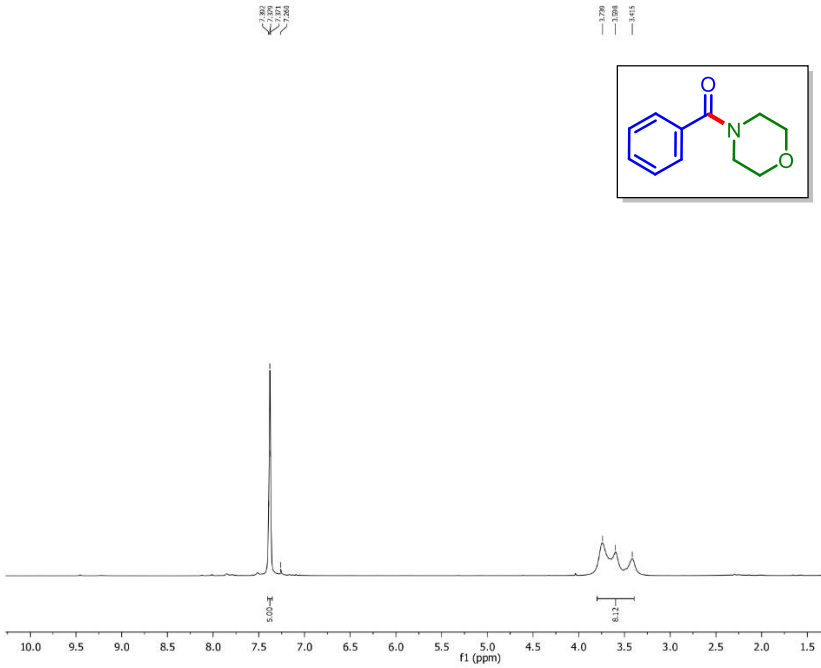

Morpholino(phenyl)methanone (1a): $^{13}C\{^{1}H\}$ NMR ($CDCl_3$, 150 MHz)

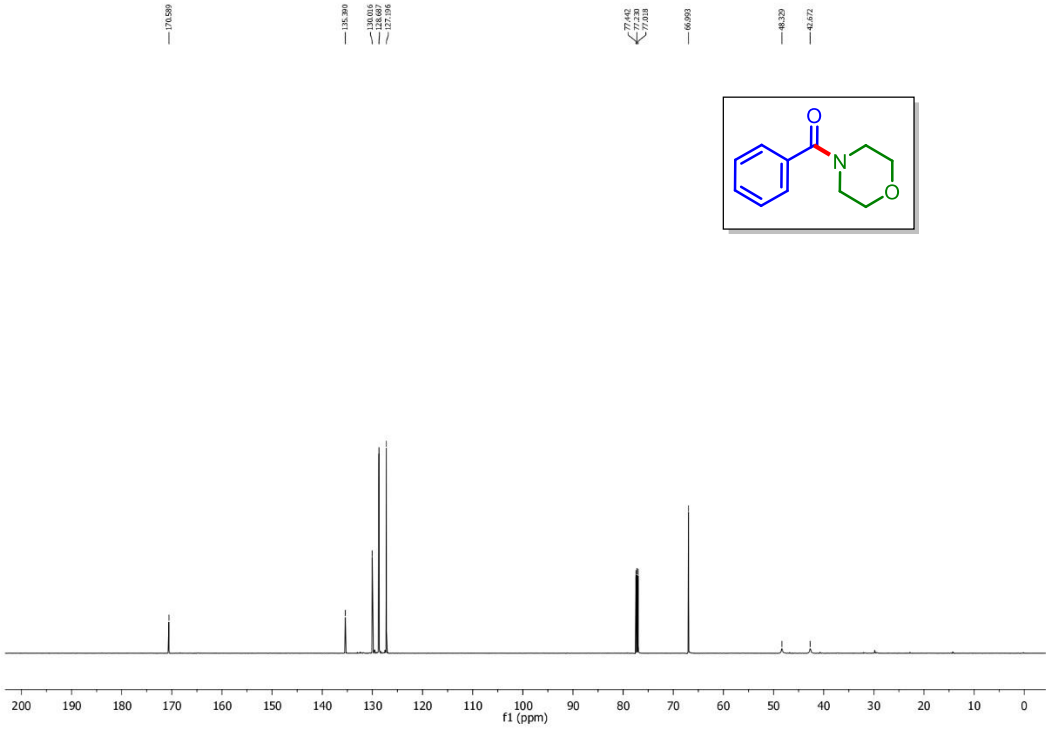

N-(Furan-2-ylmethyl)benzamide (19a): ^{1}H NMR ($CDCl_3$, 600 MHz)

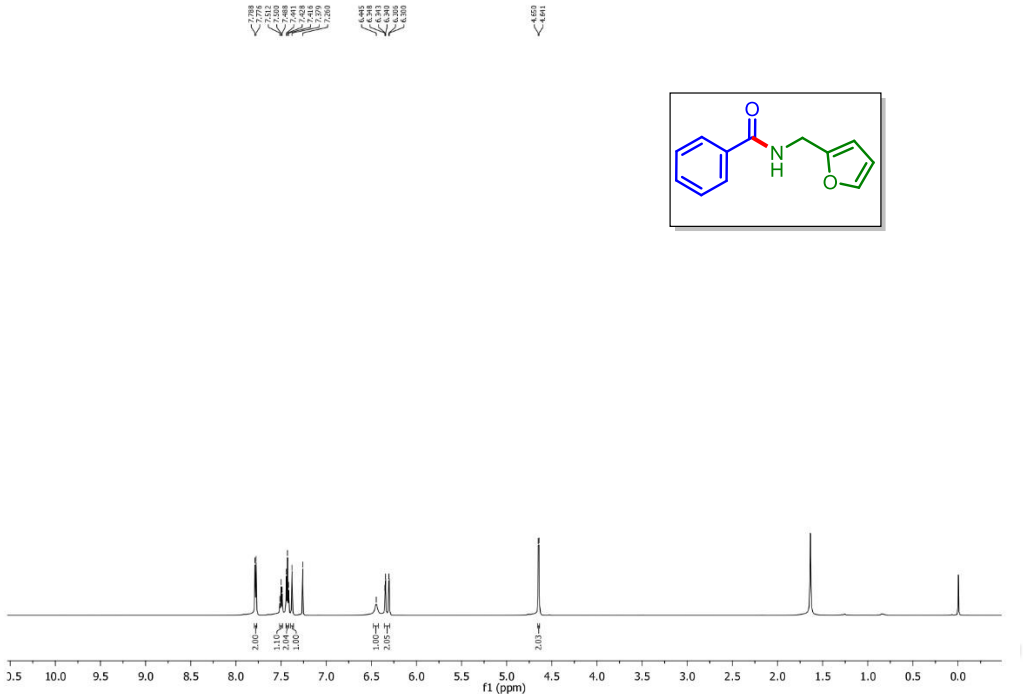

N-(Furan-2-ylmethyl)benzamide (19a): $^{13}C\{^{1}H\}$ NMR ($CDCl_3$, 150 MHz)

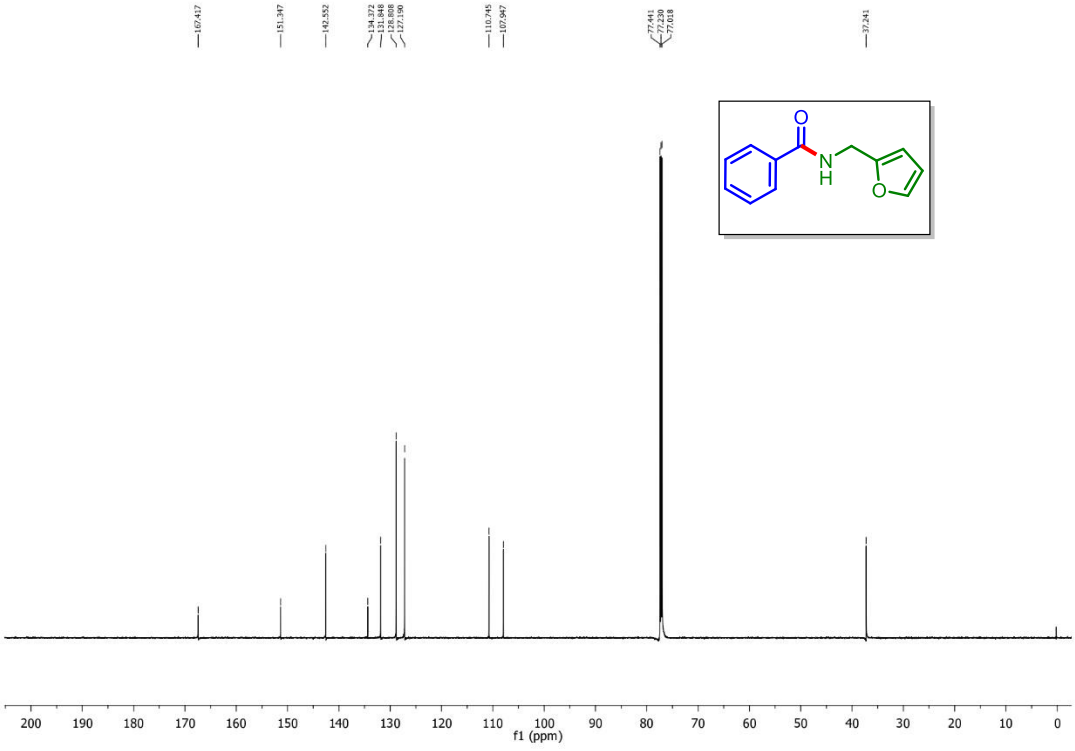

Phenyl(1H-pyrazol-1-yl)methanone (25a): ^{1}H NMR (CDCl$_3$, 600 MHz)

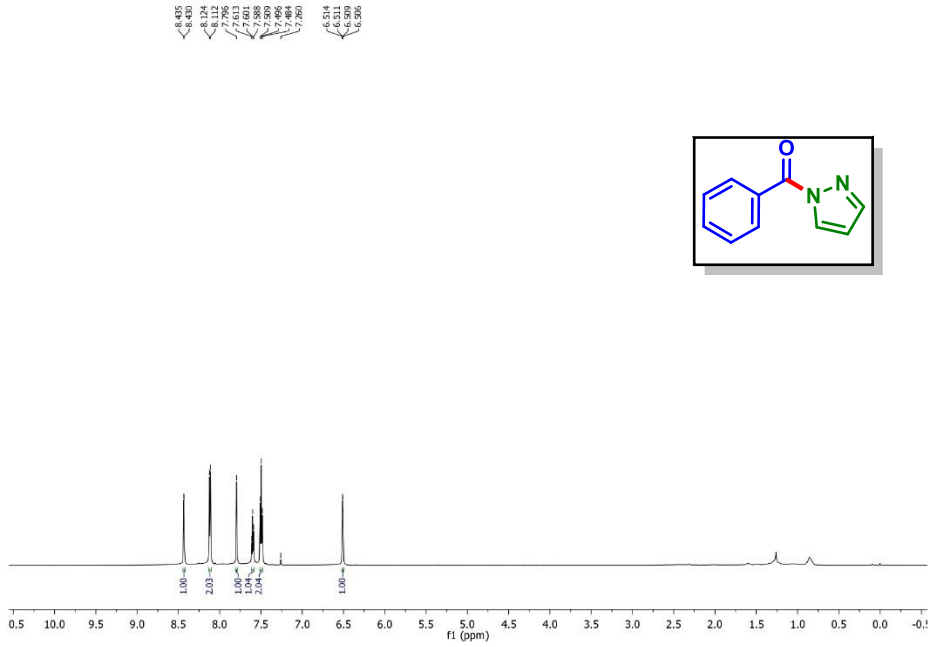

Phenyl(1H-pyrazol-1-yl)methanone (25a): ^{13}C{^{1}H} NMR (CDCl$_3$, 150 MHz)

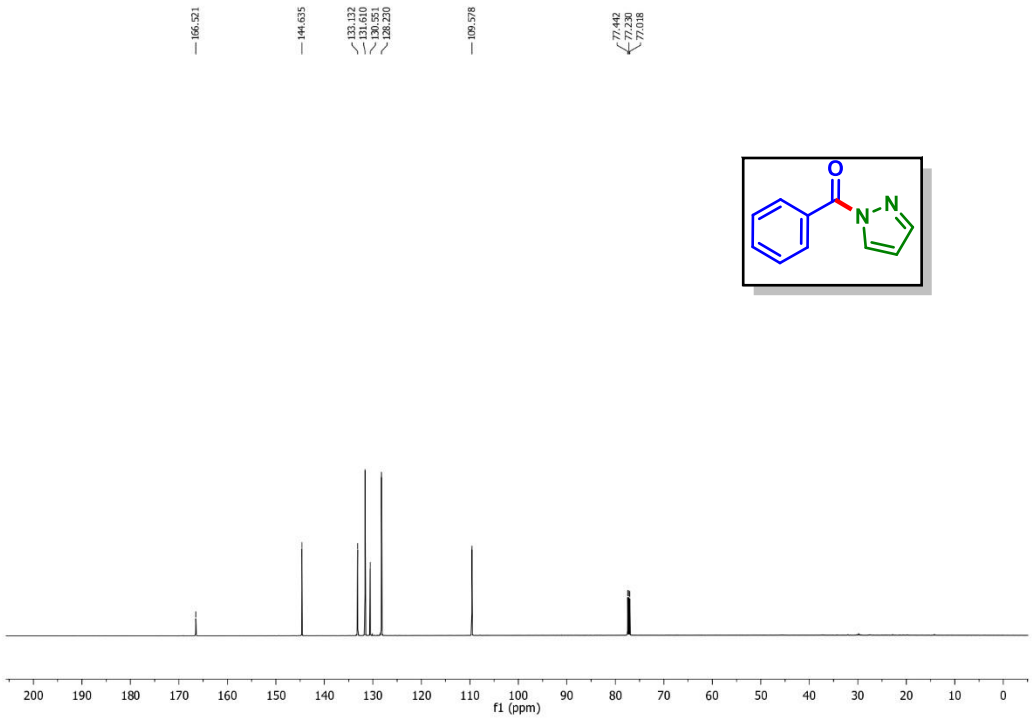

(4-Methoxyphenyl)(morpholino)methanone (1e): ^{1}H NMR (CDCl$_3$, 500 MHz)

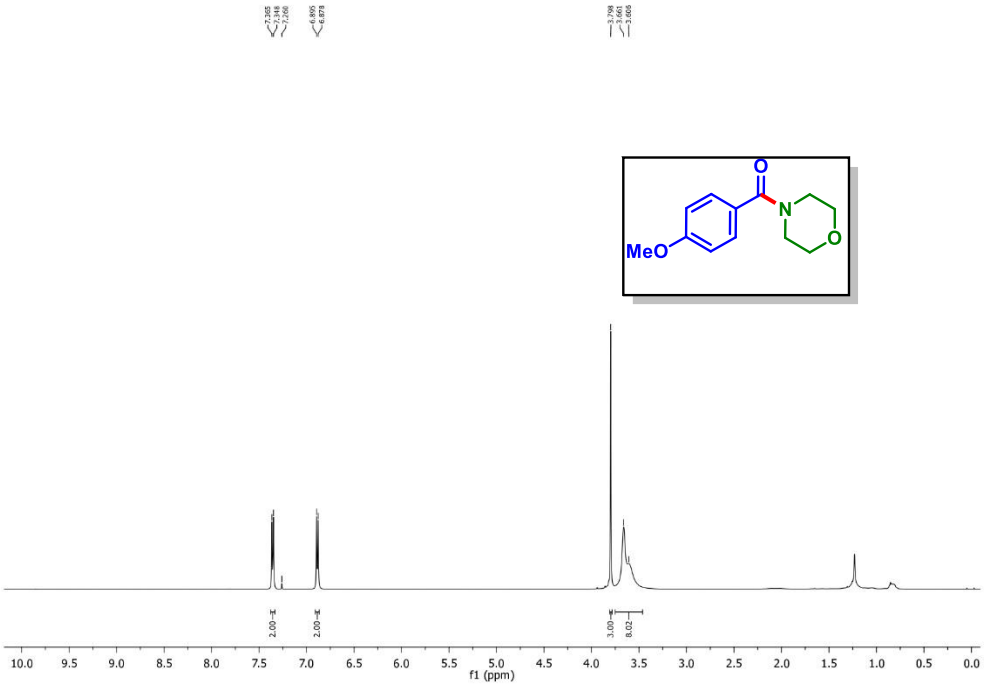

(4-Methoxyphenyl)(morpholino)methanone (1e): ^{13}C{^{1}H} NMR (CDCl$_3$, 125 MHz)

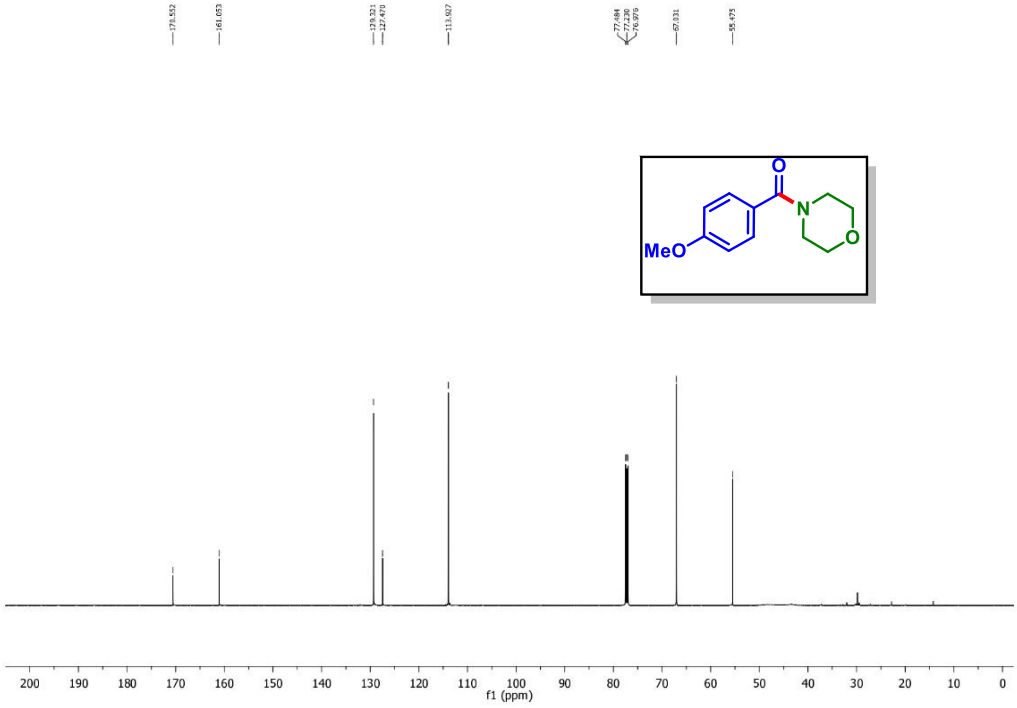

Benzofuran-2-yl(morpholino)methanone (1k): ^{1}H NMR ($CDCl_3$, 600 MHz)

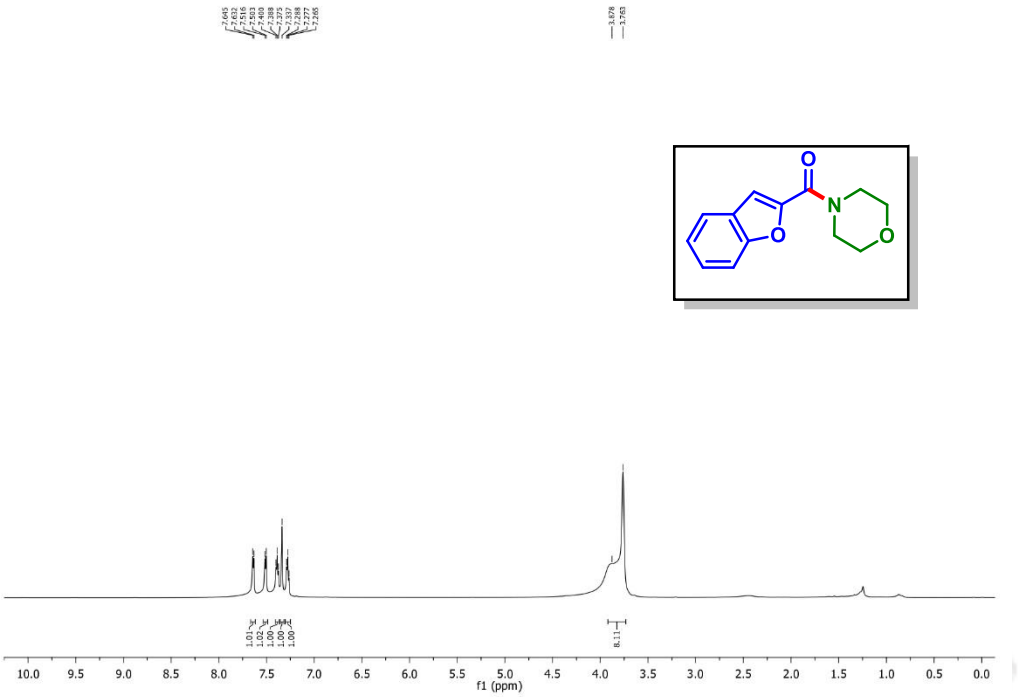

Benzofuran-2-yl(morpholino)methanone (1k): $^{13}C\{^{1}H\}$ NMR ($CDCl_3$, 150 MHz)

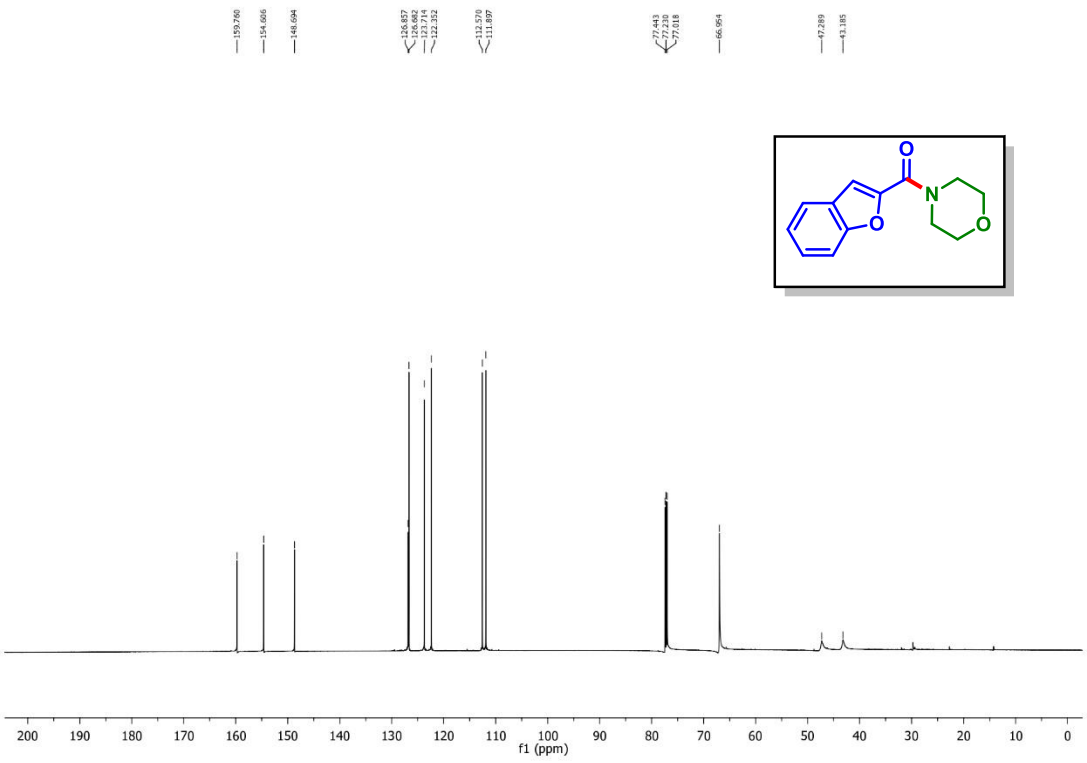

CHAPTER-V

Electrochemical *N*-Aroylation of Sulfoximines using Benzoyl Hydrazines with H_2 Generation

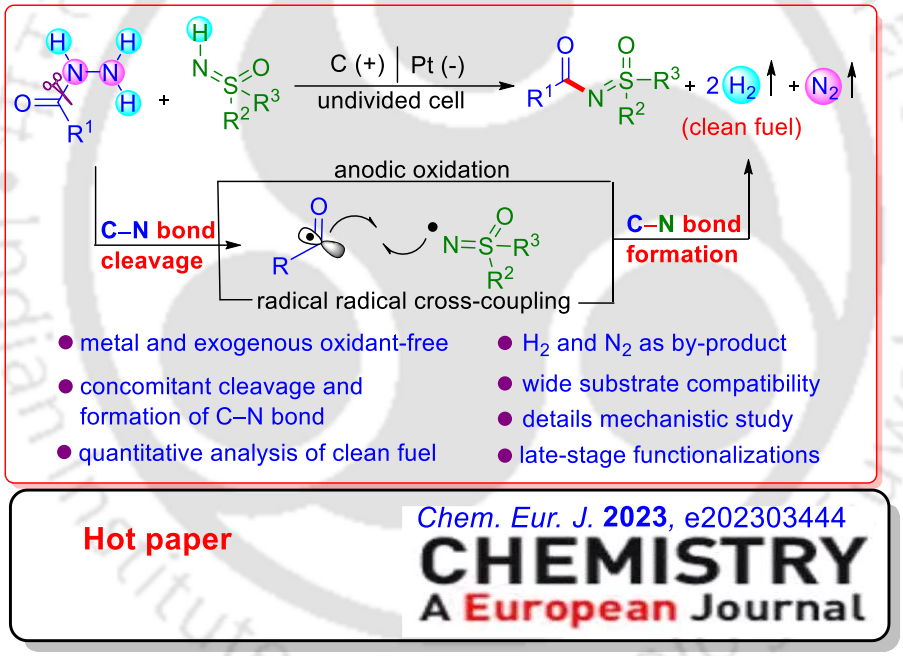

Abstract: ***Developed here is a robust electrochemical cross-coupling between aroyl hydrazine and NH-sulfoximine via concomitant cleavage and formation of C(sp^2)–N bond with the evolution of H_2 and N_2 as innocuous by-products. This sustainable protocol avoids the use of toxic reagents and occurs at room temperature. The reaction proceeds via the generation of an aroyl and a sulfoximidoyl radical via anodic oxidation under constant current electrolysis (CCE), affording N-aroylated sulfoximine. The strategy is applied to late-stage sulfoximidation of L-menthol, (–)-borneol, D-glucose, vitamin-E derivatives, and marketed drugs such as probenecid, ibuprofen, flurbiprofen, ciprofibrate, and sulindac. In addition, the present methodology is mild, high functional group tolerance with broad substrate scope and scalable.***

CHAPTER V

Electrochemical *N*-Aroylation of Sulfoximines using Benzoyl Hydrazines with H_2 Generation

V.1. Introduction

The potential applications of organosulfur compounds, *viz.* sulfoximines in pharmaceuticals[1a] and pesticides[1d] have been well recognized. Sulfoximine-containing compounds such as atuveciclib, BAY1251152, and AZD6738 have progressed into clinical trials.[1c] Sulfoxaflor, a sulfoximine-containing compound, was developed by Dow AgroSciences as a potential insecticide and introduced into the market (Figure V.1).[1] Thus, a significant effort has been devoted to establishing efficient strategies for the synthesis of *N*-acylated sulfoximines. In this context, carboxyl activating agents such as 1-ethyl-3-(3-dimethylaminopropyl)carbodiimide (EDC) or *N*,*N*′-dicyclohexylcarbodiimide (DCC) have been employed for the coupling of carboxylic acid and *NH*-sulfoxamine leading to *N*-acylated sulfoximine.[2] Similar sulfoximidation has been developed, employing other activating agents such as boric acid or 1,3-dioxa-5-aza-2,4,6-triborinane (DATB).[3] The transition-metal-catalyzed synthesis of *N*-aroyl sulfoximine has been achieved using aryl halide and carbon monoxide [Scheme V.1 (a)].[4] Considering their importance, the development of sustainable synthetic methods having (i) broad functional group tolerance and reaction scope, (ii) amenable to late-stage diversification of biologically relevant molecules, and (iii) providing clean energy source (H_2) as a by-product is highly desirable.

Due to the importance of acylated derivatives in synthetic chemistry and biochemical processes, the readily available benzoyl hydrazine is an ideal precursor for benzoyl radical, which produces N_2 and H_2 as by-products under certain conditions.[5-6] However, the existing methods for their generation rely on stoichiometric use of chemical oxidants under transition-metal catalysis, producing chemical waste making them environmentally unacceptable [Scheme V.1 (b)].[7] In this context, developing a milder and more sustainable method for generating benzoyl radicals from benzoyl hydrazine is highly desirable.

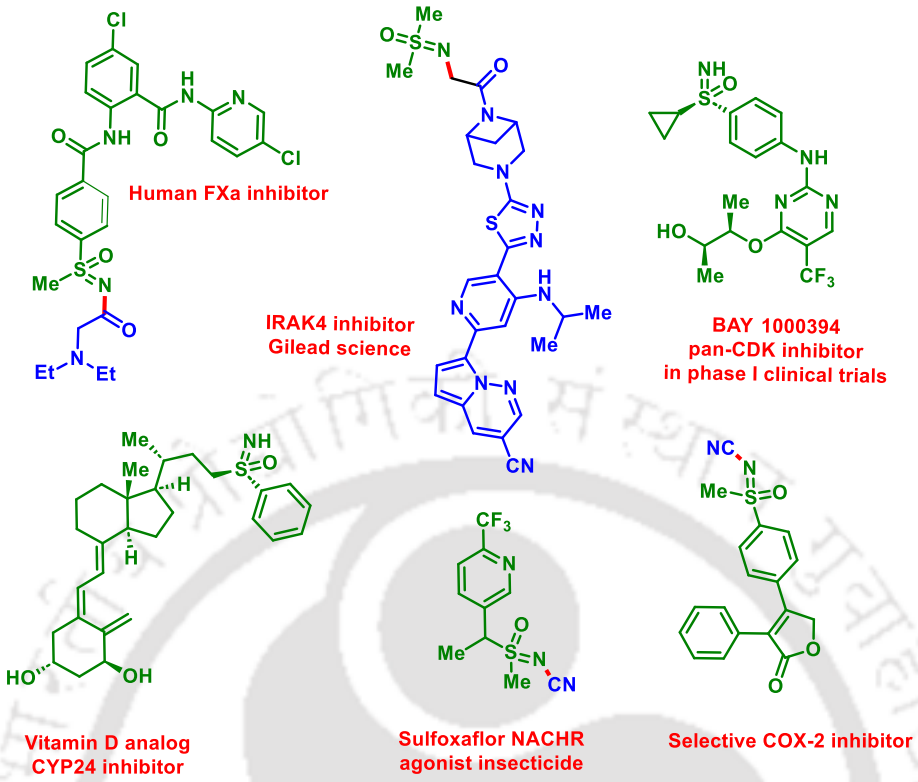

Figure V.1. *Representative bioactive sulfoximines.*

Recently, the scientific community has witnessed an upsurge in interest in organic electrosynthesis as it avoids using chemical oxidants and utilizes electrons as a reagent.[8] The application of either electric potential or current facilitates redox events leading to reactions occurring under mild conditions with improved atom economy.[9-14] The electrochemical process is more appealing, employing two different nucleophiles in an oxidative cross-coupling.[15] However, the current oxidative strategies predominantly focus on the oxidative cross-couplings of C–H and X–H (where X represents a heteroatom) bonds.[16] Despite the significant advancements in oxidative cross-coupling, the simultaneous cleavage of the C–N bond through anodic oxidation and the formation of a new C–N bond from two distinct nucleophiles under mild conditions remain attractive yet challenging.

Scheme V.1. Strategies for N-aroylation of sulfoximines

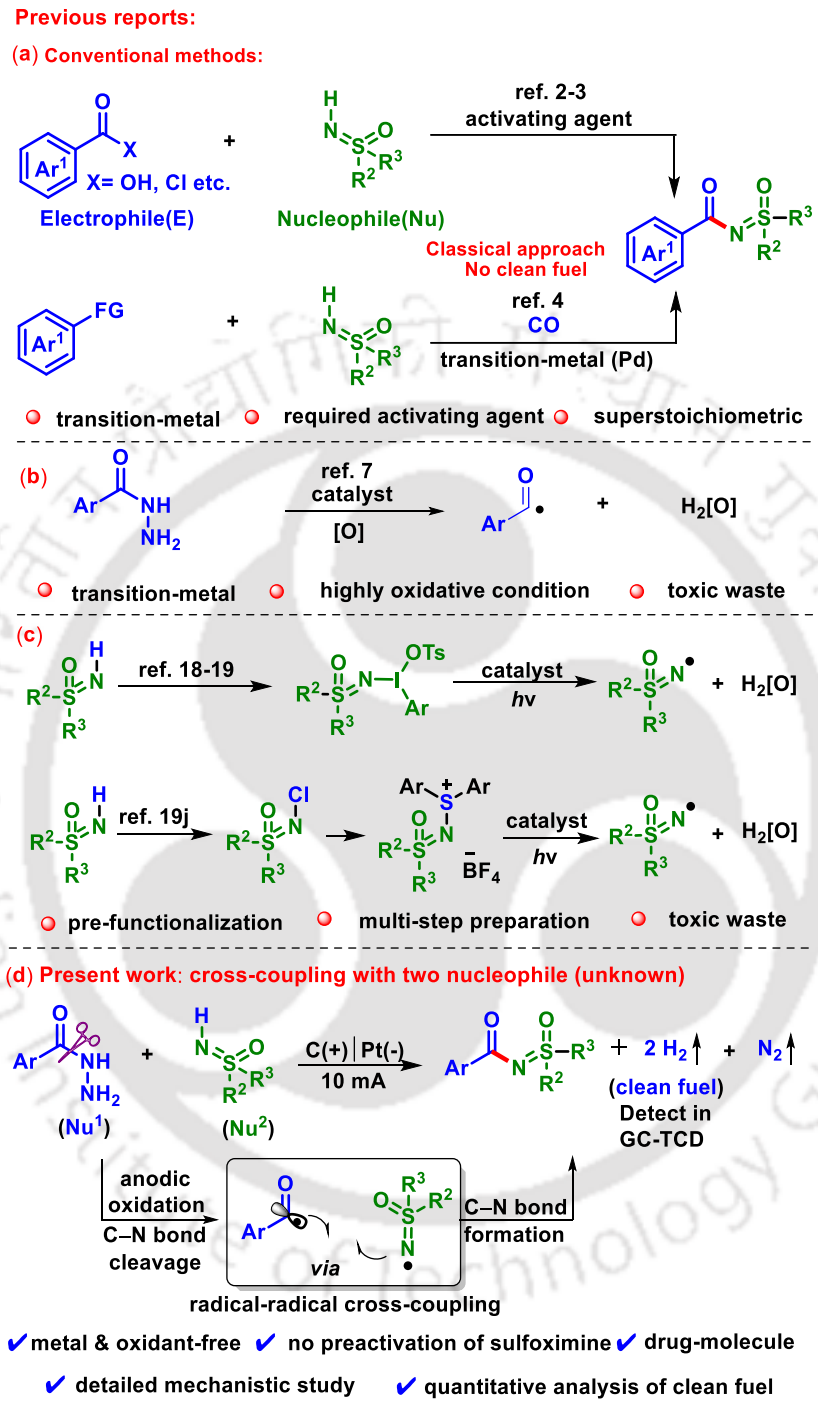

The cross-coupling of *NH*-sulfoximine under electrochemical condition is unexplored, probably due to the high oxidation potential of *NH*-sulfoximine (E_{ox} = +1.92 to +2.00 V vs. SCE) and high bond dissociation energy (BDE_{N-H} = 104−106 kcal/mol) for the generation of

N-centre radical.[17] Recently, a visible-light-induced *α*-keto acylation of sulfoximines using hypervalent iodine reagent and aryl alkynes has been achieved.[18] Following this, several other strategies involving the generation of *N*-centered sulfoximidoyl radical under photocatalytic conditions have been adopted [Scheme V.1 (c)].[19] The success of these strategies relies on the preactivation[19a] or *in situ* activation of *NH*-sulfoximines, using hypervalent iodine(III)[19b-e] and *N*-halogenated sulfoximines[19f-i] *via* mesolytic or homolytic cleavage of a weak nitrogen-heteroatom bond. Considering all these, we envisioned sulfoximidation *via* anodic oxidation of benzoyl hydrazine and *NH*-sulfoximine [Scheme V.1 (d)].

V.2. Strategies for the Synthesis of Sulfoximidation Product

In 2015 An *et al.* disclosed CuI-mediated α-ketoacylation of sulfoximines under solvent-free conditions. Both aryl- and alkyl-substituted sulfoximines and aryl-substituted acetophenones coupled smoothly, but the alkyl-substituted acetophenones failed to participate in this transformation. This protocol requires no extra solvents, bases, or additives and demonstrates outstanding compatibility with diverse functional groups (Scheme V.2).[20a]

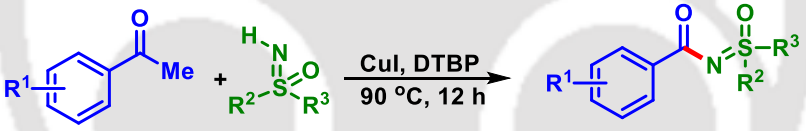

Scheme V.2. *N-Acylation of sulfoximines with acetophenones.*

In 2020 Bolm and co-workers reported an efficient strategy for the construction of α-keto-*N*-acyl sulfoximines *via* the radical coupling between sulfoximine and gemdifluoroalkenes in good to excellent yields through a C–N bond formation under photoredox catalysis. The reaction proceeds in the presence of NBS without using an additional oxidant. The mechanistic studies suggest that the two oxygens in the products originate from water and dioxygen (Scheme V.3).[20b]

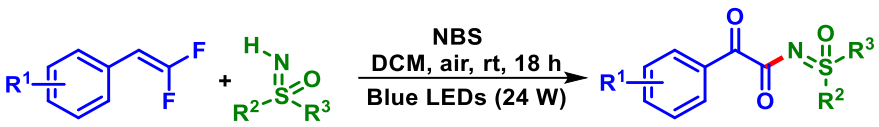

Scheme V.3. *N-Acylation of sulfoximines with gemdifluoroalkenes.*

In 2023 the Ji group disclosed an electrochemical oxidative carbonylation of NH-Sulfoximines. This electrochemical strategy proceeds under mild reaction conditions, without external oxidants, and ligands, and is easy to scale up to grams scale. Both control experiments and mechanistic studies revealed that the entire electrochemical approach proceeded through a palladium (II/IV/II) catalytic cycle (Scheme V.4).[20c]

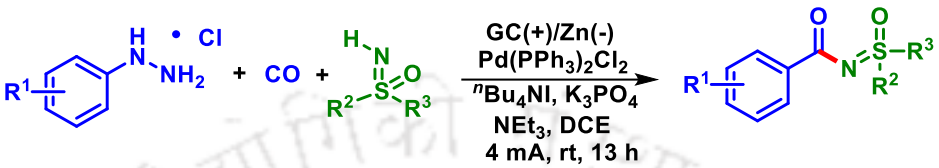

Scheme V.4. *Synthesis of N-acyl sulfoximines derivatives.*

V.3. Present Work

V.3.1. Optimization of the Reaction Conditions

As proof of our concept, a preliminary reaction was conducted between benzoyl hydrazine (**a**) and *NH*-sulfoximine (**1**). Herein, benzoyl hydrazine (**a**, 1 equiv.) and *NH*-sulfoximine (**1**, 1.5 equiv.) were treated in an electrolyte $^{n}Bu_4NOAc$ (1 equiv.) in a mixed solvent of HFIP:CH_3CN (1:4, 5 mL) having carbon rod as the anode and platinum plate as the cathode. The reaction was stirred by applying a 10 mA constant current under an N_2 atmosphere at room temperature for 10 h in an undivided cell. Gratifyingly, a new compound was isolated in a satisfactory yield of 71%. After spectroscopic (^{1}H and ^{13}C) and HRMS characterization, the structure was assigned to be *N*-aroylated sulfoximine (**1a**). The structure was further confirmed by a single-crystal X-ray diffraction analysis (CCDC-2291919) (Figure V.2).

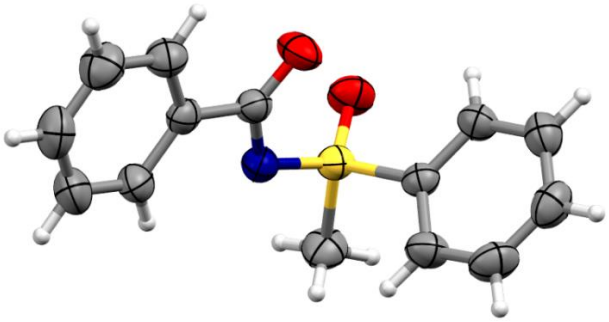

Figure V.2. *ORTEP diagram of (1a) with 50% ellipsoid probability (CCDC 2291919).*

Fascinated by the success of our anticipated electrochemical *N*-aroylation, the effect of various reaction parameters, such as solvent, electrolyte, electrode, and electric current were varied and the results are summarized in Table V.1.

Table V.1. Optimization of the reaction conditions[a,b]

Entry	Variation from the standard conditions	Yield[b] (%)
1	**None**	**71**
2	Without HFIP	30
3	Without CH_3CN	38
4	Isopropanol, MeOH, ethylene glycol instead of HFIP	N.D
5	1,4–dioxane, DMSO, DMA instead of CH_3CN	N.D
6	Nickel, RVC, platinum anode instead of C rod anode	39, 50, 56
7	Carbon cloth, stainless steel instead of platinum cathode	26, 33
8	^{n}Bu$_4$NBF$_4$,^{n}Bu$_4$NPF$_6$, ^{n}Bu$_4$NI instead of ^{n}Bu$_4$NOAc	35, 21, 26
9	0.5 Equiv., 1.5 equiv. instead of 1 equiv. ^{n}Bu$_4$NOAc	23, 63
10	1 Equiv., 2 equiv. instead of 1.5 equiv. sulfoximine	21, 59
11	15 mA, 5 mA instead of 10 mA	45, 60
12	5 h, 12 h instead of 10 h	33, 65
13	No electric current	N.D
14	No electrolyte	N.D
15	No electric current, 80 ^oC	N.D
16	air atmosphere	63

[a]Reaction conditions: **a** (0.5 mmol), **1** (1.5 equiv), ^{n}Bu$_4$NOAc (1 equiv.) in 1:4 ratios of HFIP and CH_3CN (5 mL) solvent with a carbon rod anode (Φ 6 mm), platinum plate cathode (10 mm x 10 mm x 0.3 mm), constant current = 10 mA, at room temperature under N_2 atm, 10 h in undivided cell. [b]yield of isolated product. N.D = not detected.

When CH_3CN was used as the only solvent (without HFIP), the reaction was not very efficient, resulting in a lower yield (30%) (Table V.1, entry 2). On the other hand, using only HFIP led to a slightly better yield (38%) (Table V.1, entry 3). Then, we explore various other organic co-solvents by replacing HFIP with isopropanol, MeOH, and ethylene glycol (Table

V.1, entry 4) and CH_3CN with 1,4-dioxane, DMSO, and DMA (Table V.1, entry 5). Unfortunately, none of these combinations proved effective in promoting the desired transformation. Therefore, the combination of CH_3CN/HFIP is active and ideal for this electro-catalytic process. The choice of electrode material plays a crucial role in any electrosynthesis. Thus, substituting the carbon rod anode with nickel, RVC, and platinum plate (Table V.1, entry 6) and the cathode platinum plate with carbon cloth and stainless steel showed little improvement (Table V.1, entry 7). Furthermore, our attempts to enhance the yield by replacing various electrolytes such as $^{n}Bu_4NBF_4$, $^{n}Bu_4NPF_6$, and $^{n}Bu_4NI$ were found not so productive (Table V.1, entry 8). The reaction carried out with a lower concentration (0.5 equiv.) of $^{n}Bu_4NOAc$ reduced the yield (23%), whereas the yield dropped marginally (63%) using a higher concentration (1.5 equiv.) of $^{n}Bu_4NOAc$ (Table V.1, entries 9). Thus, the use of one equivalent of electrolyte $^{n}Bu_4NOAc$ was found optimal. The use of lower (1 equiv.) or higher (2 equiv.) amounts of sulfoximine was found counterproductive, providing 21% and 59% yields, respectively, compared to the use of 1.5 equiv. of sulfoximine (Table V.1, entry 10). Additionally, altering the operating current by either decreasing (5 mA) or increasing (15 mA) was not found effective in improving the yield of (**1a**) (Table V.1, entry 11). When the reaction was stopped at 5 h and continued up to 12 h, a diminished yield of 33% and 65 % was observed (Table V.1, entry 12). In the absence of electric current or electrolyte, no product formation was observed even when the reaction mixture was heated at 80 ^{o}C, suggesting the necessity of electro-oxidation in this coupling. The reaction in an air atmosphere provided a slightly lesser yield (63%) of the product than in a nitrogen atmosphere (Table V.1, entry 16). Thus, the best-optimized condition was found to be the use of benzoyl hydrazine (**a**) (0.5 mmol), sulfoximine (**1**) (0.75 mmol, 1.5 equiv.), and $^{n}Bu_4NOAc$ (1 equiv.) in a co-solvent of HFIP/CH_3CN (1:4) 5 mL and applying a 10 mA current, carbon rod as anode and platinum plate as cathode under N_2 atmosphere at room temperature for 10 h in an undivided cell (Table V.1, entry 1).

V.3.2. Scope of the Reaction with Benzoyl Hydrazine and Sulfoximine Derivatives

Having established the optimized reaction conditions, we sought to examine the generality of this transformation by exploring the scope of various sulfoximines (**2**–**19**) with

benzoyl hydrazine (**a**) (Scheme V.5). Simple *NH*-sulfoximine (**1**), reacted with hydrazine (**a**) smoothly giving the corresponding product (**1a**, 71%). Arylsulfoximines possessing electron-donating-groups (EDGs) such as *p*-Me (**2**), *o*-Me (**3**), *p*-OMe (**4**), and *m*-OMe (**5**) coupled successfully with benzoyl hydrazine (**a**) to afford the desired *N*-aroylated products **2a**–**5a** in decent yields (63–75%). Similarly, arylsulfoximines possessing electron-withdrawing groups (EWGs) such as *p*-F (**6**), *m*-F (**7**), *m*-Cl (**8**), *o*-Br (**9**), and *p*-CN (**10**) coupled competently with hydrazine (**a**) resulting in their respective products (**6a**, 75%), (**7a**, 68%), (**8a**, 70%) (**9a**, 63%), and (**10a**, 62%). The sulfoximines bearing *S*-4-methyl benzyl and *S*-phenyl (**11**), *S*-isopropyl (**12**), and *S*-allyl (**13**) all gave products (**11a**–**13a**) in moderate yields (55–70%). Next, a heterocyclic sulfoximine (**14**), dibenzothiophene (**15**), and dibenzodithinane (**16**) also proved to be good coupling partners, giving their respective products (**14a**, 69%), (**15a**, 63%), and (**16a**, 60%) in modest yields. Further, an aliphatic sulfoximine (**17**) also participated, providing the anticipated product (**17a**) but with a lower yield (43%). On the other hand, a -NO_2 containing sulfoximine (**18**) and a symmetric diaryl sulfoximine (**19**) both failed to deliver the corresponding sulfoximidated product (**18a**) and (**19a**).

The scope of the present protocol was further extended to a range of benzoyl hydrazines having different electronic properties and functional groups (**b**–**t**) with sulfoximine (**1**) as the other coupling partner. For example, benzoyl hydrazine possessing EDGs, such as *p*-Me (**b**), *o*-Me (**c**), *m*-Me (**d**), 3,4-*di*-Me (**e**), *p*-^{t}Bu (**f**), *p*-Ph (**g**), and *p*-OMe (**h**) reacted well to provide their sulfoximidated products (**1b**–**1h**) in moderate to good yields (52–79%) (Scheme V.5). Next, benzoyl hydrazines bearing EWGs, like *p*-Cl (**i**), *p*-Br (**j**), and *p*-CF_3 (**k**) all reacted smoothly with sulfoximine (**1**) to deliver the corresponding coupling products (**1i**–**1k**) in satisfactory yields ranging from 60–66% (Scheme V.5). Bicyclic aromatics such as 1 and 2-napthylhydrazines (**l**) and (**m**), effectively underwent *N*-aroylation yielding their corresponding product (**1l**, 65%), and (**1m**, 69%) in good yield. Heteroaromatic hydrazines (**n**–**p**) were all compatible and coupled efficiently with *NH*-sulfoximine (**1**), delivering products **1n**–**1p** in good yields (60–68%). However, aliphatic hydrazine, such as hexene hydrazine (**1q**), provided the anticipated product (**1q**) with a lower yield (22%).

Scheme V.5. Substrate scope [a]

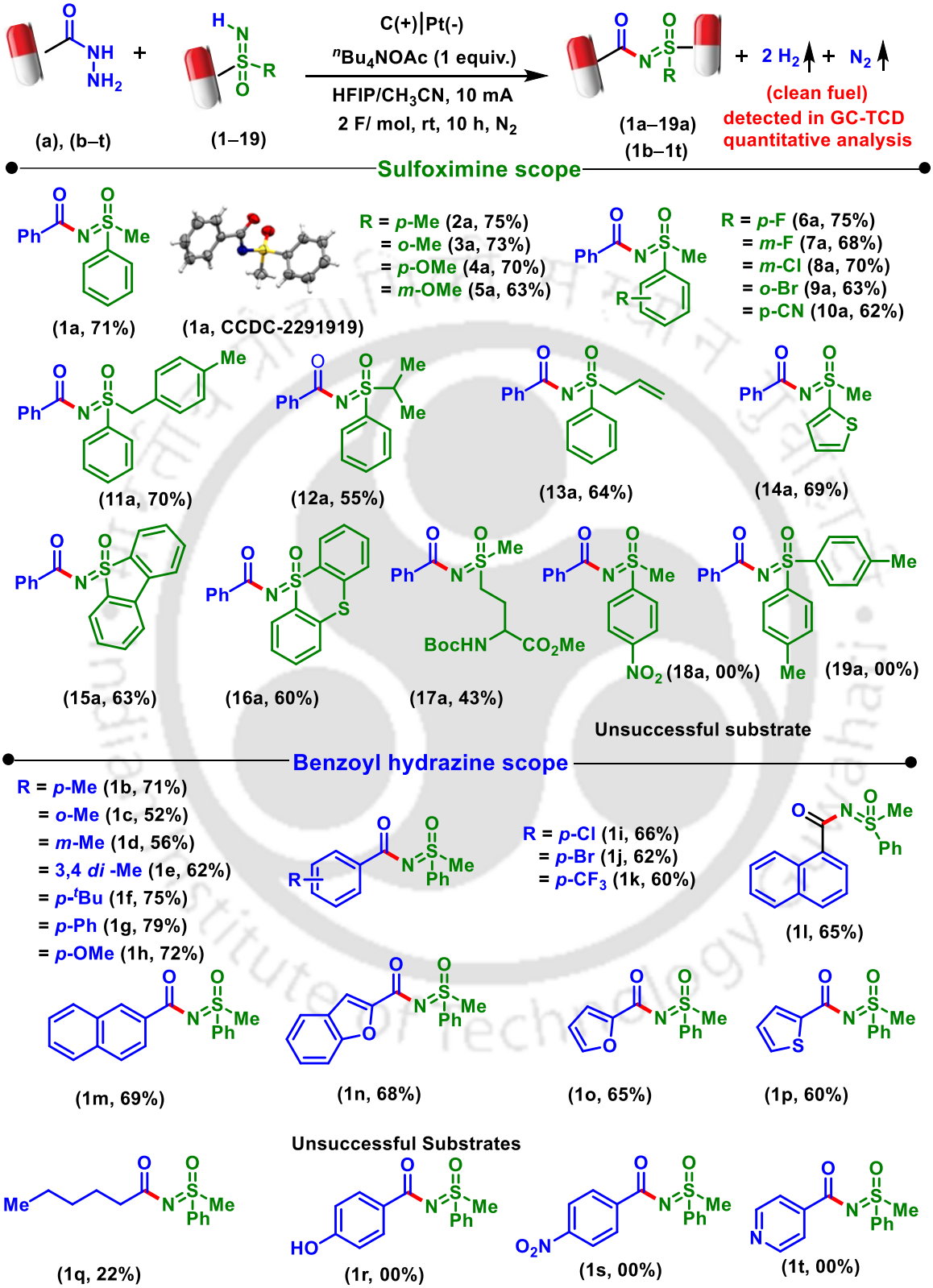

[a]Reaction conditions: (i) **1**–**19** (0.75 mmol), benzoyl hydrazine (**a–t**) (0.5 mmol), $^{n}Bu_4NOAc$ (1 equiv.) in 1:4 of HFIP and CH_3CN (5 mL) utilizing a 10 mA constant current, 2 F/ mol applied charge (**1a**), carbon rod (Φ 6 mm) as an anode and platinum plate (10 mm x 10 mm x 0.3 mm) as a cathode at room temperature under N_2 atmosphere for 10 h in an undivided cell.

Surprisingly, both strongly electron-donating and redox-active -OH (**r**), or electron-withdrawing -NO_2 (**s**) and pyridine (**t**) containing hydrazines were completely inert under the standard conditions giving no products.

Late-stage modification of complex molecules plays a crucial role in identifying potential drugs.[21] To demonstrate the applicability of the developed electrochemical strategy, uricosuric agent probenecid hydrazine (**u**) was reacted with *NH*-sulfoximine (**1**), which provided probene-sulfoxamine (**1u)** in 54% yield (Scheme V.6). Notably, *NH*- sulfoxamine of probenester (**20**), L-menthol (**21**), borneol (**22**), and D-glucose derivative (**23**) all successfully yielded their corresponding benzoylated derivative (**20a**, 48%), (**21a**, 69%), (**22a**, 65%), and, (**23a**, 58%) respectively. Similarly, *NH*-sulfoxamine of nonsteroidal anti-inflammatory drugs ibuprofen (**24**), flurbiprofen (**25**), vitamin E (**26**), fibrates drugs ciprofibrate (**27**), anti-inflammatory and analgesic agents sulindac (**28**) all furnished their respective benzoylated product (**24a**, 62%), (**25a**, 53%), (**26a**, 42%), (**27a**, 51%), (**28a**, 44%). The late-stage modification of compounds having sensitive groups demonstrates the potential of our developed electrochemical protocol in the field of drug discovery.

Scheme V.6. Substrate scope of natural product [a]

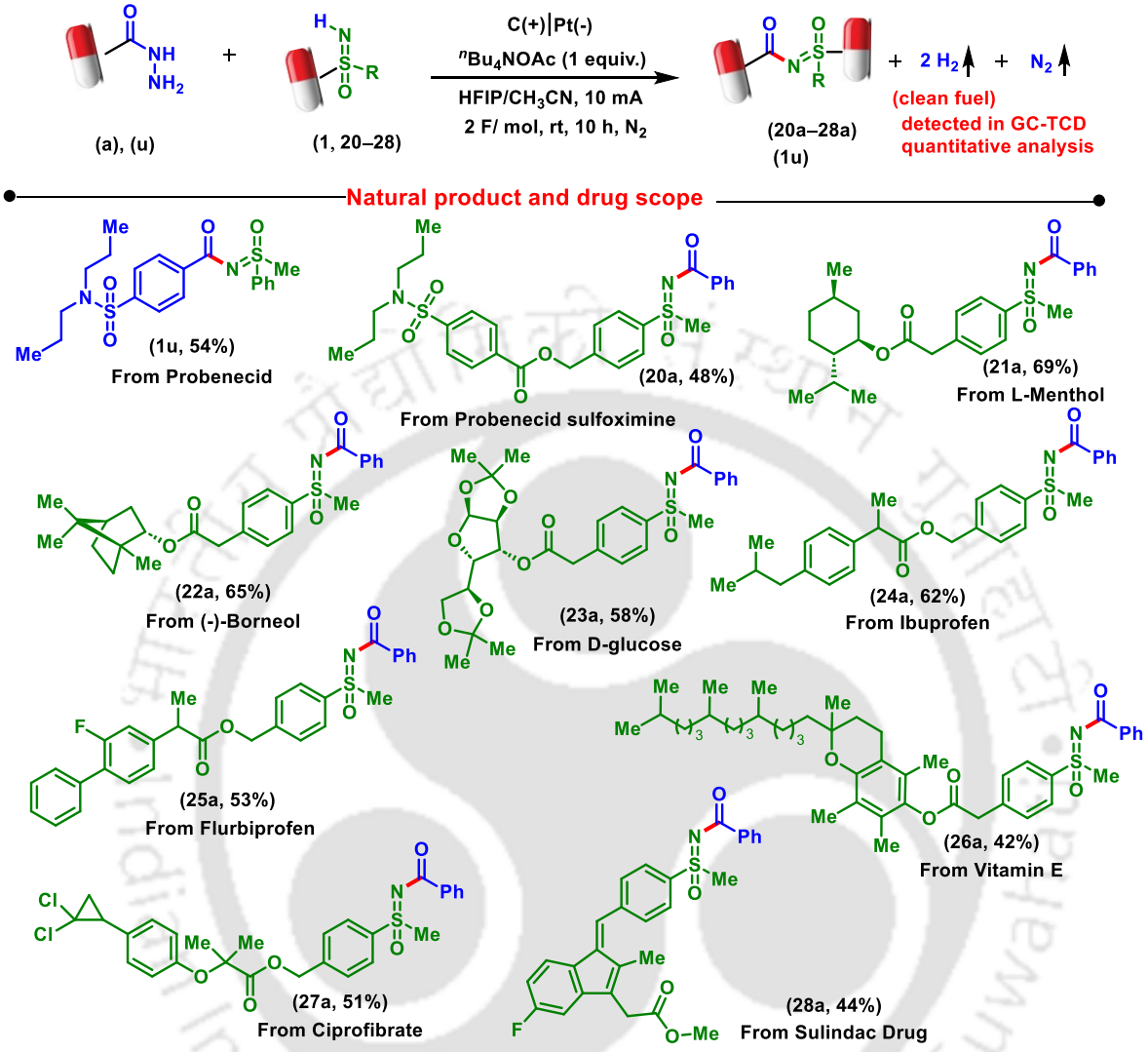

[a]Reaction conditions: (i) **20**–**28** (0.75 mmol), benzoyl hydrazine (**a,u**) (0.5 mmol), $^{n}Bu_4NOAc$ (1 equiv.) in 1:4 of HFIP and CH_3CN (5 mL) utilizing a 10 mA constant current, carbon rod (Φ 6 mm) as an anode and platinum plate (10 mm x 10 mm x 0.3 mm) as a cathode at room temperature under N_2 atmosphere for 10 h in an undivided cell.

This electrochemical sulfoximidation basically involves a series of electron transfer redox processes. Now the question arises whether other conventional oxidizing agents can carry out the ensuing oxidative cross-coupling. The coupling between benzoyl hydrazine (**a**) and *NH*-sulfoximine (**1**) was conducted in the presence of various oxidizing agents, such as

the *tetra*-butylammonium iodide (TBAI)/ *tetra*-butyl hydroperoxide (TBHP), I_2/TBHP, $K_2S_2O_8$, cerium (IV) ammonium nitrate (CAN), pyridinium chlorochromate (PCC), $KMnO_4$, and $FeCl_3$ (Table V.3). However, none of these chemical oxidants could promote the coupling reaction. These investigations highlight the essential role of the electrochemical method in achieving the desired redox potential necessary for this coupling (Table V.3).

Table V.3. Scope of the external oxidants in cross-coupling[a]

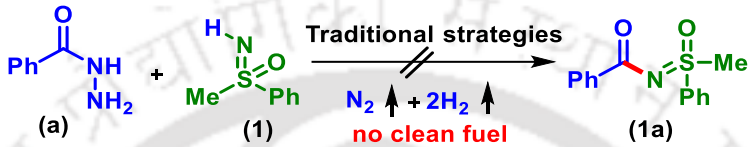

Entry	Conditions	Yield[a] (1a,%)
1	TBAI (20 mol %), TBHP (2.0 equiv.), HFIP/CH_3CN (1:4), rt, 10 h	0
2	I_2 (50 mol %), TBHP (2.0 equiv.), HFIP/CH_3CN (1:4), rt, 10 h	0
3	$K_2S_2O_8$ (2.0 equiv.), HFIP/CH_3CN (1:4), rt, 10 h	0
4	CAN (2.0 equiv.), HFIP/CH_3CN (1:4), rt, 10 h	0
5	PCC (2.0 equiv.), HFIP/CH_3CN (1:4), rt, 10 h	0
6	$KMnO_4$ (10 mol %), TBHP (2.0 equiv.), HFIP/CH_3CN (1:4), rt, 10 h	0
7	$FeCl_3$ (10 mol %), HFIP/CH_3CN (1:4), rt, 10 h	0

[a]Reaction conditions: (i) (**a)** (0.5 mmol), (**1**) (0.75 mmol), traditional oxidant (x mol%/ x equiv.) in 1:4 of HFIP and CH_3CN (5 mL) at room temperature under N_2 atmosphere for 10 h.

V.4. Mechanistic Investigations

V.4.1. Control Experiments

We proceeded further to investigate the mechanistic insight of this protocol When TEMPO (2 equiv.) was added to the coupling reaction between benzoyl hydrazine (**a**) and *NH*-sulfoximine (**1**), the formation of (**1a**) was significantly inhibited (<10%) and the benzoyl radical trapped TEMPO-adduct (**v**) was isolated in 26% yield (Scheme V.7). The identity and purity of the product were confirmed by NMR and HRMS analysis (Figure V.3), ^{1}H NMR (Figure V.4), and ^{13}C{1H} (Figure V.5) analyses suggesting the formation of benzoyl radicals during the reaction.

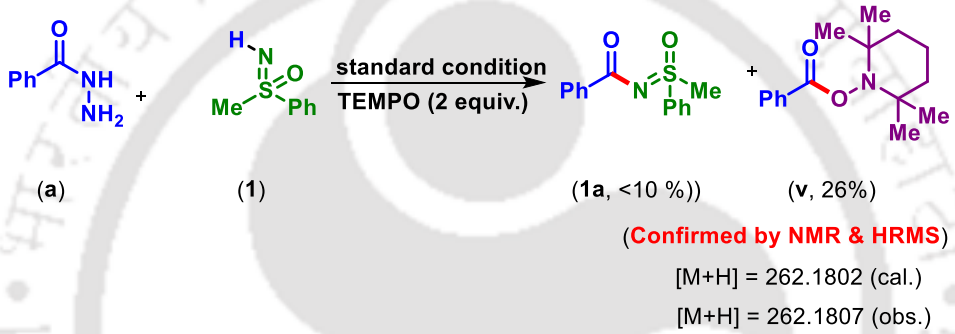

Scheme V.7. *Radical trapping experiments using TEMPO.*

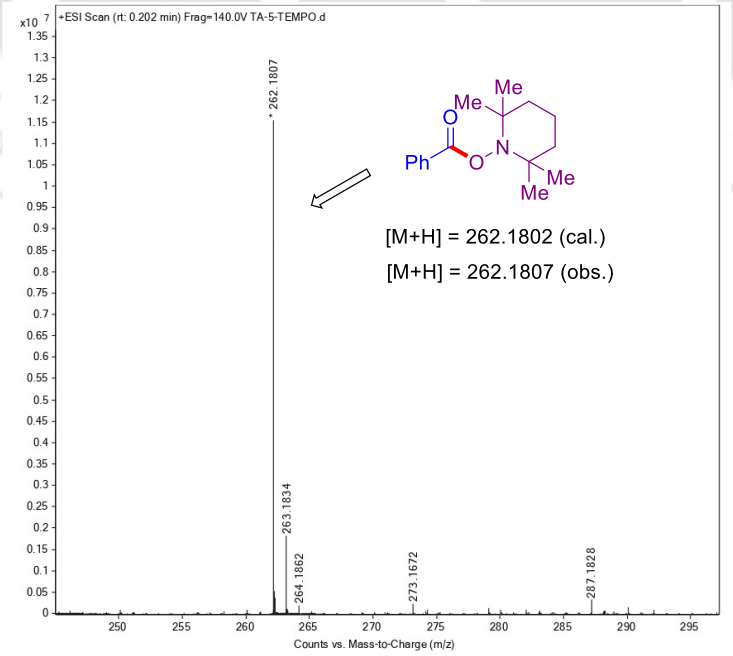

Figure V.3 *HRMS spectra of benzoyl-radical trapped adduct (**1s**).*

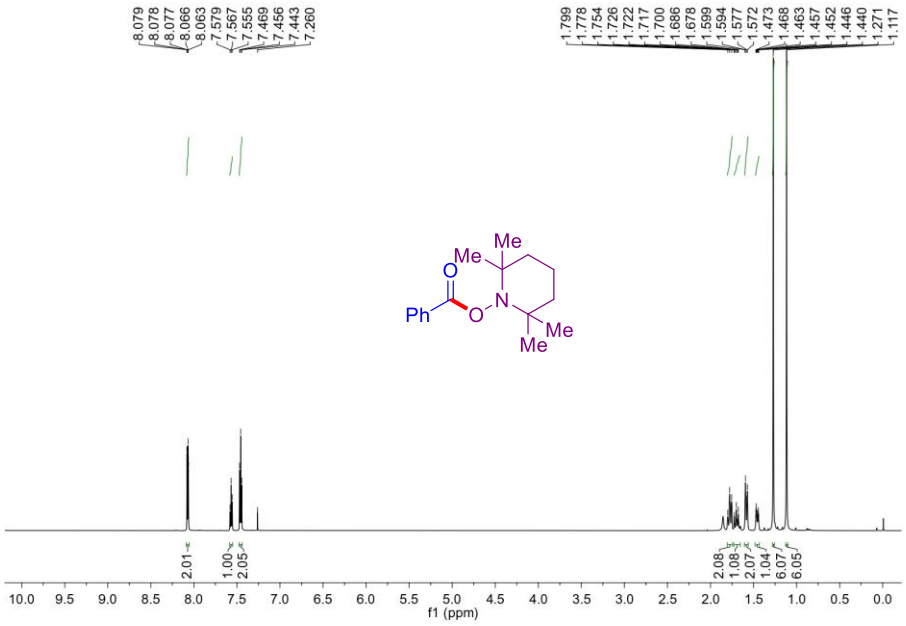

Figure V.4 *^{1}H-NMR spectra of benzoyl-radical trapped adduct (**1s**).*

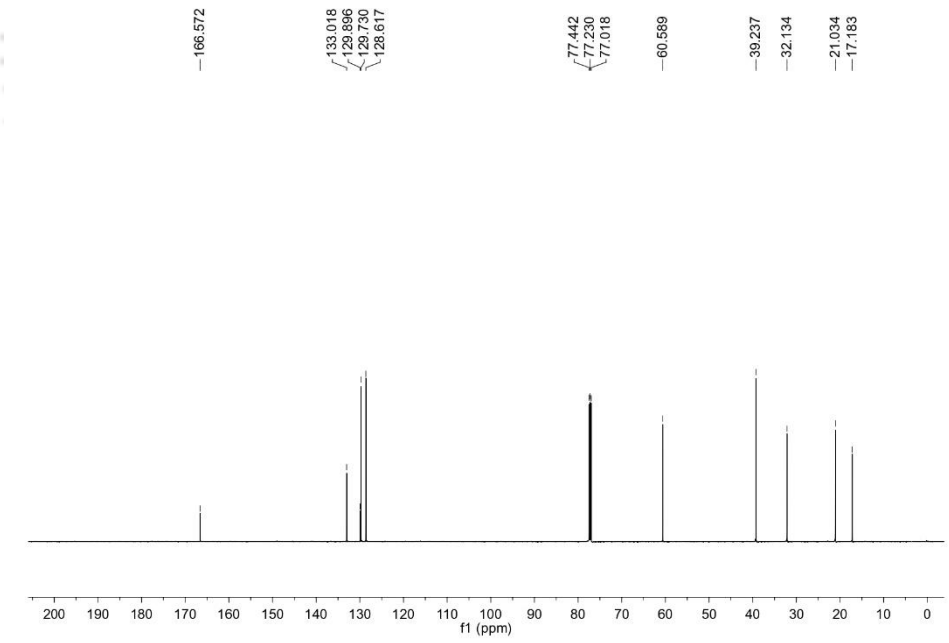

Figure V.5 *^{13}C{1H} NMR spectra of benzoyl-radical trapped adduct (**1s**).*

Similarly, the addition of another radical scavenger BHT also suppresses this reaction giving the product **1a** in <10% yield along with the formation of BHT-sulfoxamine adduct

(**w**) (Scheme V.8). The formation of the BHT-adduct, 2,6-di-tert-butyl-4(morpholinomethyl)phenol (t) was confirmed by HRMS analysis of the reaction mixture (Figure V.6).

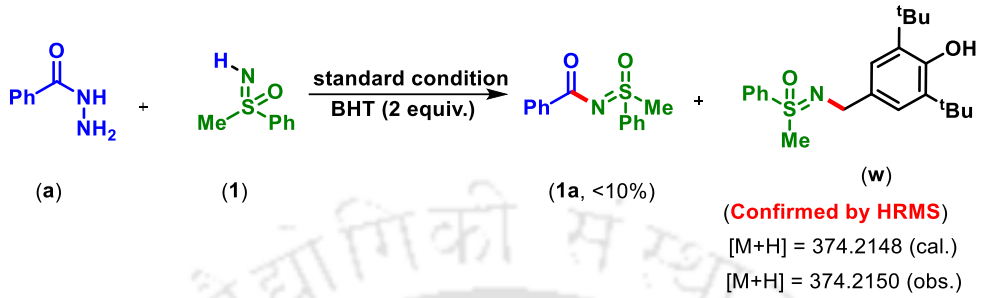

Scheme V.8. *Radical trapping experiments with BHT.*

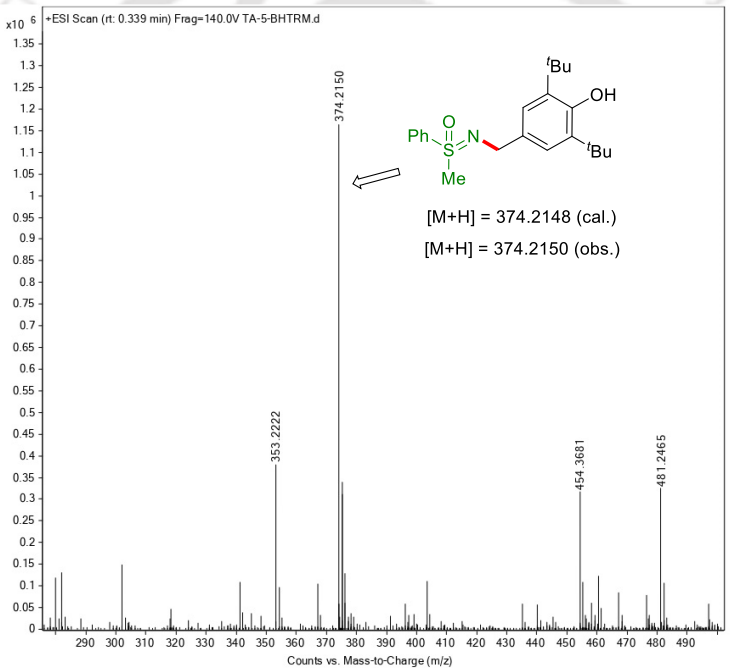

Figure V.6. *HRMS spectrum of BHT-adduct (t).*

There is a possibility that the benzoyl hydrazine (**a**) under the electrochemical conditions may generate aldehyde (**a′**), carboxylic acid (**a′′**), or benzamide (**a′′′**) as possible intermediates that may couple with *NH*-sulfoximine (**1**). To check the possibility, three independent reactions of *NH*-sulfoximine (**1**) with benzaldehyde (**a′**), benzoic acid (**a′′**), and benzamide (**a′′′**) were carried out under the present electrochemical conditions. However, none of these reactions yielded the desired product (**1a**) (Scheme V.9), thus, ruling out their intermediacy.

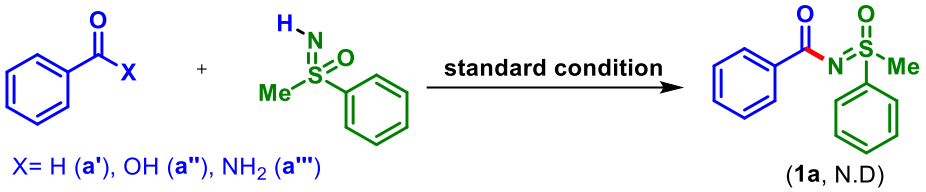

Scheme V.9. *Possible intermediate detection experiment.*

The radical nature of both these coupling intermediates, *viz.* benzoyl and sulfoxamidoyl radicals, has been further confirmed by electron paramagnetic resonance (EPR) measurements. In one experiment, benzoyl hydrazine (**a**) {without sulfoximine (**1**)} was subjected to identical electrolytic conditions for 1 hour, after which spin-trapping agent, 5,5-dimethyl-pyrroline *N*-oxide (DMPO) (50 µL) was added. After 10 minutes of further electrolysis, 500 µL of the reaction aliquot was taken in an electron paramagnetic resonance (EPR) tube and the EPR signal was recorded at liquid nitrogen temperature (Scheme V.10). The appearance of a strong EPR signal (Figure V.7) suggests the formation of benzoyl-trapped radical (**ax**) which was also confirmed by HRMS analysis of the reaction aliquot (Figure V.8). Which suggested benzoyl radical is the intermediate of this reaction.

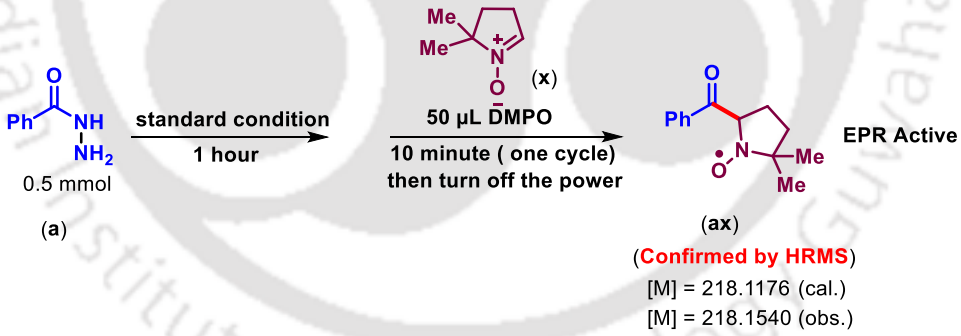

Scheme V.10. *EPR experiment with benzoyl hydrazine (**a**).*

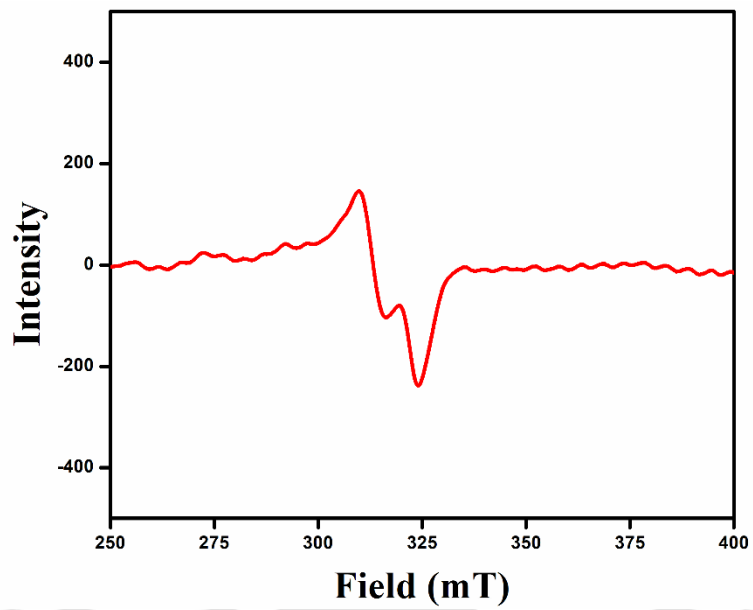

Figure V.7. *EPR spectrum of benzoyl hydrazine (**a**).*

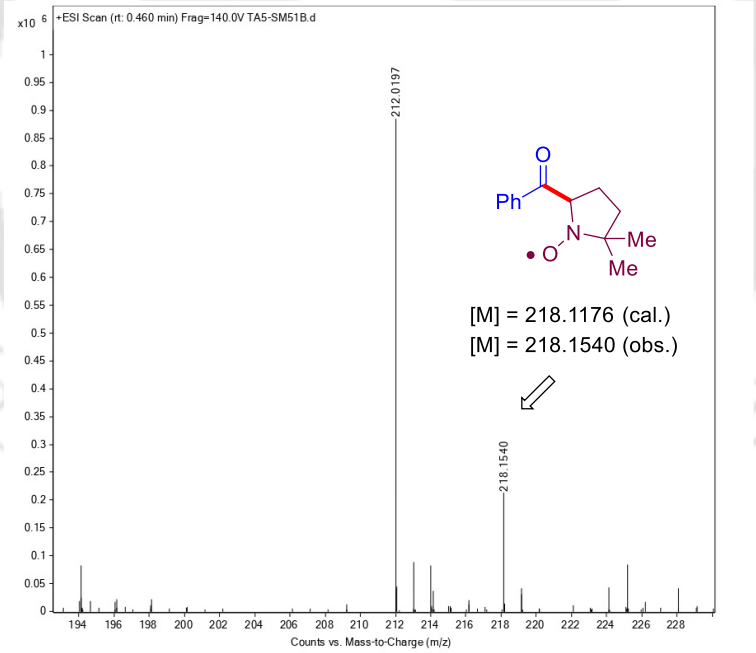

Figure V.8. *HRMS spectrum of benzoyl-adduct (**ax**).*

Similarly, in another experiment sulfoximine (**1**) {without benzoyl hydrazine (**a**)} was subjected to an identical spin-trapping experiment using DMPO (Scheme V.11). The observation of a strong EPR signal (Figure V.9) confirms the formation of sulfoxamidoyl-

trapped radical (**1x**) which was also reconfirmed by the HRMS analysis (Figure V.10). Which suggested sulfoximidoyl radical is the intermediate of this reaction.

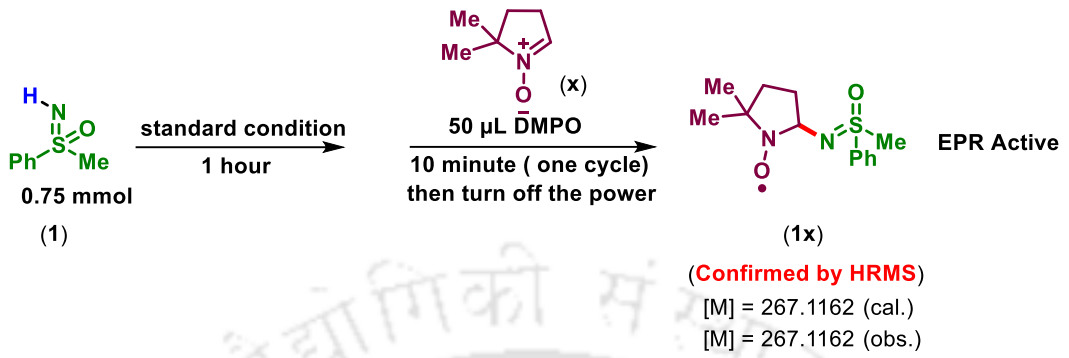

Scheme V.11. *EPR experiment with sulfoximine (**1**).*

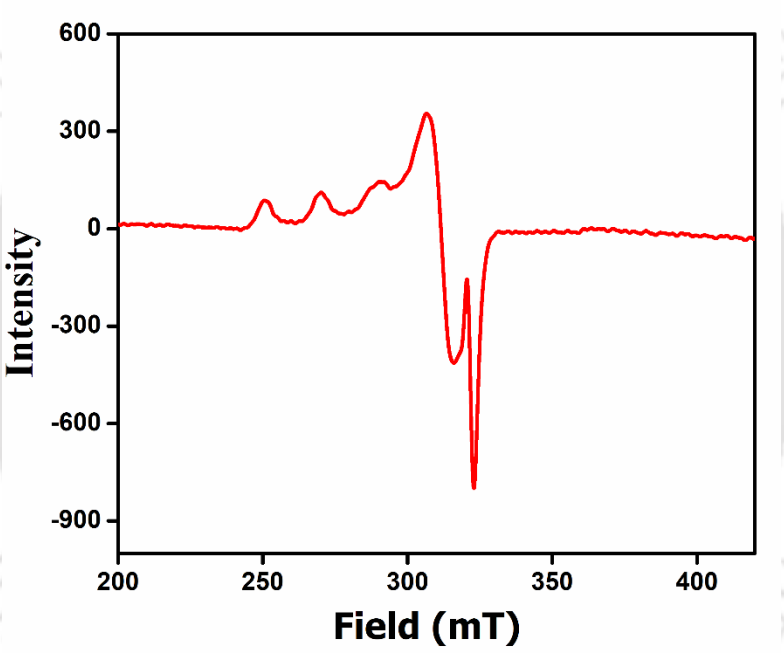

Figure V.9. *EPR spectrum of sulfoximine (**1**).*

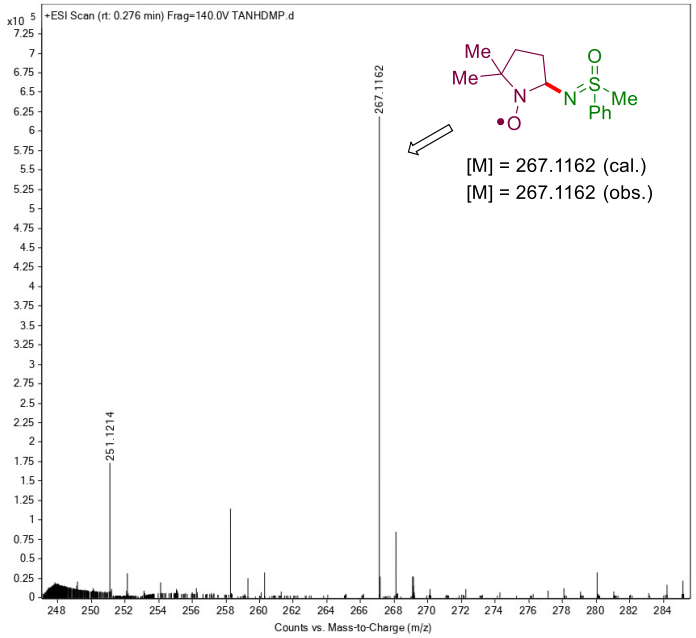

Figure V.10. *HRMS spectrum of sulfoximidoyl-adduct (**1x**).*

Finally, another spin-trapping experiment using DMPO in the presence of both the coupling partner's benzoyl hydrazine (**a**) and *NH*-sulfoximine (**1**) under the above-described conditions (Scheme V.12) also gave a strong EPR signal (Figure V.11). These experiments suggest that the generated benzoyl and sulfoxamidoyl radicals have enough lifetime to be trapped by DMPO before undergoing coupling.

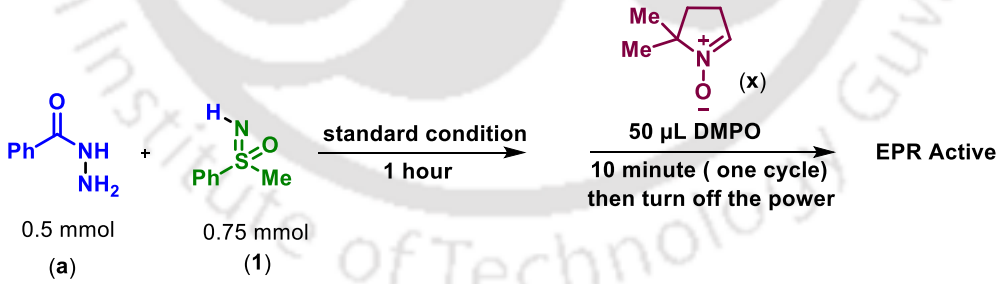

Scheme V.12. *EPR experiment with benzoyl hydrazine (**a**) and sulfoximine (**1**).*

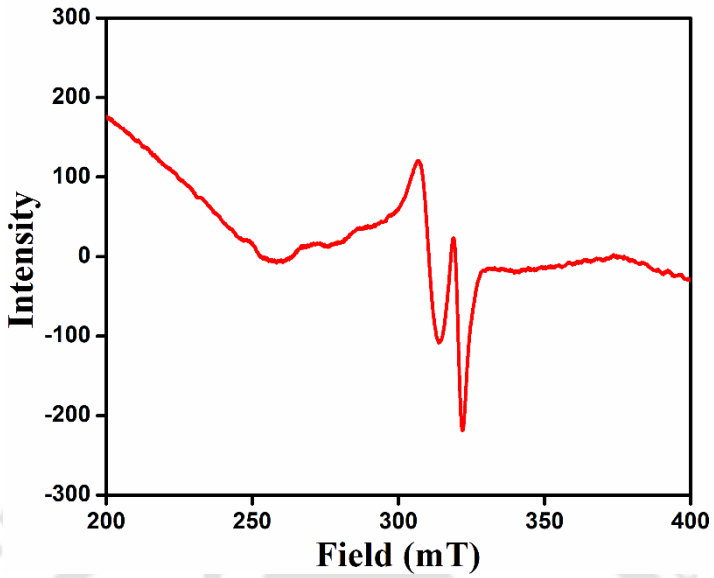

Figure V.11. *EPR spectrum of reaction mixture.*

If acyl radical is obtained from benzoyl hydrazine (**a**), then there is a possibility of the hydrazine unit undergoing a sequential SET process at the anode eliminating N_2 and H_2 as by-products. Now the question arises if hydrogen is generated, what is its time-dependent release? To find an answer to this, a time-dependent hydrogen production for the standard electrochemical reaction between benzoyl hydrazine (**a**) and NH-sulfoximine (**1**) was monitored every hour for up to 10 hours. For this, the evolved gas was syringed out at one-hour intervals from the headspace of the reaction mixture and injected into the GC-MS instrument with an Elite Plot-Q column. The GC chromatogram was recorded, and percent evaluation was calculated (Figure V.12). The hydrogen production at the cathode reached a threshold value within 5 hours and remained steady for nearly two hours. In the next three hours, the hydrogen production decreased. The quantity of hydrogen production depends on the overall oxidation of both these substrates (**a**) and (**1**) at the anode.[22]

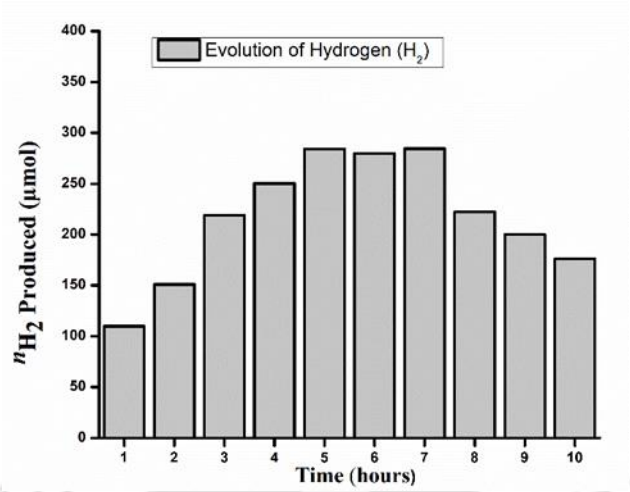

Figure V.12. *Time-dependent evolution of hydrogen (H_2).*

To investigate whether the interaction of electrolyte, $^{n}Bu_4NOAc$ has any influence on coupling partner *viz.* benzoyl hydrazine (**a**) and sulfoximine (**1**) in the formation of their respective radicals (benzoyl and sulfoximidoyl), cyclic voltammetry (CV) studies was performed (Figure V.13). In the presence of $^{n}Bu_4NPF_6$ as the supporting electrolyte, the CV of benzoyl hydrazine (**a**) showed three stepwise $1e^-$ oxidation at $E_{ox} \approx 1.5V$, 1.9V, and 2.06V respectively (vs. SCE, in saturated KCl). The addition of 20 mM of tetrabutylammonium acetate ($^{n}Bu_4NOAc$), resulted in a cathodic shift of the first oxidation wave to ≈ 1.1V (shift of 400 mV) and showed a sharp irreversible wave with a potential of ≈ 1.25 V vs. SCE for the latter two. A stepwise addition of 40, 60, and 80 mM of $^{n}Bu_4NOAc$ resulted in the overlapping of all these signals to a single peak and a continuous enhancement of the current [Figure V.13, (I)].[23a] Such a sharp change in the electrochemical behavior of benzoyl hydrazine (**a**) suggests the strong participation of $^{n}Bu_4NOAc$ during electrochemical oxidation.

Similarly, to understand the interaction between the electrolyte, $^{n}Bu_4NOAc$, and sulfoximine (**1**), cyclic voltammetry studies were performed [Figure V.13, (II)]. The observed oxidation potential of sulfoximine was found to be at $E_{ox} \approx 2.13$ V (vs. SCE in acetonitrile). Upon sequential addition of $^{n}Bu_4NOAc$, 20, 40, 60, 80, and 100 mM to sulfoximine (**1**) causes a negligible shift in the onset potential but a substantial increase in the current, thus confirming a strong interaction between $^{n}Bu_4NOAc$ with (**1**), during the electrochemical oxidation [Figure V.13, (II)].[23a-b] Further, to understand the influence of electrolyte ($^{n}Bu_4NOAc$) in the overall coupling reaction, a similar titration with $^{n}Bu_4NOAc$ (20, 40, 60,

and 80 mM) was performed in the presence of both the substrates (**a**) and (**1**) [Figure V.13, (III)]. The CV measurements of the mixture showed a new peak at 2.5V vs. SCE. The current and peak position remained virtually unchanged, with an increase in the concentration of $^{n}Bu_4NOAc$ [Figure V.13, (III)], suggesting a strong association of electrolytes with both the reacting partners.[23a-c]

Electrochemical studies were performed to gain further mechanistic insights into the anodic and cathodic processes. To monitor the effective potential of the working electrode during the electrolysis under a 10 mA current, a parallel study of potential versus time was conducted [Figure V.13, (IV)]. It was observed that the potential consistently remained around 1.46–1.75V vs. Ag/AgCl throughout the electrolytic process. This constant potential profile signifies an active and sustained electrolysis with a steady reaction rate, demonstrating the stability and effectiveness of the process.[24] Then, the constant potential electrolysis was performed, and the yield was obtained only 18%.

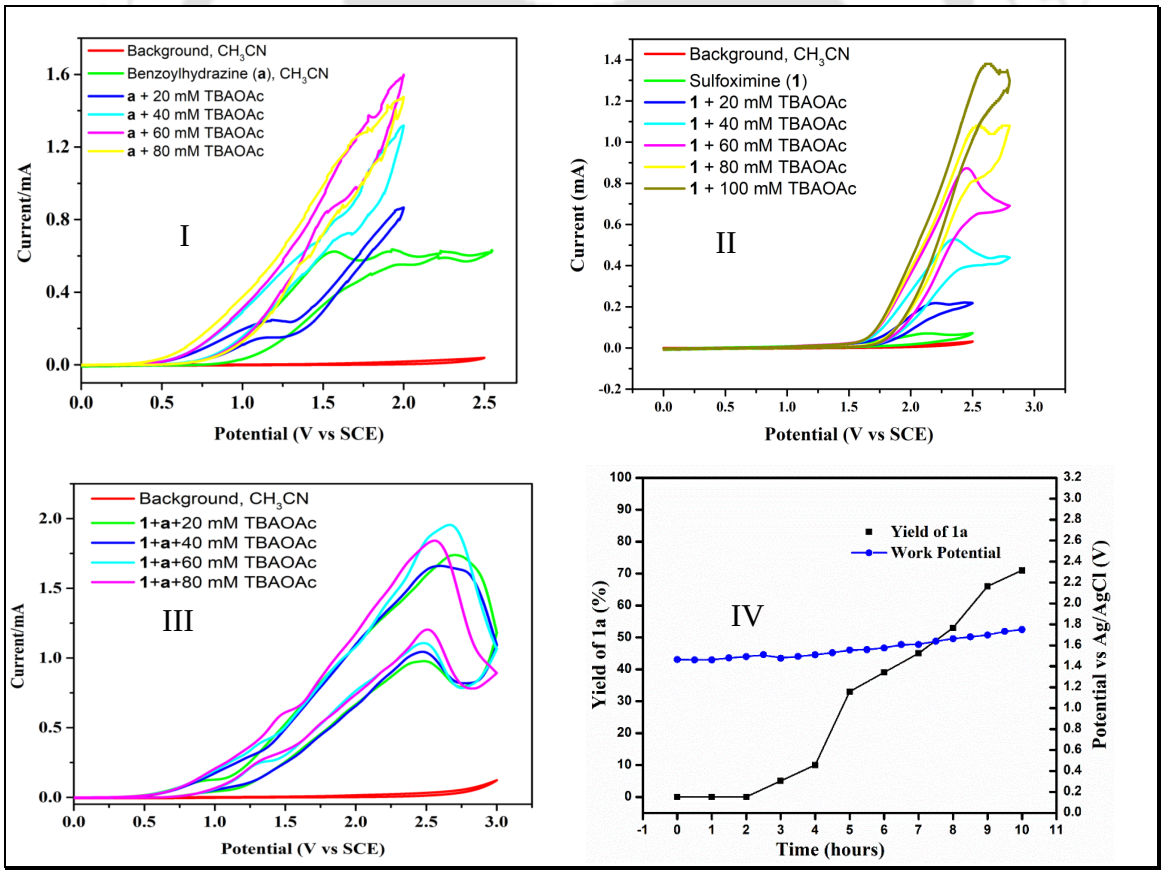

Figure V.13. *Cyclic voltammetry studies. (I) Cyclic voltammograms of benzoyl hydrazine (a). (II) Cyclic voltammograms of sulfoximine (1). (III) Cyclic voltammograms of benzoyl hydrazine (a) and sulfoximine (1). (IV) The relationship between time, yield, and potential.*

V.4.2. Plausible Reaction Mechanism

Based on the electrochemical studies, the results obtained from control experiments, and previous literature reports,[23-24] a plausible mechanism is depicted in Scheme V.13. It is well documented and demonstrated here as well, that tetrabutylammonium acetate ($^{n}Bu_4NOAc$) plays a vital role in this electrosynthesis.[23] The initial step involves hydrogen bonding between $^{n}Bu_4NOAc$ and the N–H of benzoyl hydrazine (**a**). Subsequently, the resulting adduct of benzoyl hydrazine (**a**) undergoes an electrochemical anodic oxidation, leading to selective homolysis of the amidic N–H bond.[23a] This process generates a *N*-centered diazanyl radical intermediate (**A**). Next, through a sequential two-step transformation involving intermediate (**B**), a diazene radical intermediate (**C**) is produced from radical intermediate (**A**). Further, the cleavage of the initial C–N bond of benzoyl hydrazine (**a**) releases a molecule of N_2 as the by-product and produces a benzoyl radical intermediate (**D**).

Scheme V.13. Plausible mechanisms

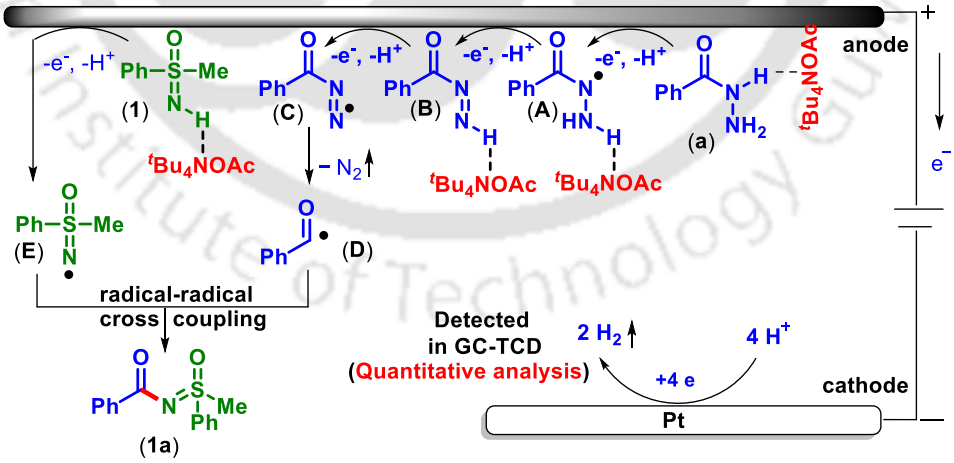

In a similar fashion, the sulfoximine (**1**) is activated by H-bonding interaction with tetrabutylammonium acetate and, *via* anodic oxidation, generates sulfoximidoyl radical intermediate (**E**).[23b] Finally, the radical–radical cross-coupling between intermediates (**D**) and

(**E**) affords the sulfoximidated product (**1a**). On the other hand, at the platinum plate cathode surface, the overall redox process is balanced by the reduction of four protons with four electrons producing hydrogen gas. Further, quantitative analysis of hydrogen production is also illustrated with the help of the GC-TCD method.

V.5. Gram-scale and Post-synthetic Modification

The feasibility of this approach is subsequently demonstrated through the synthesis of (**1a**) on a gram scale. Upon performing the standard electrochemical reaction between benzoyl hydrazine (**a**) and *NH*-sulfoximine (**1**) on a 10 mmol scale, the desired product (**1a**) was obtained in 62% yield after 20 hours (Scheme V.14).

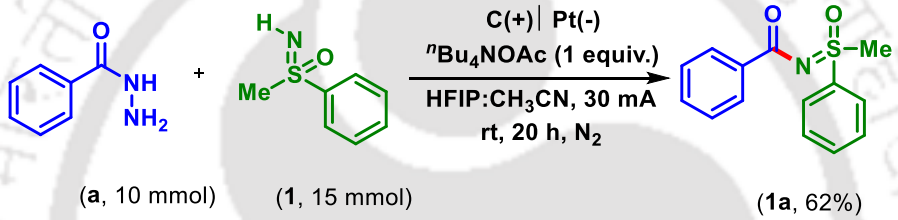

Scheme V.14. *Gram-scale synthesis.*

To demonstrate the synthetic utility of the product (**1a**), the carbonyl group was reduced using $BH_3.SMe_2$ (3 equiv.) to provide a benzyl sulfoximine (**1y**) in 76% yield (Scheme V.15).

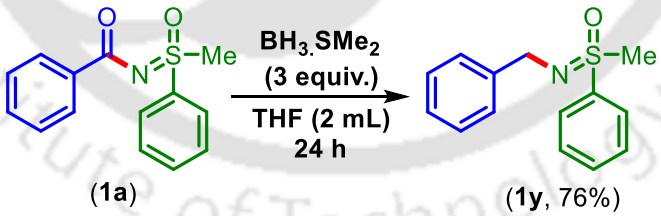

Scheme V.15. *Synthesis of benzyl derivative.*

Further, the compound (**1a**) having a sulfoximine served as *o*-C–H directing group in a Pd-catalyzed C–H activation process providing *o*-hydroxylated product (**1z**) in 60% yield (Scheme V.16).[25]

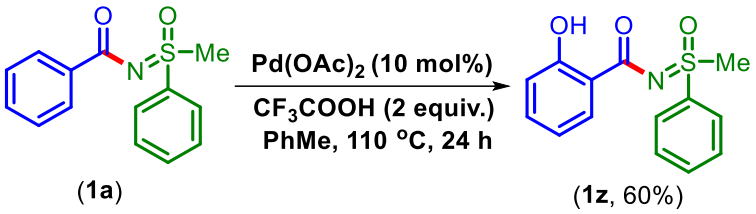

Scheme V.16. *Synthesis of o*-hydroxylated *derivative.*

V.6. Conclusion

In summary, developed here is an electrochemical sulfoximidation under metal and external oxidant-free conditions between benzoyl hydrazine and *NH*-sulfoximine. The process involves a radical–radical cross-coupling between the *in situ*-generated benzoyl and sulfoximidoyl radicals. The developed electrochemical approach features mild reaction conditions, operational simplicity, and remarkable scope, particularly in the late-stage modifications of complex and sensitive pharmaceuticals and natural products. The method is scalable and provides H_2 and N_2 as the only by-products that can be utilized as a clean energy source. The sequential cleavage and formation of a new C(sp^2)–N bond under the same condition offers opportunities to pursue fundamental mechanistic studies, which may lead to the discovery of new cross-coupling in synthetic electrochemistry.

V.7. Experimental Section

V.7.1. General Information: All the reagents were commercial grade and purified according to the established procedures. All the reagents were commercial grade and used without further purification unless otherwise stated. Preparation of the starting materials was carried out in an oven-dried 100 mL or 50 mL round bottom flask. Reactions were monitored by thin layer chromatography (TLC) on 0.25 mm silica gel plates ($60F_{254}$) and visualized under UV illumination at 254 nm. Organic extracts were dried over anhydrous sodium sulfate (Na_2SO_4). Column chromatography was performed to purify the crude product on silica gel 60–120 mesh using a mixture of hexane and ethyl acetate as eluent. The isolated compounds were characterized by spectroscopic [^{1}H, ^{13}C{1H} NMR, and IR] techniques and HRMS analysis. NMR spectra were recorded in deuterochloroform ($CDCl_3$) or deuterated dimethyl sulfoxide (DMSO-d^6). ^{1}H, ^{13}C{^{1}H} were recorded in 600 (150) or 500 (125) MHz spectrometer and were calibrated using tetramethylsilane or residual undeuterated solvent for

^{1}H NMR, deuterochloroform for ^{13}C NMR as an internal reference {$Si(CH_3)_4$: 0.00 ppm or $CHCl_3$: 7.260 ppm for ^{1}H NMR, 77.230 ppm for ^{13}C NMR or $(CH_3)_2SO$: 2.50 ppm for ^{1}H NMR, 39.50 ppm for ^{13}C NMR}. ^{19}F NMR was calibrated without any internal standard in $CDCl_3$ and DMSO-d^6 in a 500 MHz spectrometer. The chemical shifts are quoted in δ units, parts per million (ppm). ^{1}H NMR data is represented as follows: Chemical shift, multiplicity (s = singlet, d = doublet, t = triplet, q = quartet, m = multiplet), integration and coupling constant(s) *J* in hertz (Hz). High-resolution mass spectra (HRMS) were recorded on a mass spectrometer using electrospray ionization-time of flight (ESI-TOF) reflection experiments. FT-IR spectra were recorded in KBr or neat and reported in the absorption frequency (cm^{-1}). The instrument used for the electrolysis is a dual-display METRAVI RPS-6005/RPS-6002 adjustable 60V/5A DC Power Supply (Made in India). The anodic electrode was a carbon rod (Φ 6 mm), and the cathodic electrode was a platinum plate (10 mm ×10 mm × 0.3 mm). All the reactions were carried out using an oven-dried three-neck cell under a nitrogen atmosphere. IUPAC names were obtained using the ChemDraw Professional 16.0 software. The amine and benzoyl hydrazine were purchased from Sigma-Aldrich, TCI, and Alfa aesar.

V.7.2. Crystallographic Information

(A) Sample Preparation:

The single crystal of compound (**1a)** was prepared by the slow evaporation method for which 15 mg of the compound (**1a**) was dissolved in 1 mL of methanol in a clean and dry 10 mL glass vial. DCM (1 mL) was added to this solution slowly with a dropper. The mouth of the glass vial was covered with a cap having a small hole and kept for slow evaporation at room temperature. Crystals of (**1a)** were obtained as a transparent white needle-like shape after 3 days.

(B) Crystallographic Description of *N*-(Methyl(oxo)(phenyl)-λ^6-sulfaneylidene)benzamide (1a):

Diffraction data were collected at 292 K with MoKα radiation (λ = 0.71073 Å) using a Bruker Nonius SMART APEX CCD diffractometer equipped with graphite monochromator and Apex CD camera. The SMART software was used for data collection for indexing the reflections and determining the unit cell parameters. Data reduction and cell refinement were performed using SAINT[1,2] software, and the space groups of these crystals were determined

from systematic absences by XPREP and further justified by the refinement results. The structures were solved by direct methods and refined by full-matrix least-squares calculations using SHELXTL-97[3] software. All the non-H atoms were refined in the anisotropic approximation against F^2 of all reflections.

1. G. M. Sheldrick, SADABS, 1996, based on the method described in: R. H. Blessing, *Acta Crystallogr.* 1995, **A51**, 33–38.
2. SMART and SAINT, Siemens Analytical X-ray Instruments Inc., Madison, WI, 1996.
3. G. M. Sheldrick, *Acta Crystallogr.*, 2008, **A64**, 112–122.

$C_{14}H_{13}NO_2S$, crystal dimensions 0.34 x 0.24 x 0.20 mm, M_r = 259.31, monoclinic, space group P -1, a=5.8083 (9), b=8.6159 (14), c=13.536 (2) Å, α = 81.087(6), β = 88.311(6), γ = 73.433(5) , V = 641.35(17) Å^3, Z = 2, ρ_{calcd} = 1.343 mg/m^3, μ = 0.245 mm^{-1}, $F(000)$ = 272.0, refinement method = full-matrix least-squares on F^2, final R indices [$I > 2\sigma(I)$]: R_1 = 0.0370(2335), wR_2 = 0.0969(2828), goodness of fit = 1.000. CCDC 2291919 for *N*-(methyl(oxo)(phenyl)-λ^6-sulfaneylidene)benzamide (**1a**) contains the supplementary crystallographic data for this paper. These data can be obtained free of charge from The Cambridge Crystallographic Data Centre via www.ccdc.cam.ac.uk/data_request/cif.

V.7.3. General Procedure for the Synthesis of Benzoyl Hydrazines (m-n, q, u)

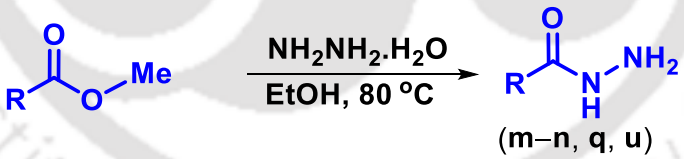

Scheme V.17. *Preparation of hydrazine derivative.*

To an oven-dried 50 mL round bottom flask was added methyl 2-naphthoate (372 mg, 2 mmol), and hydrazine hydrate (1.00 g, 20 mmol) was added in absolute ethanol (20 mL). The mixture was stirred and refluxed for 18 h. After the disappearance of the methyl 2-naphthoate, as indicated by TLC, the reaction was stopped and the solvent was evaporated under reduced pressure. When precipitation was observed, the solid was collected through filtration and washed with 20 mL of (hexane: diethylether, 1:1) to result in the product 2-naphthohydrazide in 205 mg, 55% yield. (**m**) (Scheme V.17).

V.7.4. General Procedure for the Synthesis of *NH*-Sulfoximines (1–28)

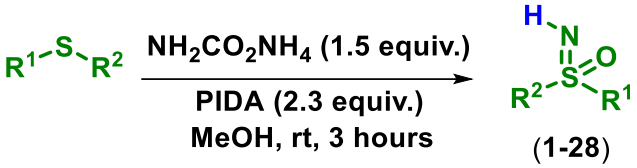

Scheme V.18. *Preparation of NH-sulfoximine derivatives.*

In an oven-dried 50 mL round bottom flask, methylphenylsulfide (2 mmol, 1 equiv, 248 mg), ammonium carbamate (3 mmol, 1.5 equiv, 234 mg), and phenyliodo diacetate (PIDA) (4.6 mmol, 2.3 equiv, 1.48 g) in 15 mL methanol are taken and stirred at room temperature for 3 hours. After the disappearance of the sulfides, as indicated by TLC, the reaction was stopped, and the solvent was evaporated under reduced pressure. Then, the mixture was admixed with ethyl acetate (40 mL), and the organic layer was washed with brine (1 x 20 mL). The organic layer was dried over anhydrous Na_2SO_4, and the solvent was evaporated under reduced pressure. The compound was purified by column chromatography and separated in 80% of EtOAc in hexane to produce S-phenyl-S-methyl-sulfoximine (**1**) in 242 mg, 78% yield (Scheme V.18).

V.7.5. General Procedure for the Synthesis of *N*-(Methyl(oxo)(phenyl)-λ^6-sulfaneylidene)benzamide (1a) from Benzoylhydrazine (a) and *NH*-Sulfoximine (1)

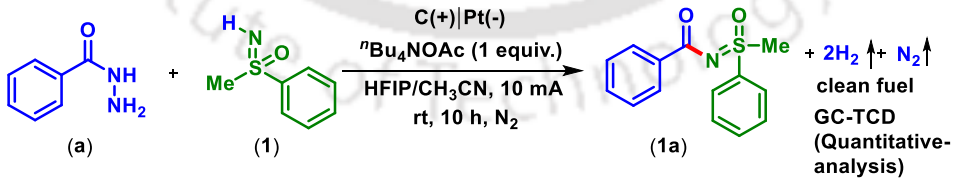

Scheme V.19. *Synthesis of N-(methyl(oxo)(phenyl)-λ^6-sulfaneylidene)benzamide (1a).*

To an oven-dried undivided three-necked flask (50 mL) equipped with a magnetic bar, was added benzoyl hydrazine (**a**) (68 mg, 0.5 mmol), and tetrabutylammonium acetate (^{n}Bu$_4$NOAc) (150.76 mg, 0.5 mmol). Then, the flask was equipped with the graphite rod (Φ 6

mm; immersion depth in solution about 15 mm) as the anode, the platinum plate (10 mm ×10 mm × 0.3 mm) as the cathode, maintaining a distance of 6 mm between the electrodes and was flushed with nitrogen (N_2). Then sulfoximine (**1**) (116.41 mg, 0.75 mmol, 1.5 equiv) in 1:4 ratios of 1,1,1,3,3,3-hexafluoro-2-propanol (HFIP) and acetonitrile (CH_3CN) (5 mL) was added via a syringe under nitrogen atmosphere. The reaction mixture was stirred and electrolyzed at a constant current of 10 mA and applied charge of 2 F/ mol at room temperature for 10 hours. After completion of the reaction (monitored by TLC analysis), the solvent was removed in vacuum, the mixture was admixed with ethyl acetate (25 mL), and the organic layer was washed with brine (1 x 10 mL). The organic layer was dried over anhydrous Na_2SO_4, and the solvent was evaporated under reduced pressure. The crude product was purified over a column of silica gel using 30% ethyl acetate in hexane to afford the *N*-(methyl(oxo)(phenyl)-λ^6-sulfaneylidene)benzamide (**1a**) in 71% yield (92 mg) (Scheme V.19). The identity and purity of the product were confirmed by spectroscopic analysis.

Reaction Set-up:

For the electrolysis, an undivided three-neck cell (40 mL), three rubber septa, a teflon-coated magnetic bar, a carbon rod (Φ 6 mm) as an anode, a platinum plate (10 mm × 10 mm × 0.3 mm) as a cathode and a dual display METRAVI RPS-6002 adjustable 60V/2A DC power supply were used (Figure V.14).

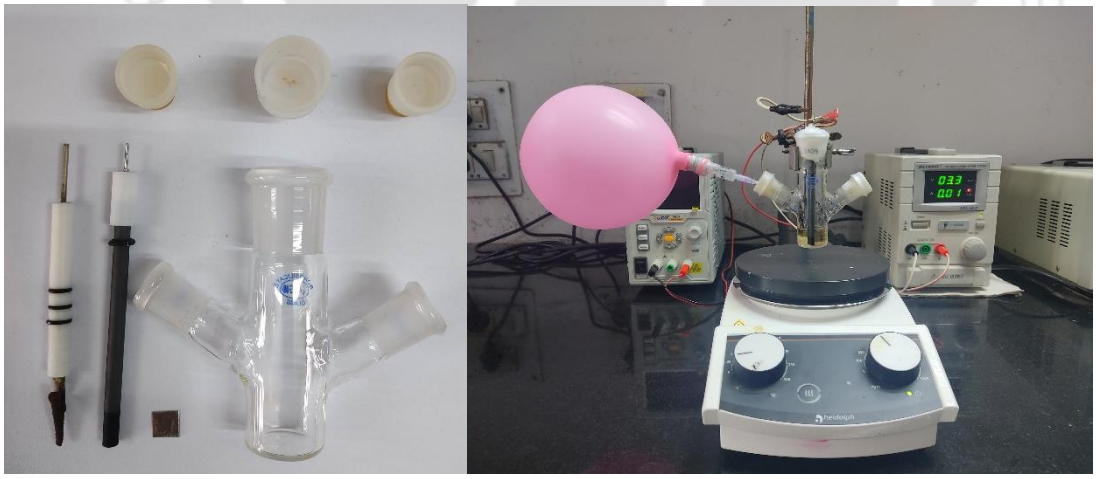

Figure V.14. *Electrochemical reaction set-up.*

V.7.6. General Procedure for 10 mmol Scale Reaction

To an oven-dried undivided two-necked flask (100 mL) equipped with a magnetic bar, was added benzoyl hydrazine (**a**) (1.36 g, 10 mmol), and tetrabutylammonium acetate ($^{n}Bu_4NOAc$) (3.01 g, 10 mmol). Then, the flask was equipped with the graphite rod (Φ 6 mm; immersion depth in solution about 15 mm) as the anode, the platinum plate (10 mm ×10 mm × 0.3 mm) as the cathode, maintaining a distance of 6 mm between the electrodes and was flushed with nitrogen (N_2). Then, sulfoximine (**1**) (2.32 g, 15 mmol, 1.5 equiv) in 1:4 ratios of 1,1,1,3,3,3-hexafluoro-2-propanol (HFIP) and acetonitrile (CH_3CN) (50 mL) was added via a syringe under N_2 atmosphere. The reaction mixture was stirred and electrolyzed at a constant current of 10 mA, and a charge of 2 F/ mol was under room temperature for 20 hours. After completion of the reaction (monitored by TLC analysis), the solvent was removed in a vacuum, the mixture was admixed with ethyl acetate (100 mL), and the organic layer was washed with brine (1 x 50 mL). The organic layer was dried over anhydrous Na_2SO_4, and the solvent was evaporated under reduced pressure. The crude product was purified over a column of silica gel using increasing 30% ethyl acetate in hexane to afford the *N*-(methyl(oxo)(phenyl)-λ^6-sulfaneylidene)benzamide (**1a**) in 62% yield (1.60 g). The identity and purity of the product were confirmed by spectroscopic analysis.

V.7.7. Post-synthetic Modification

(A) Procedure for the Synthesis of (Benzylimino)(methyl)(phenyl)- λ^6-sulfanone (1y)

A 10 mL Schlenk tube containing a stir bar was charged with *N*-(methyl(oxo)(phenyl)-λ^6-sulfaneylidene)benzamide (**1a**) (25.9 mg, 0.1 mmol, 1.0 equiv) under nitrogen atmosphere. Then BH_3 (2 M dimethyl sulfide solvent, 150 µL, 3.0 equiv) with THF (2.0 mL) was added via a syringe. The resulting mixture was stirred at room temperature for 24 hours. After completion of the reaction (monitored by TLC analysis), the reaction was quenched by H_2O (5 mL). The mixture was admixed with ethyl acetate (25 mL), and the organic layer was washed with brine (1 x 10 mL). The organic layer was dried over anhydrous Na_2SO_4, and the solvent was evaporated under reduced pressure. The crude product obtained was purified over a column of silica gel using 40% of EtOAc in hexane to afford the (benzylimino)(methyl)(phenyl)- λ^6-sulfanone (**1y**) in 76% yield (18.6 mg). The identity and purity of the product were confirmed by spectroscopic analysis.

(B) Procedure for the Synthesis of 2-Hydroxy-*N*-(methyl(oxo)(phenyl)-λ^6-sulfaneylidene)benzamide (1z)

A 10 mL Schlenk tube containing a stir bar was charged with *N*-(methyl(oxo)(phenyl)-λ^6-sulfaneylidene)benzamide (**1a**) (25.9 mg, 0.1 mmol, 1.0 equiv) $K_2S_2O_8$ (0.2 mmol, 54 mg), $Pd(OAc)_2$ (0.01 mmol, 2.24 mg), toluene (2 mL) and CF_3COOH (0.2 mmol, 0.0152 mL). Then the reaction mixture was refluxed for 24 h. After completion of the reaction (monitored by TLC analysis), cooled to room temperature. The mixture was admixed with ethyl acetate (25 mL), and the organic layer was washed with $NaHCO_3$ (1 x 10 mL). The organic layer was dried over anhydrous Na_2SO_4, and the solvent was evaporated under reduced pressure. The crude product was purified over a column of silica gel using 10% ethyl acetate in hexane to afford 2-hydroxy-*N*-(methyl(oxo)(phenyl)-λ^6-sulfaneylidene)benzamide (**1z**) in 60% yield (16.5 mg). The identity and purity of the product were confirmed by spectroscopic analysis.

V.7.8. Mechanistic Investigations

Radical-trapping Experiments

(i) To an oven-dried undivided three-necked flask (50 mL) equipped with a magnetic bar was added benzoyl hydrazine (**a**) (68 mg, 0.5 mmol), tetrabutylammonium acetate (^{n}Bu$_4$NOAc) (150.76 mg, 0.5 mmol) and (2,2,6,6-tetramethylpiperidin-1-yl)oxyl (TEMPO) (156 mg, 1.0 mmol, 2 equiv). Then, the flask was equipped with the graphite rod (Φ 6 mm; immersion depth in solution about 15 mm) as the anode, the platinum plate (10 mm ×10 mm × 0.3 mm) as the cathode, maintaining a distance of 6 mm between the electrodes and was flushed with nitrogen. Then sulfoximine (**1**) (116.41 mg, 0.75 mmol, 1.5 equiv) in 1:4 ratios of 1,1,1,3,3,3-hexafluoro-2-propanol (HFIP) and acetonitrile (CH_3CN) (5 mL) was added *via* a syringe under nitrogen atmosphere. The reaction mixture was stirred and electrolyzed at a constant current of 10 mA under room temperature for 10 h. After completion of the reaction (monitored by TLC analysis), the solvent was removed in vacuum, the mixture was admixed with ethyl acetate (25 mL), and the organic layer was washed with brine (10 mL). The organic layer was dried over anhydrous Na_2SO_4, and the solvent was evaporated under reduced pressure. The crude product obtained was purified over a column of silica gel using 10% ethyl acetate in hexane to afford the TEMPO-adduct, 2,2,6,6-tetramethylpiperidin-1-yl benzoate (**v**)

in 26% yield (34 mg) and <10% yield of *N*-(methyl(oxo)(phenyl)-λ^6-sulfaneylidene)benzamide (**1a**).

(ii) To an oven-dried undivided three-necked flask (50 mL) equipped with a magnetic bar was added benzoyl hydrazine (**a**) (68 mg, 0.5 mmol), tetrabutylammonium acetate (^{n}Bu$_4$NOAc) (150.76 mg, 0.5 mmol) and butylated hydroxytoluene (BHT) (220 mg, 1.0 mmol, 2 equiv). Then, the flask was equipped with the graphite rod (Φ 6 mm; immersion depth in solution about 15 mm) as the anode, the platinum plate (10 mm ×10 mm × 0.3 mm) as the cathode, maintaining a distance of 6 mm between the electrodes and was flushed with nitrogen. Then sulfoximine (**1**) (116.41 mg, 0.75 mmol, 1.5 equiv) in 1:4 ratios of 1,1,1,3,3,3-hexafluoro-2-propanol (HFIP) and acetonitrile (CH_3CN) (5 mL) was added via a syringe under nitrogen atmosphere. The reaction mixture was stirred and electrolyzed at a constant current of 10 mA under room temperature for 10 h. After completion of the reaction (monitored by TLC analysis), the solvent was removed in vacuum, the mixture was admixed with ethyl acetate (25 mL), and the organic layer was washed with brine (10 mL). The organic layer was dried over anhydrous Na_2SO_4, and the solvent was evaporated under reduced pressure. The crude product obtained was purified over a column of silica gel using 20% ethyl acetate in hexane to afford *N*-(methyl(oxo)(phenyl)-λ^6-sulfaneylidene)benzamide (**1a**) (Scheme S5) in <10% yield.

Electron Paramagnetic Resonance (EPR) Experiments

Figure V.15. *Reaction set-up for the EPR experiments.*

(i) The radical nature of both these coupling intermediates, *viz.* benzoyl and sulfoxamidoyl radicals has been further confirmed by electron paramagnetic resonance EPR measurements with spin-trapping regents, 5,5-dimethyl-1-pyrroline N-oxide (DMPO). To an oven-dried undivided three-necked flask (50 mL) equipped with a magnetic bar was added benzoyl hydrazine (**a**) (68 mg, 0.5 mmol), tetrabutylammonium acetate ($^{n}Bu_4NOAc$) (150.76 mg, 0.5 mmol). Then, the flask was equipped with the graphite rod (Φ 6 mm; immersion depth in solution about 15 mm) as the anode, the platinum plate (10 mm × 10 mm × 0.3 mm) as the cathode, maintaining a distance of 6 mm between the electrodes and was flushed with nitrogen. Then, 1:4 ratios of 1,1,1,3,3,3-hexafluoro-2-propanol (HFIP) and acetonitrile (CH_3CN) (5 mL) were added via a syringe under a nitrogen atmosphere. The reaction mixture was stirred and electrolyzed at a constant current of 10 mA under room temperature for 1 h. Then DMPO (50 μL, 0.8 equiv) was added into the cell (Scheme S6). After 10 minutes of further electrolysis, 500 μL of the reaction aliquot was taken in an electron paramagnetic resonance (EPR) tube, and the EPR signal was recorded at liquid nitrogen temperature.

(ii) To an oven-dried undivided three-necked flask (50 mL) equipped with a magnetic bar was added tetrabutylammonium acetate ($^{n}Bu_4NOAc$) (150.76 mg, 0.5 mmol). Then, the flask

was equipped with the graphite rod (Φ 6 mm; immersion depth in solution about 15 mm) as the anode, the platinum plate (10 mm × 10 mm × 0.3 mm) as the cathode, maintaining a distance of 6 mm between the electrodes and was flushed with nitrogen. Then sulfoximine (**1**) (116.41 mg, 0.75 mmol, 1.5 equiv) in a 1:4 ratio of 1,1,1,3,3,3-hexafluoro-2-propanol (HFIP) and acetonitrile (CH_3CN) (5 mL) was added via a syringe under a nitrogen atmosphere. The reaction mixture was stirred and electrolyzed at a constant current of 10 mA under room temperature for 1 hour. Then DMPO (50 μL, 0.8 equiv) was added into the cell (Scheme S7). After 10 minutes of further electrolysis, 500 μL of the reaction aliquot was taken in an electron paramagnetic resonance (EPR) tube, and the EPR signal was recorded at liquid nitrogen temperature.

(iii) To an oven-dried undivided three-necked flask (50 mL) equipped with a magnetic bar, was added benzoyl hydrazine (**a**) (68 mg, 0.5 mmol), and tetrabutylammonium acetate ($^nBu_4NOAc$) (150.76 mg, 0.5 mmol). Then, the flask was equipped with the graphite rod (Φ 6 mm; immersion depth in solution about 15 mm) as the anode, the platinum plate (10 mm × 10 mm × 0.3 mm) as the cathode, maintaining a distance of 6 mm between the electrodes and was flushed with nitrogen (N_2). Then sulfoximine (**1**) (116.41 mg, 0.75 mmol, 1.5 equiv) in a 1:4 ratio of 1,1,1,3,3,3-hexafluoro-2-propanol (HFIP) and acetonitrile (CH_3CN) (5 mL) was added via a syringe under nitrogen atmosphere. The reaction mixture was stirred and electrolyzed at a constant current of 10 mA under room temperature for 1 hour. Then DMPO (50 μL, 0.8 equiv) was added into the cell (Scheme S8). After 10 minutes of further electrolysis, 500 μL of the reaction aliquot was taken in an electron paramagnetic resonance (EPR) tube, and the EPR signal was recorded at liquid nitrogen temperature.

All the above results strongly supported the existence of benzoyl and sulfoximidoyl radicals in this electrochemical reaction.

Intermediate Detection Experiments

(I) Reaction with benzaldehyde

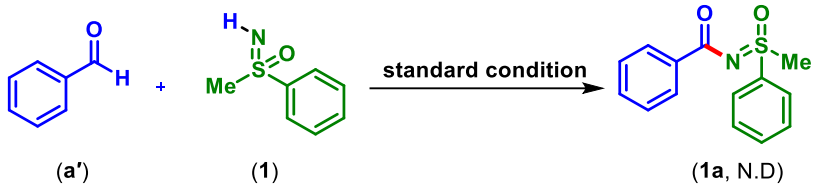

Scheme V.20. *Experiments with benzaldehyde.*

To an oven-dried undivided three-necked flask (50 mL) equipped with a magnetic bar was added tetrabutylammonium acetate ($^{n}Bu_4NOAc$) (150.76 mg, 0.5 mmol). Then the flask was equipped with the graphite rod (Φ 6 mm; immersion depth in solution about 15 mm) as the anode, the platinum plate (10 mm × 10 mm × 0.3 mm) as the cathode maintaining a distance of 6 mm between the electrodes and was flushed with nitrogen. Then benzaldehyde (**a′**) (53 mg, 0.5 mmol), and then sulfoximine (**1**) (116.41 mg, 0.75 mmol, 1.5 equiv) in 1:4 ratios of 1,1,1,3,3,3-hexafluoro-2-propanol (HFIP) and acetonitrile (CH_3CN) (5 mL) were added via a syringe under nitrogen atmosphere. The reaction mixture was stirred and electrolyzed at a constant current of 10 mA under room temperature for 10 h. The formation of *N*-(methyl(oxo)(phenyl)-λ^6-sulfaneylidene)benzamide (**1a**) was not detected (Scheme V.20), which suggested that aldehyde is not the intermediate of this reaction.

(II) Reaction with benzoic acid

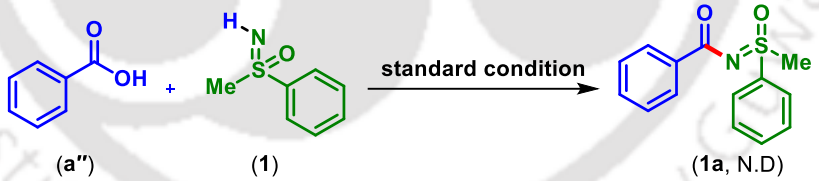

Scheme V.21. *Experiment with benzoic acid.*

To an oven-dried undivided three-necked flask (50 mL) equipped with a magnetic bar was added benzoic acid (**a″**) (61 mg, 0.5 mmol) and tetrabutylammonium acetate ($^{n}Bu_4NOAc$) (150.76 mg, 0.5 mmol). Then, the flask was equipped with the graphite rod (Φ 6 mm; immersion depth in solution about 15 mm) as the anode, the platinum plate (10 mm × 10 mm × 0.3 mm) as the cathode, maintaining a distance of 6 mm between the electrodes and was flushed with nitrogen. Then sulfoximine (**1**) (116.41 mg, 0.75 mmol, 1.5 equiv) in 1:4 ratios of 1,1,1,3,3,3-hexafluoro-2-propanol (HFIP) and acetonitrile (CH_3CN) (5 mL) were added via a syringe under nitrogen atmosphere. The reaction mixture was stirred and

electrolyzed at a constant current of 10 mA under room temperature for 10 h. The formation of *N*-(methyl(oxo)(phenyl)-λ^6-sulfaneylidene)benzamide (**1a**) was not detected (Scheme V.21), which suggested that benzoic acid is not the intermediate of this reaction.

(III) Reaction with benzamide

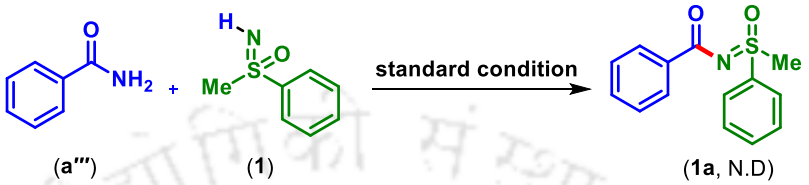

Scheme V.22. *Experiment with benzamide.*

To an oven-dried undivided three-necked flask (50 mL) equipped with a magnetic bar was added benzamide (**a‴**) (60 mg, 0.50 mmol) and tetrabutylammonium acetate (^{n}Bu$_4$NOAc) (150.76 mg, 0.5 mmol). Then the flask was equipped with the graphite rod (Φ 6 mm; immersion depth in solution about 15 mm) as the anode, the platinum plate (10 mm × 10 mm × 0.3 mm) as the cathode maintaining a distance of 6 mm between the electrodes and was flushed with nitrogen. Then sulfoximine (**1**) (116.41 mg, 0.75 mmol, 1.5 equiv) in 1:4 ratios of 1,1,1,3,3,3-hexafluoro-2-propanol (HFIP) and acetonitrile (CH_3CN) (5 mL) were added via a syringe under nitrogen atmosphere. The reaction mixture was stirred and electrolyzed at a constant current of 10 mA under room temperature for 10 h. The formation of *N*-(methyl(oxo)(phenyl)-λ^6-sulfaneylidene)benzamide (**1a**) was not detected (Scheme V.22), which suggested that benzamide is also not the intermediate of this reaction.

V.7.9. H_2 Gas Production Measurement Under the Standard Condition

A time-dependent hydrogen production electrolysis experiment was conducted under standard conditions using benzoyl hydrazine (**a**) (68 mg, 0.5 mmol), tetrabutylammonium acetate (^{n}Bu$_4$NOAc) (150.76 mg, 0.5 mmol). The flask was equipped with the graphite rod (Φ 6 mm) as the anode and the platinum plate (10 mm × 10 mm × 0.3 mm) as the cathode, maintaining a distance of 6 mm between the electrodes and was flushed with nitrogen. Then sulfoximine (**1**) (116.41 mg, 0.75 mmol, 1.5 equiv) in 1:4 ratios of 1,1,1,3,3,3-hexafluoro-2-propanol (HFIP) and acetonitrile (CH_3CN) (5 mL) was added via a syringe under nitrogen atmosphere. The reaction mixture was stirred and electrolyzed at a constant current of 10 mA under room temperature and was monitored for up to 10 hours (Scheme V.23). After every

hour, the evolved gas was syringed out from the headspace of the reaction mixture and injected into the PerkinElmer clarus-590 GC instrument using Elite Plot-Q column (30 m length x 530 µm x 20 µm ID) employing the following method: (Figure V.16). Then, the GC chromatogram was recorded and percent evaluation was calculated (Table-V.3).

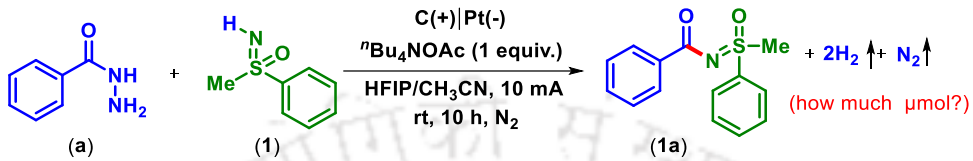

Scheme V.23. *Time-dependent hydrogen production reaction.*

Figure V.16. *Reaction set-up for the hydrogen gas (H_2) detection.*

TCD starting temperature: 40 °C

Oven temperature: 60 °C

Time at starting temperature: 0 min

Hold time: 5 min Ramp: 28 °C/ min up to 200 °C

Flow rate: 5 ml/ min (N_2)

Split ratio: 20

Inlet temperature: 40 °C

Detector temperature TCD: 200 °C

The detected gas chromatogram is shown in Figure V.17.

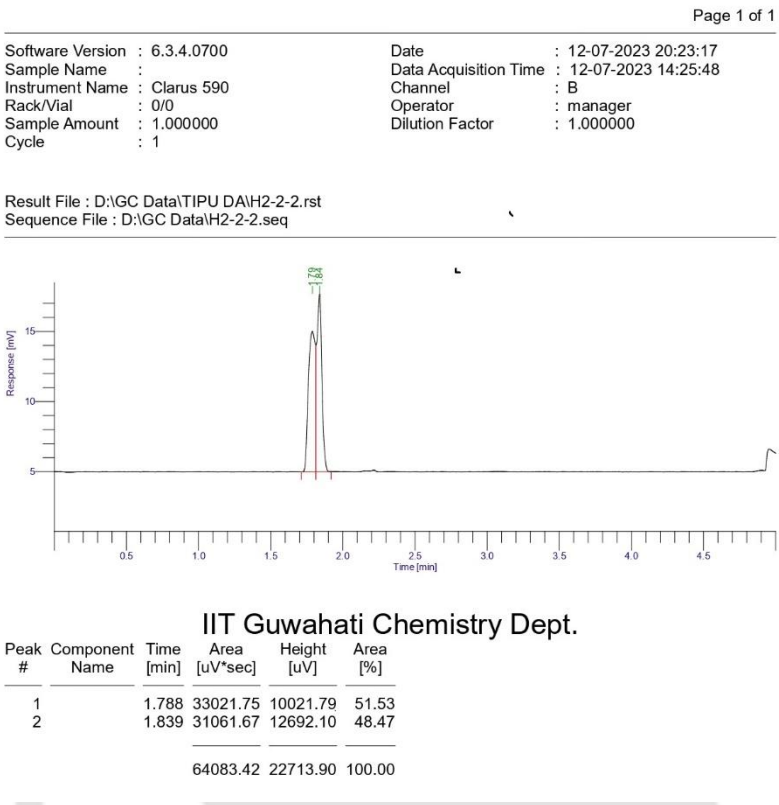

Figure V.17. *A representive chromatogram of evolved hydrogen gas during electrolysis*

Volume of gas syring: 1 mL.

Volume of headspace: 40 mL.

Standard hydrogen peak area: 522641.18

Standard hydrogen concentration: 44.6428 (μmol)

Table V.3. H_2 evaluation calculation:

Entry	Time (h)	Peak area	Concentration (μmol)	H_2 Produced (μmol)
1	1	32195.79	2.750089868	110.0035947
2	2	44162.56	3.772263666	150.8905466
3	3	64083.42	5.473857422	218.9542969
4	4	73206.52	6.25313151	250.1252604
5	5	83206.94	7.107344241	284.2937697
6	6	81918.11	6.997255366	279.8902146
7	7	83254.62	7.111416957	284.4566783
8	8	65051.76	5.556570784	222.2628314

9	9	58552.40	5.001410495	200.0564198
10	10	51505.30	4.399463523	175.9785409

The hydrogen production from the cathode reached a threshold value within 5 hours and remained steady for the next two hours. In the next three hours, the hydrogen production decreased. The quantity of hydrogen production is dependent on the overall oxidation of both these substrates (**a**) and (**1**) at the anode.

IV.7.10. Cyclic Voltammetry (CV) Experiments

Cyclic voltammetry experiments were performed using a Gamry instrument in a three-electrode cell connected to an undivided three-necked bottle with a stir bar under a nitrogen atmosphere at room temperature. The working electrode was a platinum electrode and the counter electrode was a platinum wire. The reference was a saturated calomel electrode submerged in a saturated aqueous KCl solution.

(i) Cyclic Voltammetry Studies of Benzoyl Hydrazine (a) to Explore the Reaction at the Anode

Test conditions: A cyclic voltammograms in solvent (5 mL) using platinum as the working electrode, Pt wire as the counter electrode, and saturated calomel electrode (SCE) as the reference electrode under N_2 atm. at room temperature (Figure V.18). The scan rate was 0.1 V/s.

Red line: 5 mL CH_3CN and $TBAPF_6$ (0.1 M).

Green line: 20 mM benzoyl hydrazine (**a**) with 5 mL CH_3CN solvent. The three oxidation peaks for (**a**) were observed at 1.5 V (vs SCE), 1.9 V (vs SCE), and 2.06 V (vs SCE).

Blue line: 20 mM benzoyl hydrazine (**a**) with 5 mL CH_3CN solvent. The addition of about 20 mM of tetrabutylammonium acetate, ($^nBu_4NOAc$) resulted in a cathodic shift of the first oxidation wave of ~400 mV to reach at ≈ 1.1 V vs SCE.

Cyan line to Green line: A stepwise addition of 40, 60, and 80 mM of $^nBu_4NOAc$ resulted in the overlapping of all the signals to a single peak and a continuous enhancement of the current.

Such a sharp change in the electrochemical behavior of benzoyl hydrazine (**a**) suggests the strong participation of $^{n}Bu_4NOAc$ during electrochemical oxidation.

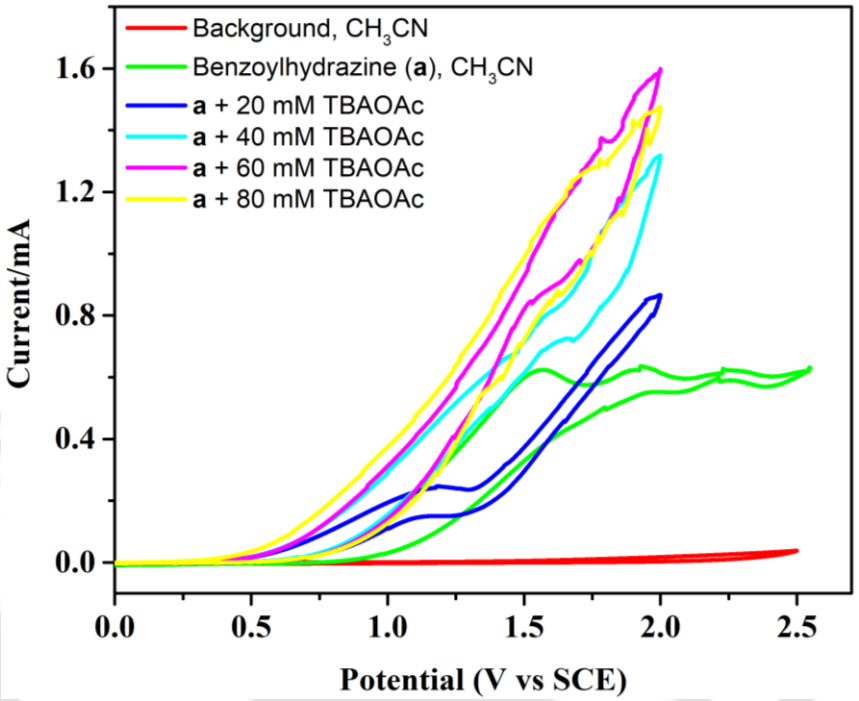

Figure V.18. *Cyclic voltammograms of benzoyl hydrazine (a).*

(ii) Cyclic Voltammetry Studies of Sulfoximine (1) to Explore the Reaction at the Anode

Test conditions: A cyclic voltammograms in solvent (5 mL) using platinum as the working electrode, Pt wire as the counter electrode, and saturated calomel electrode (SCE) as the reference electrode under N_2 atm. at room temperature (Figure V.19). The scan rate is 0.1 V/s.

Red line: 5 mL CH_3CN and $TBAPF_6$ (0.1 M).

Green line: 20 mM Sulfoximine (**1**) with 5 mL CH_3CN solvent. The oxidation peaks of (**1**) were observed at 2.13 V (vs SCE).

Blue line to Gray line: Upon sequential addition of $^{n}Bu_4NOAc$ 20, 40, 60, 80, and 100 mM to sulfoximine (**1**), causes a negligible shift in the onset potential but a substantial increase in the current.

This confirms the strong interaction between $^{n}Bu_4NOAc$ and (**1**) during the electrochemical oxidation.

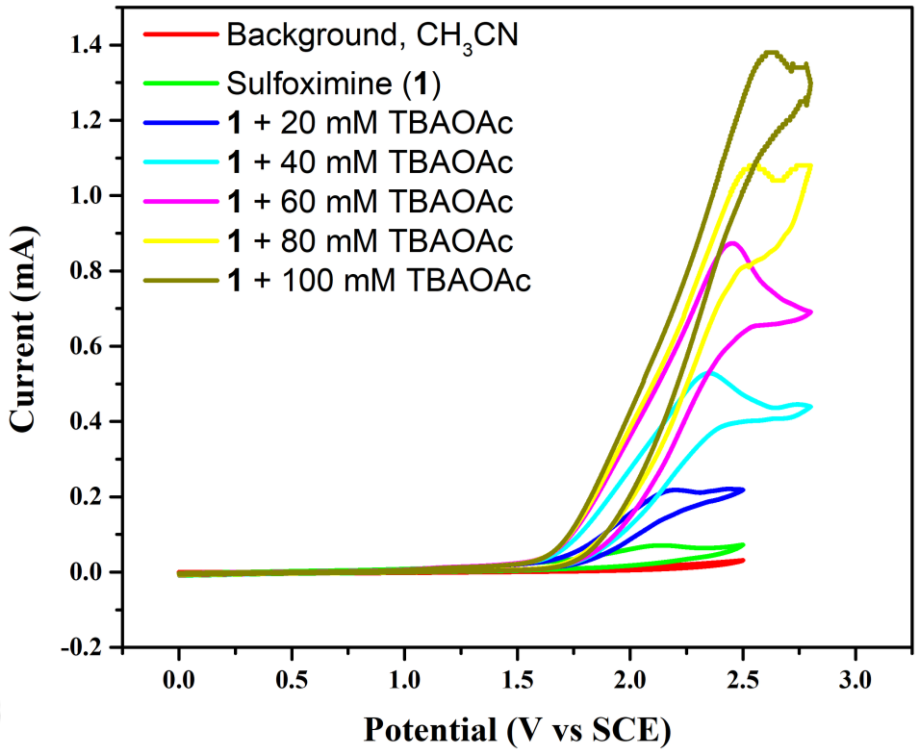

Figure V.19. *Cyclic voltammograms of sulfoximine (1).*

(iii) Cyclic Voltammetry Studies of Mixture of Benzoyl Hydrazine (a) and Sulfoximine (1) to Explore the Reaction at the Anode

Test conditions: A cyclic voltammograms in solvent (5 mL) by using platinum as the working electrode, Pt wire as the counter electrode, and saturated calomel electrode (SCE) as the reference electrode under N_2 atm. at room temperature (Figure V.20). The scan rate is 0.1 V/s.

Red line: 5 mL CH_3CN and $TBAPF_6$ (0.1 M).

Cyan line to Pink line: A similar titration with $^{n}Bu_4NOAc$ (20, 40, 60, and 80 mM) was performed in the presence of both the substrates (**a**) and (**1**). The CV measurements of the mixture show a new peak at 2.5V vs. SCE. The current and the peak position remained virtually unchanged, with an increase in the concentration of $^{n}Bu_4NOAc$.

Suggesting a strong association of electrolytes with both the reacting partners.

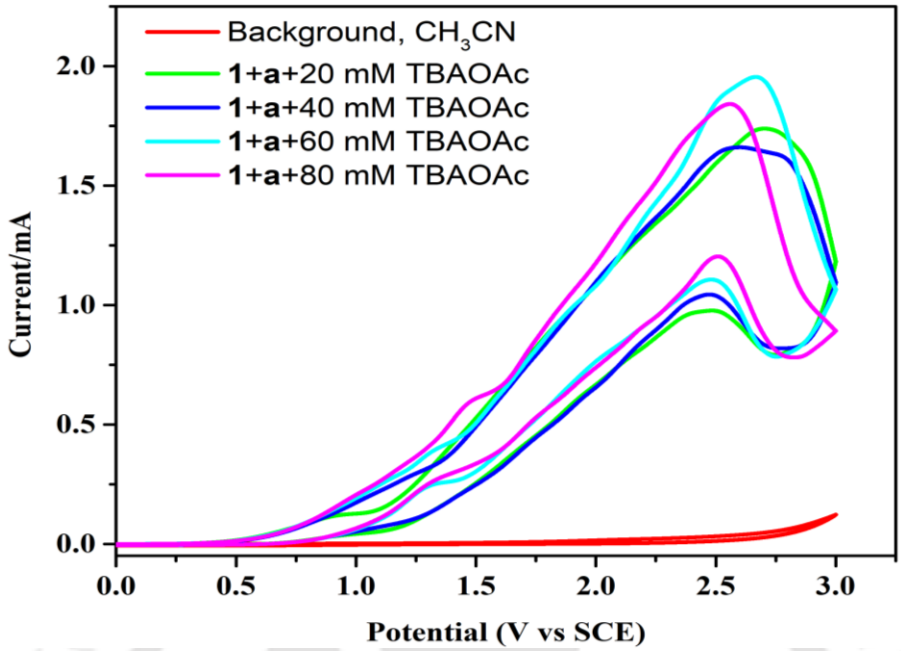

Figure V.20. *Cyclic voltammograms of benzoyl hydrazine (a) and sulfoximine (1).*

Work Potential Reaction Time Experiments

To monitor the effective potential applied to the working electrode during electrolysis under a 10 mA current, a parallel study of voltage over time was conducted under standard conditions. To an oven-dried undivided three-necked flask (50 mL) equipped with a magnetic bar, was added benzoyl hydrazine (**a**) (68 mg, 0.5 mmol), and tetrabutylammonium acetate ($^{n}Bu_4NOAc$) (150.76 mg, 0.5 mmol). Then, the flask was equipped with the graphite rod (Φ 6 mm; immersion depth in solution about 15 mm) as the anode, the platinum plate (10 mm × 10 mm × 0.3 mm) as the cathode, maintaining a distance of 6 mm between the electrodes and Ag/AgCl as the reference electrode, flushed with nitrogen (N_2). Then sulfoximine (**1**) (116.41 mg, 0.75 mmol, 1.5 equiv) in 1:4 ratios of 1,1,1,3,3,3-hexafluoro-2-propanol (HFIP) and acetonitrile (CH_3CN) (10 mL) was added via a syringe under nitrogen atmosphere. The reaction mixture was stirred and electrolyzed at a constant current of 10 mA under room temperature. The anodic working potential was measured every 5 minutes. In addition, the yield of (**1a**) was measured every 1 hour.

Constant Potential Experiment

To an oven-dried undivided three-necked flask (50 mL) equipped with a magnetic bar, was added benzoyl hydrazine (a) (68 mg, 0.5 mmol), and tetrabutylammonium acetate ($^{n}Bu_4NOAc$) (150.76 mg, 0.5 mmol). Then the flask was equipped with the graphite rod (Φ 6 mm; immersion depth in solution about 15 mm) as the anode, the platinum plate (10 mm × 10 mm × 0.3 mm) as the cathode maintaining a distance of 6 mm between the electrodes and Ag/AgCl as the reference electrode, flushed with nitrogen (N_2). Then sulfoximine (1) (116.41 mg, 0.75 mmol, 1.5 equiv) in 1:4 ratios of 1,1,1,3,3,3-hexafluoro-2-propanol (HFIP) and acetonitrile (CH_3CN) (10 mL) was added via a syringe under nitrogen atmosphere. The reaction mixture was stirred and electrolyzed at a constant potential of 1.7 V under room temperature for 10 h. After completion of the reaction (monitored by TLC analysis), the solvent was removed in vacuum, the mixture was admixed with ethyl acetate (25 mL), and the organic layer was washed with brine (1 x 10 mL). The organic layer was dried over anhydrous Na_2SO_4, and the solvent was evaporated under reduced pressure. The crude product was purified over a column of silica gel using 30% ethyl acetate in hexane to afford the *N*-(methyl(oxo)(phenyl)-λ^6-sulfaneylidene)benzamide (**1a**) in 18% yield.

V.8. References

[1] (a) Luecking, U. *Angew. Chem., Int. Ed*. **2013**, *52*, 9399–9408. (b) Frings, M.; Bolm, C.; Blum, A.; Gnamm, C. *Eur. J. Med. Chem*. **2017**, *126*, 225–245. (c) Boulard, E.; Zibulski, V.; Oertel, L.; Lienau, P.; Schäfer, M.; Ganzer, U. Lücking, U. *Chem.Eur. J*. **2020**, *26*, 4378–4388. (d) Sparks, T. C.; Watson, G. B.; Loso, M. R.; Geng, C.; Babcock, J. M.; Thomas, J. D. *Pestic. Biochem. Physiol*. **2013**, *107*, 1–7. (e) Watson, G. B.; Loso, M. R.; Babcock, J. M.; Hasler, J. M.; Letherer, T. J.; Young, C. D.; Zhu, Y.; Casida, J. E.; Sparks, T. C. *Insect. Biochem. Mol. Biol*. **2011**, *41*, 432–439.

[2] (a) Bolm, C.; Hackenberger, C. P. R.; Simić, O.; Verrucci, M.; Müller, D.; Bienewald, F. *Synthesis* **2002**, *7*, 879–887. (b) Hackenberger, C. P. R.; Raabe, G.; Bolm, C. *Chem.-Eur. J*. **2004**, *10*, 2942–2952.

[3] (a) Garimallaprabhakaran, A.; Harmata, M. *Synlett* **2011**, *3*, 361–364. (b) Noda, H.; Asada, Y.; Shibasaki, M.; Kumagai, N. *Chem. Commun*. **2017**, *53*, 7447–7450.

[4] (a) Bala, B. D.; Sharma, N.; Sekar, G. *RSC Adv*., **2016**, *6*, 97152–97159. (b) Guo, S.; Kumar, P. S.; Yuan, Y.; Yang. M. *Tetrahedron Lett*. 2017, **58**, 2681–2684. (c) Han, S. H.; Lee, K.; Noh, H. C.; Lee, P. H. *Asian J. Org. Chem*. **2021**, *10*, 1–10.

[5] (a) Banerjee, A.; Sarkar, S.; Shah, J. A.; Frederiks, N. C.; Bazan-Bergamino, E. A.; Johnson, C. J.; Ngai, M.-Y. *Angew. Chem. Int. Ed*. **2022**, *61*, e202113841. (b) Liu, J.; Liu, Q.; Yi, H.; Qin, C.; Bai, R.; Qi, X.; Lan, Y.; Lei, A. *Angew. Chem. Int. Ed*. **2014**, *53*, 502–506.

[6] (a) Braslau, R.; Anderson, M.O.; Rivera, F.; Jimenez, A.; Haddad, T.; Axon, J. R. *Tetrahedron* **2002**, *58*, 5513–5523. (b) Banerjee, A.; Lei, Z.; Ngai, M.-Y. *Synthesis* **2019**, *51*, 303–333.

[7] (a) Xie, S.; Su, L.; Mo, M.; Zhou, W.; Zhou, Y.; Dong, J. *J. Org. Chem*. **2021**, *86*, 739–749. (b) Xu, X.; Tang, Y.; Li, X.; Hong, G.; Fang, M.; Du, X. *J. Org. Chem*. **2014**, *79*, 446–451. (c) Amos, R. I. J.; Gourlay, B. S.; Yates, B. F.; Schiesser, C. H.; Lewis, T. W.; Smith, J. A. *Org. Biomol. Chem.*, **2013**, *11*, 170–176.

[8] (a) Yan, M.; Kawamata, Y.; Baran, P. S. *Chem. Rev*. **2017**, *117*, 13230–13319. (b) Xiong, P.; Xu, H.-C. *Acc. Chem. Res*. **2019**, *52*, 3339–3350. (c) Shi, S.-H.; Liang, Y.; Jiao, N. *Chem. Rev*. **2021**, *121*, 485–505. (d) Wang, Z.-H.; Gao, P.-S.; Wang, X.; Gao, J.-Q.; Xu, X.-T.; He, Z.; Ma, C.; Mei, T.-S. *J. Am. Chem. Soc.* **2021**, *143*, 15599–15605.

[9] Cantillo, D. *Chem. Commun*. **2022**, *58*, 619–628.

[10] (a) Yuan, Y.; Lei, A. *Acc. Chem. Res*. **2019**, *52*, 3309–3324. (b) Liu, Y.; Shi, B.; Liu, Z.; Gao, R.; Huang, C.; Alhumade, H.; Wang, S.; Qi, X.; Lei, A. *J. Am. Chem. Soc*. **2021**, *143*, 20863–20872. (c) Yuan, Y.; Yang, J.; Lei, A. *Chem. Soc. Rev.*, **2021**, *50*, 10058–10086. (d) Liu, X.; Yang, D.; Liu, Z.; Wang, Y.; Liu, Y.; Wang, S.; Wang, P.; Cong, H.; Chen, Y.-H.; Lu, L.; Qi, X.; Yi, H.; Lei, A. *J. Am. Chem. Soc*. **2023**, *145*, 3175–3186. (e) Yang, D.; Guan, Z.; Peng, Y.; Zhu, S.; Wang, P.; Huang, Z.; Alhumade, H.; Gu, D.; Yi, H.; Lei, A. *Nat. Commun* **2023**, *14*, 1476–1484.

[11] (a) Novaes, L. F. T.; Liu, J.; Shen, Y.; Lu, L.; Meinhardt, J. M.; Lin, S. *Chem. Soc. Rev*., **2021**, *50*, 7941–8002. (b) Han, J.; Haines, C. A.; Piane, J. J.; Filien, L. L.; Nacsa, E. D. *J. Am. Chem.Soc*. **2023**, *145*, 15680–15687.

[12] Harwood, S. J.; Palkowitz, M. D.; Gannett, C. N.; Perez, P.; Yao, Z.; Sun, L.; Abruña, H. D.; Anderson, S. L.; Baran, P. S. *Science* **2022**, *375*, 745–752.

[13] Sadowski, B.; Yuan, B.; Lin, Z.; Ackermann, L. *Angew. Chem. Int. Ed*. **2022**, *61*, e202117188.

[14] (a) Klein, M.; Waldvogel, S. R. *Angew. Chem. Int. Ed*. **2021**, *60*, 23197–23201. (b) Liu, D.; Liu, Z.-R.; Wang, Z.-H.; Ma, C.; Herbert, S.; Schirok, H.; Mei, T.-S. *Nat. Commun* **2022**, *13*, 7318–7327. (c) Panja, S.; Ahsan, S.; Pal, T.; Kolb, S.; Ali, W.; Sharma, S.; Das, C.; Grover, J.; Dutta, A.; Werz, D. B.; Paul, A.; and Maiti, D. *Chem. Sci.*, **2022**, *13*, 9432–9439. (d) Hamby, T. B.; LaLama, M. J.; Sevov, C. S. *Science*, **2022**, *376*, 410–416.

[15] Wang, H.; Gao, X.; Lv, Z.; Abdelilah, T.; Lei, A. *Chem. Rev*. **2019**, *119*, 6769–6787.

[16] (a) Zheng, H.; Liu, C.-H.; Guo, S.-Y.; He, G.-C.; Min, X.-T.; Zhou, B.-C.; Ji, D.-W.; Hu, Y.-C.; Chen, Q.-A. *Nat. Commun* **2022**, *13*, 3496–3506 (b) Sbei, N.; Martins, G. M.; Shirinfar, B.; Ahmed, N. *Chem. Rec*., **2020**, *20*, 1530–1552.

[17] Wimmer, A.; König, B. *Adv. Synth. Catal*. **2018**, *360*, 3277–3285.

[18] Wang, C.; Ma, D.; Tu, Y.; Bolm, C. *Org. Lett*. **2020**, *22*, 8937–8940.

[19] (a) Su, W.; Xu, P.; Petzold, R.; Yan, J.; Ritter, T. *Org. Lett*. **2023**, *25*, 1025–1029. (b) Wang, C.; Tu, Y.; Ma, D.; Tarint, C. A.; Bolm, C. *Org. Lett*. **2021**, *23*, 6891–6894. (c) Wang, H.; Zhang, D.; Bolm, C. *Angew. Chem. Int. Ed.* **2018**, *57*, 5863–5866. (d) Wang, C.; Tu, Y.; Ma, D.; Bolm, C. *Angew. Chem. Int. Ed*. **2020**, *59*, 14134–14137. (e) Wang, C.; Shi, P.; Bolm, C. *Org. Chem. Front*., **2021**, *8*, 2919–2923. (f) Tu, Y.; Shi, P.; Bolm, C. *Org. Lett*. **2022**, *24*, 907–911. (g) Dong, J.; Su, Q.; Li, D.; Mo, J. *Org. Lett*. **2022**, *24*, 8447–8451. (h) Chakraborty, N.; Rajbongshi, K. K.; Dahiya, A.; Das, B.; Vaishnanic, A.; Patel, B. K. *Chem. Commun*., **2023**, *59*, 2779–2782. (i) Yang, Y.-M.; Zhang, C.; Yang, H.; Tang, Z.-Y. *Chem. Commun*., **2022**, *58*, 8580–8583.

[20] (a) Zou, Y.; Peng, Z.; Dong, W.; An, D. *Eur. J. Org. Chem*. **2015**, 4913–4921. (b) Tu, Y.; Shi, P.; Bolm, C. *Org. Lett*. **2022**, *24*, 907–911. (c) Li, M.; Peng, M.; Huang, W.; Zhao, L.; Wang, S.; Kang, C.; Jiang, G.; Ji, F. *Org. Lett*. **2023**, *25*, 7529–7534.

[21] Cernak, T.; Dykstra, K. D.; Tyagarajan, S.; Vachal, P.; Krska, S. W. *Chem. Soc. Rev*., **2016**, *45*, 546–576.

[22] Wang, S.; Gao, Y.; Liu, Z.; Ren, D.; Sun, H.; Niu, L.; Yang, D.; Zhang, D.; Liang, X.; Shi, R.; Qi, X.; Lei, A. *Nat. Catal.* **2022**, *5*, 642−651.

[23] (a) Hu, X.; Zhang, G.; Nie, L.; Kong, T.; Lei, A. *Nat. Commun* **2019**, *10*, 5467. (b) Shi, Z.; Li, Y.; Li, N.; Wang, W.-Z.; Lu, H.-K.; Yan, H.; Yuan, Y.; Zhu, J.; Ye, K.-Y. *Angew. Chem. Int. Ed*. **2022**, *61*, e202206058. (c) Shi, Z.; Wang, W.-Z.; Li, N.; Yuan, Y.; Ye, K.-Y. *Org. Lett*. **2022**, *24*, 6321−6325.

[24] Yu, W.; Wang, S.; He, M.; Jiang, Z.; Yu, Y.; Lan, J.; Luo, J.; Wang, P.; Qi, X.; Wang, T.; Lei, A. *Angew. Chem. Int. Ed*. **2023**, *62*, e202219166.

[25] (a) Liu, M.-S.; Shu, W. *ACS Catal*. **2020**, *10*, 12960−12966. (b) Yadav, M. R.; Rit, R. K.; Sahoo, A. K. *Chem. Eur. J*. **2012**, *18*, 5541−5545.

V.9. Spectral Data

N-(Methyl(oxo)(phenyl)- λ⁶-sulfaneylidene)benzamide (1a):

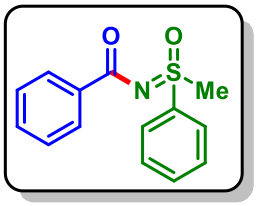

Yield: 71% (92 mg) as a white solid; Purified over a column of silica gel (30% EtOAc in hexane); ^{1}H NMR ($CDCl_3$, 600 MHz): δ 8.17 (d, 2H, J = 7.2 Hz), 8.05 (d, 2H, J = 7.8 Hz), 7.68 (t, 1H, J = 7.5 Hz), 7.61 (t, 2H, J = 7.5 Hz), 7.51 (t, 1H, J = 7.5 Hz), 7.41 (t, 2H, J = 7.5 Hz), 3.46 (s, 3H); ^{13}C{1H} NMR ($CDCl_3$, 150 MHz): δ 174.4, 139.2, 135.7, 133.9, 132.3, 129.9, 129.6, 128.2, 127.3, 44.5; IR (KBr, cm^{-1}): 3023, 2928, 1601, 1445, 970, 704; HRMS (ESI/Q-TOF) (m/z) calcd for $C_{14}H_{14}NO_2S$, $[M + H]^+$: 260.0740, found 260.0746.

***N-(Methyl(oxo)(p-tolyl)-λ⁶-sulfaneylidene)benzamide (2a)*:**

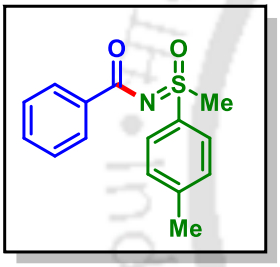

Yield: 75% (102.5 mg) as a white solid; Purified over a column of silica gel (30% EtOAc in hexane); ^{1}H NMR ($CDCl_3$, 600 MHz): δ 8.16 (d, 2H, J = 7.8 Hz), 7.92 (d, 2H, J = 8.4 Hz), 7.49 (t, 1H, J = 7.2 Hz), 7.41–7.37 (m, 4H), 3.44 (s, 3H), 2.44 (s, 3H); ^{13}C{^{1}H} NMR ($CDCl_3$, 150 MHz): δ 174.4, 145.0, 136.0, 135.8, 132.2, 130.4, 129.5, 128.1, 127.3, 44.6, 21.7; IR (KBr, cm^{-1}): 3018, 2853, 1609, 1275, 1030, 708; HRMS (ESI/Q-TOF) (m/z) calcd for $C_{15}H_{16}NO_2S$, $[M + H]^+$: 274.0896, found 274.0898.

***N-(Methyl(oxo)(o-tolyl)- λ⁶-sulfaneylidene)benzamide (3a)*:**

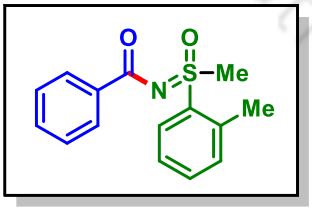

Yield: 73% (99.7 mg) as a white gummy solid; Purified over a column of silica gel (30% EtOAc in hexane); ^{1}H NMR ($CDCl_3$, 600 MHz): δ 8.15 (t, 3H, J = 10.5 Hz), 7.54–7.47 (m, 2H), 7.44–7.33 (m, 4H), 3.46 (s, 3H), 2.68 (s, 3H); ^{13}C{^{1}H} NMR ($CDCl_3$, 150 MHz): δ 174.1, 137.1, 137.0, 135.6, 133.8, 133.4, 132.3, 129.6, 129.3, 128.2, 127.2, 43.4, 20.7; IR (KBr, cm^{-1}): 3050, 2963, 1723, 1626, 1214, 708; HRMS (ESI/Q-TOF) (m/z) calcd for $C_{15}H_{16}NO_2S$, $[M + H]^+$: 274.0896, found 274.0899.

***N-((4-Methoxyphenyl)(methyl)(oxo)-λ⁶-sulfaneylidene)benzamide (4a)*:**

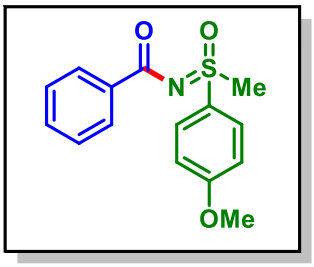

Yield: 70% (101 mg) as a white solid; Purified over a column of silica gel (30% EtOAc in hexane); ^{1}H NMR ($CDCl_3$, 600 MHz): δ 8.16 (d, 2H, J = 7.8 Hz), 7.96 (d, 2H, J = 8.4 Hz), 7.49 (t, 1H, J = 7.5 Hz), 7.40 (t, 2H, J = 7.5 Hz), 7.04 (d, 2H, J = 8.4 Hz), 3.86 (s, 3H), 3.44 (s, 3H); ^{13}C{^{1}H} NMR ($CDCl_3$, 150 MHz): δ 174.4, 164.0, 135.9, 132.2, 130.1, 129.5, 129.4, 128.1, 115.1, 55.9, 44.8; IR (KBr, cm^{-1}): 3005, 1608, 1248, 972, 825, 760; HRMS (ESI/Q-TOF) (m/z) calcd for $C_{15}H_{16}NO_3S$, $[M + H]^+$: 290.0845, found 290.0849.

***N-((3-Methoxyphenyl)(methyl)(oxo)-λ⁶-sulfaneylidene)benzamide (5a)*:**

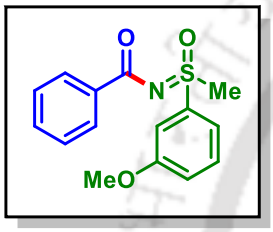

Yield: 63% (91 mg) as a white solid; Purified over a column of silica gel (30% EtOAc in hexane); ^{1}H NMR ($CDCl_3$, 600 MHz): δ 8.16 (d, 2H, J = 7.8 Hz), 7.59 (d, 1H, J = 7.8 Hz), 7.52 (s, 1H), 7.50–7.47 (m, 2H), 7.40 (t, 2H, J = 7.5 Hz), 7.17 (d, 1H, J = 7.2 Hz), 3.86 (s, 3H), 3.44 (s, 3H); ^{13}C{^{1}H} NMR ($CDCl_3$, 150 MHz): δ 174.4, 160.5, 140.3, 135.7, 132.3, 130.9, 129.5, 128.2, 120.1, 119.2, 112.2, 55.9, 44.5; IR (KBr, cm^{-1}): 3020, 2923, 1614, 1253, 1023, 715; HRMS (ESI/Q-TOF) (m/z) calcd for $C_{15}H_{16}NO_3S$, $[M + H]^+$: 290.0845, found 290.0853.

***N-((4-Fluorophenyl)(methyl)(oxo)-λ⁶-sulfaneylidene)benzamide (6a)*:**

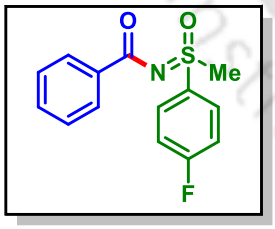

Yield: 75% (103.9 mg) as a white solid; Purified over a column of silica gel (30% EtOAc in hexane); ^{1}H NMR ($CDCl_3$, 600 MHz): δ 8.17 (d, 2H, J = 7.8 Hz), 8.10–8.08 (m, 2H), 7.54 (t, 1H, J = 7.5 Hz), 7.44 (t, 2H, J = 7.5 Hz), 7.30 (t, 2H, J = 8.1 Hz), 3.48 (s, 3H); ^{13}C{^{1}H} NMR ($CDCl_3$, 150 MHz): δ 174.3, 166.0 (d, J = 255.3 Hz), 135.5, 134.9 (d, J = 3.15 Hz), 132.4, 130.3 (d, J = 9.45 Hz), 129.6, 128.2, 117.2 (d, J = 22.6 Hz), 44.7; ^{19}F NMR ($CDCl_3$, 564 MHz): δ –103.3 (s) IR (KBr, cm^{-1}): 3025, 2918, 1625, 1272, 973, 709; HRMS (ESI/Q-TOF) (m/z) calcd for $C_{14}H_{13}FNO_2S$, $[M + H]^+$: 278.0646, found 278.0650.

***N-((3-Fluorophenyl)(methyl)(oxo)- λ⁶-sulfaneylidene)benzamide (7a)*:**

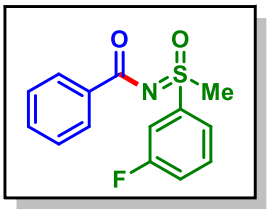

Yield: 68% (94.2 mg) as a white solid; Purified over a column of silica gel (30% EtOAc in hexane); ^{1}H NMR ($CDCl_3$, 600 MHz): δ 8.12 (d, 2H, J = 9 Hz), 7.81 (d, 1H, J = 9.6 Hz), 7.74 (d, 1H, J = 8.4 Hz), 7.59–7.54 (m, 1H), 7.49 (t, 1H, J = 8.7 Hz), 7.40–7.33 (m, 3H) 3.43 (s, 3H); ^{13}C{^{1}H} NMR ($CDCl_3$, 150 MHz): δ 174.4, 162.8 (d, J = 301.8 Hz), 141.3 (d, J = 8.1 Hz), 135.4, 132.5, 131.7 (d, J = 9.4 Hz), 129.6, 128.3, 123.1 (d, J = 4.0 Hz), 121.3 (d, J = 25.3 Hz), 114.9 (d, J = 29.8 Hz), 44.5; ^{19}F NMR ($CDCl_3$, 564 MHz): δ –108.2 (s); IR (KBr, cm^{-1}): 2928, 2858, 1614, 1476, 1215, 710; HRMS (ESI/Q-TOF) (m/z) calcd for $C_{14}H_{13}FNO_2S$, $[M + H]^+$: 278.0646, found 278.0645.

***N-((3-Chlorophenyl)(methyl)(oxo)- λ⁶ -sulfaneylidene)benzamide (8a)*:**

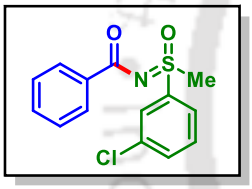

Yield: 70% (102.8 mg) as a white solid; Purified over a column of silica gel (30% EtOAc in hexane); ^{1}H NMR ($CDCl_3$, 600 MHz): δ 8.15 (d, 2H, J = 7.8 Hz), 8.02 (s, 1H), 7.92 (d, 1H, J = 7.8 Hz), 7.64 (d, 1H, J = 7.8 Hz), 7.55–7.50 (m, 2H), 7.41 (t, 2H, J = 7.8 Hz), 3.45 (s, 3H); ^{13}C{^{1}H} NMR ($CDCl_3$, 150 MHz): δ 174.3, 140.9, 136.1, 135.4, 134.1, 132.5, 131.1, 129.6, 128.2, 127.5, 125.5, 44.5; IR (KBr, cm^{-1}): 3028, 2931, 1611, 1217, 1067, 708; HRMS (ESI/Q-TOF) (m/z) calcd for $C_{14}H_{13}ClNO_2S$, $[M + H]^+$: 294.0350, found 294.0357.

***N-((2-Bromophenyl)(methyl)(oxo)- λ⁶-sulfaneylidene)benzamide (9a)*:**

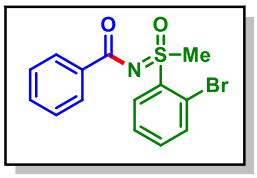

Yield: 63% (106.5 mg) as a white solid; Purified over a column of silica gel (30% EtOAc in hexane); ^{1}H NMR ($CDCl_3$, 600 MHz): δ 8.35 (d, 1H, J = 7.8 Hz), 8.13 (d, 2H, J = 7.2 Hz), 7.74 (d, 1H, J = 7.8 Hz), 7.60 (t, 1H, J = 7.5 Hz), 7.48–7.46 (m, 2H), 7.39 (t, 2H, J = 7.5 Hz), 3.58 (s, 3H); ^{13}C{^{1}H} NMR ($CDCl_3$, 150 MHz): δ 173.9, 138.0, 135.9, 135.3, 134.8, 132.3, 131.9, 129.7, 128.6, 128.1, 119.5, 42.0; IR (KBr, cm^{-1}): 3020, 2922, 1587, 1455, 1174, 713; HRMS

(ESI/Q-TOF) (m/z) calcd for $C_{14}H_{13}BrNO_2S$, $[M + H]^+$: 337.9845, found 337.9849.

***N-((4-Cyanophenyl)(methyl)(oxo)- λ⁶-sulfaneylidene)benzamide (10a)*:**

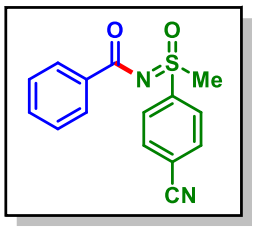

Yield: 62% (88 mg) as a white solid; Purified over a column of silica gel (30% EtOAc in hexane); ^{1}H NMR ($CDCl_3$, 600 MHz): δ 8.15 (d, 2H, J = 10.2 Hz), 8.12 (d, 2H, J = 9 Hz), 7.89 (d, 2H, J = 9.6 Hz), 7.53 (t, 1H, J = 9 Hz), 7.41 (t, 2H, J = 9 Hz), 3.45 (s, 3H); ^{13}C{^{1}H} NMR ($CDCl_3$, 150 MHz): δ 174.3, 143.7, 134.9, 133.6, 132.8, 129.6, 128.3, 128.2, 117.7, 117.2, 44.1; IR (KBr, cm^{-1}): 3095, 2933, 1625, 1215, 1094, 712; HRMS (ESI/Q-TOF) (m/z) calcd for $C_{15}H_{13}N_2O_2S$, $[M + H]^+$: 285.0692, found 285.0691.

***N-((4-Methylbenzyl)(oxo)(phenyl)- λ⁶-sulfaneylidene)benzamide (11a)*:**

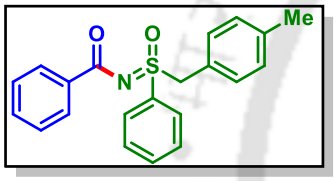

Yield: 70% (122.3 mg) as a white solid; Purified over a column of silica gel (30% EtOAc in hexane); ^{1}H NMR ($CDCl_3$, 600 MHz): δ 8.19 (d, 2H, J = 9 Hz), 7.72 (d, 2H, J = 9 Hz), 7.62 (t, 1H, J = 8.7 Hz), 7.51 (t, 1H, J = 9 Hz), 7.47 (t, 2H, J = 9 Hz), 7.42 (t, 2H, J = 9 Hz), 7.0 (d, 2H, J = 9 Hz), 6.89 (d, 2H, J = 9 Hz), 4.90 (d, 1H, J = 10.2 Hz), 4.82 (d, 1H, J = 12 Hz), 2.29 (s, 3H); ^{13}C{^{1}H} NMR ($CDCl_3$, 150 MHz): δ 174.7, 139.3, 136.1, 135.9, 133.9, 132.2, 131.3, 129.6, 129.4, 129.2, 128.7, 128.2, 124.4, 62.1, 21.4; IR (KBr, cm^{-1}): 2921, 2853, 1626, 1446, 1210, 713; HRMS (ESI/Q-TOF) (m/z) calcd for $C_{21}H_{20}NO_2S$, $[M + H]^+$: 350.1209, found 350.1212.

***N-(Isopropyl(oxo)(phenyl)- λ⁶-sulfaneylidene)benzamide (12a)*:**

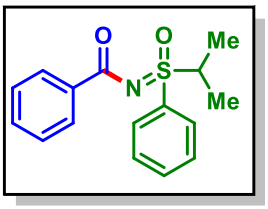

Yield: 55% (79 mg) as a yellow solid; Purified over a column of silica gel (30% EtOAc in hexane); ^{1}H NMR ($CDCl_3$, 600 MHz): δ 8.17 (d, 2H, J = 9.0 Hz), 7.93 (d, 2H, J = 9.0 Hz), 7.65 (t, 1H, J = 9.0 Hz), 7.58 (t, 2H, J = 9.3 Hz), 7.50 (t, 1H, J = 9.0 Hz), 7.40 (t, 2H, J = 9.0 Hz), 3.79–3.71 (m, 1H), 1.47 (d, 3H, J = 8.4 Hz), 1.31 (d, 3H, J = 7.8 Hz); ^{13}C{^{1}H} NMR ($CDCl_3$, 150 MHz): δ 174.2, 136.1, 134.9, 133.8, 132.1, 129.6, 128.9, 128.1, 56.5, 15.9, 15.5; IR (KBr, cm^{-1}): 3063, 2976, 1575, 1278, 1100, 704; HRMS (ESI/Q-

TOF) (m/z) calcd for $C_{16}H_{18}NO_2S$, $[M + H]^+$: 288.1053, found 288.1056.

***N-(Allyl(oxo)(phenyl)- λ⁶-sulfaneylidene)benzamide (13a)*:**

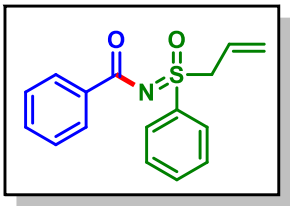

Yield: 64% (91 mg) as a yellow gummy solid; Purified over a column of silica gel (30% EtOAc in hexane); ^{1}H NMR ($CDCl_3$, 600 MHz): δ 8.19 (d, 2H, J = 9.0 Hz), 7.99 (d, 2H, J = 9.6 Hz), 7.67 (t, 1H, J = 8.7 Hz), 7.59 (t, 2H, J = 9.0 Hz), 7.51 (t, 1H, J = 8.7 Hz), 7.42 (t, 2H, J = 9.0 Hz), 5.75 (m, 1H), 5.33 (d, 1H, J = 6.6 Hz), 5.15 (d, 1H, J = 20.4 Hz), 4.46–4.42 (m, 1H), 4.33–4.29 (m, 1H); ^{13}C{^{1}H} NMR ($CDCl_3$, 150 MHz): δ 174.5, 136.5, 135.9, 134.0, 132.3, 129.6, 129.5, 128.6, 128.2, 125.9, 124.1, 60.4; IR (KBr, cm^{-1}): 3055, 2980, 1607, 1282, 924, 703; HRMS (ESI/Q-TOF) (m/z) calcd for $C_{16}H_{16}NO_2S$, $[M + H]^+$: 286.0896, found 286.0902.

***N-(Methyl(oxo)(thiophen-2-yl)- λ⁶-sulfaneylidene)benzamide (14a)*:**

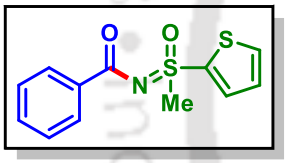

Yield: 69% (113 mg) as a white solid; Purified over a column of silica gel (30% EtOAc in hexane); ^{1}H NMR ($CDCl_3$, 600 MHz): δ 8.17–8.15 (m, 2H), 7.85–7.84 (m, 1H), 7.75–7.74 (m, 1H), 7.51 (t, 1H, J = 9.0 Hz), 7.42 (t, 2H, J = 9 Hz), 7.19–7.17 (m, 1H), 3.63 (s, 3H); ^{13}C{^{1}H} NMR ($CDCl_3$, 150 MHz): δ 174.2, 139.8, 135.5, 134.8, 133.9, 132.5, 129.6, 128.5, 128.2, 46.1; IR (KBr, cm^{-1}): 3096, 2918, 1616, 1278, 1016, 709; HRMS (ESI/Q-TOF) (m/z) calcd for $C_{12}H_{12}NO_2S_2$, $[M + H]^+$: 266.0304, found 266.0301.

***N-(5-Oxido-5 λ⁴-dibenzo[b,d]thiophen-5-ylidene)benzamide (15a)*:**

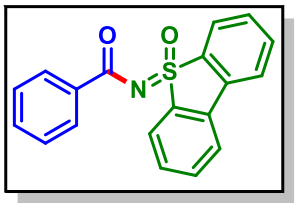

Yield: 63% (100.6 mg) as a white solid; Purified over a column of silica gel (30% EtOAc in hexane); ^{1}H NMR ($CDCl_3$, 400 MHz): δ 8.34 (d, 2H, J = 7.6 Hz), 8.14-8.11 (m, 2H), 7.84 (d, 2H, J = 7.6 Hz), 7.70–7.66 (m, 2H), 7.60–7.57 (m, 2H), 7.47–7.45 (m, 1H), 7.37 (t, 2H, J = 7.6 Hz); ^{13}C{^{1}H} NMR ($CDCl_3$, 100 MHz): δ 175.3, 137.4, 135.3, 134.6, 133.3, 132.5, 130.8, 129.8, 128.2, 125.8, 121.9; IR (KBr, cm^{-1}): 3058, 1628, 1449, 1273, 935, 753; HRMS (ESI/Q-

TOF) (m/z) calcd for $C_{19}H_{14}NO_2S$, $[M + H]^+$: 320.0740, found 320.0743.

***N-(5-Oxido-5 λ⁴-thianthren-5-ylidene)benzamide (16a)*:**

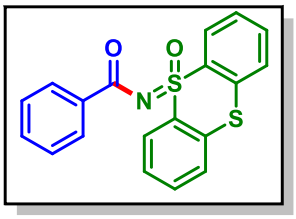

Yield: 60% (105.4 mg) as a white solid; Purified over a column of silica gel (30% EtOAc in hexane); ^{1}H NMR ($CDCl_3$, 400 MHz): δ 8.42–8.40 (m, 2H), 7.96–7.94 (m, 2H), 7.68–7.65 (m, 2H), 7.63–7.54 (m, 4H), 7.43–7.39 (m, 1H), 7.29 (t, 2H, J = 7.6 Hz); ^{13}C{^{1}H} NMR ($CDCl_3$, 100 MHz): δ 174.4, 135.5, 134.6, 133.1, 132.3, 132.2, 129.7, 129.0, 128.3, 128.1, 127.9; IR (KBr, cm^{-1}): 3060, 2924, 1628, 1226, 1048, 755; HRMS (ESI/Q-TOF) (m/z) calcd for $C_{19}H_{14}NO_2S_2$, $[M + H]^+$: 352.0460, found 352.0460.

***Methyl 4-(N-benzoyl-S-methylsulfonimidoyl)-2-((tert-butoxycarbonyl)amino)butanoate (17a)*:**

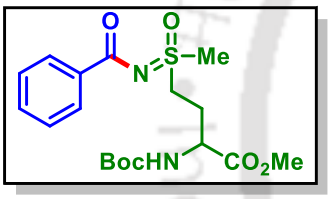

Yield: 43% (85.6 mg) as a white gummy solid; Purified over a column of silica gel (30% EtOAc in hexane); ^{1}H NMR ($CDCl_3$, 400 MHz): δ 8.10 (d, 2H, J = 8.0 Hz), 7.52–7.47 (m, 1H), 7.40 (t, 2H, J = 7.6 Hz), 5.30 (s, 1H), 4.45 (s, 1H), 3.77 (s, 3H), 3.69–3.49 (m, 2H), 3.36 (s, 3H), 2.55–2.45 (m, 1H), 2.29–2.22 (m, 1H), 1.44 (s, 9H) ; ^{13}C{^{1}H} NMR ($CDCl_3$, 100 MHz): δ 174.3, 171.7, 154.5, 135.5, 132.4, 129.5, 128.2, 80.9, 53.1, 52.2, 50.7, 40.0, 28.4, 25.5; IR (KBr, cm^{-1}): 2975, 1692, 1521, 1279, 987, 832; HRMS (ESI/Q-TOF) (m/z) calcd for $C_{18}H_{26}N_2O_6S$, $[M + Na]^+$: 421.1404, found 421.1404

***4-Methyl-N-(methyl(oxo)(phenyl)- λ⁶-sulfaneylidene)benzamide (1b)*:**

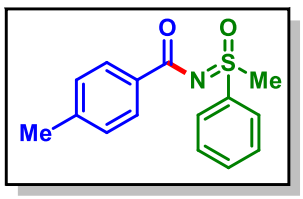

Yield: 71% (97 mg) as a white solid; Purified over a column of silica gel (30% EtOAc in hexane); ^{1}H NMR ($CDCl_3$, 600 MHz): δ 8.05 (t, 4H, J = 8.1 Hz), 7.66 (t, 1H, J = 7.5 Hz), 7.59 (t, 2H, J = 7.8 Hz), 7.20 (d, 2H, J = 8.4 Hz), 3.44 (s, 3H), 2.39 (s, 3H); ^{13}C{^{1}H} NMR ($CDCl_3$, 150 MHz): δ 174.4, 142.8, 139.3, 133.9, 133.1, 129.8, 129.7, 128.9, 127.3, 44.5, 21.8; IR (KBr, cm^{-1}): 3060, 2921,

1611, 1169, 925, 688; HRMS (ESI/Q-TOF) (m/z) calcd for $C_{15}H_{16}NO_2S$, $[M + H]^+$: 274.0896, found 274.0898.

***2-Methyl-N-(methyl(oxo)(phenyl)- λ⁶-sulfaneylidene)benzamide (1c)*:**

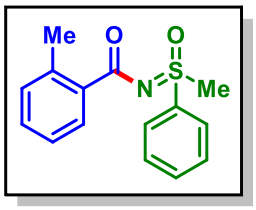

Yield: 52% (71 mg) as a white gummy solid; Purified over a column of silica gel (30% EtOAc in hexane); ^{1}H NMR ($CDCl_3$, 600 MHz): δ 8.07–8.04 (m, 3H), 7.68 (t, 1H, J = 7.5 Hz), 7.61 (t, 2H, J = 7.8 Hz), 7.35–7.32 (m, 1H), 7.24–7.19 (m, 2H), 3.43 (s, 3H), 2.59 (s, 3H); ^{13}C{^{1}H} NMR ($CDCl_3$, 150 MHz): δ 176.7, 139.5, 139.2, 135.4, 133.9, 131.7, 131.1, 130.7, 129.9, 127.3, 125.6, 44.7, 21.9; IR (KBr, cm^{-1}): 3065, 2963, 1723, 1626, 1214, 708; HRMS (ESI/Q-TOF) (m/z) calcd for $C_{15}H_{16}NO_2S$, $[M + H]^+$: 274.0896, found 274.0902.

***3-Methyl-N-(methyl(oxo)(phenyl)- λ⁶-sulfaneylidene)benzamide (1d)*:**

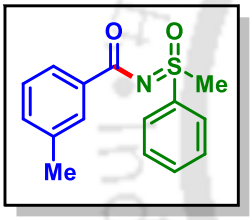

Yield: 56% (76.5 mg) as a yellow gummy solid; Purified over a column of silica gel (30% EtOAc in hexane); ^{1}H NMR ($CDCl_3$, 400 MHz): δ 8.06–8.04 (m, 2H), 7.98–7.95 (m, 2H), 7.70–7.65 (m, 1H), 7.62–7.58 (m, 2H), 7.33–7.27 (m, 2H), 3.46 (s, 3H), 2.39 (s, 3H); ^{13}C{^{1}H} NMR ($CDCl_3$, 100 MHz): δ 174.6, 139.3, 137.9, 135.7, 133.9, 133.1, 130.1, 129.8, 128.1, 127.3, 126.8, 44.5, 21.5; IR (KBr, cm^{-1}): 3069, 2930, 1626, 1445, 1223, 825; HRMS (ESI/Q-TOF) (m/z) calcd for $C_{15}H_{16}NO_2S$, $[M + H]^+$: 274.0896, found 274.0899.

***3,4-Dimethyl-N-(methyl(oxo)(phenyl)- λ⁶-sulfaneylidene)benzamide (1e)*:**

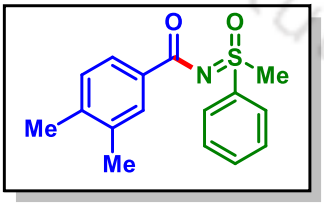

Yield: 62% (89 mg) as a white solid; Purified over a column of silica gel (30% EtOAc in hexane); ^{1}H NMR ($CDCl_3$, 600 MHz): δ 8.05–8.03 (m, 2H), 7.93 (d, 1H, J= 6 Hz), 7.91–7.89 (m, 1H), 7.68-7.65 (m, 1H), 7.61–7.58 (m, 2H), 7.16 (d, 1H, J= 6 Hz), 3.45 (s, 3H), 2.30 (s, 6H); ^{13}C{^{1}H} NMR ($CDCl_3$, 150 MHz): δ 174.6, 141.6, 139.3, 136.4, 133.9, 133.4, 130.7, 129.8, 129.5, 127.3, 127.2, 44.5, 20.1, 19.9; IR (KBr, cm^{-1}): 3020, 2856, 1603, 1225, 965,

761; HRMS (ESI/Q-TOF) (m/z) calcd for $C_{16}H_{18}NO_2S$, $[M + H]^+$: 288.1053, found 288.1052.

***4-(tert-Butyl)-N-(methyl(oxo)(phenyl)- λ⁶-sulfaneylidene)benzamide (1f)*:**

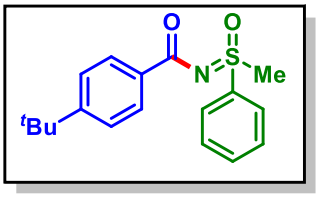

Yield: 69% (118.2 mg) as a white solid; Purified over a column of silica gel (30% EtOAc in hexane); ^{1}H NMR ($CDCl_3$, 600 MHz): δ 8.10 (d, 2H, J = 8.4 Hz), 8.04 (d, 2H, J = 7.8 Hz), 7.66 (t, 1H, J = 7.5 Hz), 7.59 (t, 2H, J = 7.8 Hz), 7.43 (d, 2H, J = 8.4 Hz), 3.4 (s, 3H), 1.33 (s, 9H); ^{13}C{^{1}H} NMR ($CDCl_3$, 150 MHz): δ 174.4, 155.9, 139.3, 133.9, 133.0, 129.8, 129.5, 127.3, 125.2, 44.5, 35.1, 31.4; IR (KBr, cm^{-1}): 2963, 1614, 1262, 957, 825, 778; HRMS (ESI/Q-TOF) (m/z) calcd for $C_{18}H_{22}NO_2S$, $[M + H]^+$: 316.1366, found 316.1370.

***N-(Methyl(oxo)(phenyl)- λ⁶-sulfaneylidene)-[1,1'-biphenyl]-4-carboxamide (1g)*:**

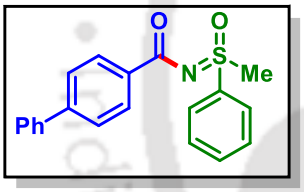

Yield: 79% (132.4 mg) as a white solid; Purified over a column of silica gel (30% EtOAc in hexane); ^{1}H NMR ($CDCl_3$, 600 MHz): δ 8.25 (d, 2H, J = 8.4 Hz), 8.07 (d, 2H, J = 7.2 Hz), 7.68–7.59 (m, 7H) 7.46 (t, 2H, J = 7.5 Hz), 7.38 (t, 1H, J = 7.5 Hz), 3.47 (s, 3H); ^{13}C{^{1}H} NMR ($CDCl_3$, 150 MHz): δ 174.2, 144.9, 140.4, 139.1, 134.6, 133.9, 130.1, 129.8, 128.9, 128.0, 127.4, 127.3, 126.9, 44.5; IR (KBr, cm^{-1}): 3005, 2923, 1606, 1285, 986, 749; HRMS (ESI/Q-TOF) (m/z) calcd for $C_{20}H_{18}NO_2S$, $[M + H]^+$: 336.1053, found 336.1053.

***4-Methoxy-N-(methyl(oxo)(phenyl)- λ⁶-sulfaneylidene)benzamide (1h)*:**

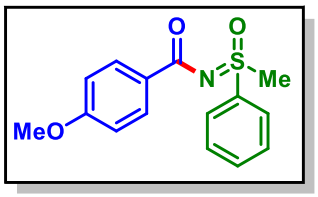

Yield: 72% (104 mg) as a white solid; Purified over a column of silica gel (30% EtOAc in hexane); ^{1}H NMR ($CDCl_3$, 600 MHz): δ 8.12 (d, 2H, J = 9.0 Hz), 8.04 (d, 2H, J = 7.8 Hz), 7.67 (t, 1H, J = 7.5 Hz), 7.60 (t, 2H, J = 7.5 Hz), 6.89 (d, 2H, J = 8.4 Hz), 3.84 (s, 3H). 3.45 (s, 3H); ^{13}C{^{1}H} NMR ($CDCl_3$, 150 MHz): δ 174.0, 163.1, 139.4, 133.9,

131.6, 129.8, 128.4, 127.3, 113.4, 55.6, 44.6; IR (KBr, cm^{-1}): 3023, 2928, 1600, 1259, 980, 750; HRMS (ESI/Q-TOF) (m/z) calcd for $C_{15}H_{16}NO_3S$, $[M + H]^+$: 290.0845, found 290.0845.

***4-Chloro-N-(methyl(oxo)(phenyl)- λ⁶-sulfaneylidene)benzamide (1i)*:**

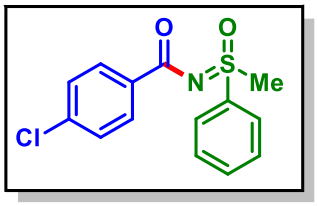

Yield: 66% (97 mg) as a white solid; Purified over a column of silica gel (30% EtOAc in hexane); ^1H NMR ($CDCl_3$, 600 MHz): δ 8.08 (d, 2H, J = 8.4 Hz), 8.02 (d, 2H, J = 7.8 Hz), 7.68 (t, 1H, J = 7.2 Hz), 7.60 (t, 2H, J = 7.5 Hz), 7.36 (d, 2H, J = 8.4 Hz), 3.45 (s, 3H); $^{13}C\{^1H\}$ NMR ($CDCl_3$, 150 MHz): δ 173.3, 138.8, 138.5, 134.2, 134.1, 131.0, 129.9, 128.4, 127.2, 44.5; IR (KBr, cm^{-1}): 3062, 2924, 1627, 1302, 985, 683; HRMS (ESI/Q-TOF) (m/z) calcd for $C_{14}H_{13}ClNO_2S$, $[M + H]^+$: 294.0350, found 294.0355.

***4-Bromo-N-(methyl(oxo)(phenyl)- λ⁶-sulfaneylidene)benzamide (1j)*:**

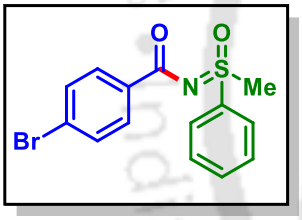

Yield: 70% (72 mg) as a white solid; Purified over a column of silica gel (30% EtOAc in hexane); ^1H NMR ($CDCl_3$, 600 MHz): δ 8.02 (t, 4H, J = 7.8 Hz), 7.68 (t, 1H, J = 7.5 Hz), 7.61 (t, 2H, J = 7.5 Hz), 7.53 (d, 2H, J = 8.4 Hz), 3.45 (m, 1H); $^{13}C\{^1H\}$ NMR ($CDCl_3$, 150 MHz): δ 173.5, 138.9, 134.7, 134.1, 131.4, 131.2, 129.9, 127.3 127.2, 44.5; IR (KBr, cm^{-1}): 3033, 2928, 1626, 1446, 1269, 740; HRMS (ESI/Q-TOF) (m/z) calcd for $C_{14}H_{13}BrNO_2S$, $[M + H]^+$: 337.9845, found 337.9845.

***N-(Methyl(oxo)(phenyl)- λ⁶-sulfaneylidene)-4-(trifluoromethyl)benzamide (1k)*:**

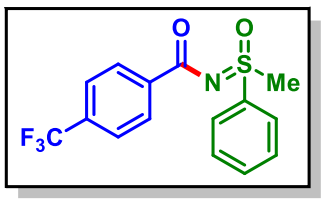

Yield: 75% (98 mg) as a white solid; Purified over a column of silica gel (30% EtOAc in hexane); ^1H NMR ($CDCl_3$, 500 MHz): δ 8.26 (d, 2H, J = 8.0 Hz), 8.04 (d, 2H, J = 7.5 Hz), 7.70 (t, 1H, J = 7.25 Hz), 7.66–7.60 (m, 4H), 3.48 (s, 3H); $^{13}C\{^1H\}$ NMR ($CDCl_3$, 125 MHz): δ 173.0, 139.0, 138.8, 134.2, 133.7 (q, J = 32.125, 32.4 Hz), 129.9 (d, J = 3.12 Hz), 125.2 (q, J = 3.6, 3.12 Hz), 123.0, 120.9, 44.54; ^{19}F NMR ($CDCl_3$, 471 MHz): δ –62.9 (s). IR (KBr, cm^{-1}): 3025, 2926, 1581, 1409, 1095, 774; HRMS (ESI/Q-TOF)

(m/z) calcd for $C_{15}H_{13}F_3NO_2S$, $[M + H]^+$: 328.0614, found 328.0620.

N-(Methyl(oxo)(phenyl)- λ⁶-sulfaneylidene)-1-naphthamide (1l):

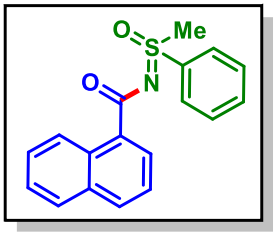

Yield: 65% (100.5 mg) as a colorless viscous liquid; Purified over a column of silica gel (30% EtOAc in hexane); ^{1}H NMR ($CDCl_3$, 600 MHz): δ, 9.00 (d, 1H, J = 10.8 Hz), 8.36–8.35 (m, 1H), 8.10 (d, 2H, J = 6 Hz), 7.96 (d, 1H, J = 6 Hz), 7.85 (d, 1H, J = 6 Hz), 7.69 (t, 1H, J = 6 Hz), 7.62 (t, 2H, J = 6 Hz), 7.55–7.52 (m, 1H), 7.50–7.47 (m, 2H), 3.49 (s, 3H); ^{13}C{^{1}H} NMR ($CDCl_3$, 150 MHz): δ 176.7, 139.1, 134.1, 134.0, 133.0, 132.6, 131.5, 130.0, 129.9, 128.5, 127.4, 127.3, 126.6, 126.1, 124.7, 44.7; IR (KBr, cm^{-1}): 3054, 2930, 1612, 1297, 973, 731; HRMS (ESI/Q-TOF) (m/z) calcd for $C_{18}H_{16}NO_2S$, $[M + H]^+$: 310.0896, found 310.0900.

N-(Methyl(oxo)(phenyl)- λ⁶-sulfaneylidene)-2-naphthamide (1m):

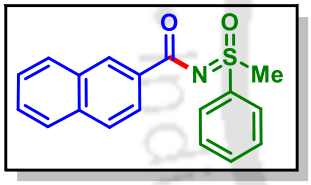

Yield: 75% (106.7 mg) as a white solid; Purified over a column of silica gel (30% EtOAc in hexane); ^{1}H NMR ($CDCl_3$, 500 MHz): δ 8.75 (s, 1H), 8.21 (d, 1H, J = 8.5 Hz), 8.09 (d, 2H, J = 7.5 Hz), 7.95 (d, 1H, J = 8.0 Hz), 7.86–7.84 (m, 2H), 7.68 (t, 1H, J = 7.2 Hz), 7.61 (t, 2H, J = 7.5 Hz), 7.53 (m, 2H), 3.50 (s, 3H); ^{13}C{^{1}H} NMR ($CDCl_3$, 125 MHz): δ 174.5, 139.2, 135.5, 133.9, 133.1, 132.8, 130.7, 129.8, 129.5, 127.9, 127.8, 127.7, 127.3, 126.4, 125.8, 44.5; IR (KBr, cm^{-1}): 3028, 2926, 1607, 1349, 1102, 763; HRMS (ESI/Q-TOF) (m/z) calcd for $C_{18}H_{16}NO_2S$, $[M + H]^+$: 310.0896, found 310.0896.

***N-(Methyl(oxo)(phenyl)- λ⁶-sulfaneylidene)benzofuran-2-carboxamide (1n)*:**

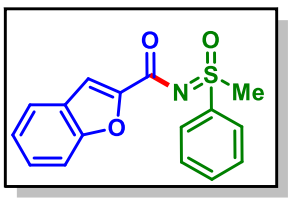

Yield: 68% (101.7 mg) as a colorless solid; Purified over a column of silica gel (30% EtOAc in hexane); ^{1}H NMR ($CDCl_3$, 400 MHz): δ 8.08-8.06 (m, 2H), 7.72–7.67 (m, 1H), 7.66–7.57 (m, 4H), 7.52 (d, 1H, J = 0.8 Hz), 7.42–7.38 (m, 1H), 7.28–7.24 (m, 1H), 3.52 (s, 3H); ^{13}C{^{1}H} NMR ($CDCl_3$, 100 MHz): δ 166.4, 155.8, 151.1, 138.7, 134.2, 129.9, 127.7, 127.4, 127.2, 123.6, 122.8, 112.9,

112.2, 44.7; IR (KBr, cm^{-1}): 3023, 2928, 1611, 1175, 902, 739; HRMS (ESI/Q-TOF) (m/z) calcd for $C_{16}H_{14}NO_3S$, $[M + H]^+$: 300.0689, found 300.0693.

N-(Methyl(oxo)(phenyl)- λ⁶-sulfaneylidene)furan-2-carboxamide (1o):

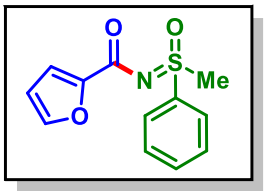

Yield: 65% (81 mg) as a white solid; Purified over a column of silica gel (30% EtOAc in hexane); ^1H NMR ($CDCl_3$, 500 MHz): δ 8.03 (d, 2H, J = 8.0 Hz), 7.67 (t, 1H, J = 7.25 Hz), 7.60 (t, 2H, J = 7.7 Hz), 7.52 (s, 1H), 7.16 (d, 1H, J = 7.0 Hz), 6.46 (s, 1H), 3.46 (s, 3H); $^{13}C\{^1H\}$ NMR ($CDCl_3$, 125 MHz): δ 165.4, 150.2, 145.7, 138.9, 134.1, 129.9, 127.3, 116.9, 111.9, 44.7; IR (KBr, cm^{-1}): 2923, 1609, 1465, 1186, 1085, 750; HRMS (ESI/Q-TOF) (m/z) calcd for $C_{12}H_{12}NO_3S$, $[M + H]^+$: 250.0532, found 250.0533.

N-(Methyl(oxo)(phenyl)- λ⁶-sulfaneylidene)thiophene-2-carboxamide (1p):

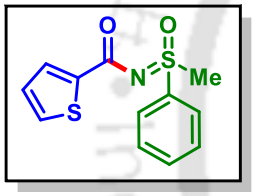

Yield: 60% (79.6 mg) as a white solid; Purified over a column of silica gel (25% EtOAc in hexane); ^1H NMR ($CDCl_3$, 600 MHz): δ 8.05–8.03(m, 2H), 7.79 (dd, 1H, J = 1.2, 1.2 Hz), 7.68 (t, 1H, J = 7.5 Hz), 7.61 (t, 2H, J = 7.8 Hz), 7.48 (dd, 1H, J = 1.2, 0.6 Hz), 7.06–7.05 (m, 1H), 3.45 (s, 3H) ; $^{13}C\{^1H\}$ NMR ($CDCl_3$, 150 MHz): δ 169.1, 141.3, 138.9, 134.1, 132.3, 131.7, 129.9, 127.9, 127.4, 44.6; IR (KBr, cm^{-1}): 3075, 2923, 1606, 1271, 985, 748; HRMS (ESI/Q-TOF) (m/z) calcd for $C_{12}H_{11}NO_2S_2$, $[M + Na]^+$: 288.0123, found 288.0124.

***N-(Methyl(oxo)(phenyl)- λ⁶-sulfaneylidene)hexanamide (1q)*:**

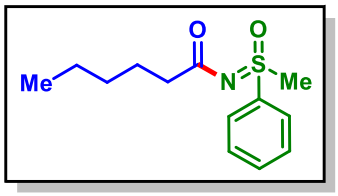

Yield: 22% (27.8 mg) as a white solid; Purified over a column of silica gel (35% EtOAc in hexane); ^1H NMR ($CDCl_3$, 600 MHz): δ 7.96 (d, 2H, J = 8.4 Hz), 7.65 (t, 1H, J = 8.7 Hz), 7.58 (t, 2H, J = 9.3 Hz), 3.32 (s, 3H), 2.38 (t, 2H, J = 9.0 Hz), 1.65–1.60 (m, 2H), 1.31–1.29 (m, 4H), 0.87 (t, 3H, J = 7.8 Hz); $^{13}C\{^1H\}$ NMR ($CDCl_3$, 150 MHz): δ 183.2, 139.2, 133.8, 129.8, 127.2, 44.3, 39.8, 31.6, 25.4, 22.6, 14.1; IR (KBr, cm^{-1}): 2928, 1618, 1446, 982, 891, 747;

HRMS (ESI/Q-TOF) (m/z) calcd for $C_{13}H_{20}NO_2S$, $[M + H]^+$: 254.1209, found 254.1214.

4-(N,N-Dipropylsulfamoyl)-N-(methyl(oxo)(phenyl)- λ⁶-sulfaneylidene)benzamide (1u):

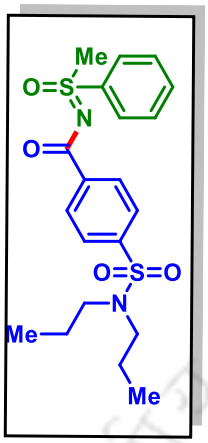

Yield: 54% (114 mg) as a colorless viscous liquid; Purified over a column of silica gel (20% EtOAc in hexane); ^{1}H NMR ($CDCl_3$, 600 MHz): δ 8.24 (d, 2H, J = 9.0 Hz), 8.03 (d, 2H, J = 7.8 Hz), 7.81 (d, 2H, J = 8.4 Hz), 7.69 (t, 1H, J = 7.2 Hz), 7.61 (t, 2H, J = 7.5 Hz), 3.47 (s, 3H), 3.07–3.05 (m, 4H), 1.54–1.48 (m, 4H), 0.84 (t, 6H, J = 7.5 Hz); ^{13}C{^{1}H} NMR ($CDCl_3$, 150 MHz): δ 172.8, 143.3, 139.1, 138.6, 134.2, 130.1, 129.9, 127.2, 126.8, 50.1, 44.5, 22.0, 11.3; IR (KBr, cm^{-1}): 3058, 2930, 2855, 1626, 1356, 741; HRMS (ESI/Q-TOF) (m/z) calcd for $C_{20}H_{27}N_2O_4S_2$, $[M + H]^+$: 423.1407, found 423.1408.

4-(N-Benzoyl-S-methylsulfonimidoyl)benzyl 4-(N,N-dipropylsulfamoyl)benzoate (20a):

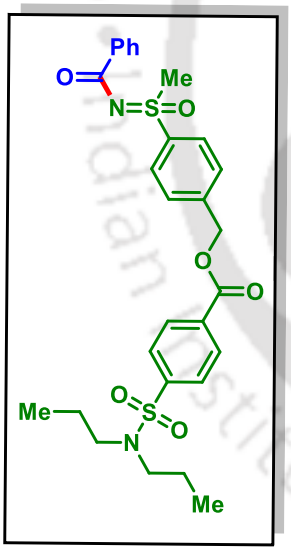

Yield: 48% (133.6 mg) as a colorless viscous liquid; Purified over a column of silica gel (40% EtOAc in hexane); ^{1}H NMR ($CDCl_3$, 600 MHz): δ 8.17 (d, 2H, J = 8.4 Hz), 8.13 (d, 2H, J = 7.2 Hz), 8.05 (d, 2H, J = 8.4 Hz), 7.87 (d, 2H, J = 8.4 Hz), 7.65 (d, 2H, J = 8.4 Hz), 7.48 (t, 1H, J = 7.2 Hz), 7.38 (t, 2H, J = 7.8 Hz), 5.44 (s, 2H), 3.43 (s, 3H), 3.08–3.06 (m, 4H), 1.55–1.48 (m, 4H), 0.84 (t, 6H, J = 7.5 Hz); ^{13}C{^{1}H} NMR ($CDCl_3$, 150 MHz): δ 174.3, 164.9, 144.8, 141.9, 139.0, 135.5, 132.9, 132.3, 130.5, 129.5, 129.2, 128.1, 127.7, 127.2, 66.0, 50.0, 44.4, 22.0, 11.2; IR (KBr, cm^{-1}): 3012, 2989, 1739, 1636, 1364, 721; HRMS (ESI/Q-TOF) (m/z) calcd for $C_{28}H_{33}N_2O_6S_2$, $[M + H]^+$: 557.1775, found 557.1779.

***(1R,2S,5R)-2-Isopropyl-5-methylcyclohexyl-2-(4-(N-benzoyl-S-methylsulfonimidoyl)phenyl)acetate (21a)*:**

Yield: 69% (157 mg) as a white solid; Purified over a column of silica gel (40% EtOAc in hexane); ^{1}H NMR ($CDCl_3$, 600 MHz): δ 8.14 (d, 2H, J = 9.0 Hz), 7.99 (d, 2H, J

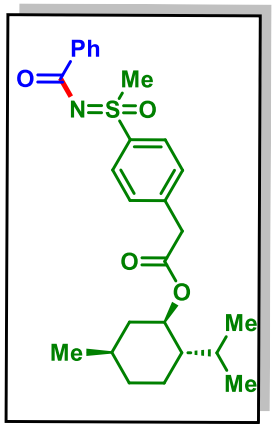

= 10.2 Hz), 7.51–7.47 (m, 3H), 7.39 (t, 2H, *J* = 9.0 Hz), 4.70–4.65 (m, 1H), 3.69 (s, 2H), 3.44 (s, 3H), 1.96–1.94 (m, 1H), 1.72–1.65 (m, 1H), 1.64–1.63 (m, 2H), 1.46–1.44 (m, 1H), 1.42–1.32 (m, 1H), 1.03–0.92 (m, 3H), 0.88 (d, 3H, *J* = 7.8 Hz), 0.84 (d, 3H, *J* = 9.0 Hz), 0.69 (d, 3H, *J* = 8.4 Hz); $^{13}C\{^{1}H\}$ NMR ($CDCl_3$, 150 MHz): *δ* 174.3, 170.0, 140.9, 137.7, 135.7, 132.3, 130.7, 129.5, 128.1, 127.5, 75.5, 47.0, 44.5, 41.5, 40.8, 34.2, 31.5, 26.4, 23.5, 22.1, 20.8, 16.4; IR (KBr, cm^{-1}): 2937, 2857, 1741, 1612, 1215, 745; HRMS (ESI/Q-TOF) (m/z) calcd for $C_{26}H_{34}NO_4S$, $[M + H]^+$: 456.2203, found 456.2203.

(2S)-1,7,7-Trimethylbicyclo[2.2.1]heptan-2-yl-2-(4-(N-benzoyl-S-methylsulfonimidoyl)phenyl)acetate (22a):

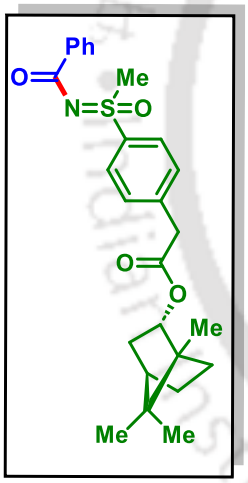

Yield: 68% (79 mg) as a colorless viscous liquid; Purified over a column of silica gel (20% EtOAc in hexane); ^{1}H NMR ($CDCl_3$, 600 MHz): *δ* 8.15 (d, 2H, *J* = 9.0 Hz), 8.01 (d, 2H, *J* = 9.6 Hz), 7.54–7.48 (m, 3H), 7.40 (t, 2H, *J* = 9.0 Hz), 4.91–4.89 (m, 1H), 3.74 (s, 2H), 3.45 (s, 3H), 2.36–2.31 (m, 1H), 1.84–1.79 (m, 1H), 1.76–1.69 (m, 1H), 1.67 (m, 1H), 1.31–1.20 (m, 1H), 1.19–1.14 (m, 1H), 0.94–0.91 (m, 1H), 0.88 (s, 3H), 0.86 (s, 3H), 0.79 (d, 3H, *J* = 7.8 Hz); $^{13}C\{^{1}H\}$ NMR ($CDCl_3$, 150 MHz): *δ* 174.4, 170.7, 140.9, 137.8, 135.7, 132.3, 130.8, 129.6, 128.2, 127.6, 81.2, 49.0, 48.0, 44.9, 44.5, 41.6, 36.9, 28.1, 27.2, 19.8, 18.9, 13.7; IR (KBr, cm^{-1}): 2927, 2841, 1712, 1618, 1260, 749; HRMS (ESI/Q-TOF) (m/z) calcd for $C_{26}H_{32}NO_4S$, $[M + H]^+$: 454.2047, found 454.2047.

(3aS,5S,6R,6aS)-5-((S)-2,2-Dimethyl-1,3-dioxolan-4-yl)-2,2-dimethyltetrahydrofuro[2,3-d][1,3]dioxol-6-yl 2-(4-(N-benzoyl-S-methylsulfonimidoyl)phenyl)acetate (23a):

Yield: 58% (162.2 mg) as a colorless viscous liquid; Purified over a column of silica gel (40% EtOAc in hexane); ^{1}H NMR ($CDCl_3$, 600 MHz): *δ* 8.15 (d, 2H, *J* = 9.0 Hz), 8.01 (d, 2H,

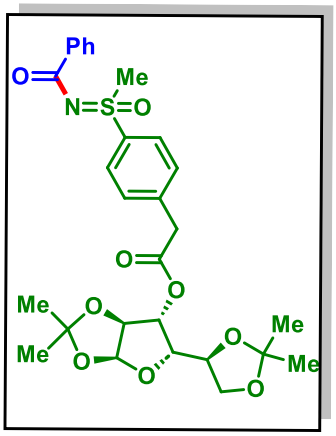

J = 10.2 Hz), 7.54–7.48 (m, 3H), 7.40 (t, 2H, *J* = 9.3 Hz), 5.86 (t, 1H, *J* = 10.2 Hz), 5.30 (d, 1H, *J* = 3.6 Hz), 4.47 (d, 1H, *J* = 4.2 Hz), 4.18–4.16 (m, 1H), 4.11–3.95 (m, 3H), 3.77 (d, 2H, *J* = 3.6 Hz), 3.45 (s, 3H), 1.51 (s, 3H), 1.38 (s, 3H), 1.27–1.24 (m, 6H); $^{13}C\{^{1}H\}$ NMR ($CDCl_3$, 150 MHz): δ 174.4, 169.1, 139.9, 138.3, 135.6, 132.4, 130.8, 129.6, 128.2, 127.7, 112.6, 109.62, 109.60, 105.2, 83.4, 80.0, 77.0, 72.5, 67.5, 44.5, 41.0, 27.0, 26.9, 26.4, 25.5; IR (KBr, cm^{-1}): 2812, 1730, 1624, 145, 1240, 713; HRMS (ESI/Q-TOF) (m/z) calcd for $C_{28}H_{34}NO_9S$, $[M + H]^+$: 560.1949, found 560.1951.

***4-(N-Benzoyl-S-methylsulfonimidoyl)benzyl 2-(4-isobutylphenyl)propanoate (24a)*:**

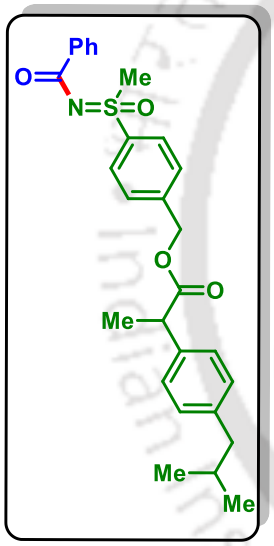

Yield: 62% (148 mg) as a colorless viscous liquid; Purified over a column of silica gel (35% EtOAc in hexane); ^{1}H NMR ($CDCl_3$, 600 MHz): δ 8.15 (d, 2H, *J* = 7.2 Hz), 7.94 (d, 2H, *J* = 8.4 Hz), 7.50 (t, 1H, *J* = 7.5 Hz), 7.41–7.36 (m, 4H), 7.21 (t, 2H, *J* = 6.9 Hz), 7.11 (d, 2H, *J* = 7.2 Hz), 5.20 (d, 1H, *J* = 13.2 Hz), 5.14 (d, 1H, *J* = 13.8 Hz), 3.79 (q, 1H, *J* = 14.4, 21.6 Hz), 3.41 (s, 3H), 2.45–2.44 (m, 2H), 1.86–1.80 (m, 1H), 1.53 (d, 3H, *J* = 7.2 Hz), 0.89 (d, 6H, *J* = 6.6 Hz); $^{13}C\{^{1}H\}$ NMR ($CDCl_3$, 150 MHz): δ 174.3, 142.7, 142.6, 140.9, 138.4, 137.3, 135.6, 132.3, 129.5, 129.4, 128.3, 128.2, 128.1, 127.4, 127.3, 64.9, 45.1, 45.0, 44.4, 30.2, 22.4, 18.3; IR (KBr, cm^{-1}): 3055, 2888, 1735, 1629, 1312, 730; HRMS (ESI/Q-TOF) (m/z) calcd for $C_{28}H_{32}NO_4S$, $[M + H]^+$: 478.2047, found 478.2053.

***4-(N-Benzoyl-S-methylsulfonimidoyl)benzyl-2-(2-fluoro-[1,1'-biphenyl]-4-yl)propanoate (25a)*:**

Yield: 53% (136.6 mg) as a white solid; Purified over a column of silica gel (30% EtOAc in hexane); ^{1}H NMR ($CDCl_3$, 500 MHz): δ 8.16 (d, 2H, *J* = 7.5 Hz), 8.00 (d, 2H, *J* = 7.5 Hz), 7.52 (t, 3H, *J* = 7.7 Hz), 7.47 (d, 2H, *J* = 8.5 Hz) , 7.44–7.36 (m, 6H), 7.16 (d, 1H, *J* = 8.0 Hz), 7.11 (d, 1H, *J* = 6.5 Hz), 5.22 (s, 2H), 3.86 (q, 1H, *J* = 7.0, 7.0

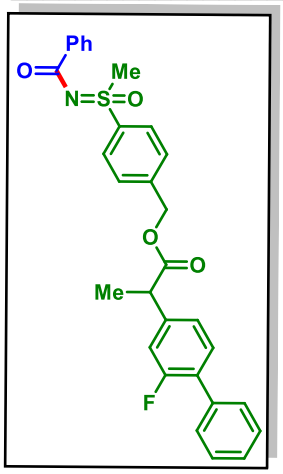

Hz), 3.41 (s, 3H), 1.58 (d, 3H, J = 7.5 Hz); $^{13}C\{^1H\}$ NMR ($CDCl_3$, 125 MHz): δ 174.4, 173.6, 159.8 (d, J = 247.2 Hz), 142.3, 141.4 (d, J = 7.5 Hz), 138.8, 135.6, 135.5, 132.4, 131.1 (d, J = 4.0 Hz), 129.6, 129.0 (d, J = 2.75 Hz), 128.8, 128.7, 128.2, 127.9, 127.6, 123.7 (d, J = 3.12 Hz), 115.4 (d, J = 23.5 Hz), 65.4, 45.1, 44.5, 18.3; ^{19}F NMR ($CDCl_3$, 471 MHz): δ –117.3 (s); IR (KBr, cm^{-1}): 3029, 2923, 1734, 1277, 977, 712; HRMS (ESI/Q-TOF) (m/z) calcd for $C_{30}H_{27}FNO_4S$, $[M + H]^+$: 516.1639, found 516.1642.

***2,5,7,8-Tetramethyl-2-(5,9,13-trimethyltetradecyl)chroman-6-yl-2-(4-(N-benzoyl-S-methylsulfonimidoyl)phenyl)acetate (26a)*:**

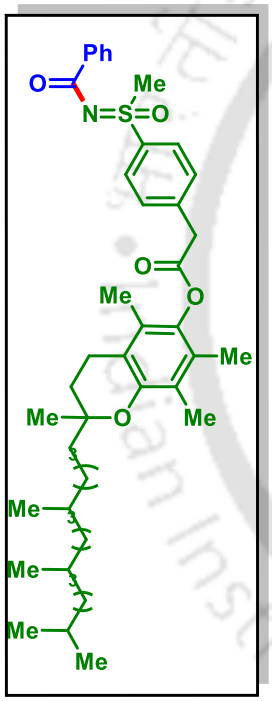

Yield: 42% (156.2 mg) as a colorless viscous liquid; Purified over a column of silica gel (35% EtOAc in hexane); ^1H NMR ($CDCl_3$, 600 MHz): δ 8.17 (d, 2H, J = 7.2 Hz), 8.06 (d, 2H, J = 8.4 Hz), 7.67 (d, 2H, J = 8.4 Hz), 7.51 (t, 1H, J = 7.2 Hz), 7.42 (t, 2H, J = 7.8 Hz), 4.01 (s, 2H), 3.48 (s, 3H), 2.56 (t, 2H, J = 6.9 Hz), 2.07 (s, 3H), 1.93 (s, 3H), 1.88 (s, 3H), 1.82–1.77 (m, 2H), 1.70–1.67 (m, 2H), 1.26 (s, 11H), 1.15–1.13 (m, 5H), 1.12–1.06 (m, 5H), 0.88–0.83 (m, 13H); $^{13}C\{^1H\}$ NMR ($CDCl_3$, 150 MHz): δ 174.4, 168.9, 149.8, 140.4, 138.3, 135.7, 132.4, 131.0, 129.6, 128.2, 127.8, 126.6, 127.8, 126.6, 124.9, 123.4, 117.7, 75.3, 49.3, 44.6, 41.1, 39.6, 37.6, 34.1, 32.9, 32.1, 28.2, 25.8, 25.1, 25.0, 24.6, 22.9, 22.8, 21.2, 20.8, 19.9, 14.3, 13.1, 12.2, 12.0; IR (KBr, cm^{-1}): 3325, 2931, 2854, 1723, 1621, 639; HRMS (ESI/Q-TOF) (m/z) calcd for $C_{45}H_{64}NO_5S$, $[M + H]^+$: 730.4500, found 730.4504.

***4-(N-Benzoyl-S-methylsulfonimidoyl)benzyl-2-(4-(2,2-dichlorocyclopropyl)phenoxy)-2-methylpropanoate (27a)*:**

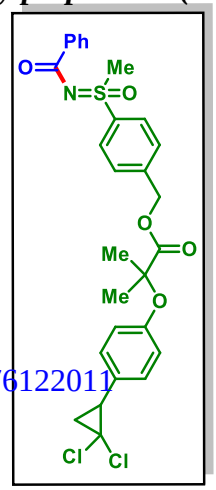

Yield: 51% (143 mg) as a white solid; Purified over a column of silica gel (25% EtOAc in hexane); ^1H NMR ($CDCl_3$, 400 MHz): 8.16 (d, 2H, J = 8.4 Hz), 7.97 (d, 2H, J = 8.4 Hz), 7.53–7.49 (m, 1H), 7.43–7.39 (m, 4H), 7.08 (d, 2H, J = 8.8 Hz), 6.76 (d, 2H, J = 8.4 Hz), 5.24 (s, 2H), 3.44 (s, 3H), 2.83–2.78 (m,

1H), 1.93–1.88 (m, 1H), 1.79–1.74 (m, 1H), 1.64 (s, 6H); $^{13}C\{^{1}H\}$ NMR ($CDCl_3$, 100 MHz): δ 174.4, 174.1, 155.0, 141.8, 139.0, 135.7, 132.4, 129.9, 129.6, 129.1, 128.3, 127.7, 118.6, 79.3, 65.9, 61.1, 44.5, 34.9, 25.9, 25.6; IR (KBr, cm^{-1}): 3015, 2928, 1734, 1610, 1275, 711; HRMS (ESI/Q-TOF) (m/z) calcd for $C_{28}H_{28}Cl_2NO_5S$, $[M + H]^+$: 560.1060, found 560.1067.

Methyl (E)-2-(1-(4-(N-benzoyl-S-methylsulfonimidoyl)benzylidene)-5-fluoro-2-methyl-1H-inden-3-yl)acetate (28a):

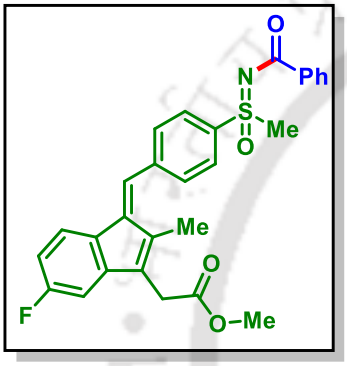

Yield: 44% (107.7 mg) green gummy solid; Purified over a column of silica gel (40% EtOAc in hexane); ^{1}H NMR ($CDCl_3$, 600 MHz): δ 8.19 (d, 2H, J = 7.8 Hz), 8.10 (d, 2H, J = 8.4 Hz), 7.52 (t, 2H, J = 7.2 Hz), 7.42 (t, 3H, J = 7.8 Hz), 7.16–7.14 (m, 1H), 7.11 (s, 1H), 6.88–6.86 (m, 1H), 6.59–6.55 (m, 1H), 3.71 (s, 3H), 3.56 (s, 2H), 3.54 (s, 3H), 2.19 (s, 3H); $^{13}C\{^{1}H\}$ NMR ($CDCl_3$, 150 MHz): δ 174.4, 170.8, 163.7 (d, J = 245.5 Hz), 147.0, 142.7 (d, J = 28.9 Hz), 138.4 (d, J = 18.4 Hz), 135.7, 132.4, 130.7, 129.6, 129.4, 128.2, 128.1, 127.6, 127.2, 123.8 (d, J = 9.0 Hz), 111.1 (d, J = 22.6 Hz), 106.5 (d, J = 23.8 Hz), 52.4, 44.5, 31.7, 10.7; IR (KBr, cm^{-1}): 3012, 2898, 1725, 1697, 1114, 697; HRMS (ESI/Q-TOF) (m/z) calcd for $C_{28}H_{25}FNO_4S$, $[M + H]^+$: 490.1483, found 490.1482.

***(Benzylimino)(methyl)(phenyl)- λ^6-sulfanone (1y)*:**

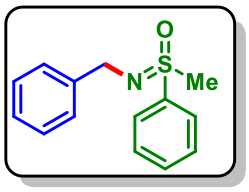

Yield: 76% (18.6 mg) as a colorless viscous liquid; Purified over a column of silica gel (10% EtOAc in hexane); ^{1}H NMR ($CDCl_3$, 600 MHz): δ 7.94 (d, 2H, J = 7.2 Hz), 7.61 (t, 1H, J = 7.8 Hz), 7.56 (t, 2H, J = 7.8 Hz), 7.35 (d, 2H, J = 7.2 Hz), 7.29 (t, 2H, J = 7.5 Hz), 7.20 (t, 1H, J = 7.2 Hz), 4.20 (d, 1H, J = 14.4 Hz), 3.97 (d, 1H, J = 13.8 Hz), 3.14 (s, 3H); $^{13}C\{^{1}H\}$ NMR ($CDCl_3$, 150 MHz): δ 141.4, 139.7, 133.1, 129.6, 128.9, 128.5, 127.8, 126.7,

47.6, 45.5; IR (KBr, cm^{-1}): 3085, 2920, 2850, 1755, 1214, 717; HRMS (ESI/Q-TOF) (m/z): calcd for $C_{14}H_{16}NOS$, $[M + H]^+$: 246.0947, found 246.0955.

2-Hydroxy-N-(methyl(oxo)(phenyl)- λ⁶-sulfaneylidene)benzamide (1z):

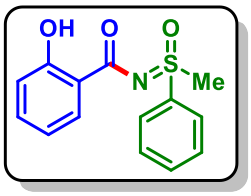

Yield: 60% (16.5 mg) as a white solid; Purified over a column of silica gel (10% EtOAc in hexane); ^1H NMR ($CDCl_3$, 500 MHz): δ 11.84 (s, 1H), 8.09 (d, 1H, J = 8.0 Hz), 8.04 (d, 2H, J = 8.0 Hz), 7.72 (t, 1H, J = 7.2 Hz), 7.64 (t, 2H, J = 7.5 Hz), 7.40 (t, 1H, J = 7.5 Hz), 6.92 (d, 1H, J = 8.5 Hz), 6.86 (t, 1H, J = 7.5 Hz), 3.47 (s, 3H); $^{13}C\{^1H\}$ NMR ($CDCl_3$, 125 MHz): δ 178.4, 162.3, 138.5, 135.2, 134.4, 131.3, 130.1, 127.3, 118.7, 117.7, 117.6, 44.9; IR (KBr, cm^{-1}): 3414, 3023, 2927, 1712, 1354, 787; HRMS (ESI/Q-TOF) (m/z): calcd for $C_{14}H_{14}NO_3S$, $[M + H]^+$: 276.0689, found 276.0690.

2,2,6,6-Tetramethylpiperidin-1-yl benzoate (v):

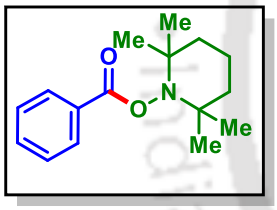

Yield: 26% (34 mg) as a white solid; Purified over a column of silica gel (10% EtOAc in hexane); ^1H NMR ($CDCl_3$, 600 MHz): δ 8.07–8.06 (m, 2H), 7.57 (t, 1H, J = 7.2 Hz), 7.46 (t, 2H, J = 7.8 Hz), 1.79–1.75 (m, 2H), 1.72–1.67 (m, 1H), 1.59–1.57 (m, 2H), 1.47–1.44 (m, 1H), 1.27 (s, 6H), 1.12 (s, 6H); $^{13}C\{^1H\}$ NMR ($CDCl_3$, 150 MHz): δ 166.6, 133.0, 129.9, 129.7, 128.6, 60.6, 39.2, 32.1, 21.0, 17.2; IR (KBr, cm^{-1}): 2937, 2816, 1755, 1254, 1123, 707; HRMS (ESI/Q-TOF) (m/z): calcd for $C_{16}H_{24}NO_2$, $[M + H]^+$: 262.1802, found 262.1807.

V.10. Representative Spectra

N-(Methyl(oxo)(phenyl)- λ⁶-sulfaneylidene)benzamide (1a) : ^{1}H NMR ($CDCl_3$, 600 MHz)

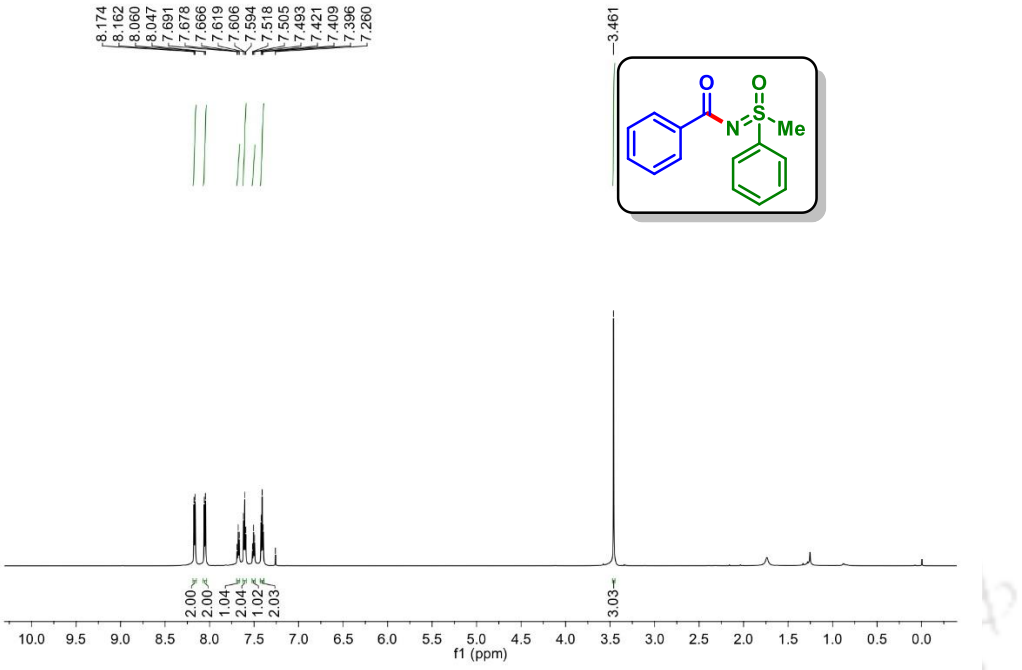

N-(Methyl(oxo)(phenyl)- λ⁶-sulfaneylidene)benzamide (1a): $^{13}C\{^{1}H\}$ NMR ($CDCl_3$, 150 MHz)

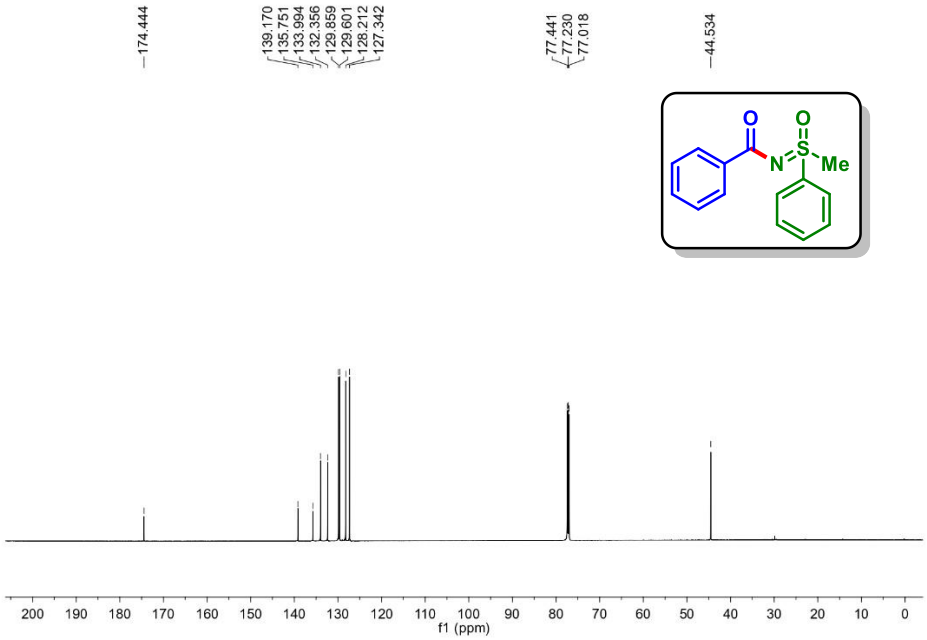

N-((4-Cyanophenyl)(methyl)(oxo)- λ⁶-sulfaneylidene)benzamide (10a): ^{1}H NMR (CDCl$_3$, 600 MHz)

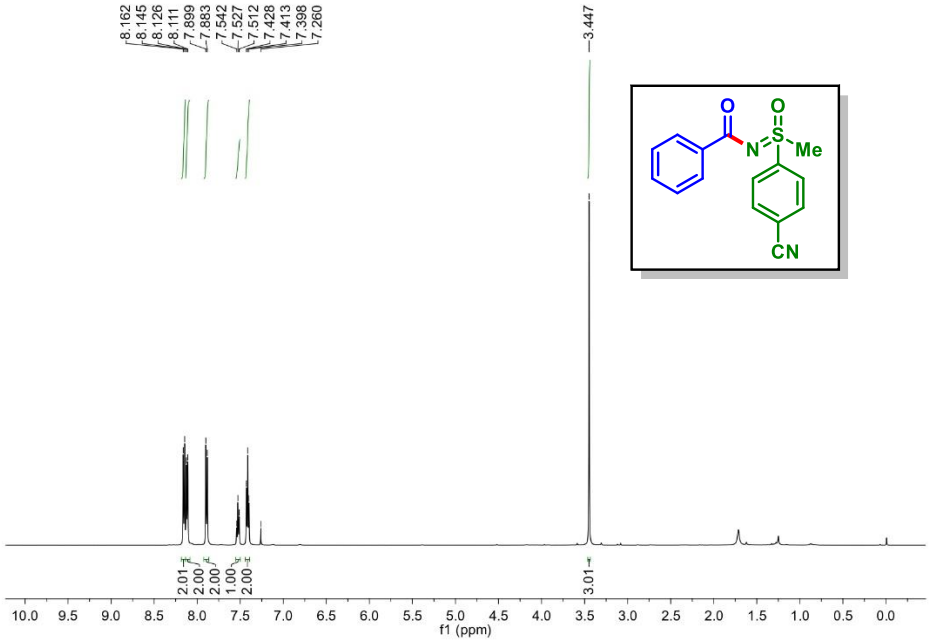

N-((4-Cyanophenyl)(methyl)(oxo)- λ⁶-sulfaneylidene)benzamide (10a): ^{13}C{^{1}H} NMR (CDCl$_3$, 150 MHz)

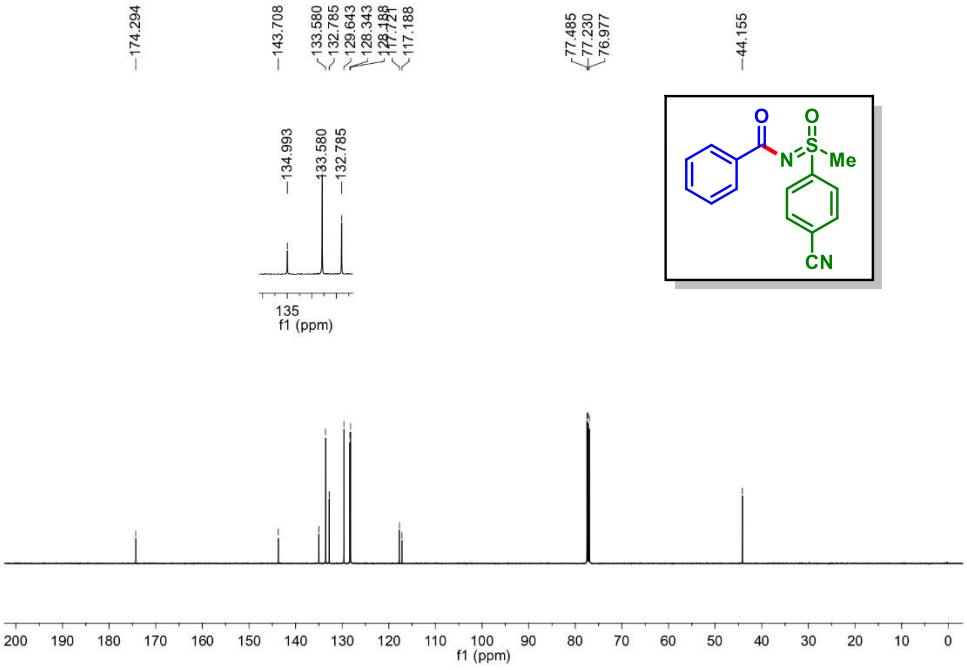

4-Methoxy-N-(methyl(oxo)(phenyl)- λ⁶-sulfaneylidene)benzamide (1h): ^{1}H NMR ($CDCl_3$, 600 MHz)

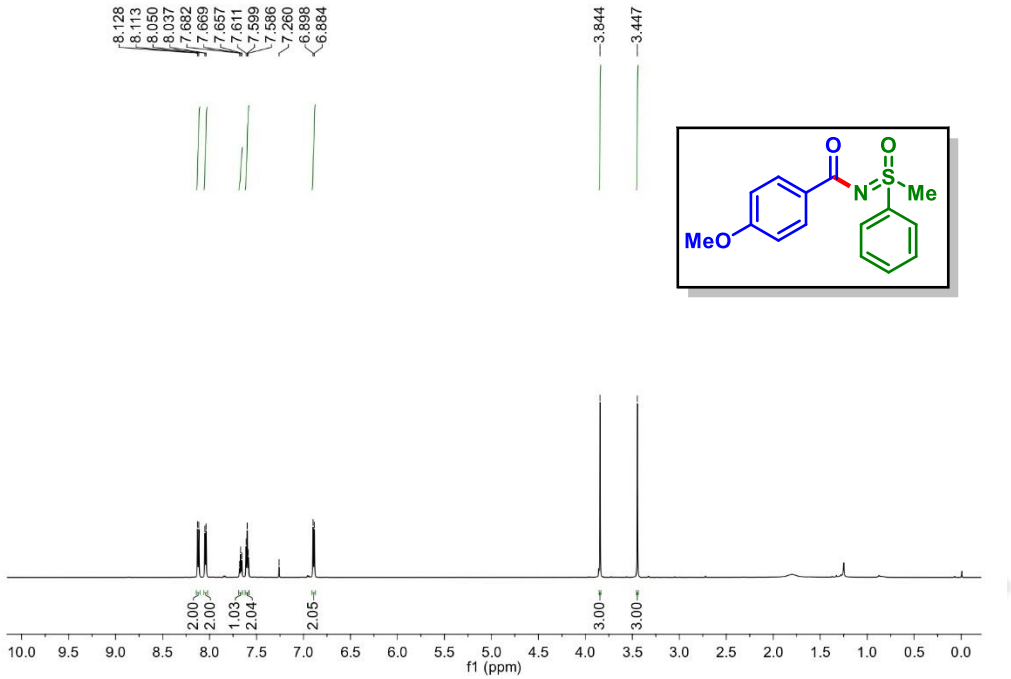

4-Methoxy-N-(methyl(oxo)(phenyl)- λ⁶-sulfaneylidene)benzamide (1h): $^{13}C\{^{1}H\}$ NMR ($CDCl_3$, 150 MHz)

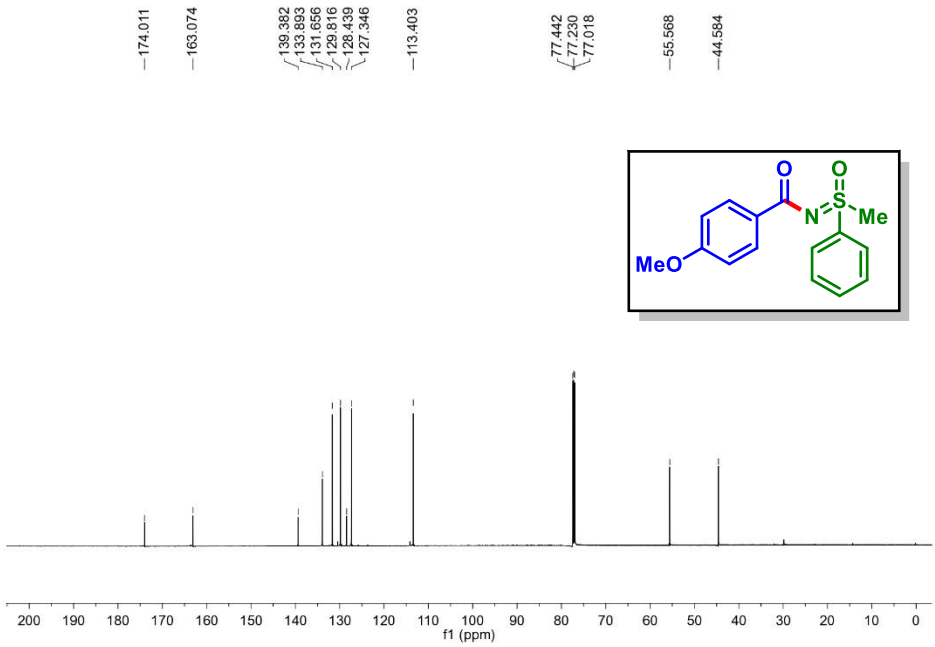

N-(Methyl(oxo)(phenyl)- λ⁶-sulfaneylidene)thiophene-2-carboxamide (1p): ^{1}H NMR ($CDCl_3$, 600 MHz)

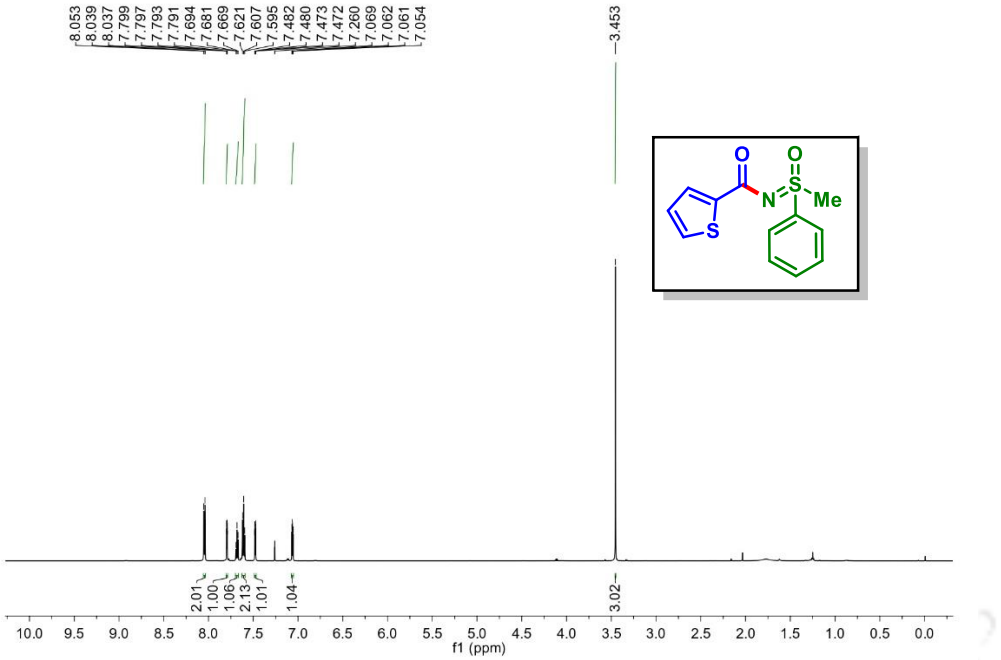

N-(Methyl(oxo)(phenyl)- λ⁶-sulfaneylidene)thiophene-2-carboxamide (1p): $^{13}C\{^{1}H\}$ NMR ($CDCl_3$, 150 MHz)

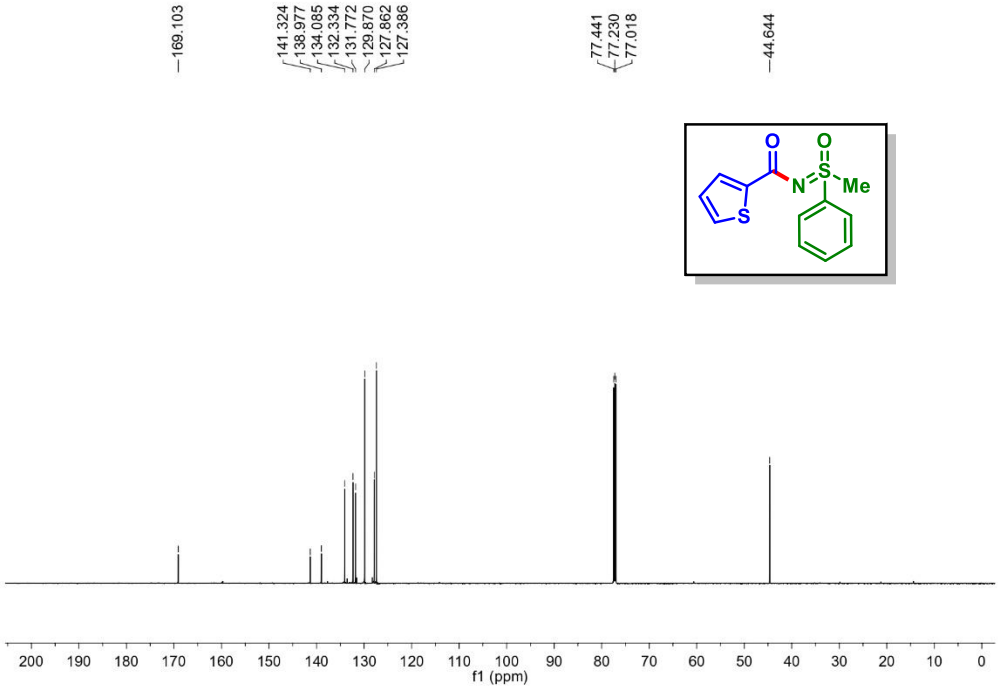

4-(N-Benzoyl-S-methylsulfonimidoyl)benzyl 2-(4-isobutylphenyl)propanoate (24a): ^{1}H NMR ($CDCl_3$, 600 MHz)

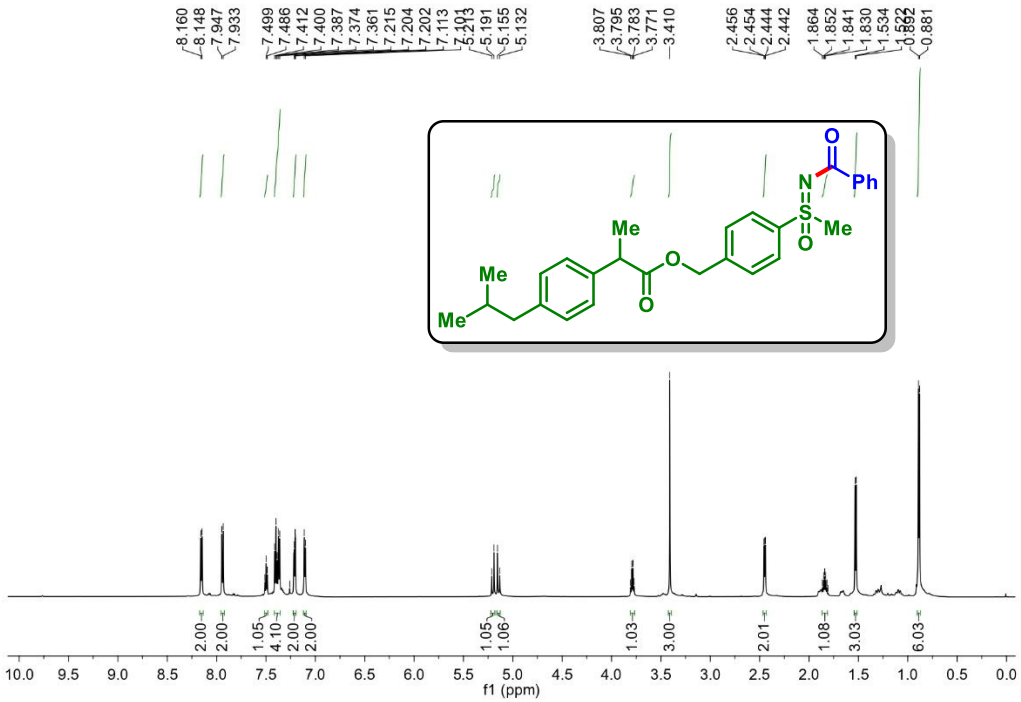

4-(N-Benzoyl-S-methylsulfonimidoyl)benzyl 2-(4-isobutylphenyl)propanoate (24a): $^{13}C\{^{1}H\}$ NMR ($CDCl_3$, 150 MHz)

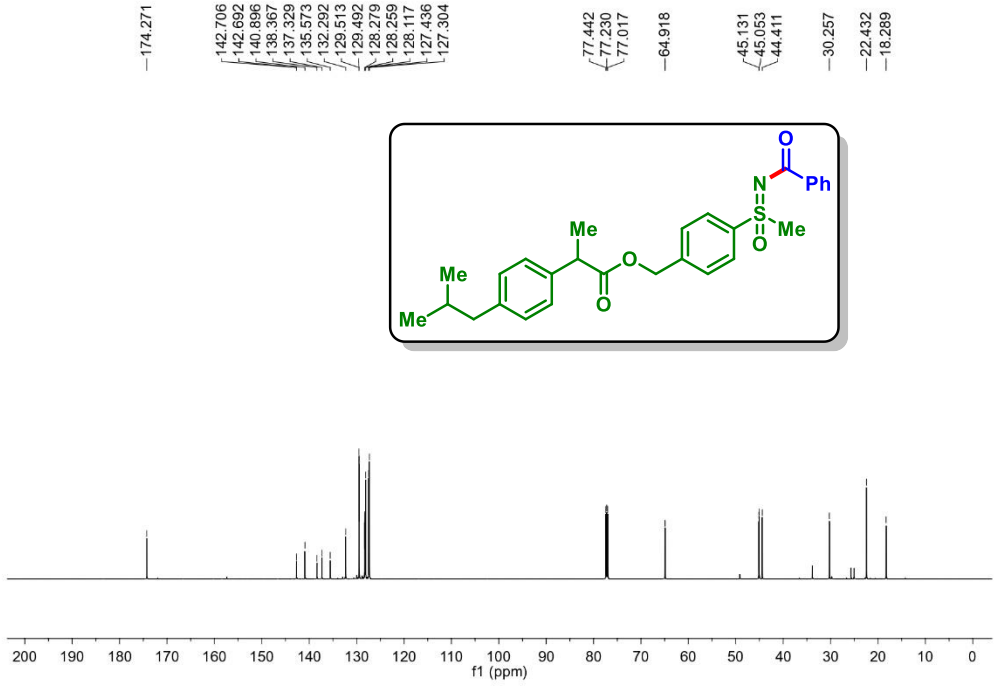

CHAPTER-VI

Electrochemical NH-Sulfoximidation with α-Keto Acids

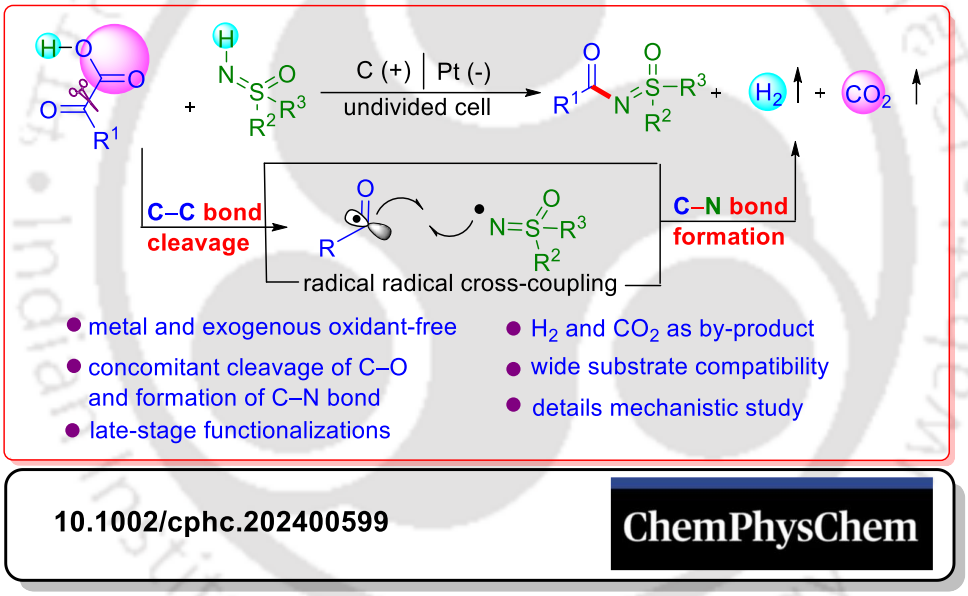

10.1002/cphc.202400599

ChemPhysChem

Abstract: ***An electrochemical N-acylation of sulfoximine has been achieved via the coupling of α-keto acids and NH-sulfoximines. This process involves the sequential cleavage of C–C bond followed by C(sp^2)–N bond formation, with the liberation of H_2 and CO_2 as the by-products. A library of N-aroylated sulfoximines is produced via the coupling of aroyl and sulfoximidoyl radicals by anodic oxidation under constant current electrolysis (CCE). The compatibility of the present protocol has been demonstrated by coupling of various bio-active compounds, such as NH-sulfoximine derived from (-)-borneol, L-menthol, D-glucose derivative, and some commercial drugs such as flurbiprofen, and ibuprofen. This late-stage functionalization highlights the importance of this sustainable protocol. Besides this, various control experiments and detection of H_2 evolution have been performed to support the proposed mechanism.***

CHAPTER VI

Electrochemical NH-Sulfoximidation with α-Keto Acids

VI.1. Introduction

Discovered from the "agenized" proteins in the early 1950s,[1] sulfoximine is recognized as isosteres of sulfones, where a "= NR substitutes one "=O" of sulfur (VI)". The sulfur (VI) linkages are subsequently expanded by the additional imino vector, bringing about unprecedented physical, chemical, and biological properties compared to sulfones.[2] Owing to the presence of sulfoximines and their functionalized derivatives in pharmaceuticals,[3] agrochemicals,[4] materials,[5] and synthesis of such molecules has grabbed the attention of chemists in modern organic synthesis (Figure-VI.1).[6]

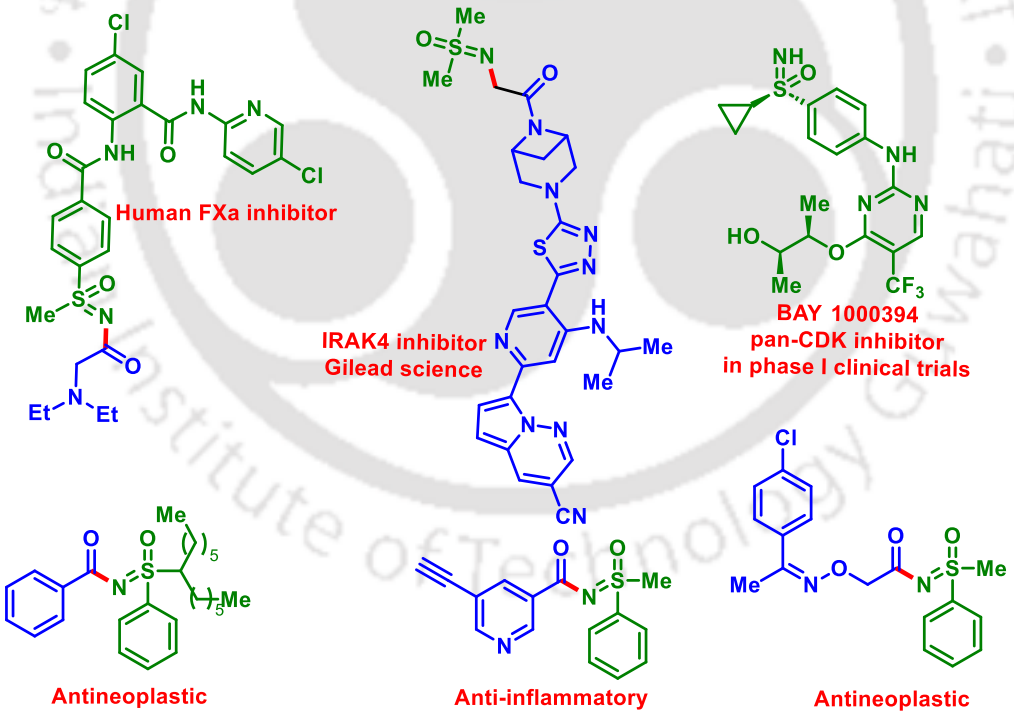

Figure VI.1. *Representative bioactive sulfoximines.*

In this regard, efforts have been made to construct *N*-acylated sulfoximines. For instance, the carboxyl activating agents like 1-ethyl-3-(3-dimethylaminopropyl)carbodiimide

(EDC) or *N*,*N*′-dicyclohexylcarbodiimide (DCC) have been used to facilitate the coupling between carboxylic acids and *NH*-sulfoximine, resulting in the formation of *N*-acylated sulfoximines [Scheme VI.1 (a)].[7]

Scheme VI.1. Strategies for N-aroylation of sulfoximines

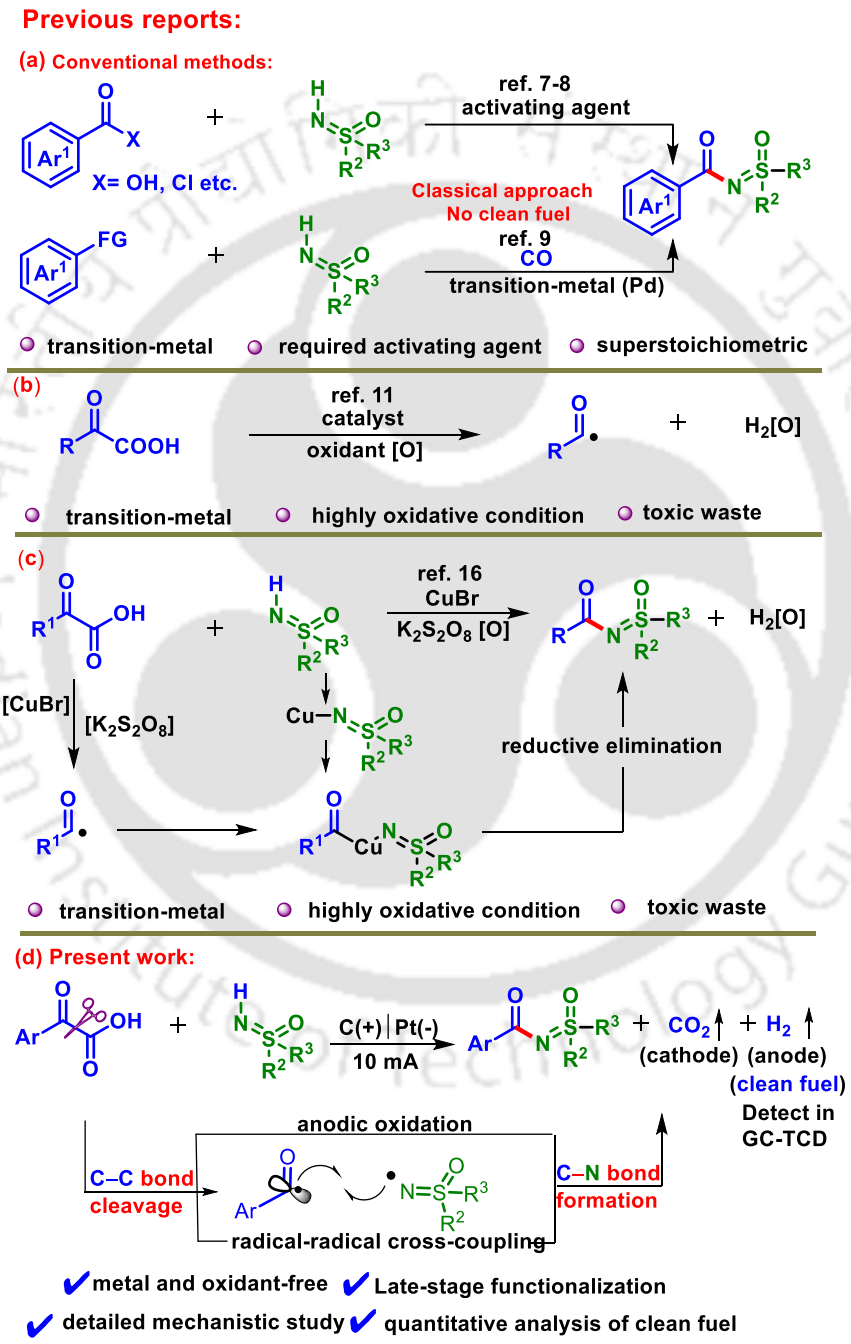

A similar sulfoximidation reaction has been established utilizing different activating agents such as boric acid or 1,3-dioxa-5-aza-2,4,6-triborinane (DATB) [Scheme VI.1 (a)].[8] The synthesis of *N*-aroyl sulfoximines has also been achieved via a transition-metal-catalyzed process using aryl halides and carbon monoxide [Scheme VI.1 (a)].[9] Given their significance, there is a strong demand for sustainable synthetic methods that possess broad functional group tolerance, allow for the late-stage modifications of biologically relevant molecules, and offer a clean energy source (H_2) as a by-product.

Considering the significance of acylated derivatives in both synthetic chemistry and biochemical processes, the readily accessible α-keto acid serves as an excellent source of aroyl radicals in many synthetic transformations. This process results in the production of H_2 and CO_2 as by-products under specific conditions. Usually, acyl radicals are generated *via* the cleavage of the C–X bond in RC(O)X[10] compounds or through the decarboxylation of α-keto acids[11a-i] in the presence of transition metals and oxidants when exposed to visible light.[11j-l] [Scheme VI.1 (b)]. However, the most frequently used strategies for producing acyl radicals typically depend on using transition metal catalysts in combination with stoichiometric chemical oxidants.[11] The above-mentioned strategies are associated with the generation of chemical wastes that are not environmentally friendly. Thus, developing a waste-free and milder method for its generation from α-keto acid is highly desirable.

Recently, electro-organic synthesis has emerged as an impressive tool for various redox transformations, offering environmentally friendly and economically viable features.[12] Electrochemistry presents a greener alternative to excessive redox reagents and minimizes the generation of hazardous waste.[13] The efficiency of electrochemical reactions can be controlled by adjusting the current flow and applied voltage.[14]

The electrochemical cross-coupling of *NH*-sulfoximine remains uncharted territory because of the high oxidation potential of *NH*-sulfoximine ($E_{ox} \geq +1.92$ to $+2.00$ V vs. SCE) and its strong N-H bond dissociation energy ($BDE_{N–H}$ = 104−106 kcal/mol), making it challenging to generate *N*-centre radicals.[15] Yotphan group developed a Cu(I)/$K_2S_2O_8$-catalyzed oxidative decarboxylative coupling of α-keto acids and sulfoximines [Scheme VI. 1 (c)].[16] These reactions proceed through an *in situ* generation of benzoyl radical involving metal complexation via an oxidative addition followed by a reductive elimination leading to *N*-acylated sulfoximines. The reported sulfoximidation strategies for synthesizing *N*-acylated

sulfoximines are neither atom-economical nor sustainable. Therefore, using any transition metal or oxidant can be avoided following this strategy. Nevertheless, designing a metal-free methodology for radical cross-coupling that accepts the challenge of generating two distinct radicals has to overcome the homo-cross-coupling reactions of two individual open-shell radicals. We envisioned sulfoximidation through anodic oxidation of readily available α-keto acids and sulfoximine [Scheme VI.1 (d)].

VI.2. Strategies for the Synthesis of sulfoximidation product

In 2020 Bolm *et al*. developed a visible-light-induced α-ketoacylation of sulfoximines using aryl alkyne. This methodology is metal and base-free, providing the diketonic products without the use of peroxides. The reaction proceeds *via* the addition of a sulfoximidoyl radical to the alkyne in the presence of blue LEDs (Scheme VI.2).[17a]

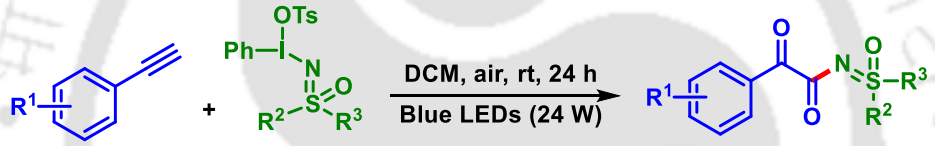

Scheme VI.2. *Synthesis of α-ketoacylations of sulfoximines derivatives.*

In 2022 the Song group disclosed a metal-, base-, and additive-free *N*-acylation of sulfoximines under mild conditions using an organic photoredox catalyst. This green strategy featured a broad substrate scope, good compatibility with air, and high yields. It was further applied to amino acid modifications and α-keto *N*-acyl sulfoximine synthesis (Scheme VI.3).[17b]

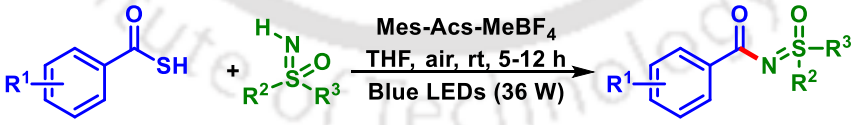

Scheme VI.3. *N-Acylation of sulfoximines with thioacid.*

The Ji group recently introduced an electrochemical approach for the *N*-acylation of sulfoximines utilizing hydroxamic acid as the acyl source. The reaction proceeds under mild conditions, without an external oxidant or catalyst. Through mechanistic investigations, key by-products such as N_2O and H_2 were identified. A large variety of functional groups having

electron-donating and electron-withdrawing substituents reacted smoothly to afford N-acylation products in moderate to good yields (Scheme VI.4).[17c]

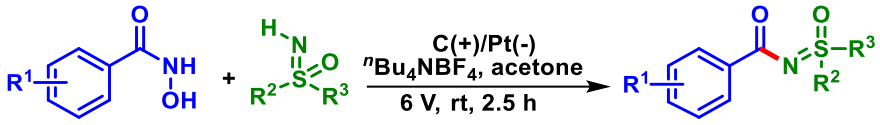

Scheme VI.4. *Electrochemical acylation of sulfoximines with hydroxamic acid.*

VI.3. Present Work

VI.3.1. Optimization of the Reaction Conditions

To validate the proposed strategy, we initiated our experiment by using α-keto acid (**a**, 2.0 equiv.) and *NH*-sulfoximine (**1**, 0.5 mmol) in the presence of electrolyte $^{n}Bu_4NClO_4$ (1.5 equiv.) in dichloromethane (DCE) having carbon rod as the anode and platinum plate as the cathode. The reaction was continued by applying a 10 mA constant current under an N_2 atmosphere at room temperature for 6 h in an undivided cell. As per the designed strategy, *N*-aroylated sulfoximine (**1a**) was obtained in 65% yield and confirmed by ^{1}H, ^{13}C, and HRMS. The predicted structure was further reconfirmed by a single-crystal X-ray diffraction study (CCDC-2332707) on one of its derivatives (Figure VI.2).

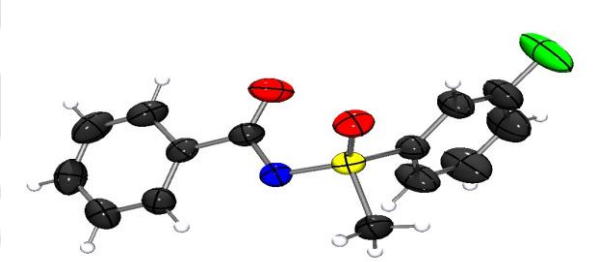

Figure VI.2. *ORTEP diagram of (8a) with 50% ellipsoid probability (CCDC 2332707)*

Encouraged by this observation, we tried to standardize the reaction condition by varying various reaction parameters, such as solvents, electrolytes, electrodes, and electric current, and the results are summarized in Table VI.1.

Table VI.1. Optimization of the reaction conditions[a,b]

Entry	Variation from the standard conditions	Yield[b] (%)
1	**None**	**65**
2	CH_3CN, DCM, MeOH, instead of DCE	12, 19, N.D
3	1, 4 –dioxane, DMSO, DMA instead of DCE	N.D
4	Nickel, RVC, platinum anode instead of C rod anode	23, 15, 42
5	Carbon cloth, stainless steel instead of platinum cathode	16, 23
6	$^nBu_4NBF_4$, $^nBu_4NPF_6$, $^nBu_4NI$, $^nBu_4NOAc$ instead of $^nBu_4NClO_4$	25, 36, 23, 33
7	1 equiv., 2 equiv. instead of 1.5 equiv. $^nBu_4NClO_4$	43, 59
8	K_3PO_4, Cs_2CO_3, DBU, instead of K_2CO_3	13, 19, N.D
9	0.5 equiv., 1.5 equiv. instead of 1 equiv. K_2CO_3	22, 43
10	0.5 equiv., 1.5 equiv. instead of 1 equiv. sulfoximine	25, 54
11	15 mA, 5 mA instead of 10 mA	52, 23
12	3 h instead of 6 h	30
13	No base	trace
14	No electric current	N.D
15	No electrolyte	N.D
16	No electric current, 80 ^oC	N.D
17	air atmosphere	63

[a]Reaction conditions: **a** (1 mmol, 2 equiv), **1** (0.5 mmol), $^nBu_4NClO_4$ (1.5 equiv), K_2CO_3 (1 equiv) in DCE (5 mL) solvent with a carbon rod anode (Φ 6 mm), platinum plate cathode (10 mm x 10 mm x 0.3 mm), constant current = 10 mA, at room temperature under N_2 atm, 6 h in undivided cell. [b]yield of isolated product. N.D = not detected.

Among various solvents tested, DCE was found to be optimal, whereas the use of other solvents, such as CH_3CN, and DCM, resulted in a lower yield of product (**1a**). Further, no product was observed using MeOH (Table VI.1, entry 2). Besides this, the use of 1,4-dioxane, DMSO, and DMA (Table VI.1, entry 3) were found less effective for the desired transformation. Subsequently, a variety of combinations of electrodes were tested. For example, replacing the anode (carbon rod) with nickel, RVC, and platinum plate (Table VI.1, entry 4) and the cathode (platinum plate) with carbon cloth and stainless steel (Table VI.1, entry 5) gave no significant improvement. Furthermore, our attempts to enhance the yield by

replacing $^{n}Bu_4NClO_4$ with various organic electrolytes such as $^{n}Bu_4NBF_4$, $^{n}Bu_4NPF_6$, $^{n}Bu_4NI$, and $^{n}Bu_4NOAc$ failed to improve the product yield (Table VI.1, entry 6). Then the use of $^{n}Bu_4NClO_4$ (1.0 equiv.) in lower concentration reduced the yield to 43%, whereas the yield dropped slightly (59%) using a higher concentration (2.0 equiv.) instead of 1.5 equiv. of $^{n}Bu_4NClO_4$ (Table VI.1, entries 7). Thus, the use of 1.5 equiv. of electrolyte, $^{n}Bu_4NClO_4$ was found ideal for this transformation. In addition, the reactions with different bases, like K_3PO_4 and Cs_2CO_3, had little effect on the yields, but the use of DBU as a base was completely ineffective (Table VI.1, entries 8). The use of fewer than 1 equiv. of the base resulted in poor conversion, but an excess amount of base (1.5 equiv.) led to the formation of benzil as the side product (Table VI.1, entry 9). The use of higher (1.5 equiv.) amounts of sulfoximine was found counterproductive providing 54% yield compared to the use of 1.0 equiv. of sulfoximine (Table VI.1, entry 10). Alternation of the operating current, i.e. decreasing to (5 mA) or increasing (15 mA), was not found effective in improving the yield of (**1a**) (Table VI.1, entry 11). When the reaction was stopped at 3 h, a diminished yield (30%) was observed (Table VI.1, entry 12). Next, without base, only a trace amount of product was formed (Table VI.1, entry 13). The absence of electric current or electrolyte resulted in no product (**1a**), even upon heating the reaction mixture to 80 ^{o}C, suggesting the importance of electro-oxidation in this coupling process (Table VI.1, entry 14-16). When the reaction mixture was performed in an air atmosphere, it provided a slightly lesser yield (52%) of the product than in a nitrogen atmosphere (Table VI.1, entry 17). Thus, the best-optimized condition was found to be the use of α-keto acid (**a**) (1 mmol, 2.0 equiv.), sulfoximine (**1**) (0.5 mmol), K_2CO_3 (1.0 equiv.) and $^{n}Bu_4NClO_4$ (1.5 equiv.) in a DCE solvent (5 mL) and applying a 10 mA current, carbon rod as anode and platinum plate as a cathode under N_2 atmosphere at room temperature for 6 h in an undivided cell (Table VI.1, entry 1).

VI.3.2. Scope of the Reaction with α-Keto Acid and Sulfoximine Derivatives

With the optimized conditions in hand, we first examined the scope of the sulfoximine. As depicted in Scheme VI.5, the present electrocatalytic system transformed an array of aromatic sulfoximine with different steric and electronic properties. Simple *NH*-sulfoximine (**1**) reacted with α-keto acid (**a**) smoothly, giving the corresponding product (**1a**, 65%). When aryl sulfoximine possessing electron-donating-groups (EDGs) such as 4-OMe

(**2**), 3-OMe (**3**), 4-Me (**4**), and 2-Me (**5**) react with α-keto acid (**a**) furnishing the desirable products (**2a**–**5a**) in moderate yields (48–62%).

Scheme VI.5. Substrate scope of the reaction

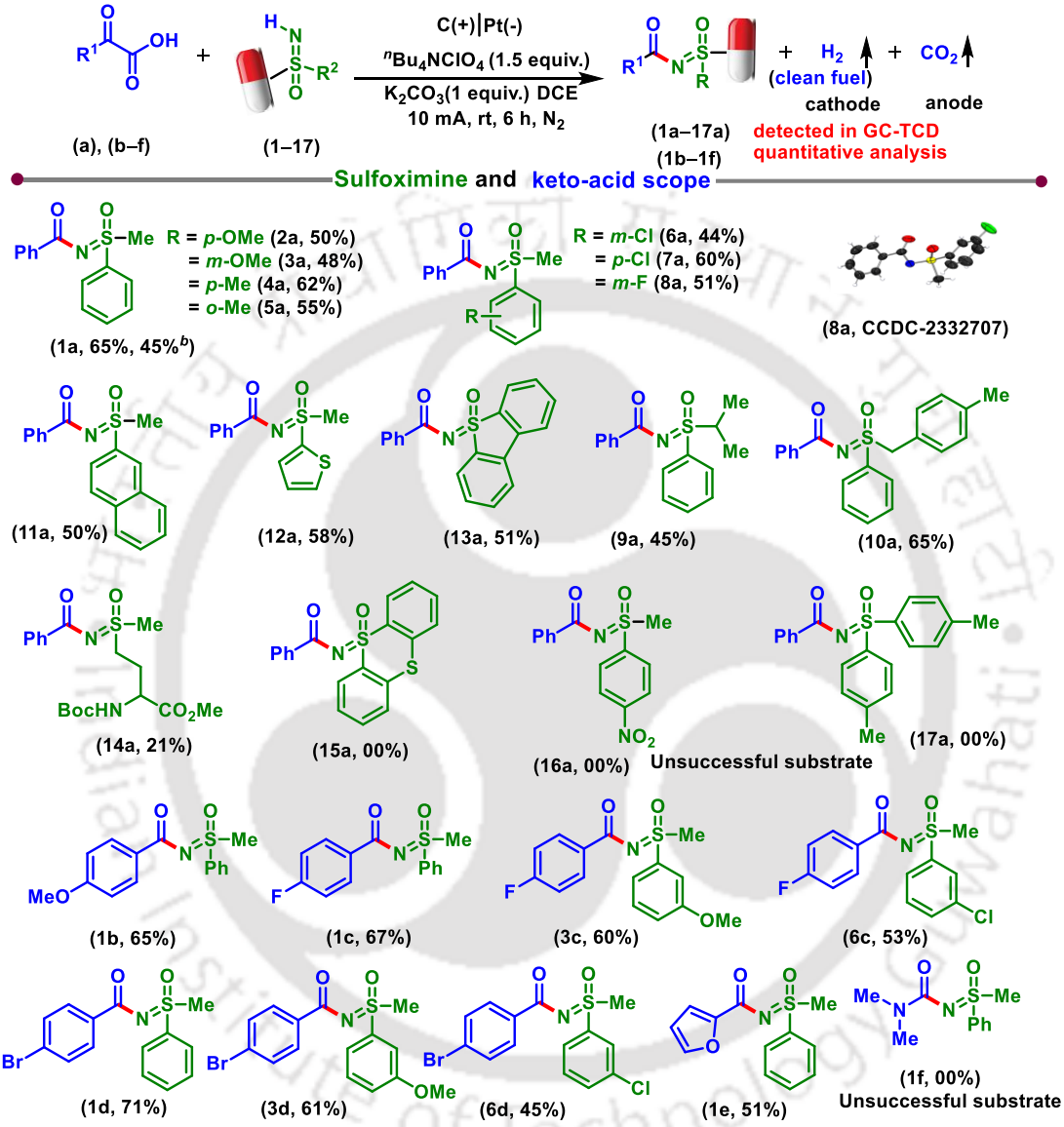

[a]Reaction conditions: (i) **1**–**22** (0.5 mmol), α-keto acids (**a–f**) (1 mmol, 2.0 equiv.), $^{n}Bu_4NClO_4$ (1.5 equiv.), K_2CO_3 (1 equiv.) in DCE (5 mL) utilizing a 10 mA constant current, carbon rod (Φ 6 mm) as an anode, and platinum plate (10 mm x 10 mm x 0.3 mm) as a cathode at room temperature under N_2 atmosphere for 6 h in an undivided cell.

Similarly, aryl sulfoximine possessing electron-withdrawing groups (EWGs) such as 3-Cl (**6**), 4- Cl (**7**), and 3-F (**8**), coupled competently with α-keto acid (**a**) resulting in their

corresponding products (**6a**, 44%), (**7a**, 60%), and (**8a**, 51%). The sulfoximine-bearing *S*-isopropyl (**9**), *S*-4-methyl benzyl, and *S*-phenyl (**10**) underwent smooth coupling, providing the desired products (**9a**–**10a**) in the range of 45% to 65%. Next, biphenyl sulfoximine was well tolerated given their product (**11a**, 50%). Besides this, heterocyclic sulfoximine (**12**) and dibenzothiophene (**13**) were efficiently *N*-aroylated giving their respective products (**12a**, 58%) and (**13a**, 51%) modest yields. However, aliphatic sulfoximine (**14**) resulted in the anticipated product (**14a**) in lower yield (21%), a dibenzodithinane (**15**), -NO_2 containing sulfoximine (**16**), and a symmetric diaryl sulfoximine (**17**) remain unsuccessful in giving their *N*-aroylated product (**15a**), (**16a**), and (**17a**). This may be due to their high oxidation potential.

After demonstrating the compatibility of various sulfoximines, we examined the nature of various substituents (EDG and EWG) present on either the α-keto acids or the phenyl rings of sulfoximine. The nature of the substituents [electron-donating 4-OMe (**b**) and electron-withdrawing 4-F(**c**), 4-Br (**d**) and heterocyclic furan (**e**) in the α-keto acids and electron donating 3-OMe (**3**) and electron-withdrawing 3-Cl (**6**) in the sulfoximine ring] or their positions of attachments all provided moderate to good yields of their products (**1b**, 65%); (**1c**, 67%); (**3c**, 60%); (**6c**, 53%); (**1d**, 71%); (**3d**, 61%); (**6d**, 45%); and (**1e**, 51%). The 2-(dimethylamino)-2-oxoacetic acid (**f**) were completely silent in giving the *N*-aroylated product (**1f**).

The late-state synthesis of complex molecules is important in identifying the potential drugs.[18] To exemplify the practicality of our electrochemical approach, the *NH*-sulfoximine of borneol (**18**), L-menthol (**19**), and D-glucose derivative (**20**) (Scheme VI.5) were all *N*-acylated, giving their desired benzoylated derivatives (**18a**, 51%), (**19a**, 55%), and (**20a**, 42%), respectively. Further, *NH*-sulfoxamine of nonsteroidal anti-inflammatory drugs flurbiprofen (**21**), and ibuprofen (**22**) all gave their desired benzoylated products (**21a**, 58%) and (**22a**, 52%). The late-stage modification of compounds with sensitive groups underscores the potential of our protocol in the realm of drug discovery.

Scheme VI.6. Substrate scope of natural product [a]

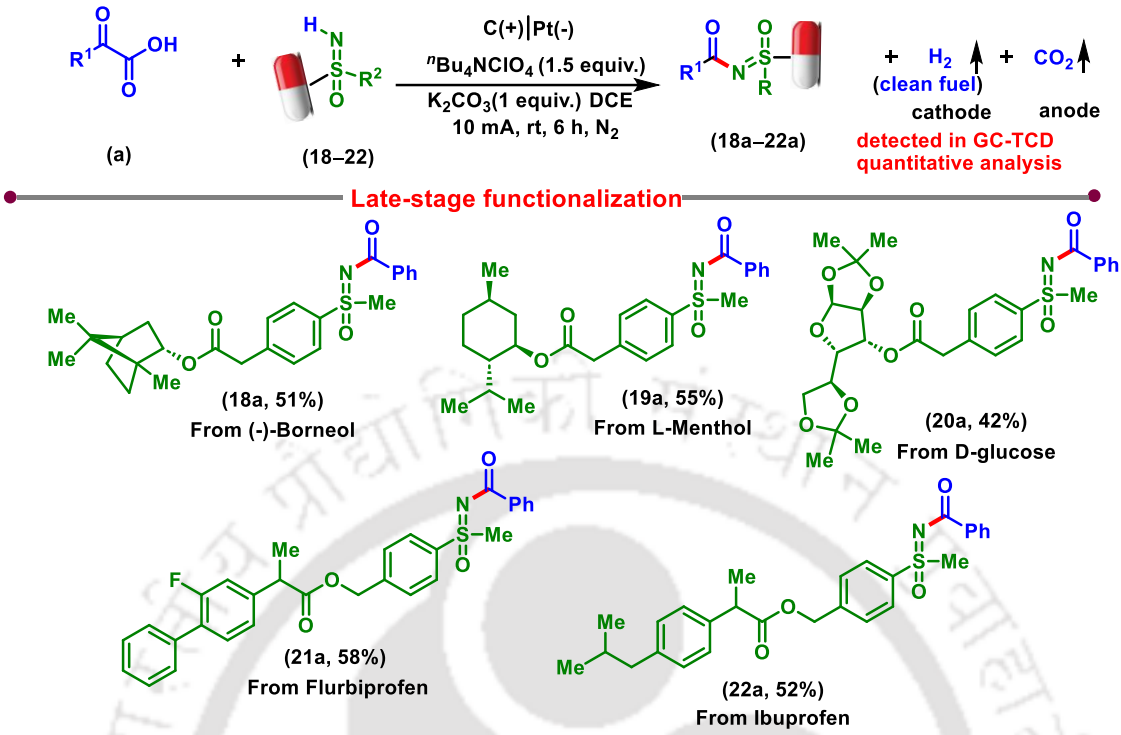

[a]Reaction conditions: (i) **18**–**22** (0.5 mmol), α-keto acids (**a**) (1 mmol, 2.0 equiv.), ^{n}Bu$_4$NClO$_4$ (1.5 equiv.), K$_2$CO$_3$ (1 equiv.) in DCE (5 mL) utilizing a 10 mA constant current, carbon rod (Φ 6 mm) as an anode, and platinum plate (10 mm x 10 mm x 0.3 mm) as a cathode at room temperature under N$_2$ atmosphere for 6 h in an undivided cell.

This electrochemical sulfoximidation primarily comprises a sequence of electron transfer redox reactions. For comparative purposes, can another traditional oxidizing agent, without any electrical current, promote oxidative cross-coupling? For this query, the coupling between α-keto acid (**a**) and *NH*-sulfoximine (**1**) was conducted in the presence of various oxidizing agents such as the K$_2$S$_2$O$_8$, I$_2$/TBHP, *tetra*-butylammonium iodide (TBAI)/ *tetra*-butyl hydroperoxide (TBHP), pyridinium chlorochromate (PCC), cerium (IV) ammonium nitrate (CAN), KMnO$_4$, and FeCl$_3$ (Table VI.2). However, none of these chemical oxidants effectively conduct the coupling reaction. Suggesting the importance of appropriate redox potential needed to carry out this reaction (Table VI.2).

Table VI.2. Comparison with traditional methods [a]

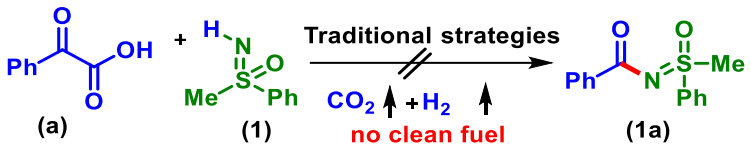

Entry	Conditions	Yield[a] (1a, %)
1	$K_2S_2O_8$ (2.0 equiv.), DCE (5 mL), rt, 6 h	0
2	I_2 (50 mol %), TBHP (2.0 equiv.), DCE (5 mL), rt, 6 h	0
3	TBAI (20 mol %), TBHP (2.0 equiv.), DCE (5 mL), rt, 6 h	0
4	PCC (2.0 equiv.), DCE (5 mL), rt, 6 h	0
5	CAN (2.0 equiv.), DCE (5 mL), rt, 6 h	trace
6	$KMnO_4$ (10 mol %), TBHP (2.0 equiv.), DCE (5 mL), rt, 6 h	0
7	$FeCl_3$ (10 mol %), DCE (5 mL), rt, 6 h	0

[a]Reaction conditions: (i) (**a**) (1.0 mmol, 2.0 equiv.), (**1**) (0.5 mmol), traditional oxidant (x mol%/ x equiv.), K_2CO_3 (1 equiv.), in DCE (5 mL) at room temperature under N_2 atmosphere for 6 h.

VI.4. Mechanistic Investigations

VI.4.1. Control Experiments

Some control experiments were performed to decipher the plausible mechanism. To confirm the radical intermediacy, when a radical scavenging experiment was carried out using TEMPO (2 equiv.) under the standard electrochemical condition, provided <15% of the product of (**1a**) and the benzoyl radical TEMPO-adduct (**u**) could be isolated in 22% yield (Scheme VI.7). The identity and purity of the product were confirmed by NMR and HRMS analysis (Figure VI.3), ^{1}H NMR (Figure VI.4), and ^{13}C{1H} (Figure VI.5) analyses suggesting the formation of benzoyl radicals during the reaction.

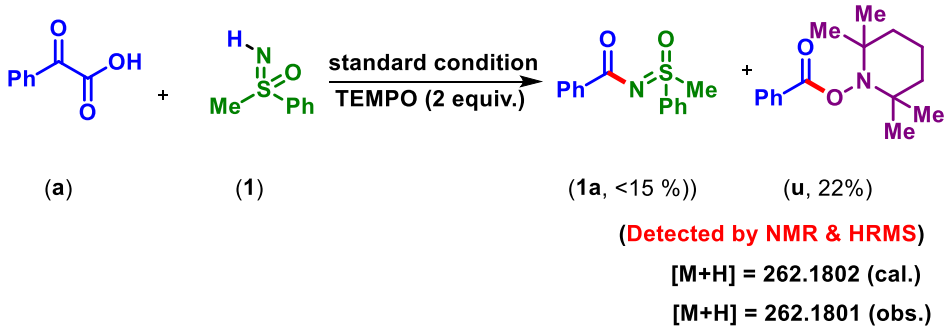

Scheme VI.7. *Radical trapping experiments using TEMPO.*

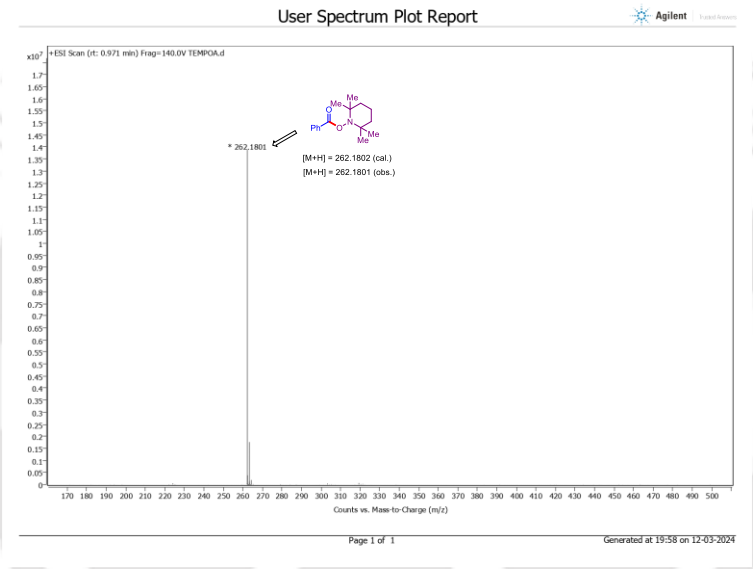

Figure VI.3 *HRMS spectra of benzoyl-radical trapped adduct (**u**)*

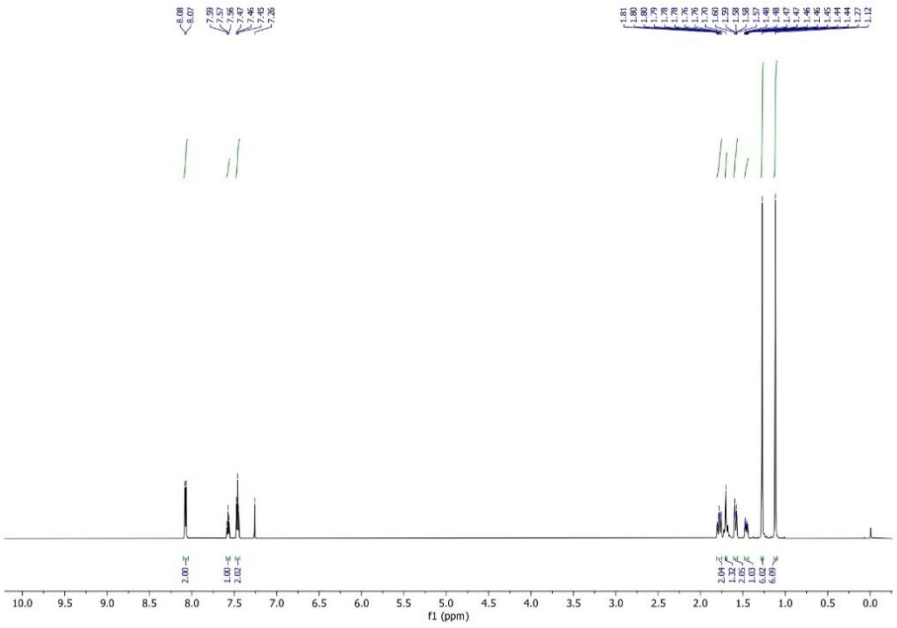

Figure VI.4 *^{1}H-NMR spectra of benzoyl-radical trapped adduct (**u**).*

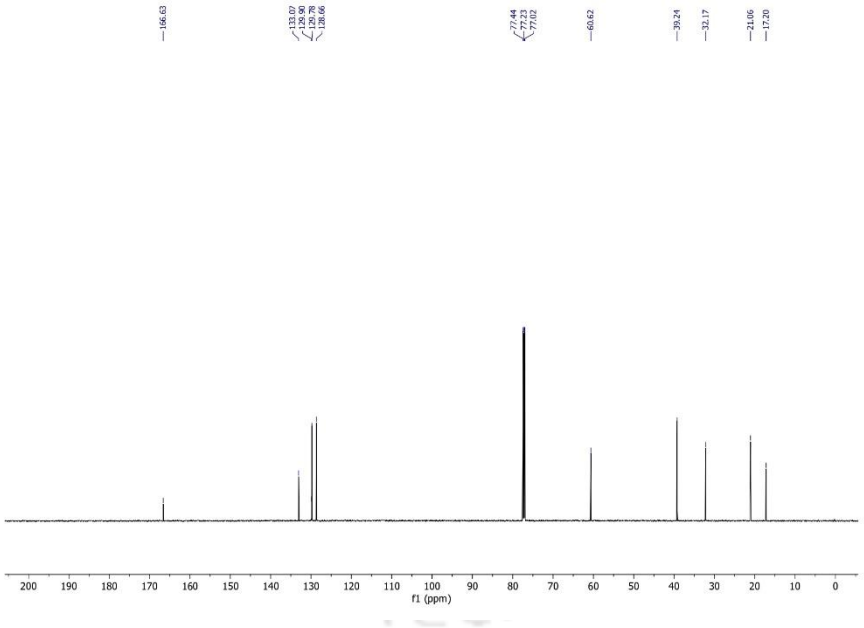

Figure VI.5 *^{13}C{1H} NMR spectra of benzoyl-radical trapped adduct (**u**).*

Similarly, the addition of BHT as a radical scavenger suppresses the reaction, giving the product **1a** in <15% yield along with the formation of BHT-sulfoxamine adduct (**v**) (Scheme VI.8). The formation of the BHT-adduct was confirmed by HRMS analysis of the reaction mixture (Figure VI.6).

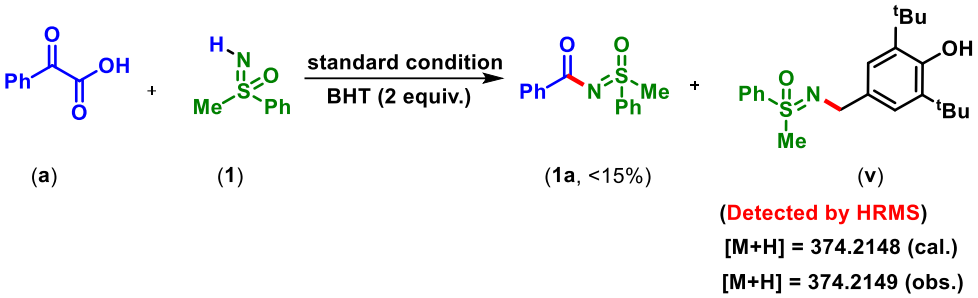

Scheme VI.8. *Radical trapping experiments with BHT*

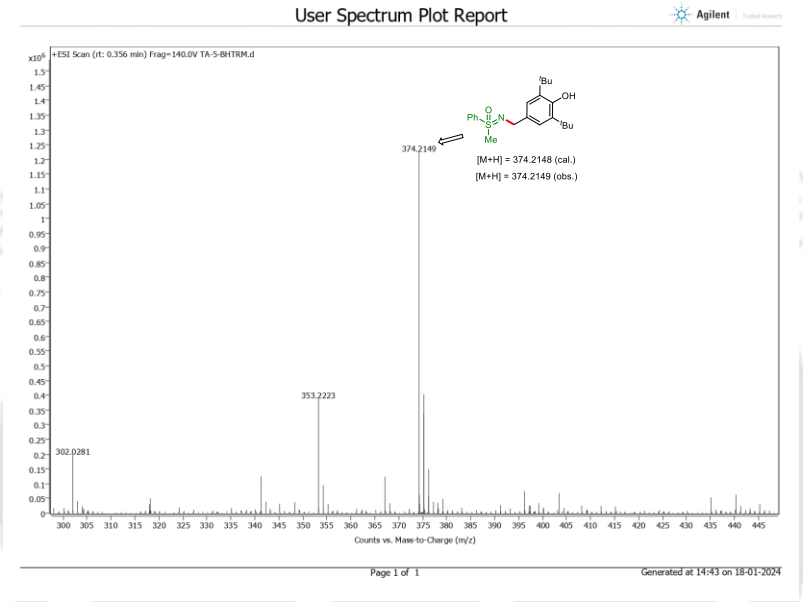

Figure VI.6. *HRMS spectrum of BHT-adduct (**v**)*

There is a possibility that α-keto acid, under the electrochemical conditions, may generate aldehyde (**x**) and carboxylic acid (y) as possible intermediates. To investigate this, two independent reactions of *NH*-sulfoximine (**1**) with benzaldehyde (**x**) and benzoic acid (**y**) were carried out under the present electrochemical conditions. However, none of these reactions yielded the desired product (**1a**) (Scheme VI.9).

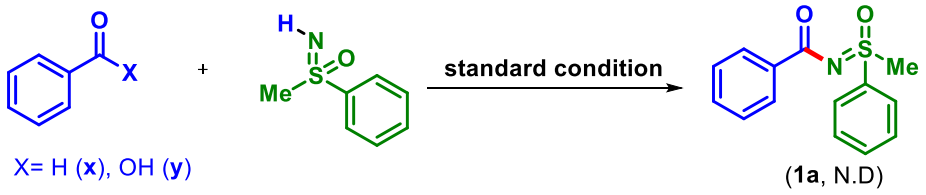

Scheme VI.9. *Possible intermediate detection experiment*

When (**a**) was subjected to electrolysis under the standard conditions without (**1**), benzil (**1a′**) was isolated in 16% yield (Scheme VI.10). These results indicate that an acyl radical might be the key intermediate. If an acyl radical is obtained, there is a possibility of CO_2 elimination via a single electron transfer (SET) process at the anode and generation of hydrogen at the cathode.

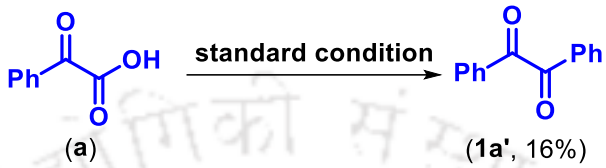

Scheme VI.10. *Possible intermediate detection experiment*

To confirm the H_2 liberation, time-dependent hydrogen production for the standard electrochemical reaction between α-keto acid (**a**) and *NH*-sulfoximine (**1**) was monitored every hour for up to 6 hours. For this, the evolved gas was syringed out at one-hour intervals from the headspace of the reaction mixture and injected into the GC-MS instrument having an Elite Plot-Q column. The GC chromatogram was recorded, and percent evaluation was calculated (Figure VI.7). The hydrogen production at the cathode reached a threshold value within 4 hours. In the next two hours, the hydrogen production decreased. The quantity of hydrogen production is dependent on the overall oxidation of both these substrates (**a**) and (**1**) at the anode.

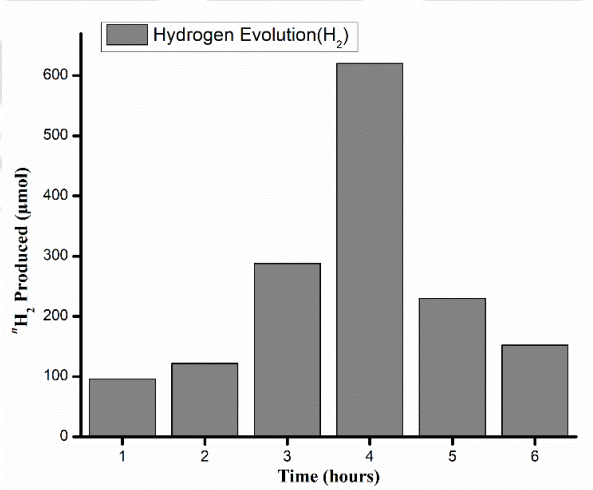

Figure V.7. *Time-dependent evolution of hydrogen (H_2).*

After that, controlled potential electrolysis (bulk electrolysis) reactions were performed under the standard reaction conditions of applying potential 1.5 V, 2 V, and 2.5 V (vs. Ag/AgCl) the reduced yield of (**1a**) was observed (Scheme VI.11).

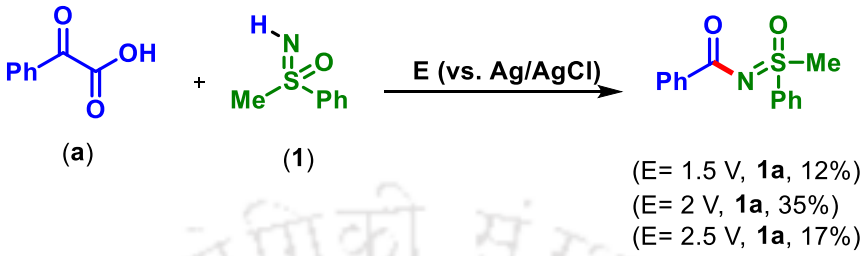

Scheme VI.11. *Controlled potential electrolysis experiment*

To confirm the necessity of the positive voltage for the reaction, the following experiments, cyclic voltammetry (CV), were conducted. One weak oxidative peak at Eox ≈1.63 V (vs. Ag/AgCl in DCE) was observed in the presence of phenylglyoxalic acid (**a**). The incremental concentrations of 10, 20, and 30 mM of K_2CO_3 resulted in the overlapping of all these signals to a single peak and a continuous enhancement of the current. This phenomenon suggests that the oxidation process becomes more facile in the presence of a base [Figure VI.8, (A)].[19a-b] Similarly, the observed oxidation potential of sulfoximine was found to be at E_{ox} ≈3.12 V (vs. Ag/AgCl in DCE). Upon sequential addition of K_2CO_3 at concentrations of 10, 20, and 30 mM to sulfoximine (**1**) causes a minimal alteration of the onset potential but a substantial increase in the current. This outcome validates a robust interaction between K_2CO_3 with (**1**) during the electrochemical oxidation process [Figure VI.8, (B)].[19c] Moreover, to gain deeper insights into the role of the base (K_2CO_3) in the overall coupling reaction, a parallel titration with K_2CO_3 (concentrations of 10, 20, and 30 mM) was carried out in the presence of both substrates (**a**) and (**1**) [Figure VI.8, (C)]. Through CV measurements of the mixture, a distinct peak emerged at Eox ≈ 2.6V vs. Ag/AgCl in DCE. Notably, the current intensity and peak position demonstrated a consistent augmentation with increasing concentrations of K_2CO_3 [Figure VI.8, (C)], indicative of an interaction between the base and the reactive partners.[19a-c]

Electrochemical studies were performed to gain further mechanistic insights into the anodic processes. A parallel study of voltage over time was conducted to monitor the effective potential applied to the working electrode during electrolysis under a 10 mA current. It was

observed that the voltage remained around 1.25–2.75 V throughout the electrolytic process. This voltage profile signifies an actively sustained electrolysis with a steady reaction rate, demonstrating the stability and effectiveness of the process [Figure VI.8, (D)].[19d].

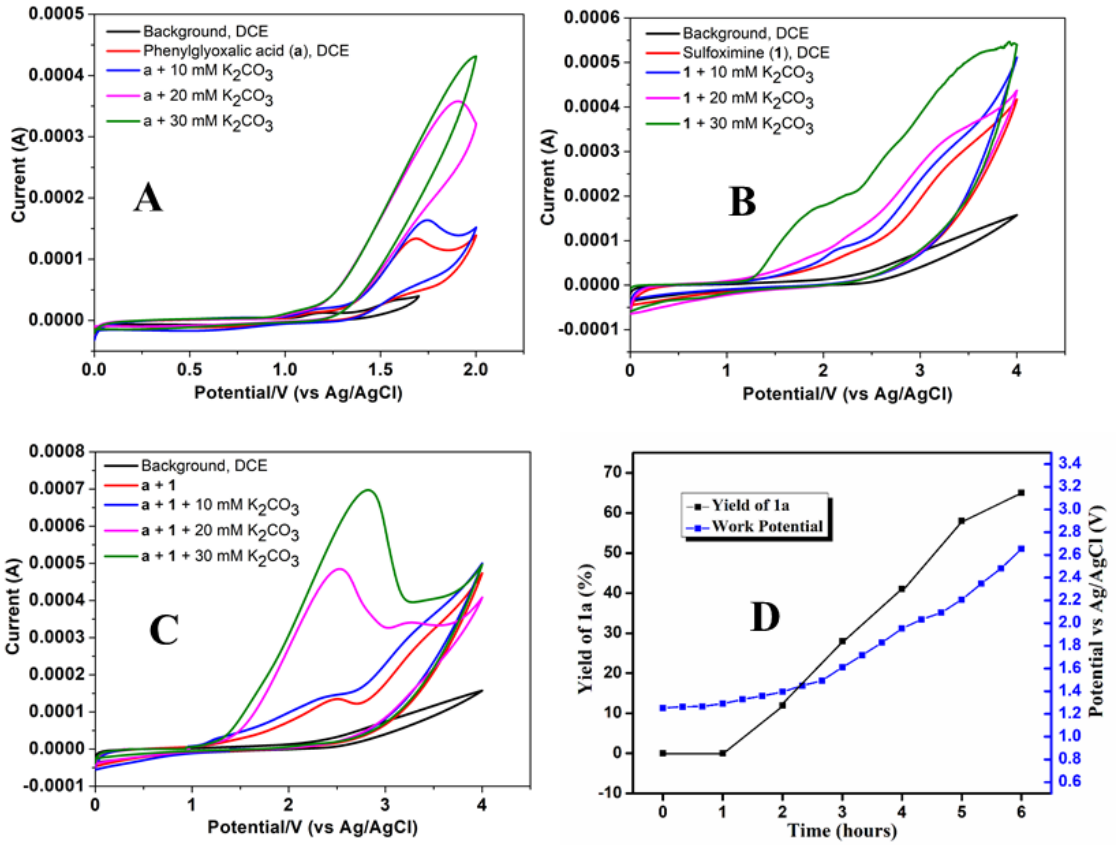

Figure VI.8. *Cyclic voltammetry studies. (A) Cyclic voltammograms of phenylglyoxalic acid (a). (B) Cyclic voltammograms of sulfoximine (1). (C) Cyclic voltammograms of phenylglyoxalic acid (a) and sulfoximine (1). (D) The relationship between time, yield, and potential.*

VI.4.2. Plausible Reaction Mechanism

Based on electrochemical studies, the results obtained from control experiments, and previous literature[19-21] reports, a mechanism for the *N*-acylated is proposed in Scheme VI.12. Initially, base-mediated deprotonation of α-keto acid provided α-oxocarboxylate intermediate (**A**). Then, anodic oxidation of α-oxocarboxylate (**A**) through a single electron transfer followed by decarboxylation gives the benzoyl radical species (**C**).[11j-l] Meanwhile, in a similar fashion, (**1**) was deprotonated to give its conjugate base (**D**), which provided the *N*-centered sulfoximidoly radical (**E**)[20] *via* anodic oxidation. Finally, the radical–radical cross-

coupling between intermediate (**C**) and intermediate (**E**) affords the sulfoximidation product (**1a**).[21] At the cathode, two H^+ were reduced to evaluate hydrogen gas. Further, quantitative analysis of hydrogen production is also illustrated with the help of the GC-TCD method.

Scheme VI.12. Plausible mechanisms

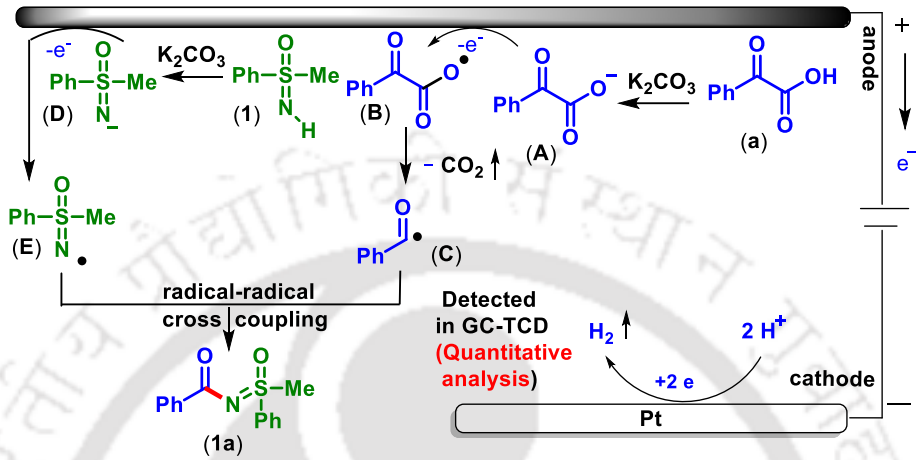

VI.5. Conclusion

In summary, we have established an operationally simple, efficient electrochemical method for the *N*-acylation of sulfoximine that operates without the use of metal catalysts or external oxidants. The mechanistic investigation reveals a cross-coupling reaction between *in situ* generated benzoyl and sulfoximidoyl radicals take place. The present strategy renders a streamlined synthesis of bio-relevant sulfoximine *via* late-stage functionalization, suggesting good functional group compatibility. This approach produces H_2 and CO_2 as the only by-products which can serve as a clean energy source. This transformation possesses general and scalable features that are expected to be utilized for wide-scale industrial and biological applications.

VI.6. Experimental Section

VI.6.1. General information: All the reagents were commercial grade and purified according to the established procedures. All the reagents were commercial grade and used without further purification unless otherwise stated. Preparation of the starting materials was carried out in an oven-dried 100 mL or 50 mL round bottom flask. Reactions were monitored by thin layer chromatography (TLC) on 0.25 mm silica gel plates ($60F_{254}$) and visualized

under UV illumination at 254 nm. Organic extracts were dried over anhydrous sodium sulfate (Na_2SO_4). Column chromatography was performed to purify the crude product on silica gel 60–120 mesh using a mixture of hexane and ethyl acetate as eluent. The isolated compounds were characterized by spectroscopic [^1H, $^{13}C\{1H\}$ NMR, and IR] techniques and HRMS analysis. NMR spectra were recorded in deuterochloroform ($CDCl_3$) or deuterated dimethyl sulfoxide (DMSO-d^6). ^1H, $^{13}C\{^1H\}$ were recorded in 600 (150) or 500 (125) MHz spectrometer and were calibrated using tetramethylsilane or residual undeuterated solvent for ^1H NMR, deuterochloroform for ^{13}C NMR as an internal reference {$Si(CH_3)_4$: 0.00 ppm or $CHCl_3$: 7.260 ppm for ^1H NMR, 77.230 ppm for ^{13}C NMR or $(CH_3)_2SO$: 2.50 ppm for ^1H NMR, 39.50 ppm for ^{13}C NMR}. ^{19}F NMR was calibrated without any internal standard in $CDCl_3$ and DMSO-d^6 in a 500 MHz spectrometer. The chemical shifts are quoted in δ units, parts per million (ppm). ^1H NMR data is represented as follows: Chemical shift, multiplicity (s = singlet, d = doublet, t = triplet, q = quartet, m = multiplet), integration and coupling constant(s) *J* in hertz (Hz). High-resolution mass spectra (HRMS) were recorded on a mass spectrometer using electrospray ionization-time of flight (ESI-TOF) reflection experiments. FT-IR spectra were recorded in KBr or neat and reported in the absorption frequency (cm^{-1}). The instrument used for the electrolysis is a dual-display METRAVI RPS-6005/RPS-6002 adjustable 60V/5A DC Power Supply (Made in India). The anodic electrode was a carbon rod (Φ 6 mm), and the cathodic electrode was a platinum plate (10 mm ×10 mm × 0.3 mm). All the reactions were carried out using an oven-dried three-neck cell under a nitrogen atmosphere. IUPAC names were obtained using the ChemDraw Professional 16.0 software. The α-keto Acids were purchased from BLD pharm.

VI.6.2. Crystallographic Information

(A) Sample Preparation:

The single crystal of compound (**8a)** was prepared by the slow evaporation method, for which 15 mg of the compound (**8a**) was dissolved in 1 mL of methanol in a clean and dry 10 mL glass vial. DCM (1 mL) was added to this solution slowly with a dropper. The mouth of the glass vial was covered with a cap having a small hole and kept for slow evaporation at room temperature. Crystals of (**8a)** were obtained as a transparent white needle-like shape after 3 days.

(B) Crystallographic Description of *N*-((3-fluorophenyl)(methyl)(oxo)- λ^6-sulfaneylidene)benzamide (8a):

Diffraction data were collected at 292 K with MoKα radiation (λ = 0.71073 Å) using a Bruker Nonius SMART APEX CCD diffractometer equipped with graphite monochromator and Apex CD camera. The SMART software was used for data collection for indexing the reflections and determining the unit cell parameters. Data reduction and cell refinement were performed using SAINT[1,2] software, and the space groups of these crystals were determined from systematic absences by XPREP and further justified by the refinement results. The structures were solved by direct methods and refined by full-matrix least-squares calculations using SHELXTL-97[3] software. All the non-H atoms were refined in the anisotropic approximation against F^2 of all reflections.

1. G. M. Sheldrick, SADABS, 1996, based on the method described in: R. H. Blessing, *Acta Crystallogr.* 1995, **A51**, 33–38.
2. SMART and SAINT, Siemens Analytical X-ray Instruments Inc., Madison, WI, 1996.
3. G. M. Sheldrick, *Acta Crystallogr.*, 2008, **A64**, 112–122.

$C_{14}H_{12}FNO_2S$, crystal dimensions 0.32 x 0.22 x 0.20 mm, M_r = 277.31, monoclinic, space group P 21/n, a= 5.6814 (3), b= 24.1630 (13), c= 9.9621 (6) Å, α =90, β = 93.063 (2), γ = 90 , V = 1365.64 (13) Å^3, Z = 4, ρ_{calcd} = 1.349 mg/m^3, μ = 0.245 mm^{-1}, F(000) = 576.0, refinement method = full-matrix least-squares on F^2, final R indices [$I > 2\sigma(I)$]: R_1 = 0.0391 (2310), wR_2 = 0.0949 (2586), goodness of fit = 1.000. CCDC 2332707 for N-((3-fluorophenyl)(methyl)(oxo)- λ^6-sulfaneylidene)benzamide (**8a**) contains the supplementary crystallographic data for this paper. These data can be obtained free of charge from The Cambridge Crystallographic Data Centre via www.ccdc.cam.ac.uk/data_request/cif.

VI.6.3. General Procedure for the Synthesis of *NH*-Sulfoximines (1–22)

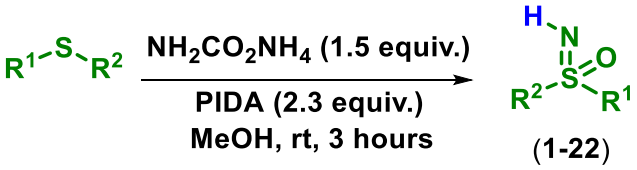

Scheme VI.13. *Preparation of NH-sulfoximine derivatives*

In an oven-dried 50 mL round bottom flask, methylphenylsulfide (2 mmol, 1 equiv, 248 mg), ammonium carbamate (3 mmol, 1.5 equiv, 234 mg), and phenyliodo diacetate (PIDA) (4.6 mmol, 2.3 equiv, 1.48 g) in 15 mL methanol are taken and stirred at room temperature for 3 hours. After the disappearance of the sulfides, as indicated by TLC, the reaction was stopped, and the solvent was evaporated under reduced pressure. Then, the mixture was admixed with ethyl acetate (40 mL), and the organic layer was washed with brine (1 x 20 mL). The organic layer was dried over anhydrous Na_2SO_4, and the solvent was evaporated under reduced pressure. The compound was purified by column chromatography and separated in 80% of EtOAc in hexane to produce S-phenyl-S-methyl-sulfoximine (**1**) in 242 mg, 78% yield (Scheme VI.13).

VI.6.4. General Procedure for the Synthesis of *N*-(Methyl(oxo)(phenyl)-λ^6-sulfaneylidene)benzamide (1a) from α-Keto acid (a) and *NH*-Sulfoximine (1)

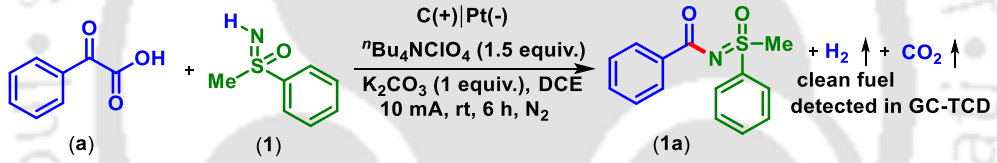

Scheme VI.14. *Synthesis of N-(methyl(oxo)(phenyl)-λ^6-sulfaneylidene)benzamide (1a)*

To an oven-dried undivided three-necked flask (50 mL) equipped with a magnetic bar, was added phenylglyoxylic acid (**a**) (150.13 mg, 1 mmol, 2.0 equiv), tetrabutylammonium perchlorate (^{n}Bu$_4$NClO$_4$) (256.43 mg, 0.75 mmol, 1.5 equiv) and potassium carbonate (K_2CO_3) (69.10 mg, 0.5 mmol, 1.0 equiv). Then the flask was equipped with the graphite rod (Φ 6 mm; immersion depth in solution about 15 mm) as the anode, the platinum plate (10 mm ×10 mm × 0.3 mm) as the cathode maintaining a distance of 6 mm between the electrodes and was flushed with nitrogen (N_2). Then sulfoximine (**1**) (77.61 mg, 0.5 mmol) in 1,2-Dichloroethane (DCE) (5 mL) was added via a syringe under nitrogen atmosphere. The reaction mixture was stirred and electrolyzed at a constant current of 10 mA at room temperature for 6 hours. After completion of the reaction (monitored by TLC analysis), the solvent was removed in vacuum, the mixture was admixed with ethyl acetate (25 mL), and the organic layer was washed with brine (1 x 10 mL). The organic layer was dried over

anhydrous Na_2SO_4, and the solvent was evaporated under reduced pressure. The crude product was purified over a column of silica gel using 25% ethyl acetate in hexane to afford the *N*-(methyl(oxo)(phenyl)-λ^6-sulfaneylidene)benzamide (**1a**) in 65% yield (84.1 mg) (Scheme IV.14). The identity and purity of the product were confirmed by spectroscopic analysis.

Reaction Set-up:

For the electrolysis, an undivided three-neck cell (50 mL) three white silicone rubber septa, a teflon-coated magnetic bar, a carbon rod (Φ 6 mm) as an anode, a platinum plate (10 mm × 10 mm × 0.3 mm) as a cathode and a dual display METRAVI RPS-6005/RPS-6002 adjustable 60V/2A DC and Gamry (interface 1010T) power supply was used (Figure VI.9).

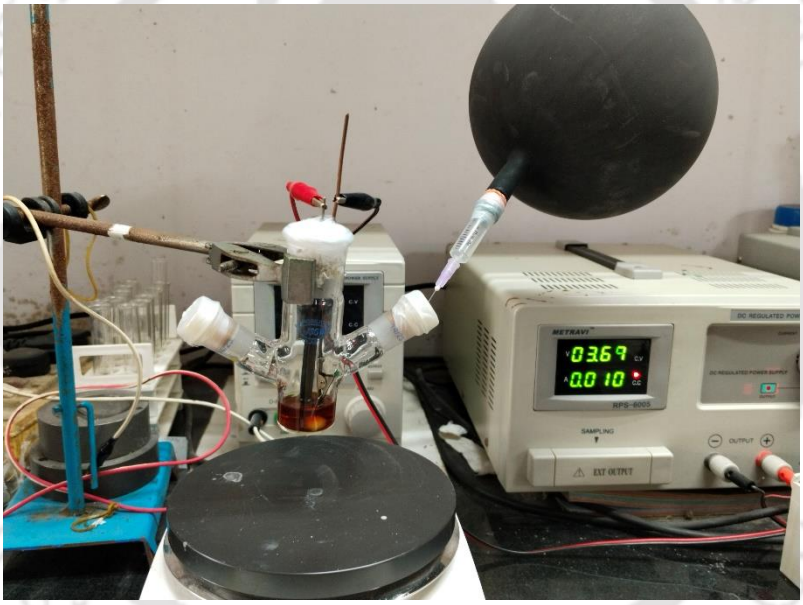

Figure VI.9. *Electrochemical reaction set-up*

VI.6.5. General Procedure for 10 mmol Scale Reaction

To an oven-dried undivided two-necked flask (100 mL) equipped with a magnetic bar, was added phenylglyoxylic acid (**a**) (3.00 g, 20 mmol), and tetrabutylammonium perchlorate ($^nBu_4NClO_4$) (5128.65 mg, 15.0 mmol, 1.5 equiv) and potassium carbonate(K_2CO_3) (1.38 g, 10.0 mmol, 1.0 equiv). Then, the flask was equipped with the graphite rod (Φ 6 mm; immersion depth in solution about 15 mm) as the anode, the platinum plate (10 mm ×10 mm × 0.3 mm) as the cathode maintaining a distance of 6 mm between the electrodes and was flushed with nitrogen (N_2). Then, sulfoximine (**1**) (1.55 g, 10 mmol) in

1,2-Dichloroethane (DCE) (50 mL) was added via a syringe under N_2 atmosphere. The reaction mixture was stirred and electrolyzed at a constant current of 10 mA at room temperature for 15 hours. After completion of the reaction (monitored by TLC analysis), the solvent was removed in a vacuum, the mixture was admixed with ethyl acetate (100 mL), and the organic layer was washed with brine (1 x 50 mL). The organic layer was dried over anhydrous Na_2SO_4, and the solvent was evaporated under reduced pressure. The crude product was purified over a column of silica gel using increasing 25% ethyl acetate in hexane to afford the *N*-(methyl(oxo)(phenyl)-λ^6-sulfaneylidene)benzamide (**1a**) in 45% yield (1.16 g). The identity and purity of the product were confirmed by spectroscopic analysis.

VI.6.6. Mechanistic Investigations

Radical-trapping Experiments

(i) To an oven-dried undivided three-necked flask (50 mL) equipped with a magnetic bar was added phenylglyoxylic acid (**a**) (150.13 mg, 1 mmol, 2.0 equiv), tetrabutylammonium perchlorate (^{n}Bu$_4$NClO$_4$) (256.43 mg, 0.75 mmol, 1.5 equiv), potassium carbonate(K_2CO_3) (69.10 mg, 0.5 mmol, 1.0 equiv) and (2,2,6,6-tetramethylpiperidin-1-yl)oxyl (TEMPO) (156 mg, 1.0 mmol, 2 equiv). Then, the flask was equipped with the graphite rod (Φ 6 mm; immersion depth in solution about 15 mm) as the anode, the platinum plate (10 mm ×10 mm × 0.3 mm) as the cathode maintaining a distance of 6 mm between the electrodes and was flushed with nitrogen. Then sulfoximine (**1**) (77.61 mg, 0.5 mmol) in 1,2-Dichloroethane (DCE) (5 mL) was added via a syringe under a nitrogen atmosphere. The reaction mixture was stirred and electrolyzed at a constant current of 10 mA under room temperature for 6 h. After completion of the reaction (monitored by TLC analysis), the solvent was removed in vacuum, the mixture was admixed with ethyl acetate (25 mL), and the organic layer was washed with brine (10 mL). The organic layer was dried over anhydrous Na_2SO_4, and the solvent was evaporated under reduced pressure. The crude product obtained was purified over a column of silica gel using 10% ethyl acetate in hexane to afford the TEMPO-adduct, 2,2,6,6-tetramethylpiperidin-1-yl benzoate (**u**) in 22% yield (28.7 mg) and <15% yield of *N*-(methyl(oxo)(phenyl)-λ^6-sulfaneylidene)benzamide (**1a**).

(ii) To an oven-dried undivided three-necked flask (50 mL) equipped with a magnetic bar was added phenylglyoxylic acid (**a**) (150.13 mg, 1 mmol, 2.0 equiv), tetrabutylammonium perchlorate ($^{n}Bu_4NClO_4$) (256.43 mg, 0.75 mmol, 1.5 equiv), potassium carbonate (K_2CO_3) (69.10 mg, 0.5 mmol, 1.0 equiv) and butylated hydroxytoluene (BHT) (220 mg, 1.0 mmol, 2 equiv). Then, the flask was equipped with the graphite rod (Φ 6 mm; immersion depth in solution about 15 mm) as the anode, the platinum plate (10 mm ×10 mm × 0.3 mm) as the cathode maintaining a distance of 6 mm between the electrodes and was flushed with nitrogen. Then sulfoximine (**1**) (77.61 mg, 0.5 mmol) in 1,2-Dichloroethane (DCE) (5 mL) was added via a syringe under a nitrogen atmosphere. The reaction mixture was stirred and electrolyzed at a constant current of 10 mA under room temperature for 6 h. After completion of the reaction (monitored by TLC analysis), the solvent was removed in vacuum, the mixture was admixed with ethyl acetate (25 mL), and the organic layer was washed with brine (10 mL). The organic layer was dried over anhydrous Na_2SO_4, and the solvent was evaporated under reduced pressure. The crude product obtained was purified over a column of silica gel using 20% ethyl acetate in hexane to afford *N*-(methyl(oxo)(phenyl)-λ^6-sulfaneylidene)benzamide (**1a**) in <15% yield.

Intermediate Detection Experiments

(I) Reaction with benzaldehyde

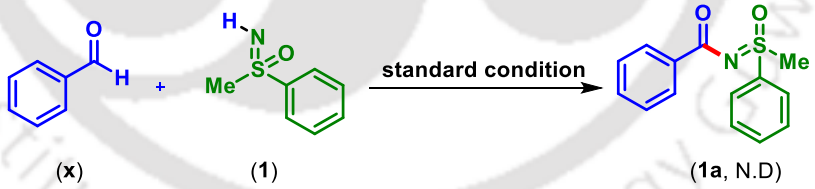

(**x**) (**1**) (**1a**, N.D)

Scheme V.15. *Experiments with benzaldehyde*

To an oven-dried undivided three-necked flask (50 mL) equipped with a magnetic bar was added tetrabutylammonium perchlorate ($^{n}Bu_4NClO_4$) (256.43 mg, 0.75 mmol, 1.5 equiv) and potassium carbonate(K_2CO_3) (69.10 mg, 0.5 mmol, 1.0 equiv). Then the flask was equipped with the graphite rod (Φ 6 mm; immersion depth in solution about 15 mm) as the anode, the platinum plate (10 mm × 10 mm × 0.3 mm) as the cathode, maintaining a distance of 6 mm between the electrodes and was flushed with nitrogen. Then benzaldehyde (**x**) (106

mg, 1 mmol, 2 equiv), and then sulfoximine (**1**) (77.61 mg, 0.5 mmol) in 1,2-Dichloroethane (DCE) (5 mL) were added via a syringe under nitrogen atmosphere. The reaction mixture was stirred and electrolyzed at a constant current of 10 mA under room temperature for 6 h. The formation of *N*-(methyl(oxo)(phenyl)-λ^6-sulfaneylidene)benzamide (**1a**) was not detected (Scheme VI.15), which suggested that aldehyde is not the intermediate of this reaction.

(II) Reaction with benzoic acid

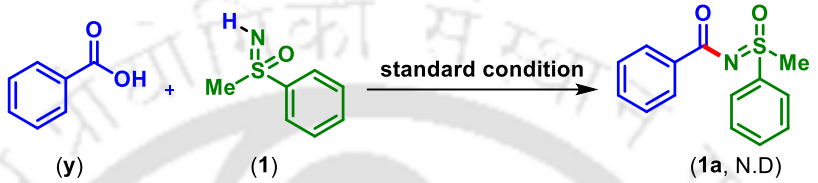

Scheme V.16. *Experiment with benzoic acid*

To an oven-dried undivided three-necked flask (50 mL) equipped with a magnetic bar was added benzoic acid (**y**) (122 mg, 1 mmol, 2 equiv) and tetrabutylammonium perchlorate (^{n}Bu$_4$NClO$_4$) (256.43 mg, 0.75 mmol, 1.5 equiv) and potassium carbonate(K_2CO_3) (69.10 mg, 0.5 mmol, 1.0 equiv). Then the flask was equipped with the graphite rod (Φ 6 mm; immersion depth in solution about 15 mm) as the anode, the platinum plate (10 mm × 10 mm × 0.3 mm) as the cathode maintaining a distance of 6 mm between the electrodes and was flushed with nitrogen. Then sulfoximine (**1**) (77.61 mg, 0.5 mmol) in 1,2-Dichloroethane (DCE) (5 mL) was added via a syringe under a nitrogen atmosphere. The reaction mixture was stirred and electrolyzed at a constant current of 10 mA under room temperature for 6 h. The formation of *N*-(methyl(oxo)(phenyl)-λ^6-sulfaneylidene)benzamide (**1a**) was not detected (Scheme VI.16), which suggested that benzoic acid is not the intermediate of this reaction.

Controlled Potential Electrolysis

The controlled potential electrolysis was performed under standard conditions. To an oven-dried undivided three-necked flask (50 mL) equipped with a magnetic bar, was added phenylglyoxylic acid (**a**) (150.13 mg, 1 mmol, 2.0 equiv), and tetrabutylammonium perchlorate (^{n}Bu$_4$NClO$_4$) (256.43 mg, 0.75 mmol, 1.5 equiv), potassium carbonate(K_2CO_3) (69.10 mg, 0.5 mmol, 1.0 equiv). Then the flask was equipped with the graphite rod (Φ 6 mm; immersion depth in solution about 15 mm) as the anode, the platinum plate (10 mm × 10 mm

× 0.3 mm) as the cathode maintaining a distance of 6 mm between the electrodes and Ag/AgCl as the reference electrode, flushed with nitrogen (N_2). Then sulfoximine (**1**) (77.61 mg, 0.5 mmol) in 1,2-Dichloroethane (DCE) (10 mL) was added via a syringe under a nitrogen atmosphere. The reaction mixture was stirred and electrolyzed at a different constant voltage (1.5 V, 2.0 V, 2.5 V) under room temperature, and the reduced yield of (**1a**) was observed.

VI.6.7. H_2 Gas Production Measurement During Electrolysis

A time-dependent hydrogen production electrolysis experiment was conducted under standard conditions using phenylglyoxylic acid (**a**) (150.13 mg, 1 mmol, 2.0 equiv), tetrabutylammonium perchlorate ($^nBu_4NClO_4$) (256.43 mg, 0.75 mmol, 1.5 equiv), potassium carbonate (K_2CO_3) (69.10 mg, 0.5 mmol, 1.0 equiv). The flask was equipped with the graphite rod (Φ 6 mm) as the anode, the platinum plate (10 mm × 10 mm × 0.3 mm) as the cathode maintaining a distance of 6 mm between the electrodes, and was flushed with nitrogen. Then sulfoximine (**1**) (77.61 mg, 0.5 mmol) in 1,2-Dichloroethane (DCE) (5 mL) was added via a syringe under a nitrogen atmosphere. The reaction mixture was stirred and electrolyzed at a constant current of 10 mA under room temperature and was monitored for up to 6 hours (Scheme VI.17). After every hour, the evolved gas was syringed out from the headspace of the reaction mixture and injected into the PerkinElmer clarus-590 GC instrument using Elite Plot-Q column (30 m length x 530 µm x 20 µm ID) employing the following method. Then, the GC chromatogram was recorded and percent evaluation was calculated.

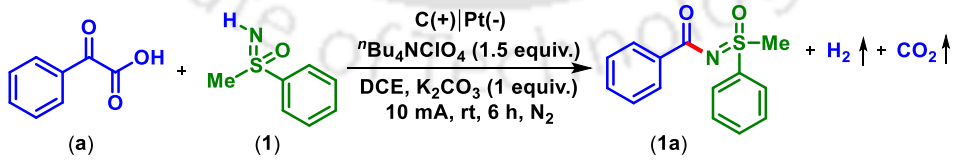

Scheme VI.17. *Time-dependent hydrogen production reaction*

TCD starting temperature: 40 °C

Oven temperature: 60 °C

Time at starting temperature: 0 min

Hold time: 5 min Ramp: 28 °C/ min up to 200 °C

Flow rate: 5 ml/ min (N_2)

Split ratio: 20

Inlet temperature: 40 °C

Detector temperature TCD: 200 °C

The detected gas chromatogram is shown in Figure VI.10.

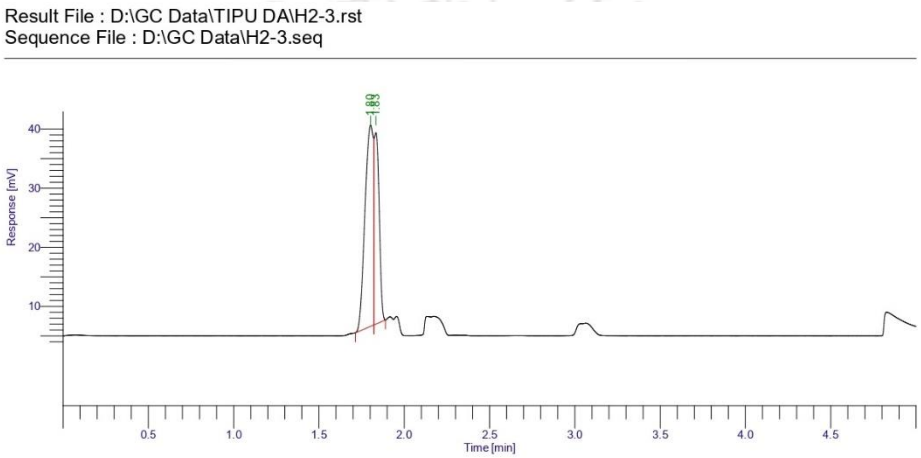

IIT Guwahati Chemistry Dept.

Peak #	Component Name	Time [min]	Area [uV*sec]	Height [uV]	Area [%]
1		1.803	114555.04	34079.91	63.04
2		1.833	67155.08	32390.80	36.96
			181710.12	66470.71	100.00

Figure VI.10. *A representative chromatogram of evolved hydrogen gas during electrolysis*

The hydrogen production from the cathode reached a threshold value within 4 hours. In the next two hours, the hydrogen production decreased. The quantity of hydrogen production depends on the overall oxidation of both these reacting partners (**a**) and (**1**) at the anode.

VI.6.8. Cyclic Voltammetry (CV) Experiments

Cyclic voltammetry experiments were performed using a Gamry instrument in a three-electrode cell connected to an undivided three-necked bottle with a stir bar under a nitrogen

atmosphere at room temperature. The working electrode was a glassy carbon electrode, and the counter electrode was a platinum wire. The reference was an Ag/AgCl electrode.

(i) Cyclic Voltammetry Studies of Phenylglyoxylic Acid (a) to Explore the Reaction at the Anode

Test conditions: A cyclic voltammograms in solvent (5 mL) using glassy carbon as the working electrode, Pt wire as the counter electrode, and Ag/AgCl as the reference electrode under N_2 atm. at room temperature (Figure VI.11). The scan rate was 0.1 V/s.

Black line: 5 mL DCE and $TBAClO_4$ (0.1 M).

Red line: 10 mM phenylglyoxalic acid (**a**) with 5 mL DCE solvent. The three oxidation peaks for (**a**) were observed at 1.63 V (vs Ag/AgCl).

Blue line to Green line: A stepwise addition of 10, 20, and 30 mM of K_2CO_3 resulted in the overlapping of all the signals to a single peak and a continuous enhancement of the current.

This phenomenon suggests that the oxidation process becomes more facile in the presence of a base.

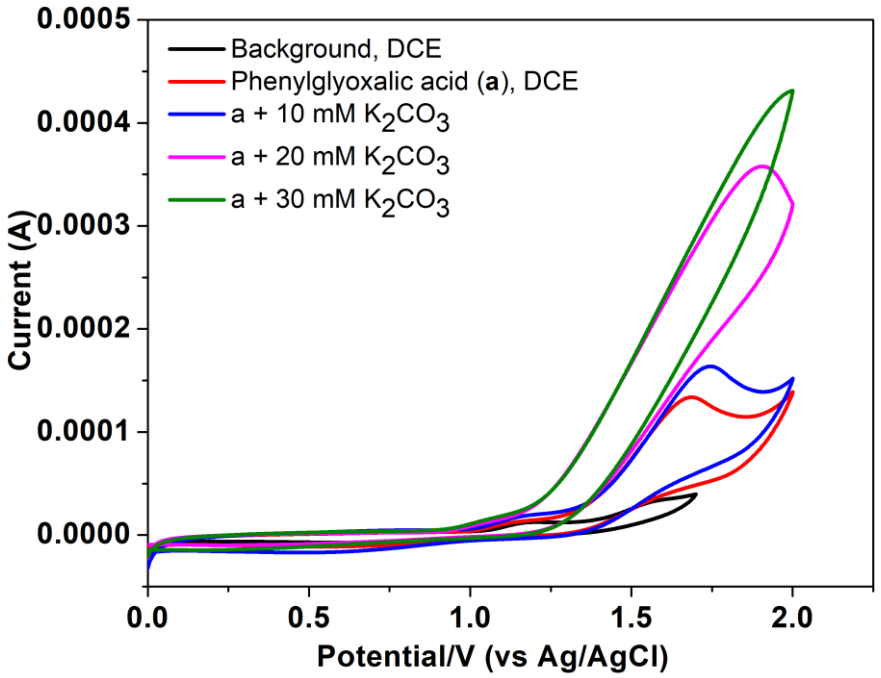

Figure V.11. *Cyclic voltammograms of phenylglyoxalic acid (a)*

(i) Cyclic Voltammetry Studies of Sulfoximine (1) to Explore the Reaction at the Anode:

Test conditions: A cyclic voltammograms in solvent (5 mL) using glassy carbon as the working electrode, Pt wire as the counter electrode, and Ag/AgCl as the reference electrode under N_2 atm. at room temperature (Figure VI.12). The scan rate is 0.1 V/s.

Black line: 5 mL DCE and $TBAClO_4$ (0.1 M).

Red line: 10 mM Sulfoximine (**1**) with 5 mL DCE solvent. The oxidation peaks of (**1**) were observed at 3.12 V (vs Ag/AgCl).

Upon sequential addition of K_2CO_3 10, 20, and 30 mM to sulfoximine (**1**), causes a negligible shift in the onset potential but a substantial increase in the current.

This outcome validates a robust interaction between K_2CO_3 with (**1**) during the electrochemical oxidation process.

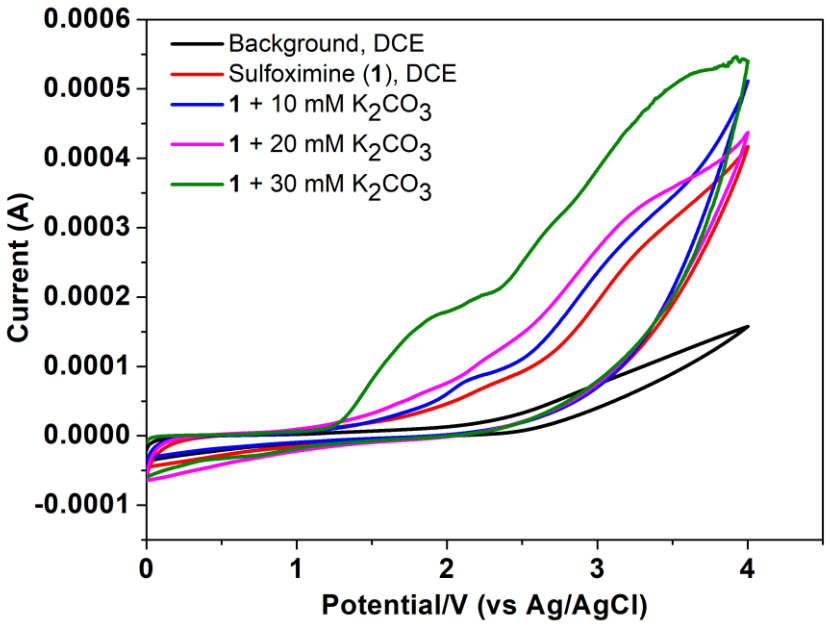

Figure V.12. *Cyclic voltammograms of sulfoximine (1)*

(iii) Cyclic Voltammetry Studies of Mixture of Phenylglyoxylic Acid (a) and Sulfoximine (1) to Explore the Reaction at the Anode:

Test conditions: A cyclic voltammograms in solvent (5 mL) by using glassy carbon as the working electrode, Pt wire as the counter electrode, and Ag/AgCl as the reference electrode under N_2 atm. at room temperature (Figure VI.13). The scan rate is 0.1 V/s.

Black line: 5 mL DCE and $TBAClO_4$ (0.1 M).

Red Line to Green Line: A similar titration with K_2CO_3 (10, 20, and 30 mM) was performed in the presence of both the substrates (**a**) and (**1**). The CV measurements of the mixture show a new peak at 2.6V vs. Ag/AgCl. The current and peak positions virtually increase with an increase in the concentration of K_2CO_3.

Suggesting a strong association of base with both the reacting partners.

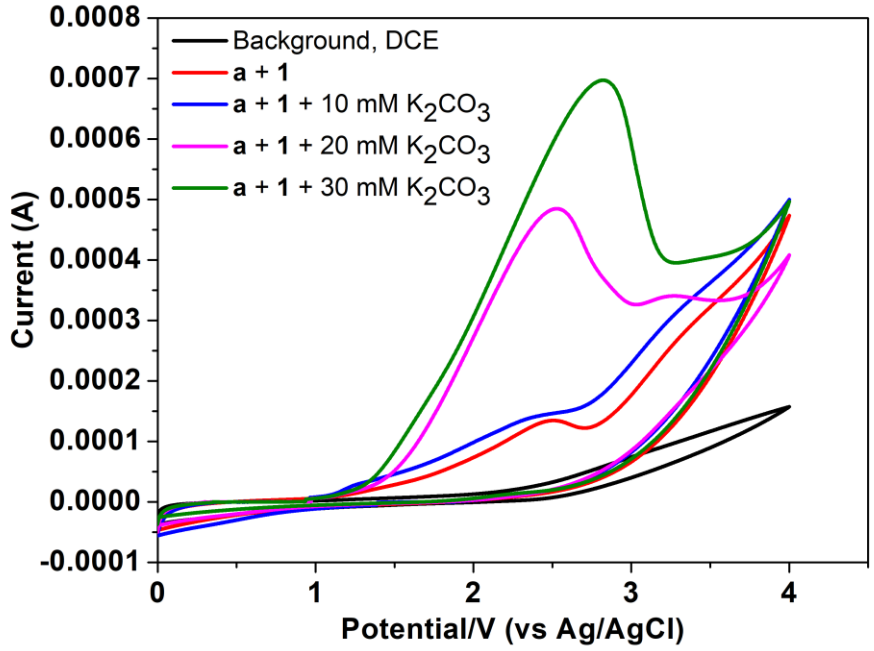

Figure V.13. *Cyclic voltammograms of phenylglyoxylic acid (a) and sulfoximine (1)*

Work Potential During Electrolysis

To monitor the effective potential applied to the working electrode during electrolysis under a 10 mA current, a parallel study of voltage over time was conducted under standard conditions (Scheme S8). To an oven-dried undivided three-necked flask (50 mL) equipped with a magnetic bar, was added phenylglyoxylic acid (**a**) (150.13 mg, 1 mmol, 2.0 equiv), and tetrabutylammonium perchlorate ($^nBu_4NClO_4$) (256.43 mg, 0.75 mmol, 1.5 equiv),

potassium carbonate(K_2CO_3) (69.10 mg, 0.5 mmol, 1.0 equiv). Then the flask was equipped with the graphite rod (Φ 6 mm; immersion depth in solution about 15 mm) as the anode, the platinum plate (10 mm × 10 mm × 0.3 mm) as the cathode maintaining a distance of 6 mm between the electrodes and Ag/AgCl as the reference electrode, flushed with nitrogen (N_2). Then sulfoximine (**1**) (77.61 mg, 0.5 mmol) in 1,2-Dichloroethane (DCE) (10 mL) was added via a syringe under a nitrogen atmosphere. The reaction mixture was stirred and electrolyzed at a constant current of 10 mA under room temperature. The anodic working potential was measured every 5 minutes. In addition, the yield of (**1a**) was measured every 1 hour.

VI.7. References

[1] Bentley, H. R.; McDermott, E. E.; Pace, J.; Whitehead, J. K.; Moran, T. *Nature* **1950**, *165*, 150–151.

[2] (a) Reggelin, M.; Zur, C. *Synthesis* **2000**, *1*, 1–64. (b) Wiezorek, S.; Lamers, P.; Bolm, C. *Chem. Soc. Rev*. **2019**, *48*, 5408–5423.

[3] (a) Luecking, U. *Angew. Chem., Int. Ed*. **2013**, *52*, 9399–9408. (b) Frings, M.; Bolm, C.; Blum, A.; Gnamm, C. *Eur. J. Med. Chem*. **2017**, *126*, 225–245. (c) Boulard, E.; Zibulski, V.; Oertel, L.; Lienau, P.; Schäfer, M.; Ganzer, U.; Lücking, U. *Chem.-Eur. J.* **2020**, *26*, 4378–4388. (d) Sparks, T. C.; Watson, G. B.; Loso, M. R.; Geng, C.; Babcock, J. M.; Thomas, J. D. *Pestic. Biochem. Physiol.* **2013**, *107*, 1–7. (e) Watson, G. B.; Loso, M. R.; Babcock, J. M.; Hasler, J. M.; Letherer, T. J.; Young, C. D.; Zhu, Y.; Casida, J. E.; Sparks, T. C.; *Insect. Biochem. Mol. Biol*. **2011**, *41*, 432–439.

[4] (a) Gnamm, C.; Jeanguenat, A.; Dutton, A. C.; Grimm, C.; Kloer, D. P.; Crossthwaite, A. J.; *Bioorg. Med. Chem. Lett*. **2012**, *22*, 3800–3806. (b) Sparks, T. C.; Watson, G. B.; Loso, M. R.; Geng, C.; Babcock, J. M.; Thomas, J. D. *Pestici. Biochem. Phys*. **2013**, *107*, 1–7.

[5] Kirsch, P.; Lenges, M.; Kühne, D.; Wanczek, K. P. Science. *Eur. J. Org. Chem*. **2005**, 797–802.

[6] (a) Simić, O.; Bolm, C. *J. Am. Chem. Soc*. **2001**, *123*, 3830–3831. (b) Okamura, H.; Bolm, C. *Chem. Lett*. **2004**, *33*, 482−487. (c) Shen, X.; Hu, J.; *Eur. J. Org. Chem*.

2014, 4437−4451. (d) Bizet, V.; Kowalczyk, R.; Bolm, C. *Chem. Soc. Rev*. **2014**, *43*, 2426–2438.

[7] (a) Bolm, C.; Hackenberger, C. P. R.; Simić, O.; Verrucci, M.; Müller, D.; Bienewald, F. *Synthesis* **2002**, *7*, 879–887. (b) Hackenberger, C. P. R.; Raabe, G.; Bolm, C. *Chem.-Eur. J*. **2004**, *10*, 2942–2952.

[8] (a) Garimallaprabhakaran, A.; Harmata, M. *Synlett* **2011**, *3*, 361–364. (b) Noda, H.; Asada, Y.; Shibasaki, M.; Kumagai, N. *Chem. Commun*. **2017**, *53*, 7447–7450.

[9] (a) Bala, B. D.; Sharma, N.; Sekar, G. *RSC Adv*., **2016**, *6*, 97152–97159. (b) Guo, S.; Kumar, P. S.; Yuan, Y.; Yang, M. *Tetrahedron Lett*. 2017, **58**, 2681–2684.

[10] Sarkar, S.; Banerjee, A.; Shah, J. A.; Mukherjee, U.; Frederiks, N. C.; Johnson, C. J.; Ngai, M.-Y. *J. Am. Chem. Soc*. **2022**, *144*, 20884–20894.

[11] (a) Reddy, C. R.; Kolgave, D. H.; Subbarao, M.; Aila, M.; Prajapti, S. K. *Org. Lett*. **2020**, *22*, 5342–5346. (b) Zhou, F.; Li, L.; Lin, K.; Zhang, F.; Deng, G.-J.; Gong, H.; *Chem. -Eur. J*. **2020**, *26*, 4246–4250. (c) Reddy, C. R.; Kajare, R. C.; Punna, N. *Chem. Commun*. **2020**, *56*, 3445–3448. (d) Bogonda, G.; Kim, H. Y.; Oh, K. *Org. Lett*. **2018**, *20*, 2711–2715 (e) Kittikool, T.; Thupyai, A.; Phomphrai, K.; Yotphan, S. *Adv. Synth. Catal*. **2018**, *360*, 3345–3355 (f) Shang, J.-Q.; Wang, X.-X.; Xin, Y.; Li, Y.; Zhou, B.; Li, Y.-M.; *Org. Biomol. Chem*. **2019**, *17*, 9447–9455. (g) Yang, K.; Chen, X.; Wang, Y.; Li, W.; Kadi, A. A.; Fun, H.-K.; Sun, H.; Zhang, Y.; Li, G.; Lu, H.; *J. Org. Chem*. **2015**, *80*, 11065-11072. (h) Zhang, N.; Yang, D.; Wei, W.; Yuan, L.; Nie, F.; Tian, L.; Wang, H.; *J. Org. Chem*. **2015**, *80*, 3258–3263. (i) Guo, L.-N.; Wang, H.; Duan, X.-H. *Org. Biomol. Chem*. **2016**, *14*, 7380–7391. (j) Cheng, Y.-Y.; Yu, J.-X.; Lei, T.; Hou, H.-Y.; Chen, B.; Tung, C.-H.; Wu, L.-Z.; *Angew.Chem.Int. Ed*. **2021**, *60*, 26822–26828. (k) Zhu, H.-L.; Zeng, F.-L.; Chen, X.-L.; Sun, K.; Li, H.-C.; Yuan, X.-Y.; Qu, L.-B.; Yu, B. *Org. Lett*. **2021**, *23*, 2976–2980. (l) Zhu, D.-L.; Wu, Q.; Young, D. J.; Wang, H.; Ren, Z.-G.; Li, H.-X. *Org. Lett*. **2020**, *22*, 6832–6837. (m) Chakraborty, N.; Rajbongshi, K. K.; Gondaliya, A.; Patel, B. K. *Org. Biomol. Chem*., **2024**, *22*, 2375–2379.

[12] (a) Yan, M.; Kawamata, Y.; Baran, P. S. *Chem. Rev*. **2017**, *117*, 13230–13319. (b) Xiong, P.; Xu, H.-C. *Acc. Chem. Res*. **2019**, *52*, 3339–3350. (c) Shi, S.-H.; Liang, Y.;

Jiao, N. *Chem. Rev*. **2021**, *121*, 485−505. (d) Li, M.; Peng, M.; Huang, W.; Zhao, L.; Wang, S.; Kang, C.; Jiang, G.; Ji, F. *Org. Lett*. **2023**, 25, 7529−7534.

[13] (a) Liu, X.; Yang, D.; Liu, Z.; Wang, Y.; Liu, Y.; Wang, S.; Wang, P.; Cong, H.; Chen, Y.-H.; Lu, L.; Qi, X.; Yi, H.; Lei, A. *J. Am. Chem. Soc*. **2023**, *145*, 3175−3186. (b) Yang, D.; Guan, Z.; Peng, Y.; Zhu, S.; Wang, P.; Huang, Z.; Alhumade, H.; Gu, D.; Yi, H.; Lei, A. *Nat. Commun* **2023**, *14*, 1476−1484. (c) Novaes, L. F. T.; Liu, J.; Shen, Y.; Lu, L.; Meinhardt, J. M.; Lin, S. *Chem. Soc. Rev*., **2021**, *50*, 7941−8002. (d) Alam, T.; Patel, B. K. *Chem.-Eur. J*. **2024**, *30*, e2023034.

[14] (a) Harwood, S. J.; Palkowitz, M. D.; Gannett, C. N.; Perez, P.; Yao, Z.; Sun, L.; Abruña, H. D.; Anderson, S. L.; Baran, P. S. *Science* **2022**, *375*, 745−752. (c) Panja, S.; Ahsan, S.; Pal, T.; Kolb, S.; Ali, W.; Sharma, S.; Das, C.; Grover, J.; Dutta, A.; Werz, D. B.; Paul, A.; Maiti, D. *Chem. Sci.*, **2022**, *13*, 9432−9439. (d) Kang, C.; Li, M.; Huang, W.; Wang, S.; Peng, M.; Zhao, L.; Jiang, G.; Ji, F. *Green Chem*., **2023**, *25*, 8838−8844.

[15] Wimmer, A.; König, B. *Adv. Synth. Catal*. **2018**, *360*, 3277−3285.

[16] Pimpasri, C.; Sumunnee, L.; Yotphan, S. *Org. Biomol. Chem*., **2017**, *15*, 4320−4327.

[17] (a) Wang, C.; Ma, D.; Tu, Y.; Bolm, C. *Org. Lett*. **2020**, *22*, 8937−8940. (b) Qiu, P.; Duan, X.; Li, M.; Zheng, Y.; Song, W. *Org. Lett*. **2022**, *24*, 2733−2737. (c) Huang, W.; Wang, S.; Li, M.; Zhao, L.; Peng, M.; Kang, C.; Jiang, G.; Ji, F. *J. Org. Chem*. **2023**, *88*,17511−17520.

[18] (a) Cernak, T.; Dykstra, K. D.; Tyagarajan, S.; Vachal, P.; Krska, S. W. *Chem. Soc. Rev*., **2016**, *45*, 546−576. (b) Mondal, K.; Mallik, S.; Sardana, S.; Baidya, M. *Org. Lett*. **2023**, *25*, 1689−1694.

[19] (a) Kong, X.; Chen, Y.; Chen, X.; Lu, Z.-X.; Wang, W.; Ni, S.-F.; Cao, Z.-Y. *Org. Lett*. **2022**, *24*, 2137−2142. (b) Kong, X.; Liu, Y.; Lin, L.; Chen, Q.; Xu, B. *Green Chem*.,**2019**, *21*, 3796−3801. (c) Li, X.; Huang, J.; Xu, L.; Liu, J.; Wei, Y. *Adv. Synth. Catal*. **2023**, *365*, 4647−4653. (d) Yu, W.; Wang, S.; He, M.; Jiang, Z.; Yu, Y.; Lan, J.; Luo, J.; Wang, P.; Qi, X.; Wang, T.; Lei, A. *Angew. Chem. Int. Ed*. **2023**, *62*, e202219166.

[20] Wan, J.-L.; Huang, J.-M. *Org. Lett.* **2022**, *24*, 8914−8919.

[21] (a) Kim, W.; Kim, H. Y.; Oh, K. *Org.Lett.***2020**, *22*, 6319–6323. (b) Wang, H.; Gao, X.; Lv, Z.; Abdelilah, T.; Lei, A. *Chem. Rev*. **2019**, *119*, 6769–6787.

VI.8. Spectral Data

N-(Methyl(oxo)(phenyl)- λ⁶-sulfaneylidene)benzamide (1a):

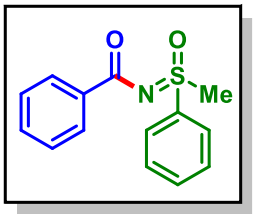

Yield: 65% (84 mg) as a white solid; Purified over a column of silica gel (25% EtOAc in hexane); ^{1}H NMR ($CDCl_3$, 600 MHz): δ 8.17 (d, 2H, J = 6.0 Hz), 8.07 (d, 2H, J = 6.0 Hz), 7.67 (t, 1H, J = 9.0 Hz), 7.62 (t, 2H, J = 6.0 Hz), 7.51 (t, 1H, J = 9.0 Hz), 7.42 (t, 2H, J = 6.0 Hz), 3.47 (s, 3H); ^{13}C{1H} NMR ($CDCl_3$, 150 MHz): δ 174.5, 139.2, 135.8, 134.0, 132.4, 129.9, 129.6, 128.3, 127.4, 44.6.

***N-((4-methoxyphenyl)(methyl)(oxo)- λ⁶-sulfaneylidene)benzamide (2a)*:**

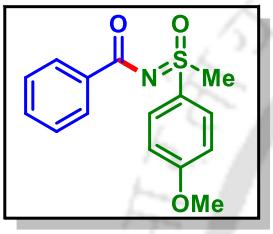

Yield: 50% (72.2 mg) as a white solid; Purified over a column of silica gel (25% EtOAc in hexane); ^{1}H NMR ($CDCl_3$, 400 MHz): δ 8.18–8.15 (m, 2H), 7.62–7.56 (m, 2H), 7.53–7.48 (m, 2H), 7.41 (t, 2H, J = 8.0 Hz), 7.20–7.17 (m, 1H), 3.88 (s, 3H), 3.45 (s, 3H); ^{13}C{^{1}H} NMR ($CDCl_3$, 100 MHz): δ 174.5, 160.5, 140.4, 135.8, 132.4, 130.9, 129.6, 128.2, 120.2, 119.3, 112.2, 55.9, 44.6.

***N-((3-methoxyphenyl)(methyl)(oxo)- λ⁶-sulfaneylidene)benzamide (3a)*:**

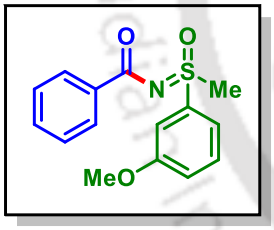

Yield: 48% (69.3 mg) as a white gummy solid; Purified over a column of silica gel (25% EtOAc in hexane); ^{1}H NMR ($CDCl_3$, 600 MHz): δ 8.16 (d, 2H, J = 6 Hz), 7.60 (d, 1H, J = 12 Hz), 7.57 (t, 1H, J = 3 Hz), 7.52–7.49 (m, 2H), 7.41 (t, 2H, J = 6 Hz), 7.20–7.18 (m, 1H), 3.88 (s, 3H), 3.45 (s, 3H); ^{13}C{^{1}H} NMR ($CDCl_3$, 150 MHz): δ 174.5, 160.5, 140.4, 135.7, 132.4, 130.9, 129.6, 128.2, 120.2, 119.3, 112.2, 55.9, 44.6.

***N-(methyl(oxo)(p-tolyl)- λ⁶-sulfaneylidene)benzamide (4a)*:**

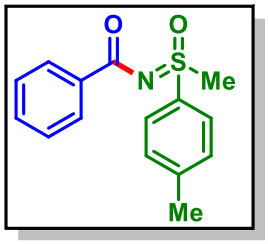

Yield: 62% (84.6 mg) as a white solid; Purified over a column of silica gel (25% EtOAc in hexane); ^{1}H NMR ($CDCl_3$, 400 MHz): δ 8.18–8.16 (m, 2H), 7.93 (d, 2H, J = 8.0 Hz), 7.53–7.48 (m, 1H), 7.41 (t, 4H, J = 6.0 Hz), 3.45 (s, 3H), 2.46 (s, 3H); ^{13}C{^{1}H} NMR ($CDCl_3$, 100 MHz): δ 174.4, 145.1, 136.1, 135.9, 132.3, 130.5, 129.6, 128.2, 127.4, 44.7.

***N-(methyl(oxo)(o-tolyl)- λ⁶-sulfaneylidene)benzamide (5a)*:**

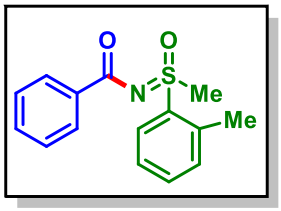

Yield: 55% (75 mg) as a white solid; Purified over a column of silica gel (25% EtOAc in hexane); ^{1}H NMR ($CDCl_3$, 400 MHz): δ 8.18–8.13 (m, 3H), 7.54–7.44 (m, 3H), 7.43–7.34 (m, 3H), 3.47 (s, 3H), 2.69 (s, 3H); $^{13}C\{^{1}H\}$ NMR ($CDCl_3$, 100 MHz): δ 174.1, 137.13, 137.10, 135.7, 133.9, 133.4, 132.3, 129.6, 129.4, 128.2, 127.3, 43.4, 20.7.

***N-((3-chlorophenyl)(methyl)(oxo)- λ^6-sulfaneylidene)benzamide (6a)*:**

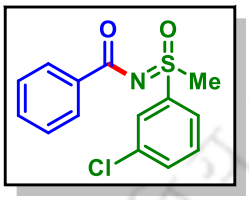

Yield: 44% (64.5 mg) as a white solid; Purified over a column of silica gel (25% EtOAc in hexane); ^{1}H NMR ($CDCl_3$, 600 MHz): δ 8.15 (d, 2H, J = 6 Hz), 8.04 (s, 1H), 7.93 (d, 1H, J = 6. 0 Hz), 7.65 (d, 1H, J = 12. 0 Hz), 7.57–7.51 (m, 2H), 7.42 (t, 2H, J = 9. 0 Hz), 3.46 (s, 3H); $^{13}C\{^{1}H\}$ NMR ($CDCl_3$, 150 MHz): δ 174.4, 141.0, 136.2, 135.4, 134.2, 132.6, 131.2, 129.7, 128.3, 127.5, 125.5, 44.6.

***N-((4-chlorophenyl)(methyl)(oxo)- λ^6-sulfaneylidene)benzamide (7a)*:**

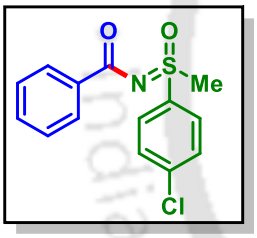

Yield: 60% (88 mg) as a white solid; Purified over a column of silica gel (25% EtOAc in hexane); ^{1}H NMR ($CDCl_3$, 600 MHz): δ 8.14 (d, 2H, J = 6.0 Hz), 7.98 (d, 2H, J = 12.0 Hz), 7.58 (d, 2H, J = 6.0 Hz), 7.52 (t, 1H, J = 9.0 Hz), 7.41 (t, 2H, J = 9.0 Hz), 3.45 (s, 3H); $^{13}C\{^{1}H\}$ NMR ($CDCl_3$, 150 MHz): δ 174.4, 140.8, 137.6, 135.4, 132.5, 130.2, 129.6, 128.9, 128.3, 44.6.

***N-((3-fluorophenyl)(methyl)(oxo)- λ^6-sulfaneylidene)benzamide (8a)*:**

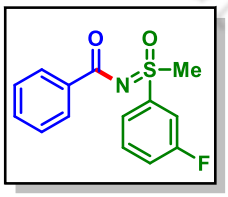

Yield: 51% (70.6 mg) as a white solid; Purified over a column of silica gel (25% EtOAc in hexane); ^{1}H NMR ($CDCl_3$, 400 MHz): δ 8.17–8.15 (m, 2H), 7.87–7.84 (m, 1H), 7.79–7.76 (m, 1H), 7.64–7.59 (m, 1H), 7.55–7.50 (m, 1H), 7.44–7.37 (m, 3H), 3.47 (s, 3H); $^{13}C\{^{1}H\}$ NMR ($CDCl_3$, 100 MHz): δ 174.7, 162.8 (d, J = 235 Hz), 140.8 (d, J = 135 Hz), 135.5, 132.6, 131.8 (d, J = 60 Hz), 129.7, 128.3, 123.2, 121.3, 115.0 (d, J = 25 Hz), 44.5.

***N-(isopropyl(oxo)(phenyl)- λ^6-sulfaneylidene)benzamide (9a)*:**

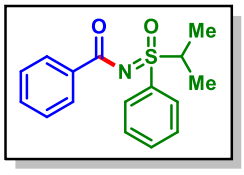

Yield: 45% (64.5 mg) as a white solid; Purified over a column of silica gel (25% EtOAc in hexane); ^{1}H NMR ($CDCl_3$, 600 MHz): δ

8.18 (d, 2H, *J* = 6.0 Hz), 7.93 (d, 2H, *J* = 6 Hz), 7.66 (t, 1H, *J* = 9.0 Hz), 7.58 (t, 2H, *J* = 9 Hz), 7.50 (t, 1H, *J* = 9 Hz), 7.41 (t, 2H, *J* = 6 Hz), 3.79–7.72 (m, 1H), 1.47 (d, 3H, *J* = 6 Hz), 1.32 (d, 3H, *J* = 6 Hz); $^{13}C\{^{1}H\}$ NMR ($CDCl_3$, 150 MHz): δ 174.3, 136.1, 134.8, 133.8, 132.2, 129.6, 129.0, 128.2, 56.5, 15.9, 15.5.

***N-((4-Methylbenzyl)(oxo)(phenyl)- λ⁶-sulfaneylidene)benzamide (10a)*:**

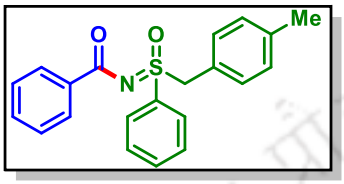

Yield: 65% (113.4 mg) as a white solid; Purified over a column of silica gel (25% EtOAc in hexane); ^{1}H NMR ($CDCl_3$, 400 MHz): δ 8.19–8.17 (m, 2H), 7.73–7.70 (m, 2H), 7.65–7.61 (m, 1H), 7.52–7.41 (m, 5H), 7.01 (d, 2H, *J* = 8 Hz), 6.89 (d, 2H, *J* = 8 Hz), 4.91 (d, 1H, *J* = 16 Hz), 4.82 (d, 1H, *J* = 16 Hz), 2.29 (s, 3H); $^{13}C\{^{1}H\}$ NMR ($CDCl_3$, 100 MHz): δ 174.8, 139.4, 135.9, 133.9, 132.3, 131.3, 129.7, 129.5, 129.3, 128.8, 128.2, 124.4, 62.2, 21.4.

***N-(methyl(naphthalen-2-yl)(oxo)- λ⁶-sulfaneylidene)benzamide (11a)*:**

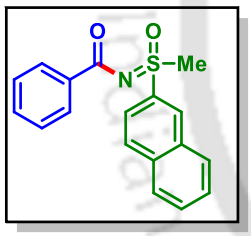

Yield: 50% (77.3 mg) as a white gummy solid; Purified over a column of silica gel (25% EtOAc in hexane); ^{1}H NMR ($CDCl_3$, 600 MHz): δ 8.66 (s, 1H), 8.20 (d, 2H, *J* = 12.0 Hz), 8.03 (t, 2H, *J* = 9.0 Hz), 7.95 (t, 2H, *J* = 12.0 Hz), 7.69 (t, 1H, *J* = 9.0 Hz), 7.64 (t, 1H, *J* = 9.0 Hz), 7.52 (t, 1H, *J* = 6.0 Hz), 7.42 (t, 2H, *J* = 9.0 Hz), 3.53 (s, 3H); $^{13}C\{^{1}H\}$ NMR ($CDCl_3$, 150 MHz): δ 174.5, 135.9, 135.8, 135.5, 132.5, 132.4, 130.3, 129.65, 129.63, 129.4, 128.21, 128.10, 121.7, 44.6.

***N-(Methyl(oxo)(thiophen-2-yl)- λ⁶-sulfaneylidene)benzamide (12a)*:**

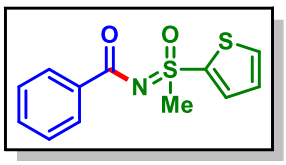

Yield: 58% (76.8 mg) as a white solid; Purified over a column of silica gel (25% EtOAc in hexane); ^{1}H NMR ($CDCl_3$, 600 MHz): δ 8.17–8.16 (m, 2H), 7.87–7.86 (m, 1H), 7.77–7.76 (m, 1H),7.53–7.51 (m, 1H), 7.42 (t, 2H, *J* = 9.0 Hz), 7.21–7.19 (m, 1H), 3.64 (s, 3H); $^{13}C\{^{1}H\}$ NMR ($CDCl_3$, 150 MHz): δ 174.3, 139.8, 135.5, 134.8, 133.9, 132.5, 129.6, 128.5, 128.3, 46.1.

***N-(5-Oxido-5 λ⁴-dibenzo[b,d]thiophen-5-ylidene)benzamide (13a)*:**

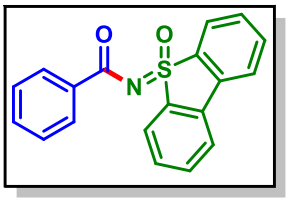

Yield: 51% (89.5 mg) as a white solid; Purified over a column of silica gel (25% EtOAc in hexane); ^{1}H NMR ($CDCl_3$, 600 MHz): δ 8.34 (d, 2H, J = 6.0 Hz), 8.12 (d, 2H, J = 6.0 Hz), 7.86 (d, 2H, J = 6.0 Hz), 7.71 (t, 2H, J = 6.0 Hz), 7.60 (t, 2H, J = 6.0 Hz), 7.48 (t, 1H, J = 9.0 Hz), 7.37 (t, 2H, J = 6.0 Hz); ^{13}C{^{1}H} NMR ($CDCl_3$, 150 MHz): δ 175.3, 137.4, 135.2, 134.6, 133.3, 132.5, 130.9, 129.8, 128.2, 125.8, 121.9.

***Methyl 4-(N-benzoyl-S-methylsulfonimidoyl)-2-((tert-butoxycarbonyl)amino)butanoate (14a)*:**

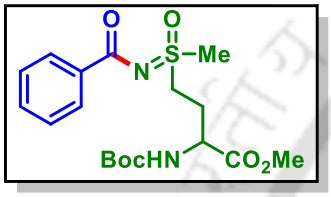

Yield: 21% (41.8 mg) as a white gummy solid; Purified over a column of silica gel (25% EtOAc in hexane); ^{1}H NMR ($CDCl_3$, 400 MHz): δ 8.11 (d, 2H, J = 8.0 Hz), 7.50 (t, 1H, J = 6.0 Hz), 7.40 (t, 2H, J = 8.0 Hz), 5.27 (s, 1H), 4.45 (s, 1H), 3.77 (s, 3H), 3.68–3.53 (m, 2H), 3.37 (d, 3H, J = 4.0 Hz), 2.54–2.47 (m, 1H), 2.29–2.20 (m, 1H), 1.44 (d, 9H, J = 4.0 Hz) ; ^{13}C{^{1}H} NMR ($CDCl_3$, 100 MHz): δ 174.2, 171.7, 135.5, 132.4, 129.54, 129.52, 128.3, 80.9, 53.1, 52.2, 50.7, 40.1, 40.0, 28.5, 25.6.

***4-Methoxy-N-(methyl(oxo)(phenyl)- λ^6-sulfaneylidene)benzamide (1b)*:**

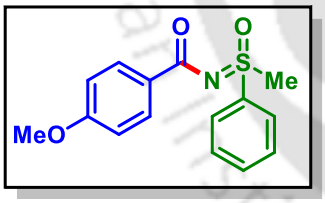

Yield: 65% (94 mg) as a white solid; Purified over a column of silica gel (25% EtOAc in hexane); ^{1}H NMR ($CDCl_3$, 600 MHz): δ 8.13 (d, 2H, J = 6.0 Hz), 8.05 (d, 2H, J = 6.0 Hz), 7.68 (t, 1H, J = 6.0 Hz), 7.61 (t, 2H, J = 6.0 Hz), 6.90 (d, 2H, J = 12.0 Hz), 3.85 (s, 3H). 3.45 (s, 3H); ^{13}C{^{1}H} NMR ($CDCl_3$, 150 MHz): δ 174.0, 163.1, 139.4, 133.9, 131.7, 129.8, 128.4, 127.4, 113.4, 55.6, 44.6.

***4-Fluoro-N-(methyl(oxo)(phenyl)- λ^6-sulfaneylidene)benzamide (1c)*:**

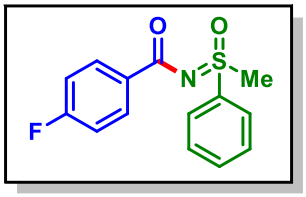

Yield: 67% (92.8 mg) as a white solid; Purified over a column of silica gel (25% EtOAc in hexane); ^{1}H NMR ($CDCl_3$, 600 MHz): δ 8.19–8.16 (m, 2H), 8.05 (d, 2H, J = 12.0 Hz), 7.70 (t, 1H, J = 6.0 Hz), 7.63 (t, 2H, J = 9.0 Hz), 7.07 (t, 2H, J = 9.0 Hz), 3.47 (s, 3H); ^{13}C{^{1}H} NMR ($CDCl_3$, 150 MHz): δ 173.4, 165.6 (d, J = 250.5 Hz),

139.1, 134.1, 132.1 (d, J = 9.0 Hz), 127.3, 115.2 (d, J = 22.5 Hz), 44.6. ^{19}F NMR ($CDCl_3$, 471 MHz): δ –107.5 (s).

***4-Fluoro-N-((3-methoxyphenyl)(methyl)(oxo)- λ⁶-sulfaneylidene)benzamide (3c)*:**

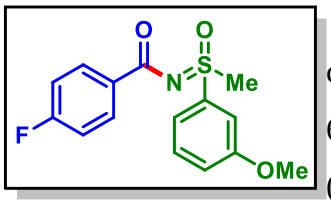

Yield: 60% (92.1 mg) as a white solid; Purified over a column of silica gel (35% EtOAc in hexane); ^{1}H NMR ($CDCl_3$, 600 MHz): δ 8.18–8.16 (m, 2H), 7.59 (d, 1H, J = 12.0 Hz), 7.55 (s, 1H), 7.51 (t, 1H, J = 6.0 Hz), 7.20 (d, 1H, J = 6.0 Hz), 7.07 (t, 2H, J = 9.0 Hz), 3.89 (s, 3H), 3.45 (s, 3H); ^{13}C{^{1}H} NMR ($CDCl_3$, 150 MHz): δ 173.4, 165.6 (d, J = 250.5 Hz), 160.6, 140.2, 132.1(d, J = 9.0 Hz), 131.0, 120.3, 119.2 115.2 (d, J = 21.0 Hz), 112.2, 56.0, 44.6. ^{19}F NMR ($CDCl_3$, 471 MHz): δ –107.6 (s); IR (KBr, cm^{-1}): 3043, 2932, 1616, 1456, 1272, 732; HRMS (ESI/Q-TOF) (m/z) calcd for $C_{15}H_{15}FNO_3S$, $[M + H]^+$: 308.0751, found 308.0748.

***N-((3-Chlorophenyl)(methyl)(oxo)- λ⁶-sulfaneylidene)-4-fluorobenzamide (6c)*:**

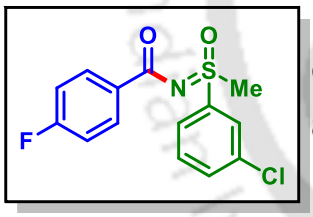

Yield: 53% (82.4 mg) as a white solid; Purified over a column of silica gel (35% EtOAc in hexane); ^{1}H NMR ($CDCl_3$, 600 MHz): δ 8.18–8.14 (m, 2H), 8.02 (s, 1H), 7.92 (d, 1H, J = 6.0 Hz), 7.66 (d, 1H, J = 12.0 Hz), 7.57 (t, 1H, J = 9.0 Hz), 7.08 (t, 2H, J = 9.0 Hz), 3.45 (s, 3H); ^{13}C{^{1}H} NMR ($CDCl_3$, 150 MHz): δ 173.3, 165.7 (d, J = 252 Hz), 140.9, 136.2, 134.3, 132.2 (d, J = 9.0 Hz), 131.6 (d, J = 3 Hz), 131.2, 127.5, 125.5, 115.3 (d, J = 22.5 Hz), 44.6; ^{19}F NMR ($CDCl_3$, 471 MHz): δ –107.1 (s). IR (KBr, cm^{-1}): 3036, 2930, 1590, 1419, 1105, 780; HRMS (ESI/Q-TOF) (m/z) calcd for $C_{14}H_{12}ClFNO_2S$, $[M + H]^+$: 312.0256, found 312.0251.

***4-Bromo-N-(methyl(oxo)(phenyl)- λ⁶-sulfaneylidene)benzamide (1d)*:**

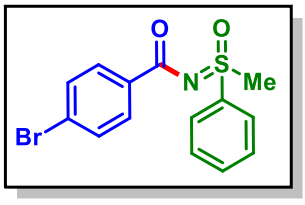

Yield: 71% (120 mg) as a white solid; Purified over a column of silica gel (30% EtOAc in hexane); ^{1}H NMR ($CDCl_3$, 600 MHz): δ, 8.05–8.02 (m, 4H), 7.70 (t, 1H, J = 9.0 Hz), 7.63 (t, 2H, J = 6.0 Hz), 7.54 (d, 2H, J = 6.0 Hz), 3.47 (s, 3H); ^{13}C{^{1}H} NMR ($CDCl_3$,

150 MHz): δ 173.6, 138.9, 134.7, 134.2, 131.5, 131.3, 129.9, 127.4, 127.3, 44.6.

4-Bromo-N-((3-methoxyphenyl)(methyl)(oxo)- λ⁶-sulfaneylidene)benzamide (3d):

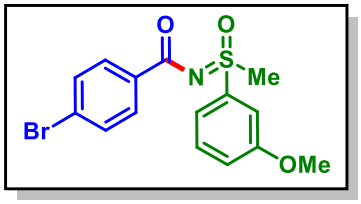

Yield: 61% (112.3 mg) as a white solid; Purified over a column of silica gel (35% EtOAc in hexane); ^{1}H NMR ($CDCl_3$, 600 MHz): δ 8.02 (d, 2H, J = 12.0 Hz), 7.58 (d, 1H, J = 6.0 Hz), 7.55–7.50 (m, 4H), 7.20 (dd, 1H, J = 6.0 Hz), 3.89 (s, 3H), 3.45 (s, 3H); ^{13}C{^{1}H} NMR ($CDCl_3$, 150 MHz): δ 173.6, 160.6, 140.1, 134.7, 131.5, 131.3, 131.0, 127.4, 120.3, 119.2, 112.2, 56.0, 44.6; IR (KBr, cm^{-1}): 3032, 2918, 1615, 1352, 1096, 773; HRMS (ESI/Q-TOF) (m/z) calcd for $C_{15}H_{15}BrNO_3S$, $[M + H]^+$: 367.9951, found 367.9953.

4-Bromo-N-((3-chlorophenyl)(methyl)(oxo)- λ⁶-sulfaneylidene)benzamide (6d):

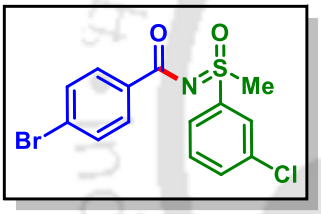

Yield: 45% (83.7 mg) as a white solid; Purified over a column of silica gel (35% EtOAc in hexane); ^{1}H NMR ($CDCl_3$, 600 MHz): δ 8.01 (d, 3H, J = 12.0 Hz), 7.92 (d, 1H, J = 12.0 Hz), 7.67 (d, 1H, J = 6.0 Hz), 7.58–7.55 (m, 3H), 3.46 (s, 3H); ^{13}C{^{1}H} NMR ($CDCl_3$, 150 MHz): δ 173.5, 140.8, 136.3, 134.3, 131.6, 131.3, 131.2, 127.6, 127.5, 125.5, 44.6; IR (KBr, cm^{-1}): 3033, 2932, 1606, 1186, 911, 742; HRMS (ESI/Q-TOF) (m/z) calcd for $C_{14}H_{12}BrClNO_2S$, $[M + H]^+$: 371.9455, found 371.9459.

N-(Methyl(oxo)(phenyl)- λ⁶-sulfaneylidene)furan-2-carboxamide (1e):

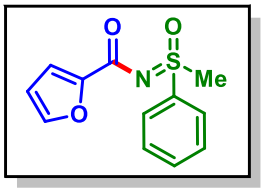

Yield: 51% (63.5 mg) as a white solid; Purified over a column of silica gel (25% EtOAc in hexane); ^{1}H NMR ($CDCl_3$, 400 MHz): δ 8.06–8.03 (m, 2H), 7.71–7.67 (m, 1H), 7.64–7.59 (m, 2H), 7.54 (s, 1H), 7.18–7.17 (m, 1H), 6.48 (d, 1H, J = 4.0 Hz), 3.47 (s, 3H); ^{13}C{^{1}H} NMR ($CDCl_3$, 100 MHz): δ 165.5, 150.2, 145.7, 138.9, 134.1, 129.9, 127.4, 116.9, 111.9, 44.8.

***(2S)-1,7,7-Trimethylbicyclo[2.2.1]heptan-2-yl-2-(4-(N-benzoyl-S-methylsulfonimidoyl)phenyl)acetate (18a)*:**

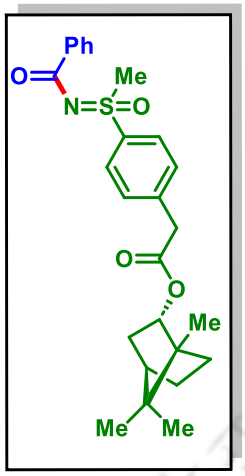

Yield: 51% (115.5 mg) as a colorless viscous liquid; Purified over a column of silica gel (20% EtOAc in hexane); ^{1}H NMR ($CDCl_3$, 600 MHz): δ 8.16 (d, 2H, J = 12.0 Hz), 8.02 (d, 2H, J = 6.0 Hz), 7.54 (d, 2H, J = 6.0 Hz), 7.51 (t, 1H, J = 6.0 Hz), 7.41 (t, 2H, J = 6.0 Hz), 4.91–4.89 (m, 1H), 3.74 (s, 2H), 3.46 (s, 3H), 2.37–2.31 (m, 1H), 1.85–1.80 (m, 1H), 1.76–1.71 (m, 1H), 1.68 (d, 1H, J = 6.0 Hz), 1.28–1.25 (m, 1H), 1.20–1.15 (m, 1H), 0.95–0.91 (m, 1H), 0.88 (s, 3H), 0.86 (s, 3H), 0.79 (s, 3H); ^{13}C{^{1}H} NMR ($CDCl_3$, 150 MHz): δ 174.4, 170.8, 141.0, 137.8, 135.7, 132.4, 130.8, 129.6, 128.2, 127.6, 81.3, 49.0, 48.0, 44.9, 44.6, 41.6, 36.9, 28.2, 27.2, 19.8, 18.9, 13.7.

***(1R,2S,5R)-2-Isopropyl-5-methylcyclohexyl-2-(4-(N-benzoyl-S-methylsulfonimidoyl)phenyl)acetate (19a)*:**

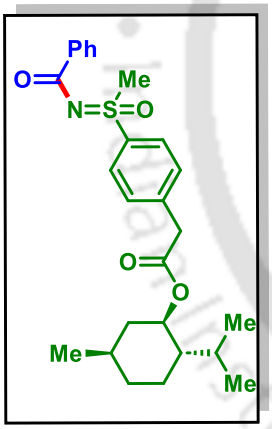

Yield: 55% (125.1 mg) as a white solid; Purified over a column of silica gel (35% EtOAc in hexane); ^{1}H NMR ($CDCl_3$, 600 MHz): δ 8.16 (d, 2H, J = 6.0 Hz), 8.01 (d, 2H, J = 12.0 Hz), 7.53–7.50 (m, 3H), 7.41 (t, 2H, J = 6.0 Hz), 4.72–4.67 (m, 1H), 3.71 (s, 2H), 3.46 (s, 3H), 1.98–1.95 (m, 1H), 1.76–1.71 (m, 1H), 1.69–1.65 (m, 2H), 1.51–1.44 (m, 1H), 1.39–1.34 (m, 1H), 1.07–0.94 (m, 3H), 0.89 (d, 3H, J = 6.0 Hz), 0.85 (d, 3H, J = 6.0 Hz), 0.70 (d, 3H, J = 6.0 Hz); ^{13}C{^{1}H} NMR ($CDCl_3$, 150 MHz): δ 174.4, 170.1, 141.0, 137.8, 135.7, 132.4, 130.8, 129.6, 128.2, 127.6, 75.6, 47.1, 44.6, 41.6, 40.9, 34.3, 31.6, 26.4, 23.5, 22.2, 20.9, 16.5.

***(3aS,5S,6R,6aS)-5-((S)-2,2-Dimethyl-1,3-dioxolan-4-yl)-2,2-dimethyltetrahydrofuro[2,3-d][1,3]dioxol-6-yl 2-(4-(N-benzoyl-S-methylsulfonimidoyl)phenyl)acetate (20a)*:**

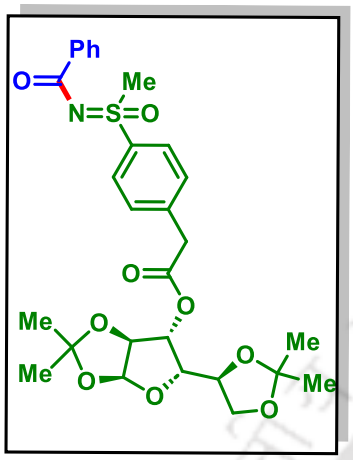

Yield: 42% (117.4 mg) as a colorless viscous liquid; Purified over a column of silica gel (35% EtOAc in hexane); ^{1}H NMR ($CDCl_3$, 600 MHz): δ 8.13–8.09 (m, 2H), 7.98–7.96 (m, 2H), 7.55–7.50 (m, 3H), 7.42–7.39 (m, 2H), 5.89–5.84 (m, 1H), 5.30–5.24 (m, 1H), 4.53–7.51 (m, 1H), 4.10–4.06 (m, 1H), 3.79–3.72 (m, 3H), 3.58–3.44 (m, 2H), 3.39–3.34 (m, 3H), 1.51–1.46 (m, 3H), 1.33–1.26 (m, 3H), 1.25 (s, 3H); ^{13}C{^{1}H} NMR ($CDCl_3$, 150 MHz): δ 174.7, 169.7, 140.1, 137.9, 135.3, 132.7, 130.9, 129.7, 128.3, 127.8, 112.6, 105.11, 105.07, 83.1, 79.5, 77.3, 69.02, 68.5, 65.0, 64.6, 44.7, 41.6, 41.4, 26.8, 26.4.

***4-(N-Benzoyl-S-methylsulfonimidoyl)benzyl-2-(2-fluoro-[1,1'-biphenyl]-4-yl)propanoate (21a)*:**

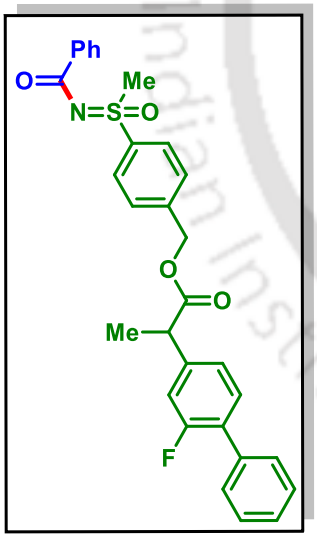

Yield: 58% (149.3 mg) as a white solid; Purified over a column of silica gel (25% EtOAc in hexane); ^{1}H NMR ($CDCl_3$, 600 MHz): δ 8.15 (d, 2H, J = 12.0 Hz), 8.00 (d, 2H, J = 12.0 Hz), 7.53–7.50 (m, 3H), 7.48 (d, 2H, J = 12.0 Hz), 7.45–7.35 (m, 6H), 7.15 (d, 1H, J = 6.0 Hz), 7.10 (d, 1H, J = 12.0 Hz), 5.22 (s, 2H), 3.84 (q, 1H, J = 6.0, 12.0 Hz), 3.42 (d, 3H, J = 6.0, Hz), 1.57 (d, 3H, J = 12.0 Hz); ^{13}C{^{1}H} NMR ($CDCl_3$, 150 MHz): δ 174.5 173.7, 159.9 (d, J = 247.5 Hz), 142.4, 141.4 (d, J = 7.5 Hz), 138.8, 135.5 (d, J = 21.0 Hz), 132.5, 131.1, 129.6 (d, J = 76.5 Hz), 128.7, 128.3, 128.0, 127.7, 123.8, 115.4 (d, J = 22.5 Hz), 65.5, 45.1, 44.6, 18.4; ^{19}F NMR ($CDCl_3$, 471 MHz): δ –117.4 (s).

4-(N-Benzoyl-S-methylsulfonimidoyl)benzyl 2-(4-isobutylphenyl)propanoate (22a):

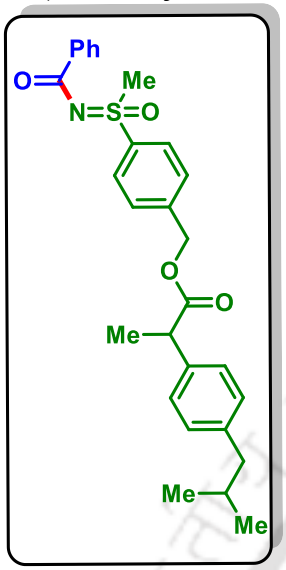

Yield: 52% (124 mg) as a colorless viscous liquid; Purified over a column of silica gel (30% EtOAc in hexane); ^{1}H NMR ($CDCl_3$, 600 MHz): δ 8.15 (d, 2H, J = 6.0 Hz), 7.95 (d, 2H, J = 12.0 Hz), 7.51 (t, 1H, J = 6.0 Hz), 7.43–7.37 (m, 4H), 7.20 (d, 2H, J = 6.0 Hz), 7.10 (d, 2H, J = 6.0 Hz), 5.21 (d, 1H, J = 12.0 Hz), 5.15 (d, 1H, J = 18.0 Hz), 3.79 (q, 1H, J = 6.0 Hz), 3.43 (s, 3H), 2.45 (d, 2H, J = 6.0 Hz), 1.86–1.81 (m, 1H), 1.53 (d, 3H, J = 6.0 Hz), 0.88 (d, 6H, J = 6.0 Hz); ^{13}C{^{1}H} NMR ($CDCl_3$, 150 MHz): δ 174.4, 142.83, 142.82, 141.0, 138.5, 137.4, 135.6, 132.4, 129.64, 129.62 128.42, 128.40, 128.25, 127.6, 127.4, 65.1, 45.3, 45.2, 44.6, 30.4, 22.5, 18.4.

2,2,6,6-Tetramethylpiperidin-1-yl benzoate (u):

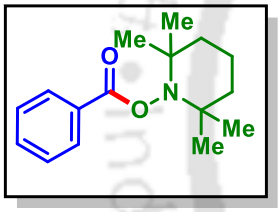

Yield: 22% (28.7 mg) as a white solid; Purified over a column of silica gel (10% EtOAc in hexane); ^{1}H NMR ($CDCl_3$, 600 MHz): δ 8.08 (d, 2H, J = 6.0 Hz), 7.57 (t, 1H, J = 9.0 Hz), 7.46 (t, 2H, J = 6.0 Hz), 1.81–1.76 (m, 2H), 1.70 (s, 1H), 1.60–1.57 (m, 2H), 1.48–1.44 (m, 1H), 1.27 (s, 6H), 1.12 (s, 6H); ^{13}C{^{1}H} NMR ($CDCl_3$, 150 MHz): δ 166.6, 133.1, 129.9, 129.8, 128.7, 60.6, 39.2, 32.2, 21.1, 17.2; HRMS (ESI/Q-TOF) (m/z): calcd for $C_{16}H_{24}NO_2$, $[M + H]^+$: 262.1802, found 262.1801.

VI.9. Representative Spectra

N-(Methyl(oxo)(phenyl)- λ⁶-sulfaneylidene)benzamide (1a) : ^{1}H NMR ($CDCl_3$, 600 MHz)

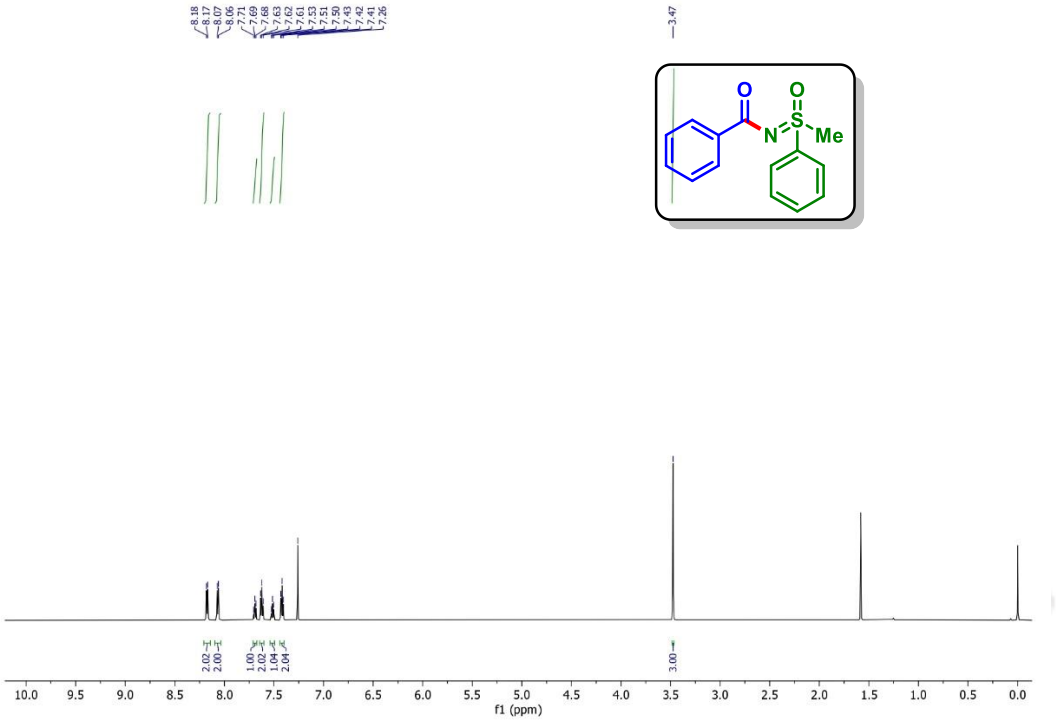

N-(Methyl(oxo)(phenyl)- λ⁶-sulfaneylidene)benzamide (1a): $^{13}C\{^{1}H\}$ NMR ($CDCl_3$, 150 MHz)

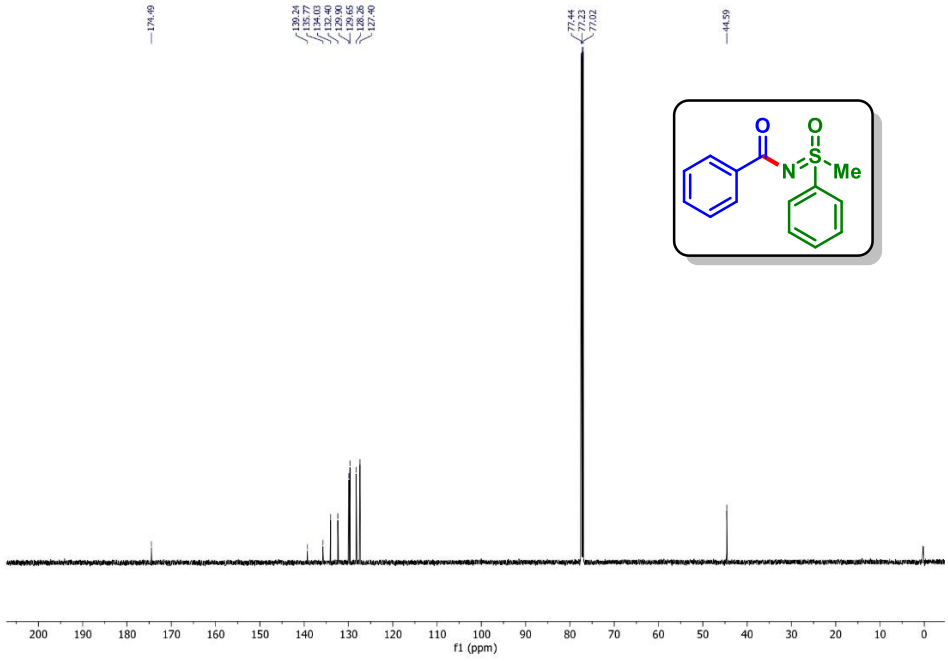

N-((4-methoxyphenyl)(methyl)(oxo)- λ⁶-sulfaneylidene)benzamide (2a): ^{1}H NMR ($CDCl_3$, 400 MHz)

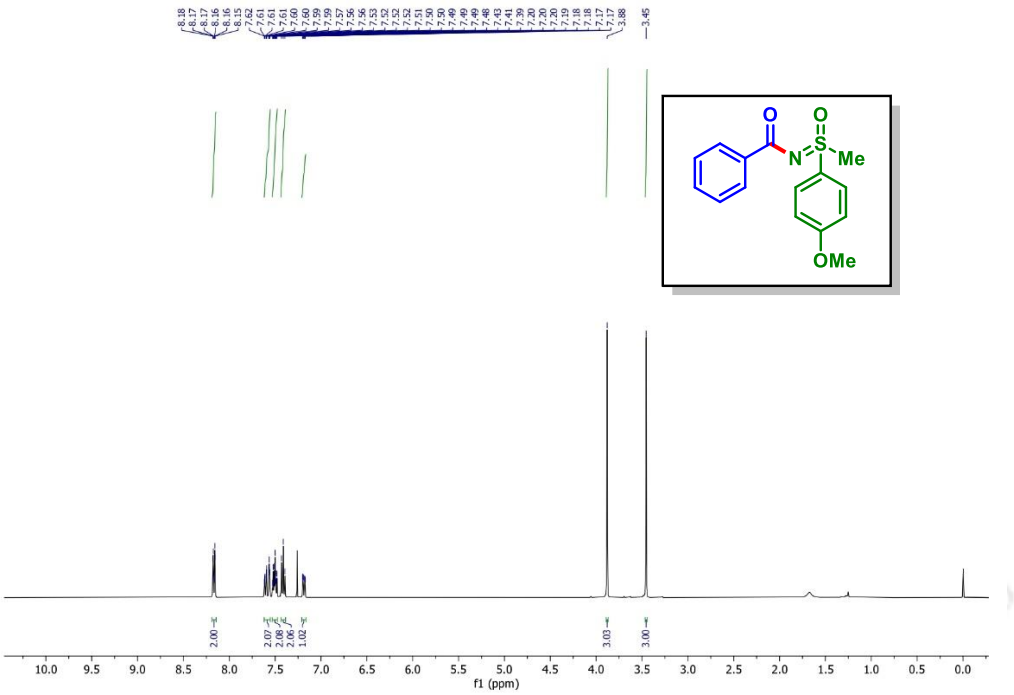

N-((4-methoxyphenyl)(methyl)(oxo)- λ⁶-sulfaneylidene)benzamide (2a): $^{13}C\{^{1}H\}$ NMR ($CDCl_3$, 100 MHz)

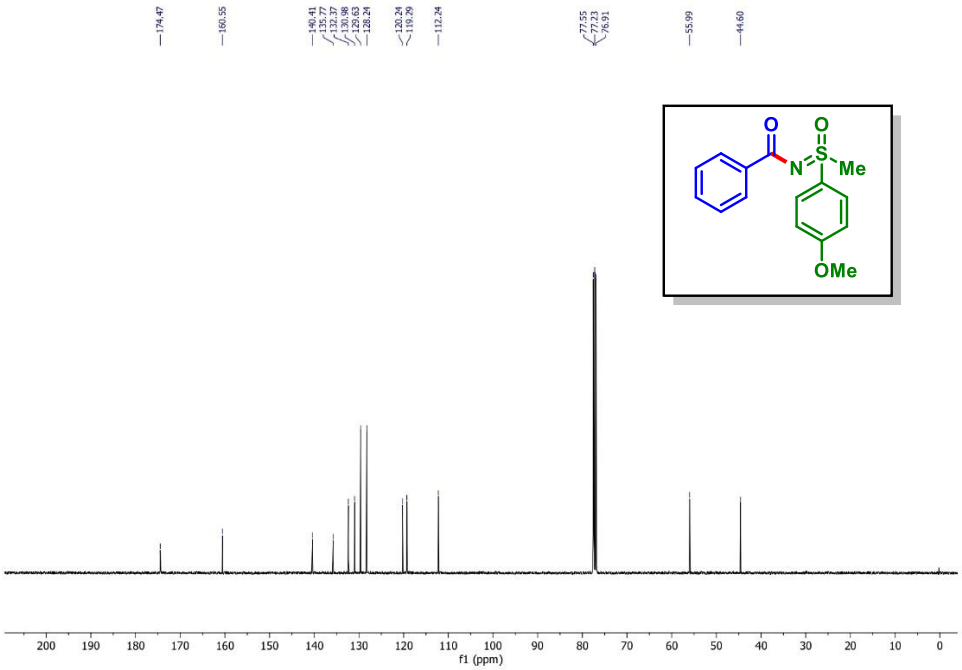

N-(Methyl(oxo)(thiophen-2-yl)- λ⁶-sulfaneylidene)benzamide (12a): ^{1}H NMR (CDCl$_3$, 600 MHz)

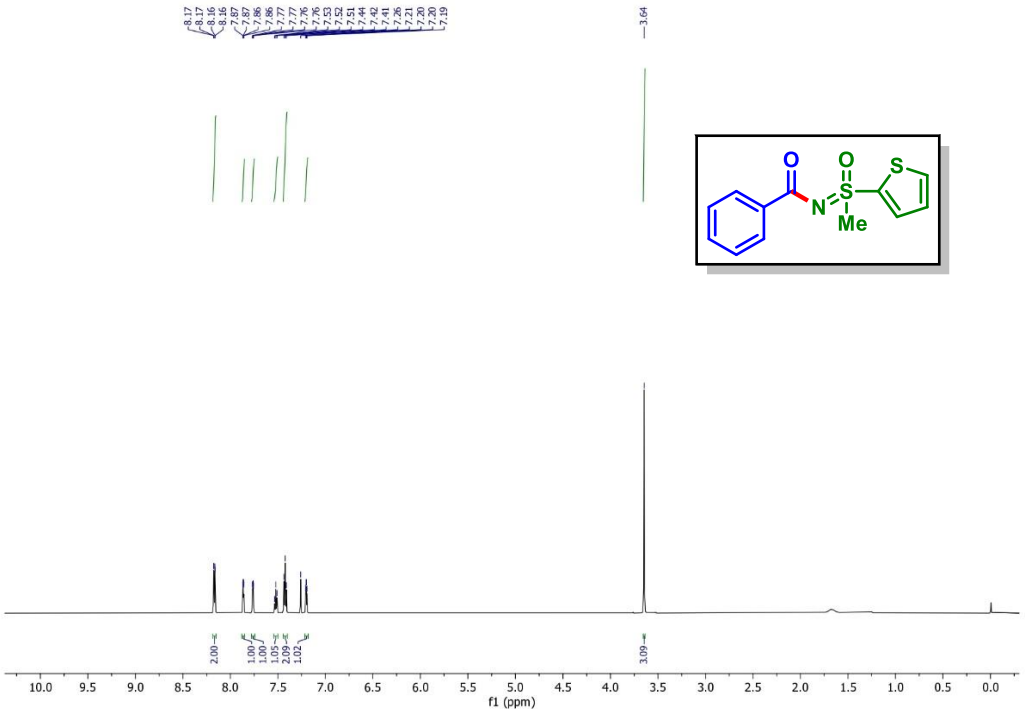

N-(Methyl(oxo)(thiophen-2-yl)- λ⁶-sulfaneylidene)benzamide (12a): ^{13}C{^{1}H} NMR (CDCl$_3$, 150 MHz)

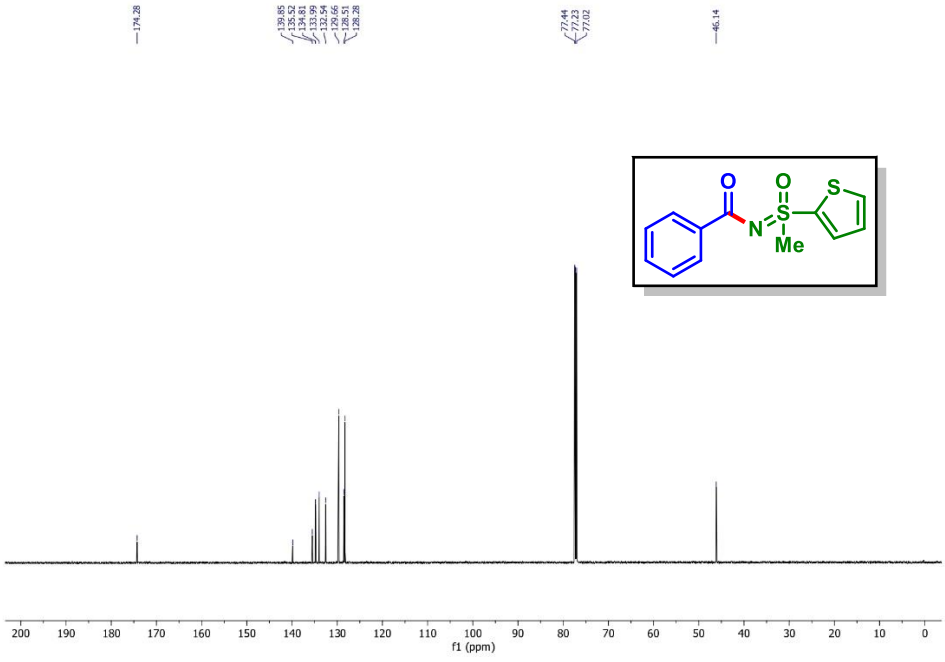

4-Bromo-N-(methyl(oxo)(phenyl)- λ⁶-sulfaneylidene)benzamide (1d): ^{1}H NMR ($CDCl_3$, 600 MHz)

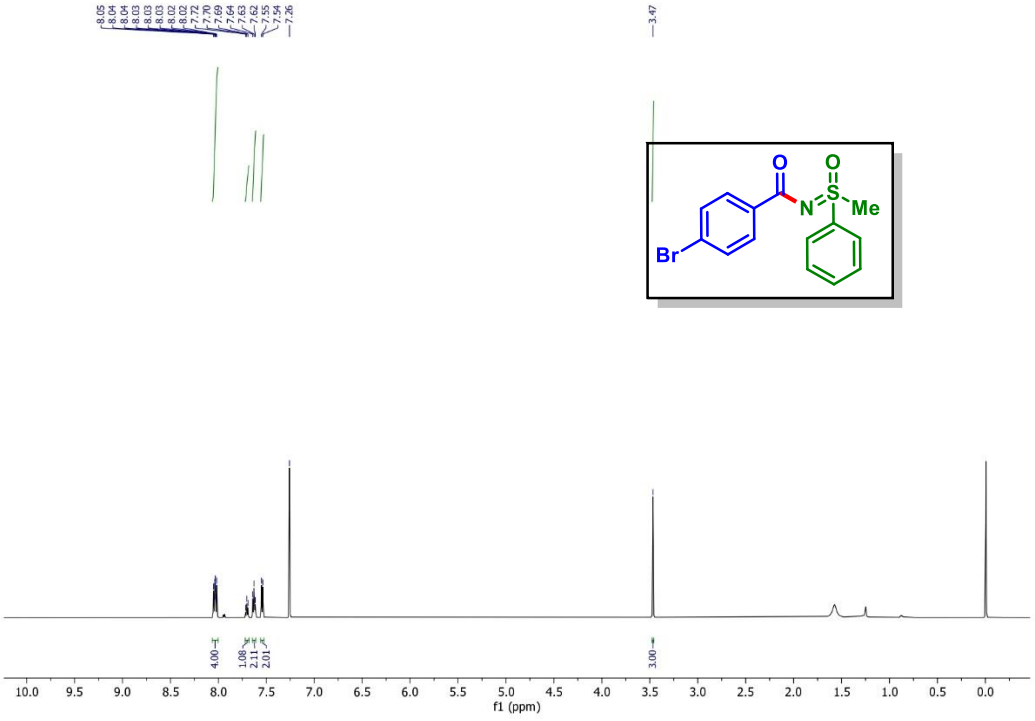

4-Bromo-N-(methyl(oxo)(phenyl)- λ⁶-sulfaneylidene)benzamide (1d): $^{13}C\{^{1}H\}$ NMR ($CDCl_3$, 150 MHz)

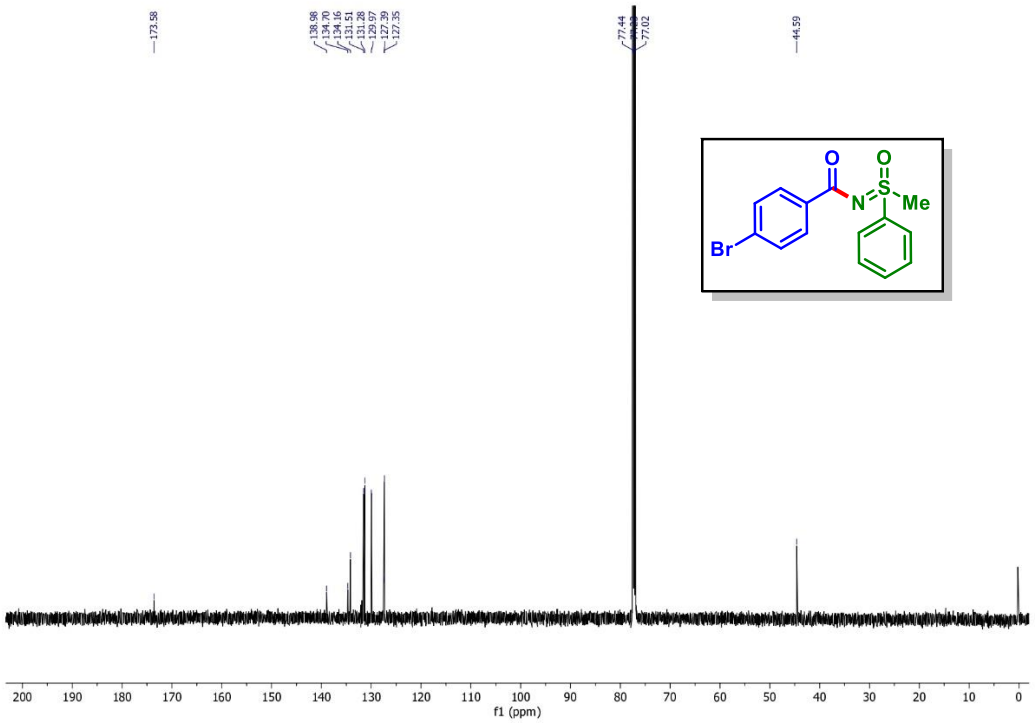

(1R,2S,5R)-2-Isopropyl-5-methylcyclohexyl-2-(4-(N-benzoyl-S-methylsulfonimidoyl)phenyl)acetate (19a): ^{1}H NMR ($CDCl_3$, 600 MHz)

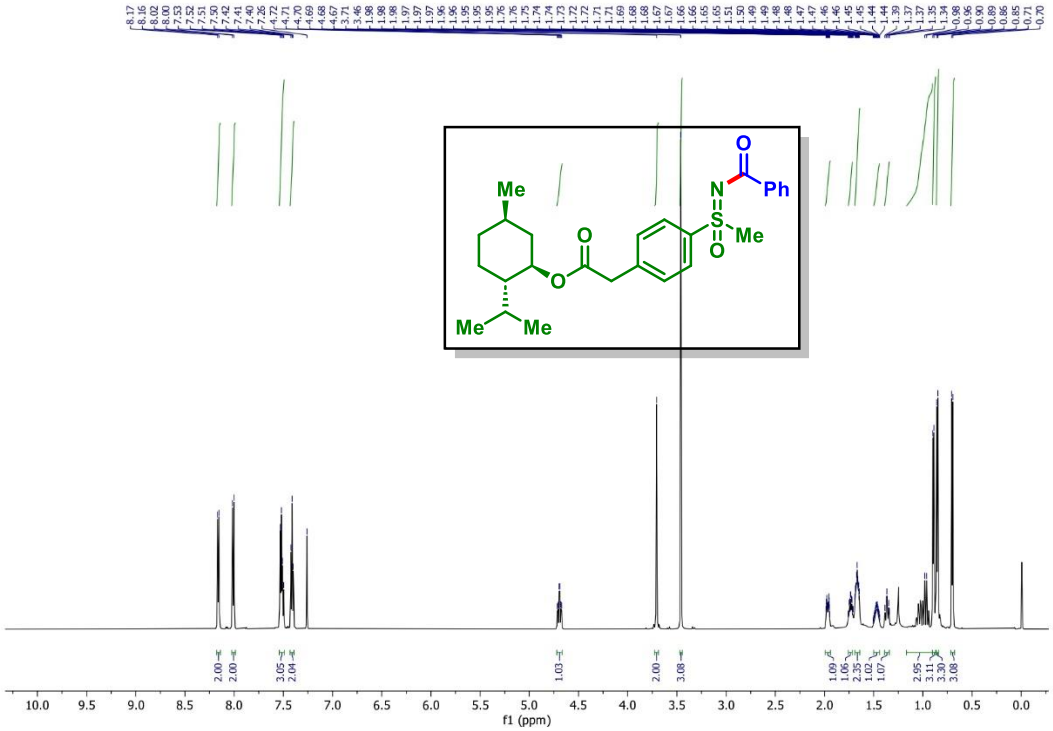

(1R,2S,5R)-2-Isopropyl-5-methylcyclohexyl-2-(4-(N-benzoyl-S-methylsulfonimidoyl)phenyl)acetate (19a): $^{13}C\{^{1}H\}$ NMR ($CDCl_3$, 150 MHz)

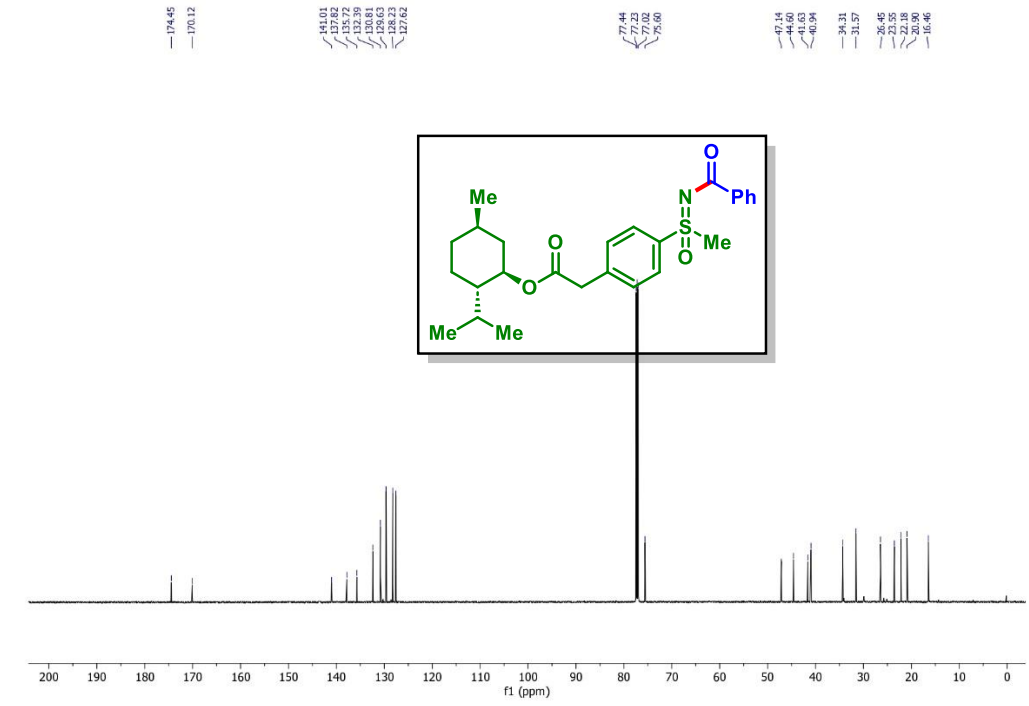

List of Publications

1. **Alam, T**.; Gupta, S.; Patel, B. K. ***(Manuscript Submitted)***.
2. **Alam, T**.; Patel, B. K. *Chem.-Eur. J.* **2023**, *e202303444*.
3. **Alam, T**.; Rakshit, A.; Dhara, H. N.; Palai, A.; Patel, B. K. *Org. Lett.* **2022,** *24*, 6619–6624.
4. **Alam, T**.; Rakshit, A.; Begum, P.; Dahiya, A.; Patel, B. K. *Org. Lett.* **2020**, *22*, 3728–3733.
5. Shukla, G., **Alam, T**., Srivastava, H.K., Kumar, R.; Patel, B. K. *Org. Lett.* **2019**, *21*, 3543–3547.
6. Dahiya, A., Ali, W., **Alam, T**.; Patel, B. K. *Org. Biomol. Chem*. **2018**, *16*, 7787–7791.
7. Ali, W., Dahiya, A., Pandey, R., **Alam, T**., Patel, B. K. *J. Org. Chem.* **2017**, *82*, 2089–2096.
8. Sau, P.; Rakshit, A.; **Alam, T**.; Srivastava, H.; Patel, B. K. *Org. Lett*. **2019**, *21*, 4966–4970.
9. Shukla, G., Dahiya, A., **Alam, T**.; Patel, B. K. *Asian J. Org. Chem*. **2019**, *8*, 1–7.
10. Rakshit, A.; Kumar, P.; **Alam, T**.; Dhara, H.; Patel, B. K. *J. Org. Chem*. **2020**, *85*, 12482−12504.
11. Rakshit, A.; Dhara, H. N.; **Alam, T**.; Dahiya, A.; Patel, B. K. *J. Org. Chem*. **2021**, *86*, 17504–17510.
12. Rakshit, A.; Dhara, H. N.; Sahoo, A. K.; **Alam, T**.; Patel, B. K. *Org. Lett*. **2022**, *24*, 3741–3746.
13. Dhara, H. N., Rakshit, A.; **Alam, T**., Sahoo, A. K.; Patel, B. K. *Org. Lett*. **2023**, *25*, 471–476.

Reviewes

1. Dahiya, A., Sahoo, A. K.; **Alam, T**.; Patel, B. K. *Chem. Asian J.* ***2019***, *14*, 4454–4492.

2 Dhara, H. N.; Rakshit, A.; **Alam, T**.; Patel, B. K. *Org. Biomol. Chem.* **2022**, *20*, 4243–4277.

Book Chapters

1 Patel, B. K.; **Alam, T**.; Rakshit, A. Alkenes-Recent Advances, New Perspectives and Applications, edited by Reza Davarnejad, IntechOpen, **2021**, 10.5772/intechopen.98949.